RADIOMETRIC PARTIAL DISCHARGE CHARACTERISATION

Carlos Ramirez Pacheco

Submitted for the degree of Doctor of Philosophy in the Department of Electric and Electronic Engineering at Strathclyde University, Glasgow

2007

COPYRIGHT

STATEMENT OF RESTRICTION

This thesis may be available for the consultation within the university library and may be photocopied or lent to other libraries for the purpose of consultation.

DECLARATION OF RIGHTS

Acknowledgements

The Author wishes to thank the follow individuals and institutions:

CONACYT (Consejo Nacional de Ciencia y Tecnologia) for financial support that allowed me to study for this Doctoral Thesis.

CFE (Comision Federal de Electricidad), especially to the **UIE** (Unidad de Ingenieria Especializada), the **Subdireccion Tecnica** and the members of the **SUTERM** (Sindicato Unico de Trabajadores Electricistas de la Republica Mexicana) for all the support for the completion of this thesis.

IPN (Instituto Politecnico Nacional) for all the kind support that allowed me to complete this thesis.

To my supervisor **Professor Phil J. Moore** for his useful advice, support and encouragement.

To the group members of Professor Phil Moore, **Iliana**, **Li**, **Sa**, **Sven** and **Myself** (☺) who have made my stay all this time smooth and happy.

Special thanks are given to **Prof. Gilberto Enriquez Haper** and **Ing, Moises Moreno Ramirez** for their support and help.

And finally thanks to **my wonderful family (Carmelita, Bonny, Paty, Vero, Mary and Nico)** this is the result of your love and care, thanks a lot.

To all **my friends** (you know who you are!).

Thanks to **God** for all your blessings.

Summary

The process of generation, transmission and distribution of electric energy appears to be very simple. However, the continuous flow of power through electric networks is affected by several factors, normally of two kinds: failures caused by ageing of insulating materials and failures caused by defective equipment or design. The energy supplied to small and big consumers can be interrupted for long periods causing disastrous economic losses. The origin of most failures normally is found in electrical insulation, which is an essential component in all electrical systems especially in power equipment such as transformers and circuit breakers, the cost of which is very high. Before the insulation fails, there are manifestations of this condition, called partial discharges (PD) and because of this, PD have been subject of an extensive study and investigation.

PD identification relies on the intrinsic characteristics of the generated discharge. This thesis shows the behaviour of radiated discharge through the analysis of the characteristic frequency spectra and pulse distribution to create pattern classification in the laboratory. This research is based on a novel technique that uses wide band, high resolution equipment, composed of an antenna array, that receives the radiated discharge, and a high resolution oscilloscope that accurately measures and samples the propagated signal. The second part of the laboratory setup comprises the characterization of partial discharges using a high voltage transformer and measurement devices that accurately apply a range of voltages to specimens containing insulation defects. The advantages of having accurate PD sources are evident: availability, free of ambiance noise, accurate AC reference and PD location. Results show that pattern recognition to identify PD's using a non invasive system and point on wave information is possible and reliable.

Table of contents

LIST OF FIGURES

LIST OF TABLES

LIST OF ABBREVIATIONS

PD	Partial discharge
SF_6	Sulfur Hexafluoride
FFT	Fast Fourier Transform
PCA	Principal Component Analysis
HV	High Voltage
LV	Low Voltage
CO_2	Carbon Dioxide
UV	Ultraviolet
EPDM	Ethylene Propylene Diene Monomer
DC	Direct Current
PE	Polyethylene
EM	Electromagnetic Radiation
UHF	Ultra High Frequency
AC	Alternating Current
GIS	Gas Insulated Substation
RIV	Radio Interference Voltage

DLA	Dielectric Loss Analyzer
PDA	Partial Discharge Analyzer
TGA	Turbine Generator Analyzer
FASE	Fault Anticipation in Substation Equipment
CEGB	Central Electricity Generating Board
VLF	Very Low Frequency
RF	Radio Frequency
TOA	Time of Arrival
ATP	Alternative Transient Program
S	Samples
CH	Channel
IEC	International Electrotechnical Commission
GUI	Graphic User Interface
CT	Current transformer

LIST OF UNITS & SIMBOLS

UNITS

dB	Decibels
Ω	Ohm
Hz	Hertz
m	Metre
mm	Millimetre
s	Seconds
V	Volts
A	Ampere
W	Watt
VAC	VoltAmpere
H	Henry

SYMBOLS

T_g	Transition temperature (degrees)
C	Capacitance (F)
s	Switch
R	Resistance (Ω)
I	Current (A)
δ	Electric charge (coulombs)
r	Distance (m)
ε_0	Relative permittivity of free space
a	Acceleration
c	Speed of light
e	Charge
P_t	Transmitted power
B	Magnetic field
Q	Pulse charge magnitude
F	Frequency (Hz)
A	Acquired signal
S	Frequency spectrum of signal
H	Frequency spectrum of nearby objects
σ	Permittivity
S_k	Skewness
k_u	Kurtosis
cc	Cross correlation factor
P_0	Average distance between pulses
D_{pn}	Average magnitude between positive and negative pulses
ABS	Absolute value

INTRODUCTION

This introduction outlines the importance of the identification and prevention of partial discharges using a non invasive system and the state of the art of the existing methods. All the relevant objectives in this project are established in order to give to the reader a clear idea of the structure of this thesis.

1.1. Importance of non invasive survey and identification of PD's.

Electrical utilities rely on the efficiency and reliance of power equipment working at different voltage levels as most power systems have three operational areas clearly identifiable: generation, transmission and distribution [1.1]. Every one of the latter areas must operate continuously within the standardized energy quality parameters to deliver power to large and small consumers. Often power equipment suffers important disruptions that lead to long lasting blackouts in service. Power systems operators avoid these disruptions using protection relays to protect against system faults that involve high currents, surge arresters for short duration transients such as lightning, and preinsertion resistors in circuit breakers for long lasting transients such as switching of transmission lines [1.2]. In spite of its efficiency power system protection is not exempt from malfunctions, thus the best method to avoid equipment failures in power systems is through proper maintenance and prevention.

A high percentage of disruptions involve insulation failure: the cause of this is a combination of external and internal factors occurring in power equipment, but it is

well know that the prime factors affecting insulation are ageing, atmospheric conditions, manufacturing defects, pollution, mechanical and electrical stress [1.3]. The manifestations of defective insulation range from corona to partial discharges and complete breakdown. Partial discharges can be difficult to detect through single observation, since insulation can be often found inside transformers, circuit breakers, generators, motors and instrument transformers. Hence, in general, it is difficult to apply prevention methods to detect partial discharges, even for external insulation.

Fortunately there are several methods to detect and prevent partial discharges. Those methods approach the inherent properties of PD's [1.4]. It can be said that there are two methods to detect PD's: invasive or direct methods, and non invasive or indirect methods, the advantages of the second method to detect and identify PD's is that it implies the complete isolation of the measurement and diagnostic system from the power equipment, thus avoiding any interruption in the service. Any PD diagnostic system must be reliable and effective to justify its application. If the power equipment is not properly diagnosed, it can lead to an unnecessary interruption of service or, in the worst case, the unnecessary replacement. The test must not give a false diagnosis of equipment deterioration since this can erode the credibility of the PD detection system which due to a single important failure it must be discarded from the PD test program [1.5]. Thus the successfully implementation of any PD monitoring system depends on the correct identification of the PD characteristics and parameters, the latter requirement can only be achieved if extensive research in the laboratory and field is made. Little is know about the intrinsic characteristics of the radiated discharges when a non invasive method using antennas is employed. This method is affected by several factors such as the propagating media, the size and configuration of structures acting as antennas, and the acquisition system. Although several research works have been made concerning the behavior of radiated discharges using antennas [1.6], it has been focused mainly on the location and discrimination of the discharge from the background noise using filtering techniques [1.7]. Hence the development of a laboratory setup for the characterization and identification of partial discharges using the properties of the radiated electromagnetic wave is sought.

1.2. Research objectives.

The prime objective in this research work is to develop a method to identify different types of partial discharge and its inherent characteristics using an experimental setup in laboratory. This research can be divided in two parts:

- Investigation of the inherent characteristics of radiated electromagnetic waves
- To develop a method to differentiate between different kinds of partial discharges (pattern classification)

1.3. Thesis structure.

The thesis structure has been designed to present the research project at different levels, from its conceptual requirements to its practical application in a transparent and simple manner. The thesis document can be divided into two parts that show information in different levels:

1. The main body of the thesis: this is divided in 9 chapters that give an overview of the research without unnecessary detail. The following is a description chapter by chapter:

   - Chapter 2 will give to the reader a general overview of the partial discharges theory, starting with a background in electrical insulation which understanding is essential for a suitable understanding of the PD mechanism. A basic explanation of the causes that trigger partial discharges and a general description of the main kinds of partial discharges is provided. After the PD description, the different kinds of partial discharge detection methods are described, following by the mathematical representation of a cavity discharge using an equivalent electric circuit. Chapter 2 ends with the explanation of PD's in SF_6.

- Chapter 3 is a summary of the importance and background of partial discharge identification; the chapter starts with the history of the monitoring and identification of PD's and a summary of the off-line and on-line PD detection systems. This chapter also surveys the modern PD detection and location systems and gives general considerations for its design. Radiofrequency transients in power systems are explained and evaluated in this chapter, the concept of sferic and its identification is provided. This chapter ends with a general overview of pattern classification of partial discharges.

- In chapter 4 a detailed explanation of the making of the laboratory test set system used in this research is provided: the description starts with the test set simulation and a description of its components; the software used for the analysis of the obtained results is described. All the system tests and verification is described step by step. Finally a general overview of the test set is given.

- Chapter 5 is a description of the tests carried out in order to asses the several factors that affect the conducted and radiated discharge in laboratory, for these tests, discharges in air and oil were generated in the developed test set and its characteristics in frequency and time were analyzed. A novel method to compensate the effect of surrounded objects and structures is included.

- Chapter 6 is a description of the tests carried out in laboratory using samples that represent several defects in insulation. The different samples using for the generation of PD's are described and the results are explained, the results of the tests conducted using the samples are explained in the context of the frequency domain analysis (FFT) and the time domain analysis (point in wave information), at the end of this chapter a comparison between different samples is analyzed.

- Chapter 7 is an analysis of the application of discrimination methods to the generated partial discharges using the obtained results; this chapter starts with the justification of the use of discrimination techniques to the conducted and radiated discharges, afterwards, the use of statistical operators as a reliable method for PD discrimination and classification is explained, and ends with the use of the principal component analysis (PCA).

- Chapter 8 provides the conclusion of the research and results conducted in the HV laboratory, the conclusions are divided for every result obtained.

- Finally chapter 9 gives the suggestions for future research concerning the results obtained so far, that were not covered by this investigation, but that could be developed for future applications.

2. Appendices: they give detailed information about the employed methods and results.

1.4. Chapter 1 references

[1.1] J. Duncan Glover, Mulukutla Sarma, *Power System Analysis and Design*, PWS, 1994.

[1.2] E. Kuffel; W. S. Zaengl; J. Kuffel, *High Voltage Engineering: Fundamentals*, Newnes, 2001.

[1.3] N. H. Malik, A. A. Al-Arainy, M. I. Qureshi, *Electrical Insulation in Power Systems*, Marcel Dekker, 1998.

[1.4] J. P. Steiner, "Partial Discharge – Part IV: Commercial PD Testing", *IEEE Electrical Insulation Magazine*, Jan/Feb 1991, Vol. 7, No. 1, pp 20 – 33.

[1.5] J. C. Stone, "Partial Discharge Part VII: Practical Techniques for Measuring PD in Operating Equipment", *IEEE Electrical Insulation Magazine*, July/August 1991, Vol. 7, No. 4, pp 9 – 19.

[1.6] E J Bartlett and P J Moore, "A system for monitoring VHF electromagnetic radiation generated by power system disturbances", Proceedings of 34th UPEC, Leicester University, Sept 1999, Vol 1, pp 249-252.

[1.7] E.J. Bartlett and P.J. Moore, "Analysis of power system transient induced radiation for substation plant condition monitoring", IEE Proc-Gener, Transm. Distrib. Vol 148, No. 3, May 2001.

PARTIAL DISCHARGES: STATE OF THE ART

This chapter provides an overview of PD basics and common diagnostic techniques to detect PD in power equipment and installations, and the introduction of new technologies as a consequence of a reliable delivery of continuous power flow to consumption centers. The description of the advantages and disadvantages of partial discharge monitoring and its characteristics is worked out and applied to the present research.

2.1. Electrical insulation

Modern power systems comprise of several components that perform a specific task in carrying power from generation plants to consumer centers. One of the tasks is to isolate the low, medium and high voltage from ground potential. In order to perform this task efficiently, insulators are used, which are made of different materials, the most common materials can be classified into five main groups [2.1]:

- Solids
- Liquids
- Gases
- Vacuum
- Composites

Further combinations of these materials can be found, but they are the basis for insulation in power equipment.

Depending on the application, the insulation of power equipment can be exposed to meteorological conditions (external insulation) i.e. to sun and uv light, rain, pollution etc, or it can be confined to internal parts of the devices (internal insulation). In both cases insulation is always exposed to high or low voltage and mechanical stress. It is very common to find combinations of these three groups in electrical devices such as transformers or circuit breakers. These combinations form insulating interfaces that can be critical for the design of power equipment as we will see in detail in the follow sections. External or internal insulation is affected in different ways, it can be noticed that external insulation is the most affected, since it is exposed to atmospheric air, but it can be diagnosed and replaced easily. The behavior and condition of internal insulation is more difficult to detect and sometimes signs of deterioration are noticed too late to avoid the complete destruction of the equipment containing the affected insulation. So different is the treatment of this insulation that its coordination must be calculated separately [2.2,2.3]. Various factors affect internal and external insulation, among this we can list the following:

- Pollution
- Acid rain
- Ageing
- Electrical and mechanical stress
- Manufacturing defects
- Quality of the insulating material

Some of the above factors are related closely, but they have to be treated separately as they present different characteristics.

- *Pollution*. - External insulation is often located in open air substations. In power plants located in industrial zones, where pollution is usually very

heavy [2.4], the surfaces of insulators accumulate layers of dust that include metallic and carbon particles. When dry these layers do not affect the performance of the insulator but when there is moisture in the air or light rain, these layers become conductive and can cause a complete breakdown.

- *Acid rain*. - Highly populated regions cause CO_2 pollution due to the consumption of fossil fuels. This gas combines with water clouds and modifies its pH balance adding acidity to the falling rain. This acidity can erode or age the surface of insulators causing surface discharges or even a complete discharge.

- *Ageing*. – The rate of deterioration of the insulation material with time depends on its quality and its manufacturing process. Ageing is normally related to polymeric insulators since the properties of this kind of material tend to be modified with use. These modifications are caused, among other things by sun and UV light or electrical stress. Cavities can be found in polymeric insulators if they are not properly manufactured in the factory. The internal walls of cavities can be eroded by electrical discharges, enlarging their size and causing damage to the insulator.

- *Mechanical and electrical stress*. - Overvoltages and electrical transients combined with mechanical effects can modify the properties of the dielectric material and cause damage or complete destruction of insulators. The application of over voltage protections and a proper mechanical design can avoid this effect.

- *Manufacturing defects*. - In the manufacturing process of polymeric insulators or power equipment, small protuberances or cavities in the boundaries between insulators of different dielectric constants or solid insulators can be created. When an electric field is applied to these defective insulators, small discharges are created (partial discharges) and in the long term they cause the failure or destruction of the equipment.

- *Quality of the insulating material.* - Even if the power equipment is well manufactured, differences exist in quality between insulators. A typical case is polymeric insulators, where different kinds of polymers are used, with Ethylene Propylene Diene Monomer (EPDM) rubber and silicon rubber the most popularly used [2.5]. Because of its characteristics, EPDM shows less resistance to degradation when compared to silicon rubber, but is less expensive.

The variety in electrical insulation employed in power systems as it can be seen, is very wide, and consequently the failures and technical problems affecting this component are very difficult to detect and hence classify. However recent advances in preventing failures in electrical equipment are mainly focused on electrical insulation, specifically in detecting partial discharges and corona.

2.2. PD Basics

The basic definition of a partial discharge is given by the international standard IEC 60270 [2.6], *A partial discharge is a discharge process that only partially bridge the distance between two electrodes*. This electric discharge could be a spark or an arc and can be originated directly at one of the electrodes or occur without electrodes in a cavity of the dielectric. Two notes accompany this definition:

"Note 1 Partial discharges are in general a consequence of local electrical stress concentrations in the insulation or on the surface of the insulation. Generally, such discharges appear as pulses having a duration of much less than 1μs. More continuous forms can, however, occur, such as the so-called pulse-less discharges in gaseous dielectrics. This kind of discharge will normally not be detected by the measurement methods described in this standard."

"Note 2 "Corona" is a form of partial discharge that occurs in gaseous media around conductors which are remote from solid or liquid insulation. *"Corona" should not be used as a general term for all forms of PD."*

Electrodes can be connected across weakness in insulation such as small voids, cracks, de-laminations, contamination, loose connections or floating pieces of metal. A voltage gradient of sufficient strength across this weakness produces partial discharges. The higher the operating voltage, the more pronounced will be the PD events. We can summarize some typical PD phenomena as follows:

- Corona discharges occurring in gaseous dielectrics in the presence of non uniform fields.
- Internal discharges occurring in voids or cavities within solid or liquid dielectrics.
- Surface discharges appearing at the boundary of different insulation materials.
- Continuous impact of discharges in solid dielectrics forming discharge channels (treeing).

2.2.1. Corona Discharges

Corona occurs in gaseous media around conductors [2.7]. Corona discharge can be formed in a high electrostatic field region caused by any sharp energized component or structure in a gaseous system. Within this partially ionized region, if the distance is increased, the electric field is decreased notably restraining the complete formation of the breakdown; however this is normally seen as a virtual extension of the adjacent conductor with respect to ground as it modifies the electric field. This increases the conductor capacitance and hence the voltage drops. This effect causes a difference in potential between the source and the conductor, as a result of which, current flows from the source to the conductor. This current exists only during the inception of corona i.e. a sporadic and random current flow. An ultra-corona occurs when the voltage is increased further above the corona threshold value, the corona current increases and the growth is proportional to the squared voltage. In a gap with large electrodes, as the voltage increases, shaped channels of light appear and disappear again within a few microseconds; this kind of corona is known as streamer corona [2.8]. The complete discharge occurs when a streamer short-circuits the

whole gap; various factors such as humidity, atmospheric pressure and humidity lead to a faster or a slower breakdown.

2.2.2. Cavity Breakdown

Sometimes solid or liquid dielectric insulators contain voids or cavities within the medium at the boundaries between the dielectric and the electrodes. Similarly, in amorphous polymers, there are vacant spaces or holes between the molecules which are called free volume. In polyethylene, below the glass transition temperature T_g, the free volume is approximately 2.5% of the total volume, which increases with temperature above T_g. Similarly, epoxy resin composites are prepared by mixing reinforcing fillers. Generally there exists between them a chemical or quasi-chemical adsorption-type bonding at the interface. But if care is not taken in fabrication, many areas of interface may have no bonding but a gap of varying thickness. These voids are generally filled with medium of a lower dielectric strength and lower permittivity; hence the electric strength in the voids will be higher than that across the dielectric. Therefore even under normal working voltages the field in the voids may exceed their breakdown value, and breakdown may occur in these small cavities, note that the effect of charge within the cavity can lead to PD without the minimum Laplacian breakdown field [2.1, 2.9].

2.2.3. Interfacial polarization in composites

The effect of interfacial polarization occurs on the application of an electric field to an insulating material that is composed of two or more different phases that contain dispersed macroscopic impurity regions. A space charge builds up at the microscopic interfaces as a result of differences in conductivities and permittivity of its individual components. It will lead to increased dielectric losses and also cause field distortion in the material [2.1].

When one of the composite components has significant ionic conductivity, then mobile charges (usually impurity ions) diffuse under the influence of the applied

field across the more conducting component up to the interface of the less conducting component. At this new interface they will become stationary and thus build up a surface charge as shown in figure 2.1. This effect will remain there until the applied field reverses, as in the case of alternating voltage. In the case of DC voltage and longer stressing time, a much larger space charge buildup continues until a very significant reverse electrical field develops from this surface charge, eventually arresting the current flow to a value that is determined by the less conducting component. This type of polarization is very common in composite insulation, since such interfaces are distributed throughout its structure. The high concentrations of traps are found at the crystalline-amorphous interfaces. Because of this, space charge accumulation in polymeric cables and solid insulation is a topic that is currently been investigated world wide.

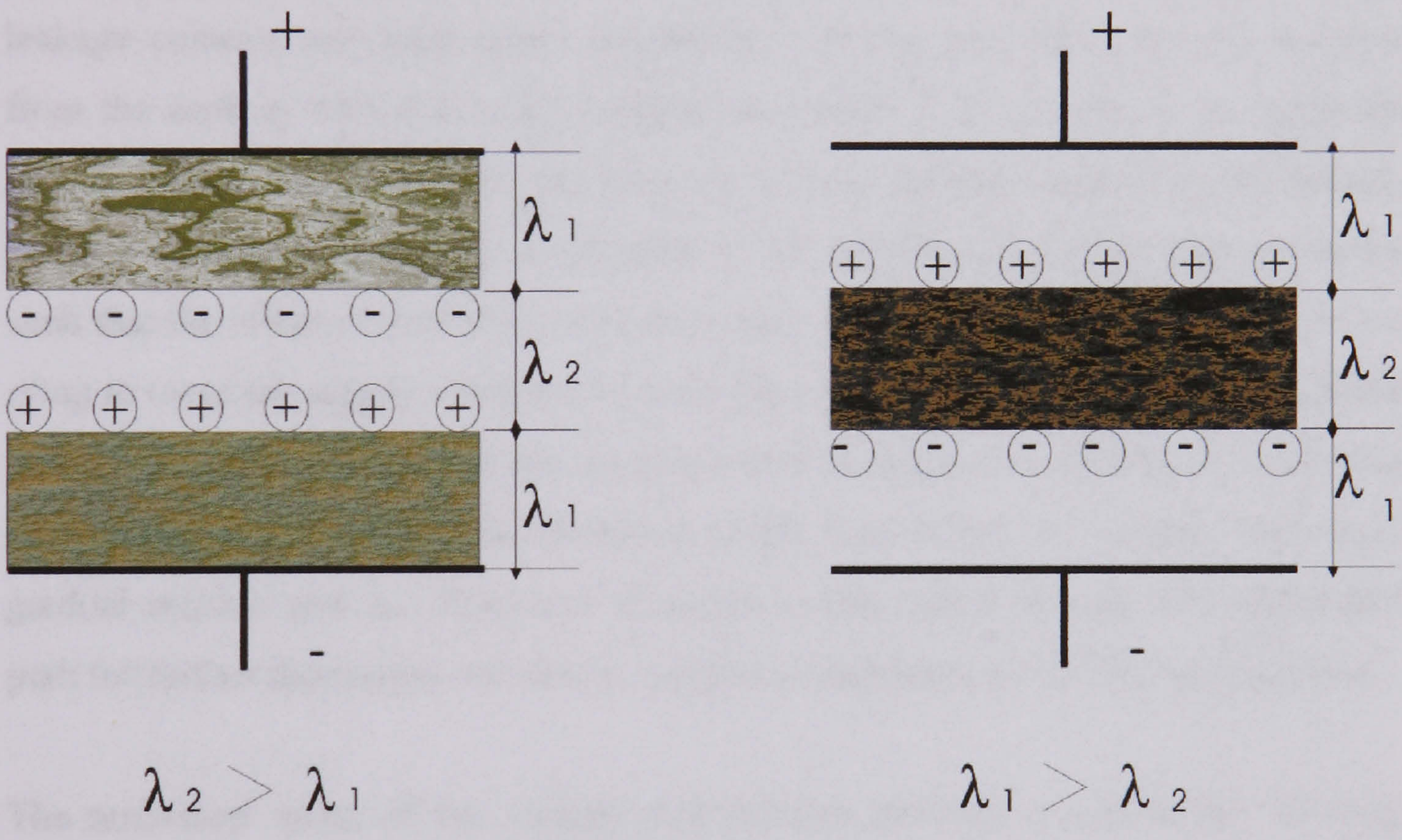

Figure 2.1 Interfacial polarization in composite dielectrics

2.2.4. Breakdown due to surface erosion and tracking

In recent years, the needs of major utilities regarding economy and reliability have encouraged the development of new materials used in high voltage equipment. Insulators have taken the lead in the use of polymeric compounds as they are tough,

light in weight and possess excellent dielectric properties [2.10]. However they are affected by erosion and tracking when in service on high voltage equipment and transmission lines. The erosion roughens the surface, causing permanent damage, which promotes the accumulation of pollution and finally leads to tracking and breakdown of the insulator.

Tracking is the formation of a permanent conducting path, carbon among other components, across the surface of the insulator, resulting from degradation due to continuous discharges and erosion [2.11]. During service, the surface of the insulator is progressively contaminated. Pollution absorbs moisture from the atmosphere and forms a wet layer of pollution that provides a continuous conducting path between the HV electrode and ground. The surface resistance decreases considerably in the presence of pollution and moisture. Low resistance, in turn, leads to high surface leakage currents and high power dissipation, causing significant loss of moisture from the surface. This loss is not uniform, and leads to the formation of dry bands [2.12]. Due to the dry band, the flow of surface leakage current is interrupted, causing inductance and stray capacitance of the system to generate high transients such that the effect is similar to a circuit breaker in which a high frequency transient of up to twice the supply voltage is sustained between the contacts. All of the applied voltage is concentrated across the dry bands and arcing occurs, causing the insulation surface to reach high local temperatures at the core of the arc column, leading to gradual erosion and the formation of carbon traces which become the established path for further discharges and then a complete breakdown of the insulation surface.

The numerical value of the voltage that initiates tracking is called the "tracking index" [2.13] and is used to quantify the surface properties of the dielectric under test.

2.3. PD Generation and detection

In general partial discharges are restricted to a region of the dielectric material, and they only partially bridge the electrodes where the voltage is applied. The insulation may consist of solid, liquid or gaseous material, or any combination of these.

Every discharge causes a progressive deterioration of the insulation material. Chemical transformations of many types take place as a consequence of the impact of high energy electrons or accelerated ions [2.14]. Deterioration of the insulator surface depends on various factors such as the type of materials and the applied voltage; because of this the relationship between the life expectancy of the insulator and the severity of the partial discharge is currently a subject of several investigations [2.15, 2.16]. Corona in air will have no influence on the expected life of an overhead line; but PD's within a thermoplastic dielectric, e. g. PE, may cause breakdown in a short time. The diagnosis of partial discharges is based on the exchange of energy taking place during the discharge. These exchanges are manifested as:

- Electrical pulse currents (with some exceptions, i. e. some types of glow discharges).
- Dielectric losses.
- E.M. radiation (light).
- Radiofrequency
- Sound (noise).
- Physical-Chemical reactions (dissolved gases)

.

Partial discharge diagnostic systems are based on the direct or indirect measurement of one or more of the phenomena mentioned above.

Methods that use sensors to detect the propagated electromagnetic wave at different frequencies such as UHF [2.17] are among the simplest ones. The sensitivity is, however, often low and hence is difficult to discriminate between partial discharges

and noise, especially when tests are carried out on line. The energy released by a partial discharge will increase the dissipation factor; a measurement of tan δ as a function of applied of voltage displays an 'ionization knee', a bending of the otherwise straight dependency. This technique has the disadvantage that the knee is blurred and not pronounced, even with a considerable amount of PD's, due to the additional losses generated in a very specific localized section. This can be very small in comparison to the volume losses resulting from polarization processes. Optical techniques are limited to discharges within transparent media and thus not applicable in most cases.

The use of ultrasonic transducers can successfully be used to localize the discharges. One of the most frequently used methods is the electrical one, which is featured in the IEC 60270 standard [2.6], these methods separate the impulse current linked with partial discharges from any other phenomena. The application of different PD detectors which is presently well defined and standardized, presupposes a fundamental knowledge about the electrical phenomena within the test samples and the test circuits, i.e. the application of gained experience by the operator in recognize visually the different patterns of partial discharges.

Other methods use the increasing gas pressure in oil filled power equipment as a result of PD activity; this is caused by the gradual deterioration and pollution of oil insulation or other organic liquids that initiate a chemical reaction that involves the disruption of the C-H C-C bonds. Oxygen and moisture initiate radical reactions that ended up in the formation of a wide range of new solid and gaseous (gases, organic compounds, waxes, soaps, etc.). These methods are better known as physical-chemical diagnostic methods [2.18].

2.4. The basic PD circuit.

As described in the last section, detection of partial discharges is based on direct or indirect measurement of discharges occurring in a test specimen (dielectric material), power equipment in a HV laboratory or in electrical installations. When the

evaluation of PD's is carried out in a laboratory, one of the aims is to evaluate the fundamental quantities related to partial discharge events for fundamental research or as a routine test. As a result the representation of the evaluated circuit is possible; the latter is one of the best ways to understand the behavior of partial discharges. In the case of PD's occurring in a void the equivalent circuit consists of a simple capacitor like arrangement, as shown in figure 2.2 [2.7, 2.19], composed of solid or fluid dielectric materials between the two electrodes A and B, and a gas-filled cavity, which can represent an imperfection in the insulation such as small voids, cracks, de-laminations, contamination, loose connections or floating pieces of metal. The electric field distribution within this test object is modeled by concentrated partial capacitances. The latter assumption is possible if space charge affecting the capacitances is not considered.

Electric field lines within the cavities are represented by C_c and those starting or ending at the cavity walls form the two capacitances $C_b^{'}$ and $C_b^{''}$ within the dielectric. Field lines outside the cavity are represented by:

$$C_a = C_a^{'} + C_a^{''}$$

Due to realistic geometric dimensions involved, and as:

$$C_b = \frac{C_b^{'} \times C_b^{''}}{C_b^{'} + C_b^{''}}$$

The magnitude of the capacitances will then be controlled by the inequality:

$$C_a \rangle\rangle C_c \rangle\rangle C_b$$

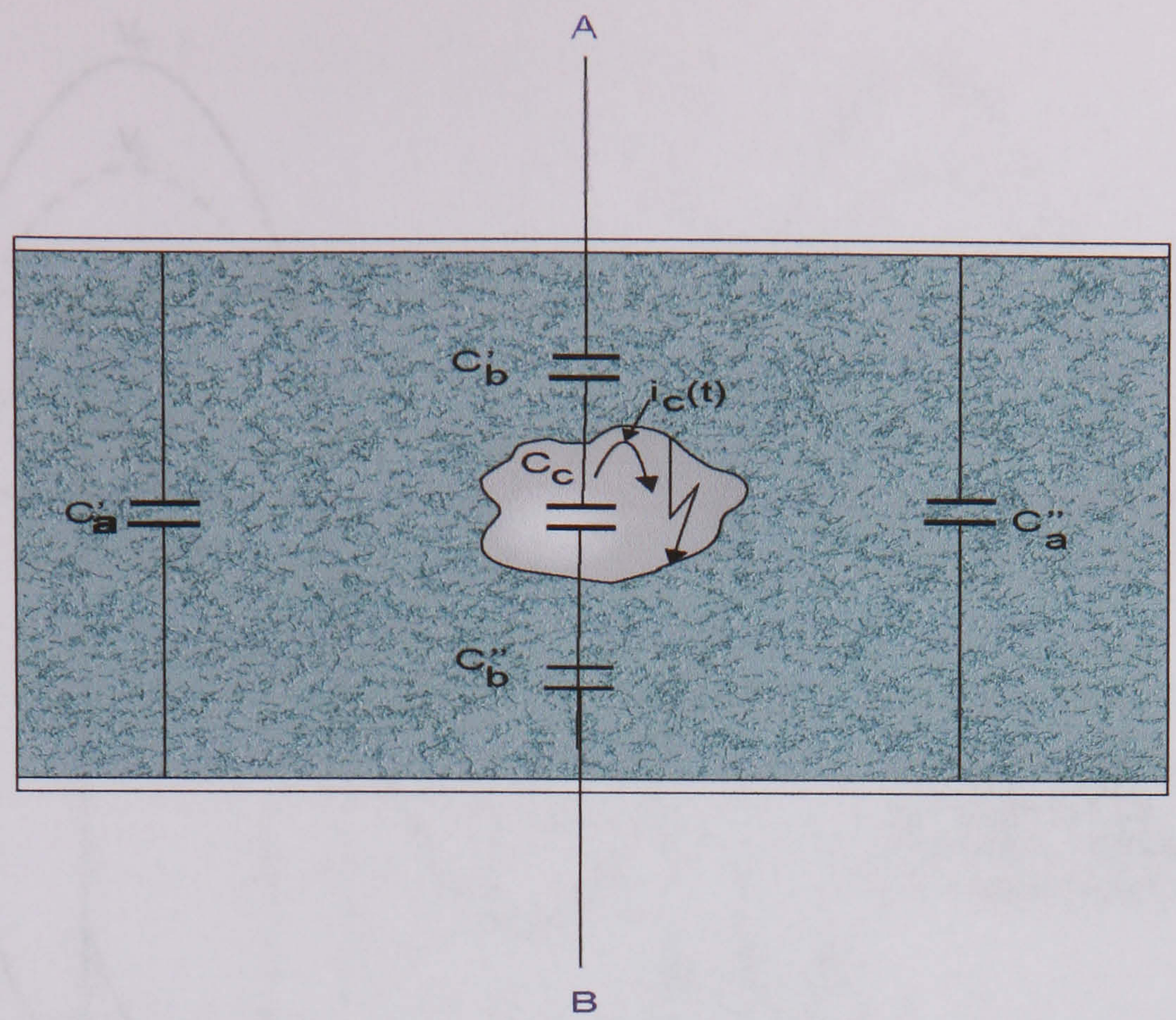

Figure 2.2. Basic PD circuit, insulation with internal cavity.

If an AC voltage is applied, the field gradients in the void start to strongly enhance due to the difference in permittivity caused by interfacial polarization [2.1] as well as by the shape of the cavity. This causes the void gas to ionize, causing a spark or discharge to appear. After this arc the capacitance Cc will rebuild until the threshold or inception voltage is again reached producing another discharge event. For an increasing value of an a.c. voltage the first discharge will appear at the crest or rising part of a half-cycle (see figure 2.3). This discharge creates electrons as well as negative and positive ions, which are driven to the surfaces of the void thus forming dipoles or additional polarization of the specimen. This physical effect reduces the voltage across the void significantly. When increased DC voltages are applied, one or only a few partial discharges will occur during the rising part of the voltage however, if the voltage remains constant, the discharges will stop as long as the surface charges as deposited on the walls of the void do not recombine or diffuse within the dielectric.

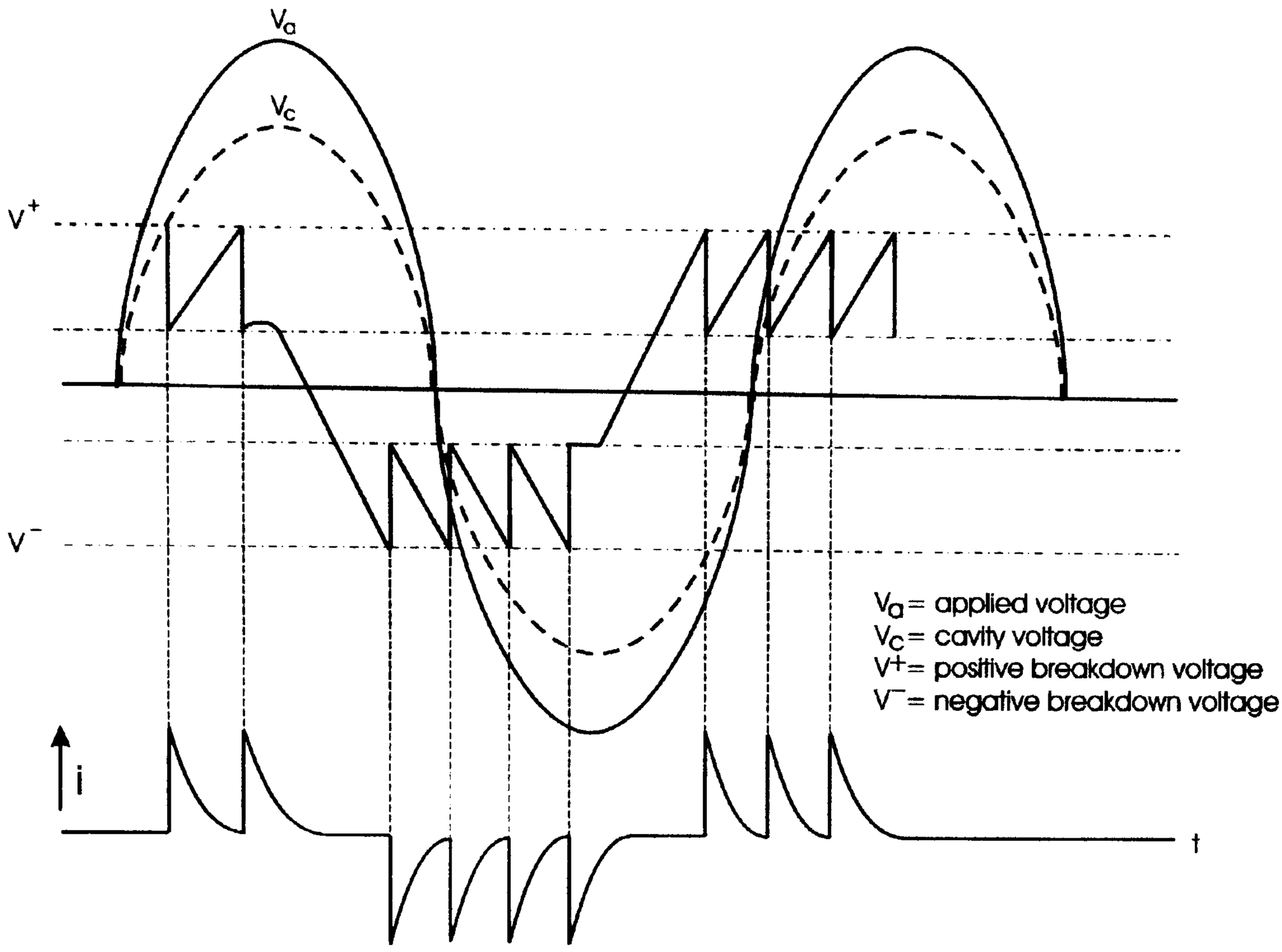

Figure 2.3 Cavity breakdown sequence when an AC voltage is applied

Figure 2.4 shows the equivalent circuit that simulates a partial discharge event. Here, the switch S is controlled by the voltage V_c across the void capacitance C_c, and S is closed only for a short time, during which the flow of a current $i_c(t)$ takes place. The resistor R_c simulates the time period during which the discharge develops and is completed. This discharge current $i_c(t)$, which can not be measured, would have a shape as governed by the gas discharge process and would be similar to a Dirac function, i.e. this discharge current is generally a very short pulse in the nanosecond range.

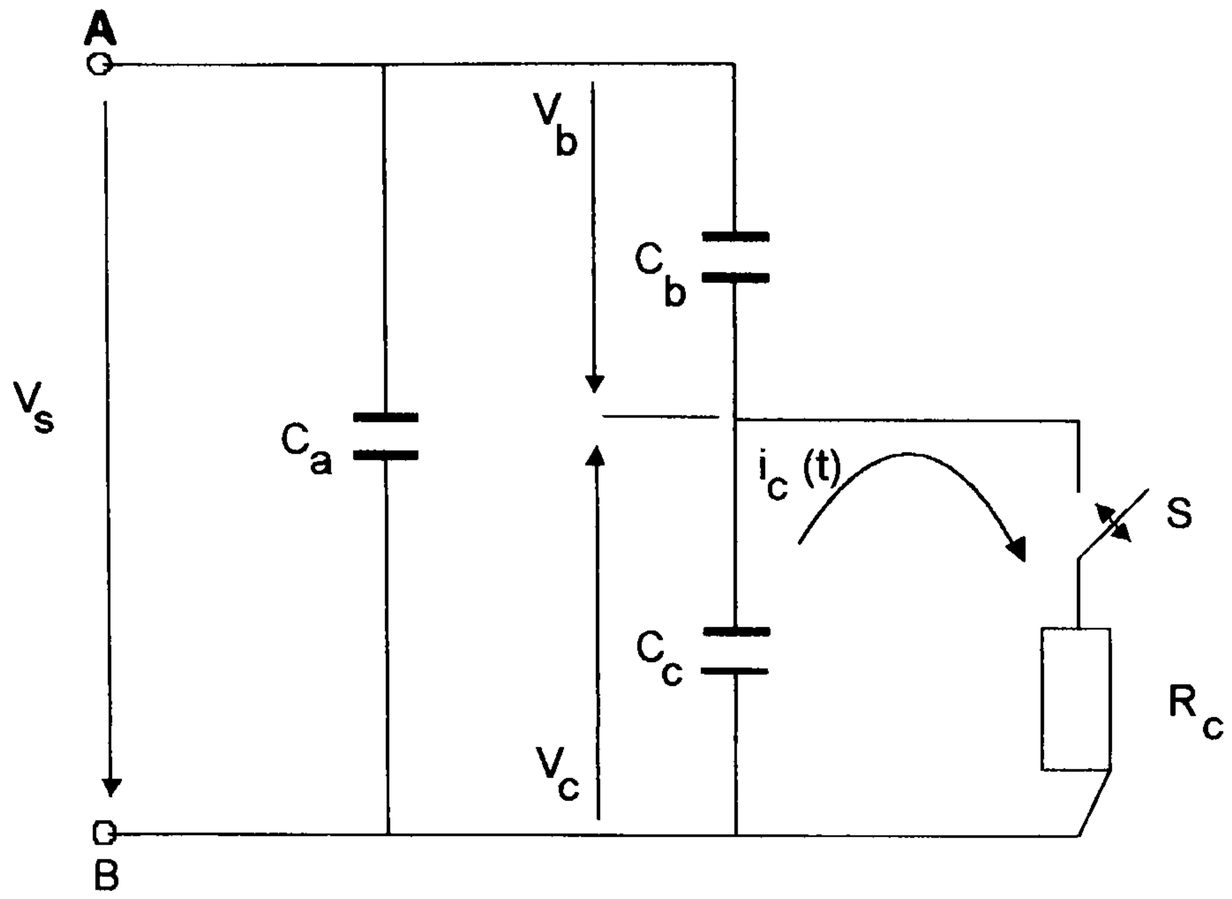

Figure 2.4 Basic PD circuit, equivalent circuit.

Let us now assume that the sample was charged to the voltage V_a but the terminals A, B are not longer connected to the source. If the switch S is closed and C_c becomes completely discharged, the current $i_c(t)$ releases a charge $\delta q_c = C_c \delta V_c$ from C_c, a charge which is lost in the whole system as assumed for this simulation. By comparing the charges within the system before and after this discharge, we receive the voltage drop across the terminal δV_a as

$$\delta V_a = \frac{C_b}{C_a + C_b} \delta V_c \tag{2.1}$$

This voltage drop contains no information about the charge δq_c, but it is proportional to $(C_b \delta V_c)$, a magnitude vaguely related to this charge, as C_b will increase with the geometric dimensions of the cavity [2.7].

PD normally involves one of the following combinations of dielectrics:

- Discharge in the gas
- Discharges involving both gas and solid insulation
- Discharges in a solid component ('electrical treeing" or "cavity discharge")

- Discharges between a system electrode and an electrical floating part

2.5. Discharges in SF_6 gas.

Conducting particles and surface roughness caused by machining or scratches are known to enhance the local field stress. As a result the intrinsic breakdown field strength of SF_6 cannot be fully exploited in practical applications. For SF_6 pressures of engineering interest and normal levels of surface roughness, PD inception and breakdown voltages are the same. However PD without breakdown can occur for protrusions above the normal surface roughness. Conducting particles are the most frequent type of imperfection in GIS. Long, thin (wire – like) particles can be lifted in the electric field and occasionally touch an electrode surface.

This worst case situation (PD without breakdown) has been investigated experimentally. Two basic types of discharge are observed. A quasi continuous corona like discharge is possible if some feedback mechanism leads to continuous production of electrons which create continuous avalanche activity. This discharge type, although possible for both polarities, is most frequent for negative polarity, where electrons can be generated by field emission from a stress enhancement. For positive polarity, where electrons are generated by detachment from negative ions in the SF_6 rather than through field emission, pulsive discharge is more common. This consists of streamer corona burst, of nanoseconds duration pulses. Such PD pulses can also occur for negative polarity but such activity is always much weaker than for positive polarity.

The polarity dependence of initiatory electron generation, together with the two types of discharge (continuous or glow discharge and pulsive discharge) usually results in substantially differing PD characteristics for the two polarities. Quasi–continuous (or glow) discharge tends to dominate for negative polarity while pulsive discharge tends to dominate for positive polarity.

Both the quasi–continuous discharge and the pulsive discharges have a distinct inception field which depends on the particle length and the tip radius. The average current associated with the quasi–continuous discharge current and the maximum charge per pulse during pulse discharge increase approximately quadratically with the background field.

2.6. Chapter 2 references

[2.1] N. H. Malik, A. A. Al-Arainy, M. I. Qureshi, *Electrical Insulation in Power Systems*, Marcel Dekker, 1998.

[2.2] Andrew R. Hileman, *Insulation Coordination for power systems*, Marcel Dekker, 1999.

[2.3] IEC Standard 60071-1 Insulation Coordination: definition principles and rules, *International Electrotechnical Commission (IEC)*, Geneva, Switzerland, 1996.

[2.4] Lamberth, P. J., "Effect of Pollution on High Voltage outdoor insulators", Proc. IEEE, No. 9, RI18, pp: 1107-1130, 1971.

[2.5] James P. Hall, "*History and bibliography of polymeric insulators for outdoor applications*", IEEE Transactions on Power Delivery, Vol.8, No.1 January, pp: 376-385, 1991.

[2.6] IEC Standard 60270 (Third edition, 2000). Partial Discharge Measurement, *International Electrotechnical Commission (IEC)*, Geneva, Switzerland, 2000.

[2.7] E. Kuffel, W. S. Zaengl, J. Kuffel, *High Voltage Engineering: Fundamentals*, Newnes, 2001.

[2.8] E. M. Bazelyan, Yu. P. Raizer, *Spark Discharge*, CRC Press LLC, 1998.

[2.9] Steven A. Boggs, "*Partial Discharge – Part III: Cavity-Induce PD in Solid Dielectrics*", IEEE Electrical Insulation Magazine, Vol.6, No.6, Nov./Dec., 1990, pp: 11-20.

[2.10] J. F. Hall, "*History and Bibliography of Polymeric Insulators for Outdoors Application*", IEEE Transactions on Power Delivery, Vol.8, No.1 January, pp: 376-385, 1993.

[2.11] R. Allen B., Randall K. N., David S. W. *Polymer Compounds Used In High Voltage Insulators*, Hubbell Power Systems, 2004.

[2.12] D. L. Williams, A. Haddad, A. R. Rowlands, H. M. Young and R. T. Waters, "*Formation and Characterization of Dry Bands in Clean Fog on Polluted Insulators*", IEEE Transactions on Dielectrics and Electrical Insulation", Vol.6, No.5 October, pp: 724-731, 1999.

[2.13] C. G. Garton, "*The Use of Materials as Electrical Insulation*", Physics Education, Vol. 3, pp. 85-91, 1968.

[2.14] T. J. Lewis, "*Ageing-A Perpective*", IEEE Electrical Insulation Magazine, Vol. 17, No. 4, July/August, pp. 6-16, 2001.

[2.15] J. Densley, "*Ageing Mechanisms and Diagnostics for Power Cables-an Overview*", IEEE Electrical Insulation Magazine, January/February, Vol. 17, No. 1, pp. 14-22, 2001.

[2.16] P. H. F. Morshuis, "*Degradation of Solid Dielectrics due to Internal Partial Discharge: Some thoughts on Progress Made and Where to Go Now*", IEEE Transactions on Dielectrics and Electrical Insulation, Vol. 12, No. 5, October, pp. 905-913, 2005.

[2.17] M. D. Judd, G. P. Clearly, C. J. Bennoch, "*Applying UHF Partial Discharge Detection to Power Transformers*", IEEE Power Engineering Review, August, pp. 57-59, 2002.

[2.18] V. G. Arakelian, "*Effective Diagnostics for Oil-Filled Equipment*", IEEE Electrical Insulation Magazine, November/December, pp. 26-38, 2002.

[2.19] Timothy J. O'Brien, "*Practical Application Discharge Testing of Insulation Systems With Emphasis on Medium Voltage Switch Gear*", Pulp and Paper Industry Technical Conference, 1998. Conference Record of 1998 Annual, pp 142-144, June 2003.

PARTIAL DISCHARGE IDENTIFICATION

This chapter outlines the importance of the identification and prevention of partial discharges using a non invasive system which allows the prevention of more serious faults. The state of the art of existing methods provides an overview of partial discharge detection and emphasizes the importance of a non invasive method for PD detection and identification. The precise identification of partial discharges as a key requirement for any diagnostic method to prevent power equipment failures is discussed.

3.1. The history of partial discharge monitoring and identification.

The history of PD measurements can be traced back to 1940 [3.1], when basic indirect on-line methods to measure PD activity were developed such as sniffers which basically consisted of radio receivers with an antenna and variable frequency in the range of MHz and an analog meter with a scale in μV and dB. These devices also called RIV (radio interference voltage) meter, measured external PD's or corona. Another earlier approach was probes attached to transformers in order to hear the ultrasonic sound activity of internally generated PD's [3.2]. An improvement in this kind of technology was to add a basic oscilloscope with limited bandwidth to visualize and classify PD wave shapes and patterns as a function of electrical phase. Nowadays, the degree of sophistication and bandwidth of electric and electronic devices has permitted the accurate detection and location of PD's.

Due to the limitations of certain types of applications, direct methods to measure discharge activity were developed, which use a different approach in measuring the dielectric loss of the insulation. This is measured using a capacitive bridge that superimpose PD pulses to the system's frequency and one oscilloscope for visualizing the dielectric "loop", this system is usually called, a DLA (Dielectric Loss Analyzer). Probably the most traditional and reliable method to measure partial discharges off - line is the method of apparent charge [3.3] (see figure 3.1). This consist of a measuring impedance, a discharge detector and a measuring system (computer aided or time resolver). Although this is the basic configuration, there exists several variations using different coupling devices and measuring instruments. Commercial and experimental prototypes are available nowadays in research centers and large utilities. The latter method is performed in the laboratory and requires standard calibration for any test to be performed.

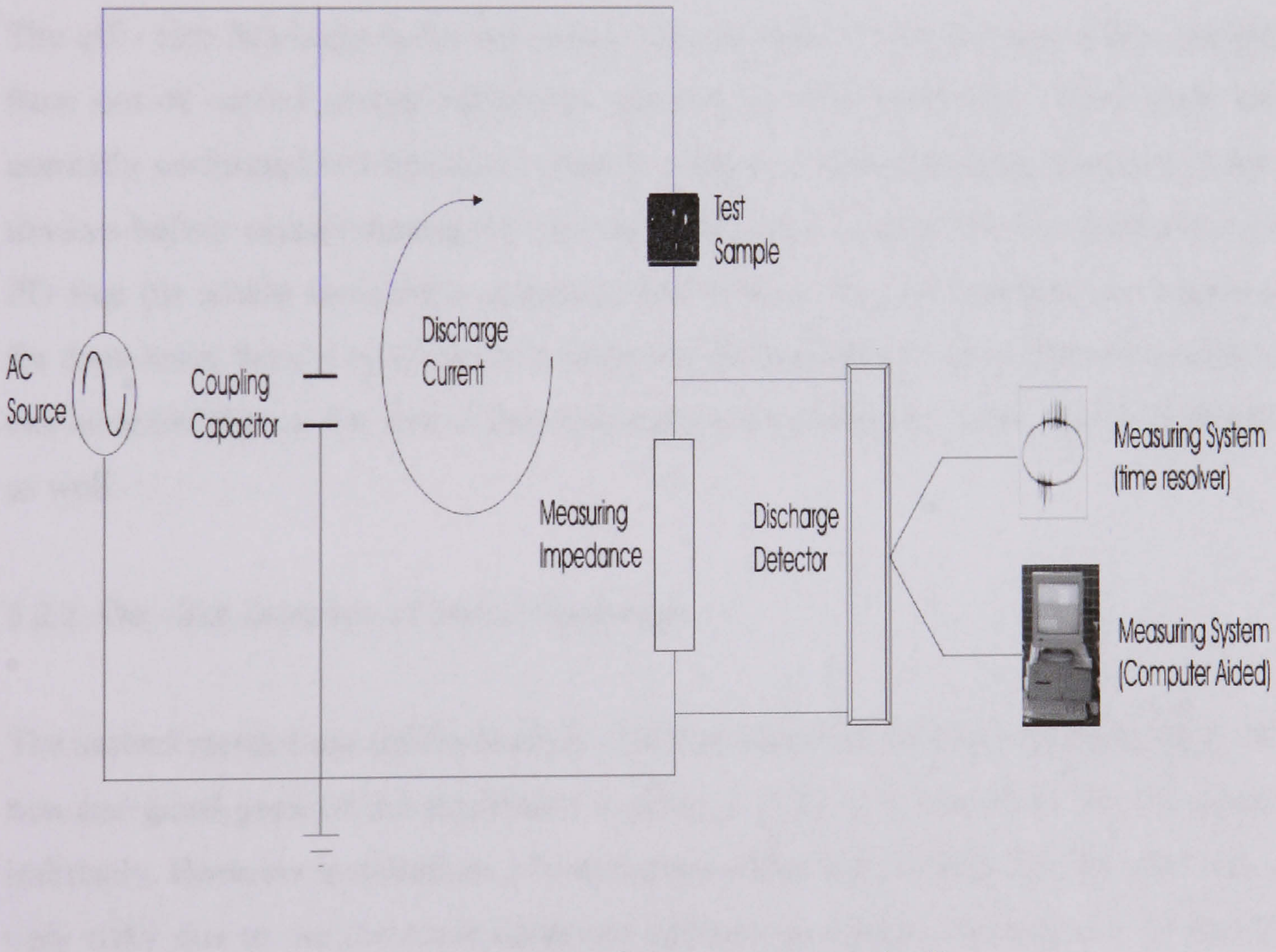

Figure 3.1. Apparent charge measurement circuit.

3.2. Partial discharge surveying systems for power substations and plants.

Several methods have been developed for the identification of partial discharges taking advantage of one specific property or a combination of them [3.4]. The methods to assess insulation through the detection of partial discharges are divided into two big groups [3.5]:

- Off - line detection of partial discharges. Where the equipment is removed from service.
- On - line detection of partial discharges. Where measurements are taken with the equipment in service.

3.2.1. Off - line detection of partial discharges

The off - line detection is the laboratory measurement of partial discharges coming from out of service power equipment under controlled conditions. These tests are normally performed in laboratory research centers or manufacturing plants of power devices before commissioning by electrical utilities to verify that the equipment is PD free (or within standards). Accuracy and a noise free environment are required for these tests, but the application is limited to the laboratory. Any kind of equipment can be tested, but as the size of the equipment grows, the cost of the test is increased as well.

3.2.2. On - line detection of partial discharges

The second method use different kinds of sensors that are coupled and attached to the non energized parts of the equipment in service [3.6], thus acquiring the PD signal indirectly. However installations of connecting cables and couplers can be sometimes very risky due to the dielectric distances between energized, floating and grounded metallic parts. Another method to detect PD on line without additional connections to the equipment is using antennas which can be placed within a safe distance [3.7].

Multipath effects as well as thermal and external noise can affect considerably the results of this kind of test.

Both methods can be applied to operate continuously or during brief periods of time according to the requirements of the test. In the past decades universities and research centers have developed several on-line and off-line methods to detect PD [3.8]. They have proved to be reliable for specific applications and they have solved problems concerning only some types of partial discharges, however there are common factors that a PD detection method must accomplish:

- The application of the partial discharge detection method must be economical compared with the cost of outages and damage to the equipment.

- The prediction of PD's occurring in electric plant and equipment must be reliable. If the system misdiagnoses it can cause significant economic losses and failure of credibility, if this happens the system may be disregarded.

- The PD system must predict efficiently or give sustainable evidence of any sign of deterioration in the insulation. It must provide sufficient time to remove the affected equipment and avoid major damage. The latter requirement must be combined with an appropriated maintenance program that helps the system to be more reliable.

- Sensitivity to measure partial discharges must be an integral requirement of the system, though this feature varies from method to method depending on the application [3.9]. The bandwidth of a specific system must be enough to detect measurable PD activity.

3.3. Modern PD detection and location systems

Due to the requirements of continuous operation of power systems, early detection of partial discharges has become important to avoid long interruptions and costly repairs or substitution of power devices. However, the development of efficient and

reliable power equipment brought about the application of more sophisticated insulation materials which as they begin to degrade cause the generation of new and different kinds of internal and external partial discharges. Recent investigations of PD in new generations of insulators, such as polymers and insulation boundaries [3.10], have caused the modification and improvement of off-line tests. A new generation of PD detectors, coupling devices and measuring instrument were introduced. The advantage of these devices is basically its capacity of storage, resolution and bandwidth beyond 2 GHz, so that they can acquire high resolution signals of the order of nanoseconds. However, off-line tests still have the disadvantage of interrupting the operation of power equipment, such as power generators in thermal or nuclear plants for several hours, weeks or even months, causing big monetary losses and security risks; this was an incentive for the improvement of reliable on-line partial discharges detection systems, though the development of this kind of systems was developed more than 50 years ago [3.11]. The basic improvements were related mainly to the reduction of noise affecting the test, and coupling devices. The most common application of these kinds of systems is made to big generators located in thermal and hydro plants. Due to the recent advances its use has also been widespread to substations and transmission lines were these detectors are not only limited to partial discharges, but to the location and detection of any kind of fault arcs [3.12]. The following are some examples of on-line PD detection systems [3.5].

- Partial discharge analyzer (PDA)
- Turbine generator analyzer (TGA)
- Fault anticipation in substation equipment (FASE)
- Metal clad switchgear monitoring system
- CEGB cable PD detector
- Radiometric identification of partial discharges

The above on-line methods utilize different approaches and they are applied to specific power equipment. The radiometric identification method is used in this investigation as the basis for the identification and discrimination of PD's.

3.4. Considerations for the design of on-line and off-line PD identification systems.

This research is focused on the identification of the intrinsic characteristics of partial discharges using the existing technology in radiometric identification. As a means of comparison, traditional methods of partial discharges measurement in the laboratory are mentioned. The following are the features of these systems:

Off-line method

- Economical and reliable
- Fast and accurate in time and sampling
- Components with a modular design to ensure different configurations and voltage levels
- Free of external noise and undesirable corona
- Safe to operate

On-line method

- Modular design
- Economical
- Mobile
- Fast and accurate in time and sampling
- Non invasive to the power equipment

- Accurate in the identification and location of partial discharges

Although the above requirements are already been partially accomplished with the existing radiometric identification methods, basic characteristics of the radiated electromagnetic wave are not well understood and a pattern recognition analysis has not yet been created.

3.5. Radiofrequency transients in power systems

Impulsive electromagnetic radiation can originate from different sources in an electric power system; these sources can be transmission lines and power equipment in substations where arcing events are likely to occur. Radiation emitted at power system frequency does not cause electromagnetic compatibility problems in most of the cases, however the impulsive nature of atmospheric radiated electromagnetic waves (also named sferics) can emit frequencies that range between VLF up to UHF [3.13] and can interfere with communications and protective equipment. The radiated sferics has a non-linear nature that is related to the properties of the plasma in the arc column once it has been established. Arc induced sferics can be classified in two categories [3.14] switching arc sferics and fault arc sferics, into the first category falls switching events such as circuit breakers, disconnectors and arc welders, in the second category events such as lightning and power system faults can be counted. Fault arcs involve high currents whose value depends on the parameters on the circuit where the fault is located; the duration of the fault depends on the operation time of the protective devices. In contrast switching arc events involve a relative smaller current whose value depend on the extinction characteristics and parameters of the breaker and the time during which the arc is established depends on the time of the related mechanism.

3.5.1. Radiation caused by an accelerated charge

Accelerating positive or negative electric charges cause radiation. The process they follow to cause this radiation is explained in figure 3.2 where a static charge and its field lines are shown.

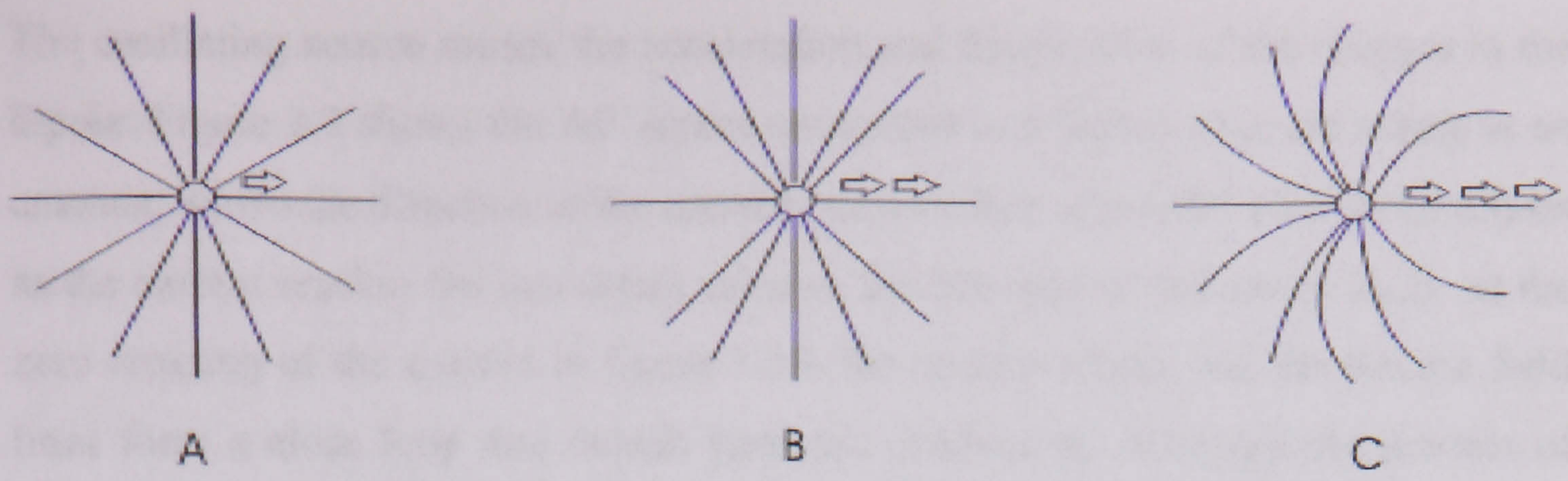

Figure 3.2. Electric charge and field lines, A) static or slow moving charge, B) fast moving charge, C) accelerated charge.

In figure 3.2A the charge can be static or slow moving; in 3.2B the charge is moving below the speed of light; in figure 3.2C when the charge is accelerated by an external force close to the speed of light causing the electric field to bend in the direction of the charge; this sole effect is responsible for electromagnetic radiation. As the charge travels along, its electric field has an associated magnetic field which moves in phase (unlike the capacitor or inductor fields which are out of phase) and they travel perpendicularly one to another; this is known as an electromagnetic wave. In an electrical wire conductor charges can suffer acceleration or deceleration and thus emit radiation, this effect is found at radiofrequency where the wire is bent, discontinuous, curved or terminated. This is illustrated in figure 6 where two electric wires of infinite (theoretically) length are connected to an AC source in the form of an electric dipole.

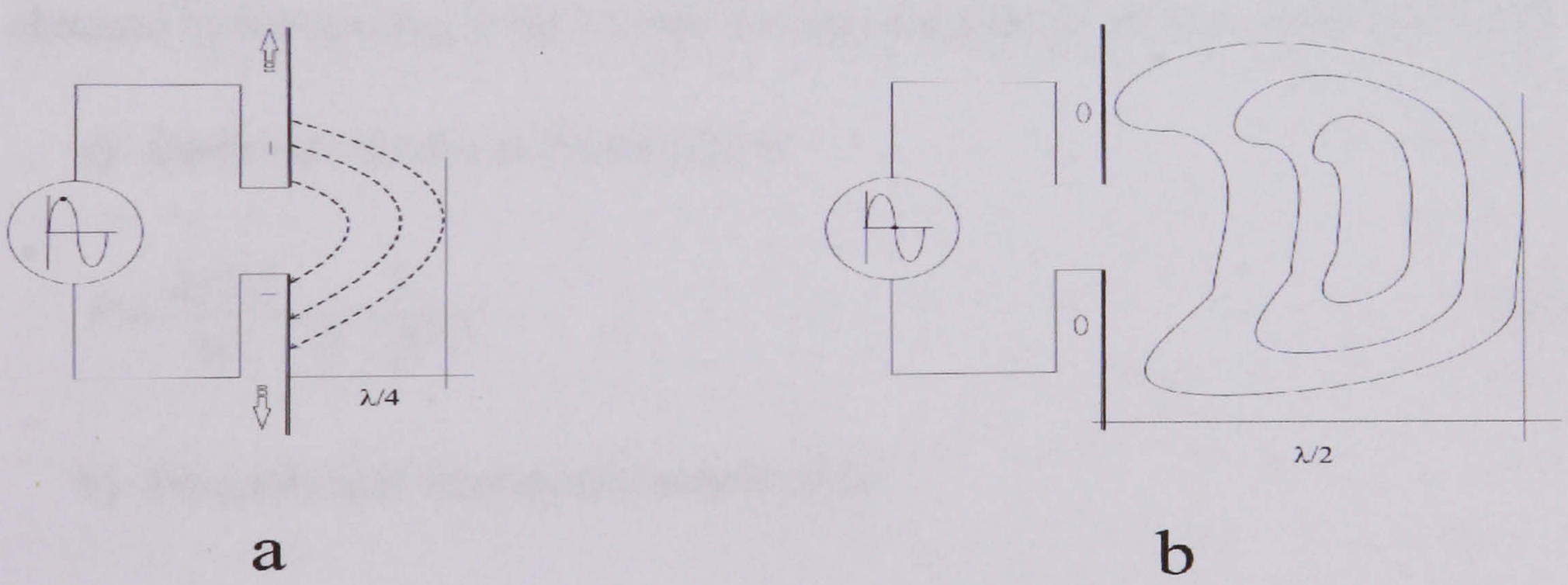

Fig. 3.3. Electromagnetic radiation by acceleration of charges due to an oscillating source, a) at maximum of the AC source, b) at zero crossing of the AC source.

The oscillating source causes the acceleration and deceleration of the charges in the dipole. Figure 3.3 shows the AC source connected to a dipole structure acting as an antenna, where the direction of the current causes a flux of parallel electric field lines as the current reaches the maximum value of the first half of the source ($\lambda/2$). At the zero crossing of the current in figure 3.3-b the current ceases and the electric field lines form a close loop and detach from the conductors. Although the process of radiating electromagnetic fields appears simple, it is a three dimensional phenomena that includes magnetic field radiating perpendicularly to the electric fields [3.15].

The radiated field can be derived from Coulomb's law, so the transverse field is:

$$E_t = \left(\frac{ar\sin\theta}{c^2}\right)\cdot\left(\frac{e}{4\pi\varepsilon_0 r^2}\right) = \frac{e}{4\pi\varepsilon_0 c^2}\cdot\frac{a\sin\theta}{r} \tag{3.1}$$

The radiation produced by moving charges well below the speed of light (non relativistic) is proportional to the square of acceleration. The mathematical representation of the radiation by an accelerated charge at low velocities can be given by *Larmor* formula [3.16],

$$P = \frac{2e^2a^2}{3c^3} \tag{3.2}$$

The radiation from an accelerated charge moving at high speed (relativistic) can be obtained by introducing in the *Larmor* formula standard relativistic equations [3.17]:

a) Co-linear velocity and acceleration:

$$P = \frac{2e^2a^2}{3c^3}\cdot\frac{1}{(1-\beta^2)^3} \tag{3.3}$$

b) Perpendicular velocity and acceleration:

$$P = \frac{2e^2a^2}{3C^3}\cdot\frac{1}{(1-\beta^2)^2} \tag{3.4}$$

The radiated power expressed in equation 4 depends on the efficiency and electrical properties of the conducting object i.e. the structures acting as antennas. The relationship between the input power P_{in} and the transmitted power P_t can be given by:

$$P_t = P_{in} - P_{loss} \tag{3.5}$$

where P_{loss} is the power absorbed by the antenna's electrical circuit. The direction and pattern of the generated radiation depends on the structures and conductor's arrangement, meanwhile the power of the radiated energy depends on the permittivity of the propagating media and dielectric interfaces. For plant evaluation the factor ε_i is added and represents the permittivity of the associated insulation.

3.5.2. Radiation caused by discharges and partial discharges in HV plants

There are different factors that cause the inception of discharges and partial discharges in high voltage installations such as the condition of external or internal insulation in power equipment, the power flowing through the plant (as it increases or decreases the non uniform magnetic or electric fields), pollution and meteorological conditions, lightning and switching of circuit breakers and disconnectors [3.18, 3.19]. All these factors contribute to the emission of radio frequency impulsive noise within the HV plant, however only high energy discharges can be detected by an antenna based system such as the one employed in this research. Still it is possible to differentiate between high and low energy discharges (as shown in the next chapter) and even noise using filtering and triggering techniques. Usually high energy discharges are caused by switching of disconnectors or circuit breakers, breakdown of solid, liquid or gas insulation and lightning. Low energy discharges are caused by partial discharges occurring in damaged internal and external insulation. Other sources of low energy RF impulsive noise are arc welding devices, electronic rectifiers, thermostatic heath equipment and electric railways [3.20]. In general HV plants are flooded with RF impulsive noise of different kinds and they can be differentiated if their intrinsic characteristics are considered. Although the partial discharge current shows a non – linear behavior, the rate of change of the generated current as the dielectric begins to breakdown is limited to

specific values as shown in figure 3.4 [3.7], where is possible to observe that strong dielectrics (SF_6 and oil) show a recovering time faster than weak dielectrics (air).

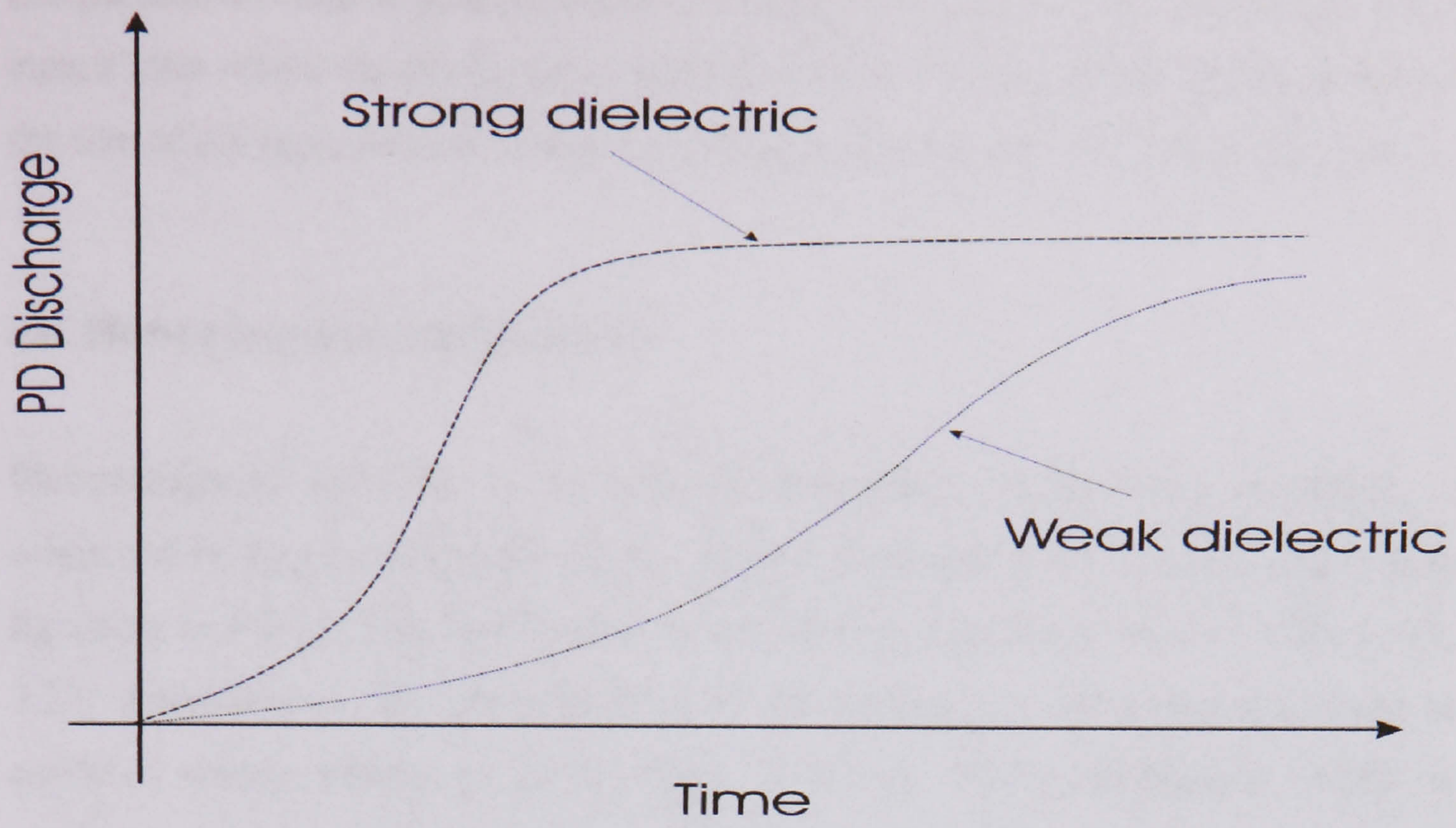

Figure 3.4. Rate of change of the PD current in relation to time

Another important characteristic of discharges and partial discharges are their frequency spectrum. According to results obtained in the laboratory and from substations in this research [3.21], discharges in atmospheric air generates a frequency spectrum with mean components below 200 MHz, where as discharges generated in dielectrics such as oil or SF_6, i.e. high dielectric strength insulators, show a spectrum that include components as high as 1 GHz. Higher frequencies are expected to be found in a substation environment since the complex arrangements of the structures and design of power equipment contribute to the scattering, reflection and fading of the original radiating signal in an effect known as multipath [3.22, 3.23]. Individual radiated partial discharges have an impulsive nature with a length that can range between several ns to few μs depending on the characteristics of the source and propagating media [3.24]. As shown later in this research, the polarity of partial discharges is another important characteristic and this can vary depending of the kind of discharge and the position within the source. Additional to noise, the original radiated signal is affected by the frequency response of the structures acting as antennas and the surrounding objects [3.25] thus the final power spectrum of the

received signal is in fact a combination between the spectrum of the structures and the spectrum of the current discharge, this research also considers a method to compensate this effect. Studies carried out in this research show that the length of the circuit loop where the discharge is generated, affects its frequency spectra, however the size of the gap does not have any significant effect in terms of frequency [3.26].

3.6. Sferic generation and detection

Electromagnetic radiation in the form of atmospheric radio waves or sferics, is originated in power equipment when a electric discharge is involved (i.e. fault arcs, lightning or PD's). The bandwidth of such sferics range from VLF to UHF [3.13, 3.27] depending on the characteristics of the discharge. The propagated sferic is analyzed taking advantage of the time of arrival (TOA) information which is recorded using antennas with a special array as a receiver, making it possible to locate the PD and its characteristics without physical connection.

Partial discharges are discharges and hence they emit electromagnetic radiation that can travel long distances through the atmosphere. This radio wave energy is related to the non-linear characteristics of the source (plasma arc) that can be regarded as a non-linear conductance of the arc column. The amount of energy released by the source depends on the transient current flowing thought the arc, however it is possible to distinguish different frequency bands through the radio spectrum due to sferic, these are: the VLF band that is common for high energy fault arcs, the VHF band for some arcs occurring in power equipment and UHF and above for small arcs generated inside or outside power devices.

When arc inception occurs between two electrodes at different potentials in air, the resulting current causes electromagnetic radiation in the form of noise; the sinusoidal power frequency signal from the source ignites an arc twice every cycle and causes a broadband noise signal with an envelope modulated at 100 Hz. This results in and causes frequency components that extend from the fundamental generation frequency to the UHF region.

The VLF radio wave has significant energy when it is propagated in a homogeneous medium which is bounded by the earth and an ionizing layer that commences at some 60 – 90 km above earth surface. The ionized layer acts to guide the VLF electromagnetic energy between the upper interface and that of the earth's surface, this results in a very low absorption rate of the radio wave. It is believed that high current arcs can be detected over long distances using the VLF band.

In the VHF band the transmission of arcing induced sferics requires a structure to radiate electromagnetic energy with a wavelength from 1m to 10 m [3.14]. Power equipment or earthed structures in the path of the fault current can act like antennas and emit radio wave energy.

Partial discharges of remarkably low energy compared to fault arcs in air, originate inside the power equipment such as transformers and circuit breakers in the form of cavities, in the boundaries between insulators of different dielectric constant or insulators and conductors. The radiated wave caused by the PD is attenuated by the surrounded insulation and the enclosed structure of the equipment, this insulation can be liquid, gas or solid such as oil, SF_6, air or polymer. The radio wave travels from inside, using the internal conductors towards the external terminals, bus bars and cables that act as antennas and then is radiated through the air. This directional characteristic of the radiated wave coming from inside power equipment can be used to distinguish PD from external noise, which travels in the opposite direction along the bus bars into the power equipment. This is known as directional sensing [3.28].

It will be shown that small internal PD's have different characteristics compared to fault arcs, such as the amount of radiated energy, the propagation frequency and polarization. These characteristics can be determined by the type of associated power equipment.

This research is focused on the non invasive monitoring and characterization of radiated PD's in the VHF and UHF frequency band. Results shows that radiated

PD's occur at frequencies of around 30 MHz (VHF) and 400 MHz (UHF). Lower frequencies that have been used for monitoring and locating arcing faults in overhead transmission and distribution lines [3.29, 3.30], are outside the aims of this research.

3.6.1. Identification of partial discharges using the properties of the radiated electromagnetic wave

The inherent characteristics of the sferics depend on several factors such as the configuration of the associated power equipment, the propagation media (solid, gases and liquids dielectrics), the gap arrangement etc. This research is focused on these characteristics in order to identify and classify the radiated discharges using experimental arrangements in a high voltage laboratory and field measurements.

This PD identification is expected to be used as a means of early radiometric identification of PD's ocurring in power substations at all voltage levels. However a possible limitation is very small PD's occurring inside power equipment that may trigger a serious failure in a long term, since the coupling system (antenna) is not sensitive enough to receive them. Normally this kind of PD failure requires invasive or laboratory PD detection methods to be assessed.

3.7. Pattern classification of partial discharges

A number of methods for the pattern classification and recognition of partial discharges have been developed for on-line and off-line PD detection systems. Analogue methods are based on the data visualization of PD's and are still in use nowadays [3.31], the newest methods are based on the digital data processing of the distribution and magnitude of pulses along the sinusoidal signal taken from the source at the power frequency (point on wave information) once partial discharges have been detected. The parameters considered to analyze and discriminate PD's depend on the method of detection. For instance, if a wideband discharge detector is used, the evaluated parameters using data visualization are the shape and distribution of the discharges in an elliptical trace that represent one cycle of the power frequency

[3.32]. If UHF PD detection is used [3.33], the parameters to be evaluated are the UHF energy, time of flight difference and count rate. For the apparent charge method [3.34], the pulse charge magnitude (Q), the phase angle and the discharge count rate are considered. After digitalization, statistical methods (statistical operators) are used and applied to those parameters for discharge recognition [3.35]. A classification of the distribution of the parameters is possible using different laboratory configurations and samples of possible PD sources; this classification is automated using simple algorithms which calculate the recognition rate [3.36]. The resulting data base is verified and complemented with field data in HV installations. This research considers different statistical operators such as the pulse magnitude (average), the pulse recurrence (difference in degrees between adjacent pulses), phase angle, difference between positive and negative pulses (average), skewness, kurtosis and number of analyzed cycles, among others.

3.7.1. Advantages of pattern recognition of the radiated electromagnetic wave

Current research concerning the radiometric identification of partial discharges has been focused solely in the location of PD and the creation of software and mobile equipment, but little is known about the fundamental properties of the radiated PD's. As pointed out earlier the reliability of the system is vital to avoid the triggering of false alarms and the unnecessary interruption of service with the consequent economical losses and lack of credibility. To achieve this, a non invasive method must rely on a research background concerning the fundamental properties of partial discharges and accomplish the regulations of international standards, however for radiometric detection of partial discharges there are not regulations concerning such standards. With an adequate background the feasibility of the system and the range of applications is increased considerably. Despite its limitations the radiometric identification of PD's using a mobile system can prevent the failure of a wide range of power equipment with a fast survey around the electrical installation. The following attributes can be considered for this system:

- On line diagnostic of external and internal partial discharges
- Fixed and mobile system for continuous or fast surveys

- Fast, accurate and feasible digital sampling and processing of PD signals
- Safe operation distance with respect to the power equipment

The latter issues will be considered in detail during the process of design and implementations of the system. The advantages of pattern recognition shall be taken into account as a means of improving the efficiency of the existing system as it can discriminate between harmless PD event (noise, occasional surface discharges and corona) and damaging PD's.

3.8. Chapter 3 references

[3.1] David A. Nattrass, "Partial Discharge XVII: The Early History of Partial Discharge Research", *IEEE Electrical Insulation Magazine*, July/August 1993, Vol. 9, No. 4, pp 27 – 31.

[3.2] Harrold R., "Partial Discharge XVI: Ultrasonic Sensing of PD within Large Capacitors", *IEEE Electrical Insulation Magazine*, May/June 1993, Vol. 9, No. 3, pp 21 – 28.

[3.3] E. Lemke, P. Schmiegel, "Fundamentals of the PD probe Measuring Technique", *Lemke Diagnostics*, website: http://www.hvtechnologies.com/images/publications/funda-us.pdf.

[3.4] *IEC Standard 60270 (Third edition, 2000). Partial Discharge Measurement*, International Electrotechnical Commission (IEC), Geneva, Switzerland, 2000.

[3.5] J. C. Stone, "Partial Discharge Part VII: Practical Techniques for Measuring PD in Operating Equipment", *IEEE Electrical Insulation Magazine*, July/August 1991, Vol. 7, No. 4, pp 9 – 19.

[3.6] Martin D. Judd, Li Yang, Ian B. B. Hunter "Partial Discharge Monitoring for Power Transformers Using UHF Sensors Part I: Sensors and Signal Interpretation", *IEEE Electrical Insulation Magazine*, March/April 2005, Vol. 21, No. 2, pp 5 – 14.

[3.7] Moore P J, Portugues I, Glover I A, "A Non-Intrusive Partial Discharge Measurement System Based on RF Technology", *Power Engineering Society Meeting*, June 2003, pp 627 – 633.

[3.8] T. Stherl, "On and Off-Line Measurement, Diagnostics and Monitoring of Partial Discharges on High Voltage Equipment", *Lemke Diagnostics Workshop,* September 2000, paper no. 4.

[3.9] S A Boggs, "Partial Discharge Part II: Detection Sensitivity", *IEEE Electrical Insulation Magazine*, September/October 1990, Vol. 06, No. 5, pp 35 – 44.

[3.10] Cherney A Edward, "Partial Discharge Part V: PD in Polymer Type Line Insulators", *IEEE Electrical Insulation Magazine*, March/April 1991, Vol. 07, No. 2, pp 28 – 32.

[3.11] G. C. Stone, "Partial Discharge Diagnostics and Electrical Equipment Insulation Condition Assessment", *IEEE Transactions on Dielectrics and Electrical Insulation*, October 2005, Vol. 12, No. 5, pp 891 – 903.

[3.12] E.J. Bartlett, M. Vaughan and P.J. Moore, "A System for Monitoring VHF Electromagnetic Radiation Generated by Power System Disturbance", *Proceedings of the 34th Universities Power Engineering Conference (UPEC)*, Leicester, September, 1999, Vol. 1, pp 249-252.

[3.13] M. Vaughan et al, 1998, "Remote Monitoring of Power System Faults Using VLF Waves", *International Conference on Electrical Engineering*, Vol. 2, p. 614.

[3.14] E.J. Bartlett, M. Vaughan and P.J. Moore, "Investigations into electromagnetic emissions from power systems arcs", *Electromagnetic Compatibility Conference EMC,* York, July 1999, pp 47-52.

[3.15] Fawwas T. Ulaby, *Electromagnetics for Engineers*, Pearson Education, 2005.

[3.16] F. H. Read, *Electromagnetic Radiation*, John Wiley & Sons, 1980.

[3.17] Jerry B. Marion, Mark A. Heald, *Classical Electromagnetic Radiation*, Academic Press, 1965, 1980.

[3.18] C. M. Wiggings, D. E. Thomas, F. S. Nickel, T. M. Salas, and S. E. Wright, "Transient Electromagnetic Interference in Substation", *IEEE Transactions on Power Delivery*, Vol. 9, No. 4, October 1994, pp 1869-1884.

[3.19] C. M. Wiggings, F. S. Nickel, A. J. Haney, and S. E. Wright, "Measurement of switching transients in a 115 kV substation", *IEEE Transactions on Power Delivery*, Vol. 4, No. 1, January 1989, pp 756-769.

[3.20] Railway Technical Center, Code of Practice for EMC Between the Railway and its Neighborhood, *Published by Railway Safety and Standard Directorate*, 1994.

[3.21] W. Ariastina, T.R. Blackburn, "Frequency Characteristics of Partial Discharges in Aged Insulation Systems", *Australasian Universities Power Engineering Conference*, AUPEC2001, Curtin University, September 2001, Volume 1, pp 543-547.

[3.22] Thereza Macnamara, *Handbook of Antennas for EMC*, Artech House Inc., 1995.

[3.23] Edward C. Jordan Editor in Chief, Reference Data for Engineers: Radio, Electronics, Computer and Communications, Howard W. Sams & Company, Seventh Edition, 1988.

[3.24] H. Debruyne and O. Lesaint, "About the significance of PD Measurements in Liquids", *IEEE Transactions on Dielectrics and Electrical Insulation*, Vol 10, No. 3, June 2003.

[3.25] Moore P J, Portugues I, Glover I A, "Pollution of the Radio Spectrum from the Generation of Impulsive Noise by High Voltage Equipment", *IEE Conference on Getting the Most Out of the Radio Spectrum*, Oct 2002, pp 37/1 – 37/5.

[3.26] C. Ramirez, P.J. Moore, "The Influence of Electrical Connection Arrangements in The Radiometric Identification of Partial Discharges", *International Symposium in High Voltage Engineering*, August 2005, session G-057.

[3.27] Electric Power Research Institute (EPRI), April 1993, "Electromagnetic Transients in Substations Vol 1: Project Summary and Recommendations", *EPRI*, Palo Alto, TR-102006.

[3.28] Su Q.; Sack K, "New Techniques for On-line Partial Discharge Measurements", *Multi Topic Conference IEEE INMIC 2001*. Technology for the 21st Century. Proceedings. IEEE International, 28-30 Dec. 2001, pp: 49 - 53.

[3.29] T.S. Sidhu et al, Oct 1998, 'Microprocessor based instrument for detecting and Locating Electric Arcs', *IEEE Transactions on Power Delivery*, Vol. 13, No. 4, pp. 1079-1085.

[3.30] J. Partanen & P. Eskelinen, "Possibilities for Power Distribution Network Fault Location With Radio Frequency Direction Finding", *IEEE 23rd National Convention on Radio Sciences and Remote Sensing Symposium*, 1998.

[3.31] David A. Nattrass, "Partial Discharge Measurement and Interpretation", *IEEE Electrical Insulation Magazine*, May/June 1988, Vol. 4, No. 3, pp 10 – 23.

[3.32] J. P. Steiner, "Partial Discharge – Part IV: Commercial PD Testing", *IEEE Electrical Insulation Magazine*, Jan/Feb 1991, Vol. 7, No. 1, pp 20 – 33.

[3.33] M. D. Judd, G. P. Clearly, C. J. Bennoch, "Applying UHF Partial Discharge Detection to Power Transformers", *IEEE Power Engineering Review*, August 2002, pp 57 – 59.

[3.34] E. Lemke, P. Schmiegel, "Introduction to Fundamentals of PD diagnostics", Lemke, Diagnostics, website: http://www.hvtechnologies.com/images/publications/intro-us.pdf.

[3.35] E. Gulski, F. H. Kreuger, "Computer –aided recognition of discharge sources", *IEEE Transactions on Electrical Insulation*, Feb 1992, pp 82 – 92.

[3.36] A. Krivda, *Recognition of discharges: Discrimination and Classification*, Coronet Books Inc., 1995.

DEVELOPMENT OF THE LABORATORY TEST SET SYSTEM

This chapter explains the basis of the developed laboratory test set system for detection and characterization of radiated partial discharges waveforms; it will describe the different stages in the construction of the laboratory test set system, from its simulation to its practical verification.

4.1. Test set simulation

It is a great advantage not having a physical connection between the power systems devices and the monitoring system. This makes possible the continuous operation of power systems and reduces costs and losses since no outage is necessary to perform a general PD survey. Another advantage is that the monitoring system is not limited to specific equipment within the power installation until some PD activity has been detected. Normally PD's occurring inside power equipment are caused by failures in insulation boundaries and start as minor discharges that evolve slowly into catastrophic damage. Sometimes these PD's are undetectable to conventional PD monitoring systems since they have to work within an environment where strong noise and electromagnetic interference is usually found [4.1]. In order to achieve a first approach in the development of a monitoring system, a laboratory test set where all the previously mentioned factors affecting the performance can be controlled, simulated and eliminated, and then adapted to normal working conditions is necessary. However the basic advantage of the laboratory test set is the

characterization of different types of partial discharges. Once a reliable test set system is achieved, the next step is the development of discrimination methods and a subsequent validation via field tests. Before the development of a laboratory test set a computer simulation that includes the connected components is used to assess equipment and personal risks involved in the case of failure. In addition the capabilities of the connected components under high voltage conditions (current and voltage limit ranges) can be evaluated.

Due to the non linear characteristics of electric arcing and its transient behaviour, the Alternative Transient Program was used for this simulation (ATP); this is a software package widely used for power system transients studies. It has a graphic user interface (ATPDRAW) that makes it relatively easy to use, and has the advantage of incorporating non linear elements which can be customized [4.2]. The equivalent test set circuit in figure 4.1 was used for the ATP simulation circuit shown in figure 4.2.

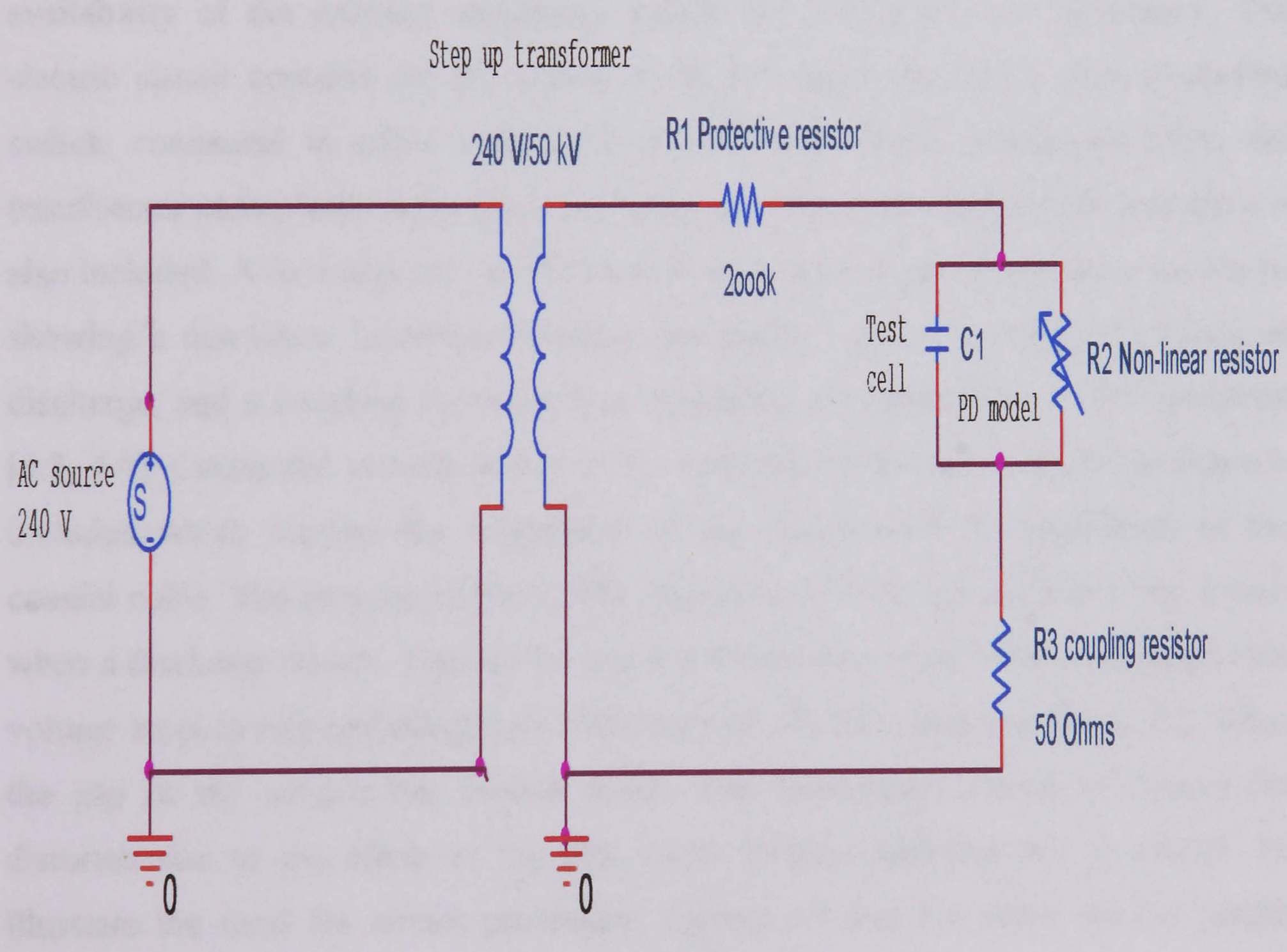

Figure 4.1. PD Test set equivalent circuit

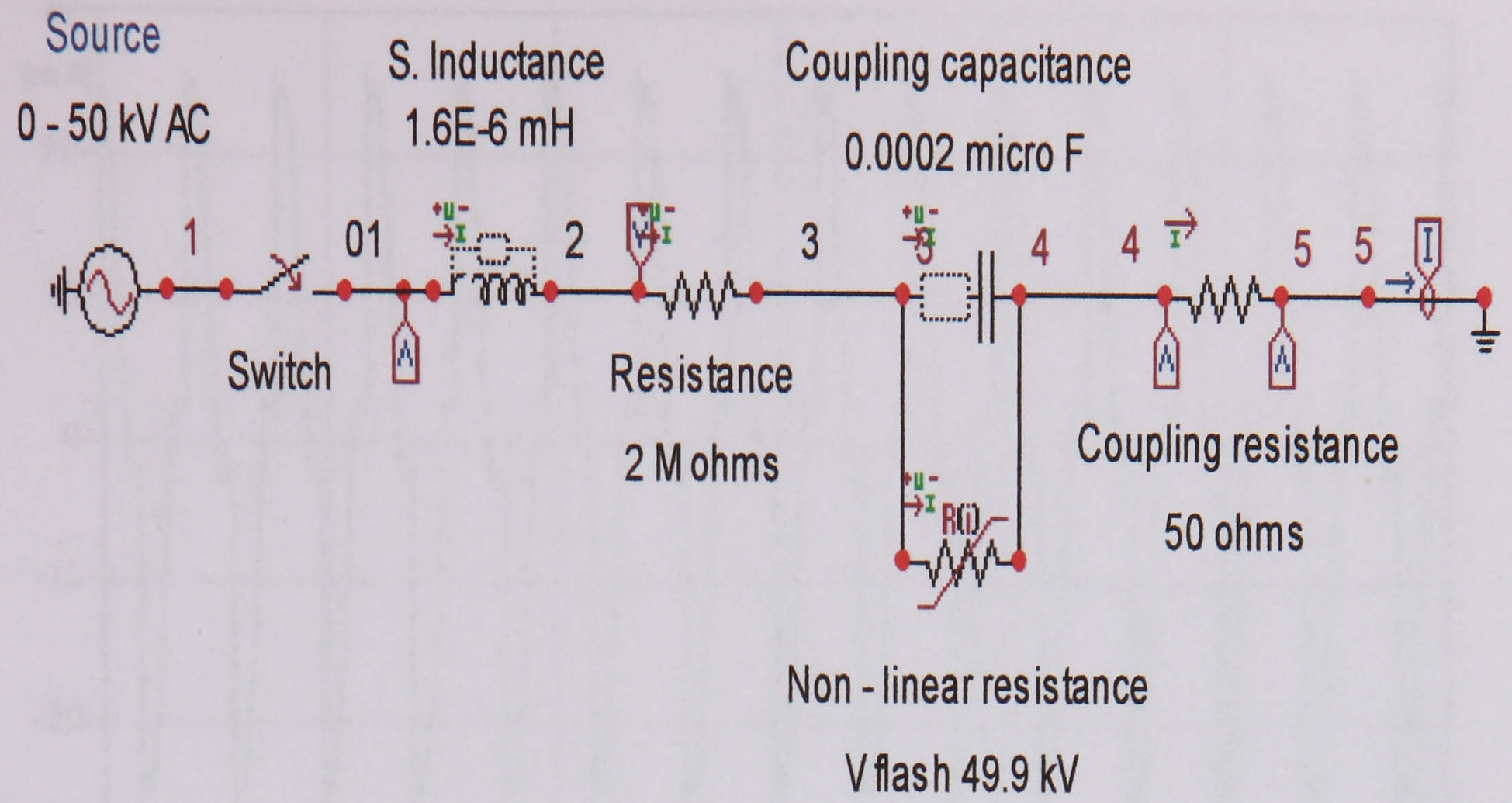

Figure 4.2. PD Test set ATP equivalent circuit

The electric components of the circuit in figure 4.1 were selected accordingly to the availability of the existent equipment within the University HV laboratory. The electric circuit contains an AC source of 50 kV maximum and a time controlled switch, connected in series with a 1.6 X 10^{-6} mH internal inductance (from the transformer nameplate). After the transformer, a series connected 2 MΩ resistance is also included. A first approach to PD simulation can be made by placing a resistance showing a non-linear behaviour between the nodes 3 and 4 (see fig 4.2) acting as discharge, and a coupling capacitor that represents the capacitance of the specimen [4.3, 4.4]. Connected to earth and in series with the PD circuit, a 50 Ω resistance is included which couples the impedance of the circuit with the impedance of the coaxial cable. The purpose of the 2 MΩ resistor is to limit the current of the circuit when a discharge occurs. Figures 4.3 and 4.4 shows the values of the current and the voltage respectively including the 2 MΩ resistor, for the circuit of figure 4.2, when the gap in the sample has broken down. The waveforms shown in figures are distorted due to the effect of the non linear resistor included in the circuit. To illustrate the need for circuit protection, figures 4.5 and 4.6 show similar results where the 2 MΩ resistor is replaced by a short circuit.

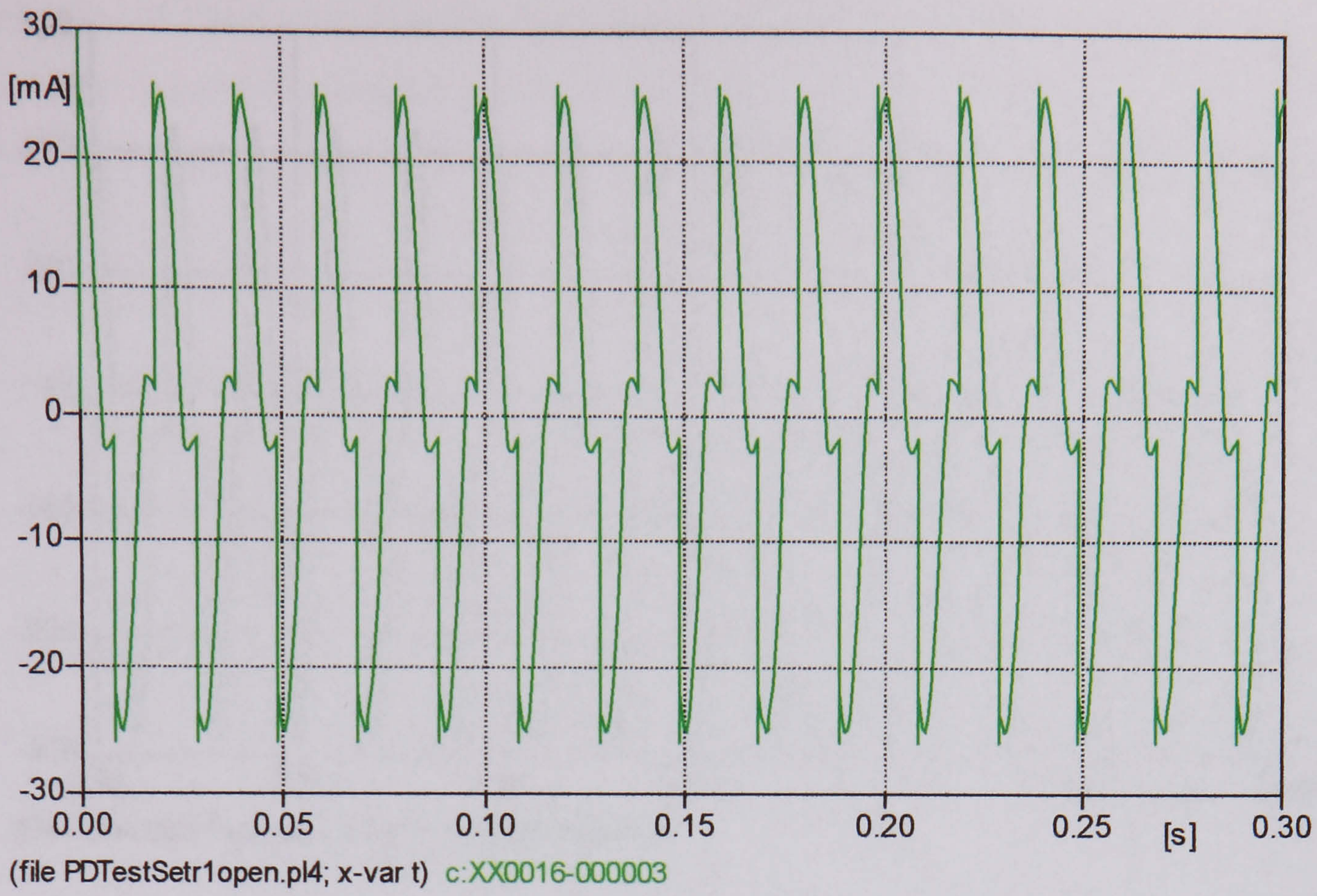

Figure 4.3. Current flowing through the 2MΩ resistor of the PD test set circuit.

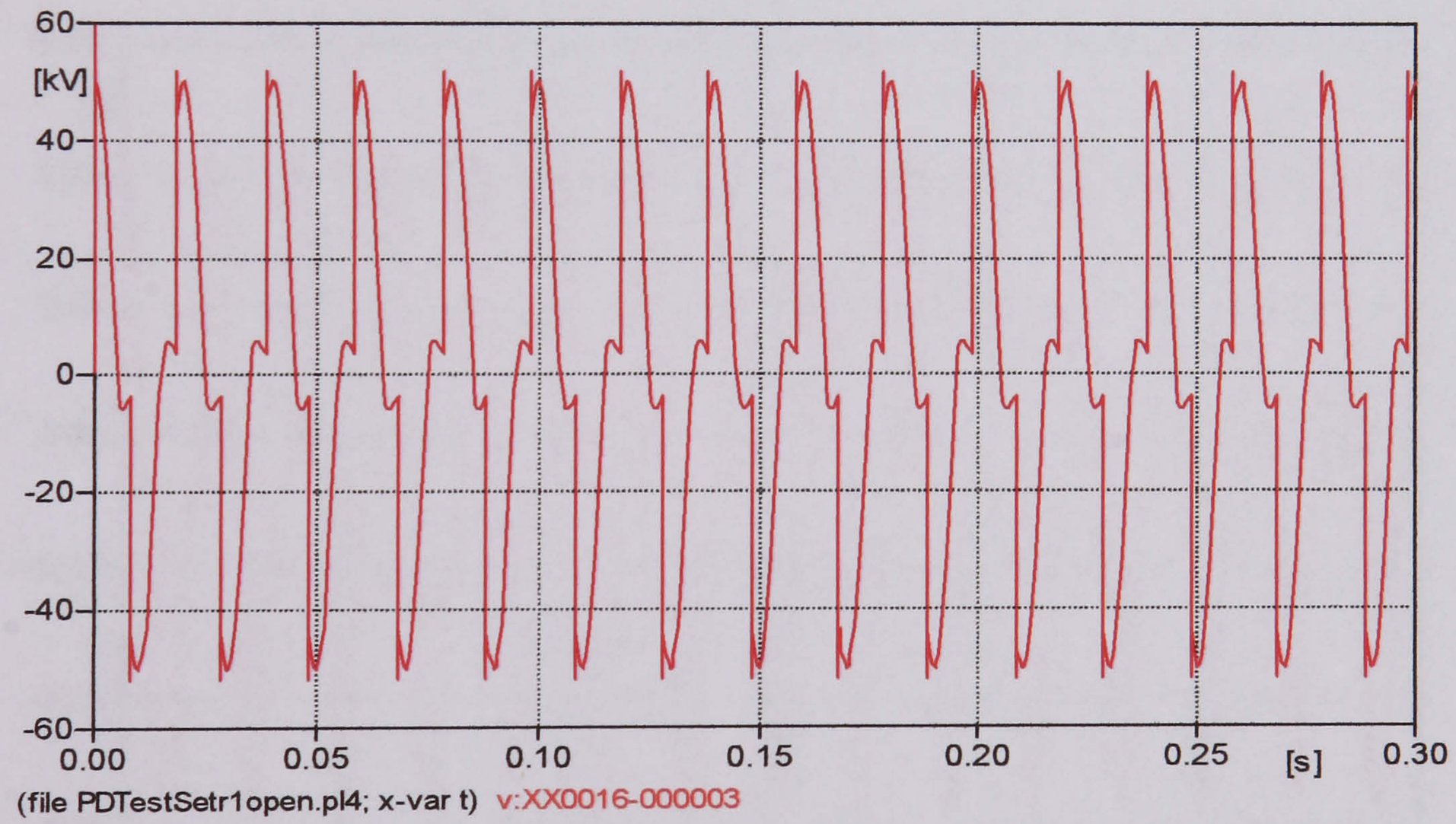

Figure 4.4. Voltage across the 2MΩ resistor of the PD test set circuit.

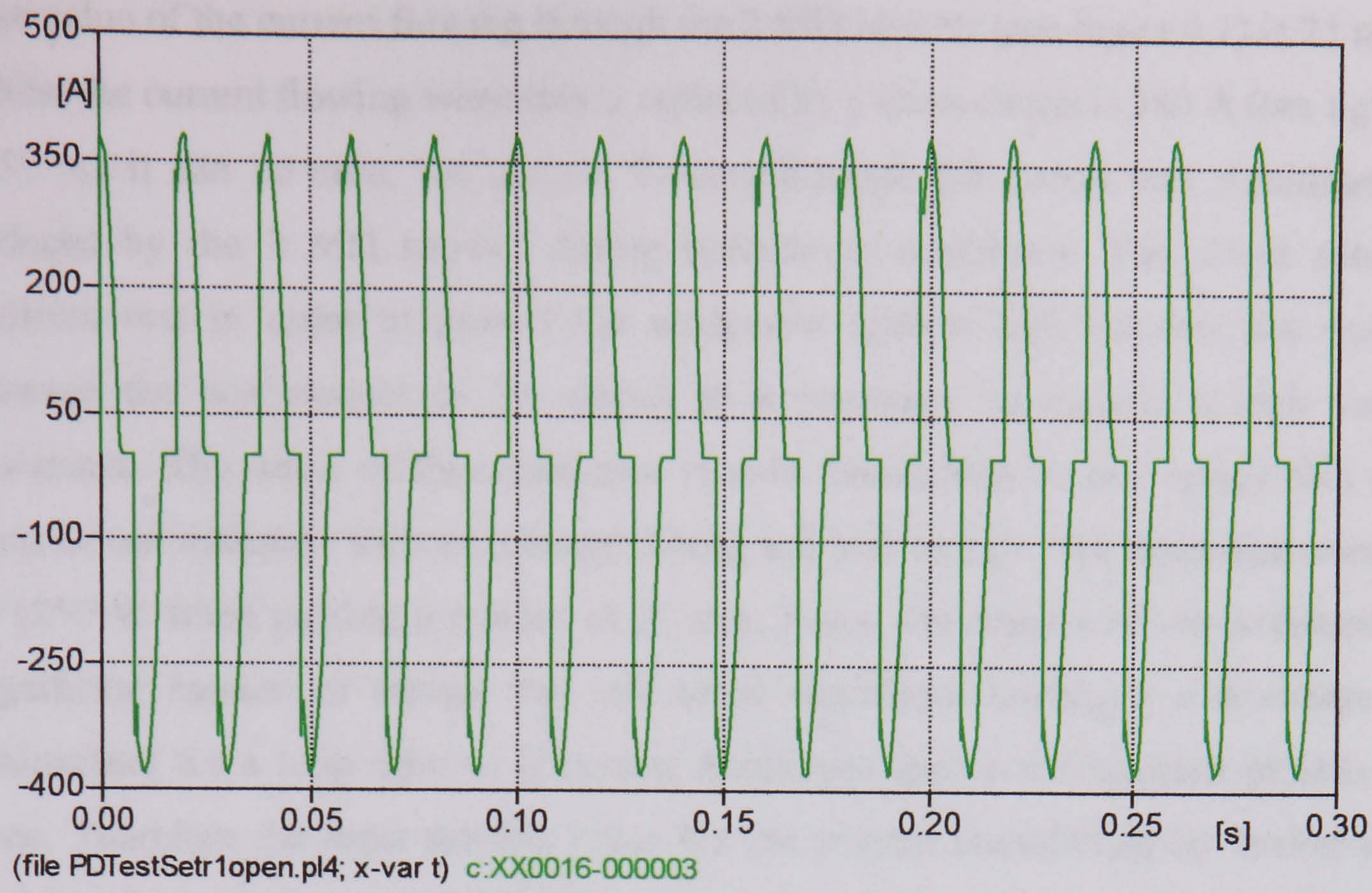

Figure 4.5. Current flowing through the PD test set circuit resistor (2MΩ resistor replaced by short circuit).

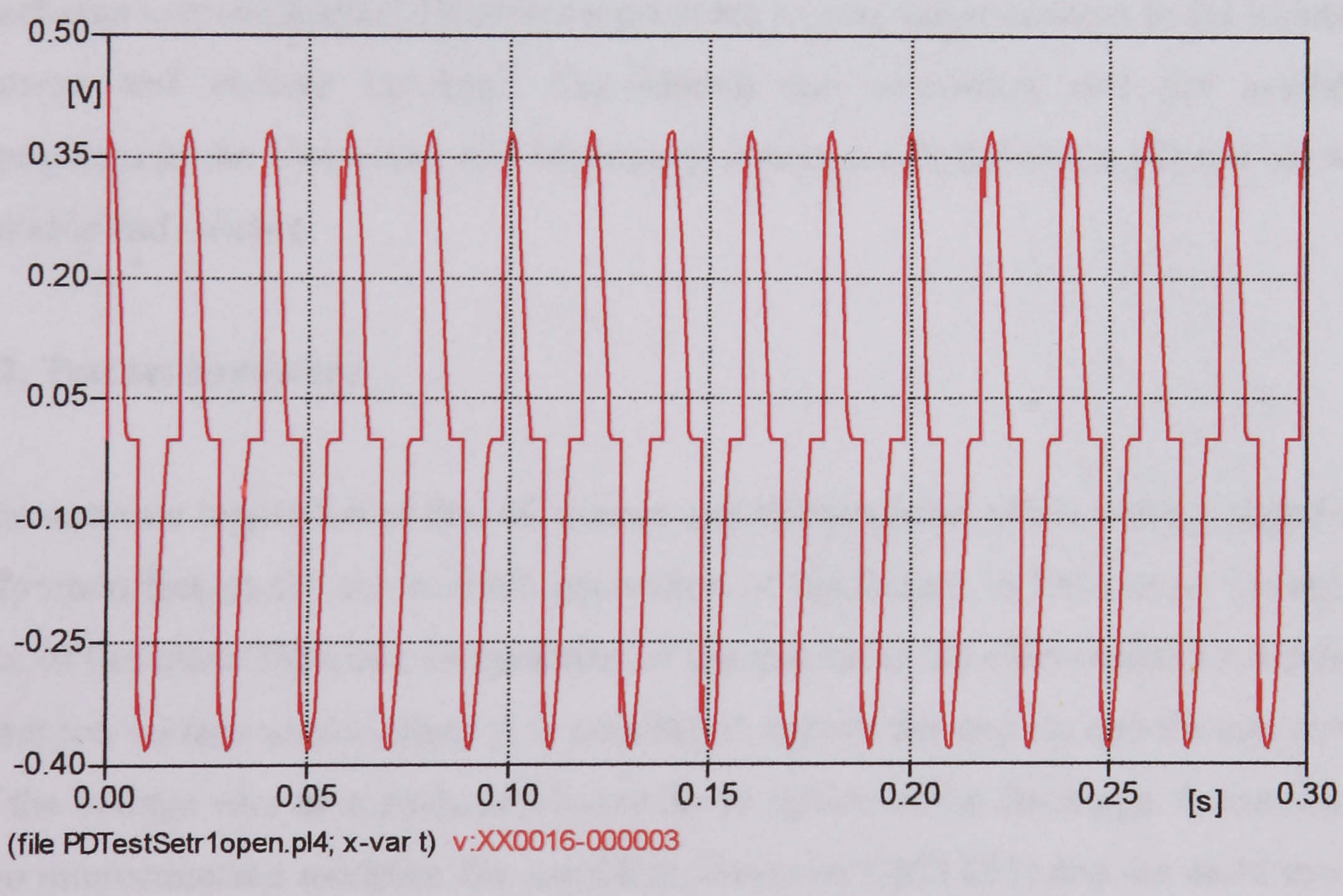

Figure 4.6. Voltage in the terminals of the PD test set circuit resistor (2MΩ resistor replaced by short circuit).

The value of the current flowing through the 2 MΩ resistor (see figure 4.1) is 25 mA, whilst the current flowing when this is replaced by a short circuit is 380 A (see figure 4.5). As it can be seen, the current flowing through the circuit was significantly reduced by the 2 MΩ resistor during breakdown conditions. The above results indicate that in order to protect the equipment against high currents that could damage the components of the circuit it is necessary to include a high value resistance. The value of this resistance is only determined by the energy that the resistor can dissipate without damage. Using a 2 MΩ resistor, the dissipated energy is 1250 W when passing a current of 25 mA; hence, the resistor has to withstand a significant amount of energy that will cause significant heating if a discharge is maintained for a long time or if several discharges appear during short periods of time. Therefore the most suitable value for the resistor considering the availability and the above factors was 2 MΩ. The current drained to earth was also considered, since the signal to the oscilloscope will be obtained from the 50 Ω resistor connected to earth.

In this simulation only a general approach to the non-linear behavior of the partial discharge was considered. However it provides a good approximation to the transient current and voltage involved. Considering the simulation and the available equipment in the University HV laboratory, it was concluded that a PD test set was suitable and reliable.

4.2. Test set hardware

The accurate regulation of the AC source and the precision of the voltage signal are important factors for the suitable generation of discharges in laboratory. Therefore one of the most important components of the test set is the electronically controlled Omicron voltage source, since it is possible to control the step up and the step down of the voltage very accurately and hence the inception of the discharge. It consists of two interconnected modules: the amplifier (Omicron CMS 251) and the multi source (Omicron 56) which is connected to a digital computer that hosts the Omicron software for the digital regulation of the source voltage.

The 240 VAC are supplied by the mains in the HV laboratory and then applied to the Omicron 56. The output voltage of the CMS 251 is monitored by a digital multimeter, with the aim to maintain a visual control of the low side voltage of the circuit. Since the maximum output of the CMS 251 is 125 VAC, a transformer with a ratio 125/240 V is used to step up the voltage and then apply it to the low voltage side of a 240V/50kV transformer. Finally, the high voltage side of the latter transformer is applied to a needle-plate gap configuration which is firmly connected to earth. The high voltage side is monitored by a capacitive divider with a voltage ratio of 10000/1. This configuration can be re-arranged according to the test requirements, and permits the accurate generation of corona and a wide range of discharges. Figure 4.7 shows a general arrangement of the described equipment.

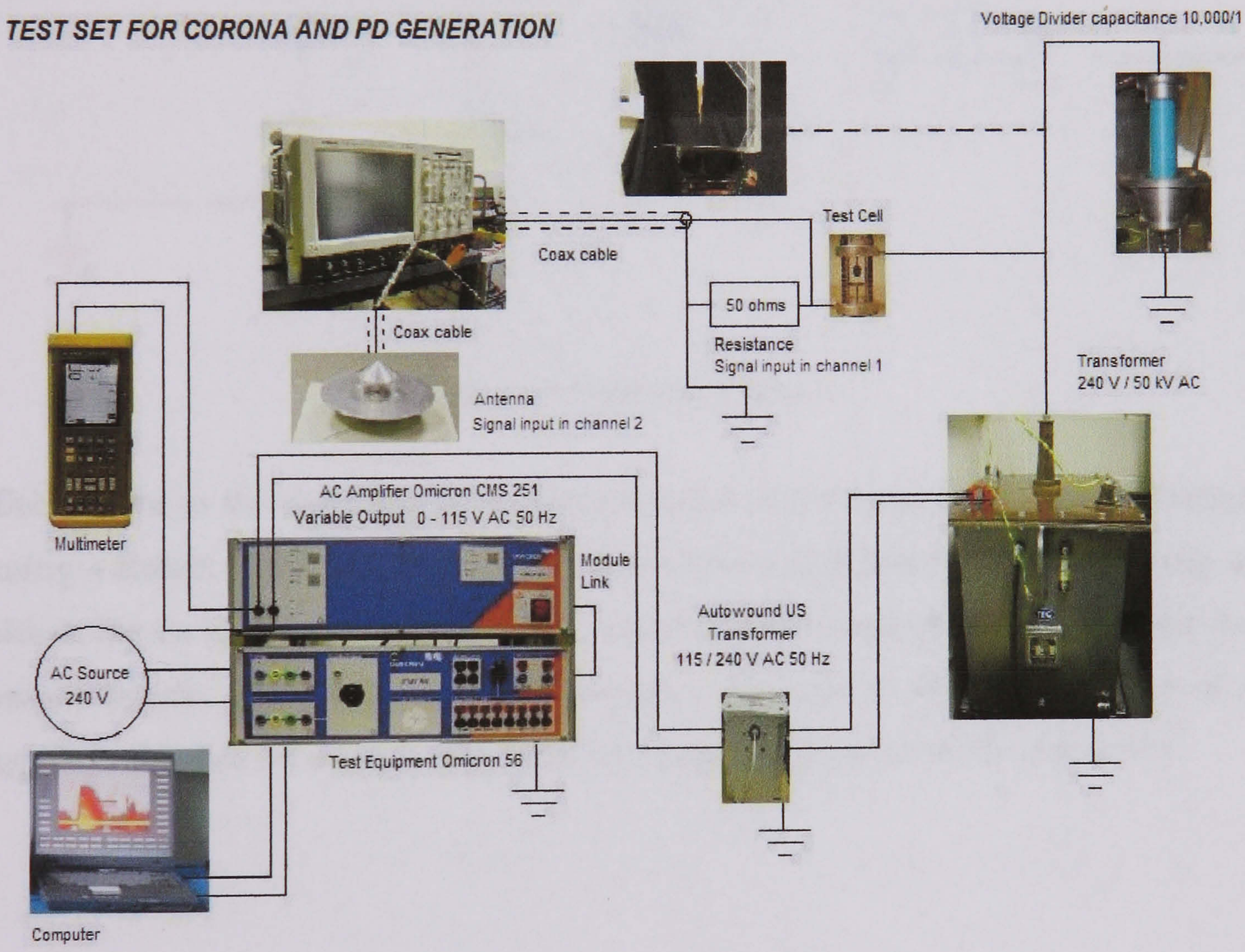

Figure 4.7. General array of the PD and discharge test circuit.

A critical part of the data acquisition system is the coupler and the protection box which includes the 50 Ω resistor. The latter is necessary to protect the oscilloscope

against high voltage discharges and high currents, and such protection is achieved by means of a transient suppression diode and a surge arrester with a breakdown voltage below the oscilloscope maximum input voltage. However, the addition of protective elements can modify the frequency spectra of the original signal. For this reason a protection circuit with a nearly flat frequency response up to 1 GHz was developed. It includes the 50 Ω resistor and rigid ground connections. Figure 4.8 show the protection box circuit.

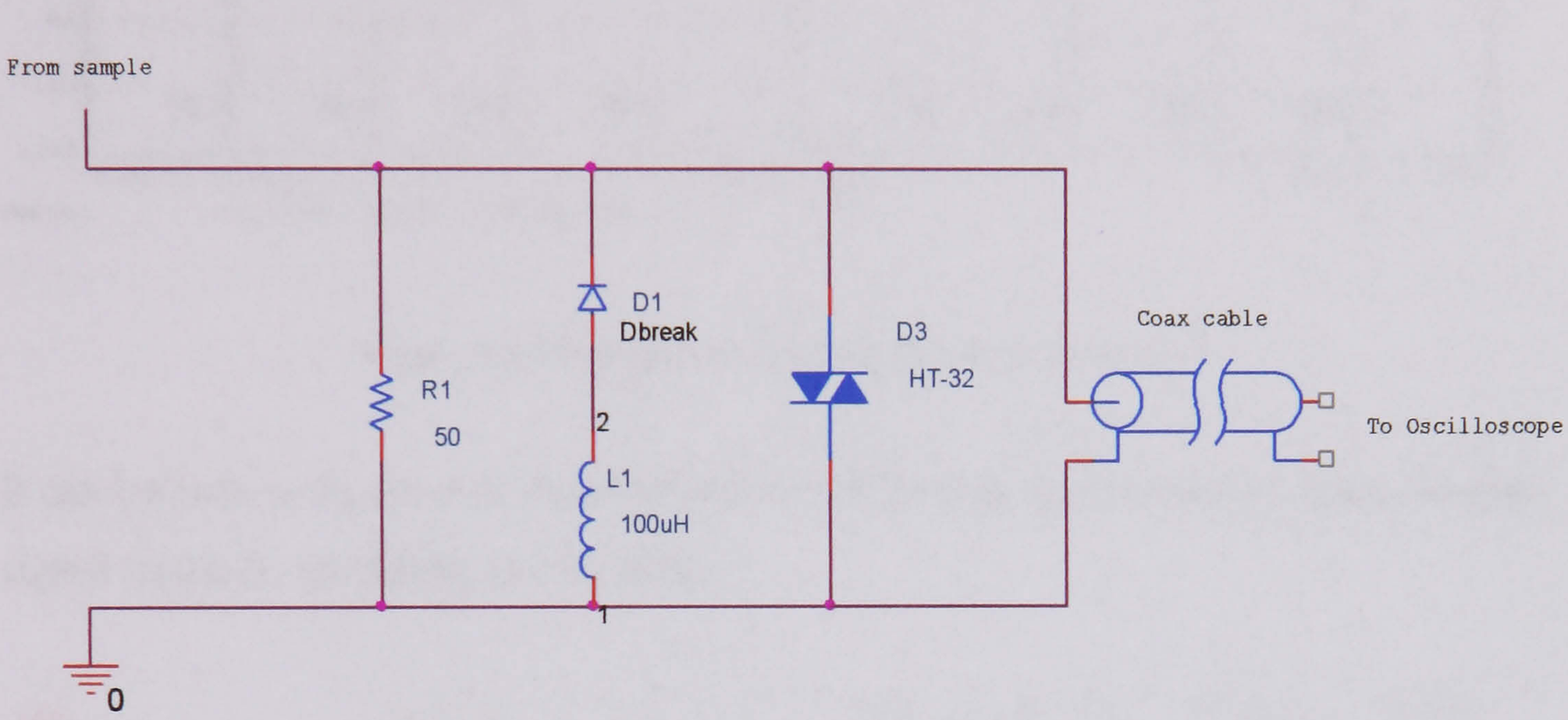

Figure 4.8. Protection box circuit

Subsequent to the development of the protection box several tests were performed using a Rohde & Schwarz FSEK 30 Signal Generator/Digital Spectrum Analyzer to determine its frequency response. The response was compared before and after the improvements. Ideally the desirable frequency response is similar to the one of a quick form cable i.e. a nearly flat frequency response as shown in the figure 4.9.

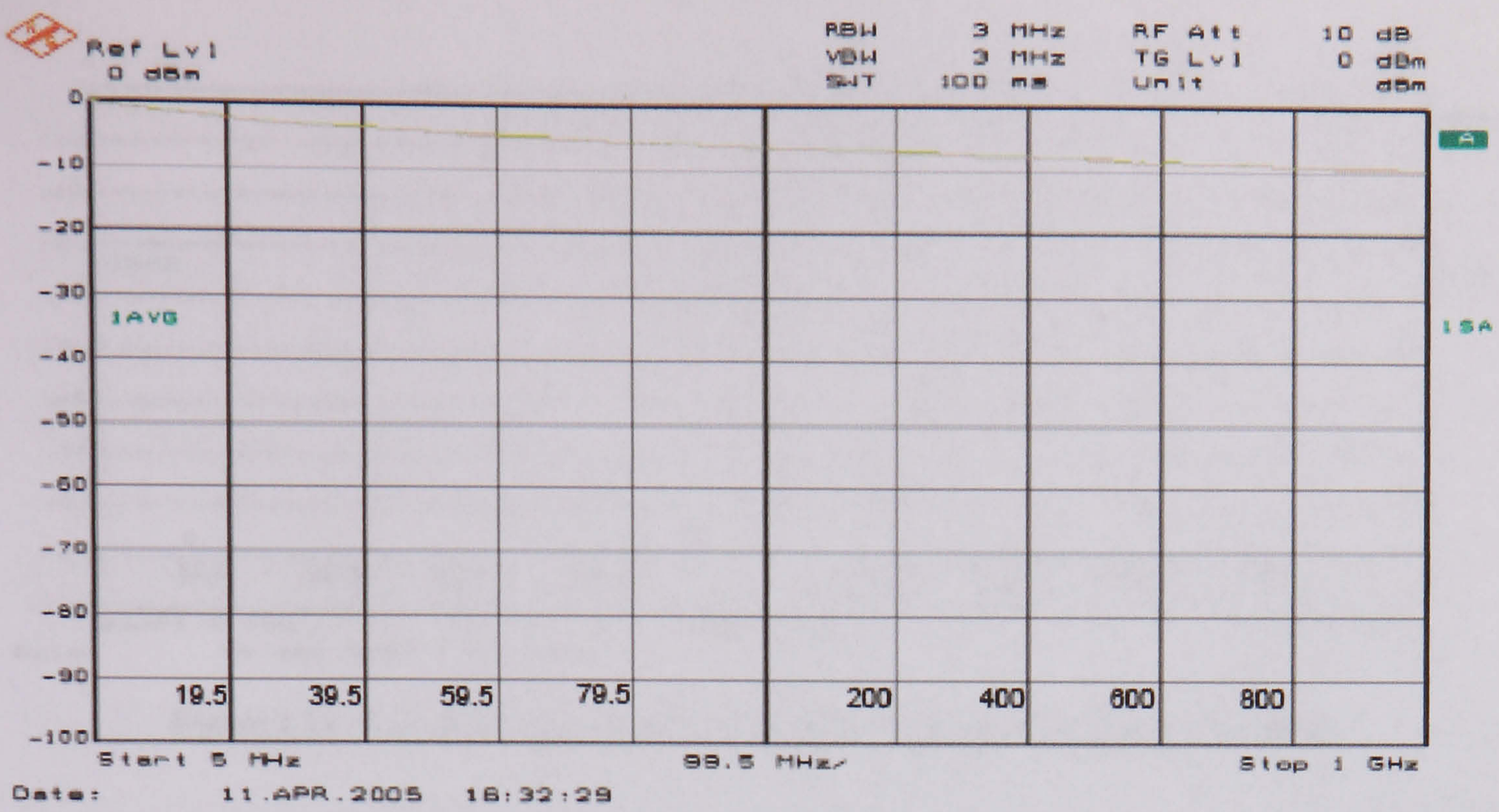

Figure 4.9. Frequency response of the quick form cable

It can be seen in figure 4.10 that the circuit without the improvements has a damped signal (around -40 dB) below 20 MHz.

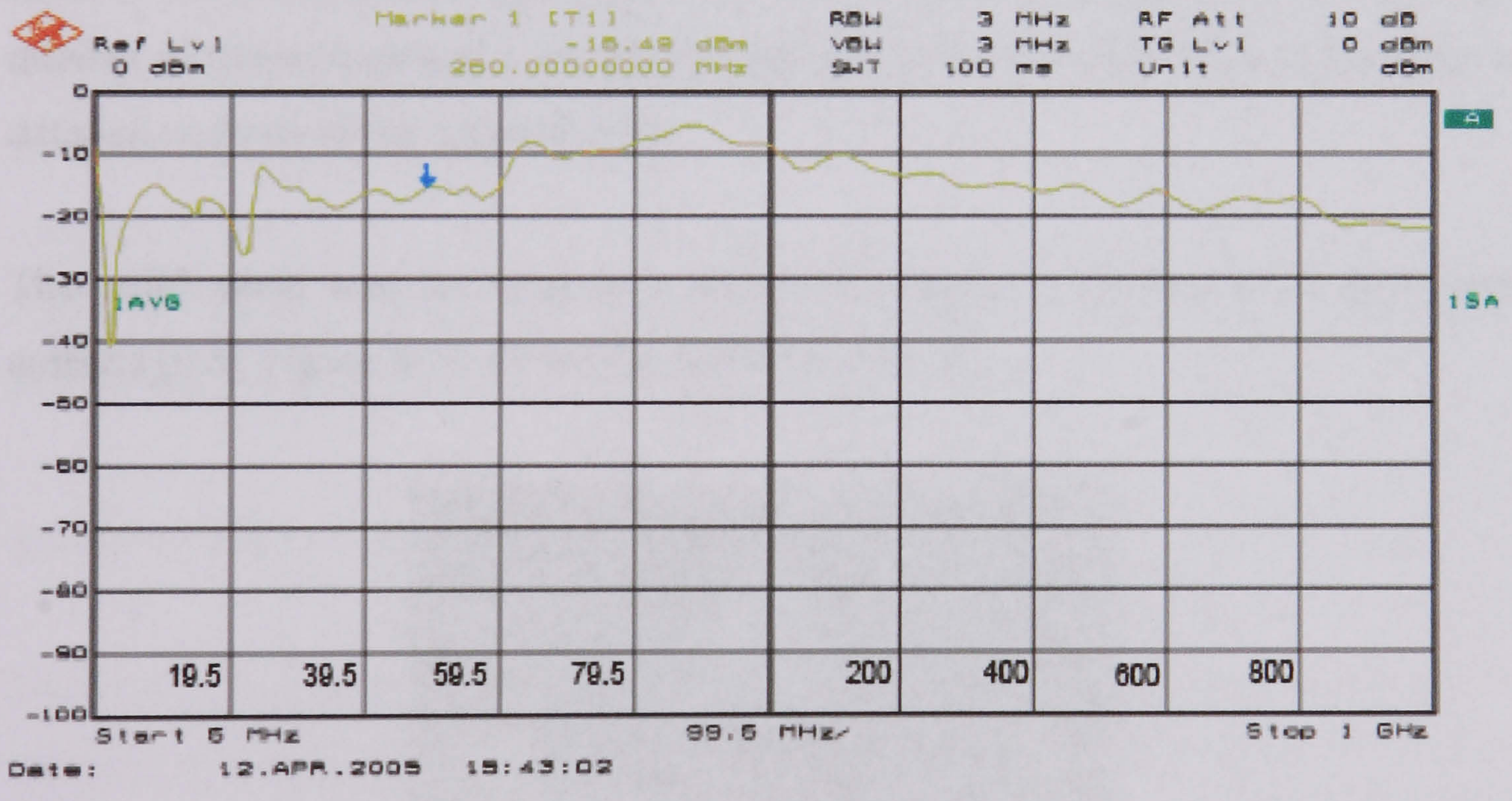

Figure 4.10. Frequency response of the protection box without the improved circuit

The latter effect was corrected by adding a 100 μH inductor which compensates the capacitance of the coaxial cable [4.4]. Figure 4.11 shows the frequency response of the improved protection box.

Figure 4.11. Frequency response of the protection box with the improved circuit.

When an electric discharge is generated, the transient current flows through the 50 Ω resistor and causes a voltage drop that is transferred to the oscilloscope via the coaxial cable. The radio wave generated by the discharge is received in the antennas and transferred to the oscilloscope. In order to analyze the relevant characteristics of the generated discharge, a state-of-the art oscilloscope (Tektronix TDS 7104) was used. It has an analogue bandwidth of 1 GHz that allows the analysis of a relevant number of frequencies and a maximum sampling frequency of 10 GS/s that permits a detailed analysis of the radiated wave.

The radio wave was received in a wideband frequency unidirectional disk-cone antenna [4.5]. Figure 4.12 shows the described antenna.

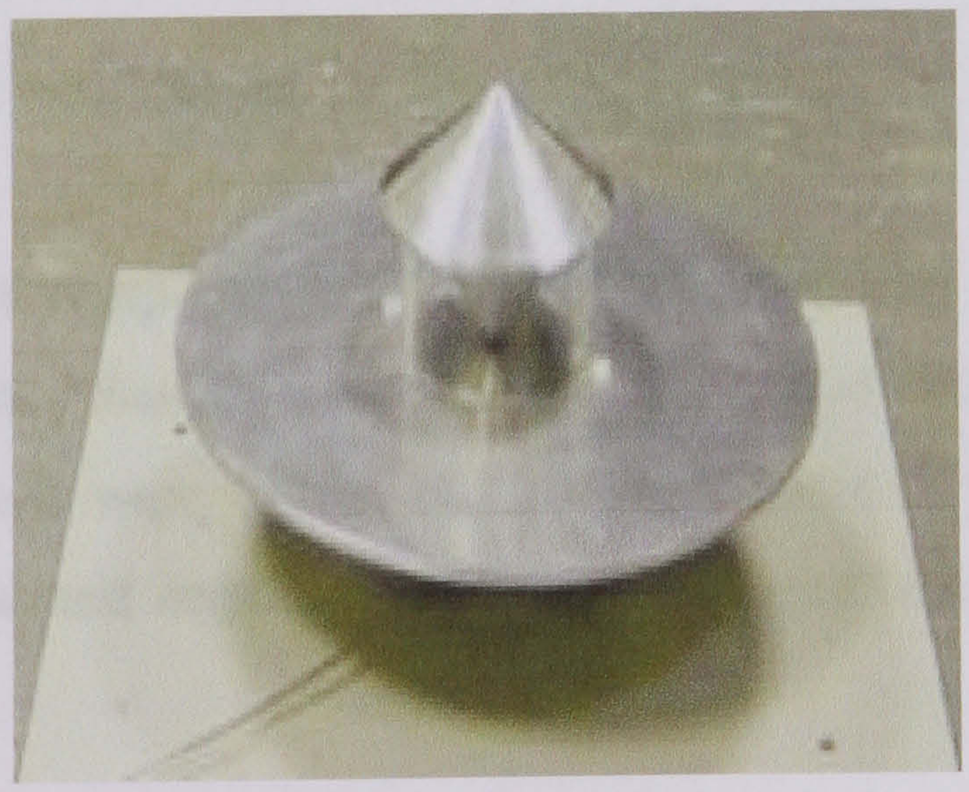

Figure 4.12. Disk – Cone antenna.

All the equipment for the experimental test was installed in a designated cage in the University HV laboratory. Strict safety measures for the operation of the test set were enforced such as interlocks between the control equipment and the HV equipment, warning signs both inside and outside the laboratory cage and risk assessment in handling dangerous materials.

4.3. Test set software

The Electrical Plant and Diagnostics Group of the University of Strathclyde have already worked on the development of software systems that locates and analyzes PD's using MATLAB [4.6]. Based on this previous work dedicated software for data acquisition and frequency domain signal analysis was developed. The relevant characteristics of this software are: four channels data acquisition for the Tektronix oscilloscope, frequency domain analysis and plotting of the acquired data using Fast Fourier Transformer (FFT). For time domain analysis a MATLAB program was developed that processes the point on wave information and pulse data. After the point on wave information has been processed, the program computes the necessary statistical operators and stores them in a Microsoft Access database file. Another program calls the database file and processes it in order to apply discrimination methods. The basic advantage of this software is the automatic analysis and plotting of the acquired data stored in the oscilloscope, which saves time and resources.

4.4. System tests and verification

Once the required test equipment was selected, the next step was its installation in the HV laboratory facilities following strict safety measures established by the University. Several tests were carried out; however some of them were considered critical due to the cost and importance of the equipment. The critical tests were as follows:

- Circuit tests

- Test set corona and PD free
- Corona and discharge generation
- Oscilloscope test
- Oscilloscope settings

The following sections describe each of the above tests.

4.4.1. Circuit test.

The installed equipment was energized and tested, the most important activity in this test was to determine the ratio between the low voltage side and the high voltage side in order to record the measured voltage. This measurement was performed using a voltmeter installed in the low voltage side and the capacitive divider connected to the high voltage side. These values served as reference during all the tests. Another important factor was the exact inception voltage value of the discharge which must be known accurately. During this stage the integrity and behavior of the electric equipment was verified.

4.4.2. Test set corona and PD free.

For this circuit, it is critical that in the LV and HV section all the components are free from any form of discharge or corona effect. The only regions where corona or discharge was allowed to occur was in the sample or gap configuration. Otherwise corona, noise or discharges occurring in other parts of the circuit can interfere with the quality of the test. Several improvements were made in order to achieve this requirement such as the use of components with Rogowski profile in the HV side [4.3], and a multipoint grounding system. Once energized, the HV side of the circuit was verified through the use of an image intensifier device to localize possible corona or undesirable small PD's. At this point the circuit was tested without any sample and a gap separation of 125 mm.

4.4.3. Corona and discharge generation.

With the absence of undesirable corona and PD, the next step was to generate corona in the tip of the needle of the gap configuration. The verification of the generated corona was made with the help of an image intensifier device and naked eye. After several tests with corona activity the breakdown voltage was reached at 35.3 kV. All the values and activities were registered in an electronic spreadsheet. Figure 4.13 a) show the generated corona and figure 4.13 b) a complete gap breakdown.

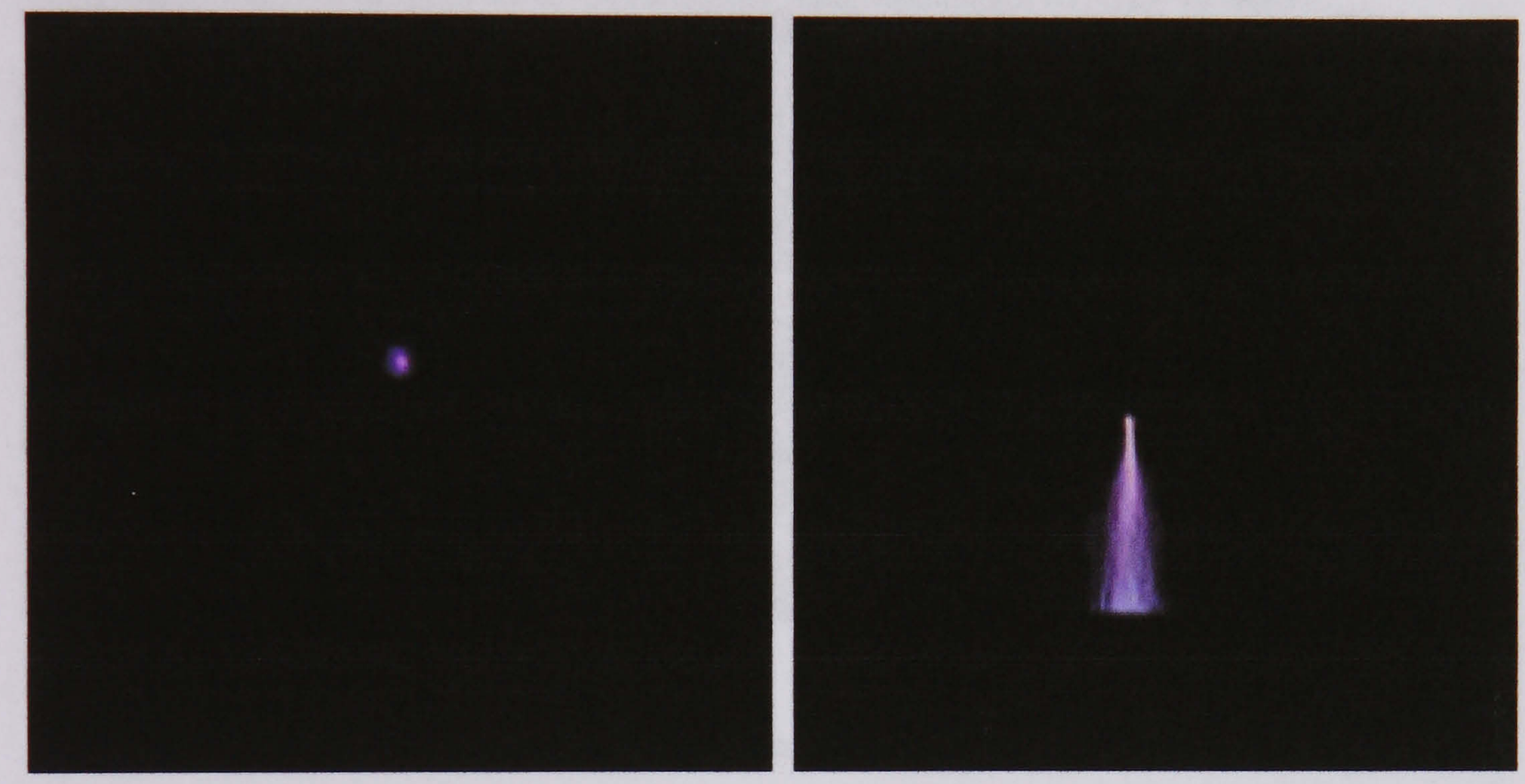

a) b)

Figure 4.13. Generated a) corona and b) gap breakdown at 35.3 kV

4.4.4. Oscilloscope tests.

Probably the most expensive and important component of the test set is the oscilloscope; therefore it is a priority to ensure the integrity of this component through several protective components and tests. Two factors were considered for the protection of the oscilloscope: the reliability of the protection and its frequency response. Several tests were performed using 20 dB attenuators for the protection of the two channels of the oscilloscope. The attenuators give acceptable frequency response and sufficient protection to the oscilloscope. A 50 Ω coupler was placed in the input of channel 1 to match the cable impedance with the oscilloscope

impedance. When required the configuration of the protective devices is as follows, 2x20 dB attenuators placed in channel 1 (input from 50 Ω earthed resistor) and a 20 dB attenuator placed in channel 2 (input from the antenna). Figure 4.14 show the latter configuration.

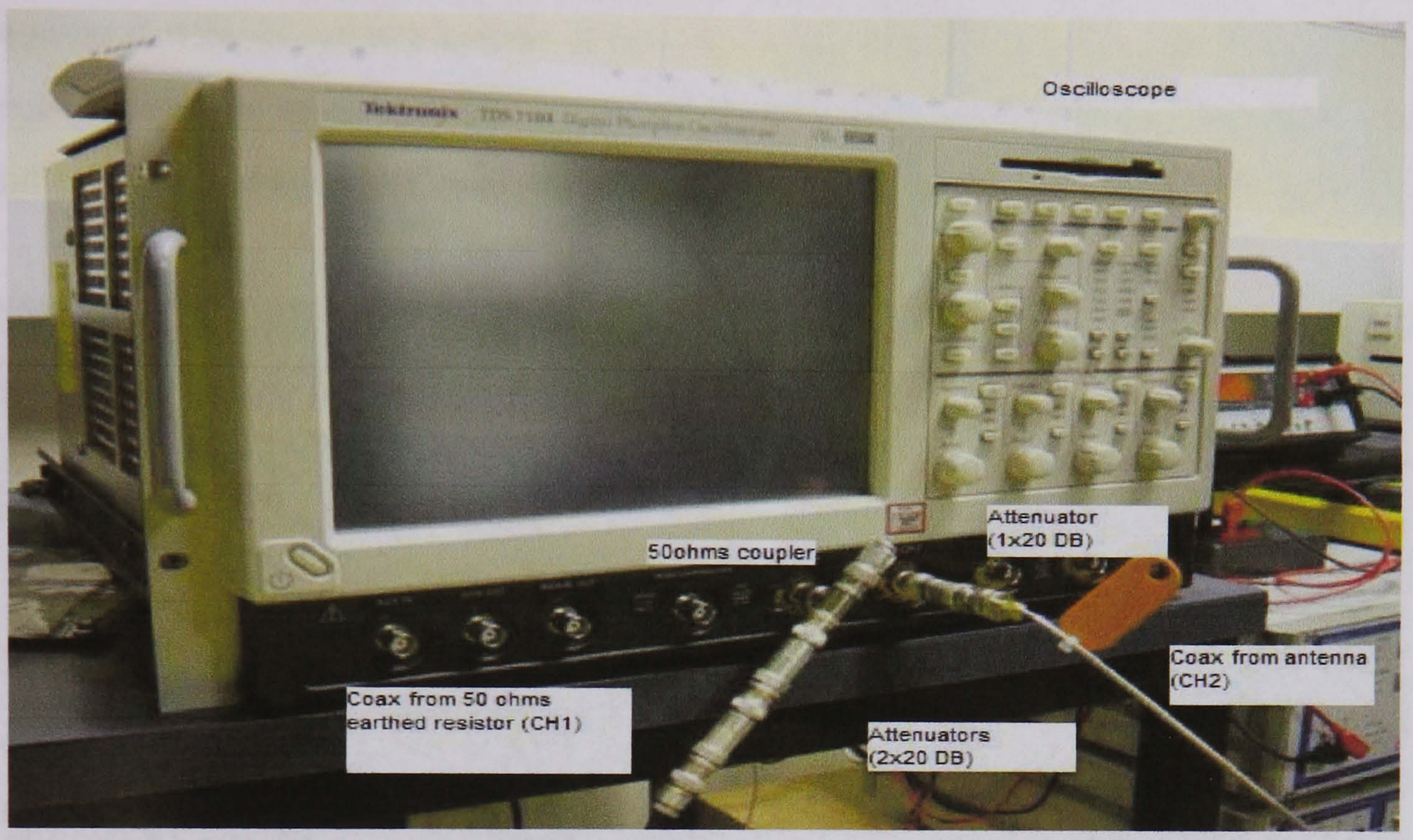

Figure 4.14. Oscilloscope configuration.

The selected protections ensure the safe connection and isolation of the oscilloscope from the HV section of the test circuit. The attenuation of the acquired signal is compensated later using the data acquisition and analysis software that was described in the previous section.

4.4.5. Oscilloscope settings.

The successful acquisition of the data from the test set depends in part on the correct functioning of all the components, and the accuracy of the results depends to a certain extent on the oscilloscope settings. The different adjustments in the oscilloscope such as volt-per-division, resolution, time, sampling etc, are recorded and registered in an electronic spreadsheet as the settings of the oscilloscope change according to the requirements of each experiment.

4.5.General layout of the laboratory test set.

All the HV equipment was placed inside a protected cage equipped with an interlock system to increase personal security when the equipment is operated. This cage is equipped with an earthed system of low resistivity value. Ground connections to live equipment are made of flat strips of copper to avoid stray capacitances and reflections. The antennas were distributed inside the cage as illustrated in figure 4.15.

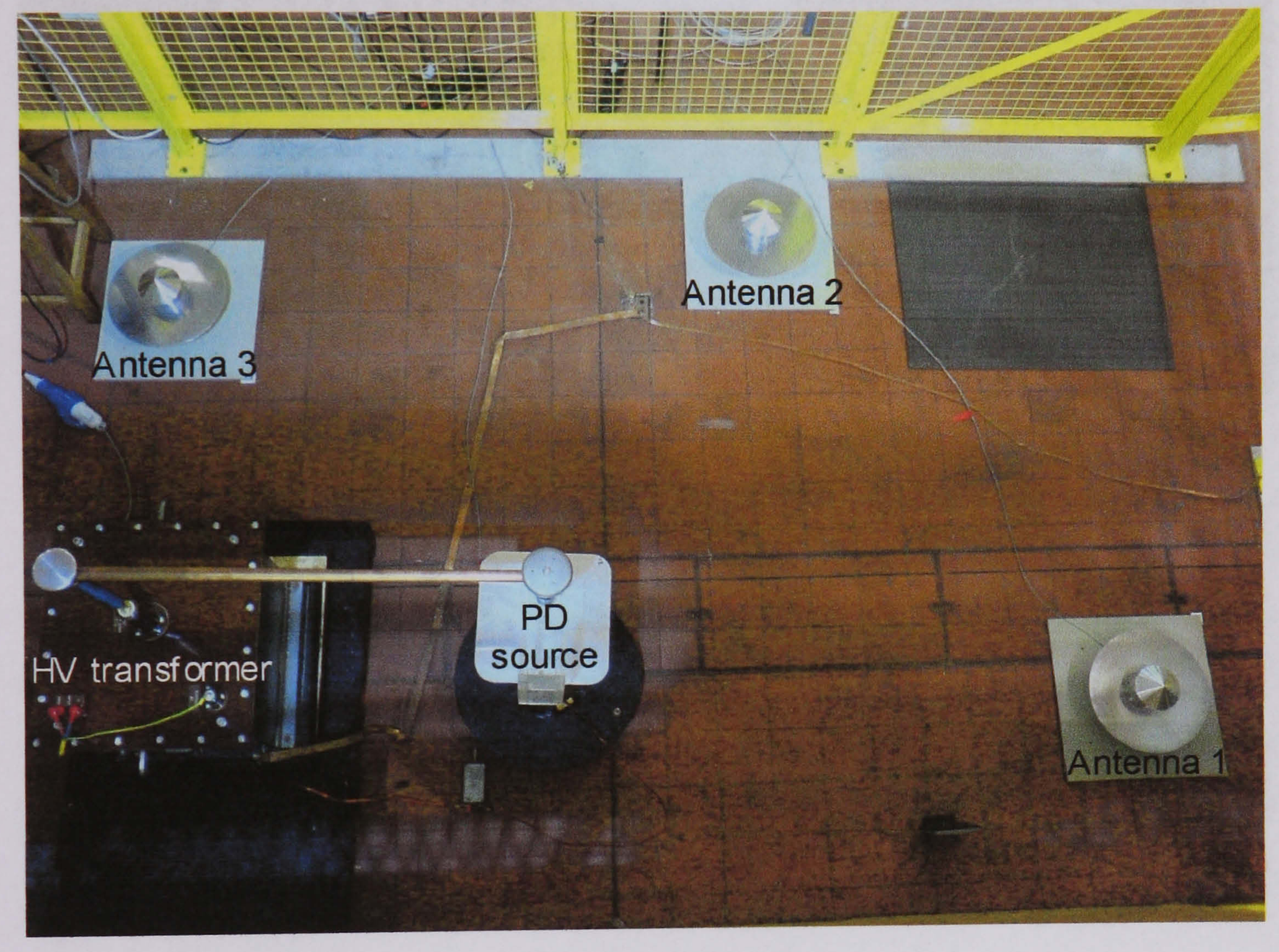

Figure 4.15. Antennas in different positions with respect to the source discharge

All the measurement equipment such as computer and oscilloscope were placed outside the cage (see figure 4.16).

Figure 4.16. Measurement and acquisition equipment

The conducted signal from the sample to the oscilloscope was coupled using a protection box whose characteristics were described previously. The characteristic of this protection box is a nearly flat frequency response and direct connection path to earth. The data acquisition system consists of 3 antennas and one oscilloscope. After the acquisition of the signals the data was stored and classified for further analysis.

4.6. Chapter 4 references

[4.1] Steven A. Boggs, "Partial Discharge – Part VII: Practical Techniques for measuring PD in operating Equipment", *IEEE Electrical Insulation Magazine*, Vol.7, No.4 Jul/Aug, 1991, pp: 9-19.

[4.2] Leuven EMTP center. *Alternative Transient Program Theory Book*. July 1987.

[4.3] E. Kuffel; W. S. Zaengl; J. Kuffel, *High Voltage Engineering: Fundamentals*, Newnes, 2001.

[4.4] M.A. Elborki, P. A. Crossley, MIEEE, Z. D. Wang, A. Darwin, SMIEEE and G. Edwards, "Detection and Characterization of Partial Discharges in Transformer defect Models", *IEEE Power Engineering Society Summer Meeting*, 2002, Volume: 1 , 21-25 July 2002, pp: 405 – 410.

[4.5] Moore P J, Portugues I, Glover I A, "A Non-Intrusive Partial Discharge Measurement System Based on RF Technology", *Power Engineering Society Meeting*, June 2003, pp 627 – 633.

[4.6] Portugues I, Glover I A, Moore P J, Sept 2002, "An investigation into effect of receiver bandwidth for the interpretation of partial discharge impulses using remote radio sensing", *Proceedings of International Universities Power Engineering Conference 2002 (UPEC'02)*, pp. 529–533

INFLUENCE OF THE SURROUNDING ENVIRONMENT ON RADIATED DISCHARGES

This chapter explains and analyzes the different tests that were carried out using the developed test set in the HV laboratory to determine the relevant characteristics of the air and oil discharges. This chapter also assesses the influence of the surrounding objects, structures and also the length of the test set circuit. It includes a novel frequency response test to evaluate and filter the frequency spectra of the PD signal to allow differentiation between oil and air discharges.

5.1. Tests description.

The purpose of the tests carried out in the HV laboratory was to investigate the intrinsic characteristics of radiated discharge signals and compare the results with conducted discharge signals. As the latter are taken directly from a 50 Ω resistor, they will serve as a reference when compared with radiated discharges and serve as the base for a discrimination method. The tests were divided in two parts:

I. Evaluation of the influence of the structures of the circuit loop and gap length over the radiated and conducted discharges.

II. Evaluation of the frequency response of the test set.

In general the methodology was to capture screenshots of the oscilloscope using the fast acquisition function for future reference and using one channel as AC reference. Another channel is used to acquire the signal coming from the 50 Ω resistor, and the remaining two channels were reserved for the antennas. The information on the four channels was recorded using a long acquisition time (typically between 4ms and 10 ms long). Once acquired, the information of several AC cycles (typically 3 or more) acquisitions of individual discharges were recorded. The oscilloscope was adjusted to 2.5 GS/s and 200 ns for each discharge. The acquired information was classified and stored in an external hard disk.

5.2. Length of the gap and circuit loop influence over the generated discharge

There are several factors that affect the frequency and shape of the radiated wave, such as the propagation media, attenuation and the structures acting as antennas [5.1]. The latter effects are analyzed in a HV laboratory using a test set in order to reproduce controlled discharges in air and oil using different gap sizes and circuit loop lengths. Figure 5.1 shows the test set configuration (air gap, oil test cell) for the mentioned tests.

a) 10 mm Air gap

b) 10 mm oil gap

Figure 5.1 a) Air gap configuration of the test set, b) oil cell configuration of the test set.

From high-voltage laboratory investigations, the impulsive radio-frequency radiation from air and oil discharges is presented as a function of the experimental

arrangement. The results show that the frequency response of radiometric data is influenced more by the experimental arrangement than by the nature of the discharge. The influence of the gap length is also assessed. Figure 5.2 shows two different lengths arrangements of the test set, in total three arrangements were used at different loop lengths see Table I.

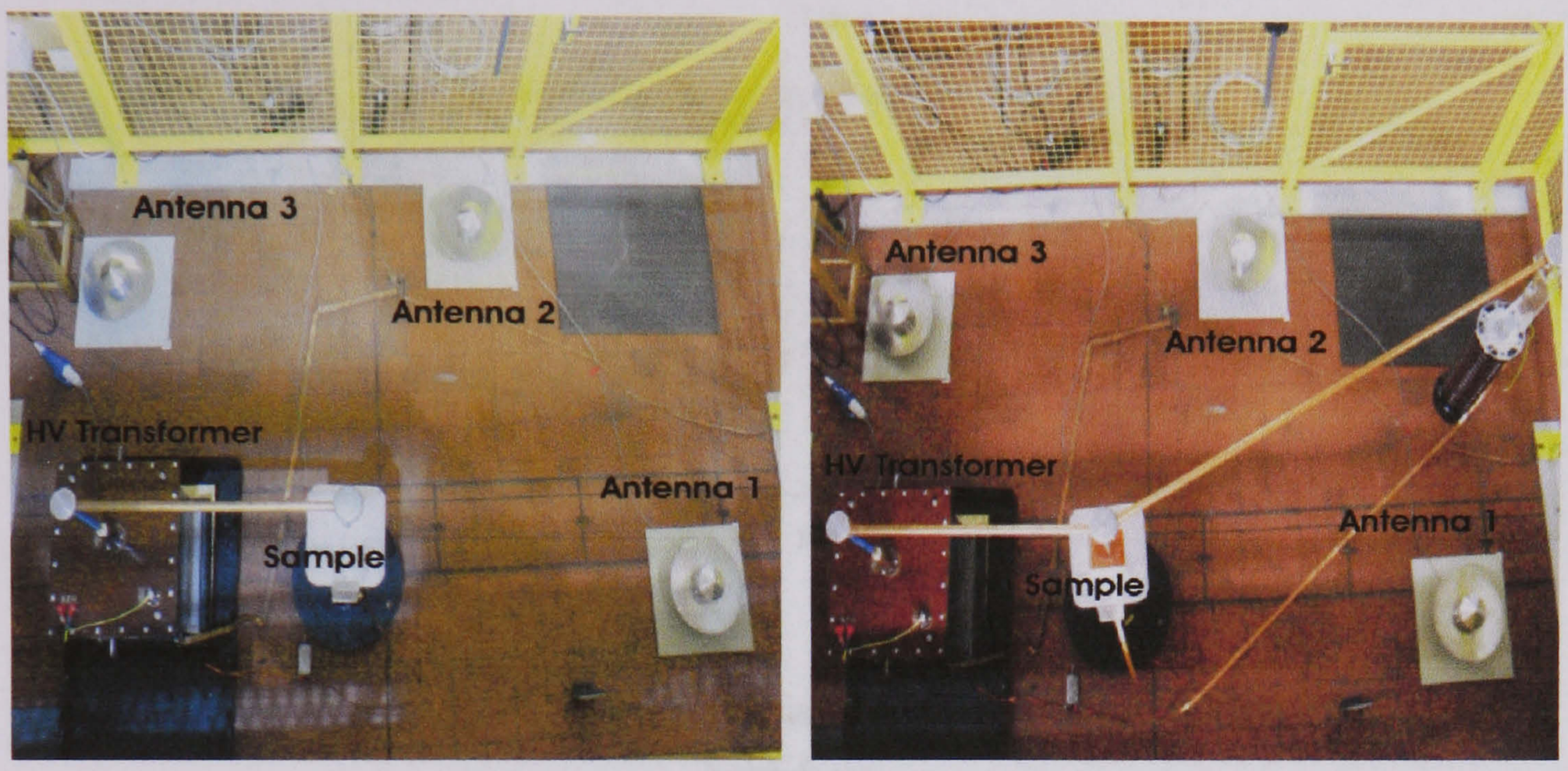

a) Short length configuration of the test set

b) Long length configuration of the test set

Figure 5.2 a) Short configuration of the test set, b) Long configuration of the test set.

Several tests were conducted and the parameters of the circuit (i.e. length of the circuit loop, air gap and dielectric media) were varied. The high resolution digital oscilloscope was adjusted to receive a sequence of five radio frequency impulses of short duration. The frequency response of the acquired signal was calculated using the FFT taken from the largest amplitude waveform recorded in the sequence. Figure 5.3 shows the simultaneous time domain recordings of the discharge current (i.e. voltage across a 50 ohm resistor) and antenna signal for an air-gap discharge. For these results the gap was set to 20 mm, the circuit loop (normal or reference loop) to 2.34 m and the voltage to 21.9 kV.

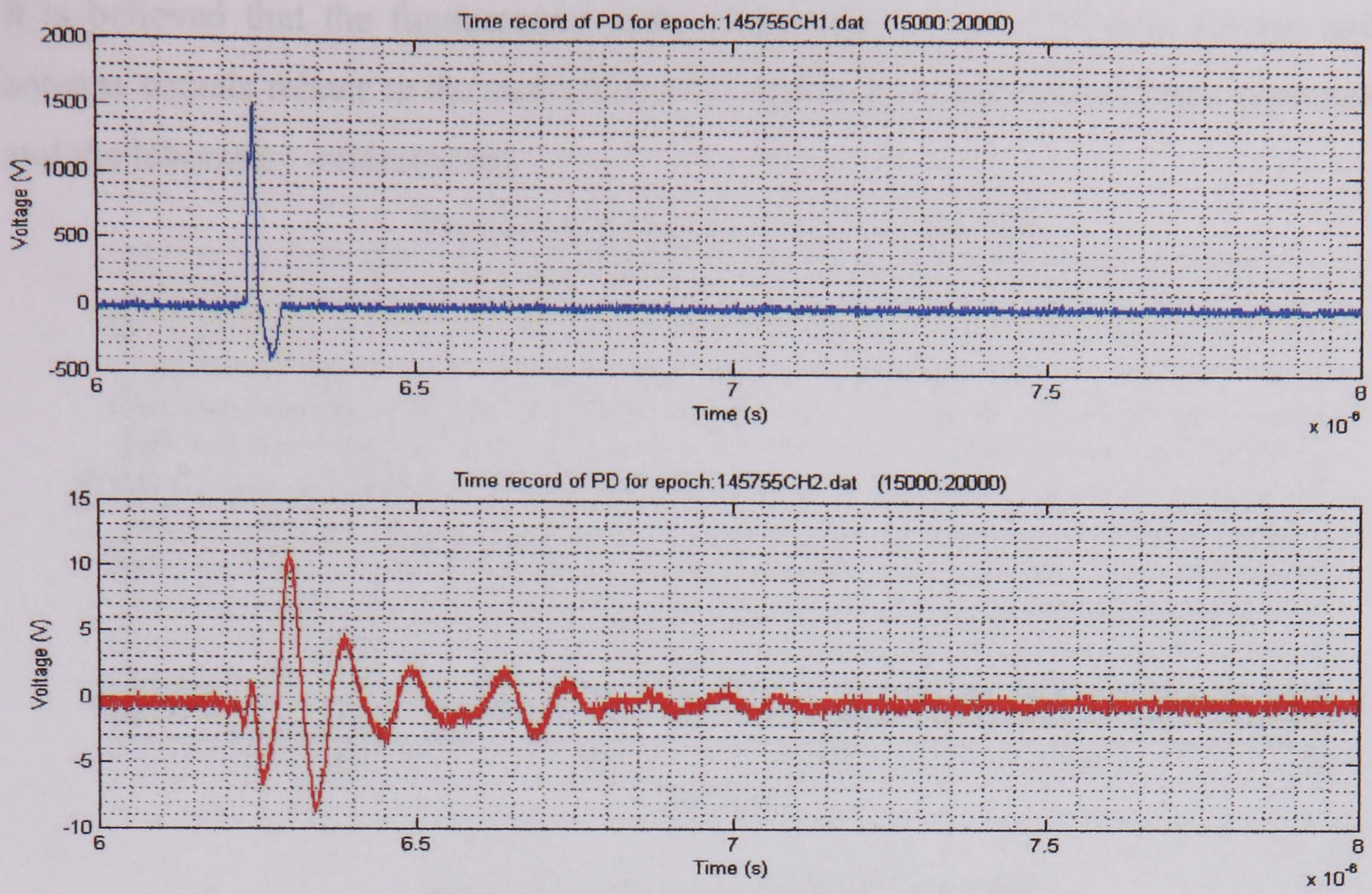

Figure 5.3 Recorded waveforms of discharge current (upper) and antenna signal (lower) for air breakdown.

There is clearly a difference in shape between the two signals in figure 5.1. The discharge current contains an initial positive pulse with a very sharp rise-time and short damping; the entire impulse is 50 ns. By comparison, the antenna signal does not display a steep-fronted impulse; the waveform has a negative initial displacement which increases in an oscillatory manner, the total width is 1000 ns.

Figure 5.4 shows the frequency responses for the waveforms of figure 5.3. Again differences can be seen between the two signals. For the discharge current signal the response is relatively smooth, having a peak at 30 MHz, with the majority of the energy occurring below 150 MHz. In the case of the antenna signal, the response displays peaks, with the majority of the energy occurring below 50 MHz; the two predominant peaks in the response occur at 20 and 25 MHz respectively.

It is believed that the fundamental differences between the discharge current and antenna signals relates to the radio frequency response of the high-voltage apparatus and the laboratory environment.

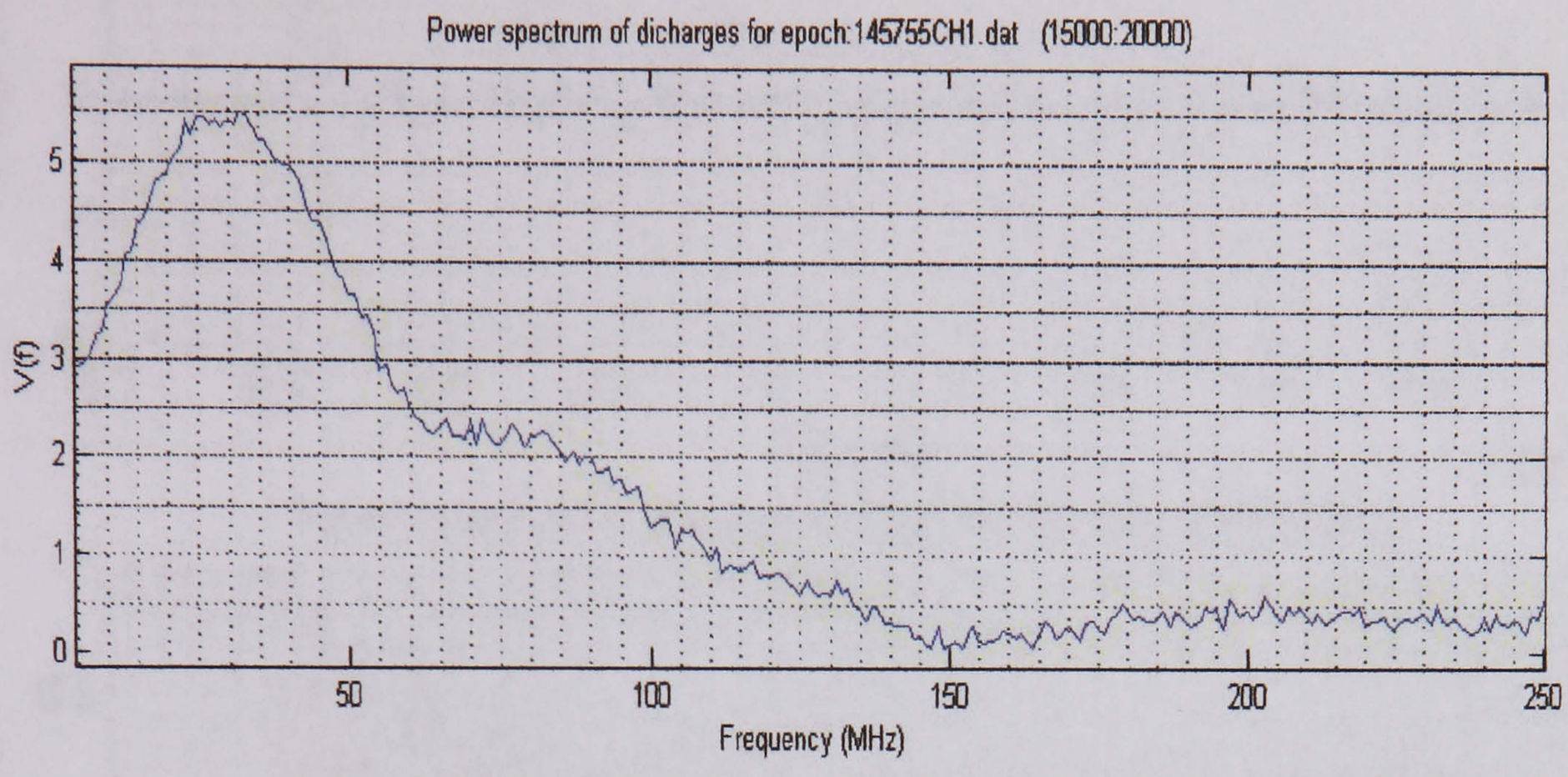

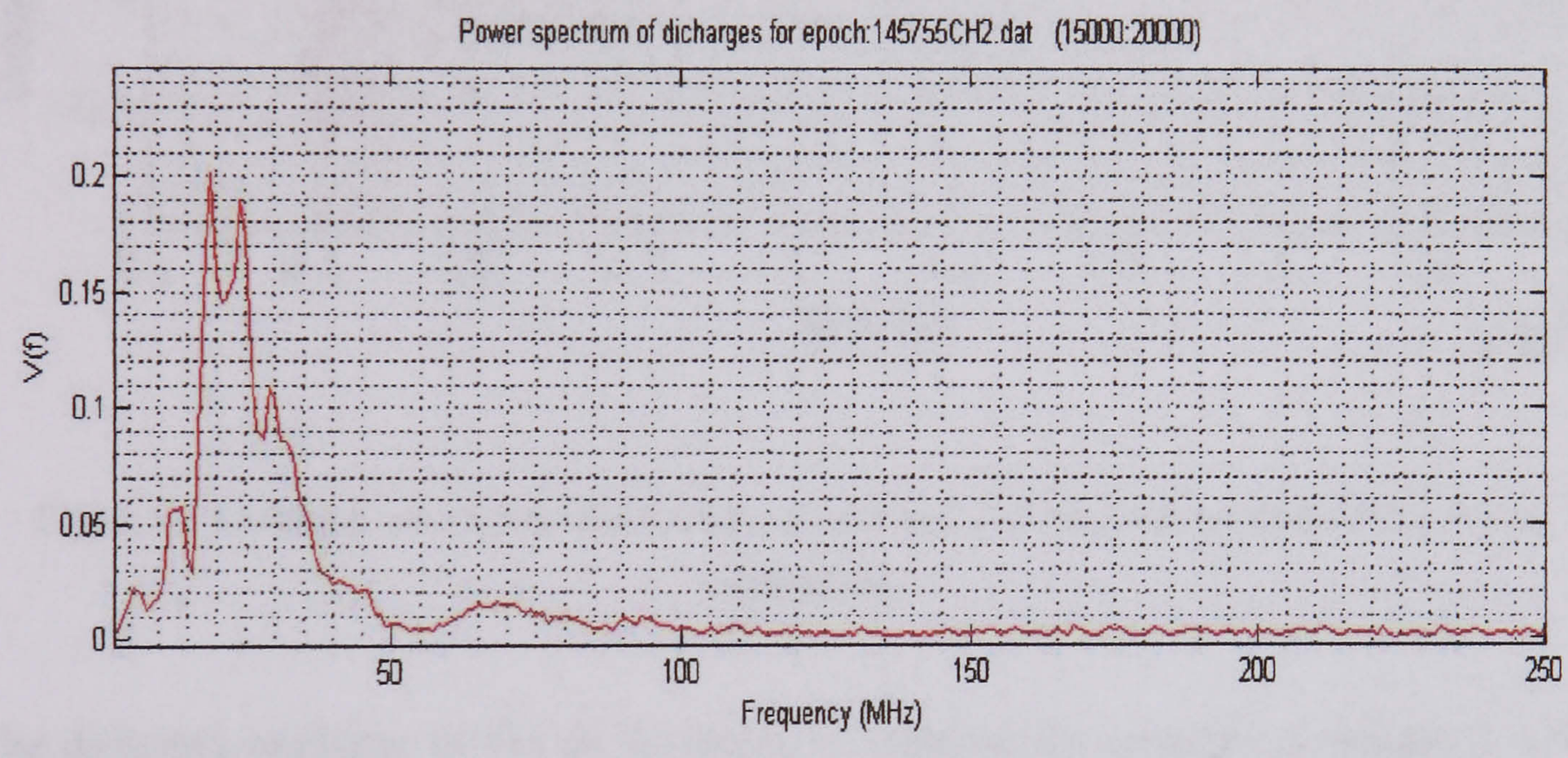

Figure 5.4 Frequency response of discharge current (upper) and antenna signal (lower) for air discharge.

The same procedure was applied to a typical discharge for the same circuit configuration using a test cell filled with oil dielectric (see figure 5.1b). Figure 5.5 shows the time domain waveforms, and figure 26 show the frequency responses.

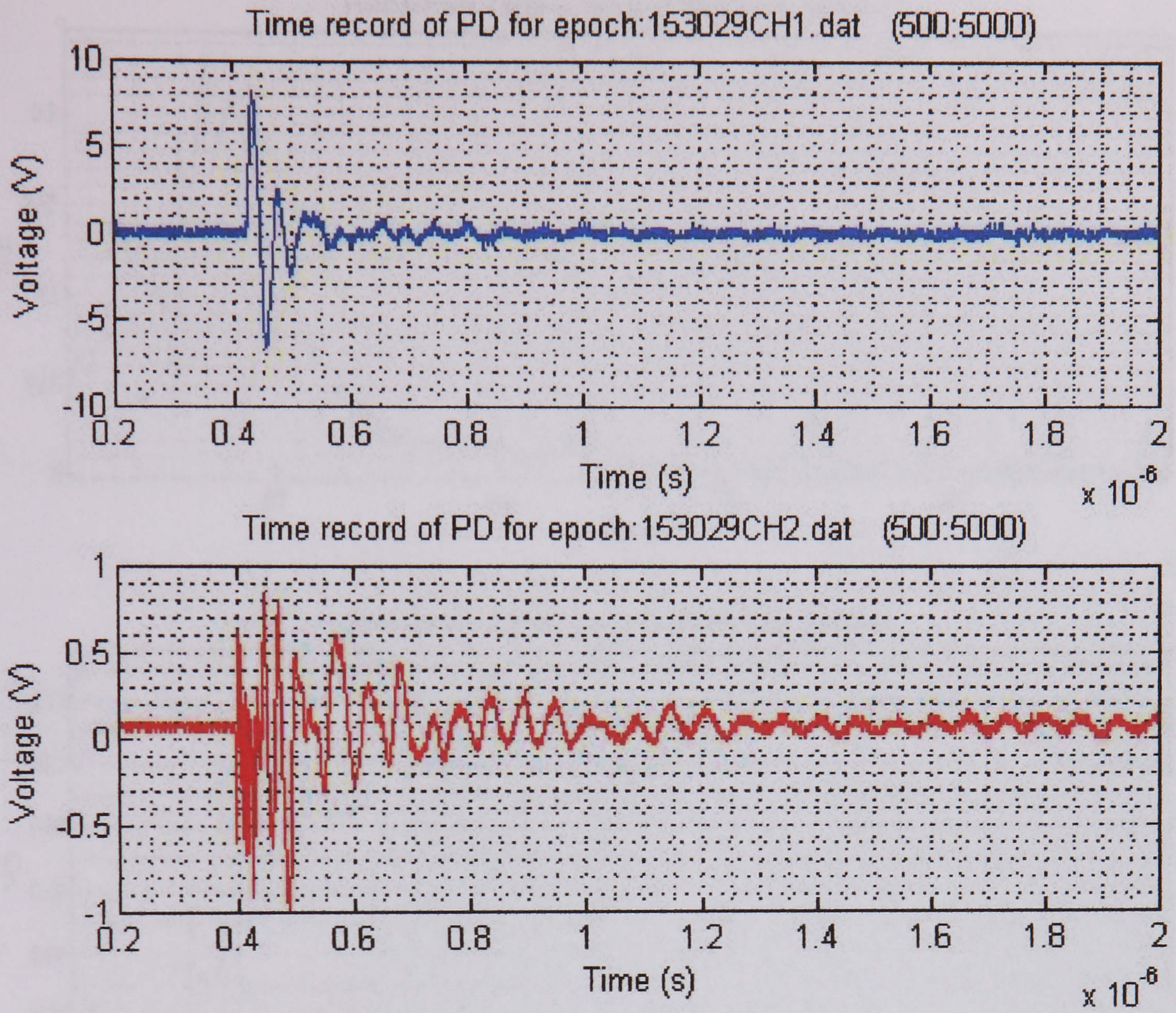

Figure 5.5 Recorded waveforms of discharge current (upper) and antenna signal (lower) for oil breakdown.

The differing response of the oil dielectric is apparent by comparing figures 5.3 and 5.5, the oil discharge current shows less damping than the air discharge and displays a slower initial rise-time. In the frequency domain (see figure 5.6), the oil discharge current is less smooth compared to the air results, and has a peak at 35 MHz. The antenna signal for the oil discharge again shows two predominant peaks in the frequency domain at 29 MHz (larger) and 35 MHz (smaller). It is noted that the overall signal magnitude for the oil discharge is smaller compared to the air discharge.

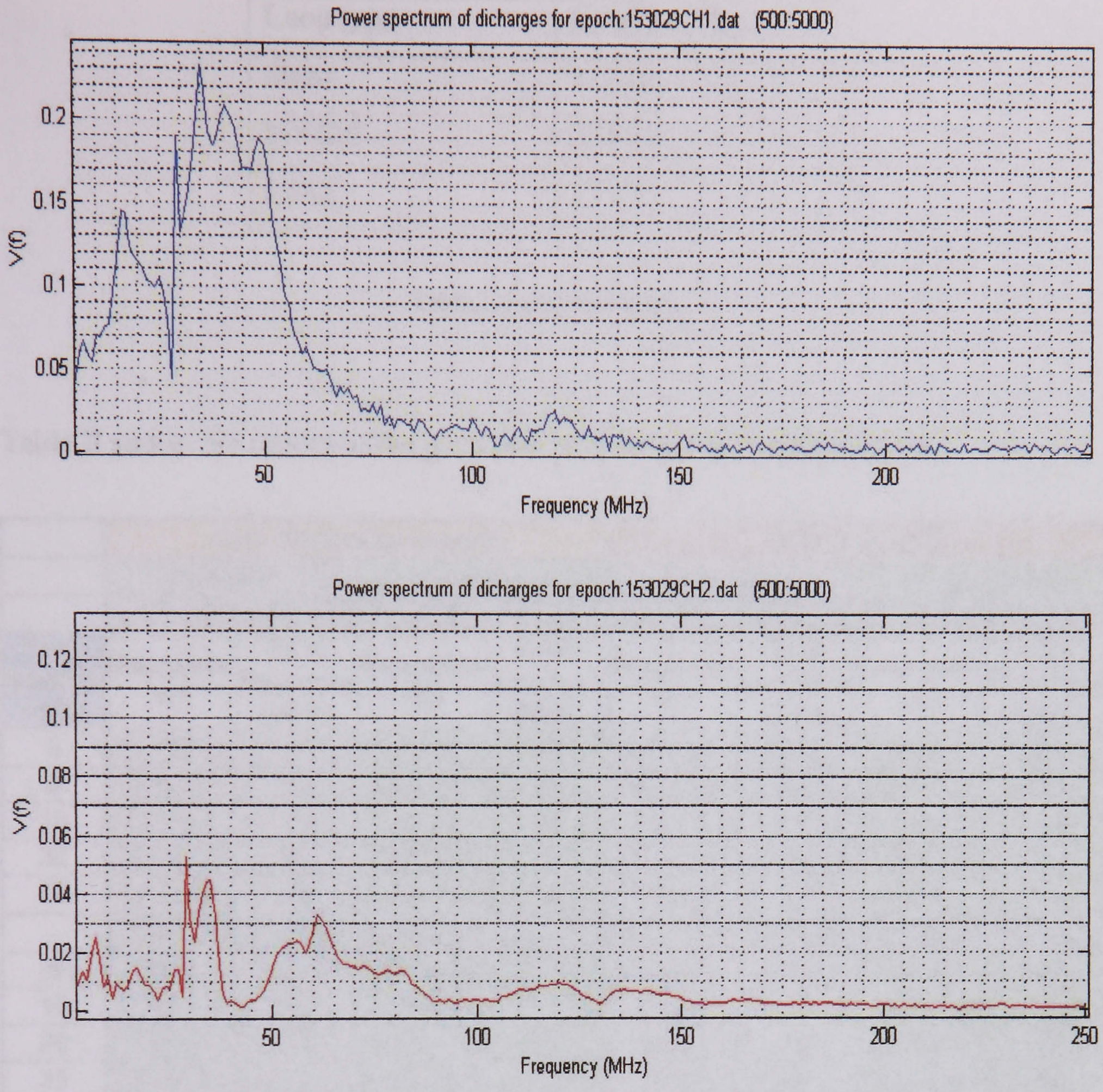

Figure 5.6 Frequency response of discharge current (upper) and antenna signal (lower) for oil discharge.

The determination of the peak frequency of the antenna signal was repeated for several tests using different gap lengths and loop sizes. A description of the loop size is presented in table I.

Loop type	Length of loop
Short	172 cm
Normal	234 cm
Long	372 cm

Table I.-Loop description.

Table II shows the results of the performed test for air gap configuration.

	CH1 (Discharge current)				CH2 (Antenna)			
	Acquisition 1		Acquisition 2		Acquisition 1		Acquisition 2	
	Short Loop CH1				Short Loop CH2			
Gap distance (mm)	Magnitude V(t)	Peak frequency (MHz)	Magnitude V(t)	Peak frequency (MHz)	Magnitude V(t)	Peak frequency (MHz)	Magnitude V(t)	Peak frequency (MHz)
5	$6x10^{1}$	19	6.4 x101	19	$6.75x10^{2}$	37	$7.6 x10^{2}$	37.5
8	$9.5x10^{1}$	19	9.6 x101	19	$1.41x10^{3}$	38	$1.37 x10^{3}$	38.5
10	$2.2x10^{2}$	19	2.4 x102	19	$3.1x10^{3}$	37.5	$2.85 x10^{3}$	37.5
20	$3.0x10^{2}$	19.1	3.22 x102	19	$2.60x10^{3}$	37	$3.32 x10^{3}$	37.2
35	$1.45x10^{2}$	19	1.35 x102	19	$1.1x10^{3}$	38	$1 x10^{3}$	38
	Normal Loop CH1				Normal Loop CH2			
5	$1.01x10^{2}$	17.5	1.03 x102	17.5	$8x10^{2}$	16.5	$7.5 x10^{2}$	16.5
10	$3.95x10^{2}$	17.5	3.85 x102	17.7	$4.1x10^{3}$	16	$4.35 x10^{3}$	16
20	$1.35x10^{5}$	16	1.46 x105	17	$4x10^{3}$	16	$6.2 x10^{3}$	16
35	$4x10^{4}$	15	1.07 x105	19	$4x10^{3}$	16	$4.94 x10^{3}$	16
	Long Loop CH1				Long Loop CH2			
5	$4.45x10^{1}$	9.4	5.4 x101	8.4	$4.1x10^{2}$	30	$4.2 x10^{2}$	30
10	7.1	11	7.75 x105	11	$3.87x10^{3}$	29	$3.51 x10^{3}$	29.3
20	$1.12x10^{6}$	10.9	1.25 x106	11	$6.1x10^{3}$	29.3	$3.28 x10^{3}$	29.3
35	$5.30x10^{6}$	12	5.95 x105	10.5	$4x10^{3}$	29.3	$1.48 x10^{3}$	29.3

Table II.- Resume of the results for air gap test.

Figures 5.7 shows the variation between peak frequency, gap size and loop type for air discharges.

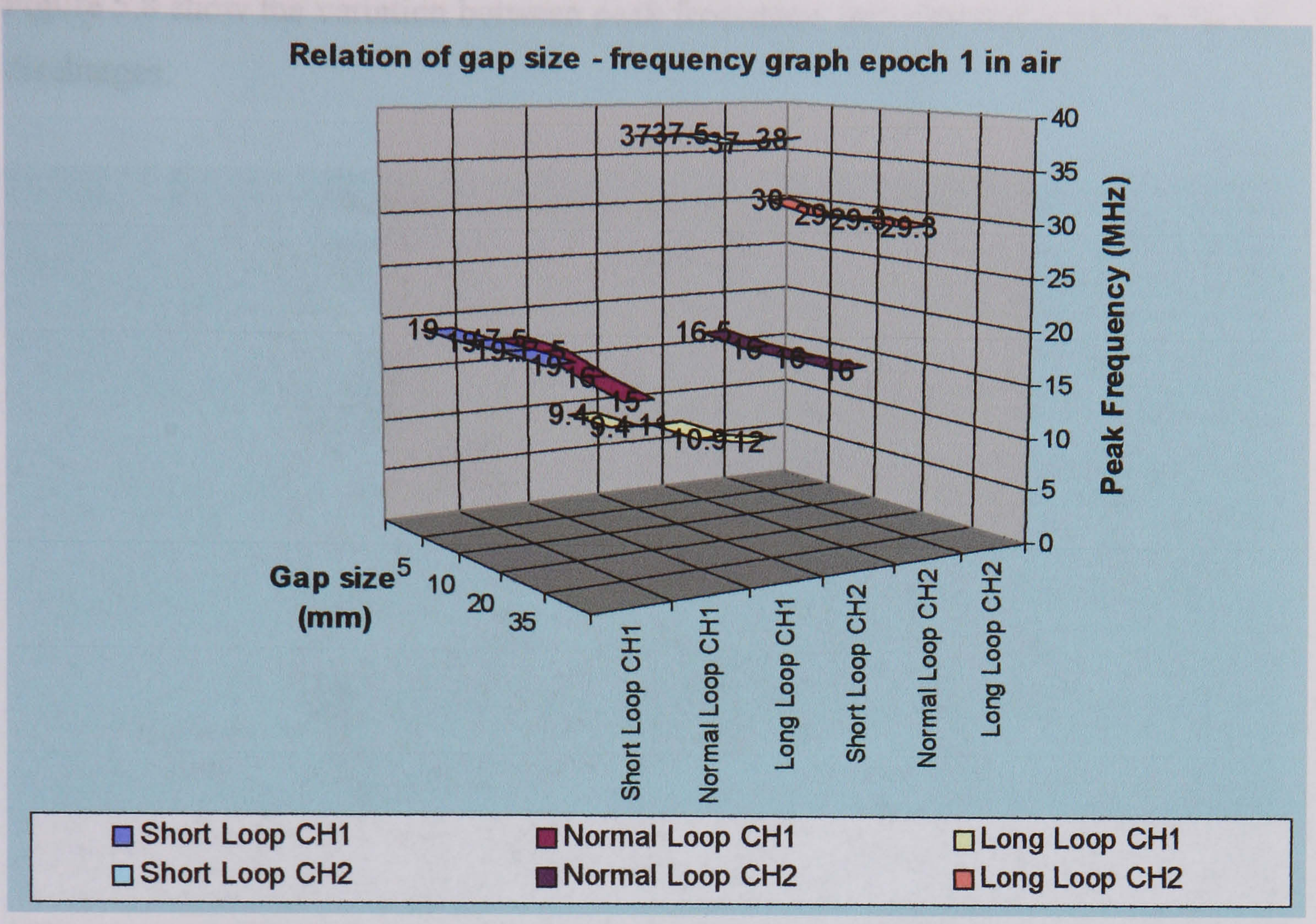

Figure 5.7 Graph of results using air dielectric (CH1 = discharge current, CH2 = antenna).

Table III show the results of the performed test for oil gap configuration.

	CH1 (Discharge current)				CH2 (Antenna)			
	Acquisition 1		Acquisition 2		Acquisition 1		Acquisition 2	
	Short Loop CH1				Short Loop CH2			
Gap distance (mm)	Magnitude V(t)	Peak frequency (MHz)	Magnitude V(t)	Peak frequency (MHz)	Magnitude V(t)	Peak frequency (MHz)	Magnitude V(t)	Peak frequency (MHz)
5	6×10^{5}	22.5	4×10^{13}	22.5	3.7×10^{4}	34	1.42×10^{8}	34
10	2.4×10^{45}	22.5	2.6×10^{9}	22.5	1.2×10^{24}	34	6.2×10^{5}	34
20	4.4×10^{29}	31	1×10^{17}	31.2	2.2×10^{16}	31.5	5×10^{9}	30
	Normal Loop CH1				Normal Loop CH2			
5	8.2×10^{9}	18.8	7×10^{9}	18.8	3.3×10^{6}	18.8	2.9×10^{6}	18.8
10	3.5×10^{9}	18.4	5.5×10^{9}	18.8	1.55×10^{6}	18.8	2.4×10^{6}	18.4
20	1.59×10^{10}	8.8	1.35×10^{18}	8.8	1.7×10^{6}	8.8	1×10^{10}	8.8
	Long Loop CH1				Long Loop CH2			
5	1.15×10^{14}	8.8	1.65×10^{14}	8.8	2.55×10^{8}	15	4.4×10^{8}	16.3
10	1.45×10^{10}	7.5	1.95×10^{10}	7.5	2.6×10^{6}	8.8	3.8×10^{6}	8.8
20	1.70×10^{10}	8.8	2.80×10^{10}	8.8	1.55×10^{8}	8.8	2.8×10^{8}	8.8

Table III.- Summary of the results for oil gap cell.

Figure 5.8 show the variation between peak frequency, gap size and loop type for oil discharges.

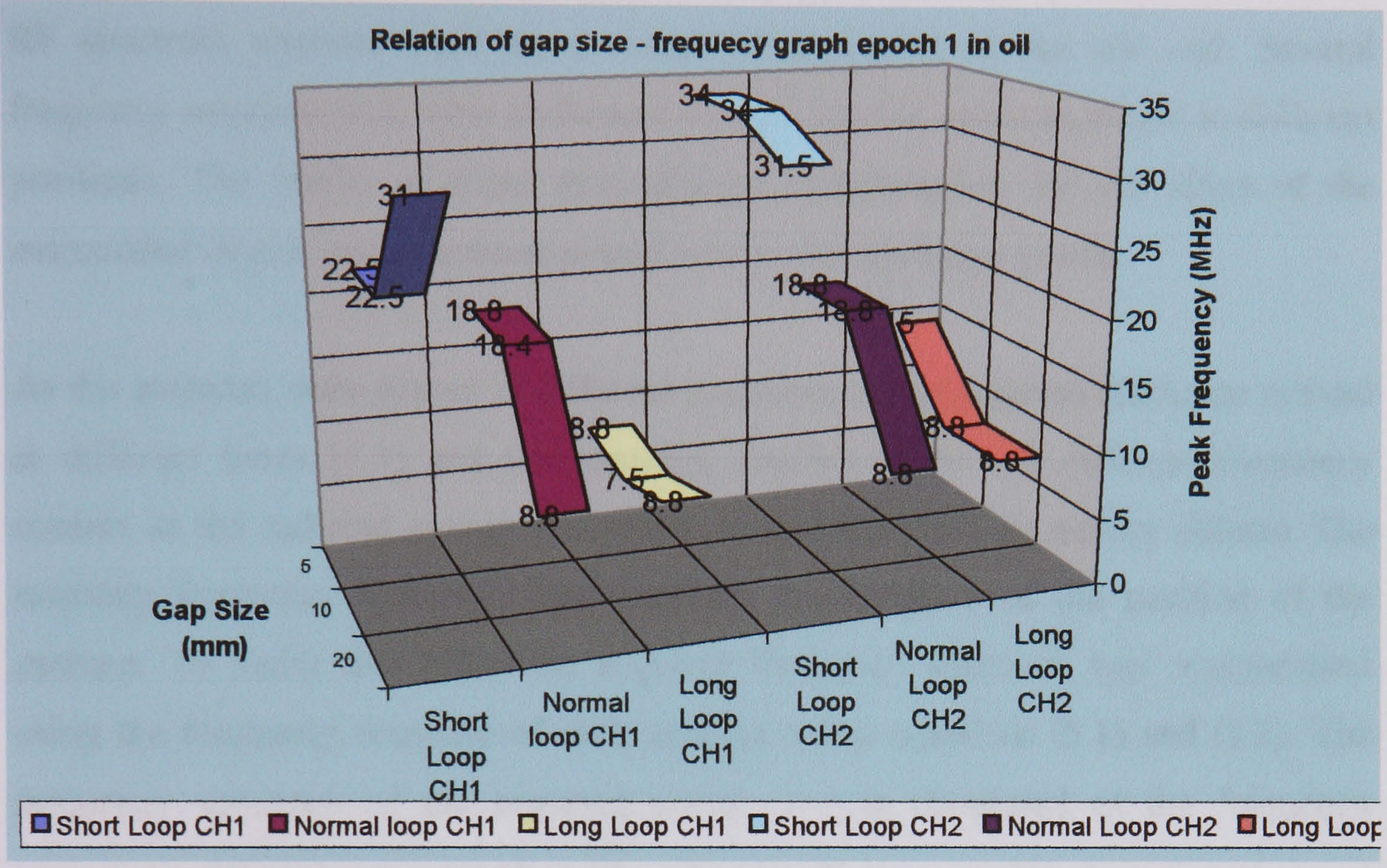

Figure 5.8 Graph of results using oil gap cell (CH1 = discharge current, CH2 = antenna).

In figures 5.7 and 5.8 it can be seen that the length of the loop affects the radiated and conducted signals both in air and oil, with a general tendency for the larger loop to yield lower peak frequencies. This is consistent with radiation efficiency of a loop antenna, where the resonant frequency is lowered with increasing enclosed area, however an inconsistence is observed in the long loop for channel 2 in air discharges, where the values are higher that the expected, this can be caused by the background noise which affects the original signal received in the antenna. The effect of the gap length can be seen to have virtually no effect on the air discharge, but changes the peak frequency for the oil discharge, as the oil cell capacitance affects the response of the radiated discharge. The influence of the gap length on waveform properties is consistent with reported results from other researchers [5.2]. This variation is due to the radio frequency response of the structures of the experimental apparatus that radiate the discharge.

5.3. Frequency response test.

The response of the experimental apparatus at radio frequency was measured with a RF spectrum analyzer used as a source of excitation at the test cell. Several frequency response tests were performed using 3 conical antennas placed in different positions. The results of these tests allowed compensation for the effect of the surrounded objects and structures placed near to the discharge source.

As the antennas were placed in different positions, the propagated discharge arrived at different times [5.3] and the resulting discharges showed different frequency content as the radiated energy was reflected and absorbed by nearby objects. The resulting frequency spectrum was therefore characteristic of the position of the antenna. To verify this effect the acquired frequency spectrum was compensated using the frequency response of each antenna using equations (5.1) and (5.2). The frequency spectrum of the acquired signal $A(f)$ is composed of the frequency spectrum of the structures and nearby objects effect $S(f)$ plus the original signal frequency spectrum $H(f)$ then:

$$H(f)xS(f) = A(f) \tag{5.1}$$

To compensate the original frequency spectrum the following relationship must be established:

$$H(f) = \frac{A(f)}{S(f)} \tag{5.2}$$

Hence, to apply (5.2) is necessary to obtain $S(f)$ for each antenna. This was possible through the use of a spectrum analyzer with sweep generator function connected to the unenergized test set with the oil test cell and air gap. Figure 5.9 shows the test set configuration for the frequency response test.

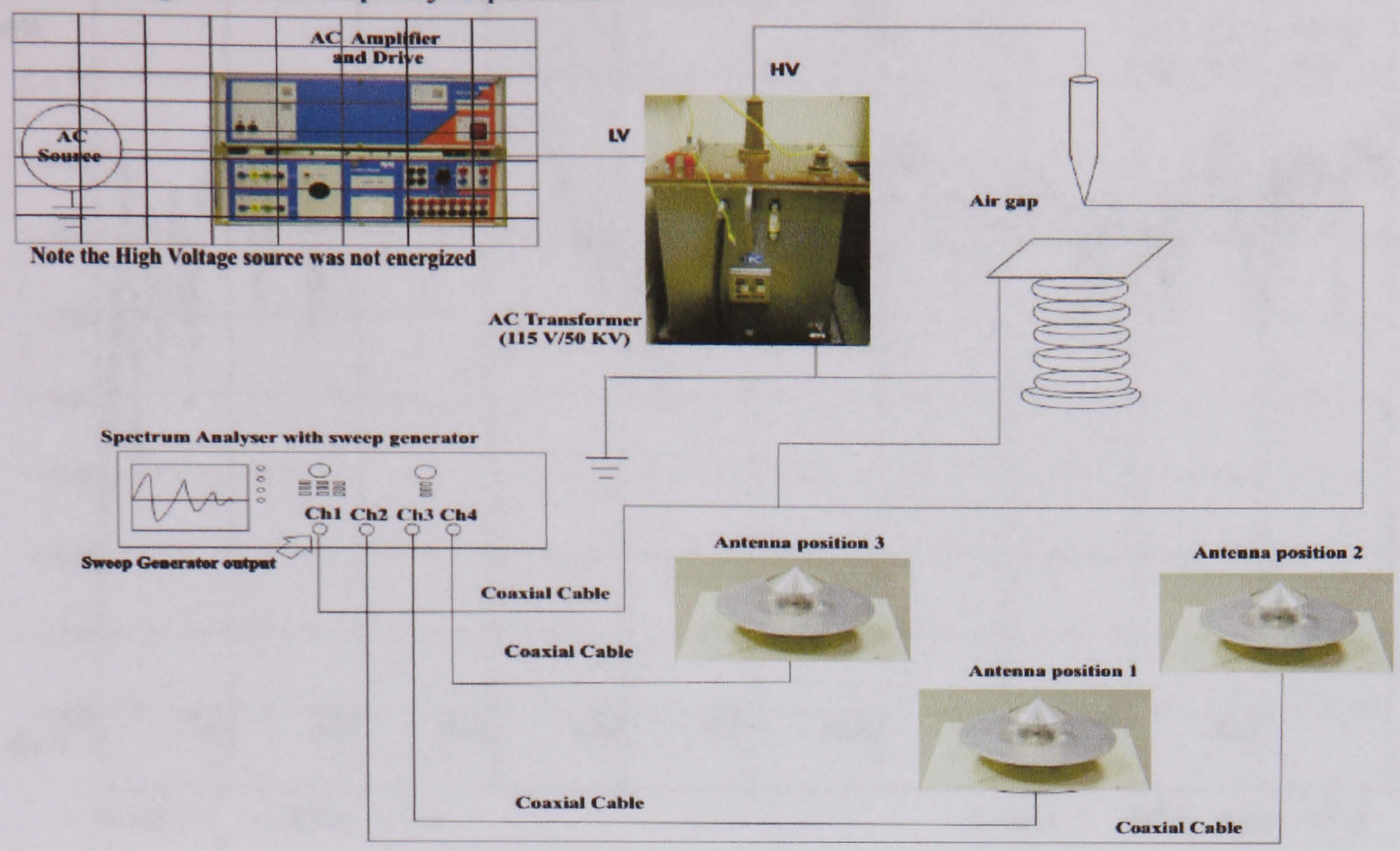

Figure 5.9 Test set configuration for frequency response test.

Figures 5.10 and 5.11 show the frequency response obtained from the spectrum analyzer, of antenna 1 using air gap and oil gap respectively.

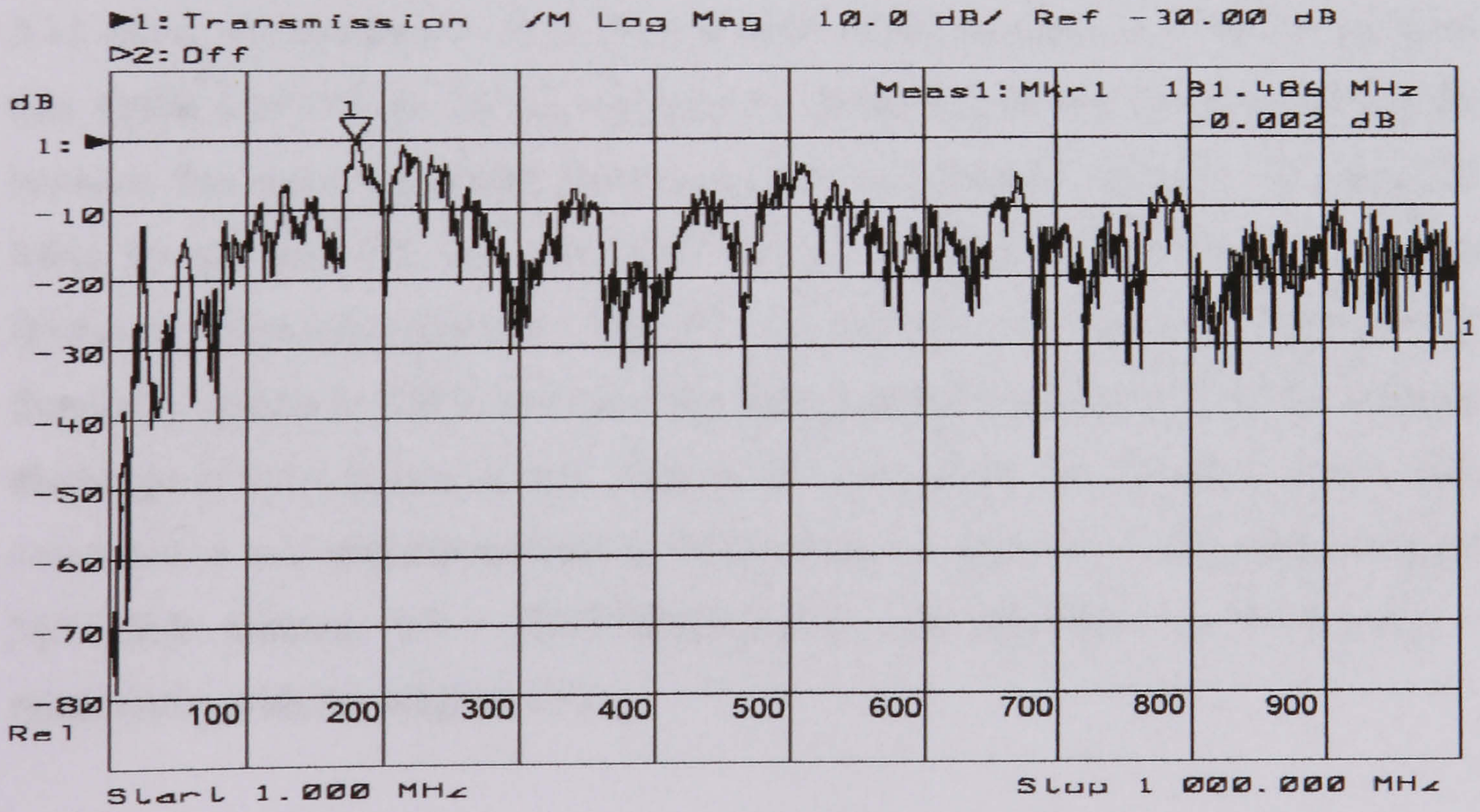

Figure 5.10 Typical frequency response in the spectrum analyzer of antenna in position 1 using a 10mm air gap sample.

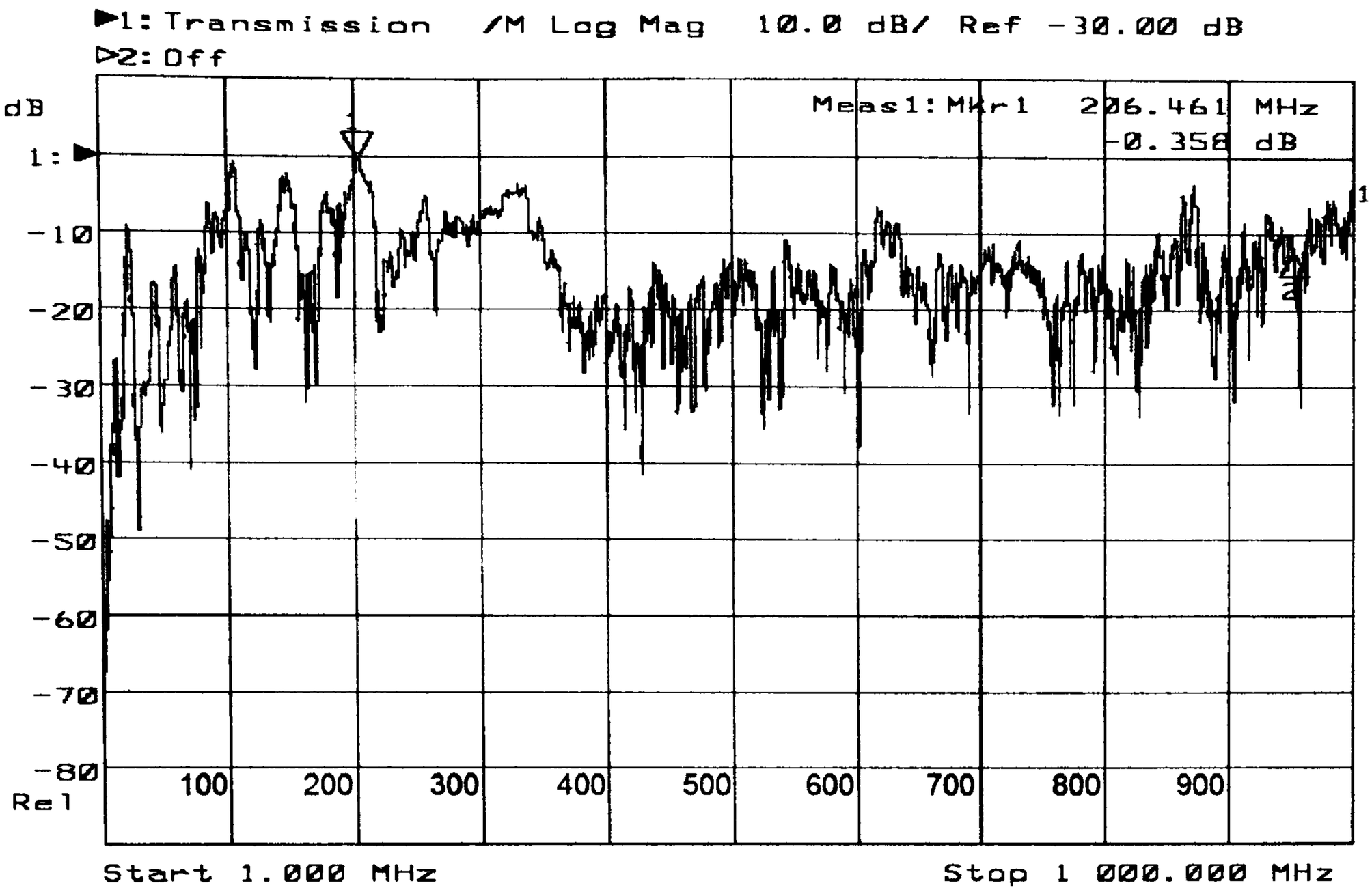

Figure 5.11 Typical frequency response in the spectrum analyzer of antenna in position 1 using a 10mm oil gap sample

The previous figures show the frequency spectra in dB's; and in order to compare the different positions in volts the measured data was processed. Figures 5.12 and 5.13 shows the conversion from dB's to volts of the antennas in different positions (see figure 4.15) for air and oil respectively. Some similarities can be observed, for instance the more significant frequencies are concentrated between 100 and 300 MHz for air and 100 and 400 MHz for oil; however the distribution of those frequencies is notably different. The data file obtained consists of 500 points of the frequency spectra in DB's: however, the data obtained from the FFT of the acquired discharge is 5000 points in mV. Due to this limitations the 500 data points were converted to mV and interpolated to 5000 points in steps of 0.5 (500 Hz) using the MATLAB function YI = INTERP1(X,Y,XI), (see appendix A) to maintain a relationship with the original FFT.

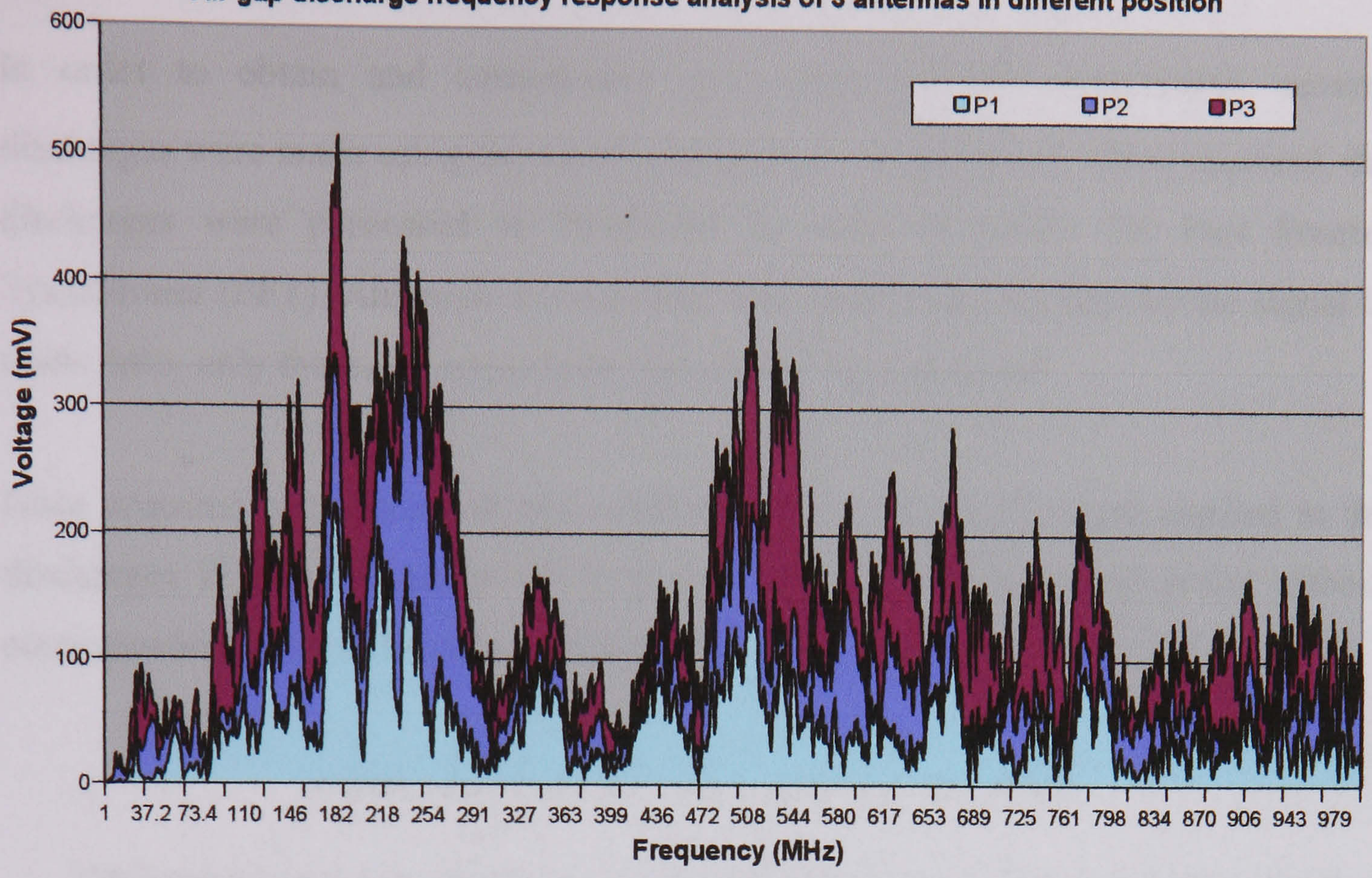

Figure 5.12 Frequency responses of antennas 1, 2 and 3 in different positions using a gap in air as sample

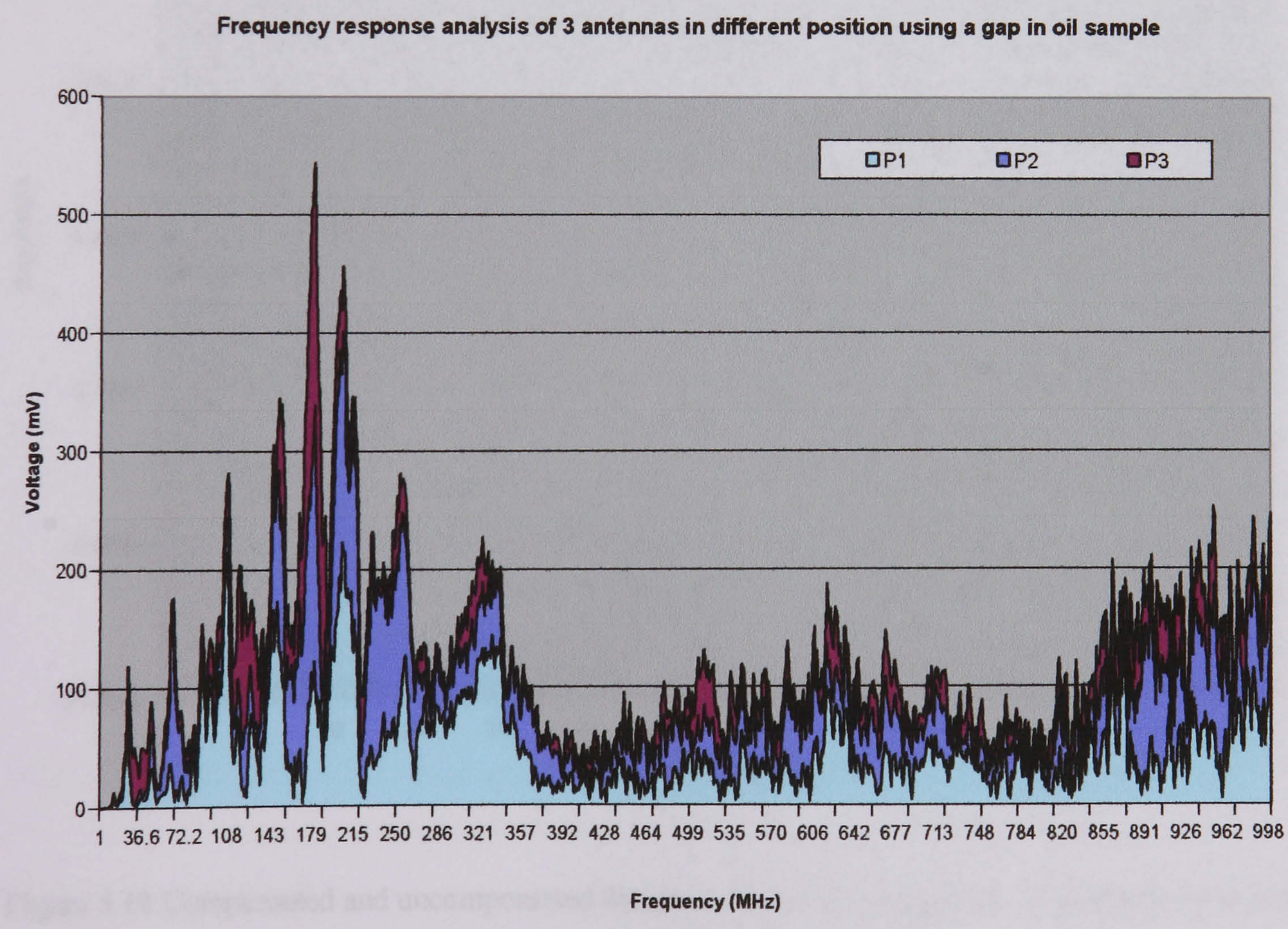

Figure 5.13 Frequency responses of antennas 1, 2 and 3 in different positions using a gap in oil as sample

In order to obtain and compensate $A(f)$ (the acquired discharges), several discharges were made using the same configuration in air and oil. Once acquired, the discharges were processed in MATLAB in order to obtain the Fast Fourier Transformer (FFT). Although several tests were performed, to improve the signal to noise ratio, only the larger magnitude waveforms were analyzed.

Once acquired and processed, the relationship of equation (5.2) was applied to the discharges. Figure 5.14 shows the frequency spectra with compensation and without compensation using antenna in position 3 for oil gap.

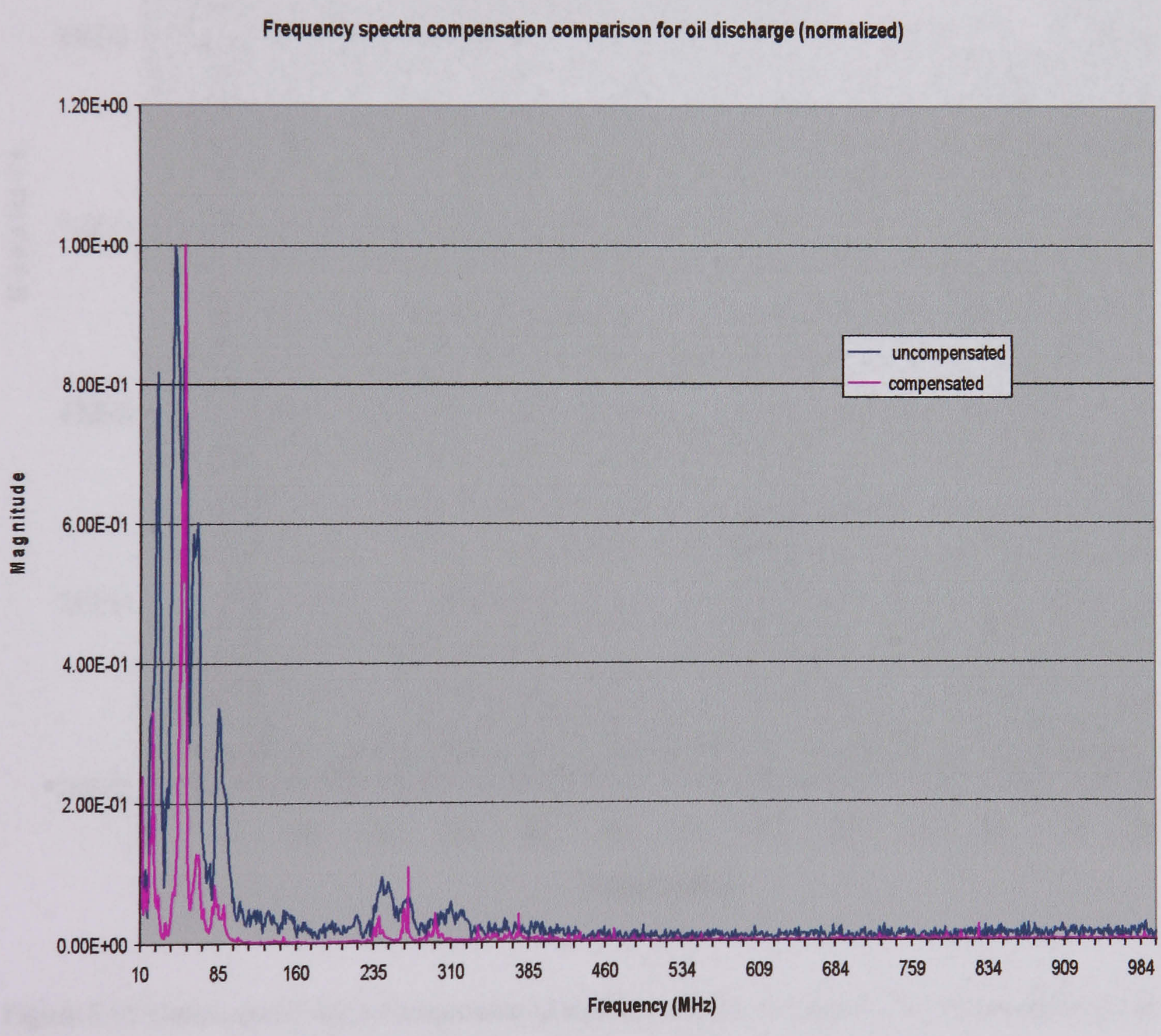

Figure 5.14 Compensated and uncompensated frequency spectra normalized for a discharge in oil and the antenna in position 3 for epoch 160257.

Figure 5.15 shows the frequency spectra with compensation and without compensation of the radiated spectra using antenna in position 1 for air gap.

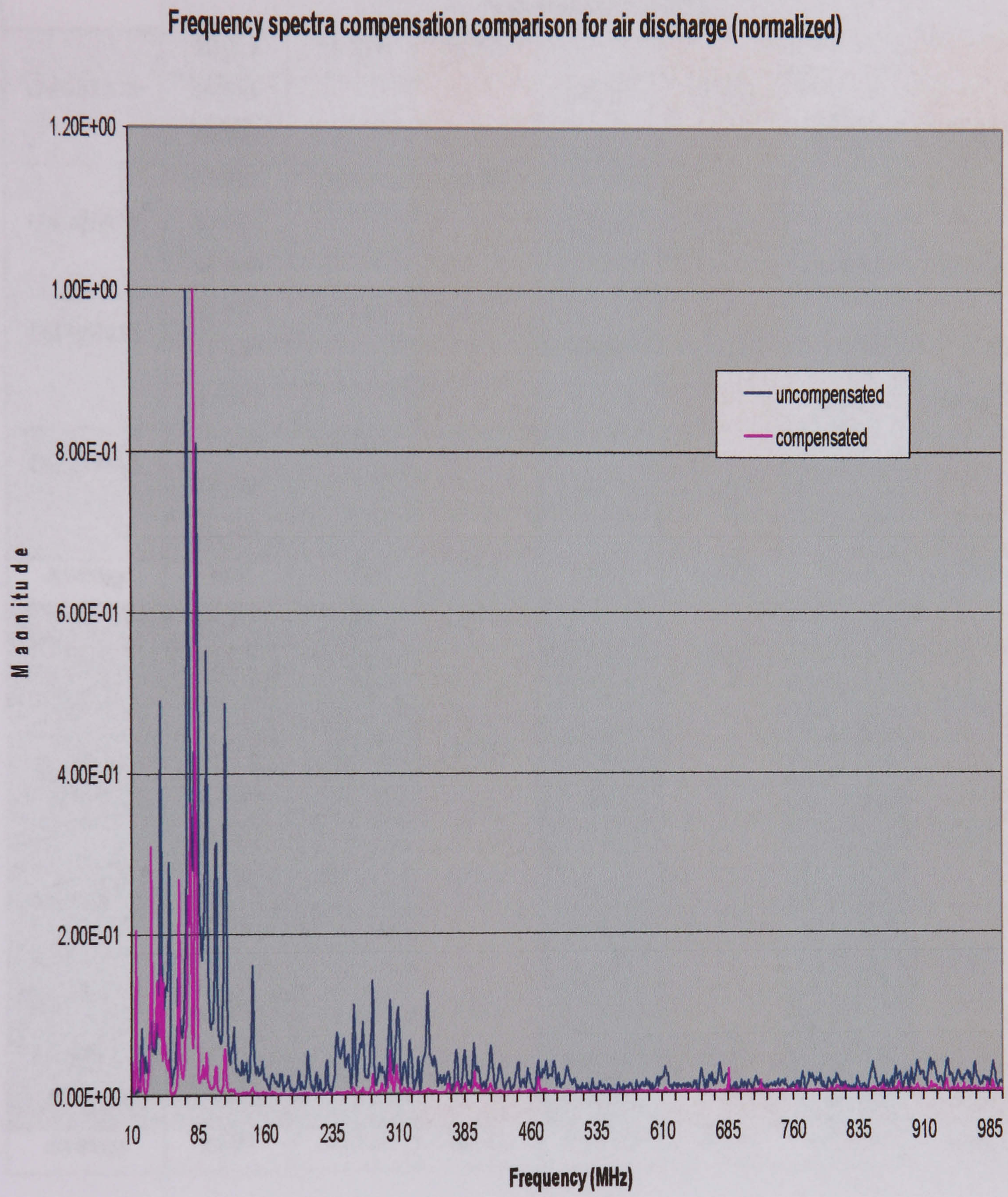

Figure 5.15 Compensated and uncompensated frequency spectra normalized for a discharge in air and the antenna in position 1 for epoch 170332.

Table IV summarizes the performed frequency response tests in the HV laboratory using equation (5.2).

Sample/ epoch	Ch1	Ch 2(antenna P1)		Ch3 (antenna P2)		Ch4 (antenna P3)	
	50 Ω res.	Not comp.	Comp.	Not comp.	Comp.	Not comp.	Comp.
	Peak frequency (MHz)						
Oil 151238	39.961	51.949	51.949				
	39.961			24.976	18.483		
	39.961					48.952	52.948
Oil 160257	53.967	51.949	51.949				
	53.947			125.88	13.987		
	53.947					43.957	52.947
Oil 120411	53.947	51.949	49.451				
	53.947			105.9	13.987		
	53.947					48.952	52.948
Oil 122541	32.968	51.949	49.451				
	32.968			24.976	13.987		
	32.968					41.959	49.951
Average	45.2	51.949	50.7	70.433	15.11	45.955	52.1985
Air 170332	50.85	72.928	80.92				
	50.85			115.89	130.87		
	50.95					34.966	80.92
Air 170537	52.984	72.928	80.92				
	52.948			116.88	130.87		
	52.948					34.966	80.92
Air 170713	56.944	83.917	80.92				
	56.944			115.89	130.87		
	56.944					34.965	80.92
Air 171238	58.942	83.917	80.92				
	58.942			116.88	130.87		
	58.942					37.963	80.92
Average	54.93	78.42	80.92	116.385	130.87	35.715	80.92

Table IV.- Summary of tests

The first column of table IV shows the dielectric and the selected acquired discharge (epoch), whilst the peak frequency of the current discharge is shown in the second column. It can be seen that an important change in peak frequency occurs when the frequency spectra is compensated both in air and oil samples. After compensation,

the peak frequency measured by the antenna in position 2, both in air and oil, differs from position 1 and 3 due to the greater distance although the original frequency is present, its peak magnitude is lower than adjacent peak frequencies. Meanwhile the peak frequency magnitude in position 1 and 2 is similar after compensation. It can be notice an important change after compensation between air and oil discharges, in oil discharges the frequency tend to be lower than in air discharges, and the same effect can be observe in the current discharge (50 Ω resistor) these results appears to contradict common knowledge [5.4]. Another feature of compensating the radiated discharge can be observed in figures 5.14 and 5.15, where the additional background noise and adjacent frequencies to the main peak have been eliminated, leaving a clear peak frequency. The frequency of the conducted current discharge (resistor) is constant for the same dielectric and different when comparing air and oil discharges. From table IV it can be seen that the peak frequency, and hence the entire spectrum, of air or oil discharges differs across the three antennas following compensation. This shows that the radiation from the PD is not isotropic, even after compensation for the test set response. However, following compensation, the difference between air and oil discharges can be reliably determined from the peak frequency since oil discharge has a peak frequency below approximately 53 MHz. It can be seen from table IV that differentiation between oil and air discharges was not possible before compensation using this simple value (excluding position 2). The results also show a variation between compensated spectra and the spectra of the electrical measurement made across a 50 Ω resistor; however, this is likely to be related to an unfavorable radio frequency response of the overall circuit.

5.4. Chapter 5 references

[5.1] Moore P J, Portugues I, Glover I A, Oct 2002, "Pollution of the Radio Spectrum from the Generation of Impulsive Noise by High Voltage Equipment", *IEE Conference on Getting the Most Out of the Radio Spectrum*, pp 37/1 – 37/5

[5.2] M.A. Elborki, P. A. Crossley, MIEEE, Z. D. Wang, A. Darwin, SMIEEE and G. Edwards, "Detection And Characterization of Partial Discharges in Transformer defect Models", *Power Engineering Society Summer Meeting, 2002 IEEE*, Volume: 1, July 2002, pp: 405 – 410

[5.3] E J Bartlett and P J Moore, "A system for monitoring VHF electromagnetic radiation generated by power system disturbances", *Proceedings of 34th UPEC*, Leicester University, Sept 1999, Vol 1, pp 249-252.

[5.4] Moore P J, Portugues I, Glover I A, "A Non-Intrusive Partial Discharge Measurement System Based on RF Technology", *Power Engineering Society Meeting*, June 2003, pp 627 – 633.

EVALUATION OF RADIATED AND CONDUCTED DISCHARGES

This chapter explains the tests that were carried out using the developed test set for the characterization of corona, surface and cavity discharges using a point-plane configuration in air and polymeric insulators samples. The basis of this analysis is pulse counting and point on wave information. At the end of this chapter a comparison of the most relevant results is shown in order to give to the reader a more clear idea of the differences found between samples.

6.1. Experimental overview

An evaluation of the intrinsic characteristics (frequency spectra, magnitude, pulse distribution etc.) of corona, surface and cavity discharges (conducted and radiated) has been made as they represent common discharges occurring in substation equipment and transmission lines. The FFT and point on wave information techniques were used as described in an earlier chapter (see section 5.1). The tests were divided as follow:

- Corona in air discharges
- Surface discharges on a new insulator
- Surface discharges on an aged insulator

- Surface discharges on a pressboard submerged in oil

- Cavity discharges

6.2. Corona in air evaluation

It is commonly accepted that small corona discharges occurring in all types of power equipment and transmission lines do not cause any important adverse effect on the performance of electrical insulation [6.1]. However, corona at one or several points on insulated equipment, can lead to a complete breakdown and hence the partial or entire damage of power equipment. Although the corona mechanism in air is well known [6.2, 6.3] the physics in other media is still not very well established. There are several new methods for corona detection, some of which require the equipment to be decommissioned from service and tested in laboratory, whilst others detect corona in situ or using on line methods such as UV cameras [6.4, 6.5] but most of these methods disregard the pulse nature of corona in air. Several tests were made in the HV laboratory in order to assess the behavior and characteristics of the conducted and radiated corona in an air gap. The test to evaluate corona consisted of a point plane gap configuration in air, the gap size selected was 10 mm and a tip of 0.5mm diameter. Figure 6.1 shows the configuration of the test and the resulting corona in air.

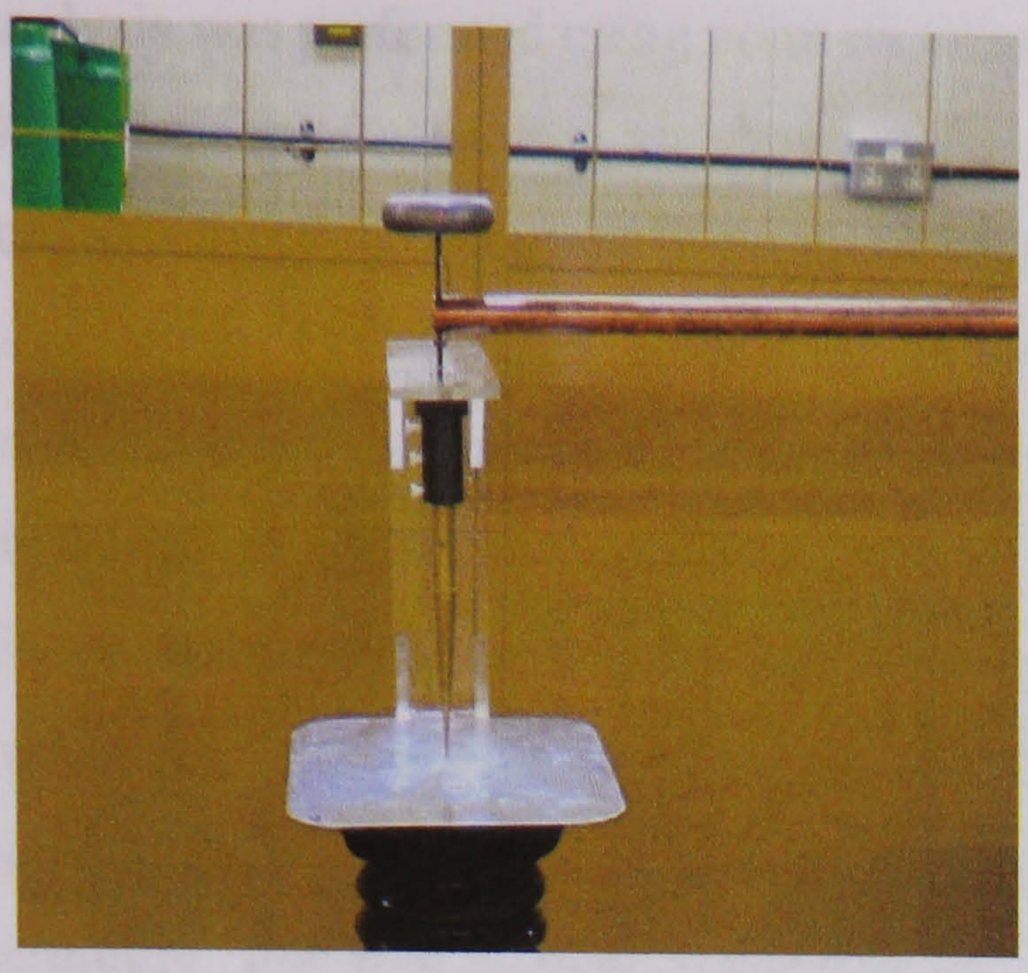

Air gap for corona and discharge generation

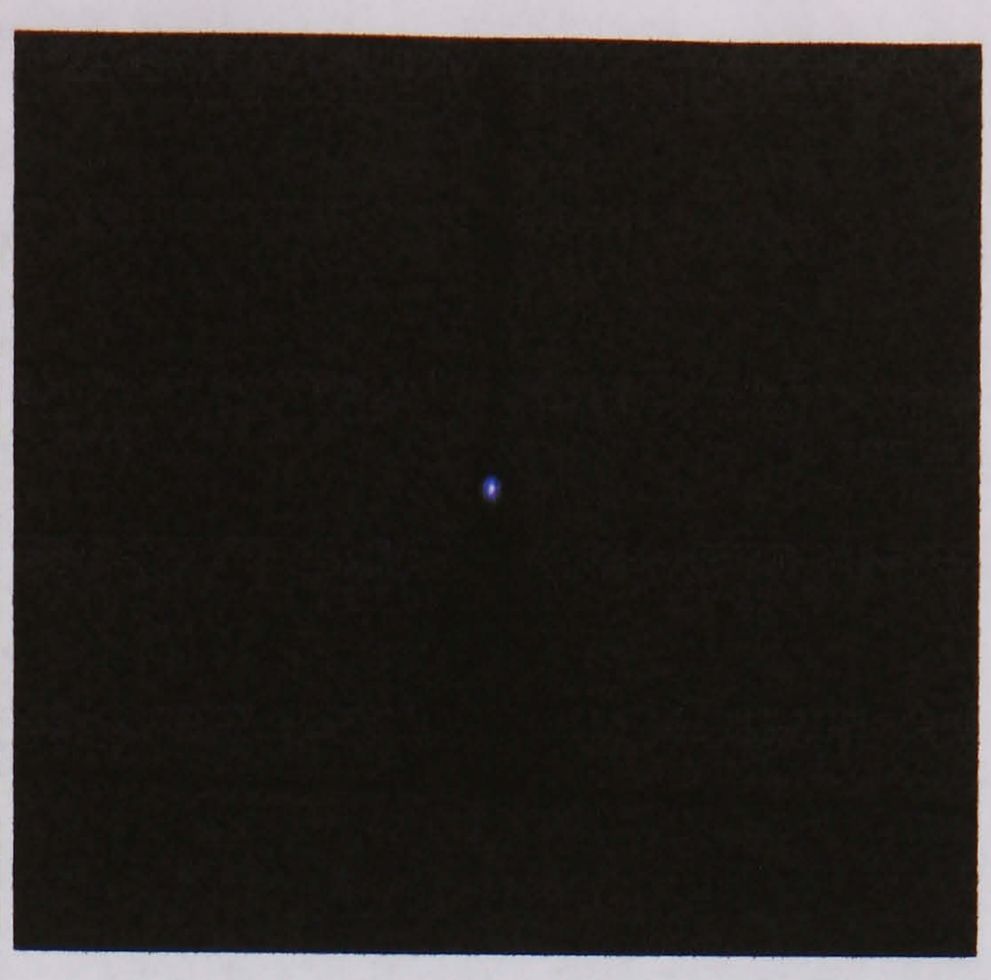

Generated corona in 10 mm air gap

Figure 6.1 Configuration used for corona in a 10mm air gap and generated corona

The conducted (current discharge) corona signal was acquired using a high resolution oscilloscope, in which channel 1 was connected to the signal coming from the 50 Ω resistor, and channel 2 to the AC signal for point on wave information. *In the evaluation of corona, disk cone antennas were used but their sensitivity and the radiated corona energy were not strong enough to be properly recorded as it will be shown, except for relatively large magnitude discharges*. Point on wave information is important since the PD's, including corona, occurred in different points of the positive and negative sinusoidal signal, in other words *PD's show a negative and positive nature*. This additional information can lead to important conclusions on *how corona or PD's can be differentiated* [6.6]. The point on wave measurement was made using the AC signal from the AC amplifier and verified using a capacitive voltage divider connected to the HV circuit. The measured difference in phase between the AC amplifier and the high voltage applied to the sample is 6 degrees which is predominantly due to the phase shift in the test set HV transformer (see figure 5.9). Screenshots of several discharges were acquired using the high resolution feature of the oscilloscope. For the frequency domain analysis, samples 200μs long and 2.5 GS/s sampling rate were acquired, and subsequently a frequency domain analysis using MATLAB was performed. For the time domain analysis, samples of 4 ms and 10 ms length and 25 MS/s sampling rate were acquired, the time domain

analysis was performed using point on wave information and MATLAB software. As the behavior of corona in air shows different features according to applied voltage, an analysis of corona using different voltages (2860, 5740, 6540 and 7370 volts) was performed. The voltage level that showed a significant change in shape and magnitude was selected and recorded before an analysis in frequency and time was made. It is important to mention that, although the voltage level is an important factor influencing corona in air, other physical variables exist which play an important role such as temperature, humidity and atmospheric pressure; however, temperature and humidity were maintained at approximately 21^0 C and 45 % humidity. For this analysis, different epochs (see appendix B) were selected that represent the acquired signal at the specific voltage, each was processed and the frequency registered. The analyzed figures show the acquired screenshots of a typical corona in air using an AC reference.

6.2.1. Frequency domain analysis

Figure 6.2 shows the generated corona discharges using different, selected voltage values. Individual positive and negative discharges were acquired and the frequency spectra analyzed for each applied voltage. Figure 6.3 and 6.4 show the acquired and processed positive and negative discharge and its frequency spectra at 2860 V, acquired signal in antenna show only a positive segment corresponding to the AC wave form used as reference when the discharge happens i.e. no radiated pulse is present in the antenna. The same procedure was applied to the other voltages.

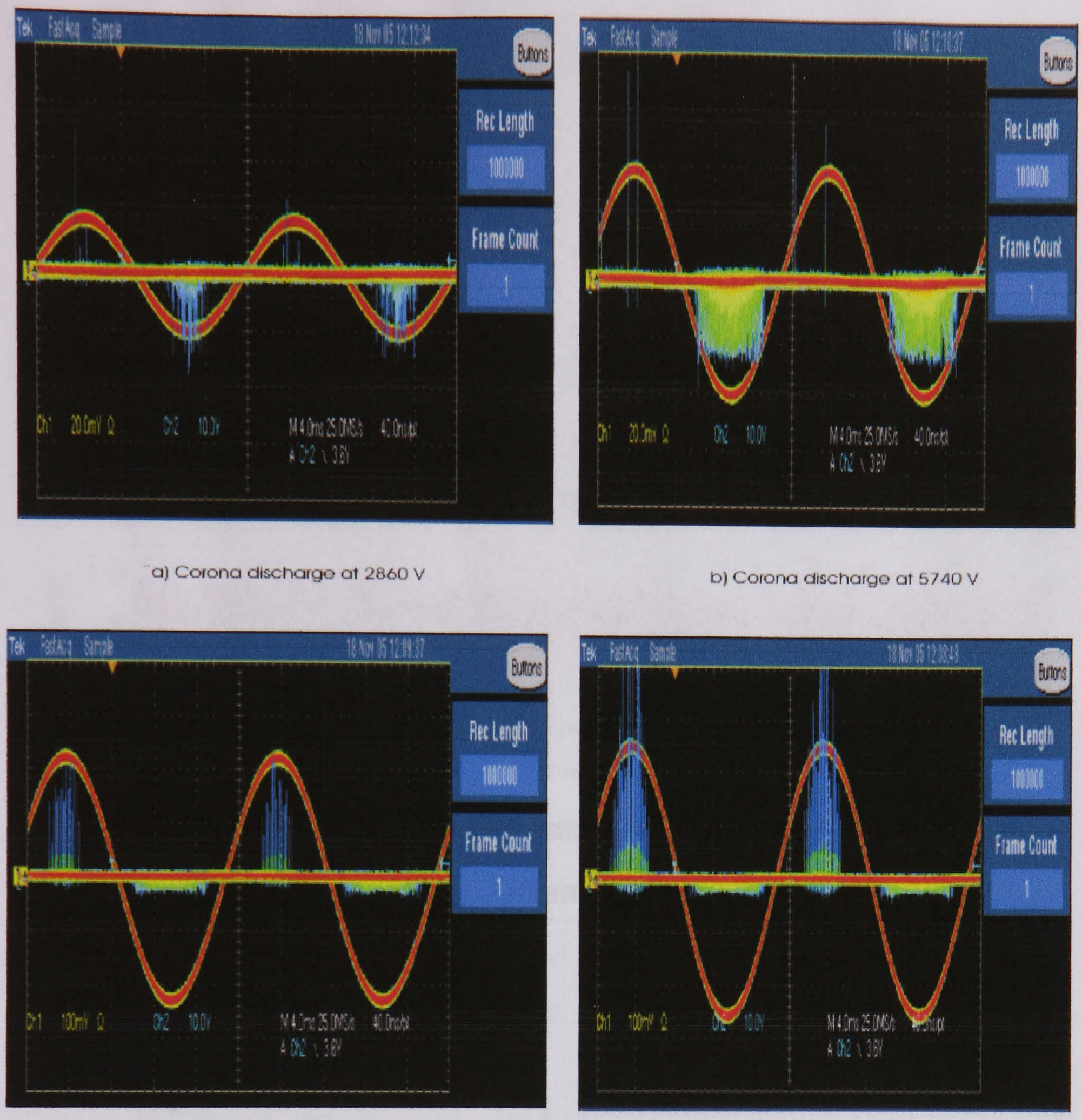

a) Corona discharge at 2860 V

b) Corona discharge at 5740 V

c) Corona discharge at 6540 V

d) Corona discharge at 7370 V

Figure 6.2 AC corona activity and AC reference signal at different voltage levels, note the different scales for CH1 (discharge current).

It is important to mention that the transition from negative to strong positive pulses is gradual, i.e. with a transition region in which positive pulses start to appear and eventually increase in magnitude and recurrence. *Strong positive pulses reach their maximum magnitude and recurrence just before the breakdown of the air gap*. Negative pulses also increase in recurrence but the magnitude remains constant. Positive pulses tend to cluster following the shape of the voltage waveform in the

positive half cycle. Note that below 3 kV, the positive and negative pulses have approximately the same magnitude.

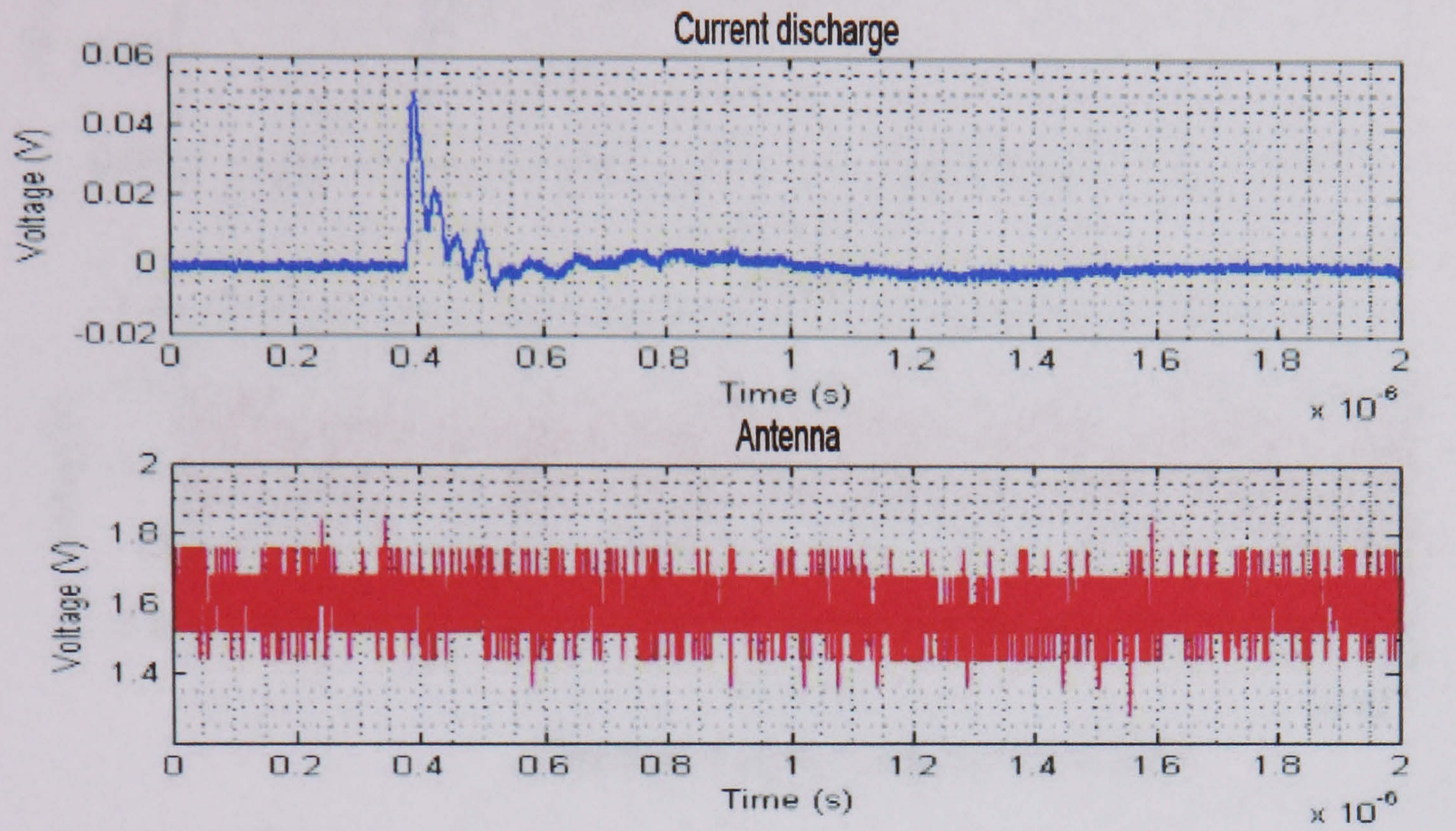

a) Positive corona discharge at 2860 V

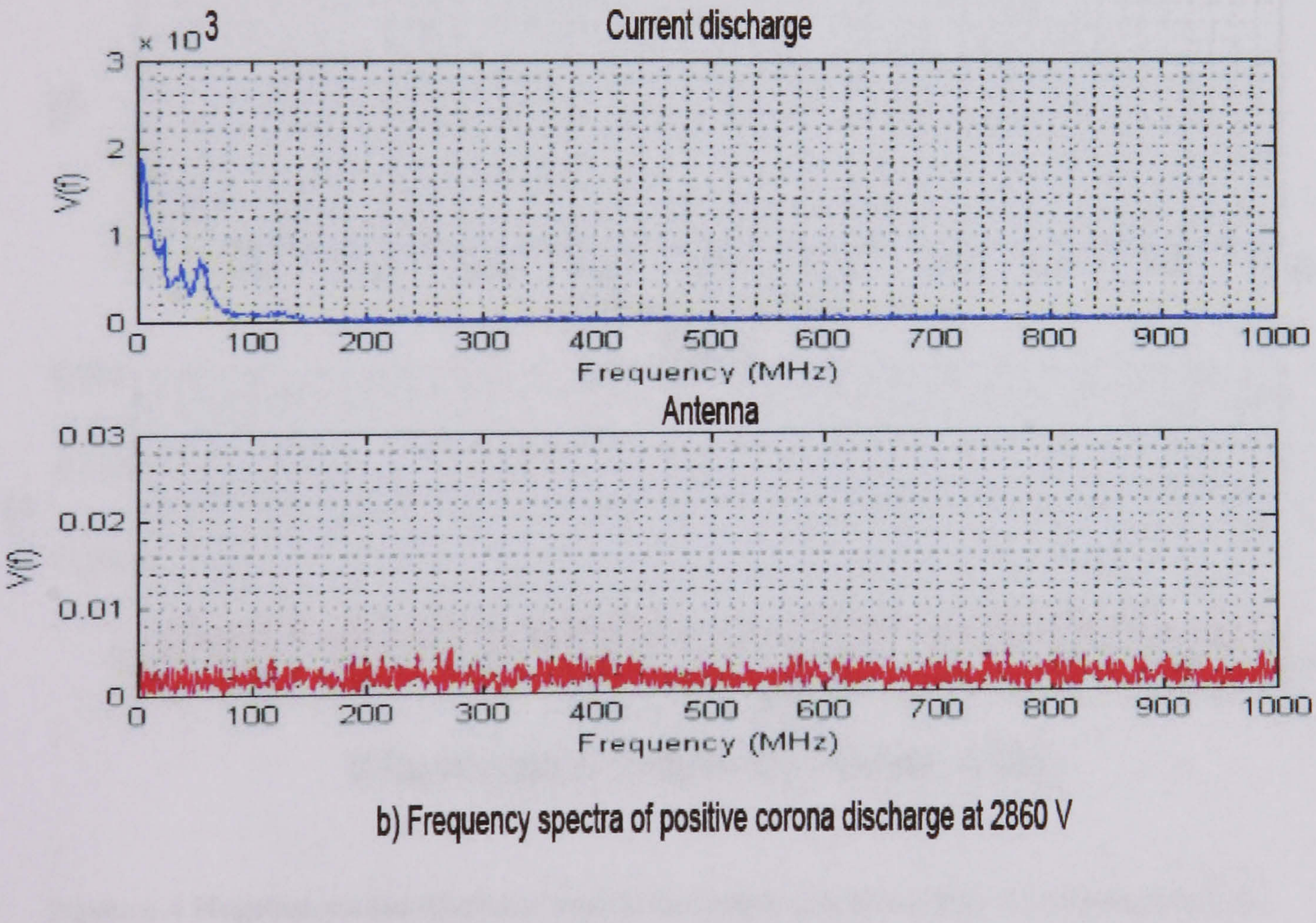

b) Frequency spectra of positive corona discharge at 2860 V

Figure 6.3 Positive corona discharge and its frequency spectra at 2860 V, a) Time record, b) frequency spectra.

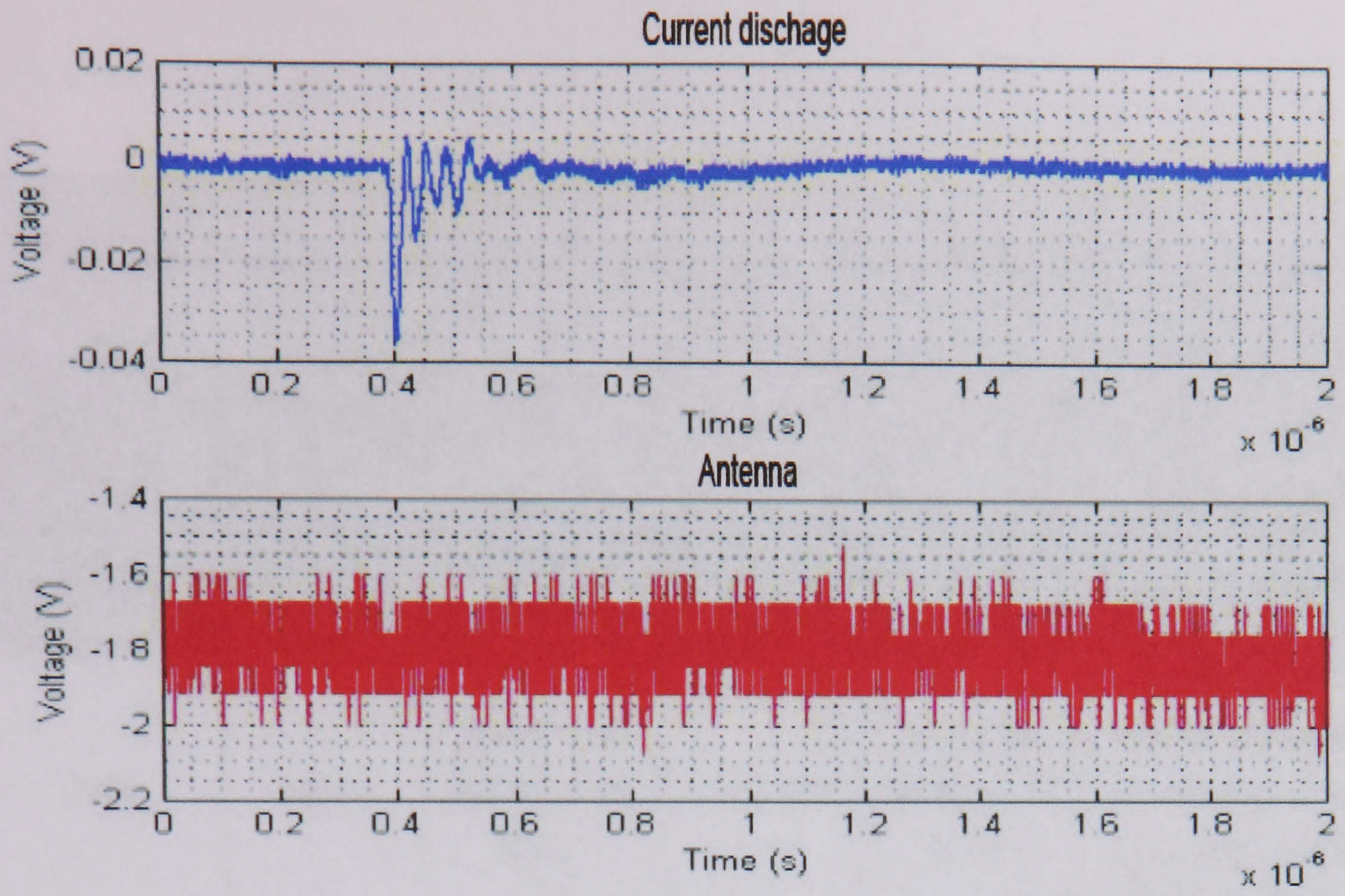

a) Time record of negative corona discharge at 2860 V

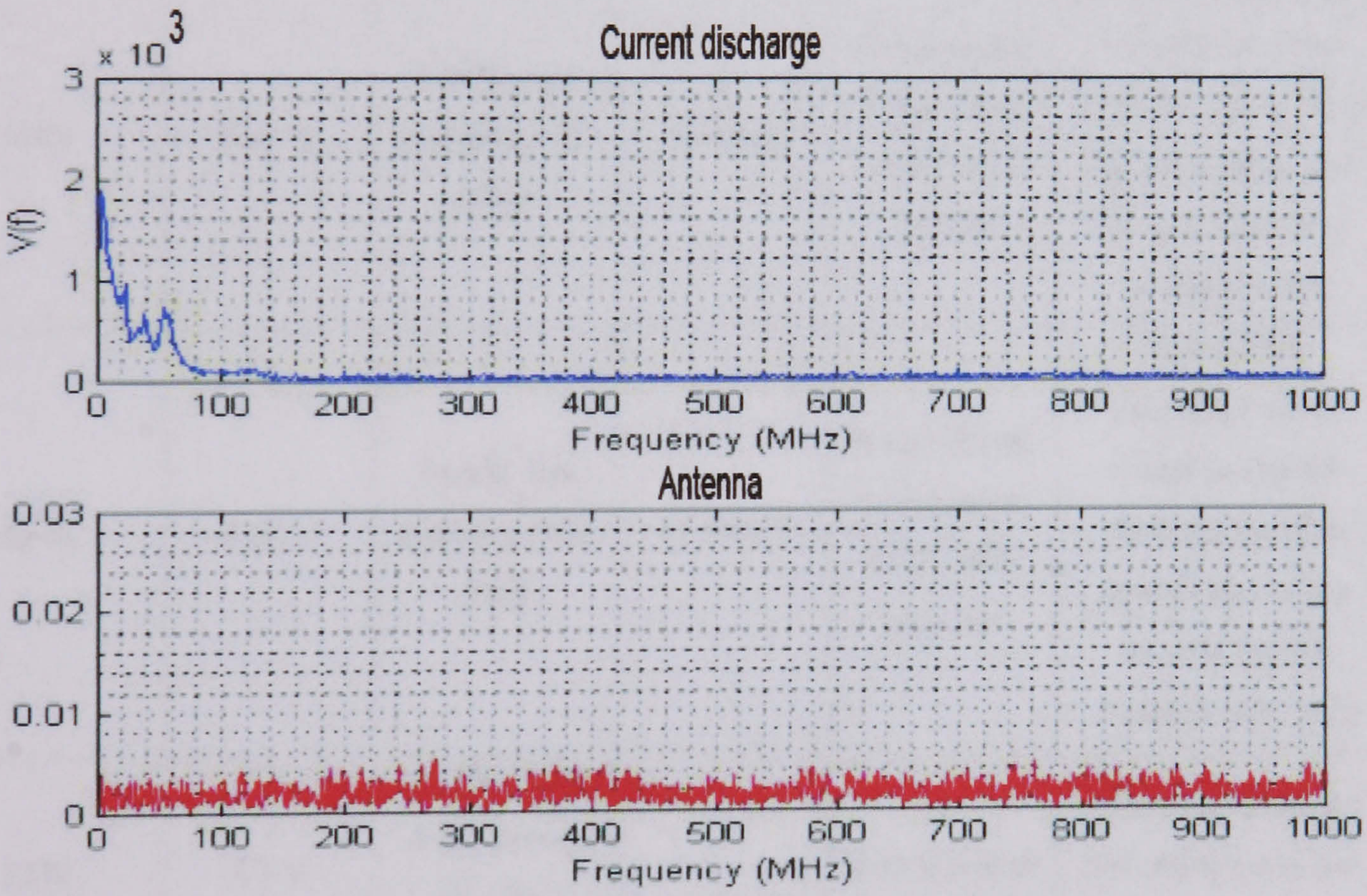

b) Frequency spectra of negative corona discharge at 2860 V

Figure 6.4 Negative corona discharge and its frequency spectra at 2860 V, a) time record, b) frequency spectra.

Summary of results for the frequency spectra of the positive and negative corona discharges					
Applied voltage (V)	**Positive corona discharge magnitude**	**Frequency content of positive corona discharge**	**Negative corona discharge magnitude**	**Frequency content of negative corona discharge**	**Observations**
2860	45 mV	Nearly flat and below 80 MHz	35-40 mV	Nearly flat and below 80 MHz	The majority of negative pulses are concentrated around the maximum of the negative half cycle.
5740	0.13 V	Nearly flat and below 80 MHz	35-40 mV	A significant component of 50 MHz appears	Pulses remain at the maximum of the negative half cycle of the AC voltage and the pulses tend to spread around.
6540	0.36 V	Nearly flat and below 80 MHz	35-40 mV	A significant component of 50 MHz appears	Pulses with maximum value (which is slightly increased) tend to concentrate to the sides of the AC negative half cycle
7370	0.7 V	A significant component of 50 MHz appears	-	Not recorded	Negative pulses are not important at this voltage level
8610 (at breakdown)	0.28 V (at breakdown)	Not recorded	-	Not recorded	At breakdown no signal was recorded

Table V.- Summary of test results for corona discharge analysis

6.2.2. Time domain analysis

As mentioned before, long time acquisitions were recorded using 4 channels of the oscilloscope, the signals recorded were: the 50Ω resistor, 2 conical antennas and the AC reference. Once recorded, the data was stored in a portable hard disk; afterwards the data was processed and analyzed using a MATLAB program. The developed program used for this analysis has the following characteristics: peak detection of individual pulses per cycle, point on wave, negative and positive average of the detected pulses, positive and negative threshold of pulses, (the threshold value is the minimum and maximum value of the acquired discharges i.e. scope trigger level that was used to capture pulses of interest), average difference between pulses and graphical/numerical output of the results. Figure 6.5a shows the typical pattern of corona in air at 2860 V where several negative pulses appear distributed along the negative AC half cycle; at the same time, a few positive pulses are noticeable in the positive half cycle of the AC reference waveform. Figure 6.7a shows the statistical distribution of the acquired pulses at 2860 V, where it can be seen that most of the pulses are located between 230 and 300 degrees and their magnitude is negative, the peak magnitude occurs at the negative peak. Positive pulses are fewer (less than 10) with a maximum magnitude similar to the negative pulses.

In figure 6.5b the applied voltage was raised to 6540 V, it can be observed that more positive pulses with a higher magnitude appear, the occurrence of negative pulses is increased, but the magnitude remains the same. The highest magnitude negative pulses tend to group at the extremes of the half negative cycle and the smallest at the centre. Figure 6.7b shows the statistical distribution of the acquired pulses, an important increase in the number of negative pulses is evident. They are distributed between 170 and 340 degrees (negative half cycle) and their magnitude show a small increase. The appearance of positive pulses is also noticeable; although they are fewer, their magnitude is much higher. If the voltage is raised to 7370 V, (see figure 6.6a) more positive pulses appear with higher magnitude (maximum 0.5 V) at this point, the pulses reach their maximum value before breakdown. The statistical

distribution of pulses at this voltage level (see figure 6.8a) shows that the distribution of positive pulses is between 170 and 340 degrees i.e. nearly the same that the previous voltage, but the recurrence of the pulses is higher. An increase in the recurrence of negative pulses is noticeable at breakdown, but their magnitude remains nearly the same (-0.05 V).

When the voltage is increased to 8610 V a breakdown in the air gap occurs. Figure 6.6b shows the generated pulses of the discharge, where it can be observed that only few pulses appear but their maximum magnitude is less than the previous voltage (7370 V). This effect is expected since the breakdown current cause a voltage drop. The statistical distribution of the discharge (see figure 6.8b) shows that the pattern has changed when compared to the previous corona voltages; the quantity of pulses has been reduced dramatically since every pulse represents a breakdown of the gap. Most of the breakdown discharges occurs at 90 degrees, i.e. the maximum of the positive half cycle of the AC reference waveform. Few negative pulses occur in the negative half cycle of the AC waveform. Appendix C shows patterns of corona discharge at all applied voltages.

Note that the negative pulses observed in these experiments correspond to Trichel pulses [6.7]. These are characterized by a constant pulse magnitude but the pulse repetition frequency increases with voltage magnitude.

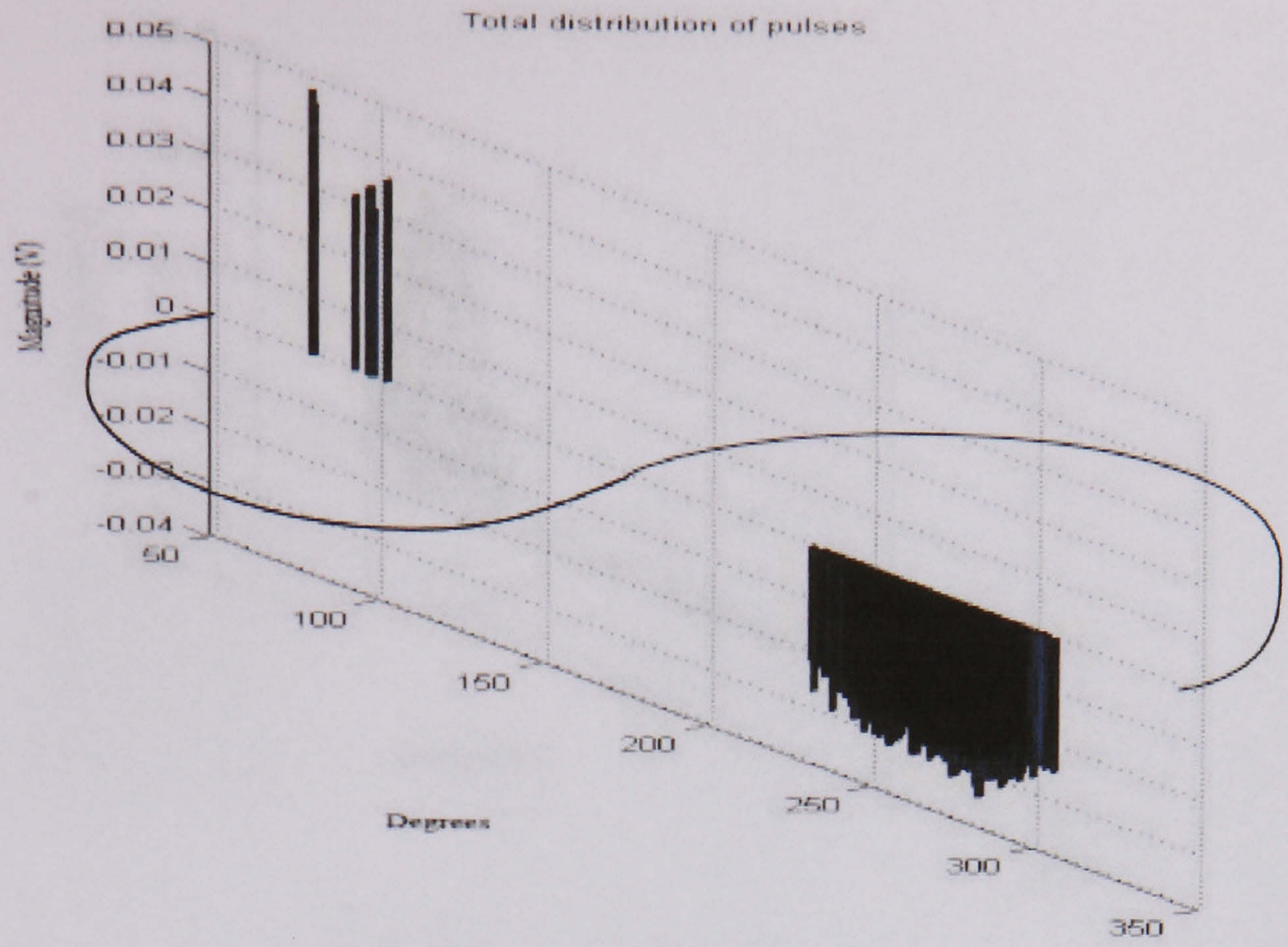

a) Pulse distribution of corona discharge
at 2860 V and 10 mm gap

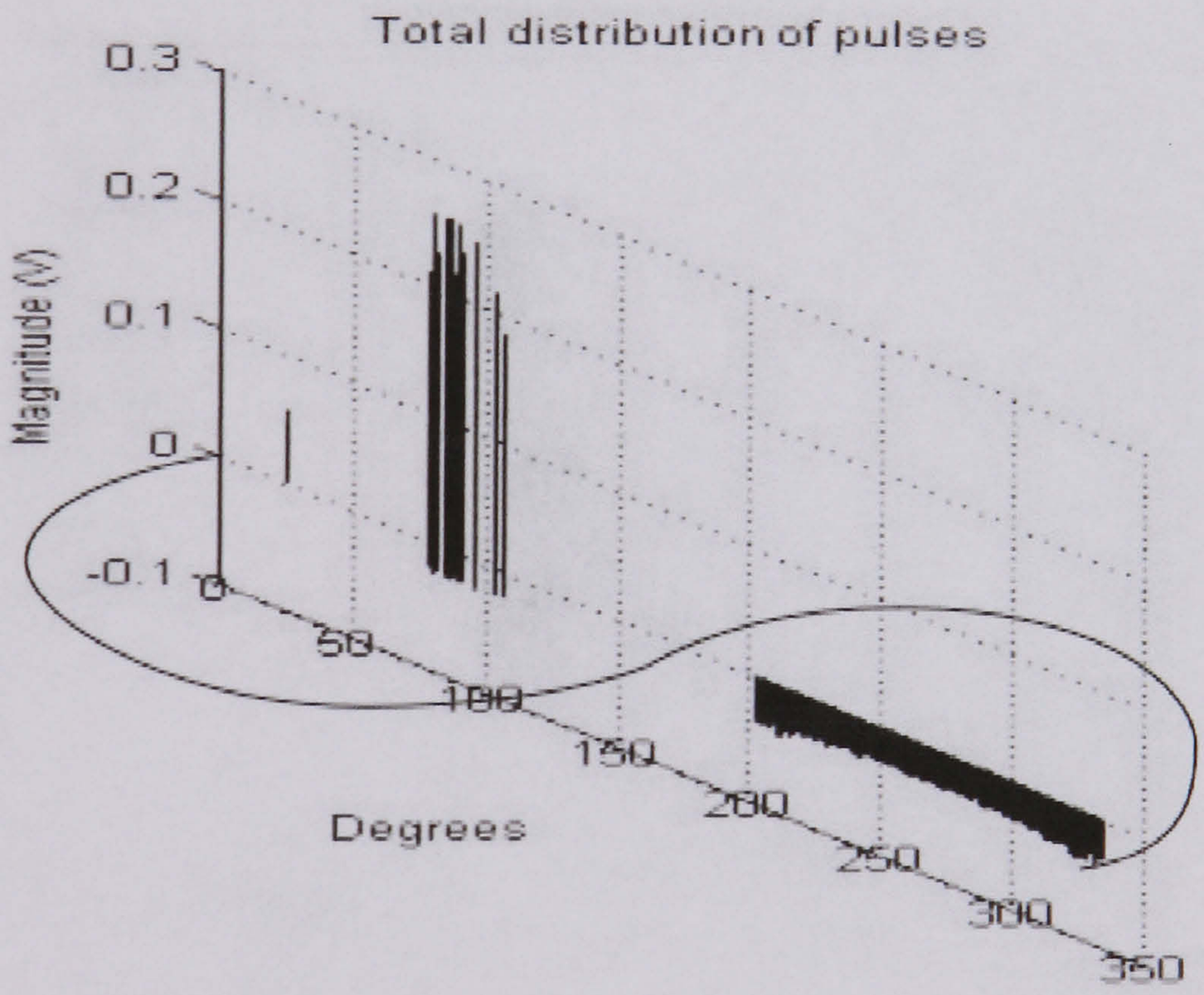

b) Pulse distribution of corona discharge
at 6540 V and 10 mm gap

Figure 6.5 Pulse distribution of corona discharge in a 10 mm gap, a) corona at 2860 V, b) corona at 6540V

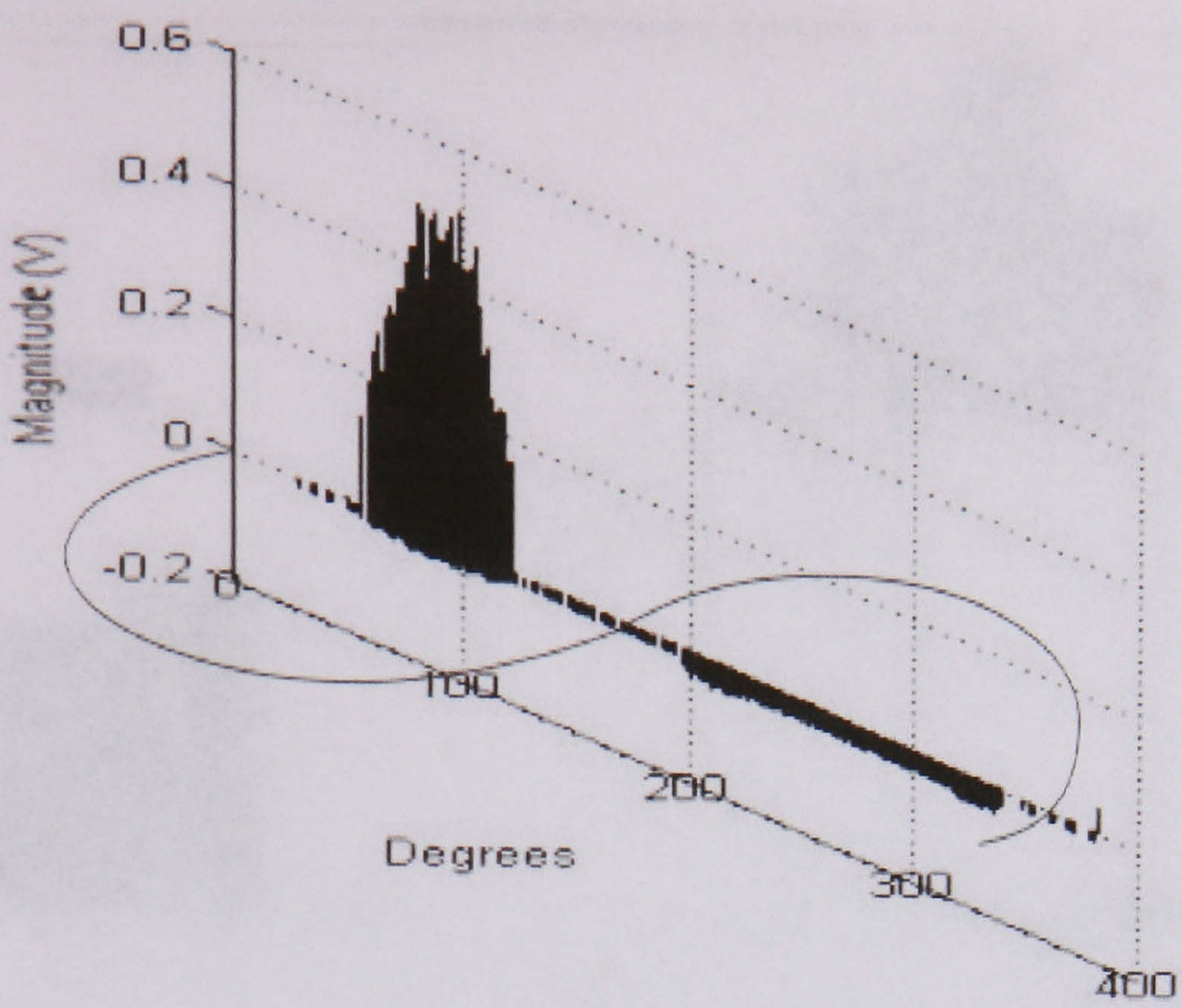

a) Pulse distribution of corona discharge
at 7370 V and 10 mm gap

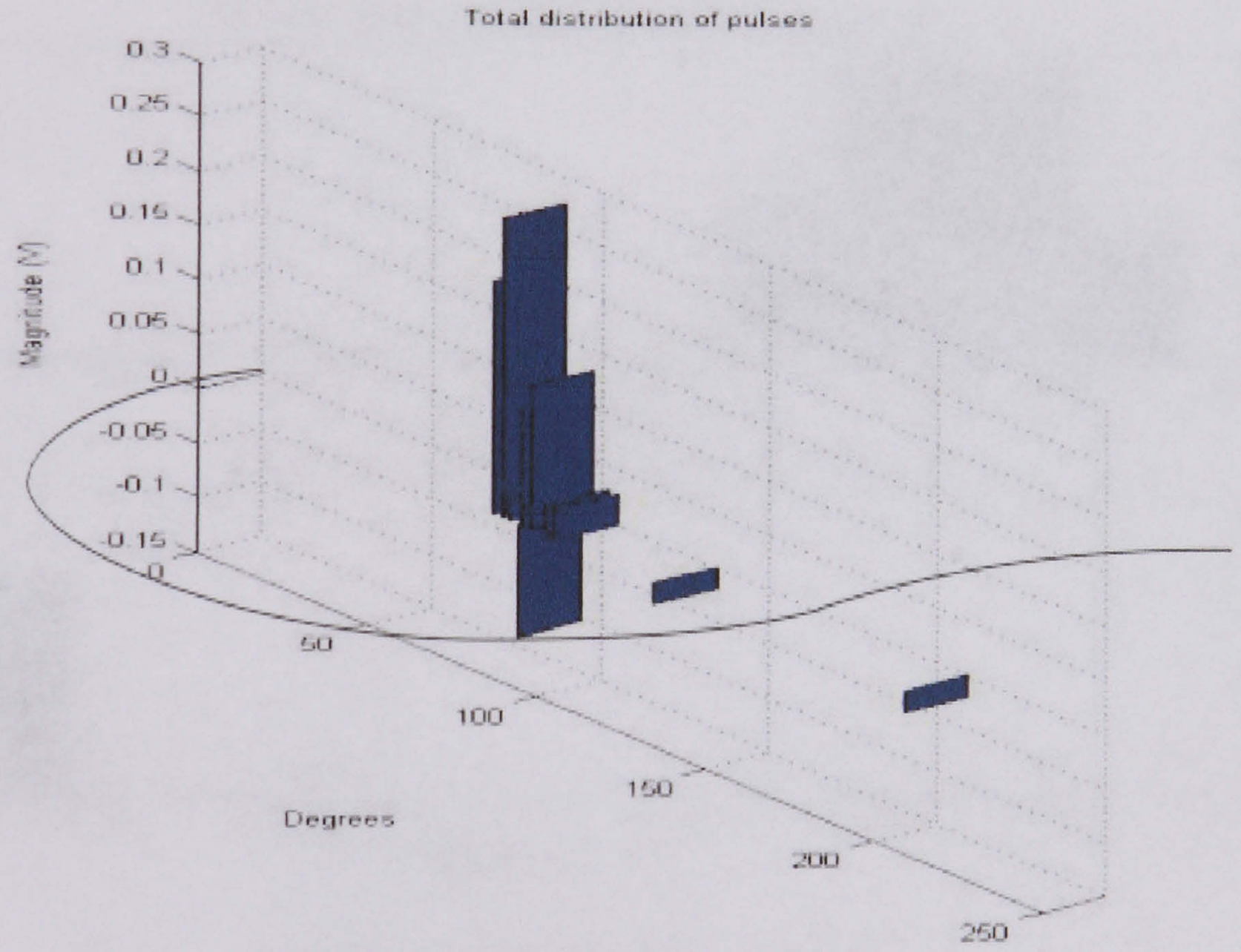

b) Pulse distribution of air discharge
at 8610 V and 10 mm gap

Figure 6.6 Pulse distribution of corona discharge in a 10 mm gap, a) corona at 7370 V, b) corona at 8610 V (breakdown).

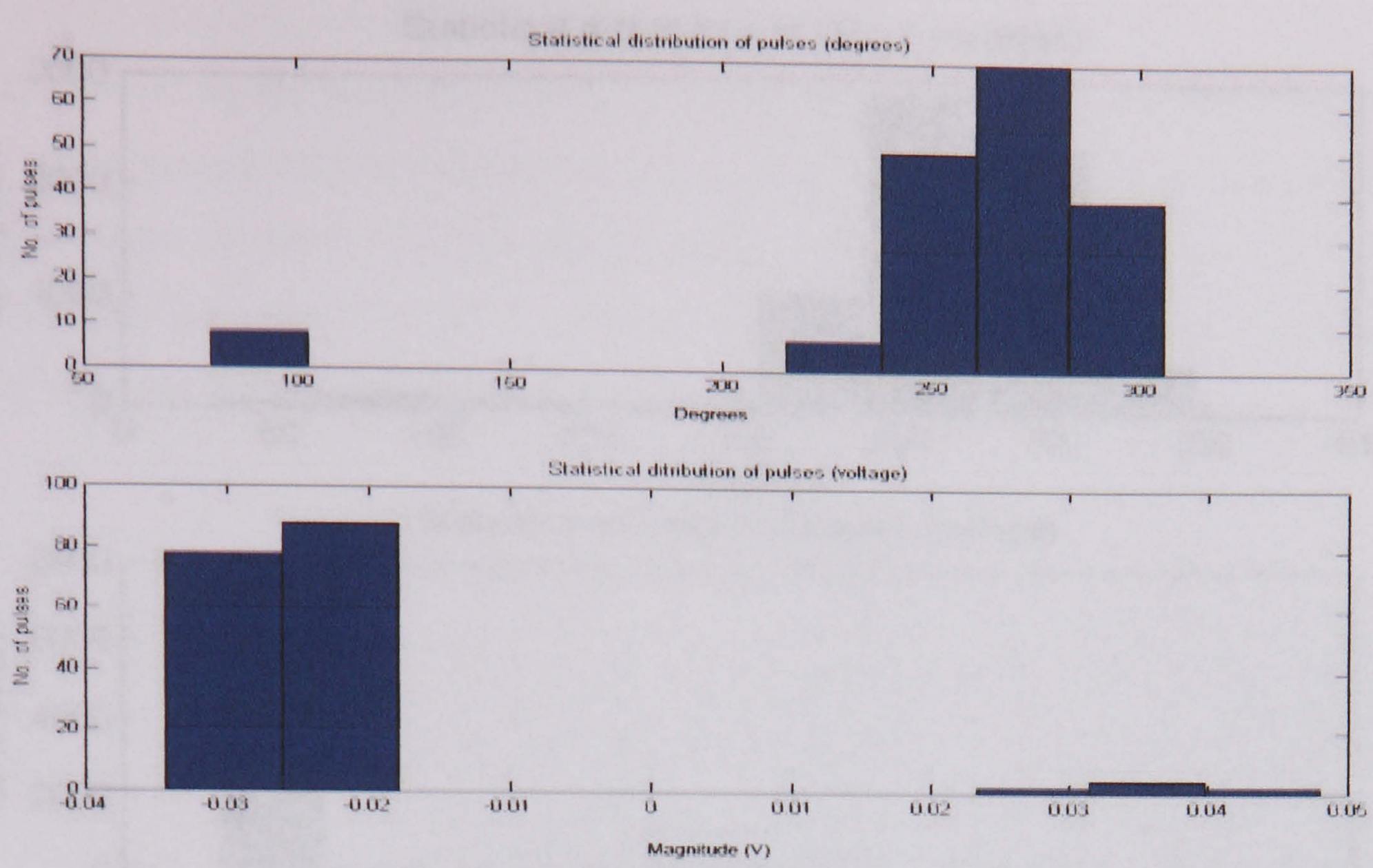

a) Statistical distribution of corona pulses
at 2860 V with a 10 mm air gap

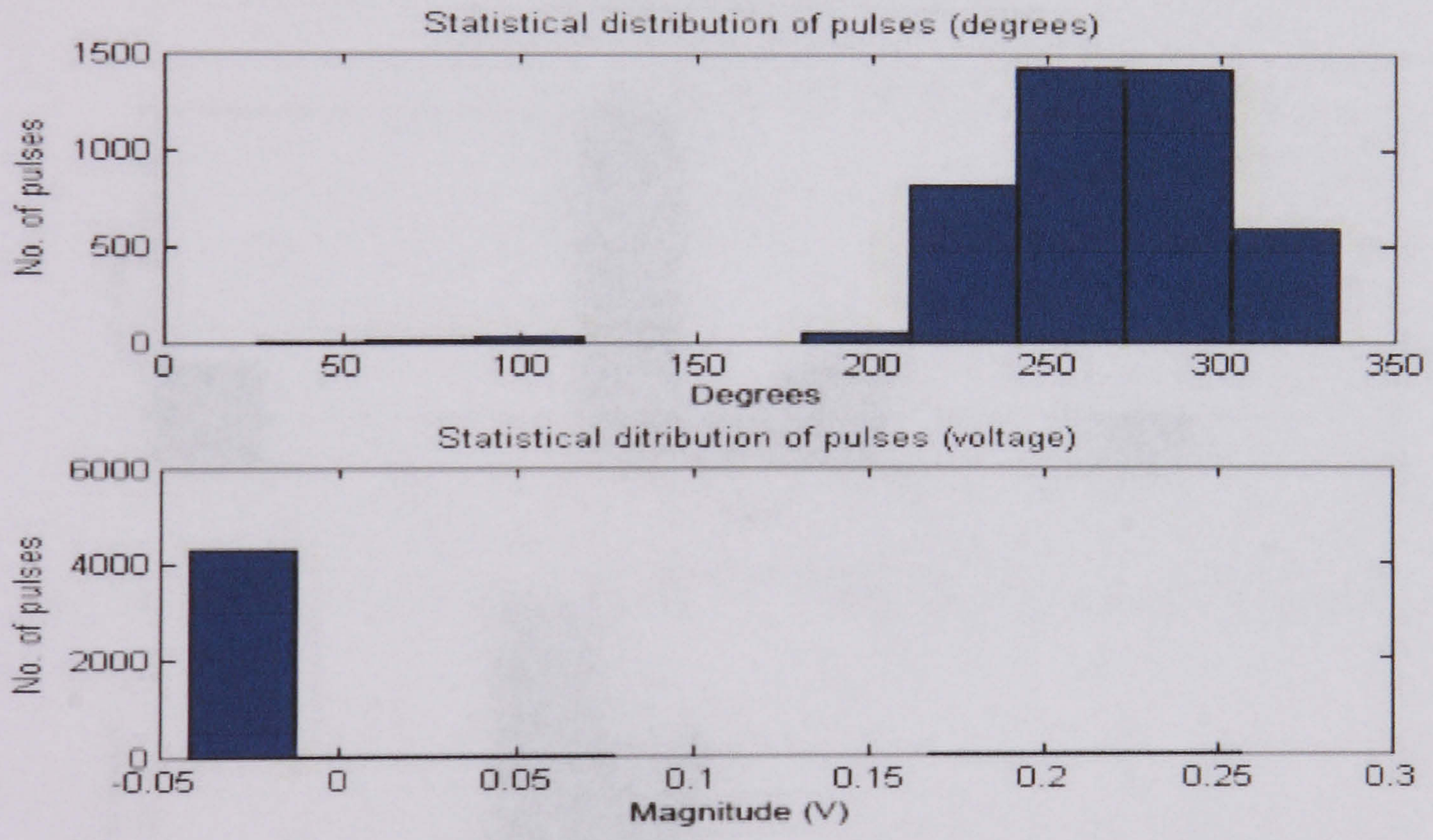

b) Statistical distribution of corona pulses
at 6540 V with a 10 mm air gap

Figure 6.7 Statistical distribution of corona pulses at a) 2860 V, b) 6540 V

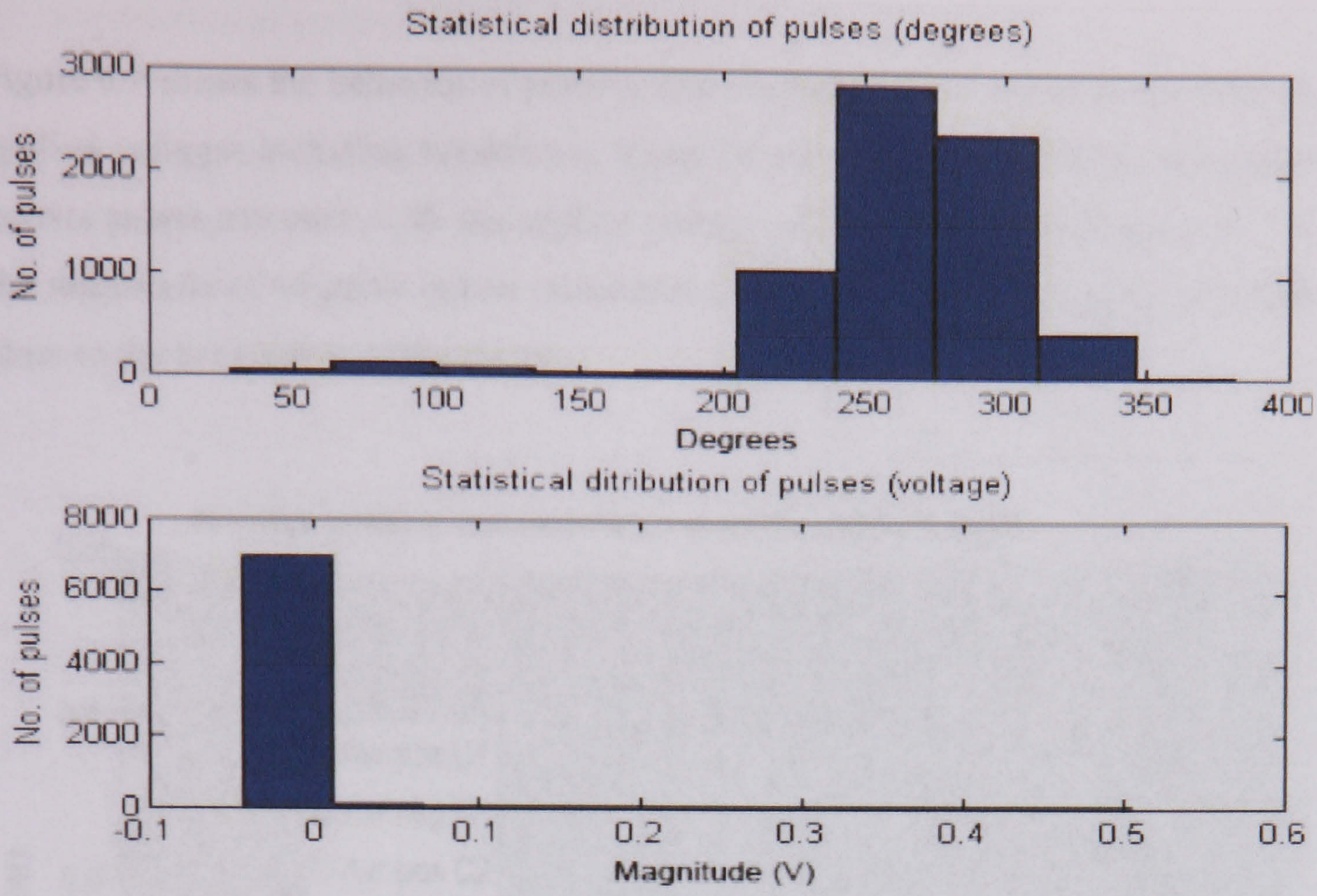

a) Statistical distribution of corona pulses
at 7370 V with a 10 mm air gap

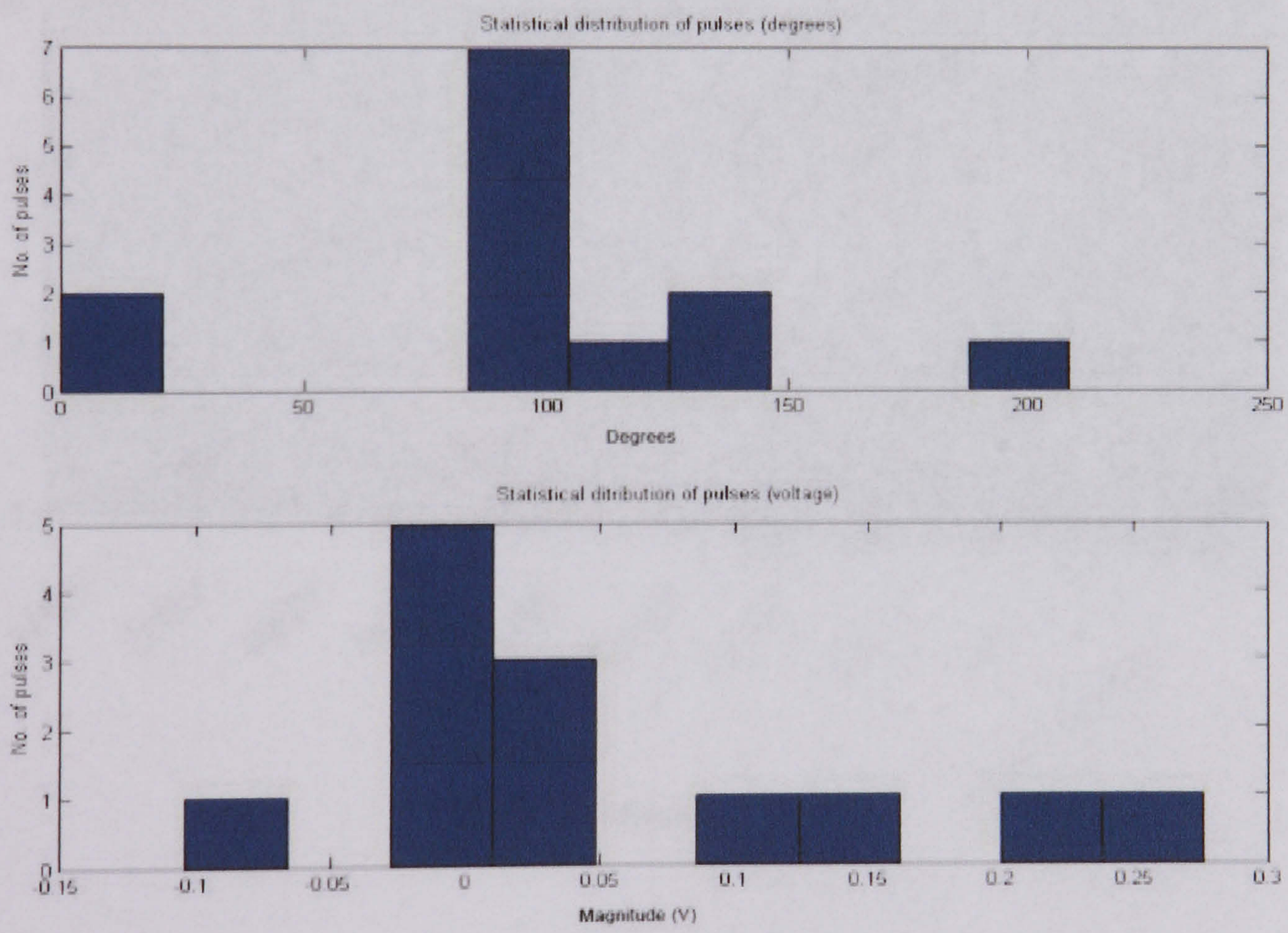

b) Statistical distribution of corona pulses
at 8610 V with a 10 mm air gap

Figure 6.8 Statistical distribution of corona pulses at a) 7370, b) 8610 V

Figure 6.9 shows the behavior of positive and negative corona pulses at the different applied voltages including breakdown. It can be seen that the magnitude of positive corona pulses increases with the applied voltage until a maximum voltage of 0.5 V, the magnitude of negative pulses remains constant with a slight tendency to reduce close to the breakdown of the air gap.

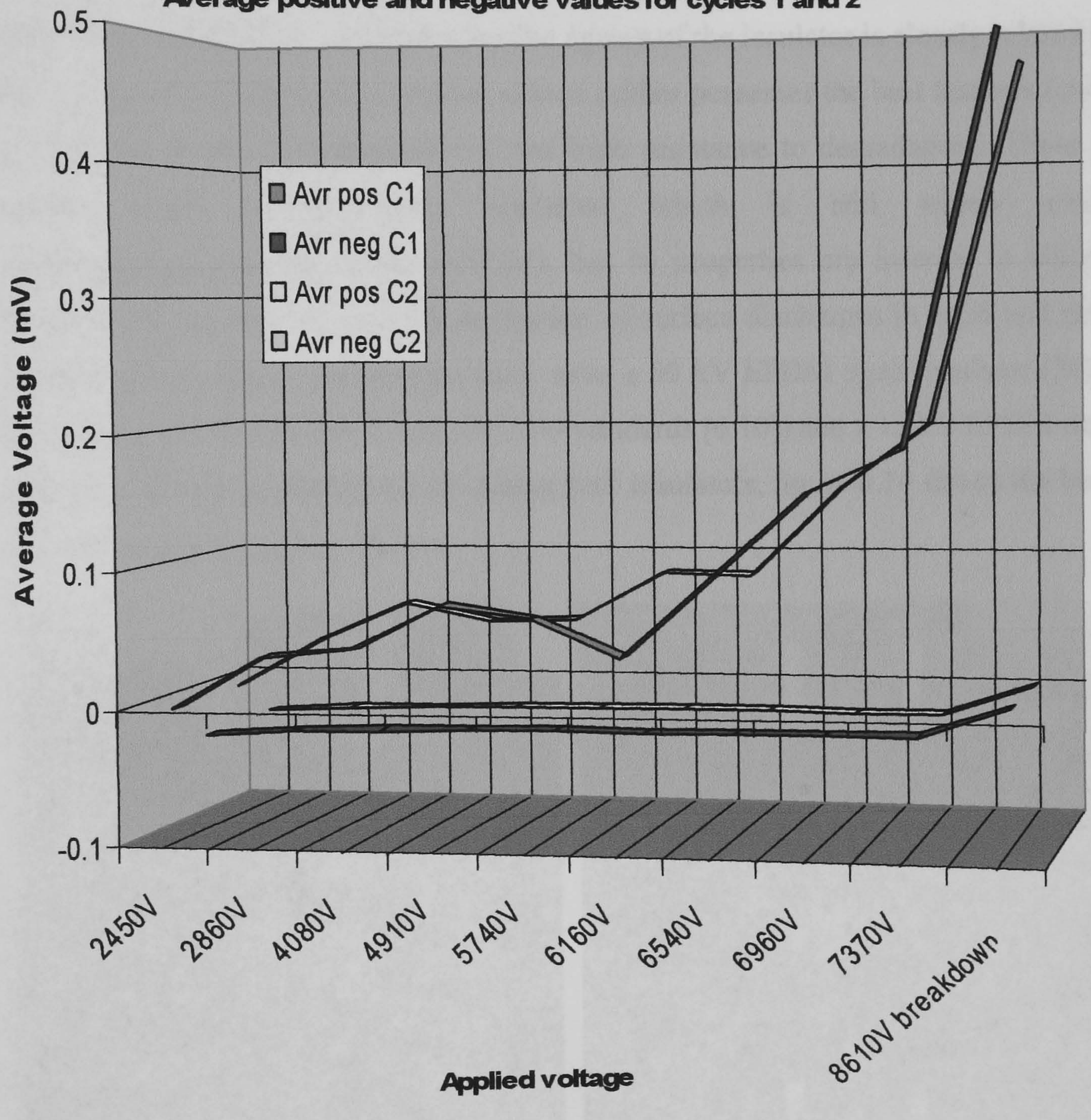

Figure 6.9 Average values of positive and negative corona pulses for cycles 1 and 2 with respect to the applied voltage

6.3. Evaluation of surface discharges over new and aged insulators.

Corona is present in different primary equipment in substations and transmission lines. The equipment most commonly affected are polymeric insulators, such as chain insulators or base insulators, where the eventual development of corona over the insulator high field regions leads to surface discharge and in severe cases the complete failure of the insulator. The inception of corona and surface discharges over the polymeric insulator is caused by several factors such as ageing and eventual loss of hydrophobicity [6.8], pollution etc. The ageing of the insulator is closely related to the quality of the insulating material; silicon rubber possesses the best features (such as fast recovering of hydrophobicity and high resistance to degradation). There is another kind of polymeric insulation which is still widely used; ethylenepropylenediene rubber (EPDM), but its properties are inferior to silicon rubber [6.9]. In this research the evaluation of surface discharges in aged and new insulators was made. The samples used were a 50 kV EPDM aged insulator (5000 hours aged in a fog chamber under IEC 60 standards [6.10]) and a 15 kV EPDM new insulator. A base was designed for testing both insulators, figure 6.10 shows the base and the insulators used in this test.

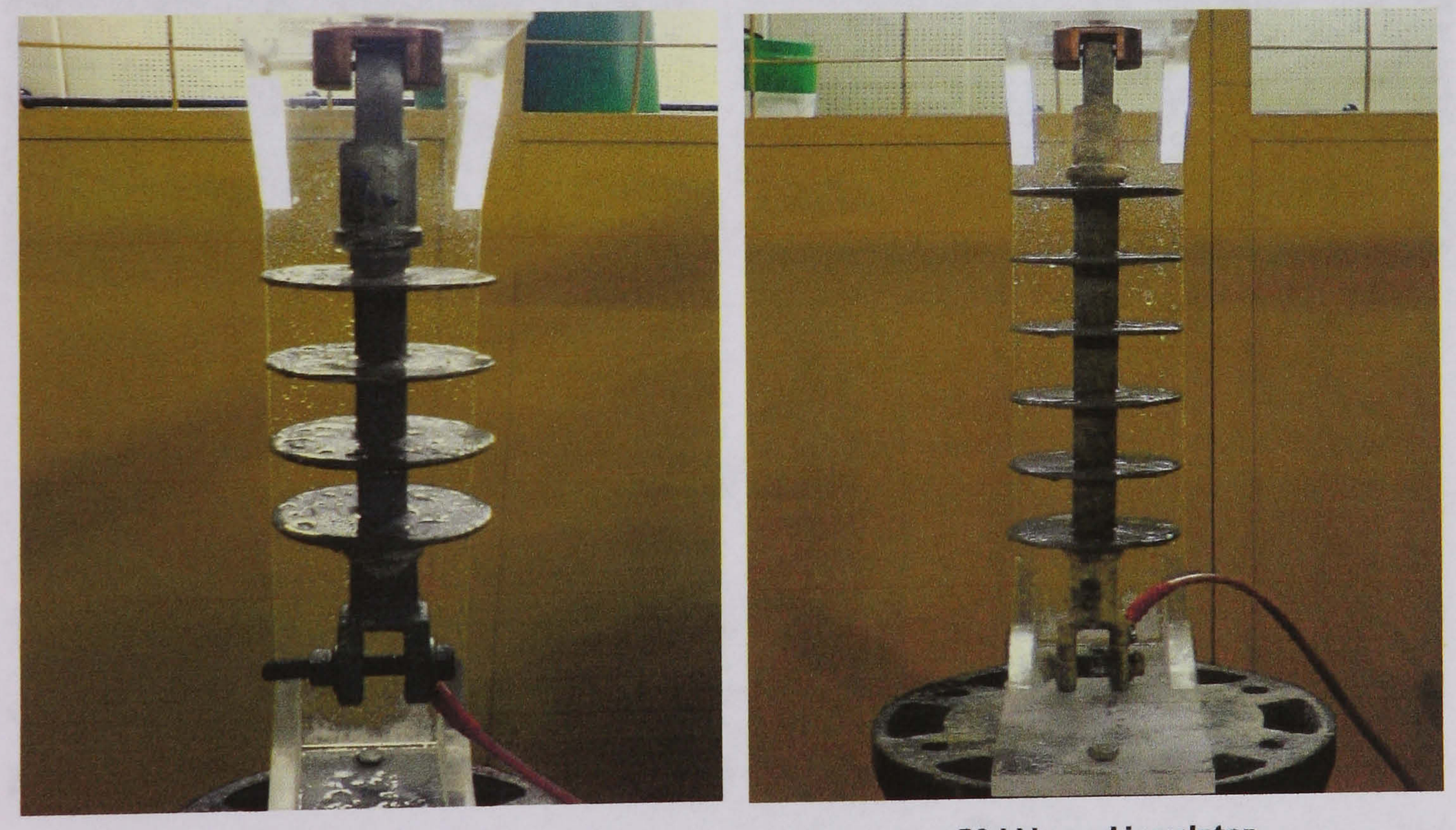

15 kV new insulator

50 kV aged insulator

Figure 6.10 Used insulators and designed base

In order to increase the inception of corona and surface discharges over both insulators, a mixture of dissolved common salt and water in a proportion of 1 to 3 was sprayed. As it was mentioned earlier, the effect of hydrophobicity plays an important role in the inception of corona, this effect can be observed on the surface of the new insulator as it tends to reject water (i.e. has little or no tendency to adsorb water) and form discrete droplets [6.8] as is shown in figure 6.11.

15 kV new insulator

50 kV aged insulator

Figure 6.11 New and aged insulator showing the hydrophobicity effect

The implications of the hydrophobicity on the corona inception will be evident in the context of the implemented tests. Once the water/salt mixture was sprayed, a gradual high voltage was applied in order to stress the insulator and eventually incept corona and surface discharges. The measured signal was acquired using the conducted current through the 50 Ω resistors, the radiated energy through the conical antennas and the AC point on wave information. Figure 6.12 shows screenshots of the

acquired surface discharges for a new insulator. It is important to notice that *there was no reception of any radiated signal in the antenna using the new insulator*, and figures in this case were not included. The applied voltage was notably higher compared to the one applied to corona in air because of the required inception voltage for surface discharges over the insulator, the complete breakdown was not achieved as the breakdown voltage of the insulator exceed the voltage of the source. The acquired signals correspond only to positive discharges as they are the most relevant.

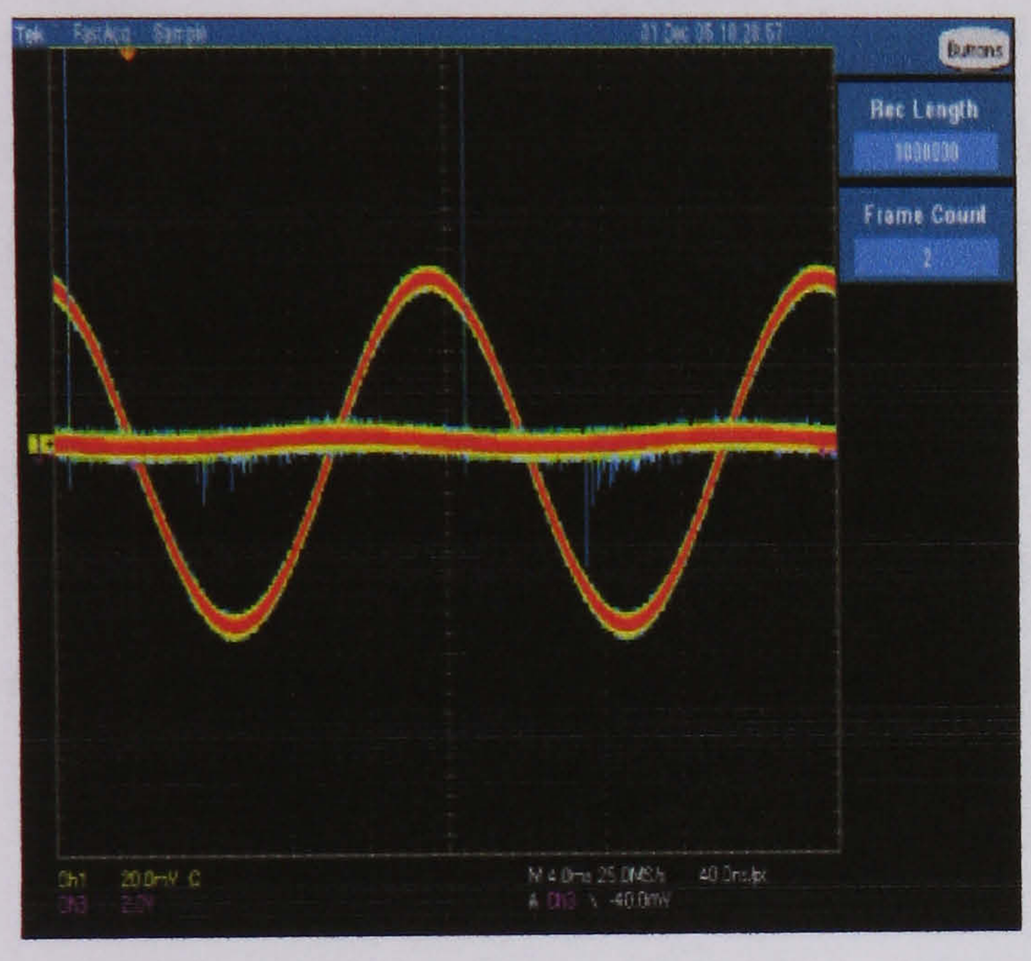

a) Surface discharges over a new insulator at 32800 V

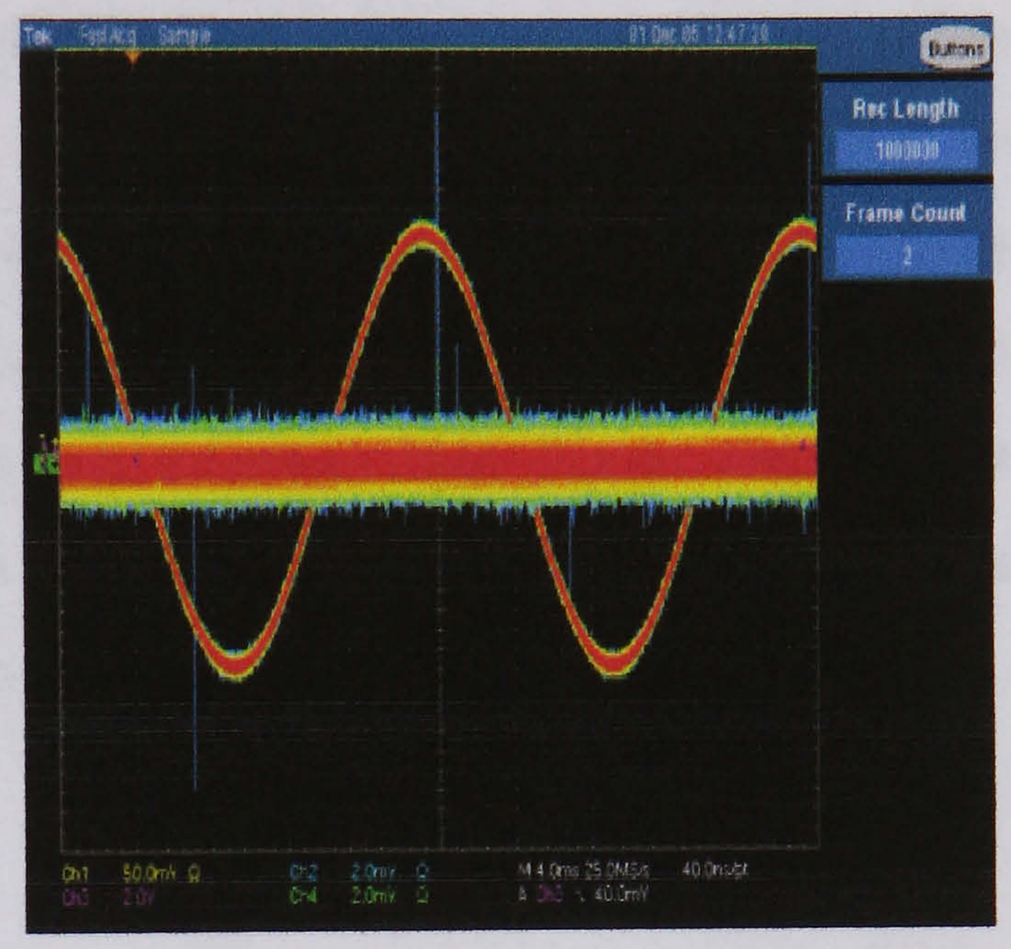

c) Surface discharges over a new insulator at 40800 V

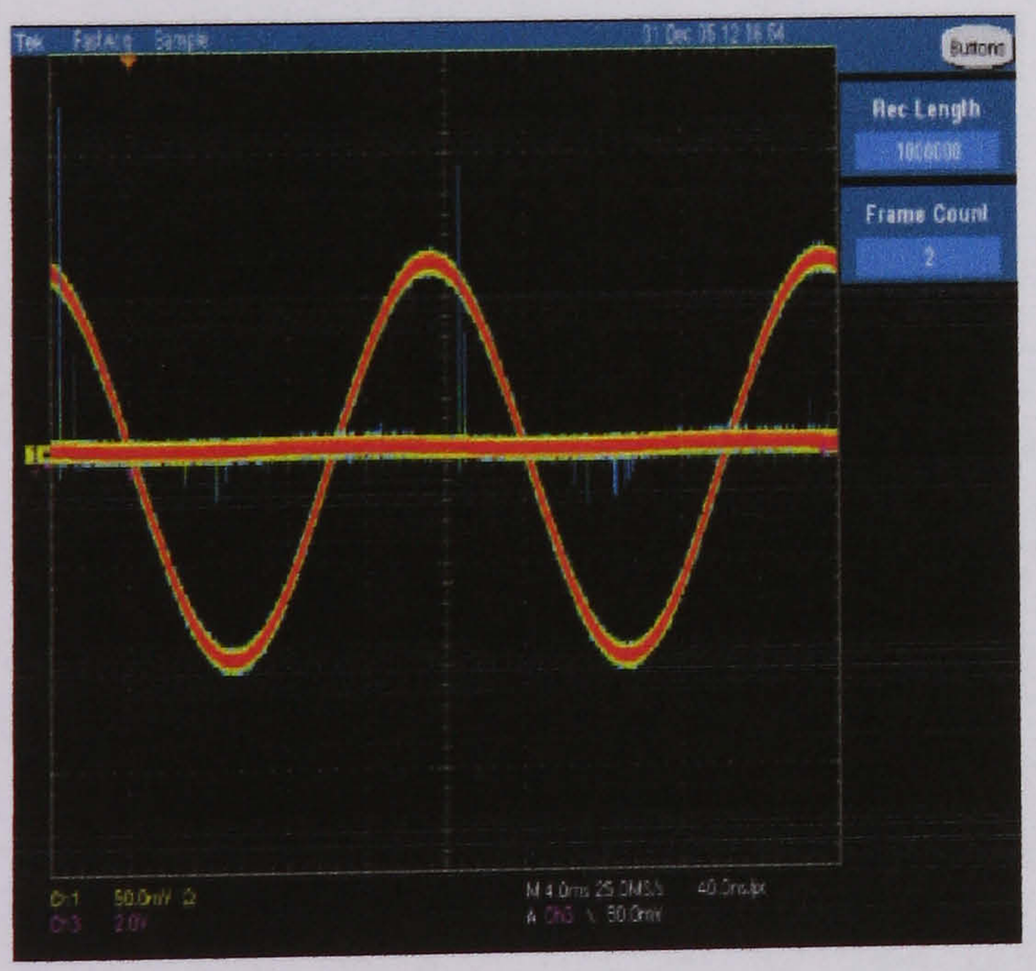

b) Surface discharges over a new insulator at 36900 V

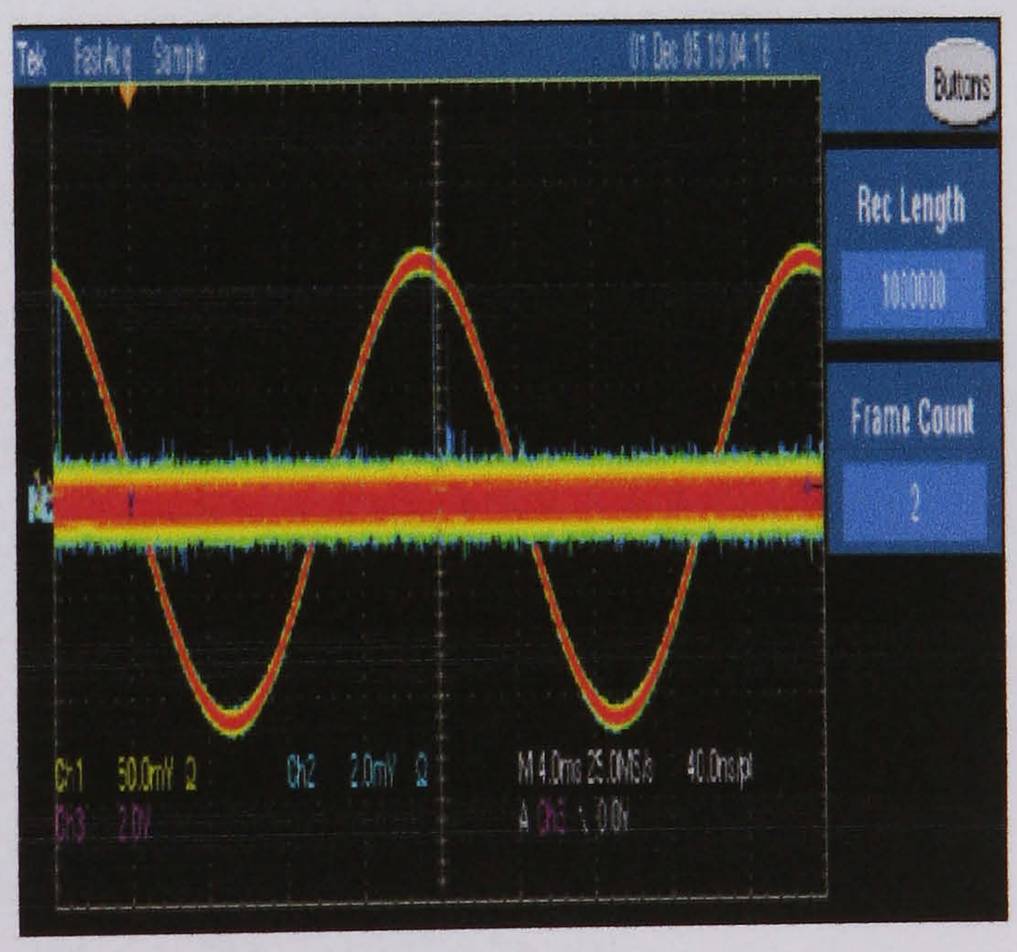

d) Surface discharges over a new insulator at 42500 V

Figure 6.12 Surface discharges over a new insulators acquired in the 50 Ω and AC reference at a) 32800 V, b) 36900 V, c) 40800 V and d) 42500 V.

6.3.1. Frequency domain analysis of the acquired signals in a new insulator

As pointed out before, for these chain insulators the applied voltage is higher compared to the air gap. The aim of this test was to generate surface discharge activity; it was not possible to generate the voltage needed to breakdown the insulator. Note that the required inception voltage for corona and surface discharge is affected by the physical conditions of the insulator. In the new insulator at 40800 V, it is possible to observe (figure 6.13a) that some discharge activity *appears (positive polarity)*, with most of the activity occurring in the negative half cycle but its magnitude is very low (0.02 volts). The frequency spectra of the acquired positive discharges at 40800 V (see figure 6.13b) shows their pulsating nature (almost no frequency content) *and no signal is received at the antennas at this point.* A similar effect is observed when the voltage is raised to 42500, i.e. positive polarity pulses appears and no reception is observed at the antennas (see figure 14a), scarce frequency content is observe as well (see figure 6.14b). Table VI summarize the results of the analyzed surface discharges over the new insulator.

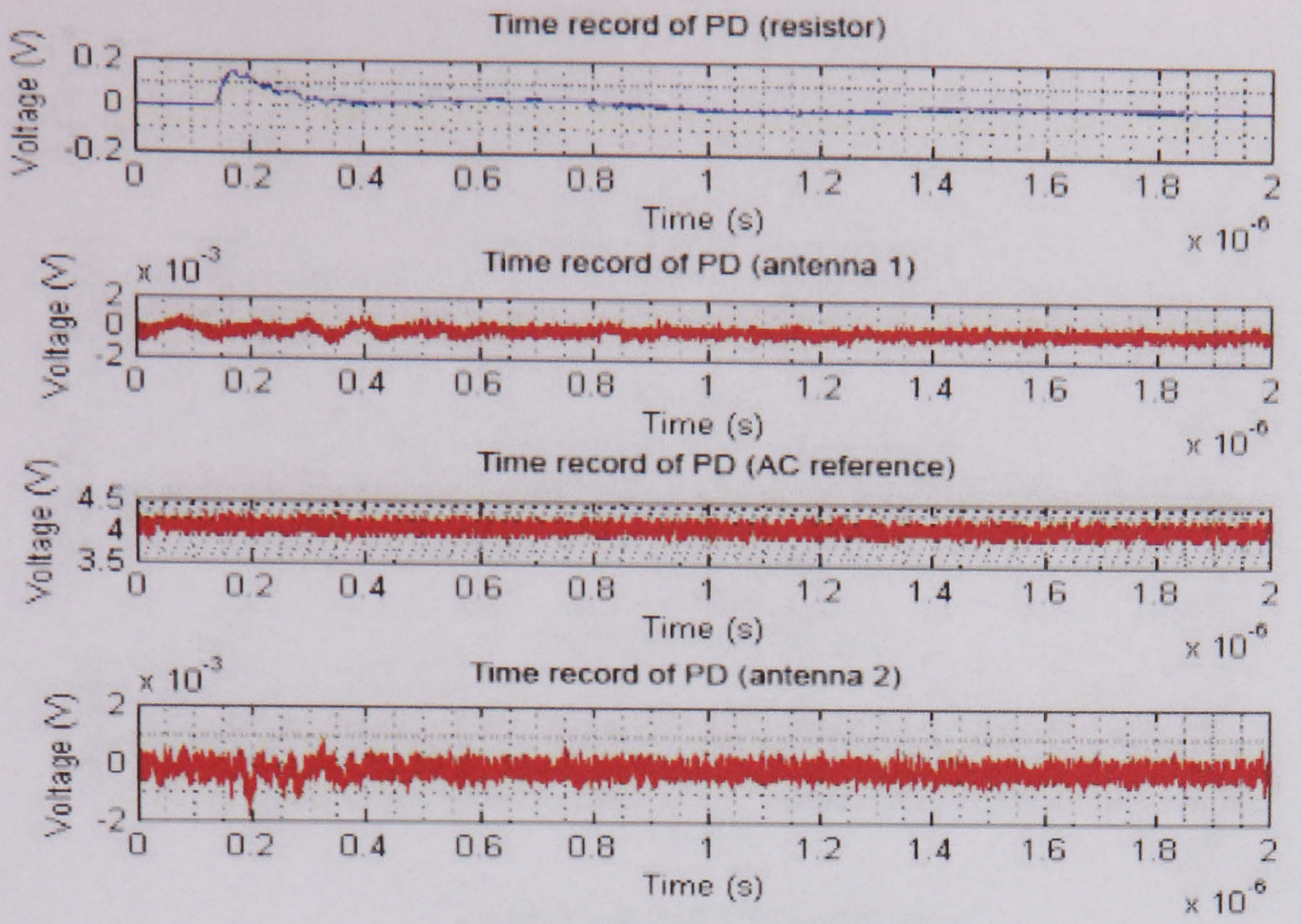

a) Surface discharge acquisition over a new insulator at 40800 V

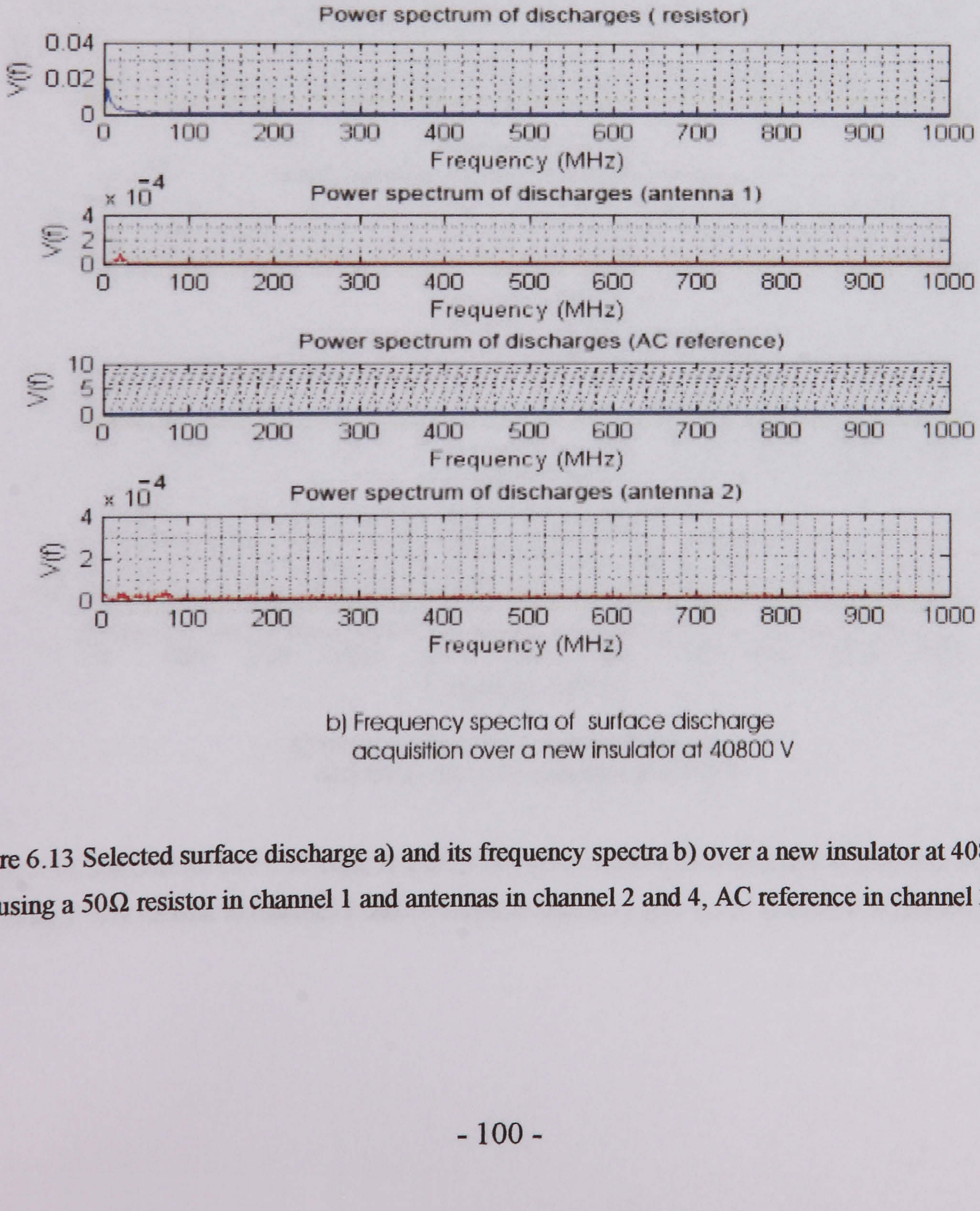

b) Frequency spectra of surface discharge acquisition over a new insulator at 40800 V

Figure 6.13 Selected surface discharge a) and its frequency spectra b) over a new insulator at 40800 V using a 50Ω resistor in channel 1 and antennas in channel 2 and 4, AC reference in channel 3.

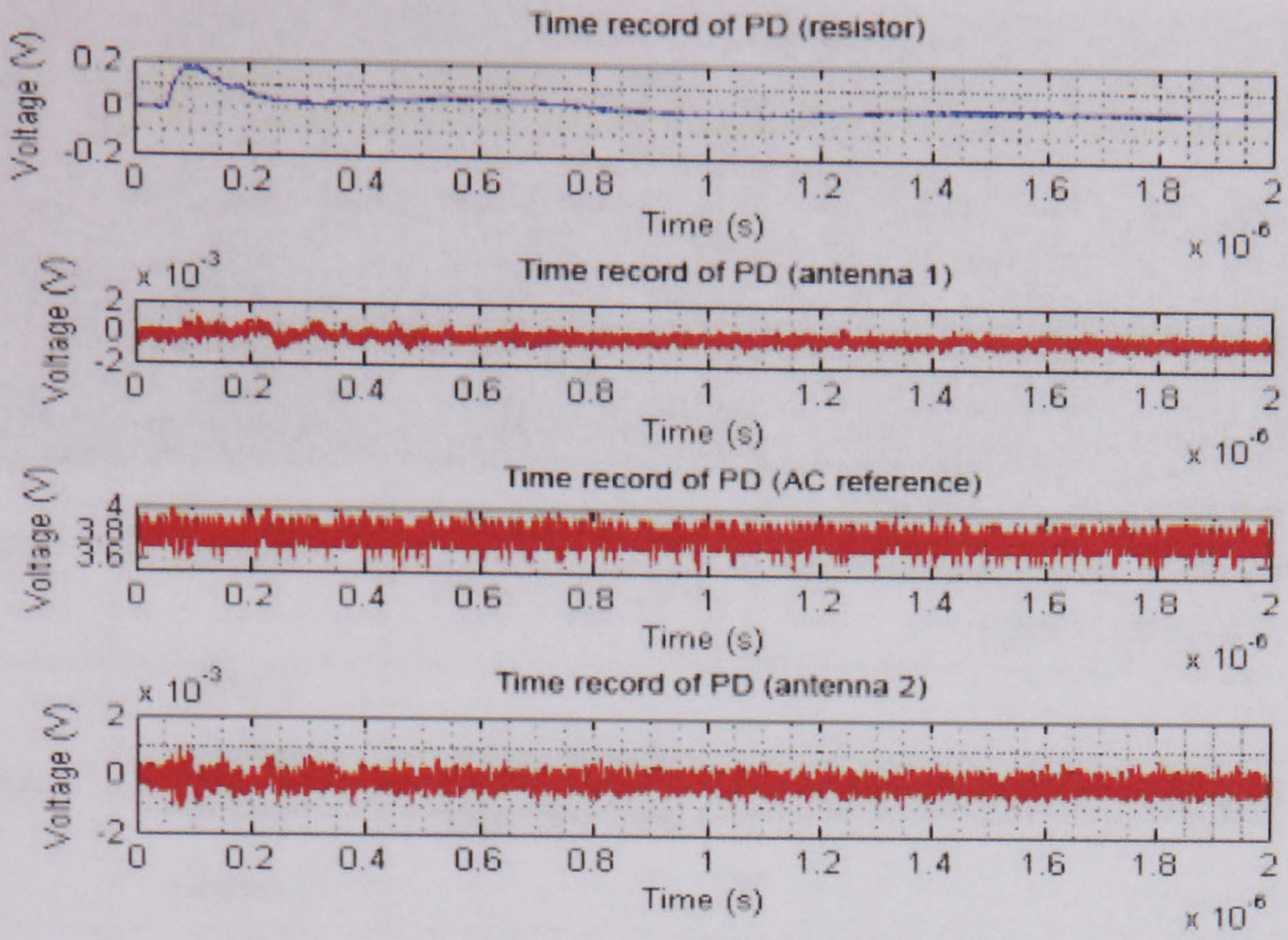

a) Surface discharge acquisition over a new insulator at 42500 V

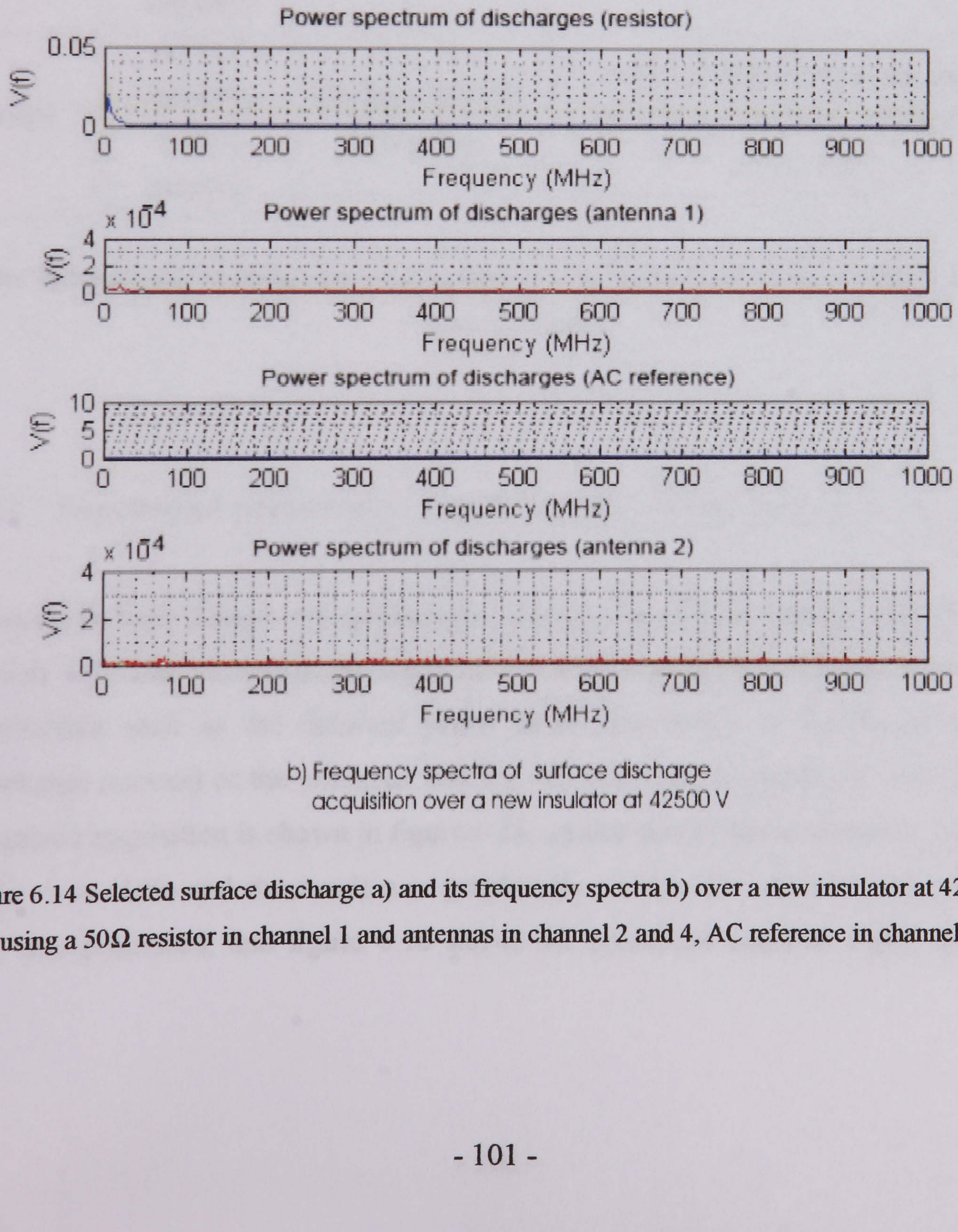

b) Frequency spectra of surface discharge acquisition over a new insulator at 42500 V

Figure 6.14 Selected surface discharge a) and its frequency spectra b) over a new insulator at 42500 V using a 50Ω resistor in channel 1 and antennas in channel 2 and 4, AC reference in channel 3.

Summary of results for the frequency spectra of the positive and negative surface discharges over a new insulator			
Applied voltage (V)	**Surface discharge magnitude**	**Frequency content of positive corona discharge**	**Observations**
32800	0.02 V	Nearly flat, no frequency content	Appearance of negative and positive discharge activity most of the activity in the negative half cycle
36900	0.15 V (positive) 0.26 V (negative)	Nearly flat, no frequency content	Discharge activity remains the same.
40800	0.170 V (positive) 0.180 V (negative)	Nearly flat, no frequency content	Decrease in negative discharge activity
42500	0.170 V (positive) 0.180 V (negative)	Components of 100 MHz appears	Positive activity increases, magnitude remains the same and weak radiated signals are received

Table VI Summary of results for the frequency spectra of the positive and negative surface discharges over a new insulator

6.3.2. Time domain analysis of the acquired signals in a new insulator

Analysis in time domain was performed using the MATLAB program described in section 4.3. The methodology consisted of acquiring several samples containing information such as the detected peaks of the discharges in the 50 Ω resistor (discharge current) or the antennas and the AC reference (normally 80 ms). A non processed acquisition is shown in figure 6.15, an analysis of this acquisition, cycle by cycle, was made and the result was graphically shown. The statistical distribution was also processed, and figure 6.16 shows the processed acquired signal (surface

discharge from the 50 Ω resistor) for cycle number 4, showing the detected peaks in the positive and negative half cycles. The discharge activity in the new insulator at 42500 V is low and is more likely to be related to corona activity and occasional surface discharges of low energy. Figure 6.17 shows the total pulse counting of the analyzed cycles and their characteristic pattern. Figure 6.18 shows the statistical distribution of the acquired pulses. It shows that most of the pulses are distributed in the positive half cycle of the AC reference (50-100 degrees) and that they have a positive polarity; few negative pulses appear in the negative half cycle (250-270 degrees). (The complete set of figures showing the pattern of discharges and its statistical distribution in a new insulator at different voltage levels in resistor and antennas is shown in appendix D)

At different applied voltages the average value of positive pulses possesses a random behaviour as pulses may or may not occur in some cycles at some voltage levels. The incidence of positive pulses occurs at all voltage levels, the value of negative discharges is constant at any voltage level.

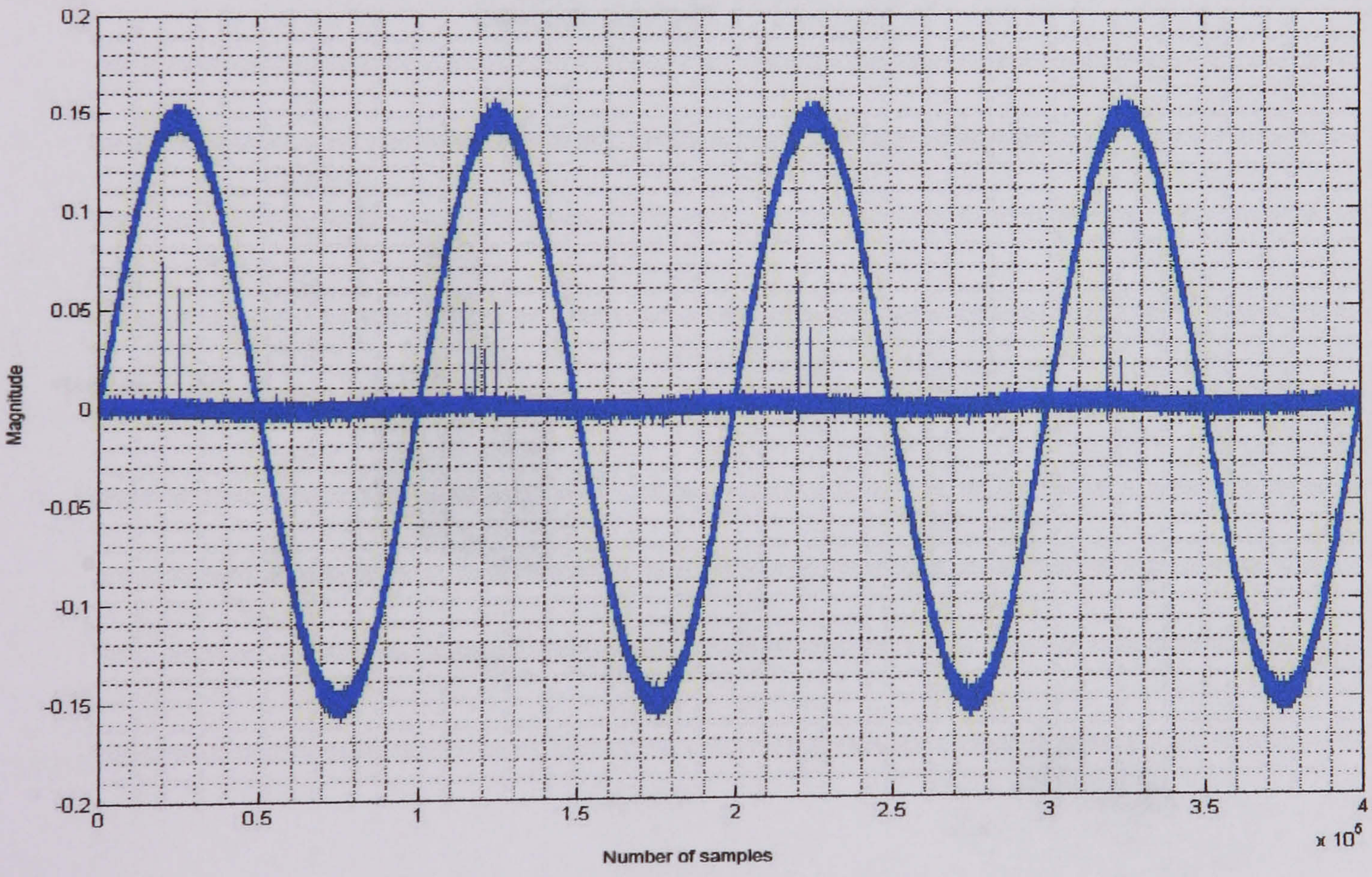

Figure 6.15 Typical unprocessed acquisition (4 cycles, 80ms), showing the received current discharge (50 Ω resistor) in a new chain insulator at 42500 V and the AC reference.

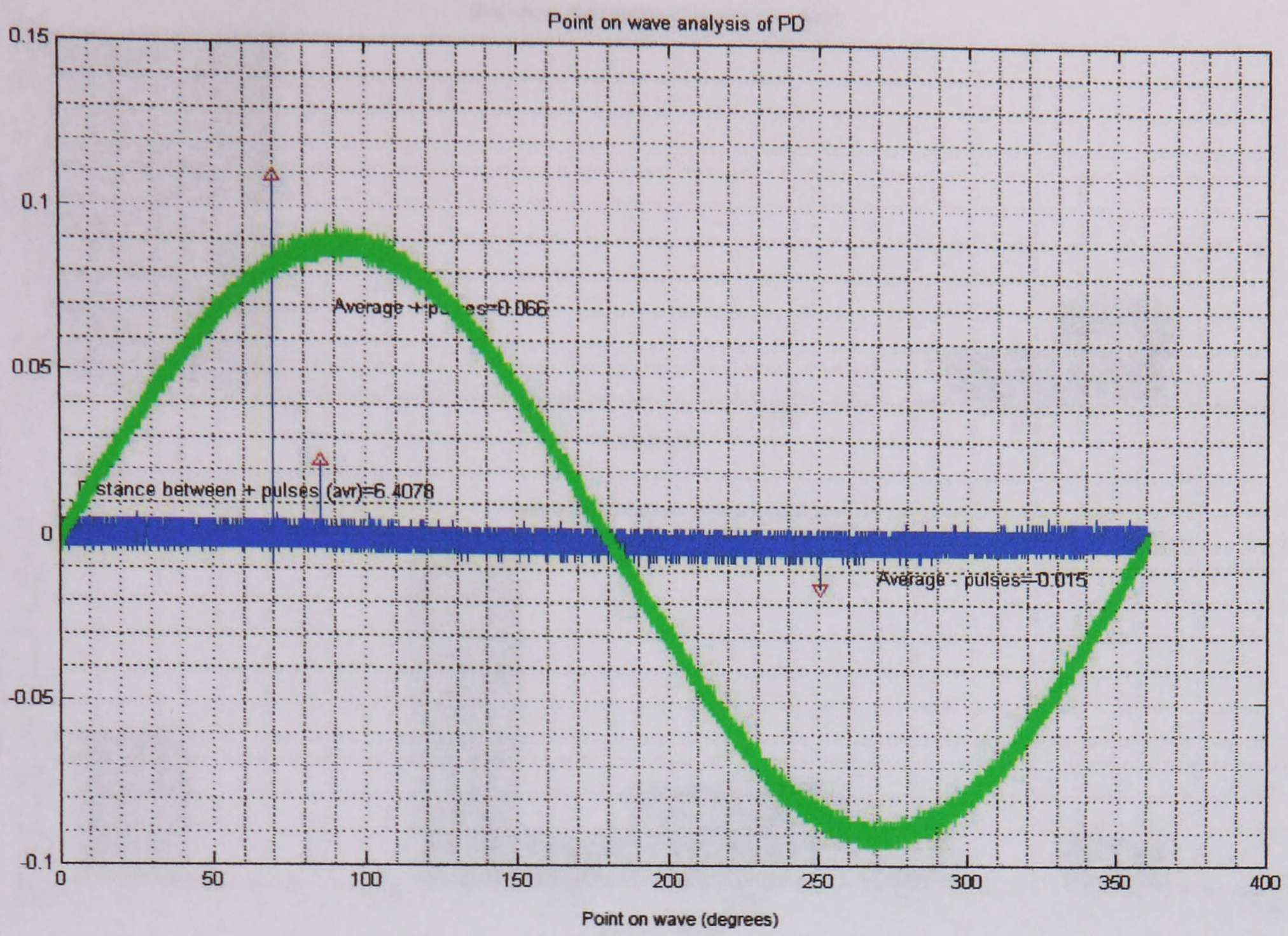

Figure 6.16 Processed acquisition of surface discharges in the 50 Ω resistor and AC reference in a new insulator at 42500 V (one cycle).

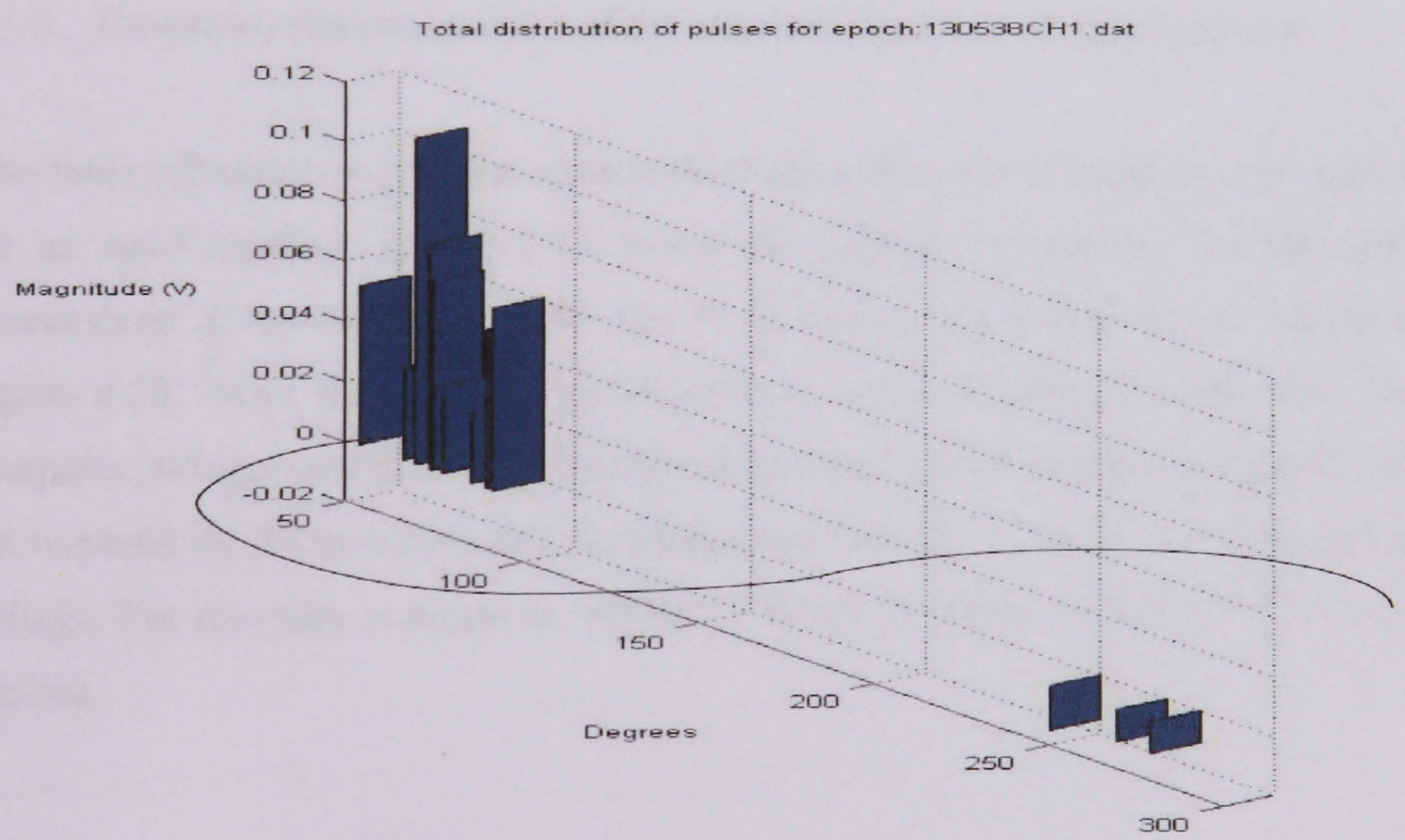

Figure 6.17 Pulse analysis of surface discharges over a new insulator at 42500 V in the 50 Ω resistor a) Pulse distribution and b) statistical distribution.

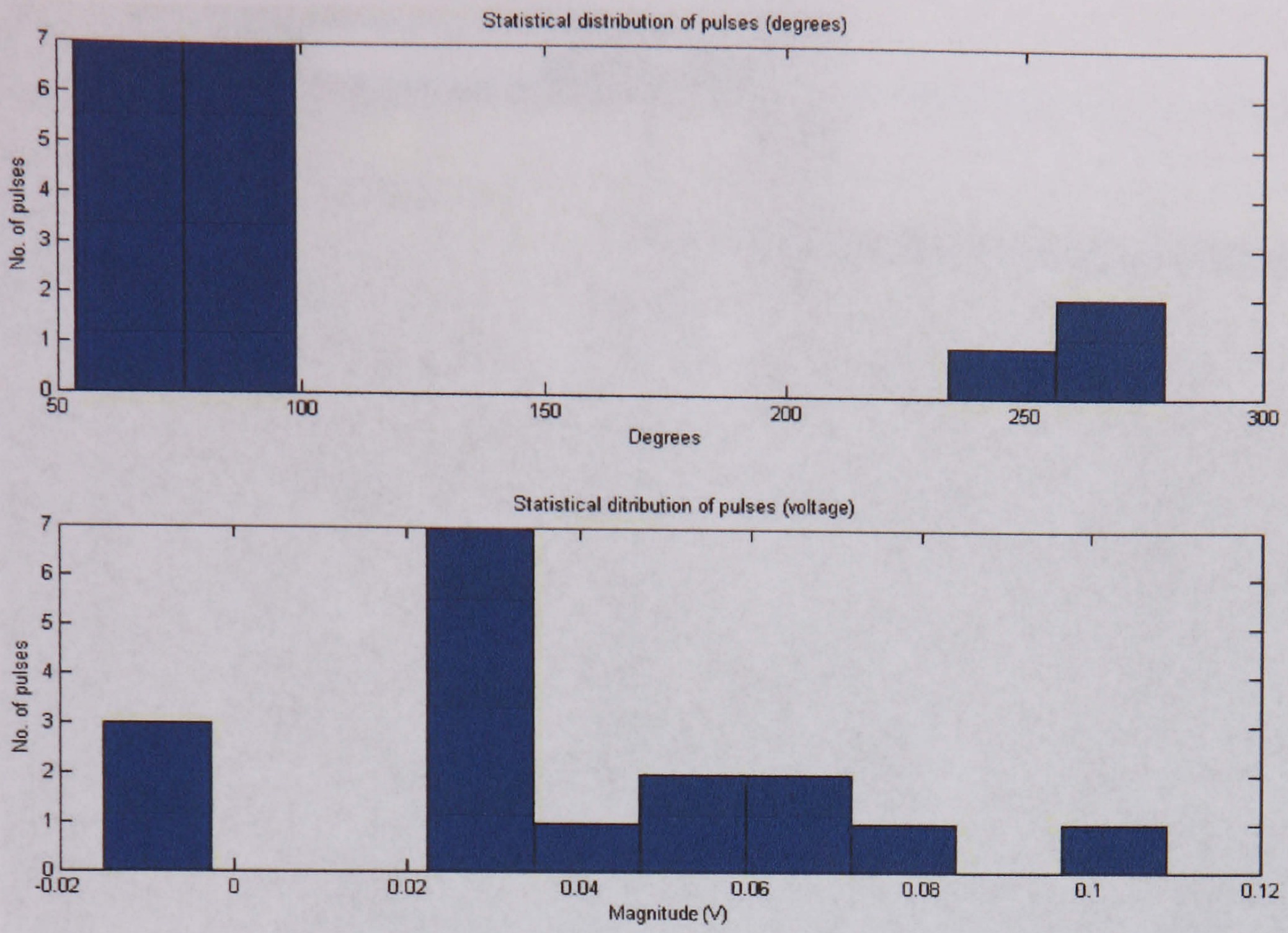

Figure 6.18 Pulse analysis of surface discharges over a new insulator at 42500 V in the 50 Ω resistor a) Phase distribution and b) pulse magnitude distribution.

6.3.3. Frequency domain analysis of the acquired signals in an aged insulator

The same procedure to produce surface discharges over a new insulator was applied for an aged insulator (figure 6.19 shows the general arrangement for this test). Screenshots of the oscilloscope for the 50 Ω resistor measurements are shown in figure 6.20. Note that antenna measurements were possible for this test. The inception voltage needed to create surface discharges is relatively low compared with the required for the new insulator; discharges are evident at low levels of the applied voltage. For this test, voltages of 34830 V, 36900 V, 40800 V and 42500 V were applied.

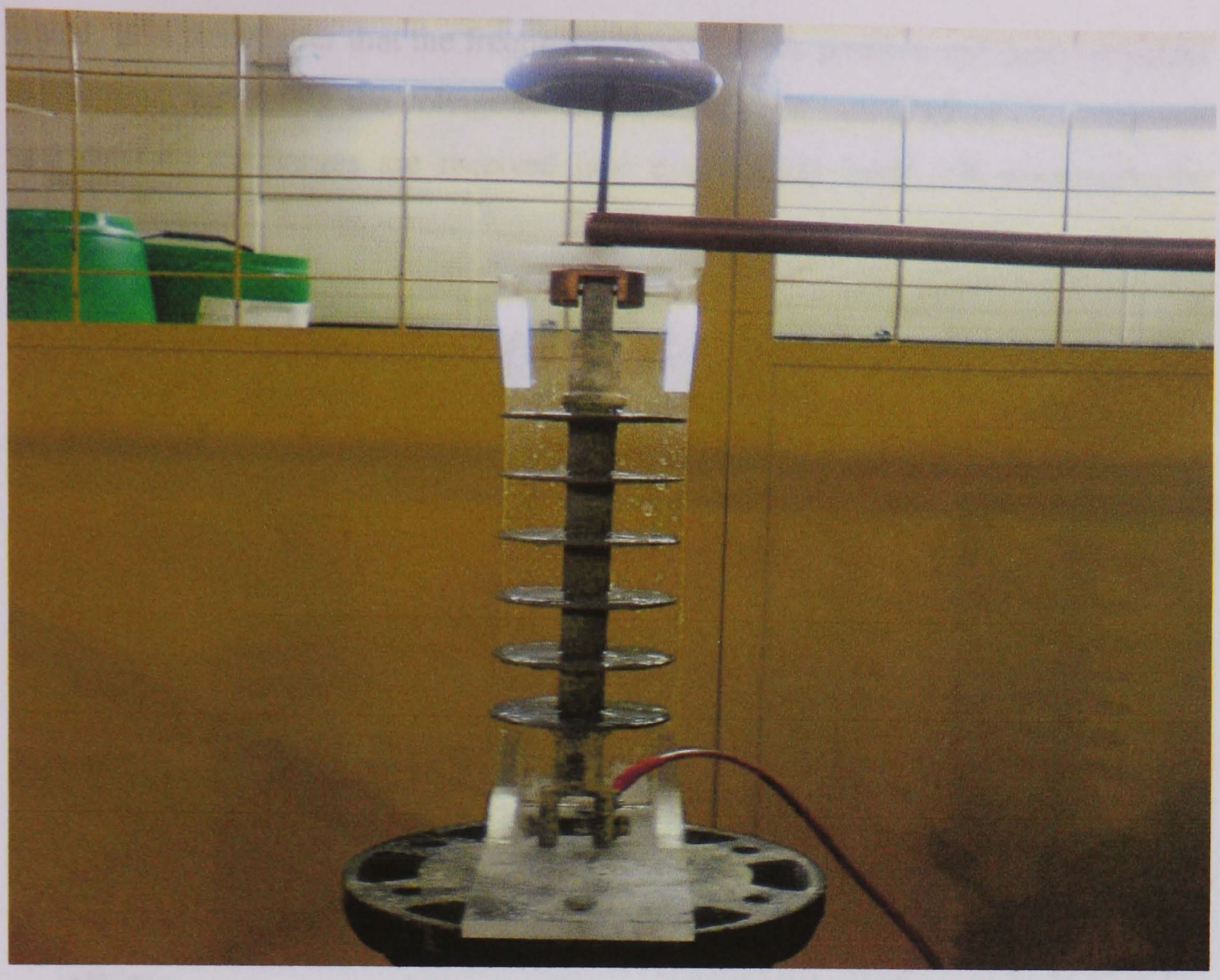

Figure 6.19 General arrangements for the aged insulator test

At 34830 V (see figure 6.20a) it is possible to observe positive and negative activity in the 50 Ω resistor but no signal is received at the antennas; discharges appear in the positive half cycle of the AC reference, negative discharges appear as well but with small magnitude when compared to the positive. The magnitude of the conducted discharge is high (0.2 V) with frequency components below 200 MHz. At 40800 V (see figure 6.21a) the magnitude of positive discharges has increased significantly (0.8 V). Negative discharges remain with the same magnitude at this voltage, but due to the high magnitude of positive discharges, it is not possible to observe any activity. At 40800 V it is possible to receive radiated surfaces discharge signals from the antenna (see figure 6.21a antenna 2). Although the magnitude is very small, the polarity of the radiated discharge is negative in distinction to the conducted discharge which has positive polarity. This condition was observed for all the radiated discharges received by the disk cone antenna and is attributed to the intrinsic design of the antenna. Apart from this effect, the radiated signal is similar to the conducted

signal. It is show latter that the frequency spectra of the positive and negative pulses is identical. Increasing the voltage to 42500 V causes a similar effect i.e. conducted and radiated discharges are received (see figure 6.22) Table VII summarize the obtained results.

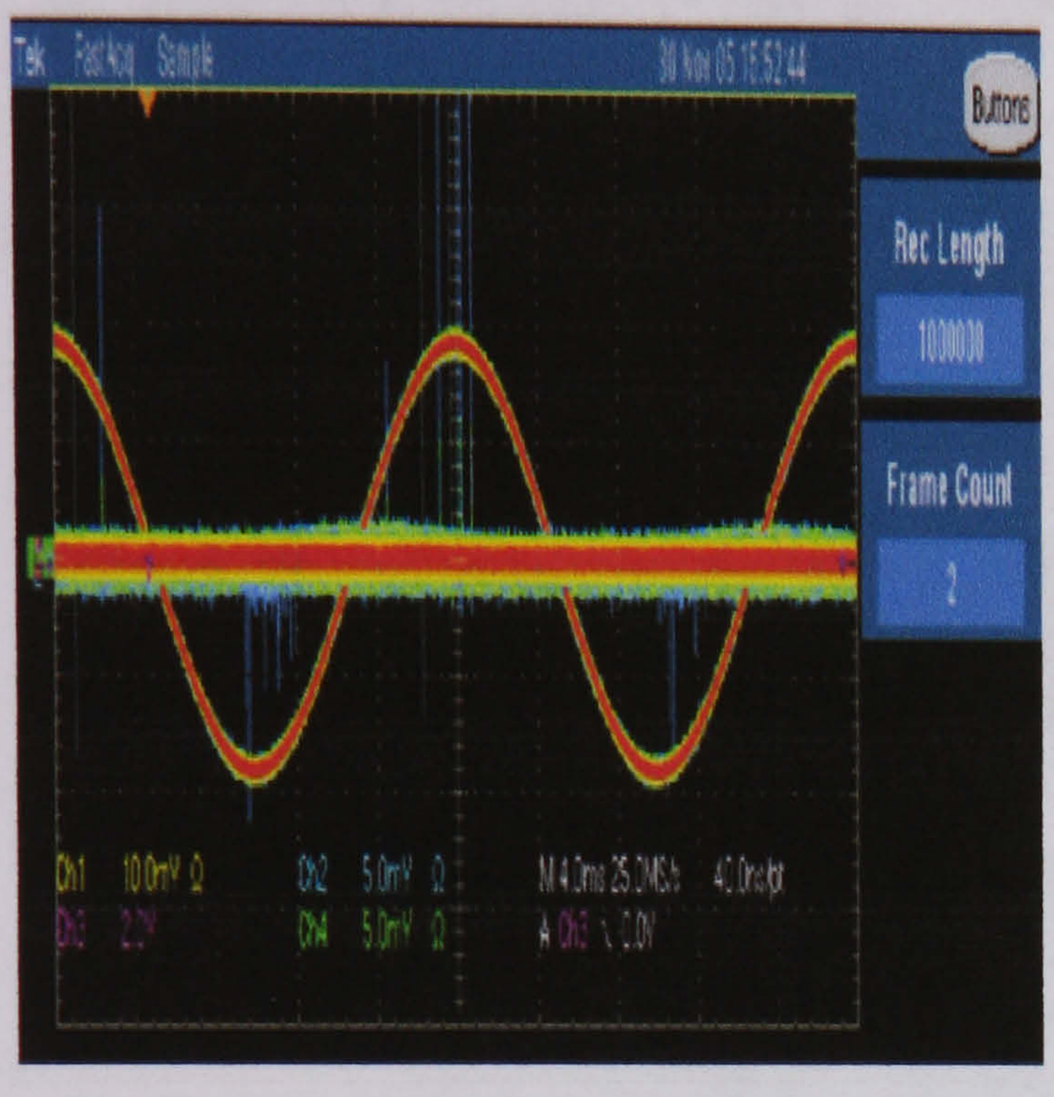

a) Surface discharges using antenna and AC reference signal at 34830 Volts

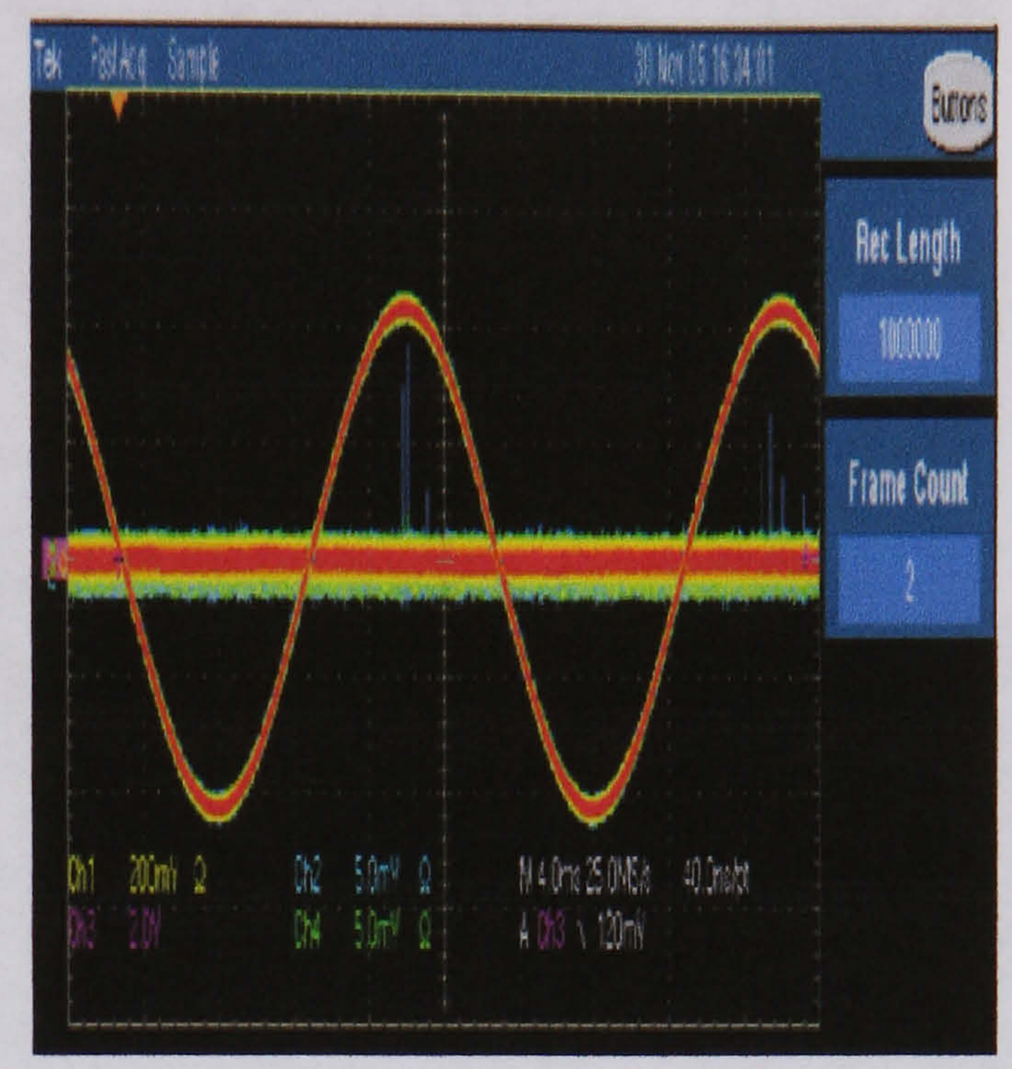

c) Surface discharges using antenna and AC reference signal at 40800 Volts

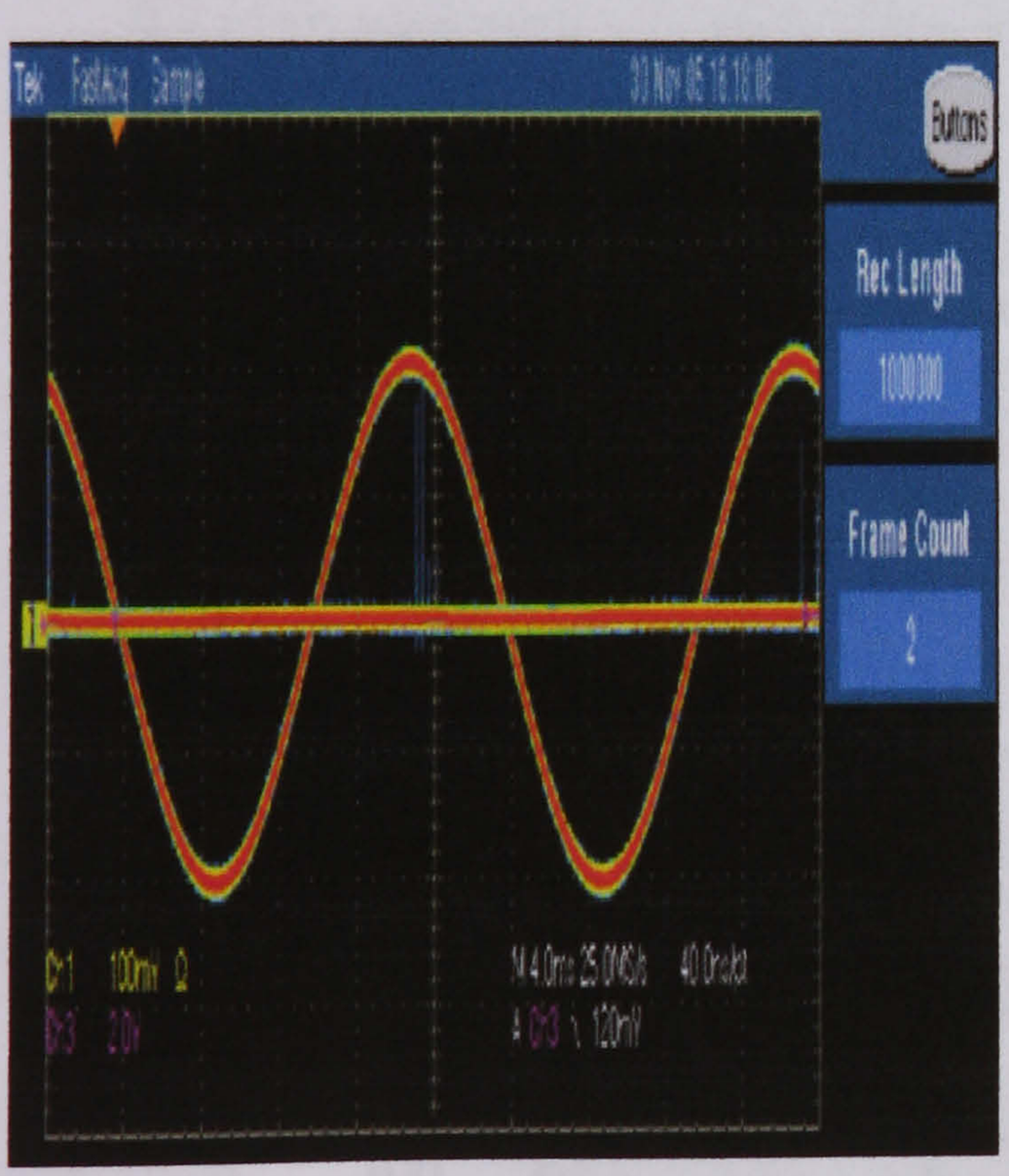

b) Surface discharges using antenna and AC reference signal at 36900 Volts

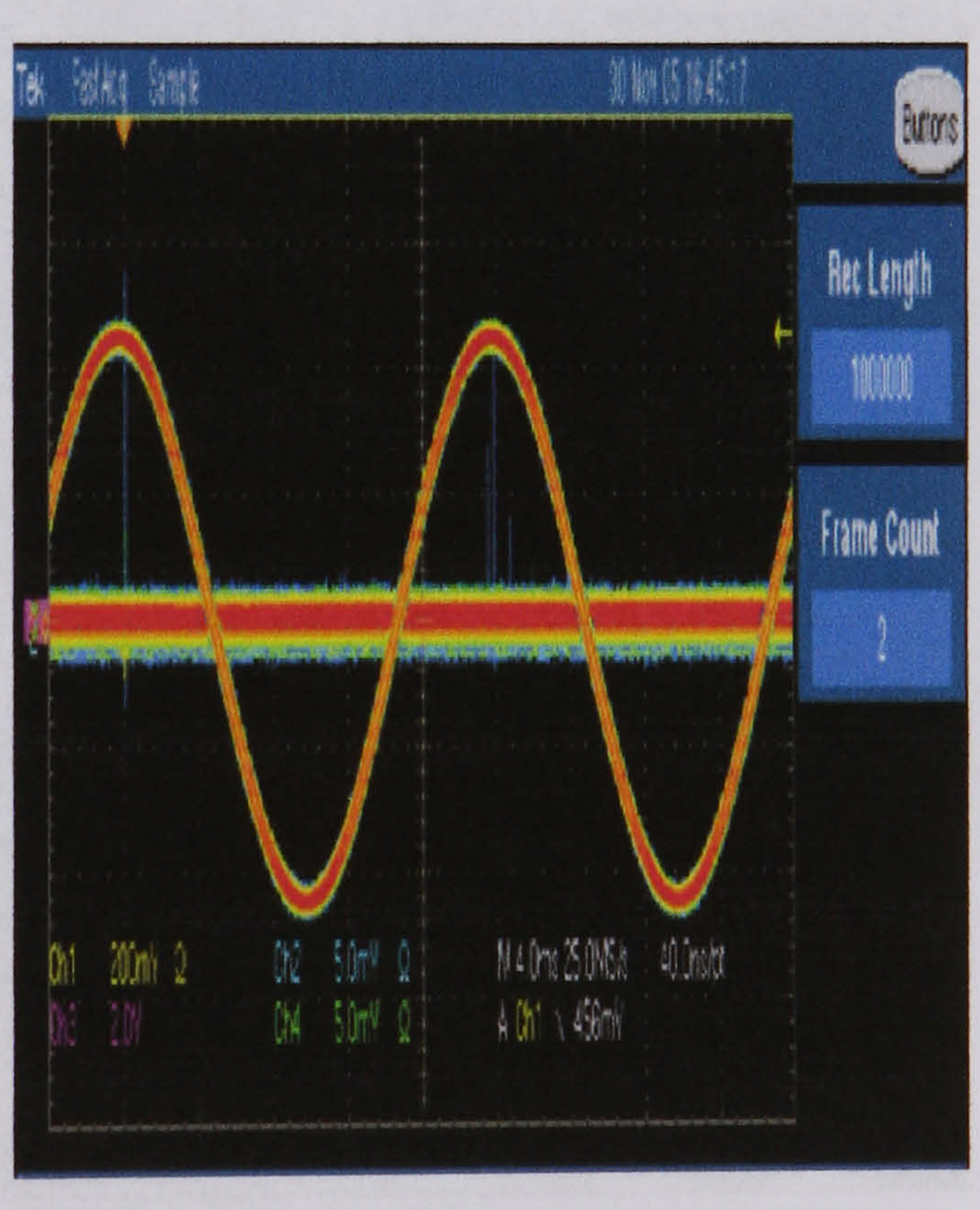

d) Surface discharges using antenna and AC reference signal at 42500 Volts

Figure 6.20 Acquired surface discharges using a 50 Ω resistor in channel 1 and AC reference in channel 2 at a) 34830 V, b) 36900 V, c) 40800 V and d) 42500 V.

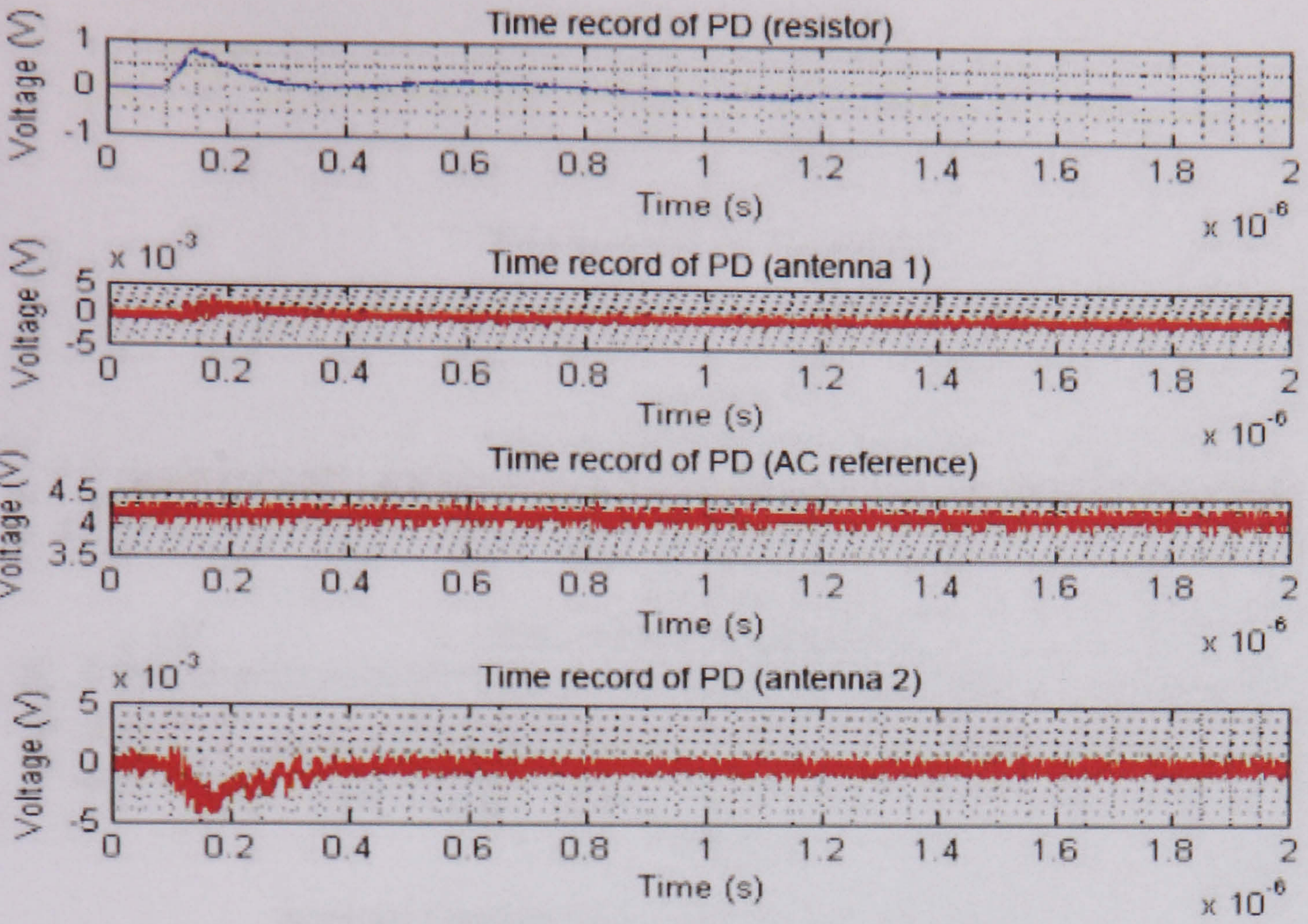

a) Selected surface discharge in an aged insulator at 40800 V

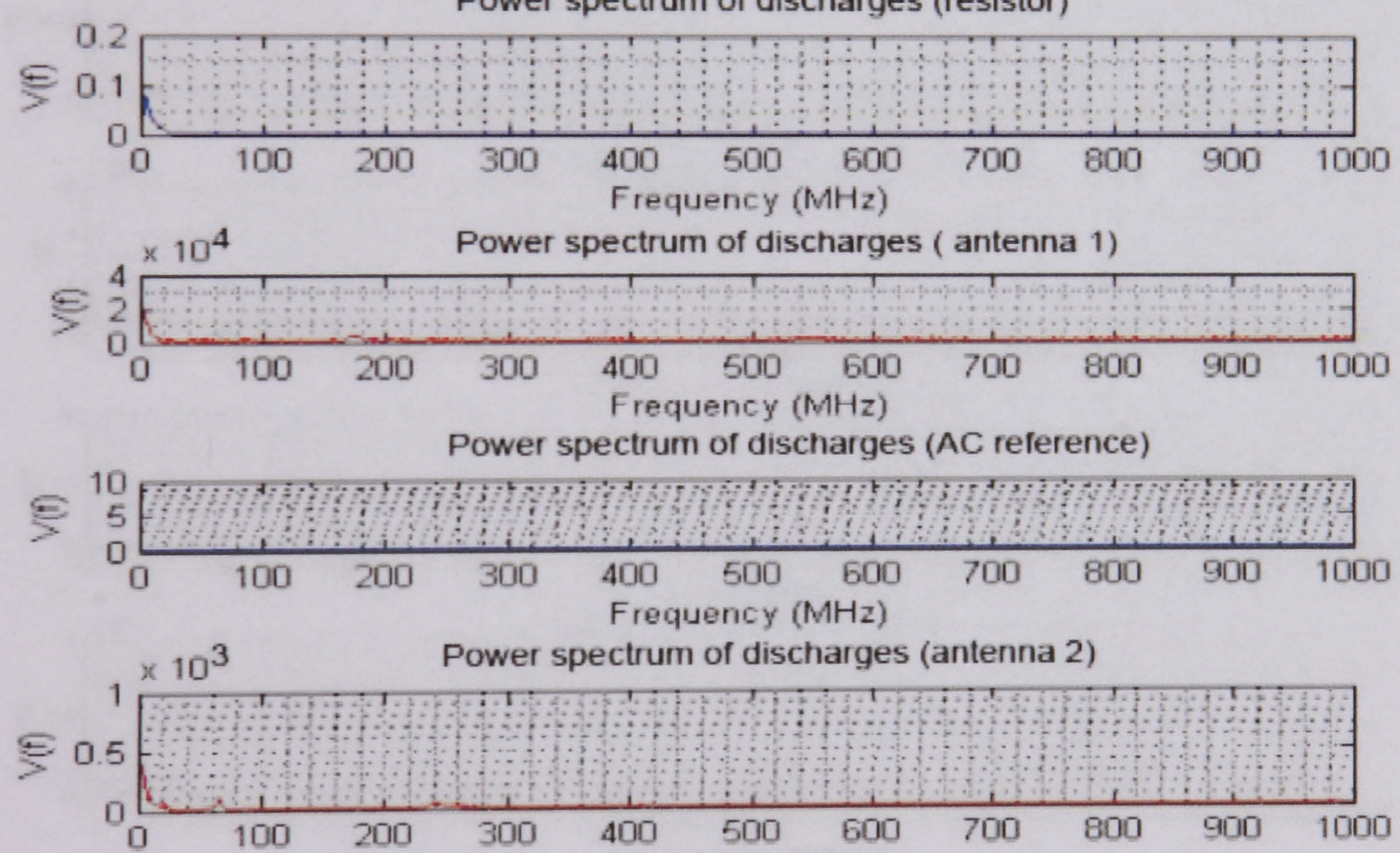

b) Frequency spectra of the selected surface discharge over an aged insulator at 40800 V

Figure 6.21 Acquired surface discharge a) and its frequency spectra b) using a 50 Ω resistor in channel 1, AC reference in channel 2, antenna 1 in channel 3 and antenna 3 in channel 4, at 40800 V

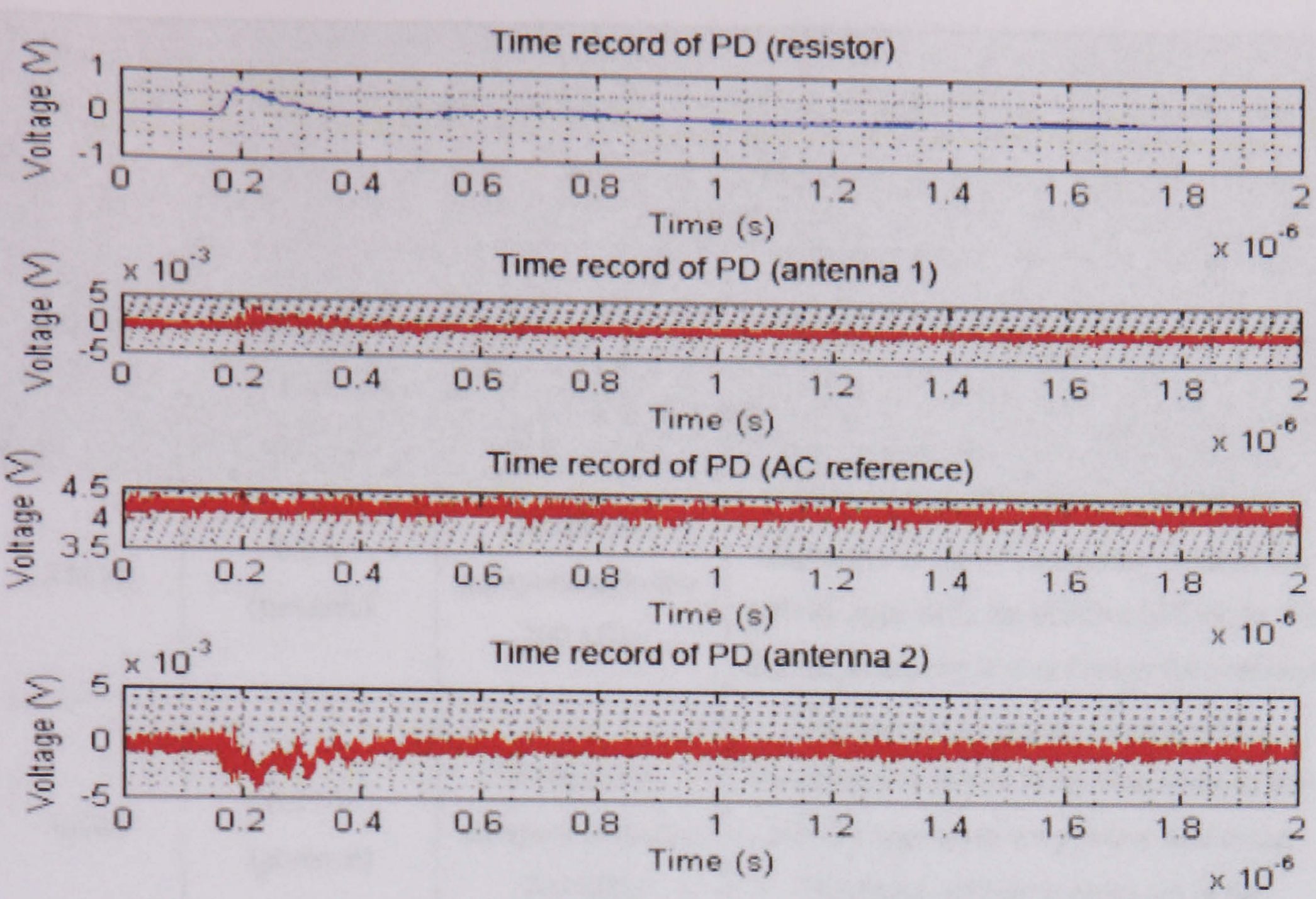

a) Selected surface discharge in an aged insulator at 42500 V

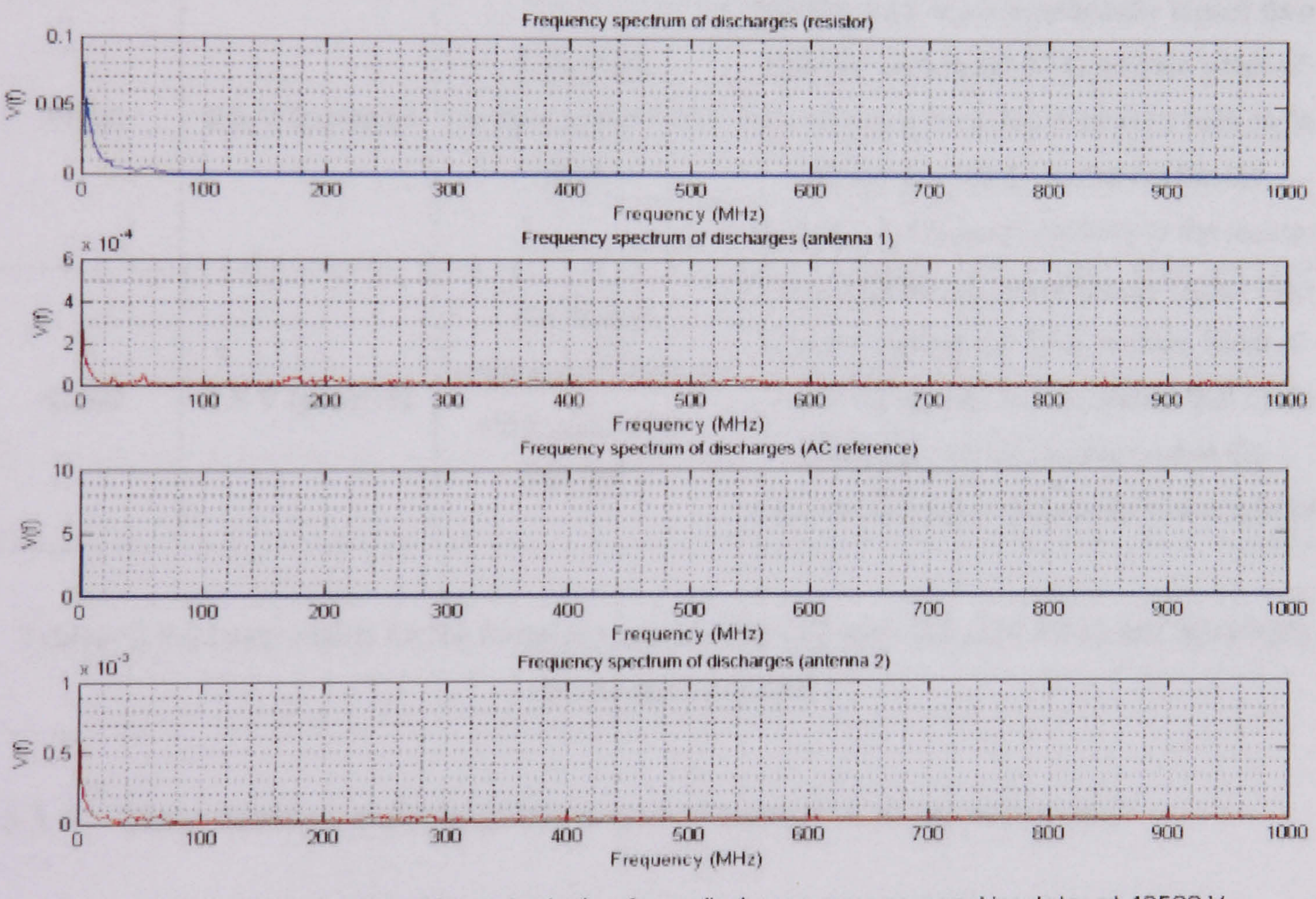

b) Frequency spectra of the selected surface discharge over an aged insulator at 42500 V

Figure 6.22 Acquired surface discharge a) and its frequency spectra b) using a 50 Ω resistor in channel 1, AC reference in channel 2, antenna 1 in channel 3 and antenna 3 in channel 4, at 42500 V

Summary of results for the frequency spectra of the positive and negative surface discharges over an aged insulator			
Applied voltage (V)	**Surface discharge Magnitude (50 Ω resistor)**	**Frequency content of positive corona discharge**	**Observations**
34830	0.2 V (positive)	Frequency components below 200 MHz	Appearance of negative and positive discharges in the 50 Ω resistor. Most of the activity appears in the positive half cycle. No discharge activity is observed in the antennas
36900	0.35 V (positive)	Frequency components below 200 MHz	Appearance of negative and positive discharges in the 50 Ω resistor. Most of the activity appears in the positive half cycle. Discharge activity is observed in the antennas, but opposite polarity to the resistor
40800	0.8 V (positive)	Frequency components of 100 MHz	Positive discharges significantly higher than negative ones in the 50 Ω resistor. Most of the activity appears in the positive half cycle. Discharge activity is observed in the antennas, but opposite polarity to the resistor
42500	0.8 V (positive)	Frequency components of 200 MHz and below 100 MHz	Positive discharges significantly higher than negative ones in the 50 Ω resistor. Most of the activity appears in the positive half cycle. Discharge activity is observed in the antennas, but opposite polarity to the resistor

Table VII Summary results for the frequency spectra of the positive and negative surface discharges over an aged insulator

6.3.4. Time domain analysis of the acquired signals in an aged insulator

The inception voltage of surface discharges in the aged insulator is constant from 40800 V onwards. Due to this effect, for the time domain analysis only surface discharges incepting at 42500 V were considered. The signal processing was made using the coded MATLAB program. There were acquired conducted and radiated

signals as well as the AC reference signal. Figure 6.23 shows the processed acquired signals for the 50 Ω resistor and antenna 1 (one cycle). In these figures, detected positive and negative pulses are shown as well as the AC waveform used as point on wave information. It can be seen that positive and negative pulses appears and tend to group in the first half of the positive and negative half cycles of the AC waveform. The magnitude of the acquired signal is higher in the conducted discharge signal than in the antenna signal. This effect is expected and is due to the attenuation of the radiation from the surface discharge. The characteristic pattern of the acquired pulses within the processed cycles can be seen in figure 6.24 for the current discharge and antenna 1, note the differences in the magnitude of the discharges measured by the 50 Ω resistor compared with the ones received in the antennas. Discharges tend to group between 20 and 125 degrees, 160 and 300 degrees and some components around 350 degrees. The statistical distribution of the acquired discharges (see figure 6.25) shows that the distribution of the conducted and radiated discharges remain the same along the AC reference waveform. However the number of acquired discharges change, the statistical distribution of discharges also shows that the polarity of the acquired pulses is erratic. The number of positive discharges is higher compared to the negative ones in the 50 Ω resistor and the number of negative discharges is higher in the antennas, i.e. the inverse polarity of the pulses occurring in the resistor, that effect was mentioned before in the corona analysis.

Figure 6.24 also shows differences between positive pulses in the 50 Ω resistor, and antenna 1. The tendency in the resistor and antenna 1 when high voltage is applied gradually is to reduce the distance between pulses. Figure 6.25 a) and b) shows the differences between negative pulses, and it is possible to observe that the behavior of the pulses in the resistor is very similar to the one in the antenna 1, i.e. both show a similar distribution of the acquired pulses along the point on wave information (AC waveform). The complete set of figures showing the pattern of discharges and its statistical distribution in an aged insulator at different voltage levels in resistor and antennas is shown in appendix E.

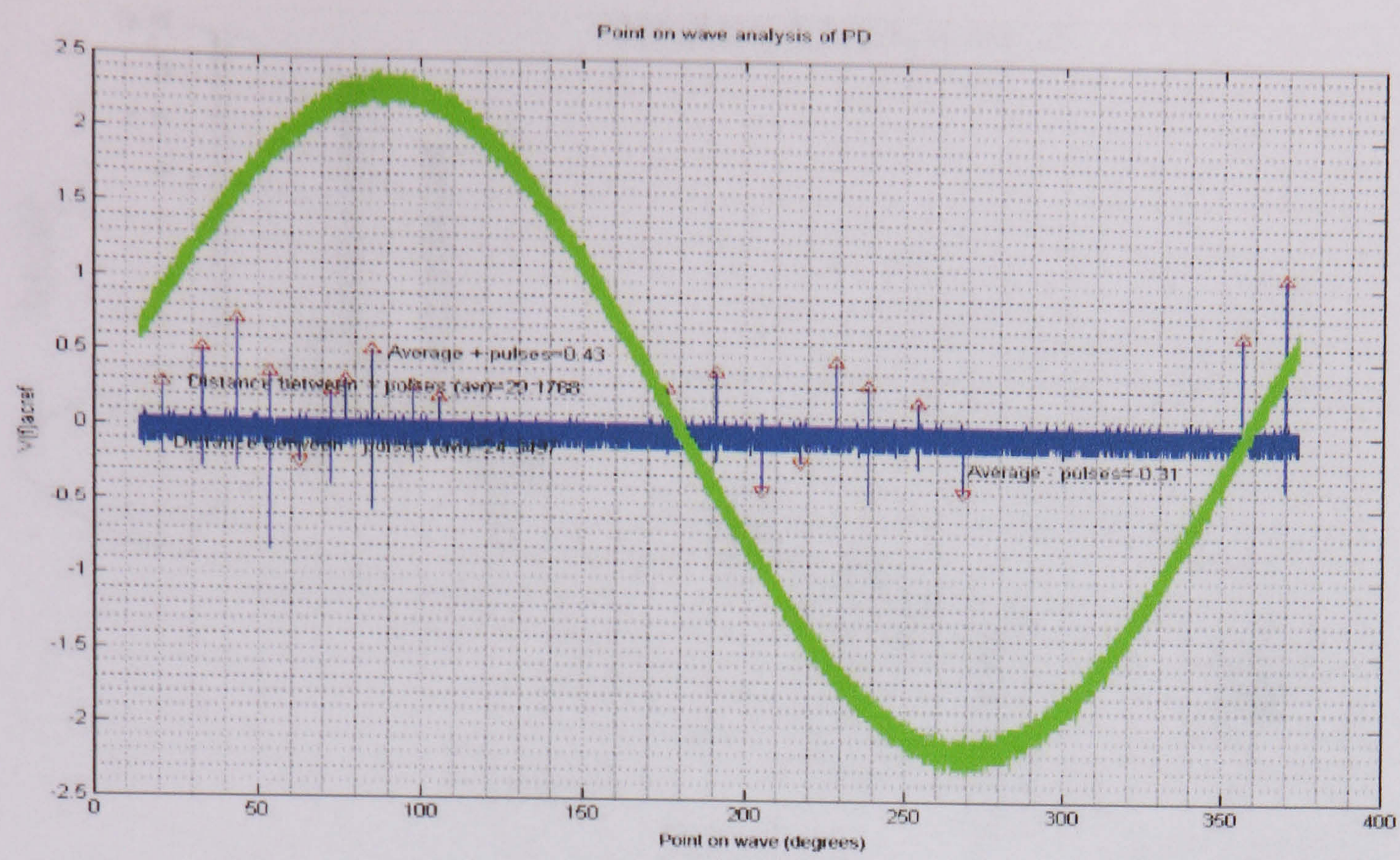

a) Aged insulator at 42500 V (resistor)

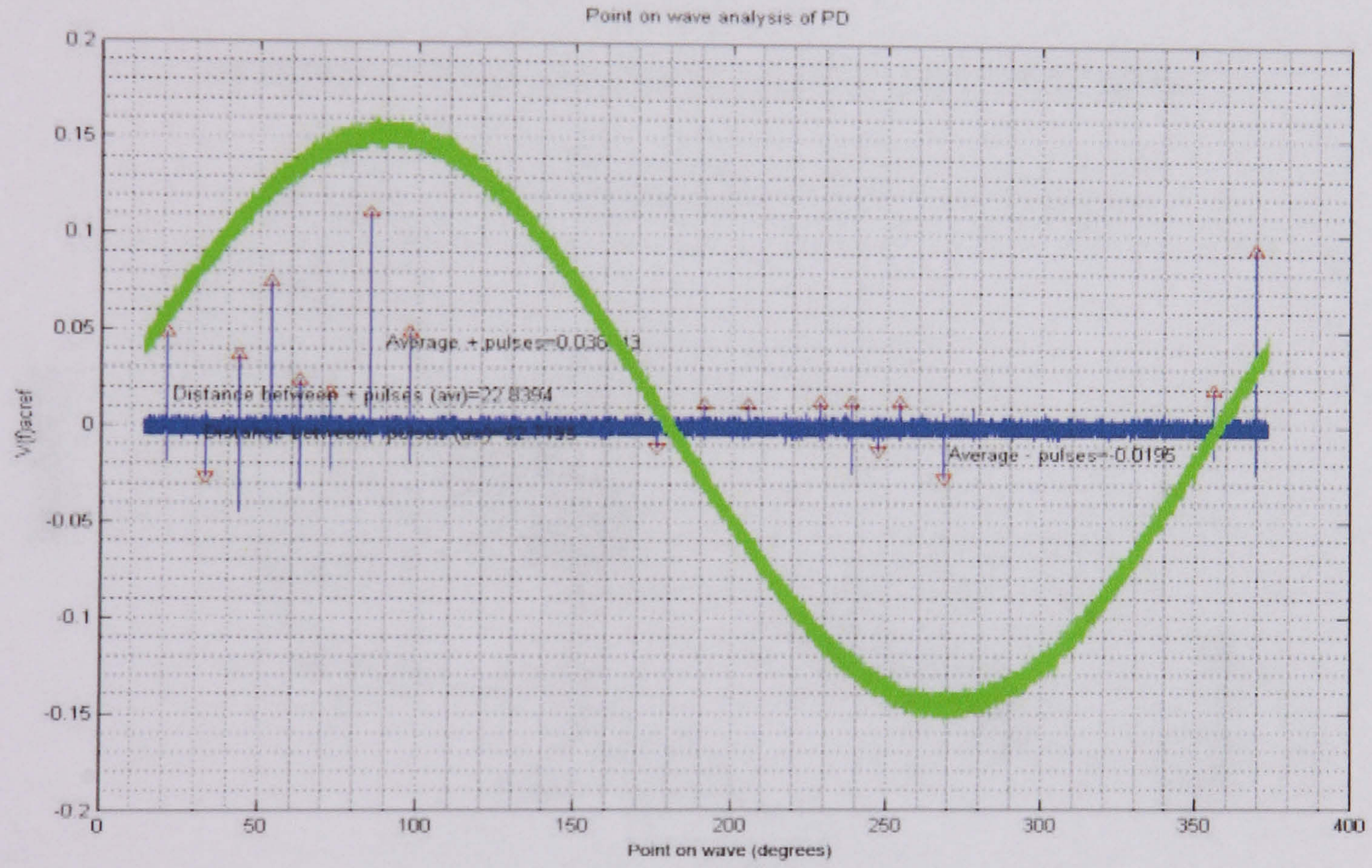

b) Aged insulator at 42500 V (antenna 1)

Figure 6.23 Processed acquisition of surface discharges and AC reference in an aged insulator at 42500 V (one cycle) in, a) 50 Ω resistor and b) antenna 1

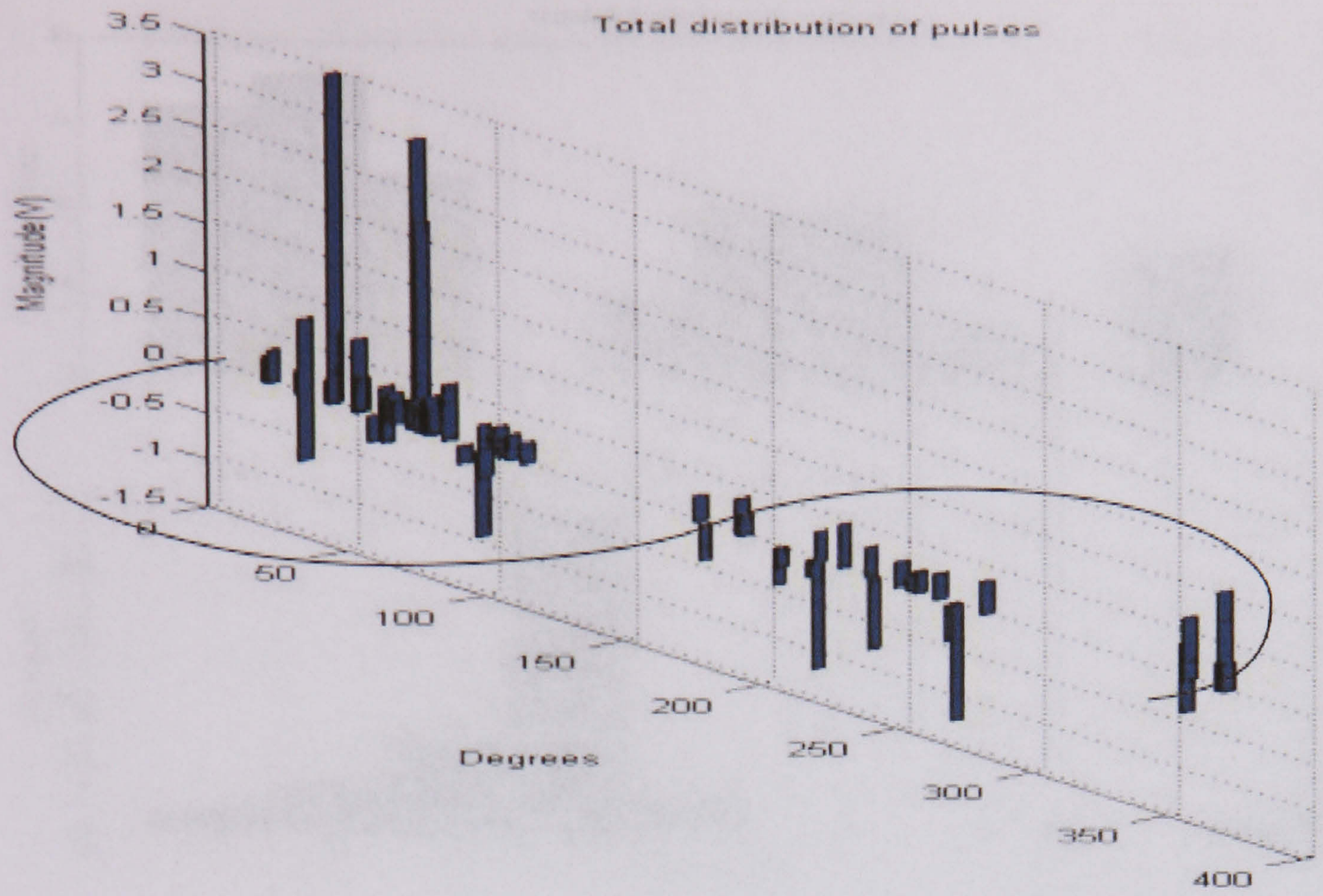

a) Distribution of surface discharges over an aged insulator at 42500 V (resistor)

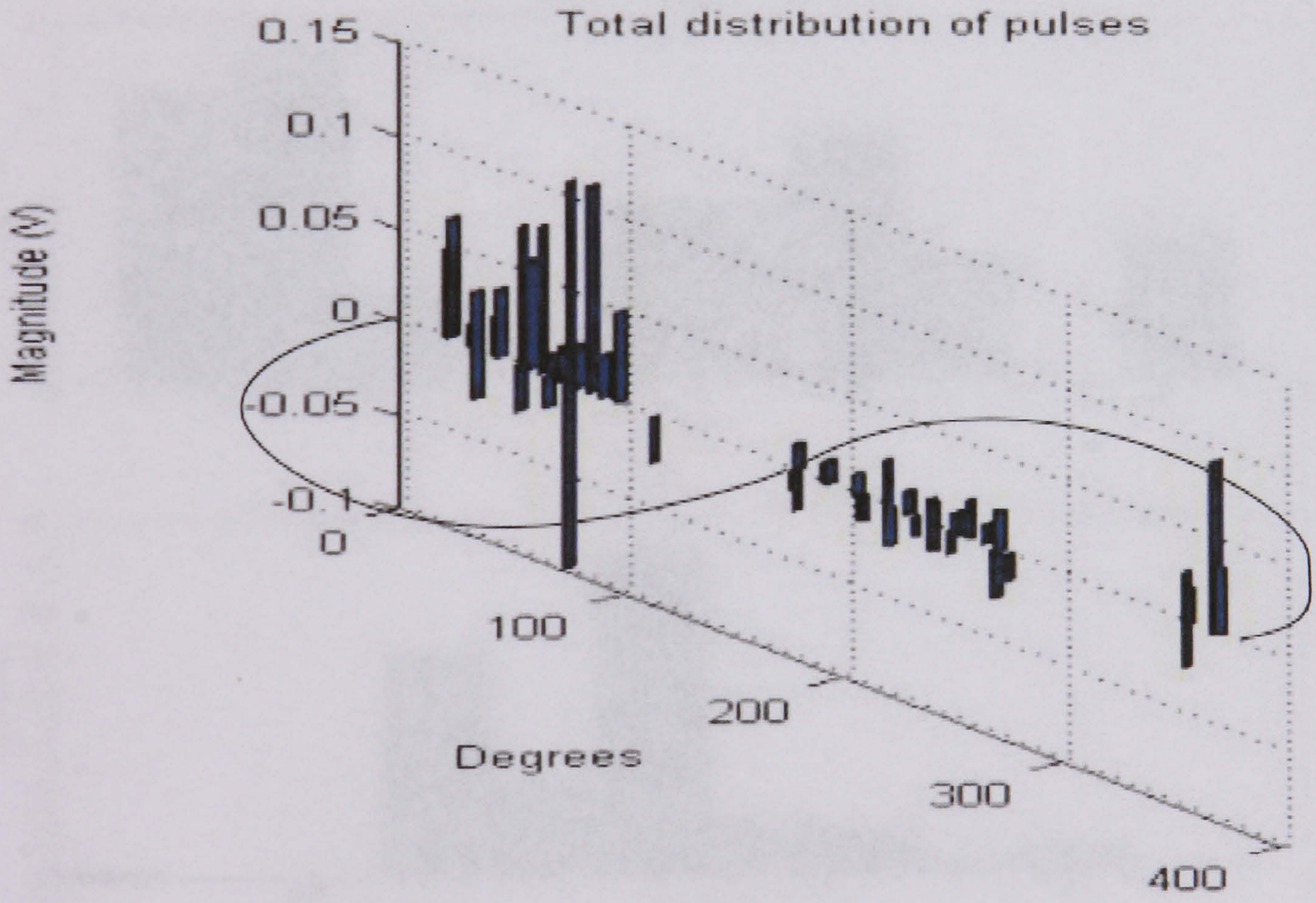

b) Distribution of surface discharges over an aged insulator at 42500 V (antenna 1)

Figure 6.24 Distribution of surface discharges over an aged insulator at 42500 V in a) 50 Ω resistor, and b) antenna 1

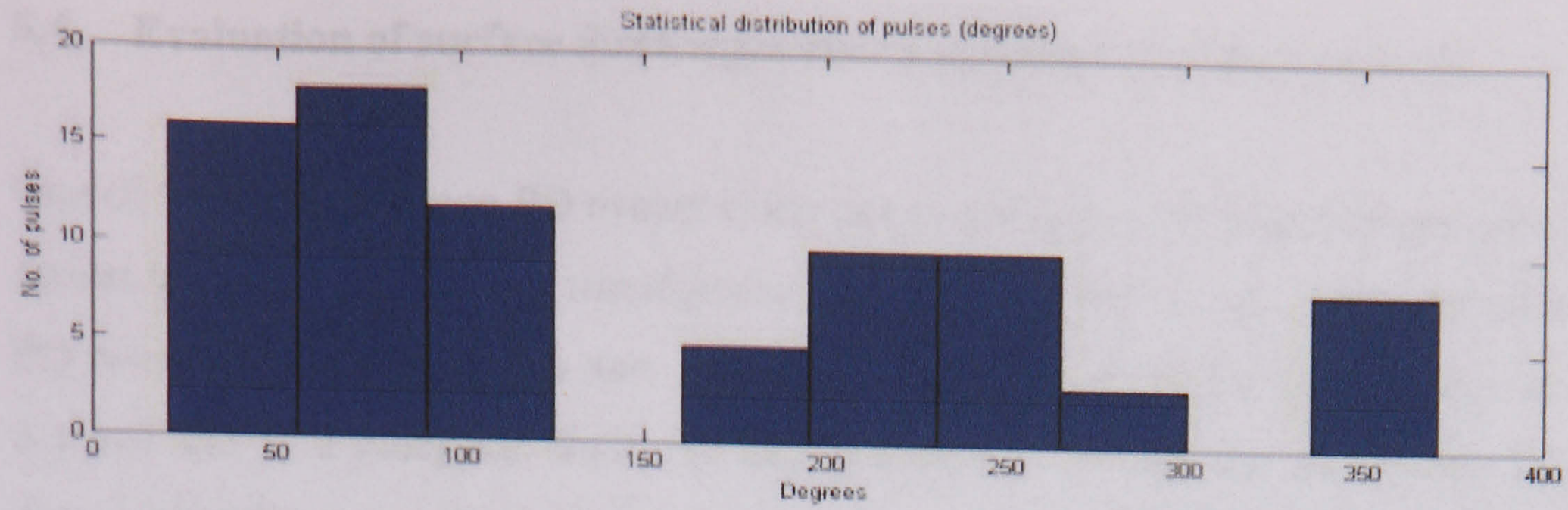

a) Statistical distribution of surface discharges over an aged insulator at 42500 V (resistor)

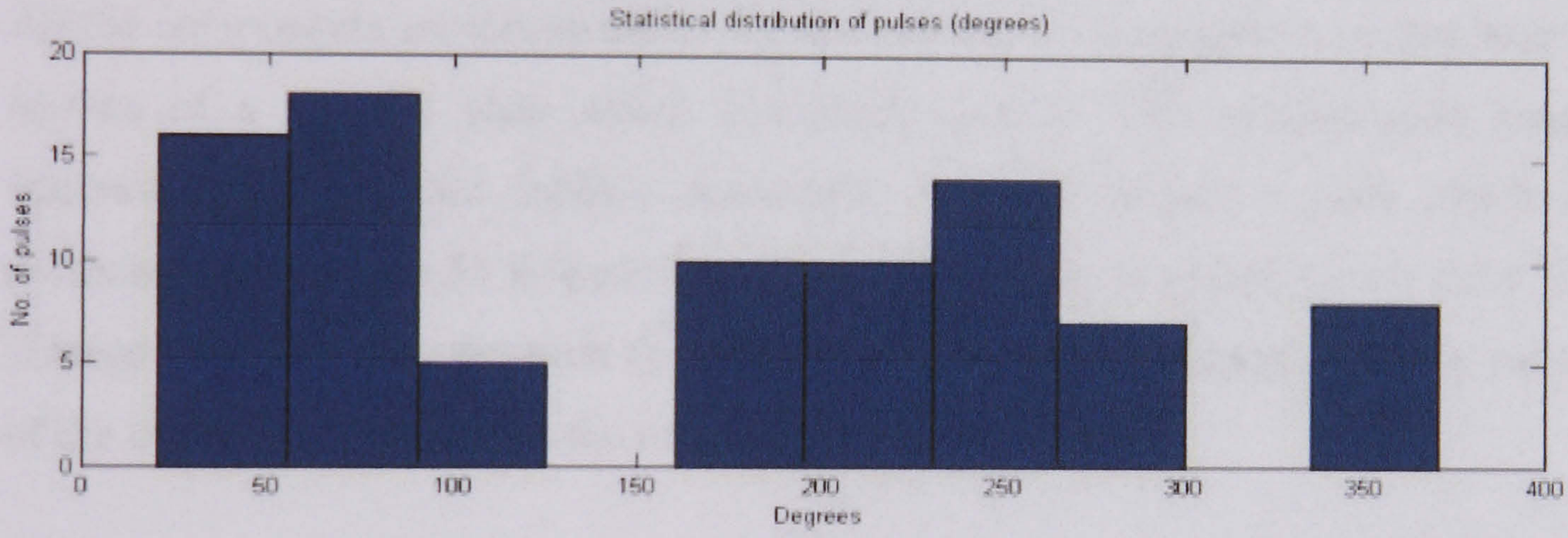

b) Statistical distribution of surface discharges over an aged insulator at 42500 V (antenna 1)

Figure 6.25 Statistical distribution of surface discharges over an aged insulator at 42500 V in a) 50 Ω resistor and b) antenna 1

6.4. Evaluation of surface discharges over a pressboard immersed in oil

One of the most common PD events is the one occurring in HV transformers such as power transformers, voltage transformers, current transformers etc. Although certain PD content is allowed within new and used transformers [6.10], the fast evolution of a small PD to a complete discharge can completely damage the equipment. Most power transformers utilize oil as insulating media, and PD developing inside this power equipment shows different behavior compared to PD's in air, as it was described in chapter 5. PD's from within power transformers normally cause discharges over the surface of solid dielectrics due to interfacial polarization effect where an intense electrical field is applied [6.12]. In order to assess this kind of PD and its radiated electromagnetic wave, a laboratory test was designed. This test consisted of a transparent container filled with dielectric oil and a solid dielectric plate (pressboard) in the bottom of the container. The high voltage is applied using a rod with a sharp tip (5mm diameter) which touches the surface of the dielectric plate. All the components are immersed in dielectric oil and the container is placed over the surface of a metallic plate which is directly earthed. This configuration creates conducted and radiated surface discharges over the dielectric plate which are measured through the 50 Ω earth resistor and the antennas placed on the floor. The voltage level was selected such that it does not create any discharge over the surface of the oil. Figure 6.26 shows the described test configuration.

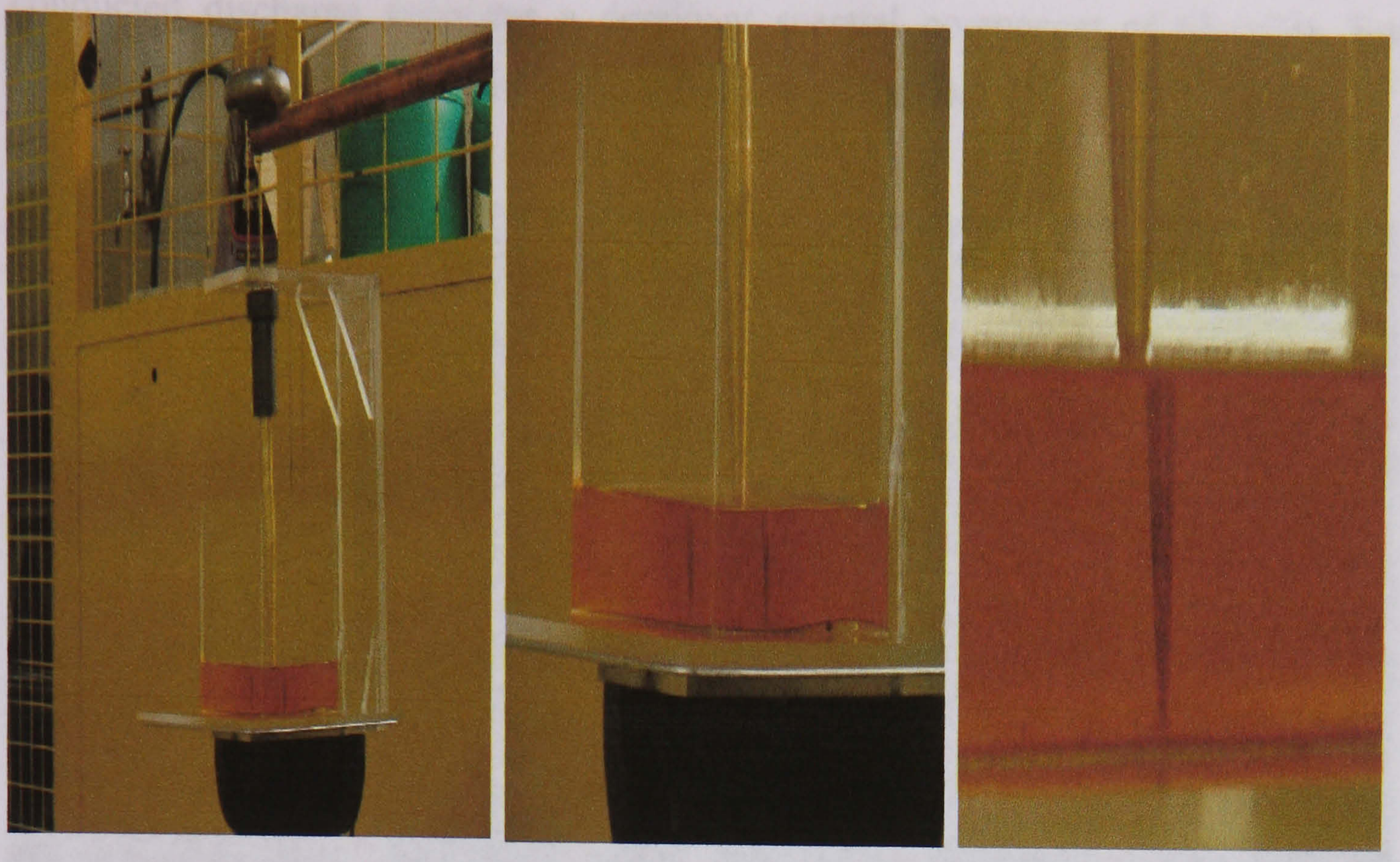

Figure 6.26 Configuration point-oil-pressboard interface

6.4.1. Frequency domain analysis

The applied voltage for this test was fixed at 18440 V since at this voltage the inception of surface discharges on the pressboard was achieved. Three methods to acquire the conducted and radiated discharges were used using the 50Ω resistor, and three antennas in different position, acquisitions consisting of 2 AC cycles were used for this analysis. Figure 6.27 show a screenshot of the oscilloscope showing the AC reference and the 50 Ω resistor of the selected acquisitions.

Applying a voltage of 18440 V to the pressboard immersed in oil causes positive and negative pulses with a notably frequency content, clustering in the first half of the positive and negative AC reference. Spaces between discharges are wider when comparing to the ones of the surface discharges over insulators in air. Conducted discharges were acquired in the 50 Ω resistor and *radiated discharges were received at the antennas* (see figure 6.28 antennas 1, 2, 3). When the frequency spectrum of the acquired signal is analyzed (see figure 6.29) dominants components of 80 MHz of the antenna in channel 1 and 138 MHz of the antenna in channel 2 are found. The

conducted discharge generates a dominant spectral component of 58 MHz. For antenna 3 no important spectral components are noticeable.

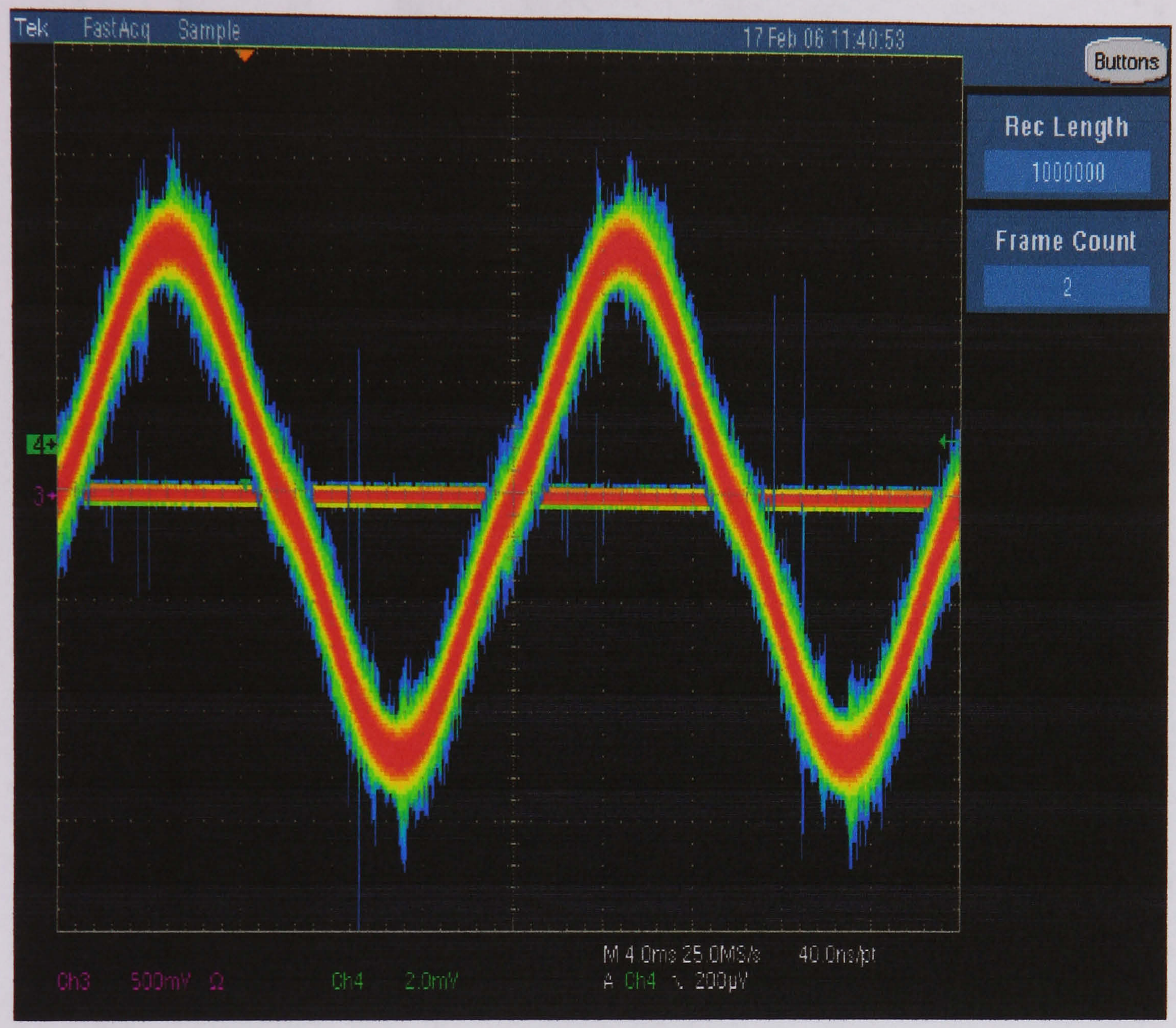

Figure 6.27 Surface discharges using 50 Ω resistor and AC reference signal at 18440 Volts

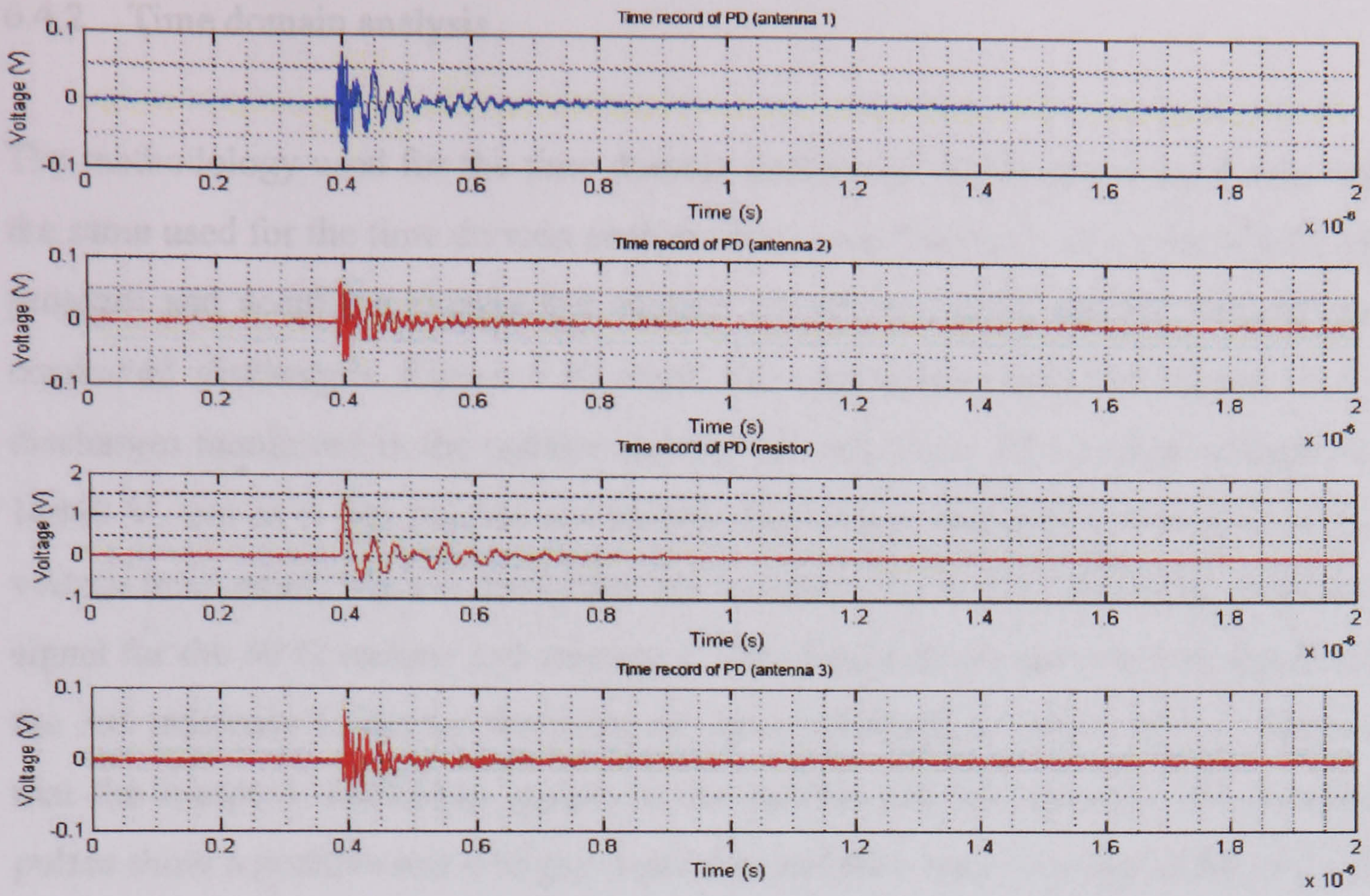

Figure 6.28 Selected surface discharge at 18440 V using a 50 Ω resistor in channel 3 and antennas in channel 1, 2 and 4

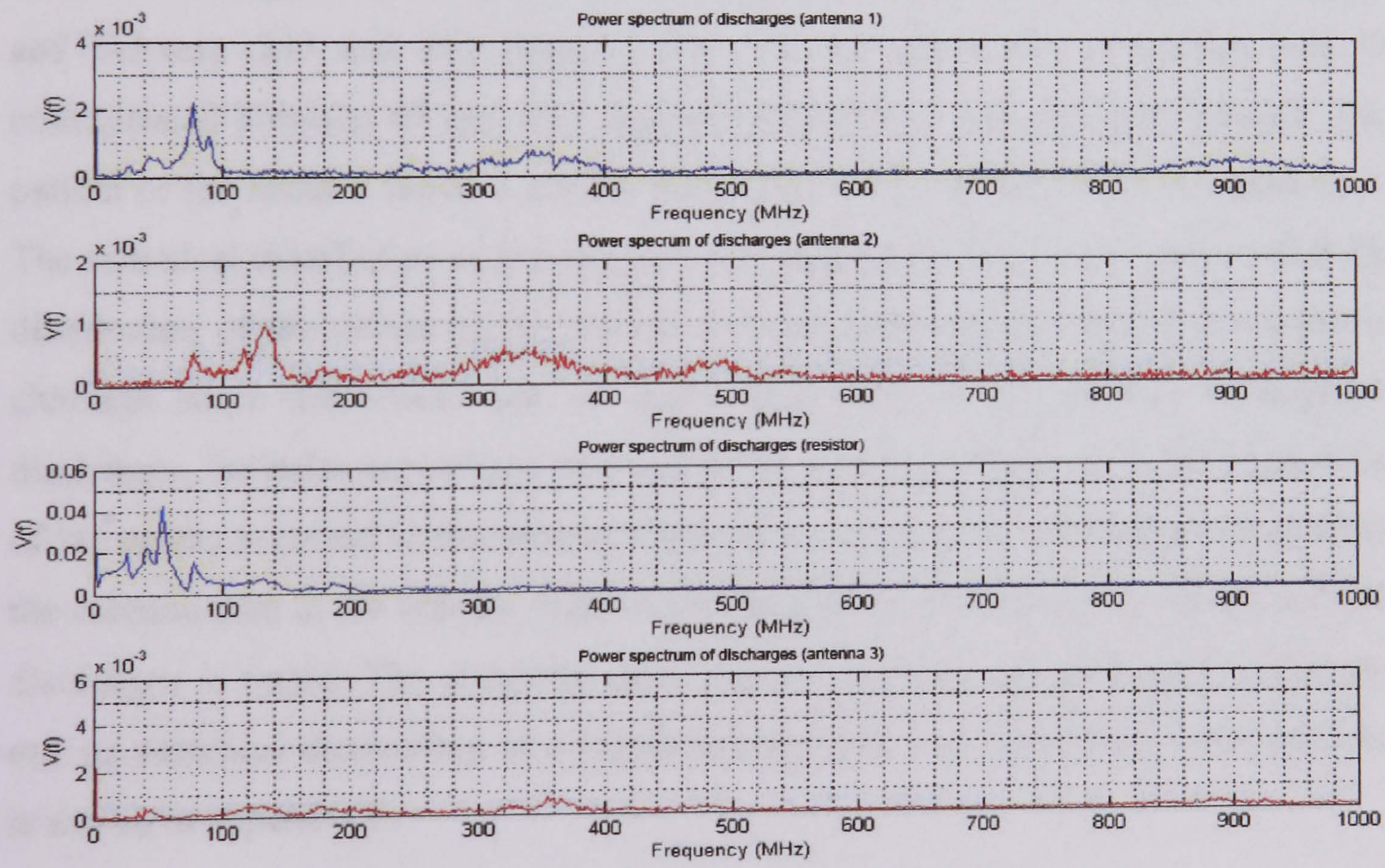

Figure 6.29 Frequency spectra of the selected surface discharge at 18440 using a 50 Ω resistor in channel 3 and antennas in channel 1, 2 and 4

6.4.2. Time domain analysis

The methodology used for the time domain analysis of discharges in insulators was the same used for the time domain analysis for a pressboard, i.e. using the MATLAB program and acquiring signals that include the AC reference and the radiated and conducted discharges. Figure 6.30 show the unprocessed acquired signal of the discharges monitored in the resistor and the AC reference. The applied voltage was 18440 V, and as it was pointed out before, this voltage was selected because at this voltage level steady surface discharges are incepted. Figure 6.31 shows the processed signal for the 50 Ω resistor and antenna 1. This figure shows the acquired signal and the AC reference to extract the point on wave information, and it can be observed that the incepted discharges appear in the resistor and the antenna. The detected pulses show a positive and a negative polarity and they tend to group in the first half of the positive and negative half cycle of the AC reference and are more spaced than the ones appearing in the insulators. The total distribution of the discharges along the AC waveform used as a reference is shown in figure 6.32 for the resistor and antenna 1. The discharges in the resistor are concentrated mainly between 30 and 60 degrees and between 240 and 260 degrees. For the antenna 1 the discharges tend to concentrated between 40 and 100 degrees and between 240 and 260 degrees. The pattern of the resistor shows a similar pulse distribution to the one in the antenna 1. The statistical distribution of the acquired discharges (see figure 6.33) shows that the distribution of the pulses in the resistor is very similar to the one of the antenna, although some differences can be appreciated such as the number of acquired discharges, the pulse occurrence received in the antenna is higher than the occurrence of the pulses acquired in the resistor. There are more positive discharges received in the antenna than in the resistor, again an inverse effect in the polarity of the received discharges is found. The complete set of figures showing the pattern of discharges and its statistical distribution in a pressboard for tests 1 to 5 in resistor and antennas is shown in appendix F.

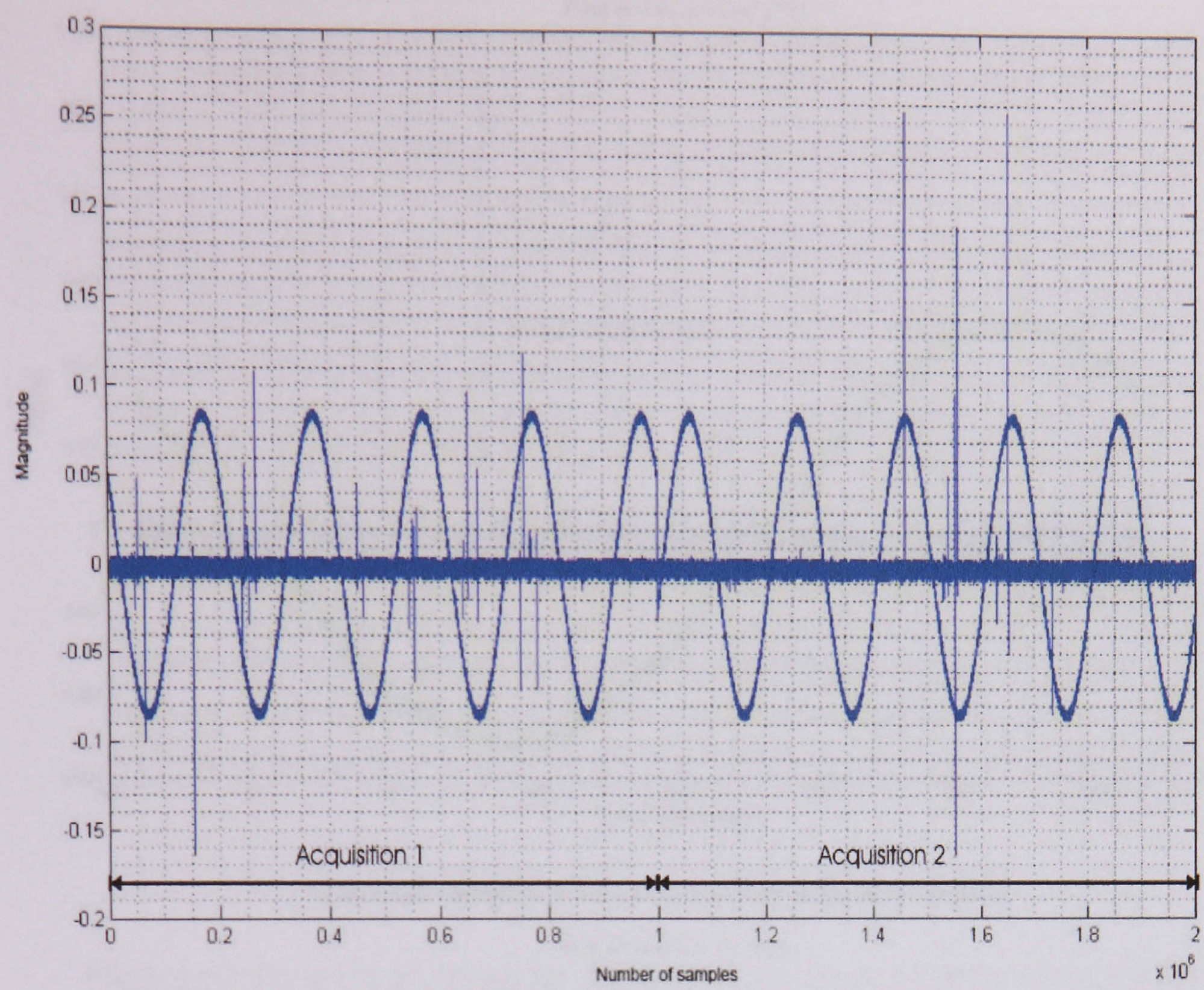

Figure 6.30 Unprocessed acquired signal of a pressboard submerged in oil

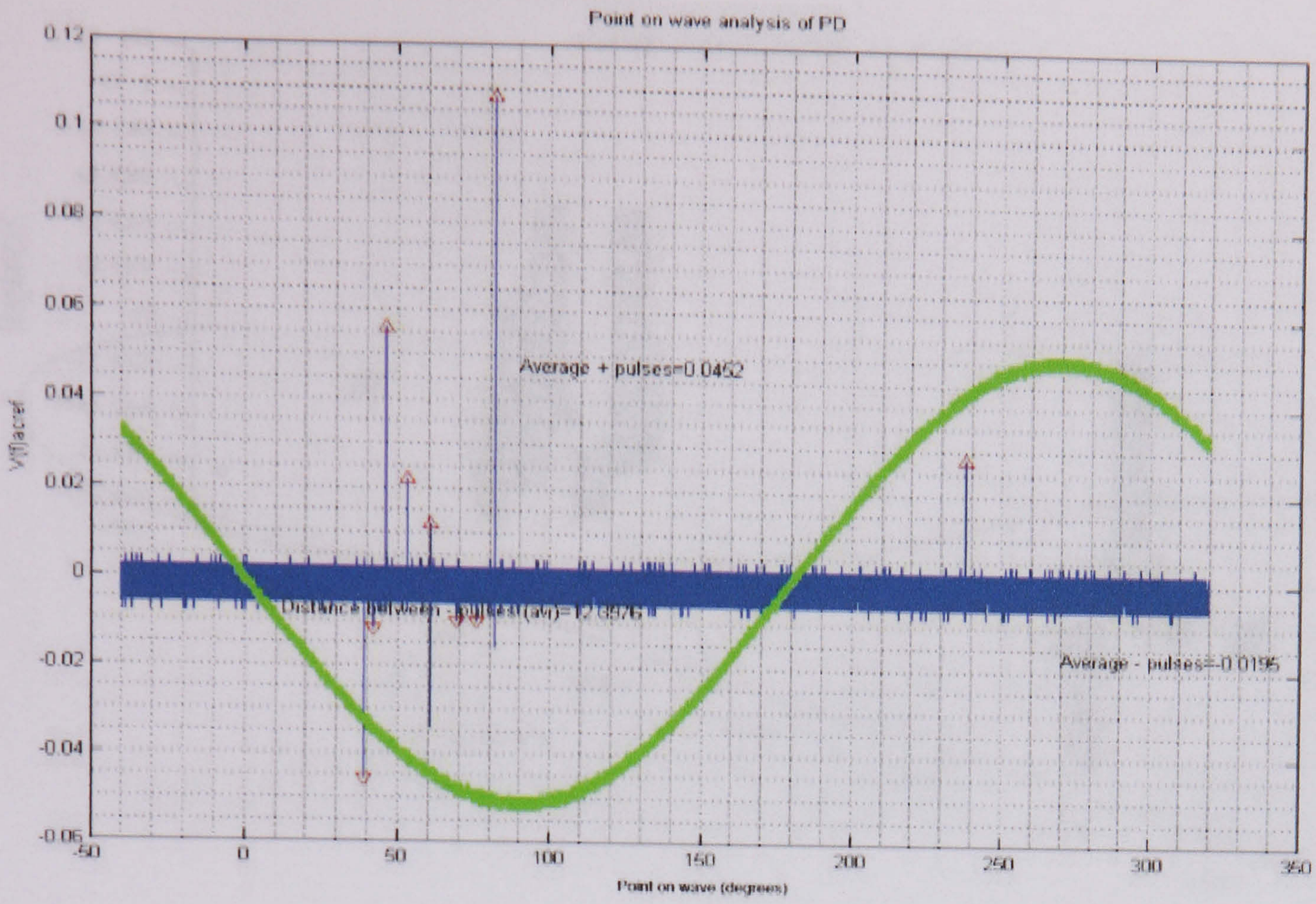

a) Surface discharges over a pressboard at 24210 V (resistor)

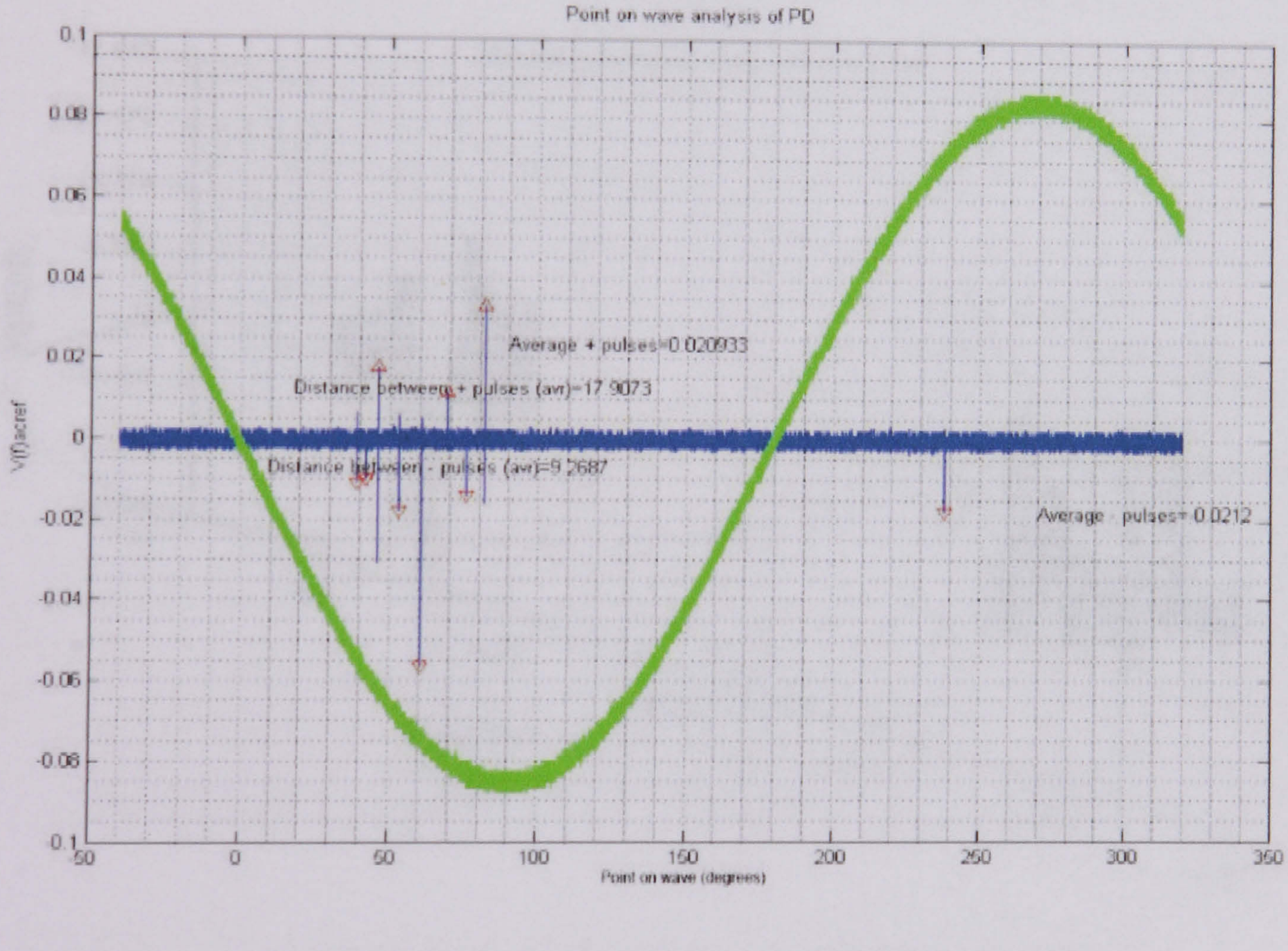

b) Surface discharges over a pressboard at 24210 V (antenna 1)

Figure 6.31 Surface discharges and AC reference over a pressboard submerged in oil at 24210 V acquired in a) resistor and b) antenna 1

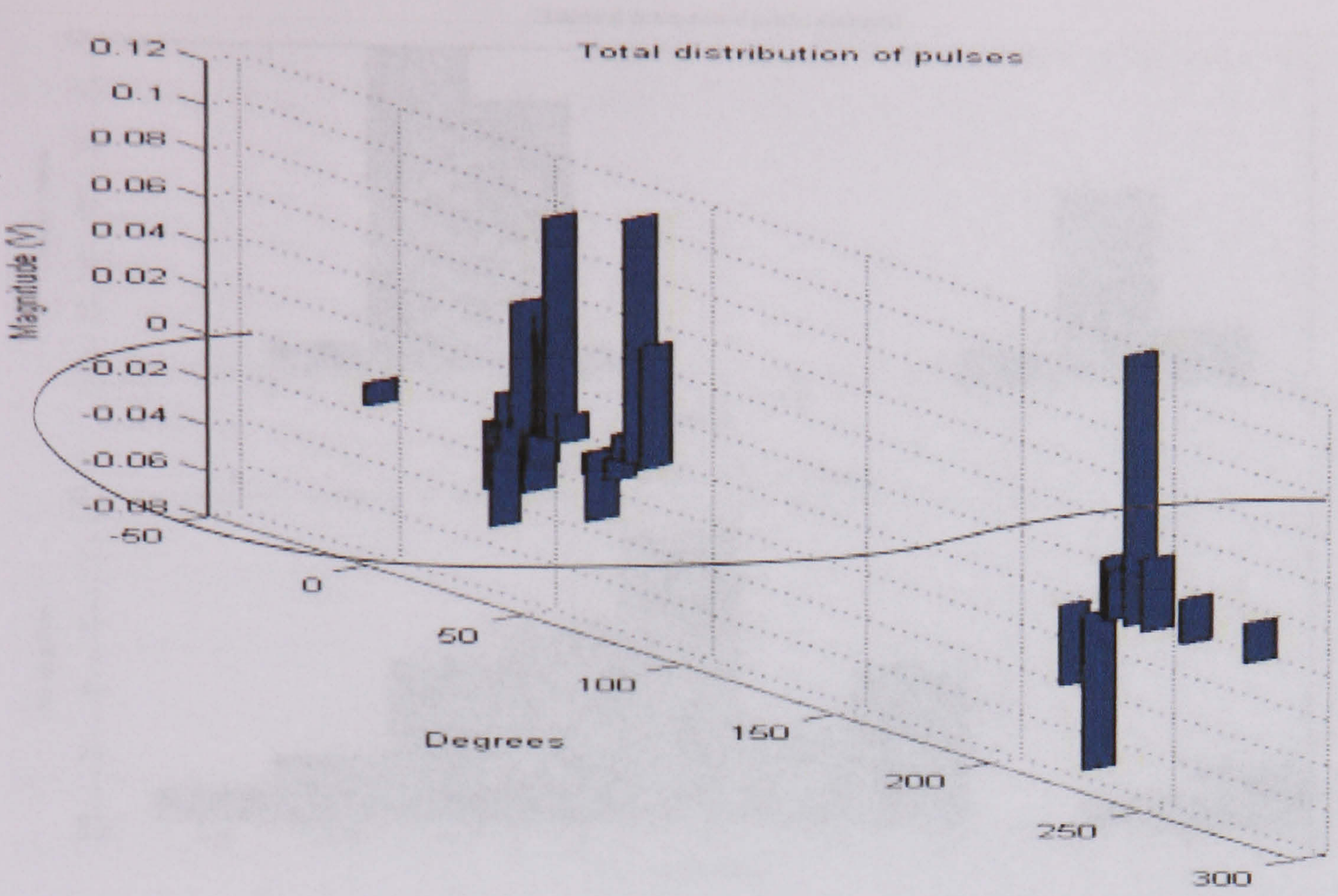

a) Distribution of surface discharges over a pressboard at 24210 V (resistor)

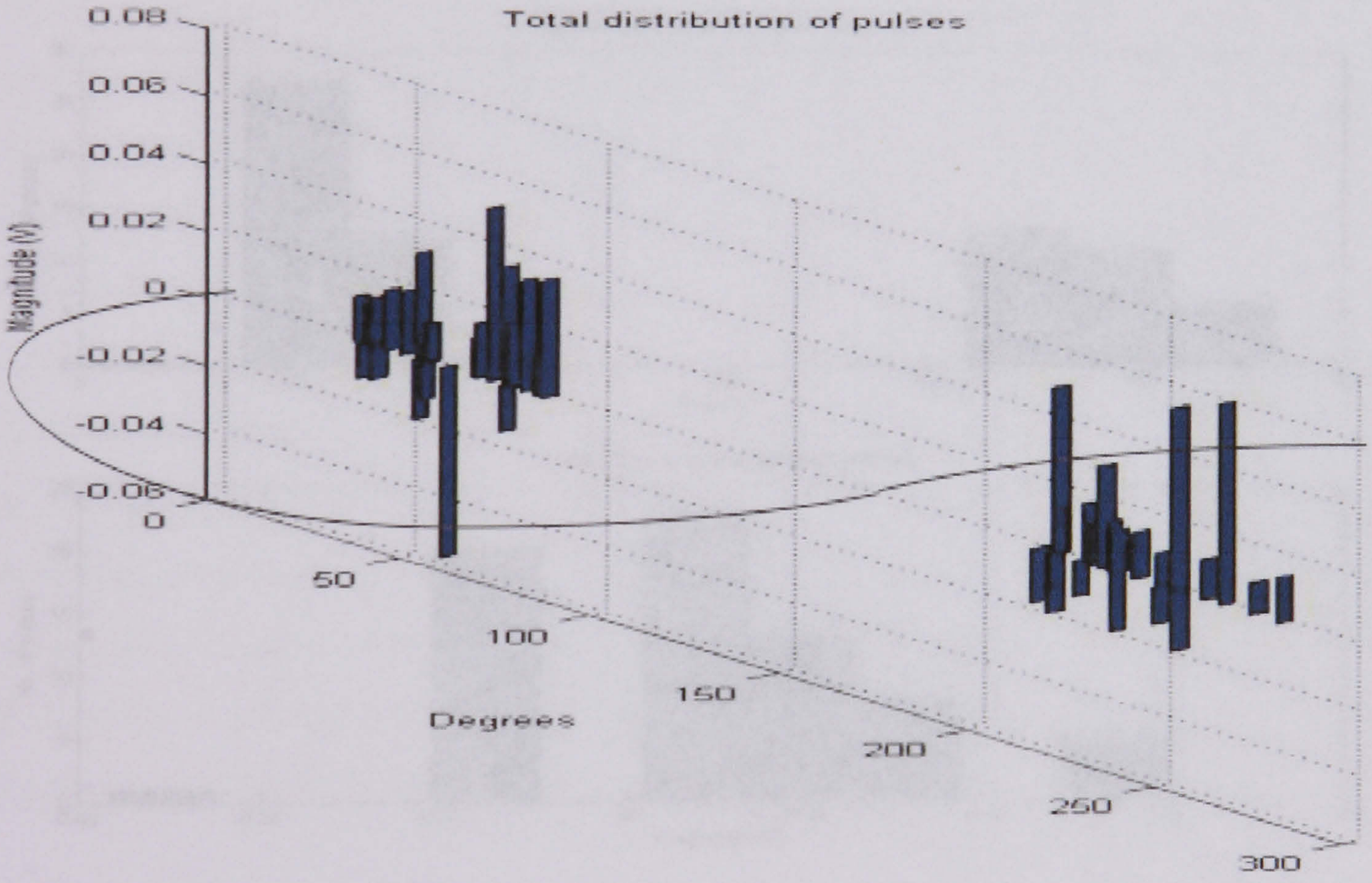

b) Distribution of surface discharges over a pressboard at 24210 V (antenna 1)

Figure 6.32 Distribution of surface discharges over a pressboard at 24210 V acquired in a) 50 Ω resistor and b) antenna 1.

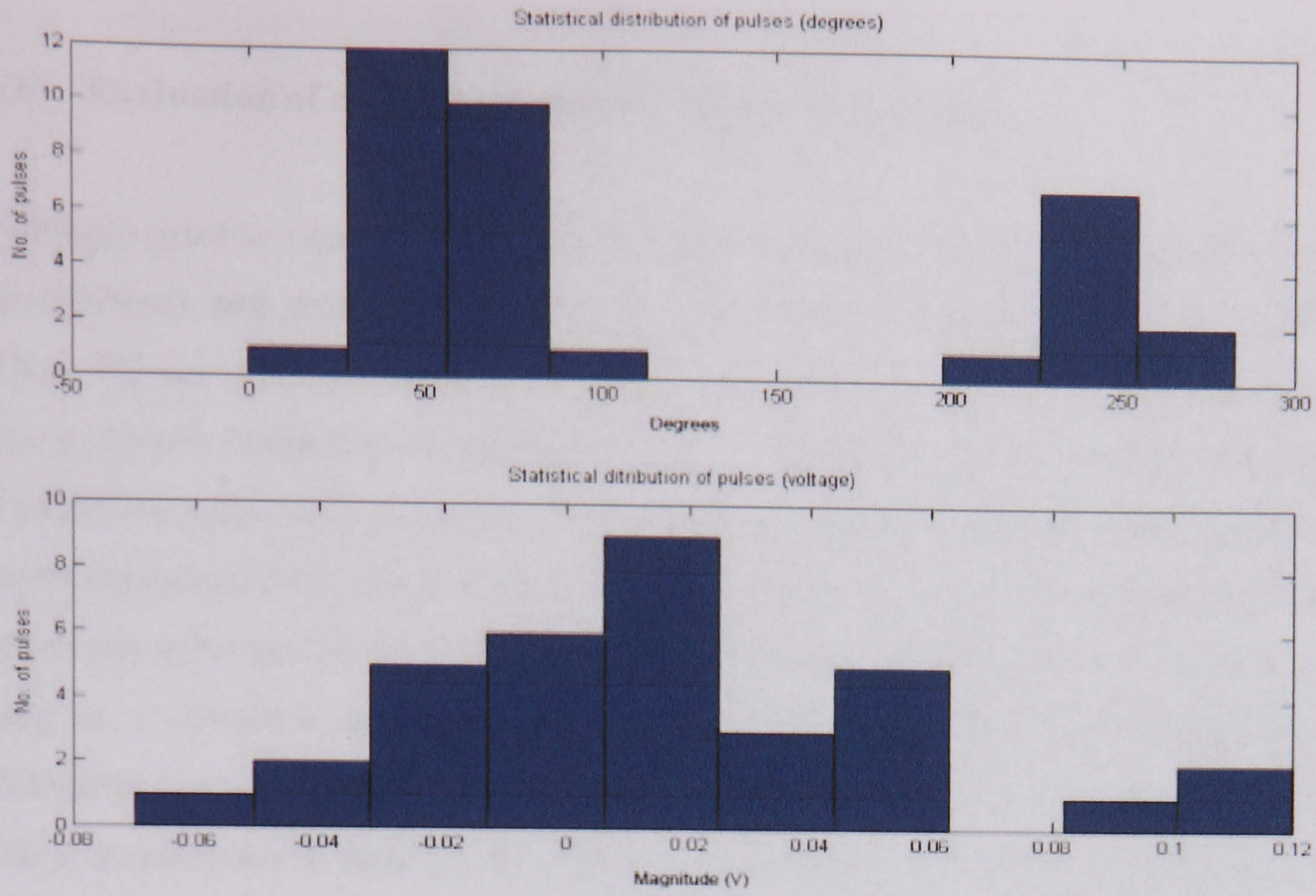

a) Statistical distribution of surface discharges over a pressboard at 24210 V (resistor)

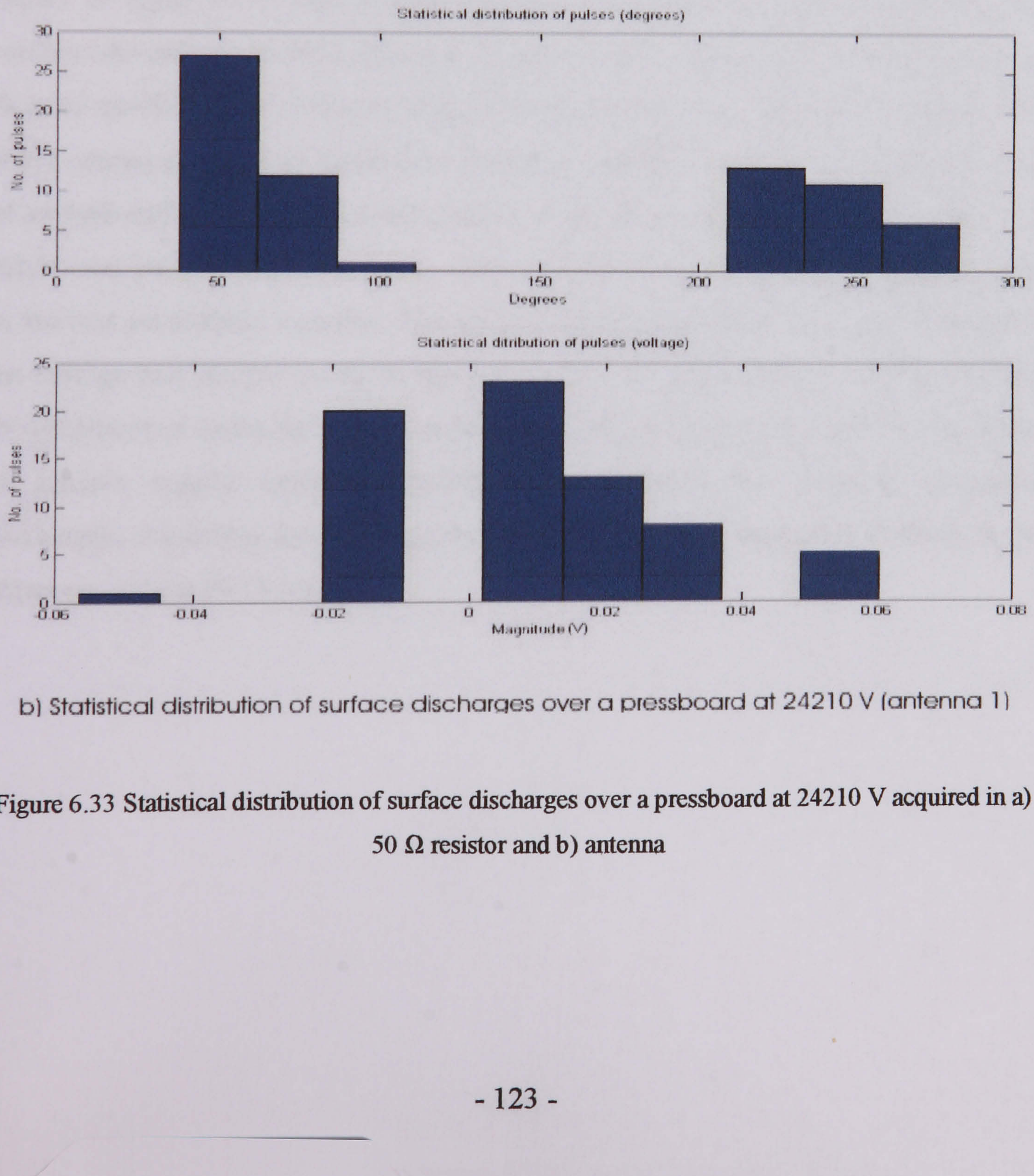

b) Statistical distribution of surface discharges over a pressboard at 24210 V (antenna 1)

Figure 6.33 Statistical distribution of surface discharges over a pressboard at 24210 V acquired in a) 50 Ω resistor and b) antenna

6.5. Evaluation of cavity discharges in a polymeric sample

Another common type of PD occurs in solid dielectrics such as found inside power transformers and external insulation in substations and transmission lines [6.13]. These PD occur when a small cavity containing gas is created inside solid insulation due to defects in the manufacturing process or degradation of the insulation material. The different dielectric constant (ε) between the air cavity and the insulator triggers a small discharge (PD) which if not detected in time, may cause the internal walls of the cavity to be eroded. This can lead to an increase in the size of the cavity wich can lead to a complete failure of the equipment containing the affected insulation. Defective insulation can contain several cavities and hence partial discharges, which can jeopardize the integrity of the power equipment. For this reason it is important to prevent this type of PD before they might cause total damage. For the evaluation of cavity discharges, a laboratory sample was used; the configuration of the test is shown in figure 6.34. This sample is made of a polymeric material (EPDM) and contains several air cavities (the sample was made by injecting air into the polymer, thus the cavities are of unknown size). The connection to the sample was designed to avoid corona and surface discharges, the latter effects were achieved through the use of smooth surfaces and Rogowski profiles to create an uniform electrical field [6.1]. Additional tests were carried out to verify the absence of detectable discharge events in the test set without samples. The applied voltage was fixed at 14320 V as this is the voltage that incepts cavity discharges steadily. It is important to mention that the development of cavity discharges requires a certain period of time that can last hours to achieve regular emissions [6.14]. Once achieved the inception of partial discharges, conducted discharge currents and radiated discharge were detected by the antennas and the 50 Ω resistor.

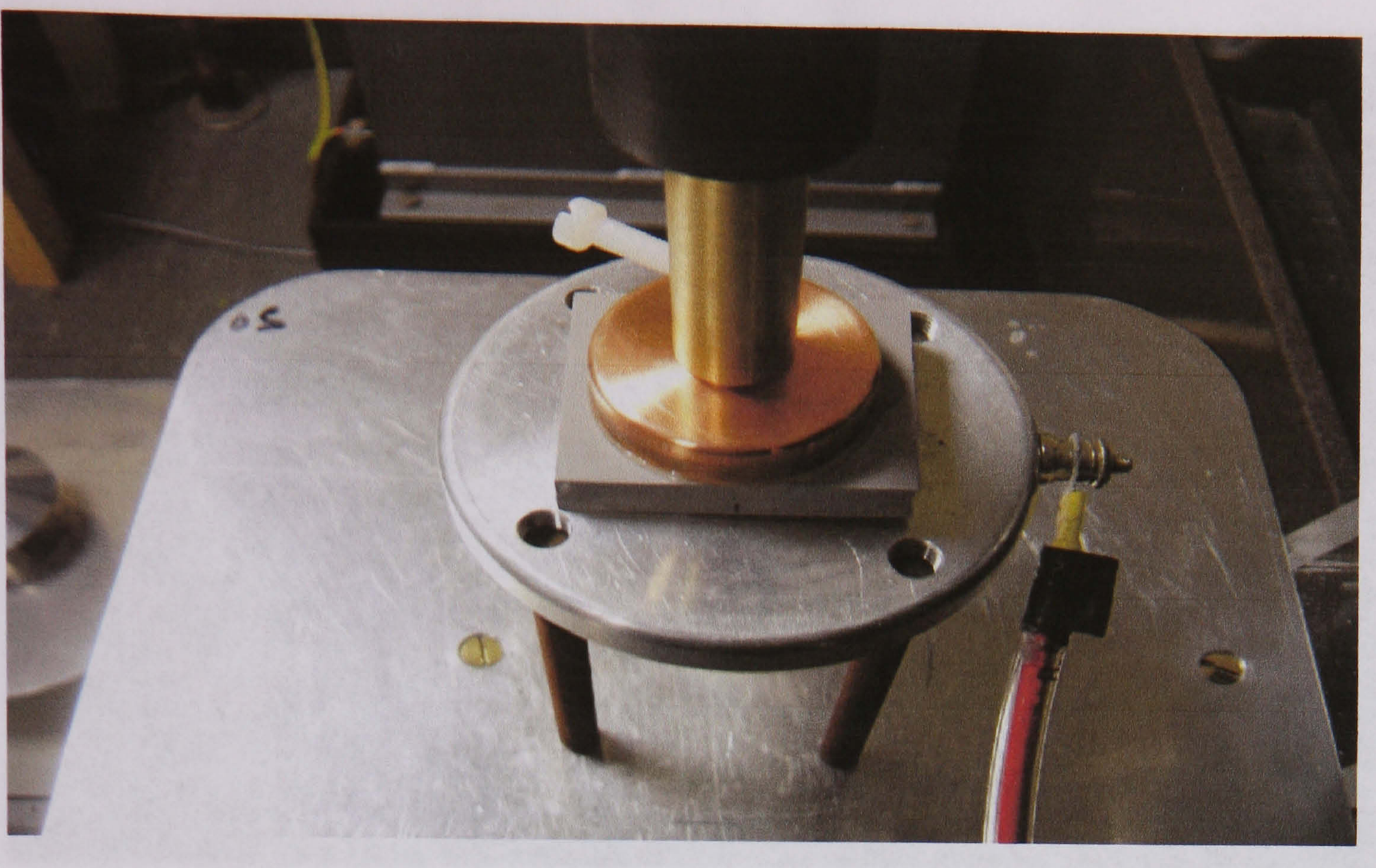

Figure 6.34 General arrangement of cavity evaluation test

6.5.1. Frequency domain analysis

Two acquisitions were selected to be analyzed, and figure 6.35 shows a screenshot of the acquired samples as seen by the oscilloscope. The screenshot show the AC reference and the cavity discharges from the 50Ω resistor. Cavity discharges show a regular occurrence and relative constant value with both positive and negative polarities. Individual conducted and radiated discharges were acquired and frequency analyzed; figure 6.36 shows an individual discharge and figure 6.37 shows the FFT of the selected discharge. The FFT analysis shows the dominant spectral components in antennas 1, 2, 3 and the resistor, to be 43, 120, 120 and 55 MHz respectively. Comparatively the value of the received conducted discharge is higher than the value of the signals received in the antennas.

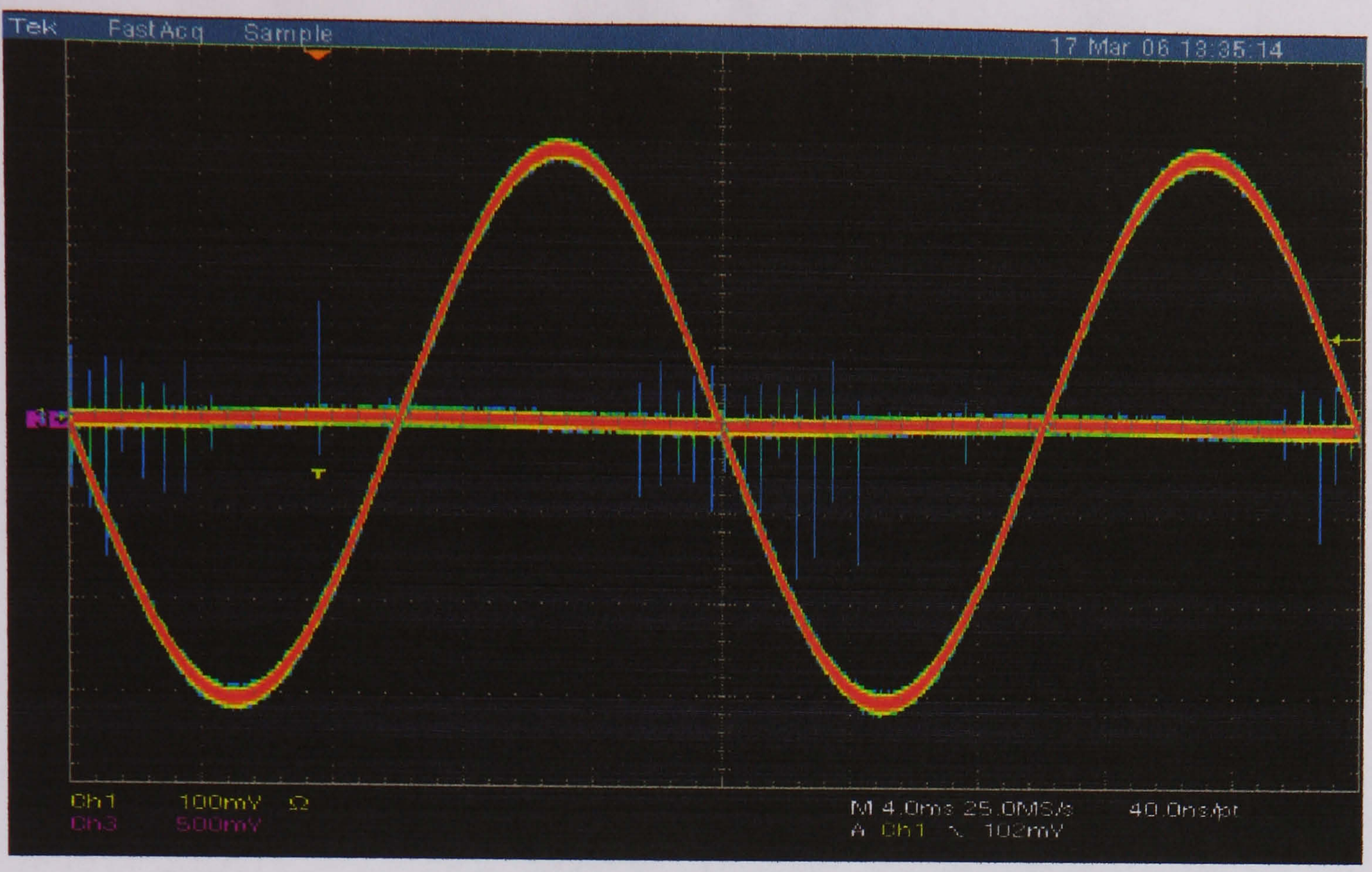

Figure 6.35 Cavity discharges using 1 antenna and AC reference signal at 14320 Volts

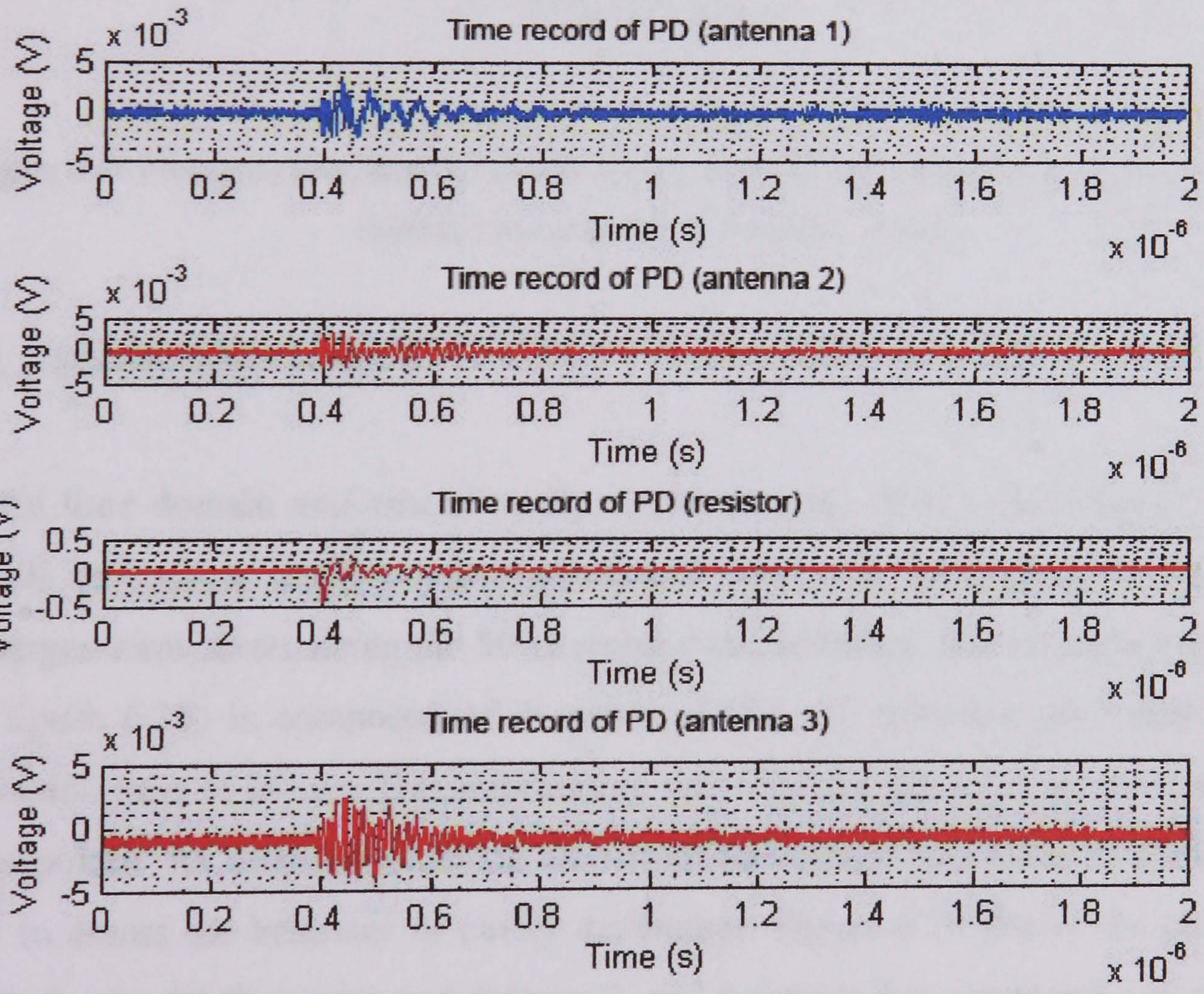

Figure 6.36 Selected cavity discharge at 14320 V using a 50 Ω resistor in channel 3 and antennas in channel 1, 2 and 4

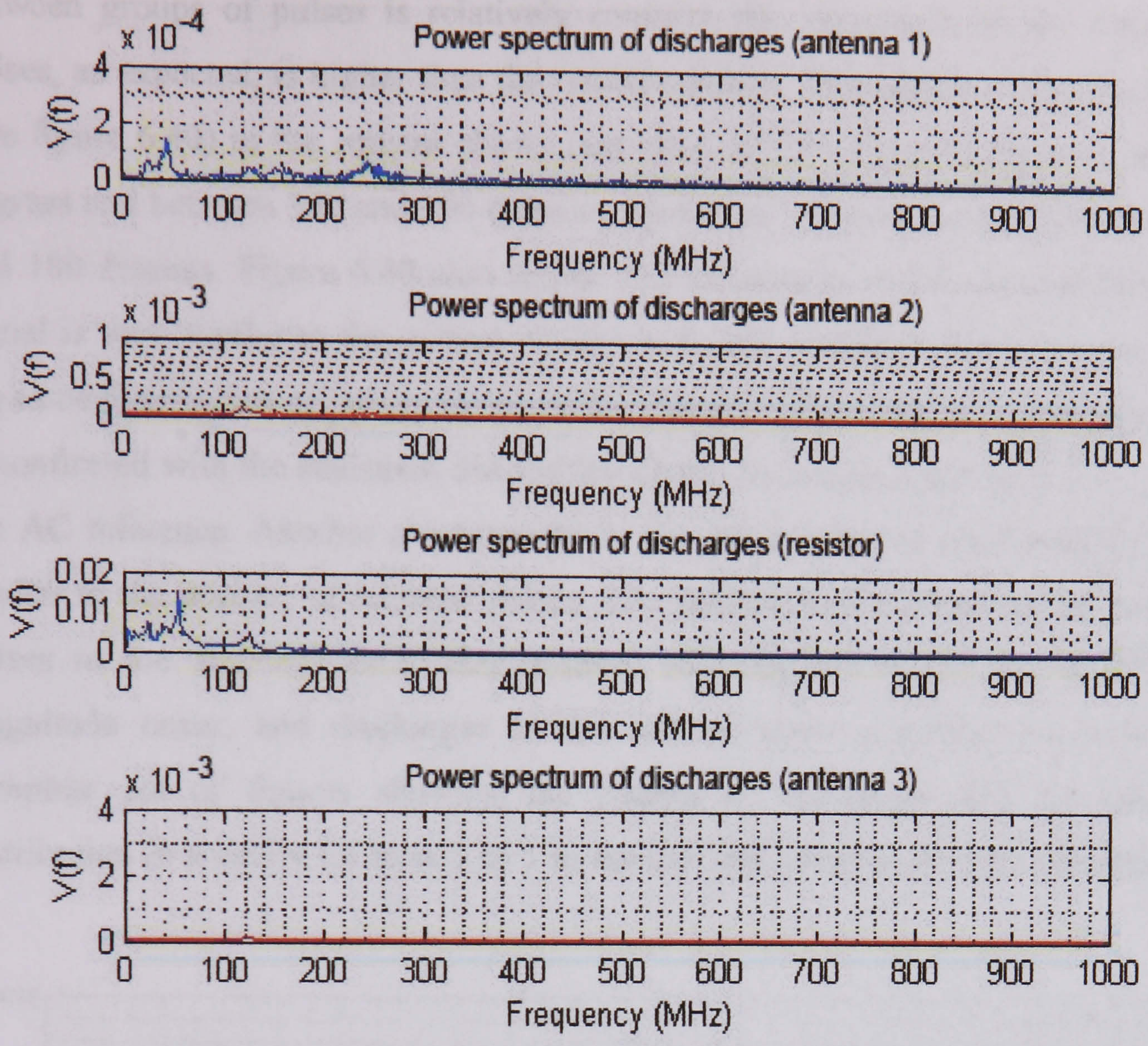

Figure 6.37 Frequency spectra of the selected cavity discharge at 14320 using a 50 Ω resistor in channel 3 and antennas in channel 1, 2 and 4

6.5.2. Time domain analysis

For the time domain analysis of cavity discharges, the MATLAB program for the analysis of corona, insulators and pressboard was used. Samples of the acquired discharges were taken, using the 50 Ω resistor and antennas. The unprocessed signal (see figure 6.38) is composed of 4 cycles of the AC reference and represent an acquisition time of 80 ms. This information was used for the point on wave analysis of the pulses. As mentioned before the inception voltage was fixed at 14320 V in order to assess the behavior of cavity discharges. Figure 6.39 shows the processed signals for the 50 Ω resistor and antenna 1, and indicates that conducted and radiated cavity discharges of positive and negative polarity are received. They tend to group around the zero crossing of the descending slope of the AC reference. The spacing

between groups of pulses is relatively constant, the magnitude of the conducted pulses, as expected, is higher than the radiated pulses. The pattern of the discharges (see figure 6.40) in the resistor shows that most of PD's occurs between 0 and 80 degrees and between 300 and 360 degrees, whilst few discharges occur between 120 and 180 degrees. Figure 6.40 also shows that the pattern of the radiated discharge signal is very similar to the pattern of the conducted discharge signal as they share the same distribution of pulses. However the radiated pulse magnitude is smaller, this is confirmed with the statistical distribution of the discharges (see figure 6.41) along the AC reference. Another characteristic is that the number of conducted pulses is similar to the number of radiated pulses. The statistical distribution of the acquired pulses in the antennas show that positive and negative discharges of different magnitude occur, and discharges in the resistor show a similar behavior. The complete set of figures showing the pattern of discharges and its statistical distribution in a cavity for tests 1 to 5 in resistor and antennas is shown in appendix G.

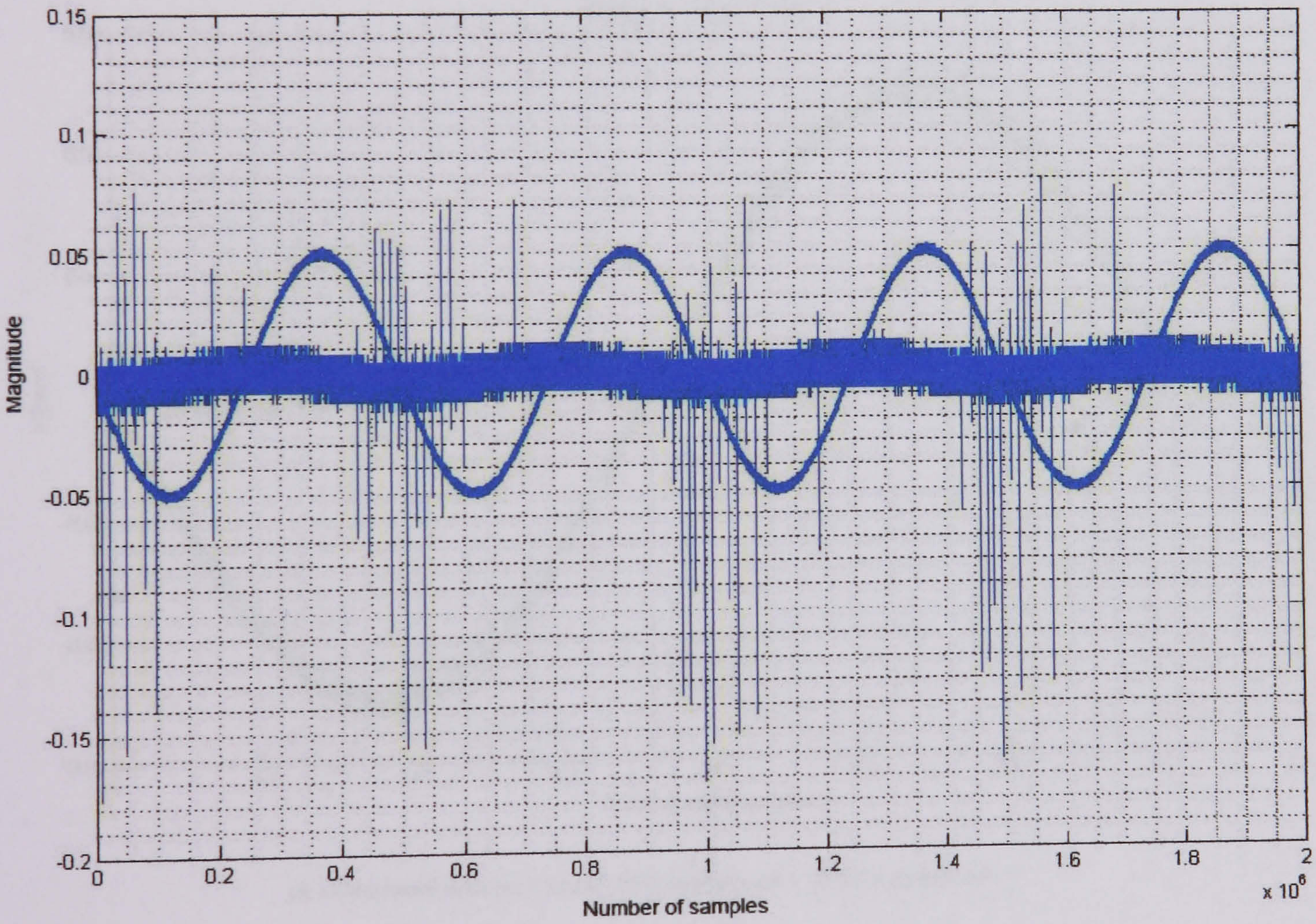

Figure 6.38 Unprocessed acquired signal of cavity discharges (resistor)

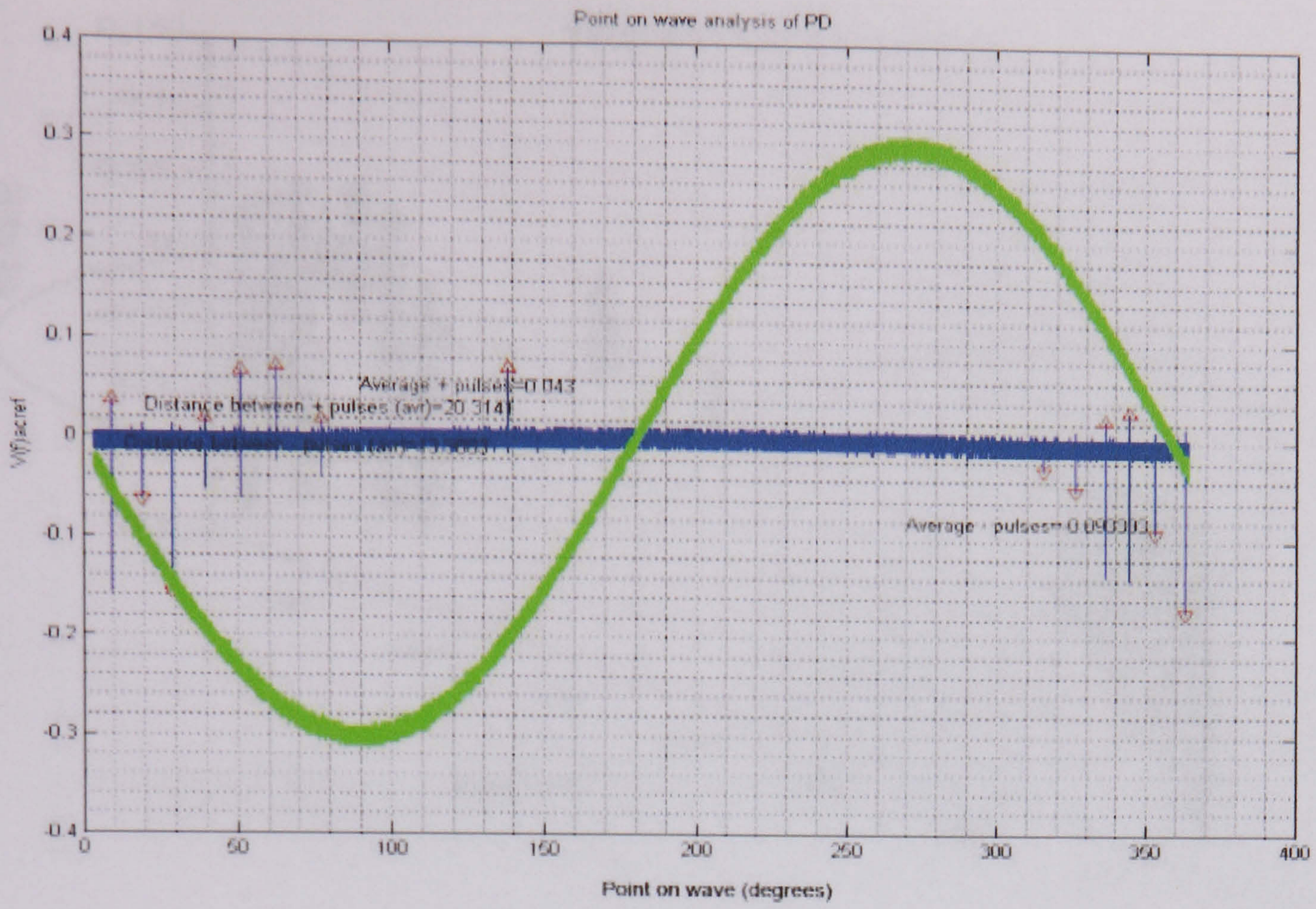

a) Pulse distribution of cavity discharges at 14230 V (resistor)

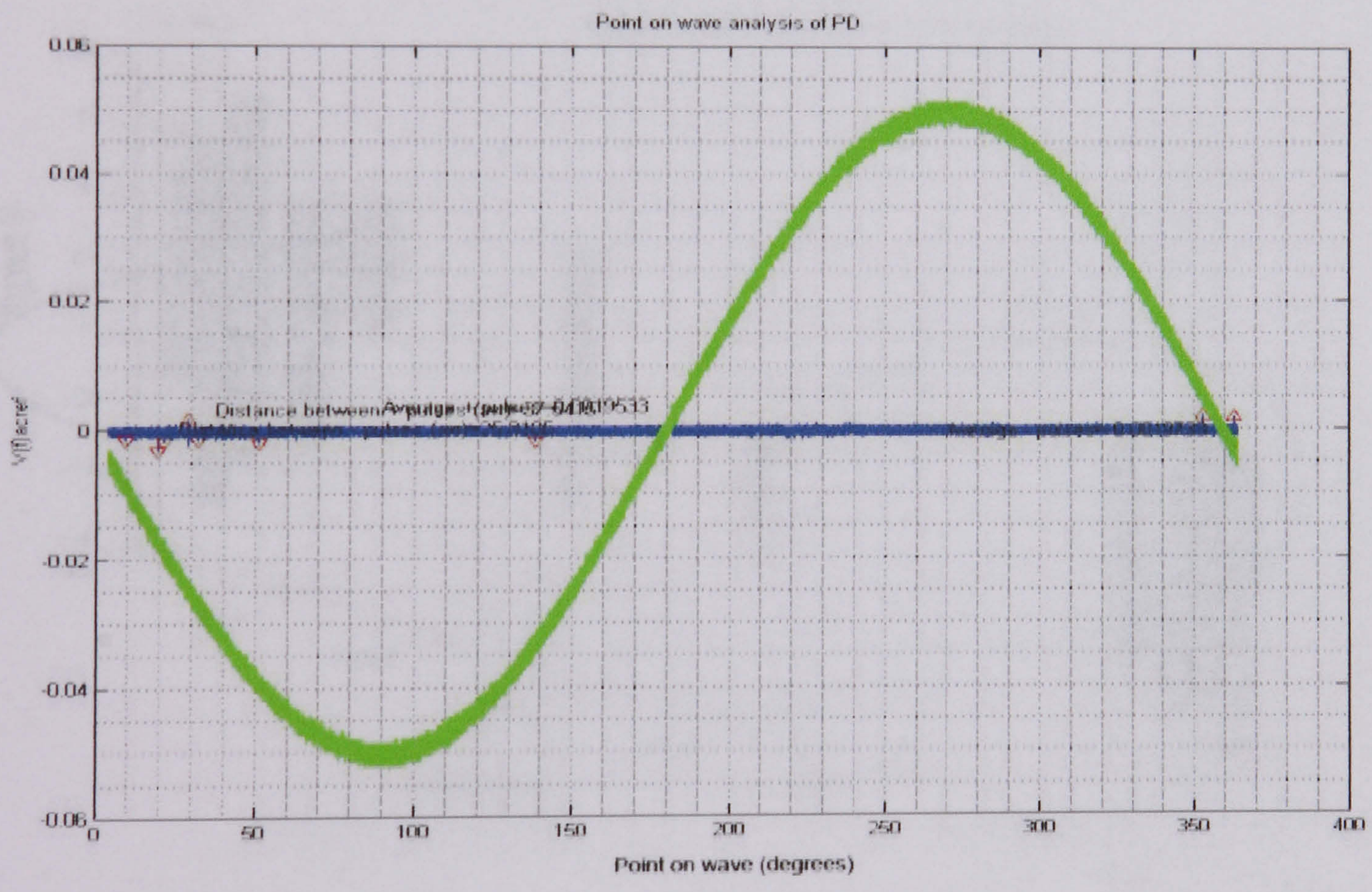

b) Pulse distribution of cavity discharges at 14230 V (antenna 1)

Figure 6.39 Pulse distribution and AC reference of cavity discharges at 14230 V acquired in a) 50 Ω, and b) antenna 1

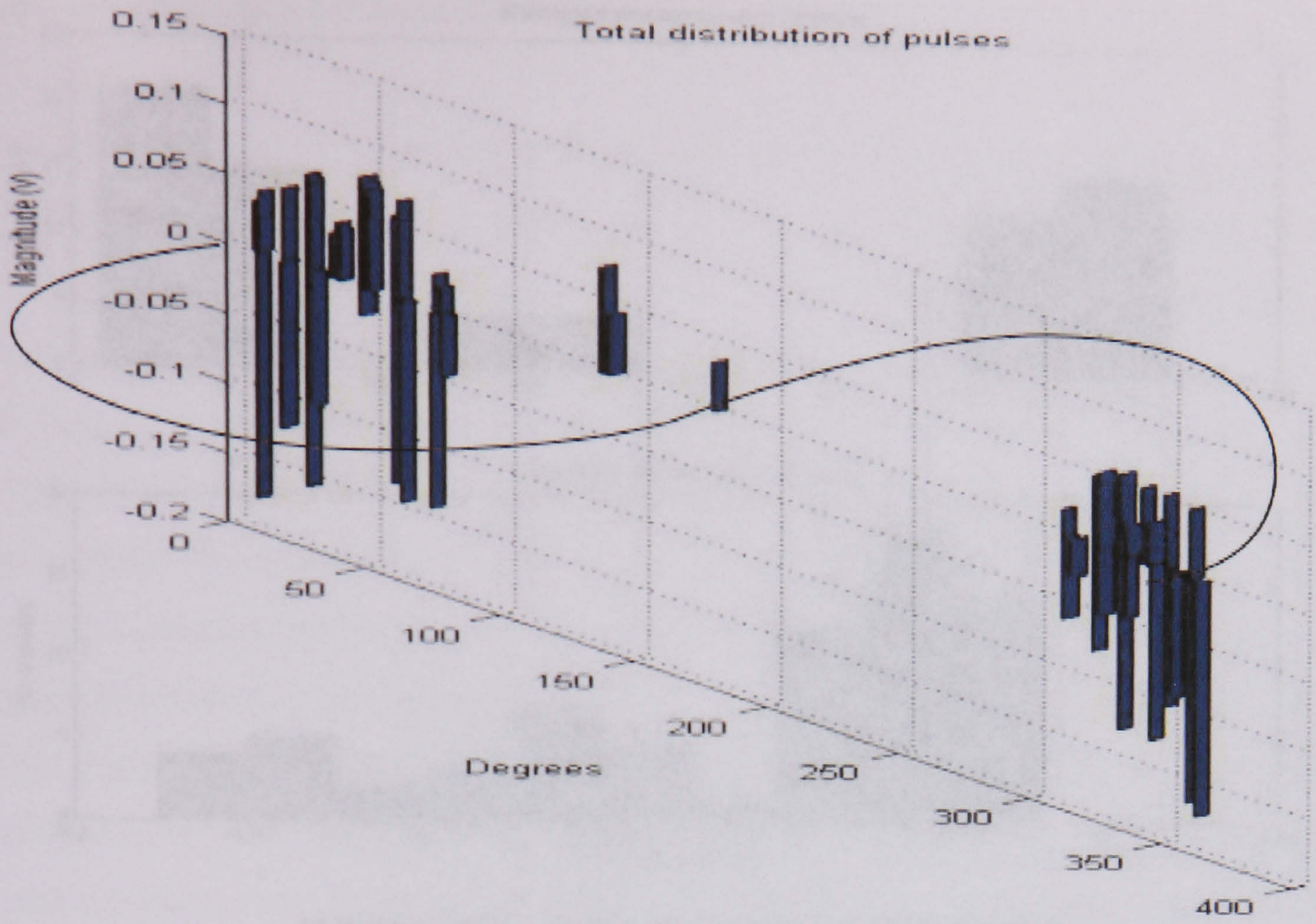

a) Pulse distribution of cavity discharges at 14320 V (resistor)

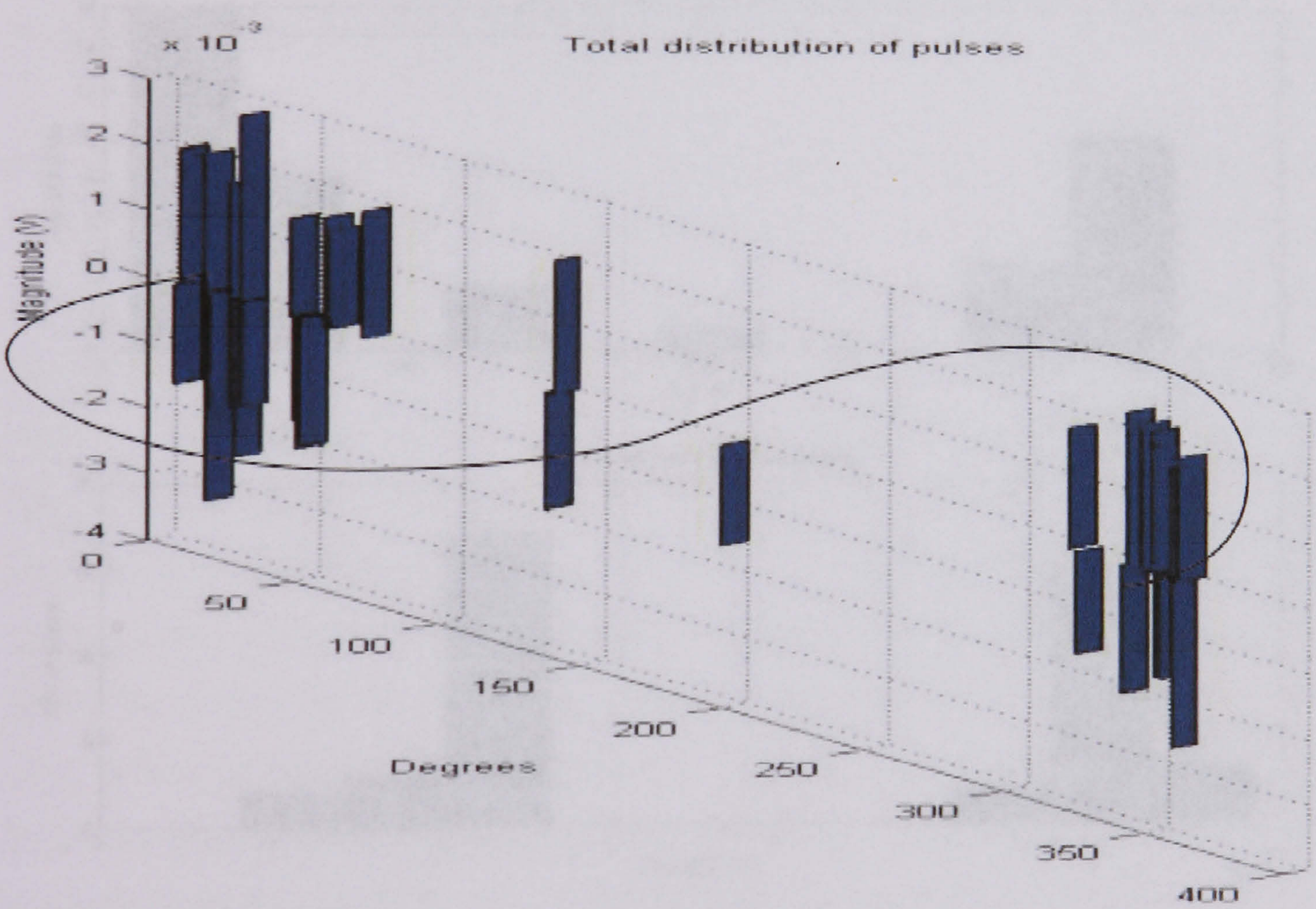

b) Pulse distribution of cavity discharges at 14320 V (antenna 1)

Figure 6.40 Pulse distribution of cavity discharges at 14320 V acquired in a) 50 Ω resistor, b) antenna 1.

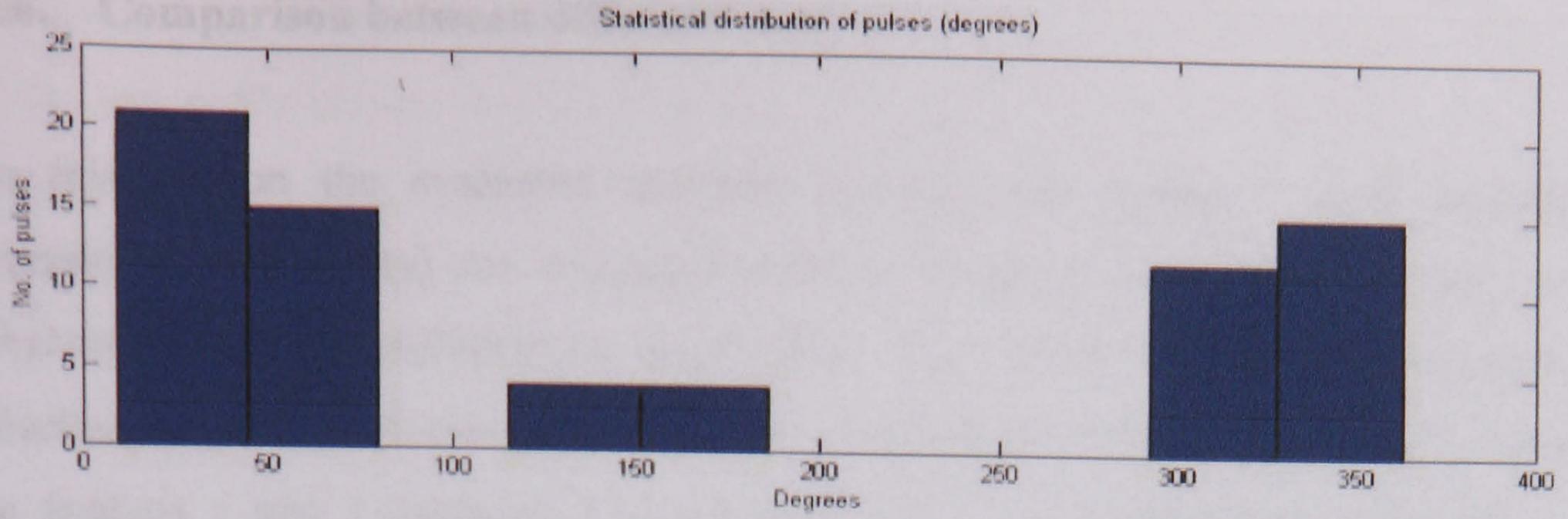

a) Statistical distribution of cavity discharges at 14230 V (resistor)

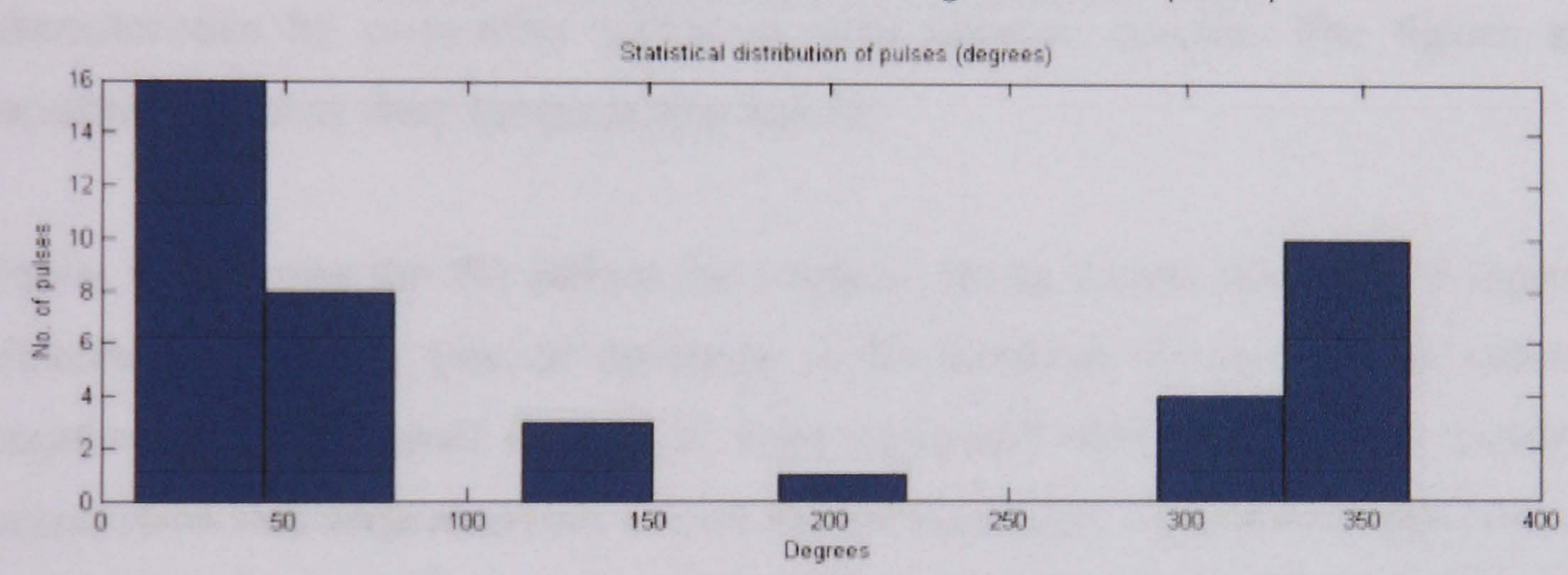

b) Statistical distribution of cavity discharges at 14230 V (antenna 1)

Figure 6.41 Statistical distribution of cavity discharges at 14230 V acquired at a) 50 Ω resistor, and b) antenna 1.

6.6. Comparison between different samples

In this section the evaluated samples (corona, new insulator, aged insulator, pressboard and cavity) are compared in order to assess the different patterns and characteristics that differentiate each other. This assessment includes conducted discharges (current discharges in the 50 Ω resistor) and radiated discharges received in antenna 1 and 3 (antenna 2 is not included as the oscilloscope is limited to 4 channels). The physics that describe the development of partial discharges determine its intrinsic characteristics [6.11, 6.12, 6.13]. Although some discharge phenomena remains undetermined, some attempts to characterize partial discharges according to pulse distribution and magnitude have been made [6.14, 6.15]. The latter technique only assesses the conducted partial discharge signals (current discharge) using a PD detector [6.6], thus the relationship between the conducted and radiated discharges remains unknown. This section aims to identify some of these fundamental characteristics by comparing typical patterns between samples. The figures are repeated for clarity from the preceding figures.

Figure 6.42 shows the PD pattern for a typical strong corona discharge. A typical characteristic of this type of discharge is the incidence of several well defined negative pulses of small magnitude when compared with positive ones; positive pulses show less occurrence but a much higher magnitude. Corona discharges have a very well defined distribution along the complete acquire AC waveform as shown in figure 6.47. Due to very small discharge magnitude, and the sensitivity of the antennas, it is not possible to receive the radiated corona above the background noise and its pattern does not have a relationship with other analyzed samples. Figure 6.43 shows the pattern for the conducted surface discharge in a new insulator, there is a clear difference between positive and negative pulses and they are more spaced with little recurrence, and again the magnitude of the acquired discharges is too small to be received by the antennas. The pattern of surface discharges over an aged insulator (see figure 6.44) shows that the distribution of the discharges is more spaced than the ones in the new insulator and they are distributed around the maximum of the half negative and positive cycle of the AC waveform, the magnitude of some pulses is

relatively high. The statistical distribution of the new and aged insulator (see figures 6.48 and 6.49) shows the latter effect, and they also show that there is little correlation between them. Figure 6.45 shows the pattern of surface discharges over a pressboard. The discharges are spaced and distributed around the maximum positive and negative half cycles of the AC reference; the discharge magnitude is relatively small. This pattern is very similar in discharge distribution and number of generated pulses to the aged insulator. Comparing the statistical distribution of surface discharges in pressboard (see figure 6.50) with the distribution of the aged insulator (figure 6.49), a similarity is noticeable. Figure 6.46 shows the typical pattern of a cavity discharge and it can be observed that discharges are distributed around the zero crossing of the AC reference at 0/360 degrees. This characteristic is the major distinction of this type of discharge, and its pattern is distinctive compared to the other analyzed samples. Its statistical distribution (see figure 6.51) also show a considerable generation of positive and negative discharges.

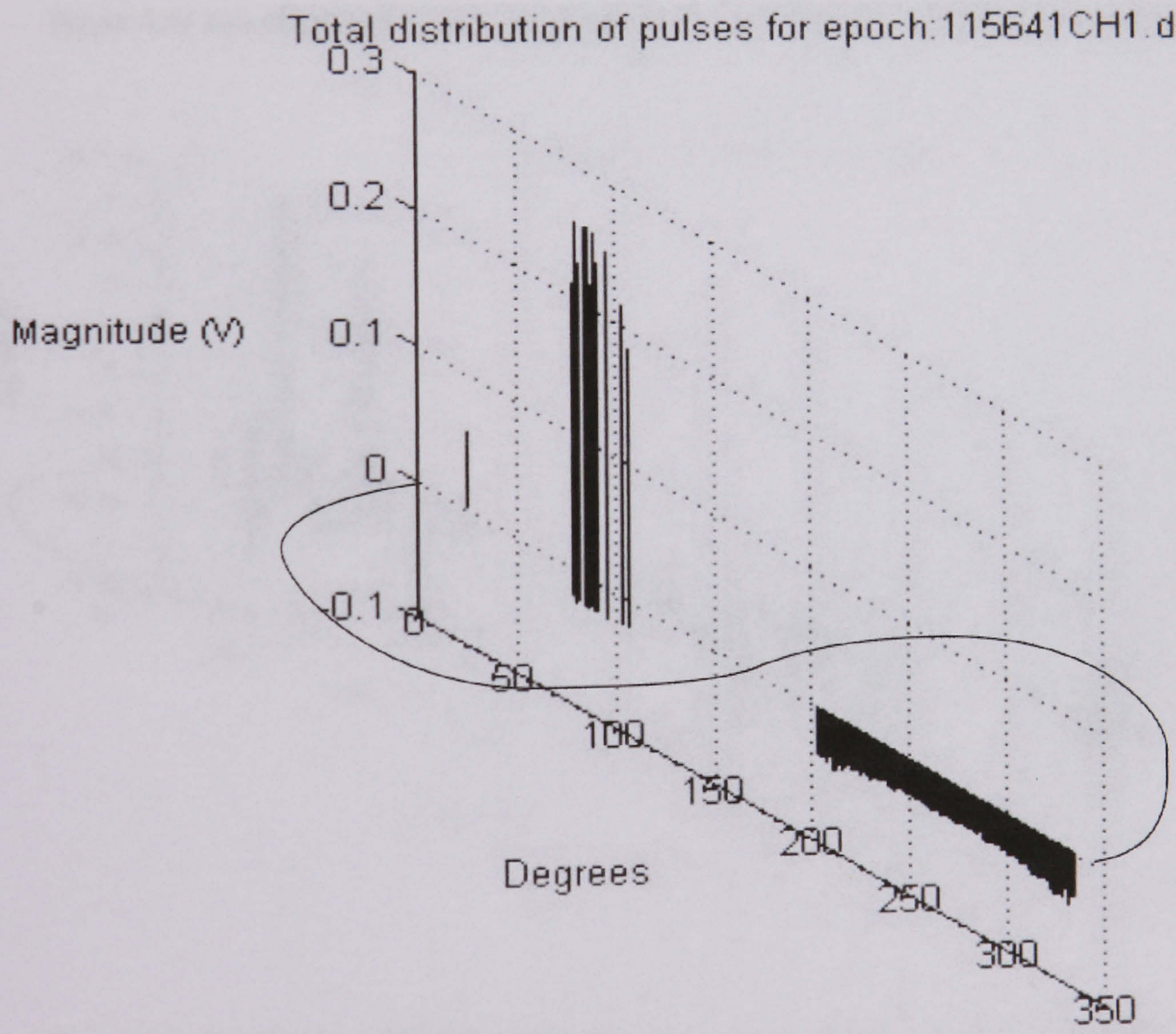

Figure 6.42 Distribution of corona pulses at 6540 V with a 10mm air gap (resistor)

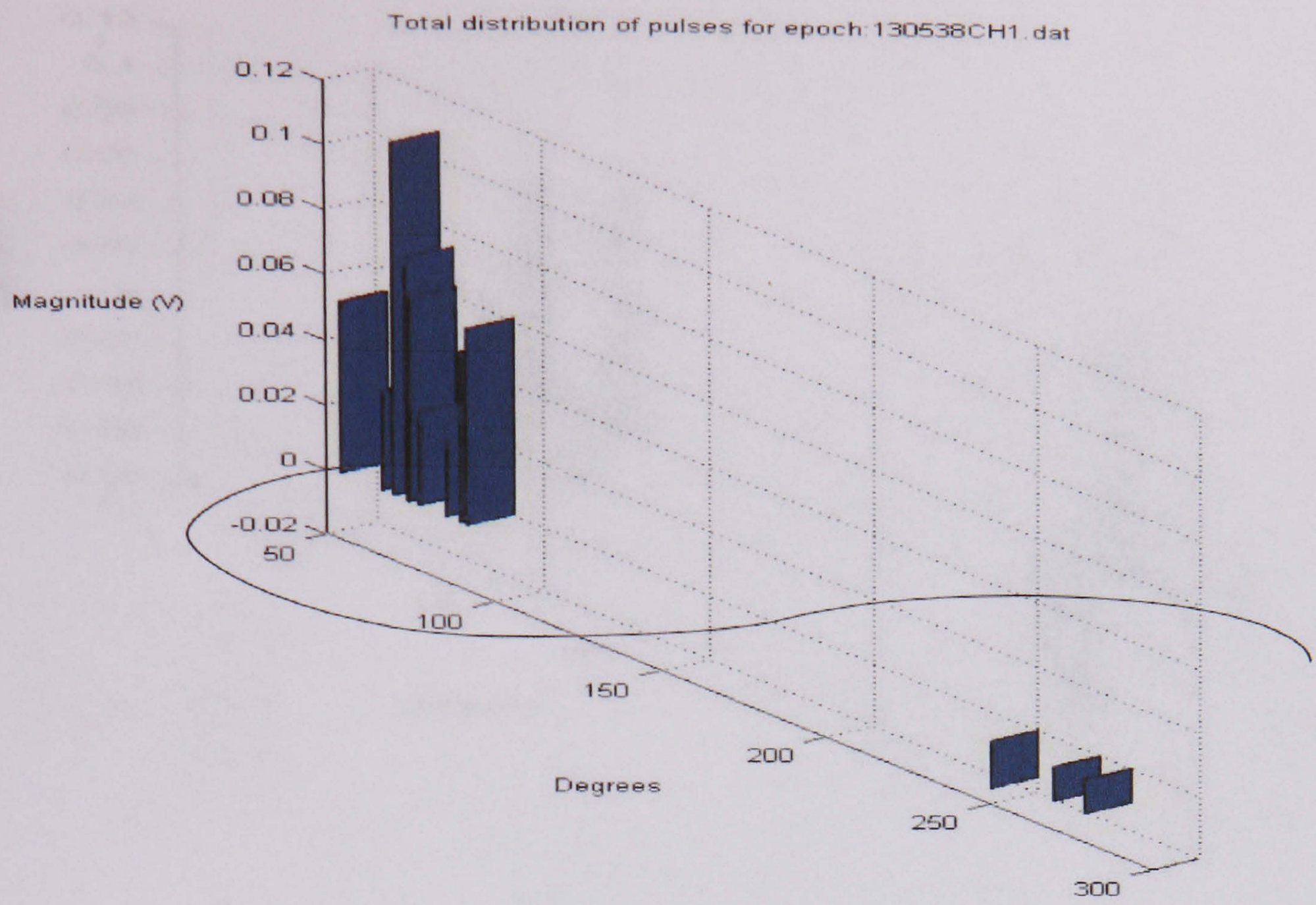

Figure 6.43 Distribution of surface discharges over a new insulator at 42500 V (resistor)

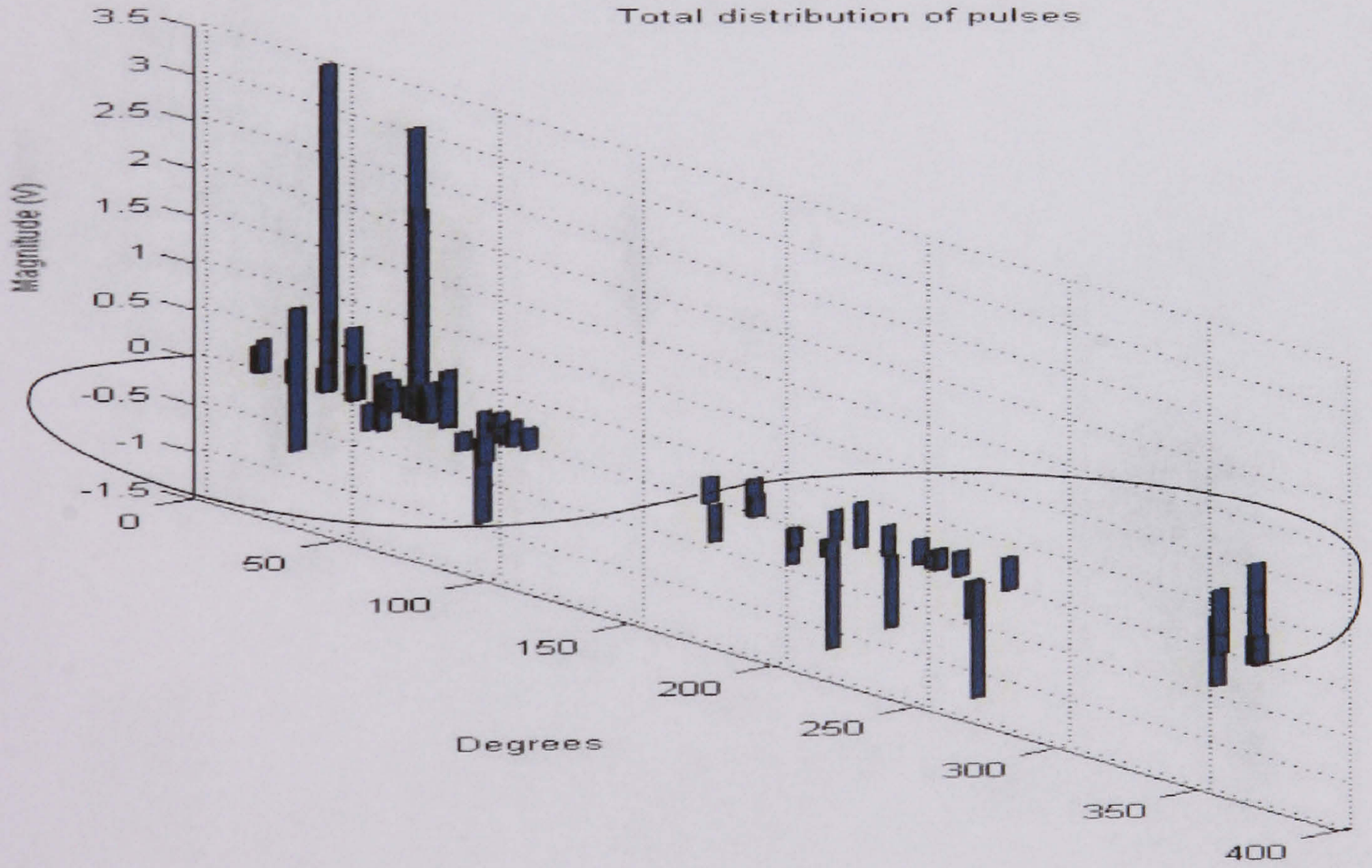

Figure 6.44 Distribution of surface discharges over an aged insulator at 42500 V (resistor)

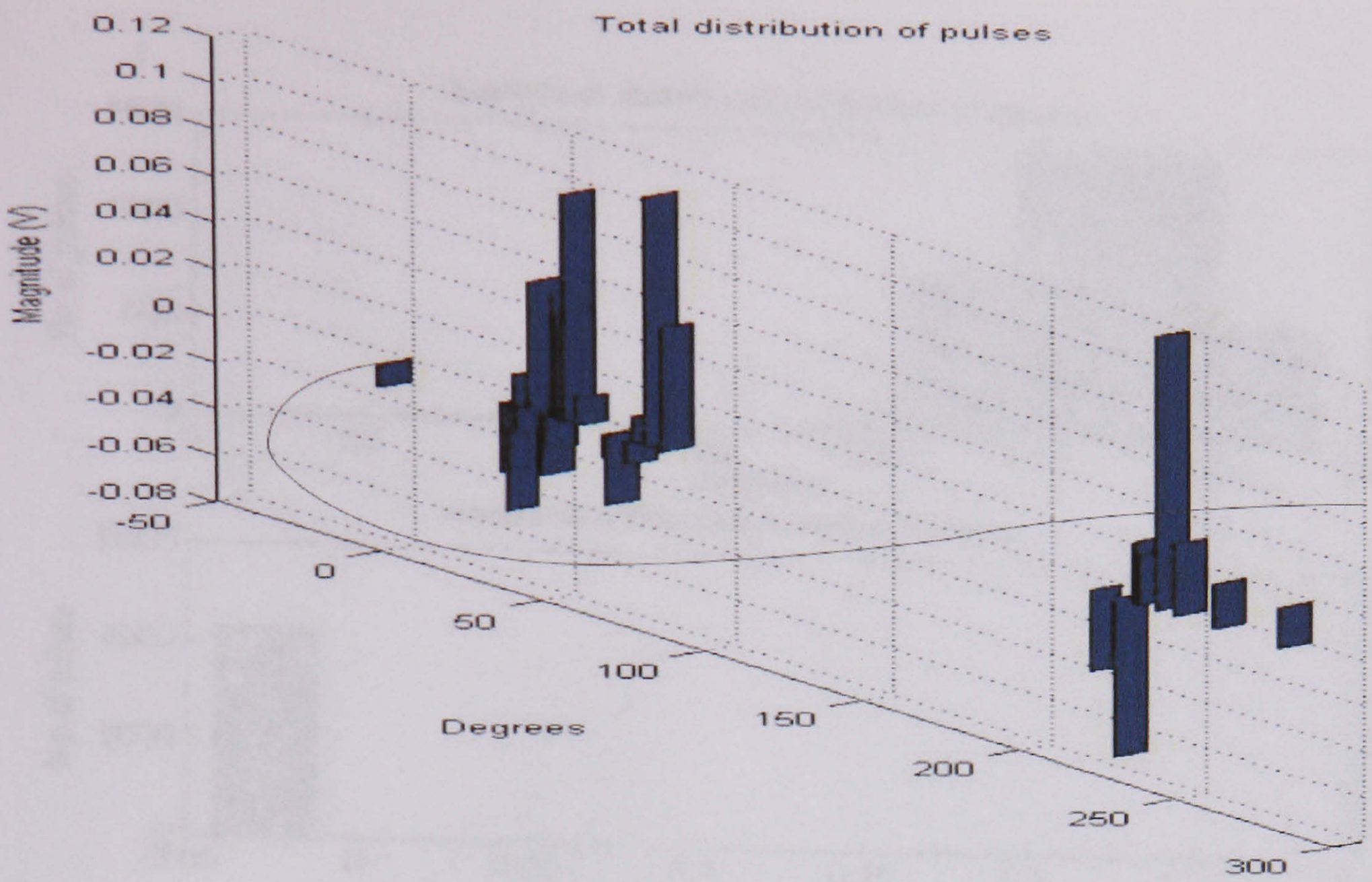

Figure 6.45 Distribution of surface discharges over a pressboard at 24210 V (resistor)

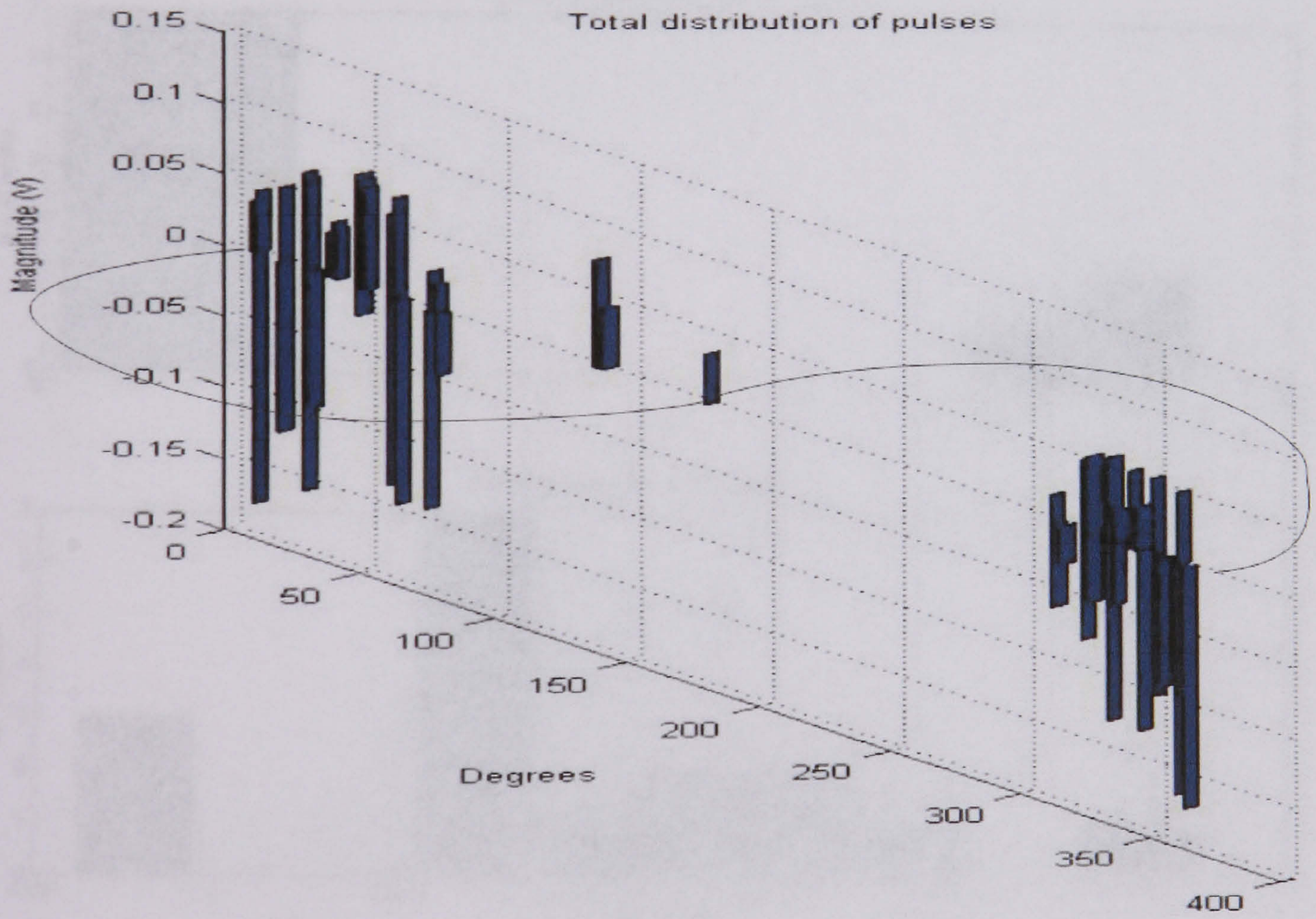

Figure 6.46 Distribution of cavity discharges at 14320 V (resistor)

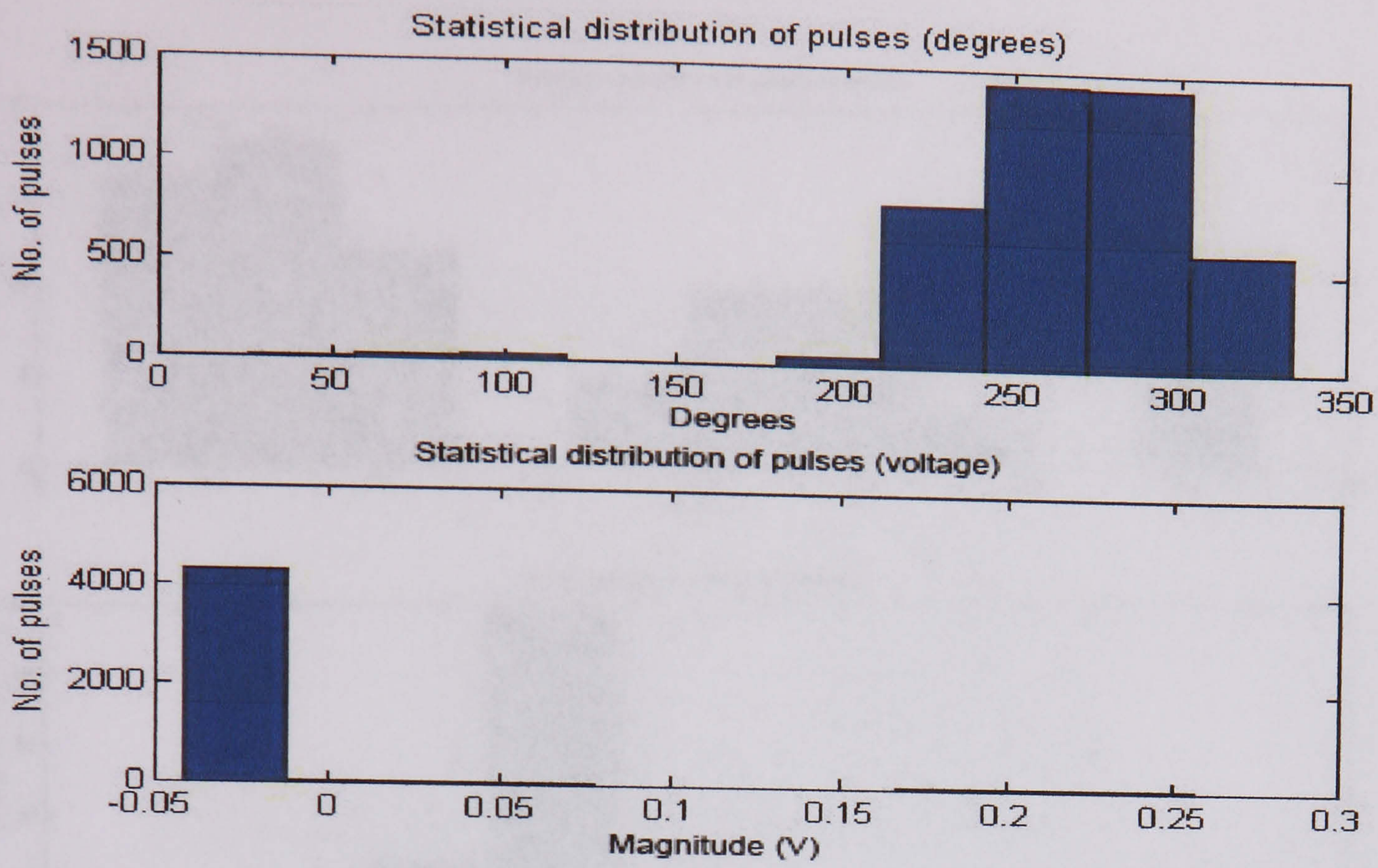

Figure 6.47 Statistical distribution of corona pulses at 6540 V with a 10mm air gap (resistor)

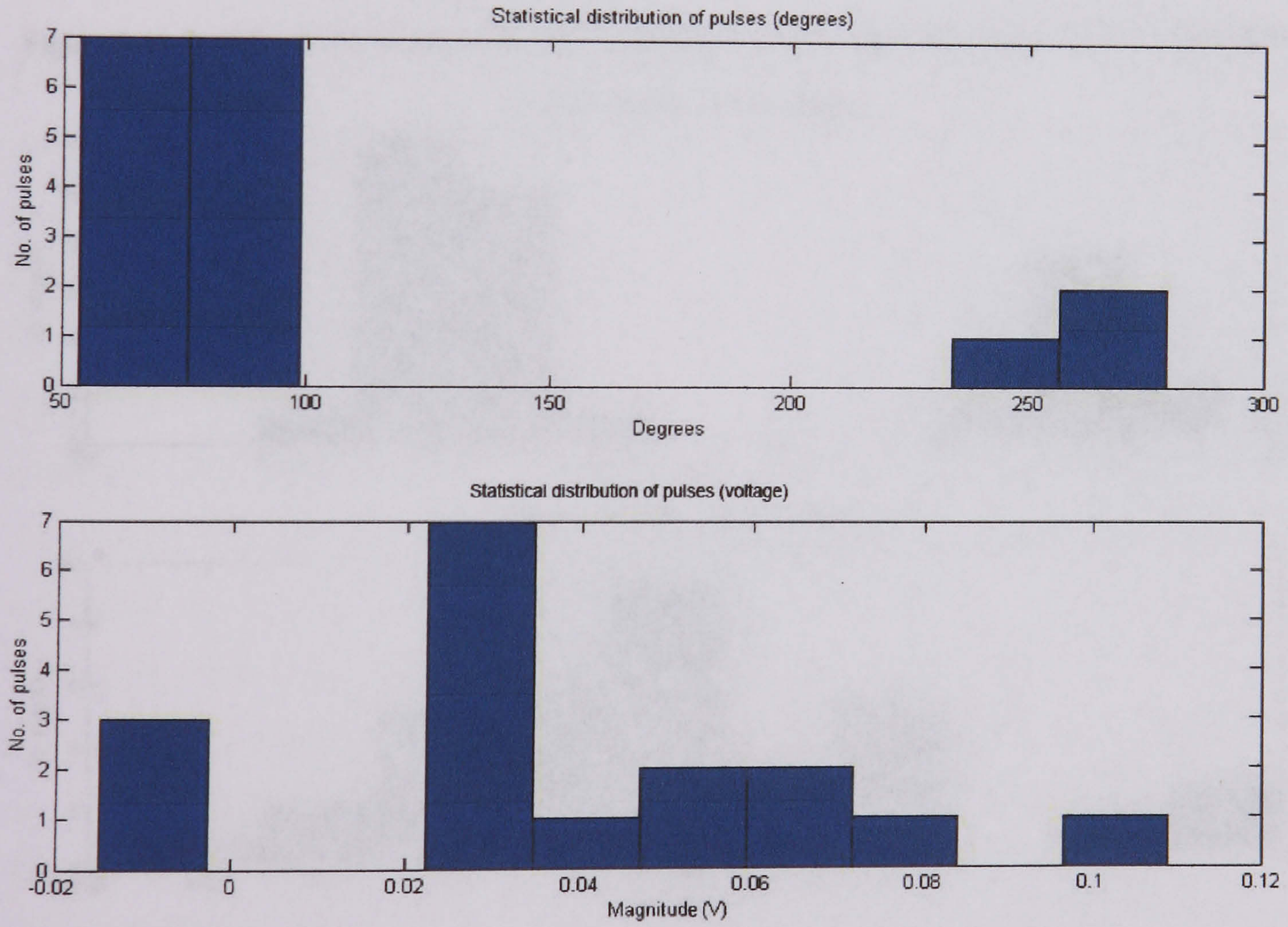

Figure 6.48 Statistical distribution of surface discharges over a new insulator at 42500 V (resistor)

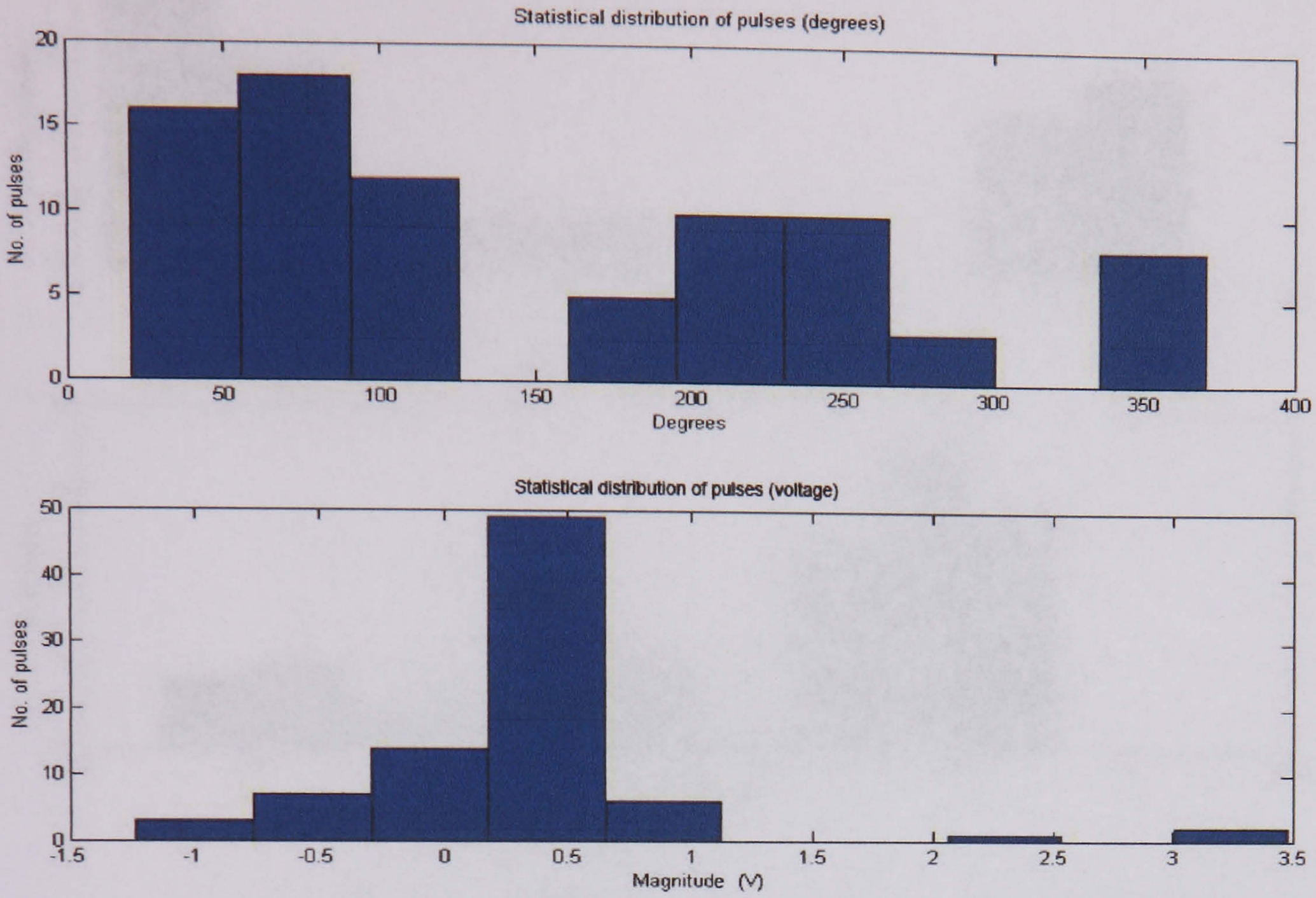

Figure 6.49 Statistical distribution of surface discharges over an aged insulator at 42500 V (resistor)

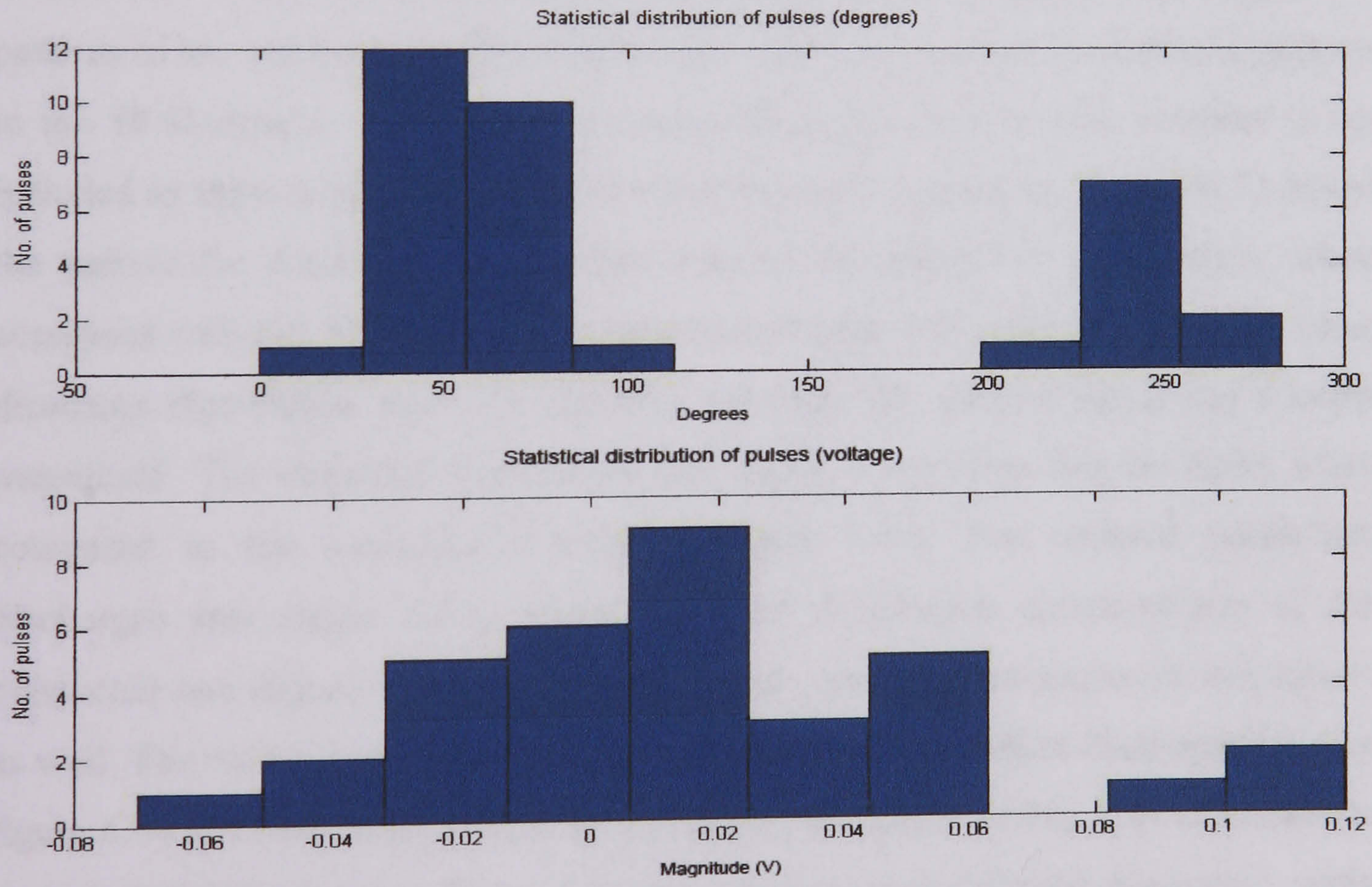

Figure 6.50 Statistical distribution of surface discharges over a pressboard at 24210 V (resistor)

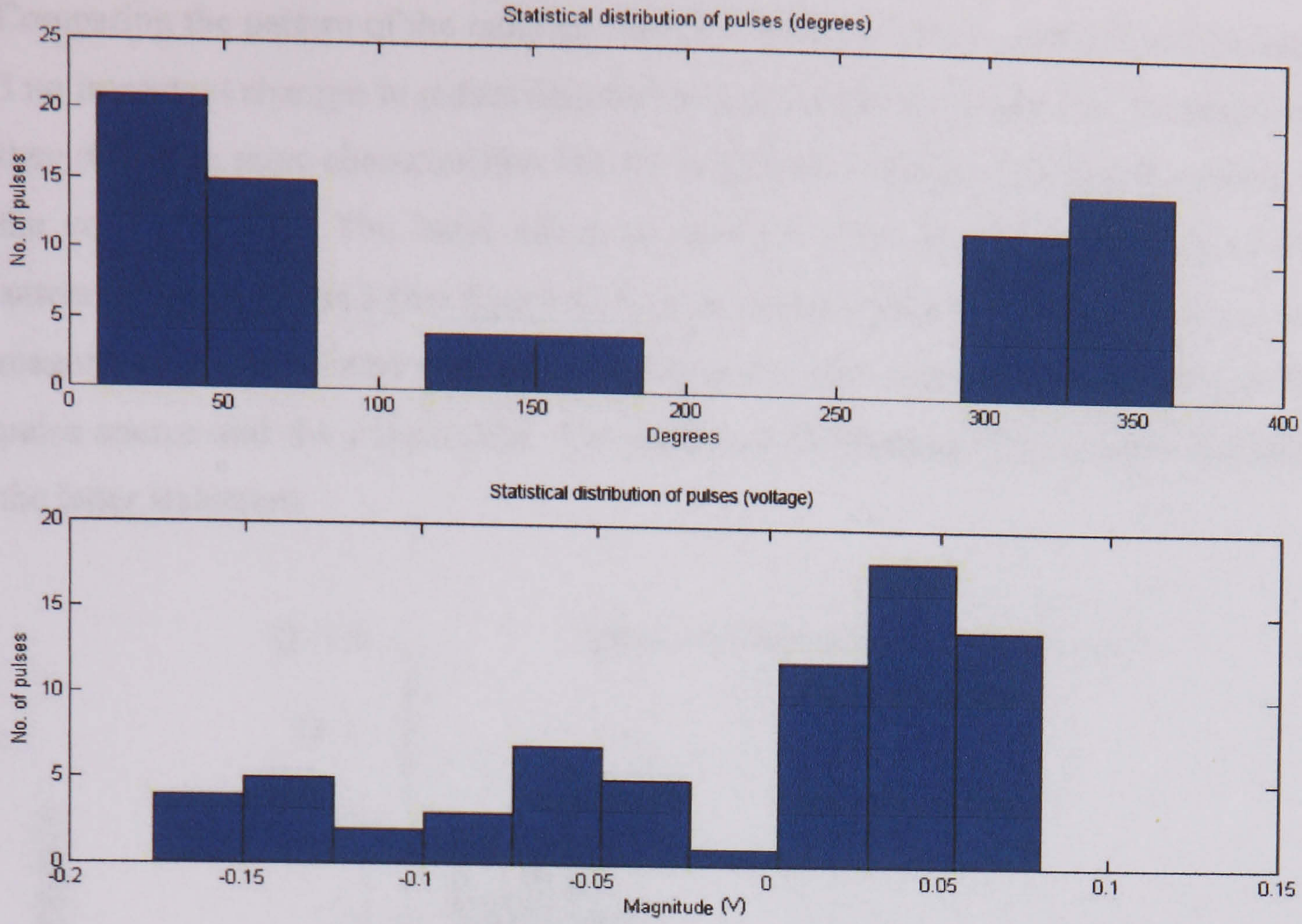

Figure 6.51 Statistical distribution of cavity discharges at 14230 V (resistor)

In order to assess the similarity between radiated and conducted discharges, the patterns of the analyzed samples in antenna 1 and 3 are compared against the patterns in the 50 Ω resistor. The pattern of corona discharge and the new insulator is not included as there is no reception of this discharge at the antennas. Figure 6.52 shows the pattern for discharges in an aged insulator in antenna 1. This pattern, when compared with the 50 Ω resistor measurement (figure 6.44) pattern, shares the same discharge distribution and characteristics although the antenna signal has a lower magnitude. The statistical distribution (see figure 6.55) show this similarity when compared to the conducted discharge (figure 6.49). The radiated pressboard discharges (see figure 6.53) share the same distribution characteristics of the conducted one (figure 6.50) at minor magnitude, more pulses appear in this sample as well. The radiated cavity discharges do not vary its distribution characteristics (see figure 6.54 and 6.60) compared to the conducted one (figure 6.46), they share similar statistical distribution (see figure 6.57 and 6.63) but with different magnitude, again the occurrence of more cavity pulses is observe in the radiated discharge.

Comparing the pattern of the radiated analyzed samples of the antenna 1 and antenna 3 no important changes in pulses distribution and statistical distribution are observed, they share the same characteristics but the magnitude is slight different, but minor to the conducted one. The latter effect is caused by the change in position of the antenna 1 and antenna 3 (see figure 4.15) with respect to the discharge source, i.e. the magnitude of the radiated discharge is a function of the relative distance between the pulse source and the antennas(s). The statistical distribution of the pulses confirms the latter statement.

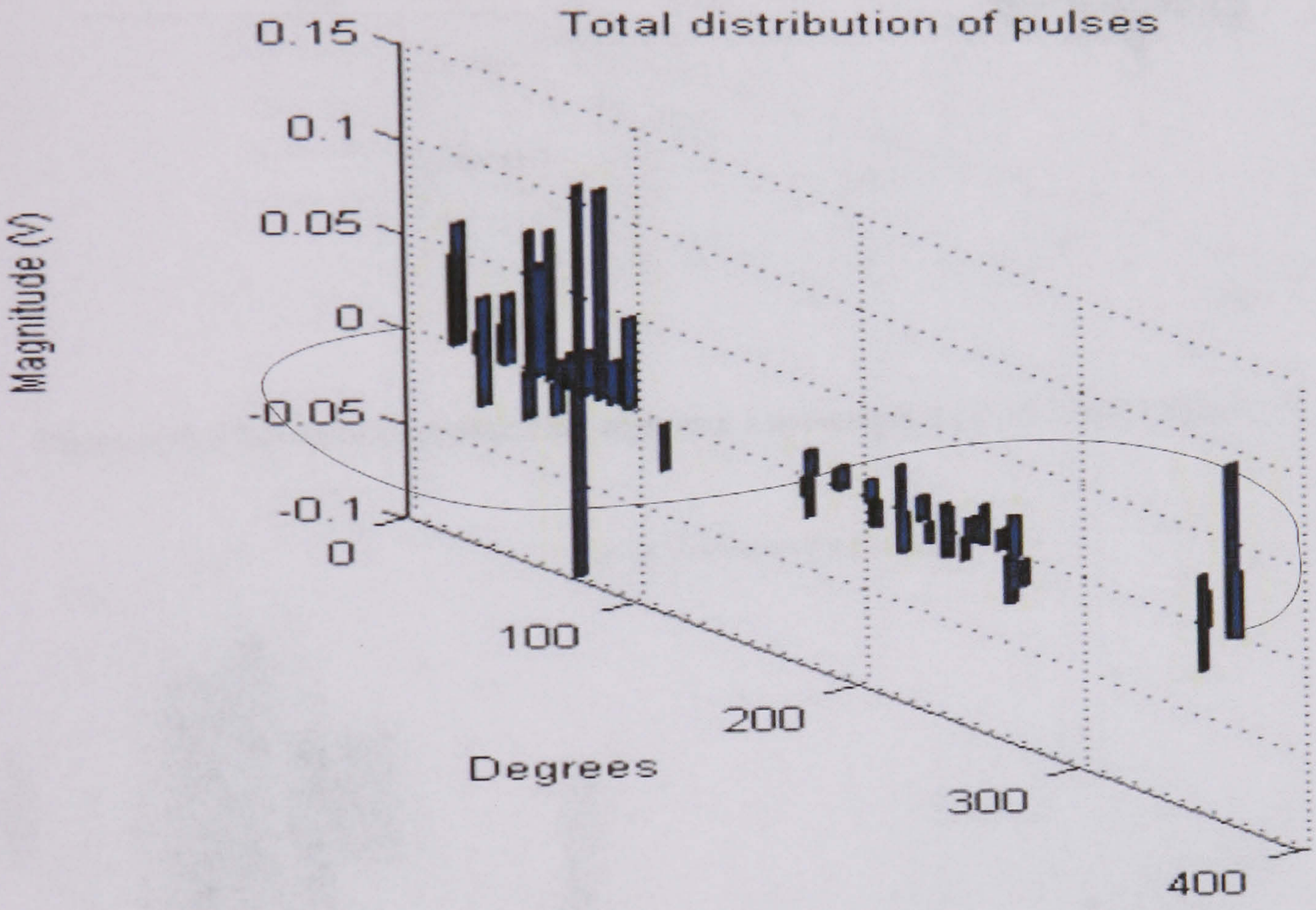

Figure 6.52 Distribution of surface discharges over an aged insulator at 42500 (antenna 1)

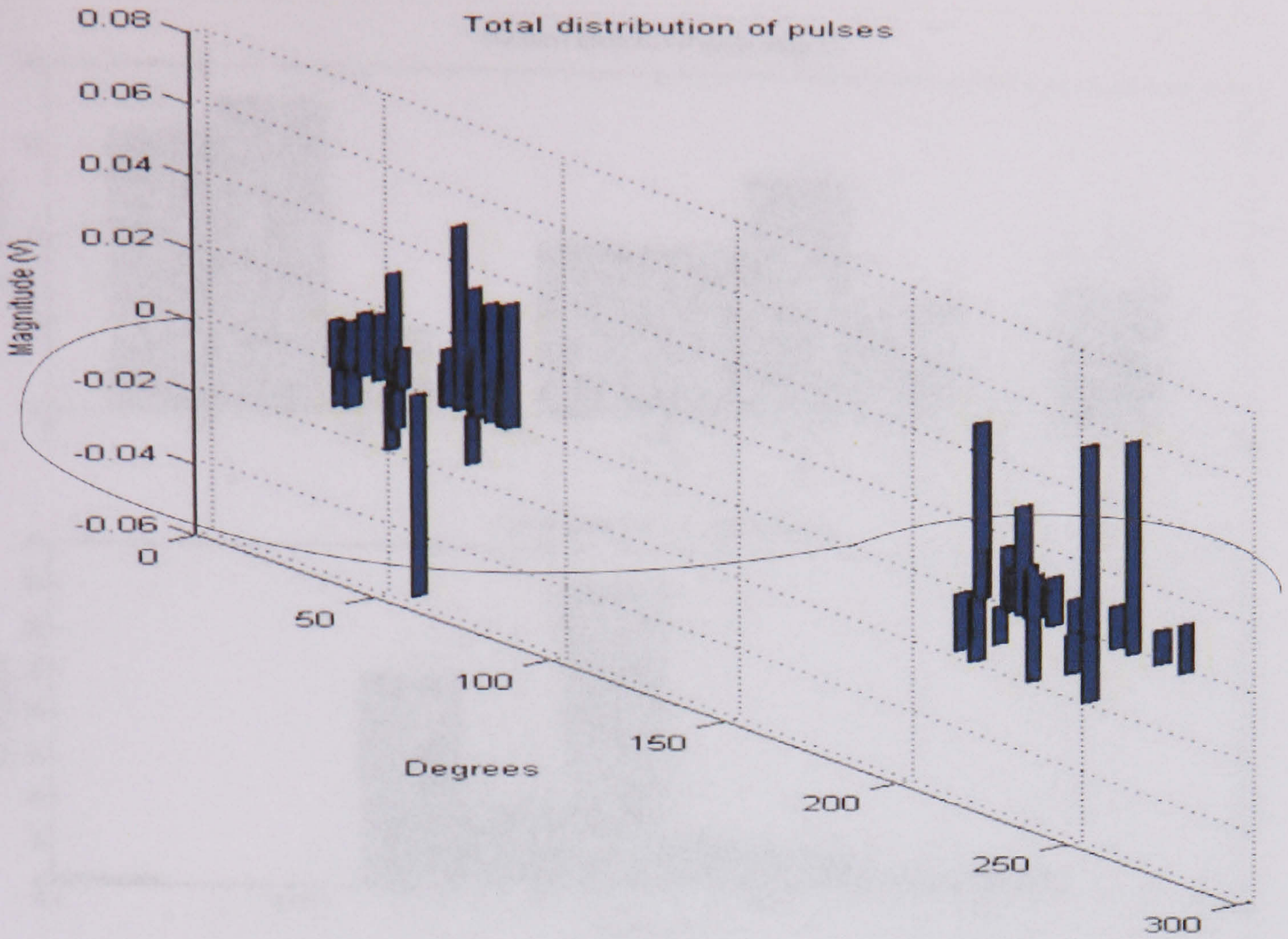

Figure 6.53 Distribution of surface discharges over a pressboard at 24210 V test 5 (antenna 1)

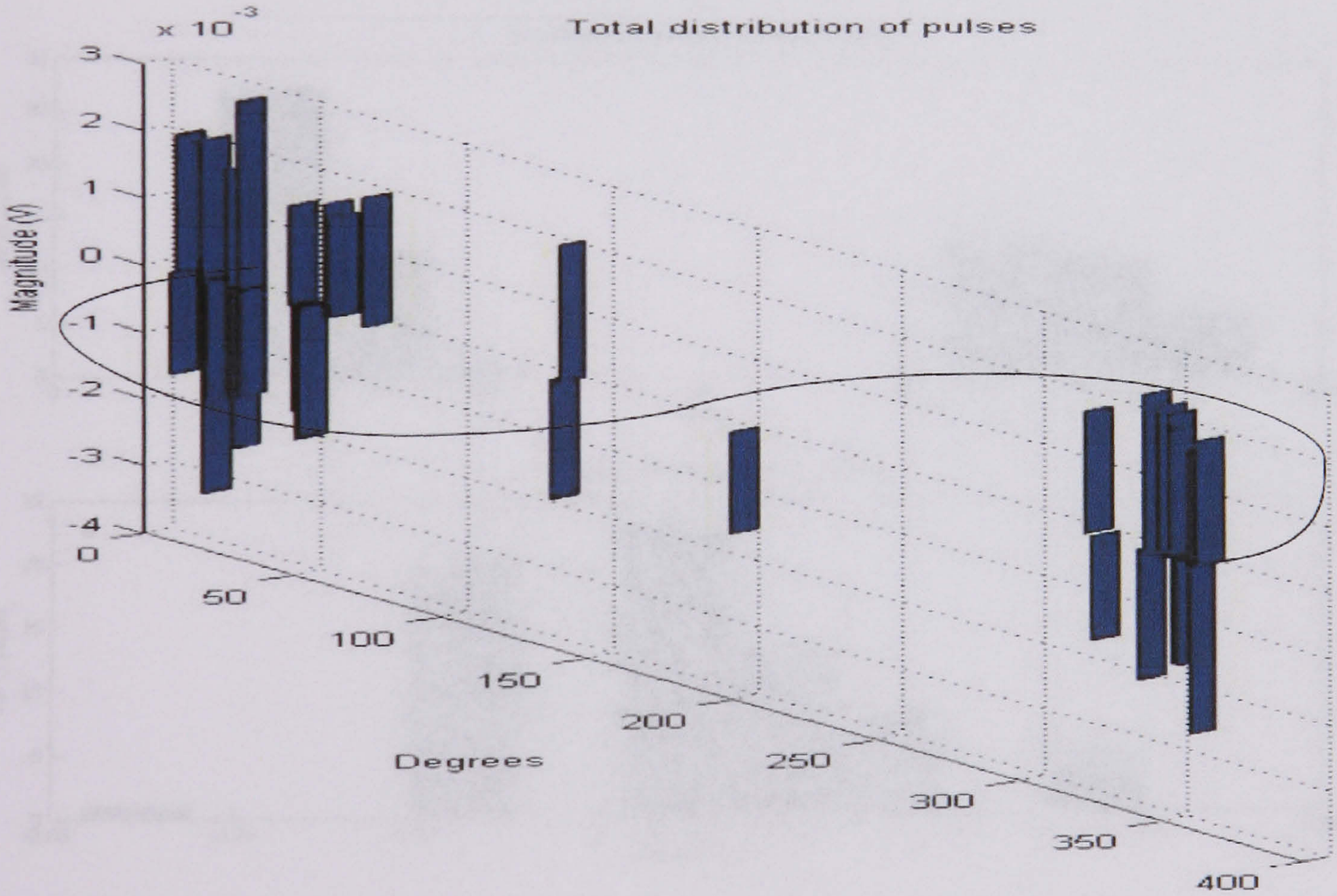

Figure 6.54 Distribution of cavity discharges at 14320 V test 5 (antenna 1)

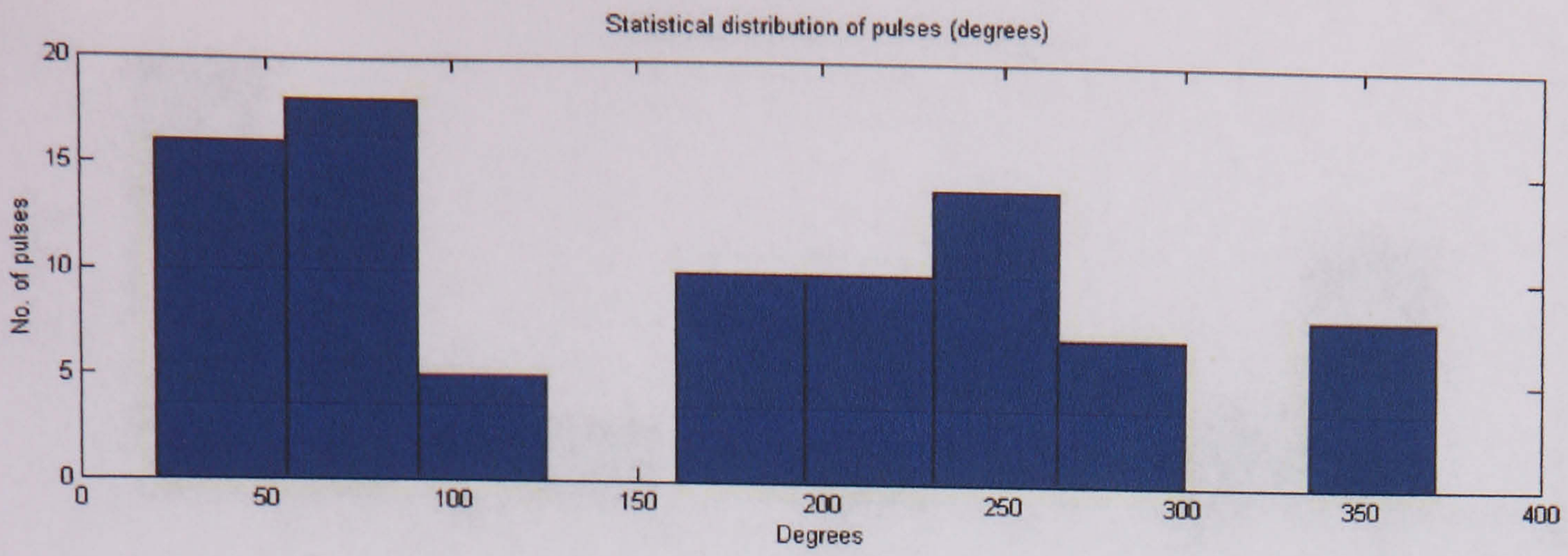

Figure 6.55 Statistical distribution of surface discharges over an aged insulator at 42500 V (antenna 1)

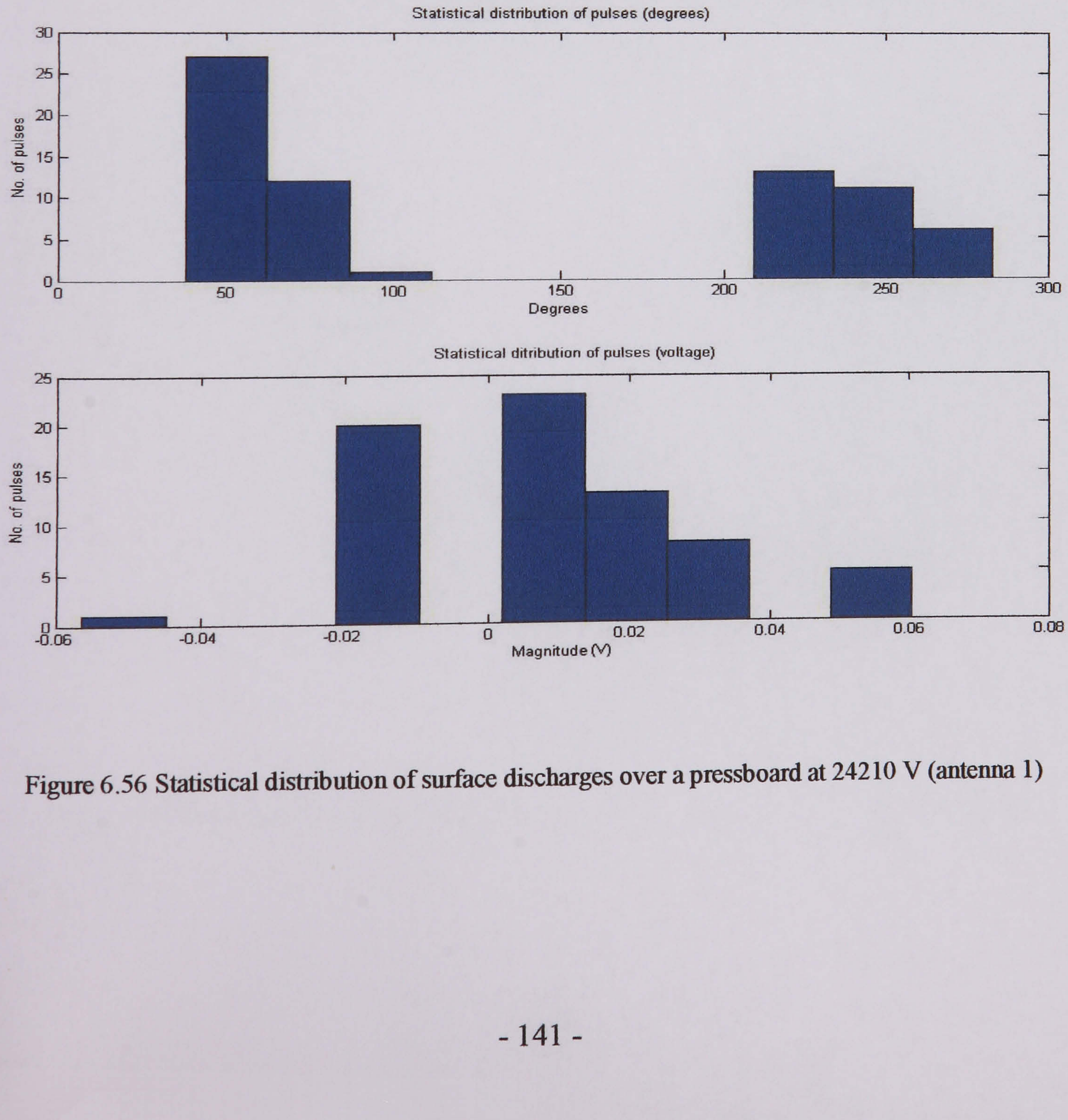

Figure 6.56 Statistical distribution of surface discharges over a pressboard at 24210 V (antenna 1)

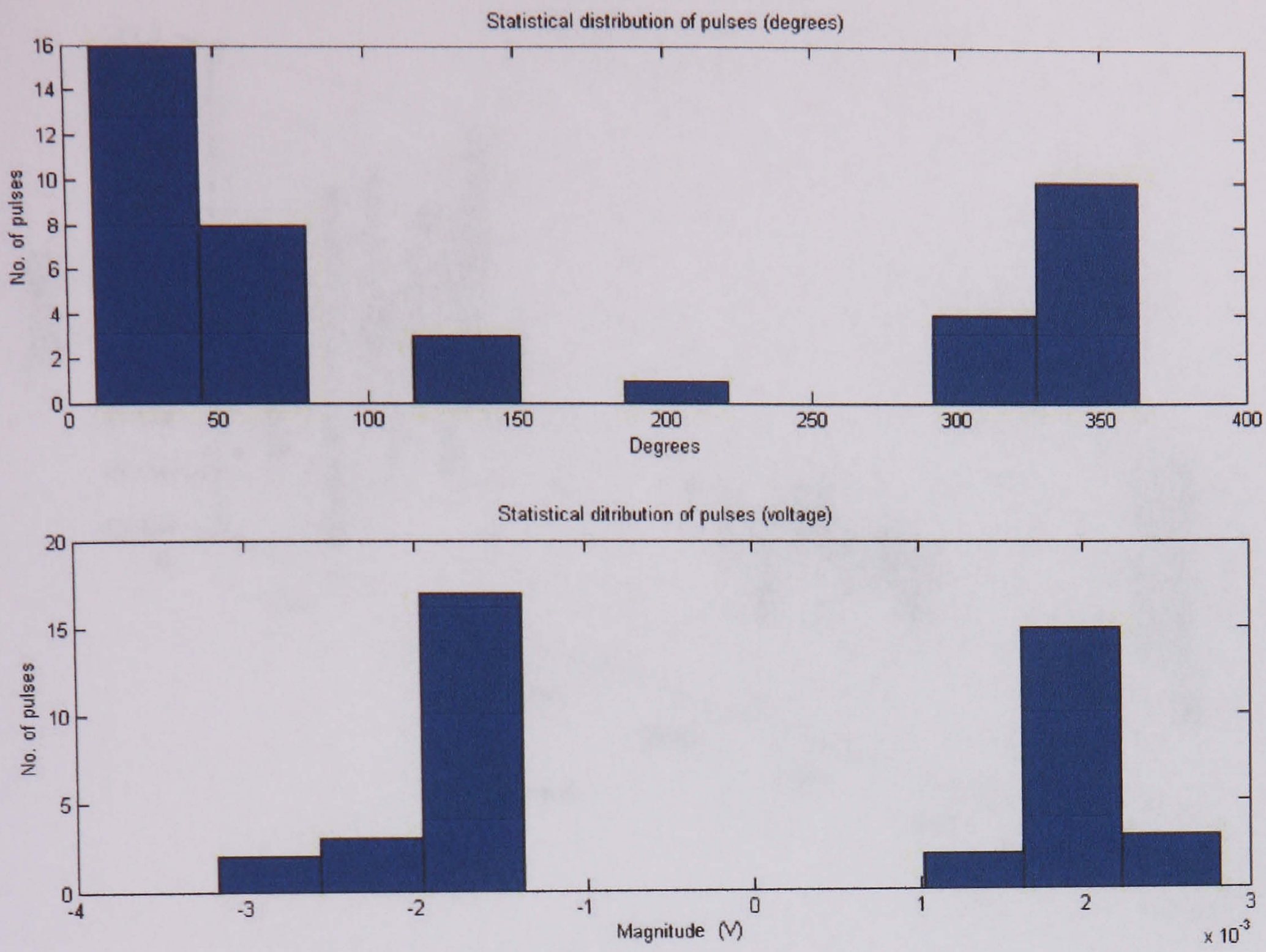

Figure 6.57 Statistical distribution of cavity discharges at 14230 V test 5 (antenna 1)

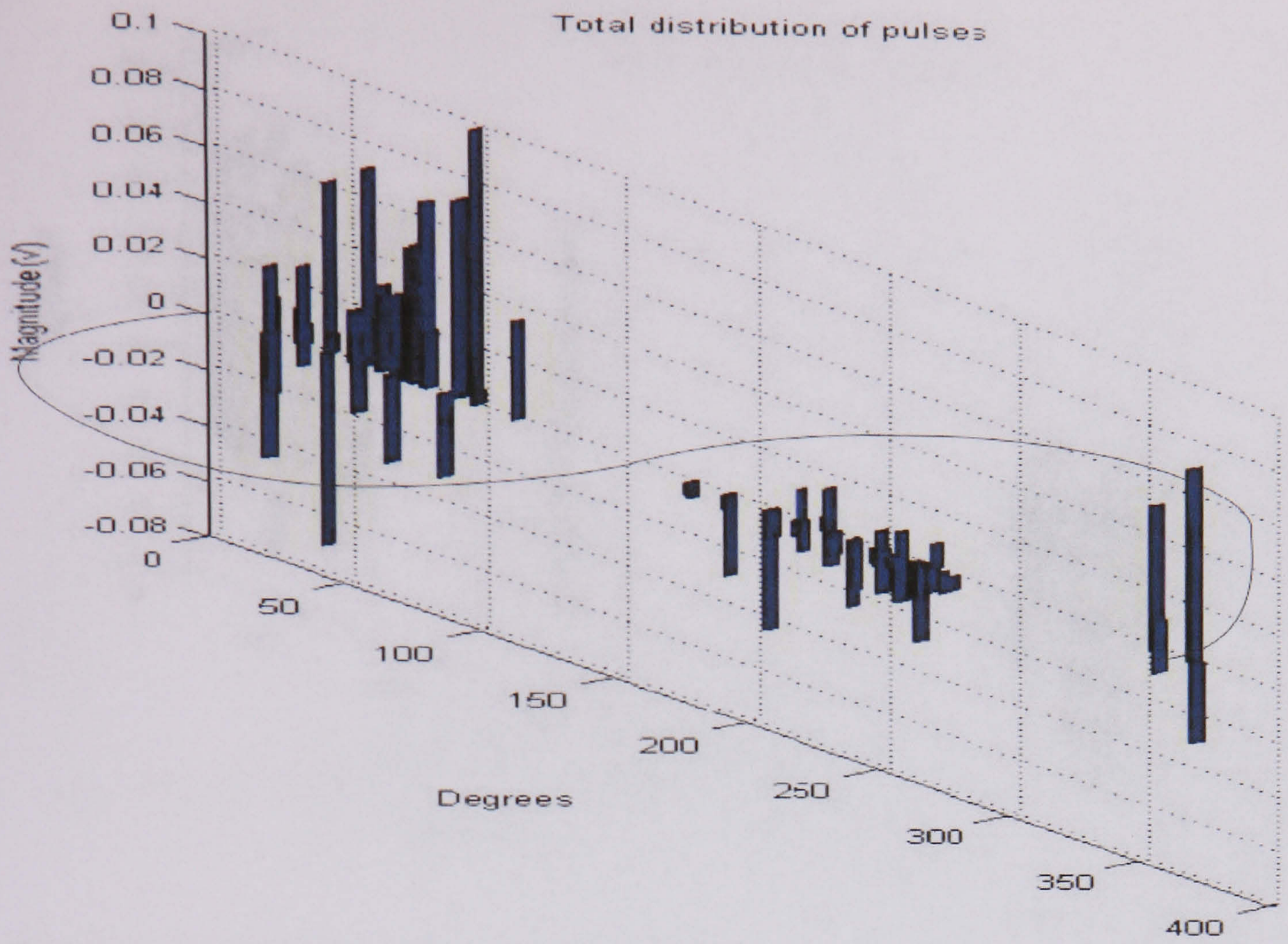

Figure 6.58 Distribution of surface discharges over an aged insulator at 42500 V (antenna3)

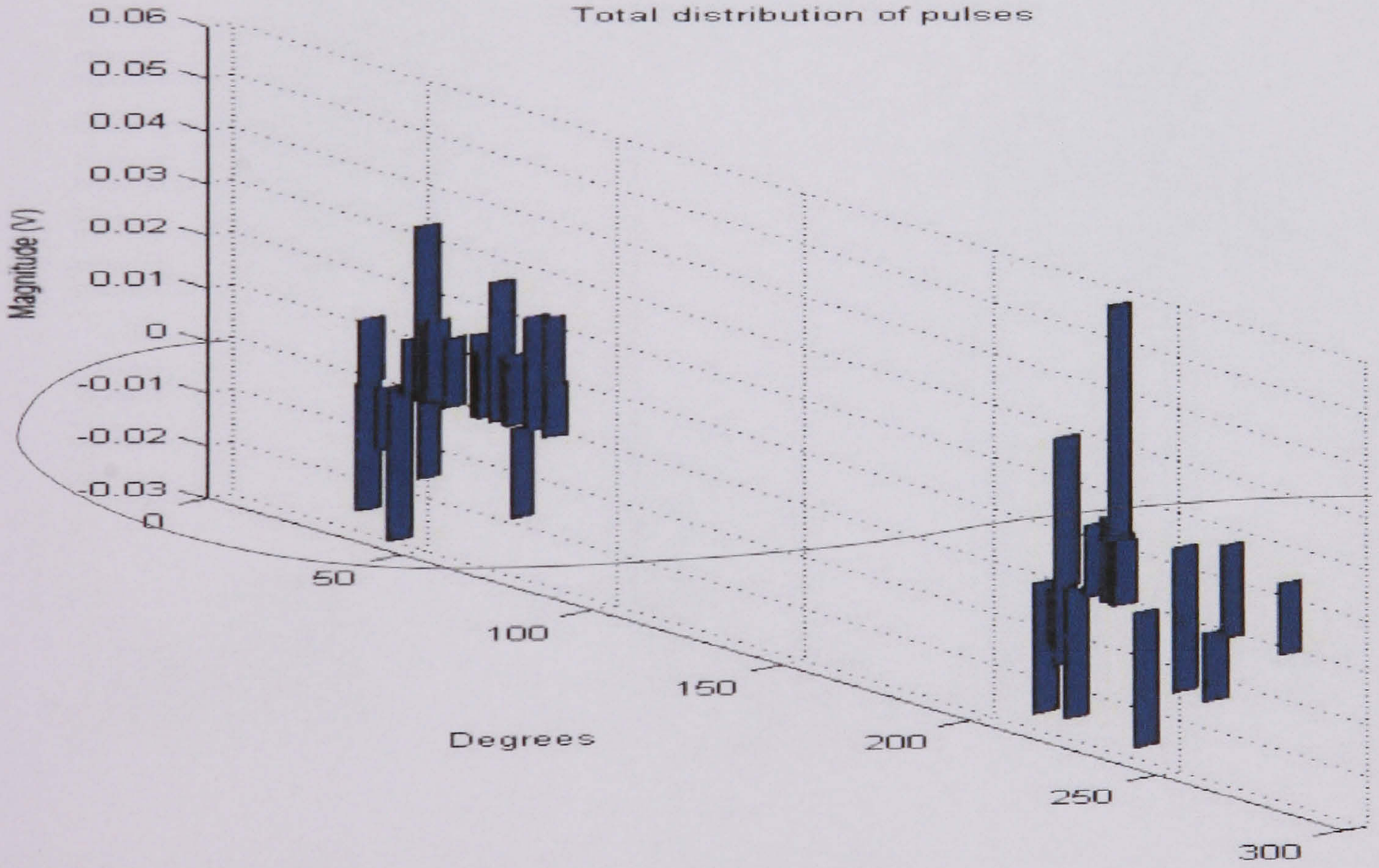

Figure 6.59 Distribution of surface discharges over a pressboard at 24210 V test 5 (antenna 3)

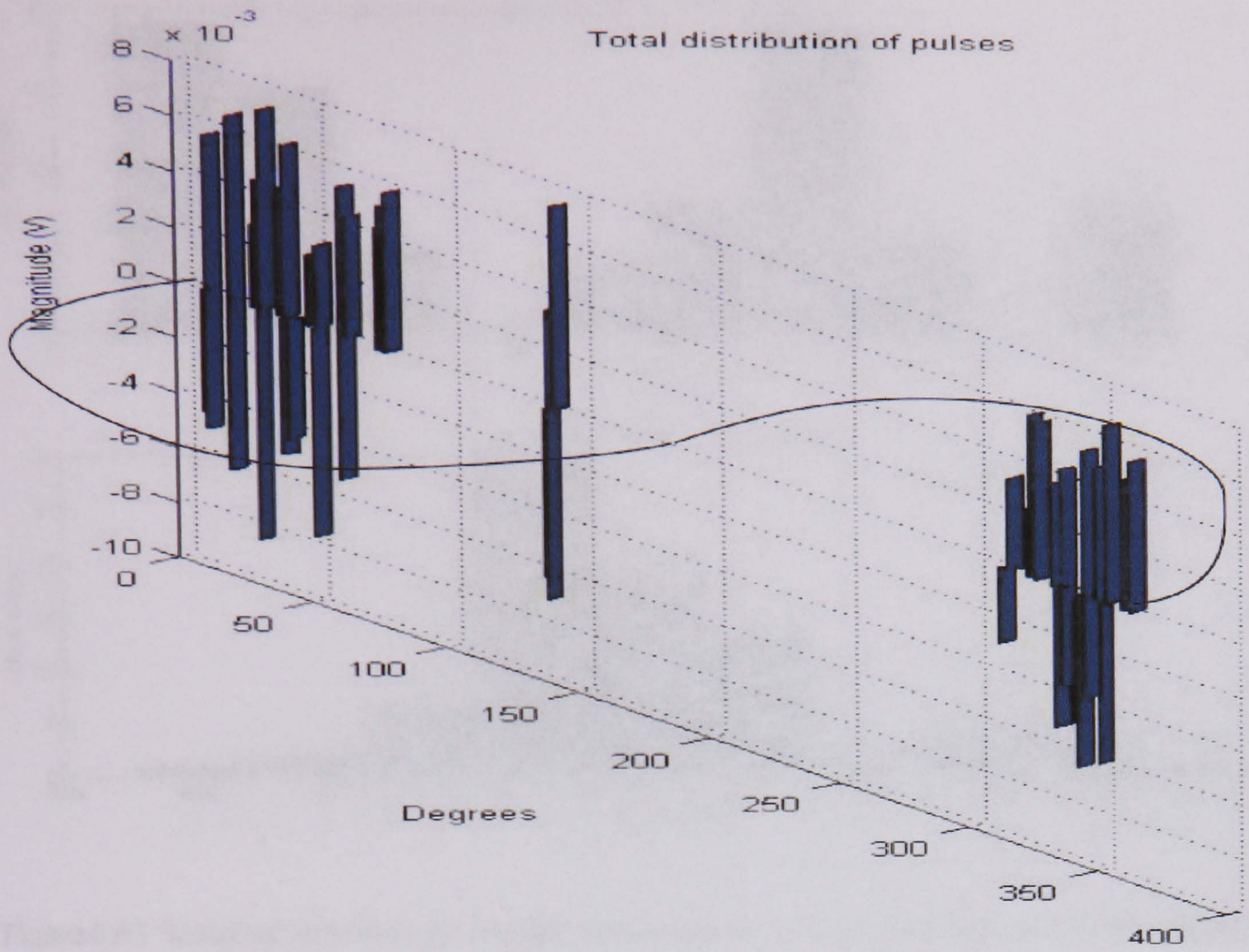

Figure 6.60 Distribution of cavity discharges at 14320 V test 5 (antenna 3)

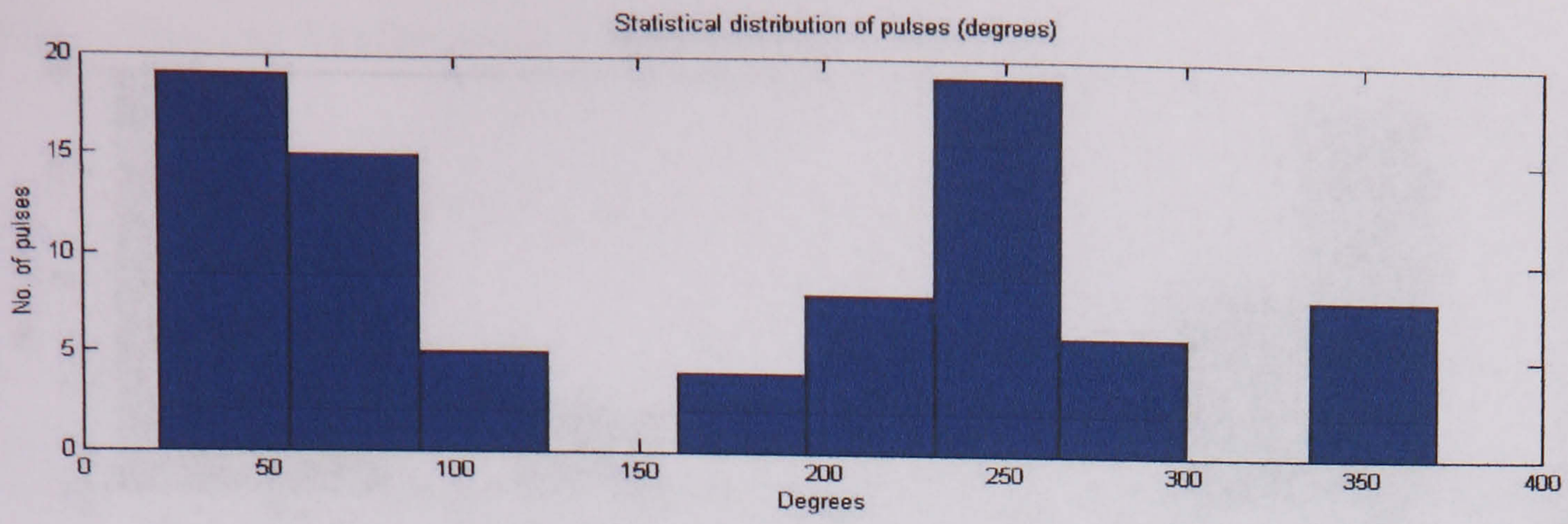

Figure 6.61 Statistical distribution of surface discharges over an aged insulator at 42500 V (antenna3)

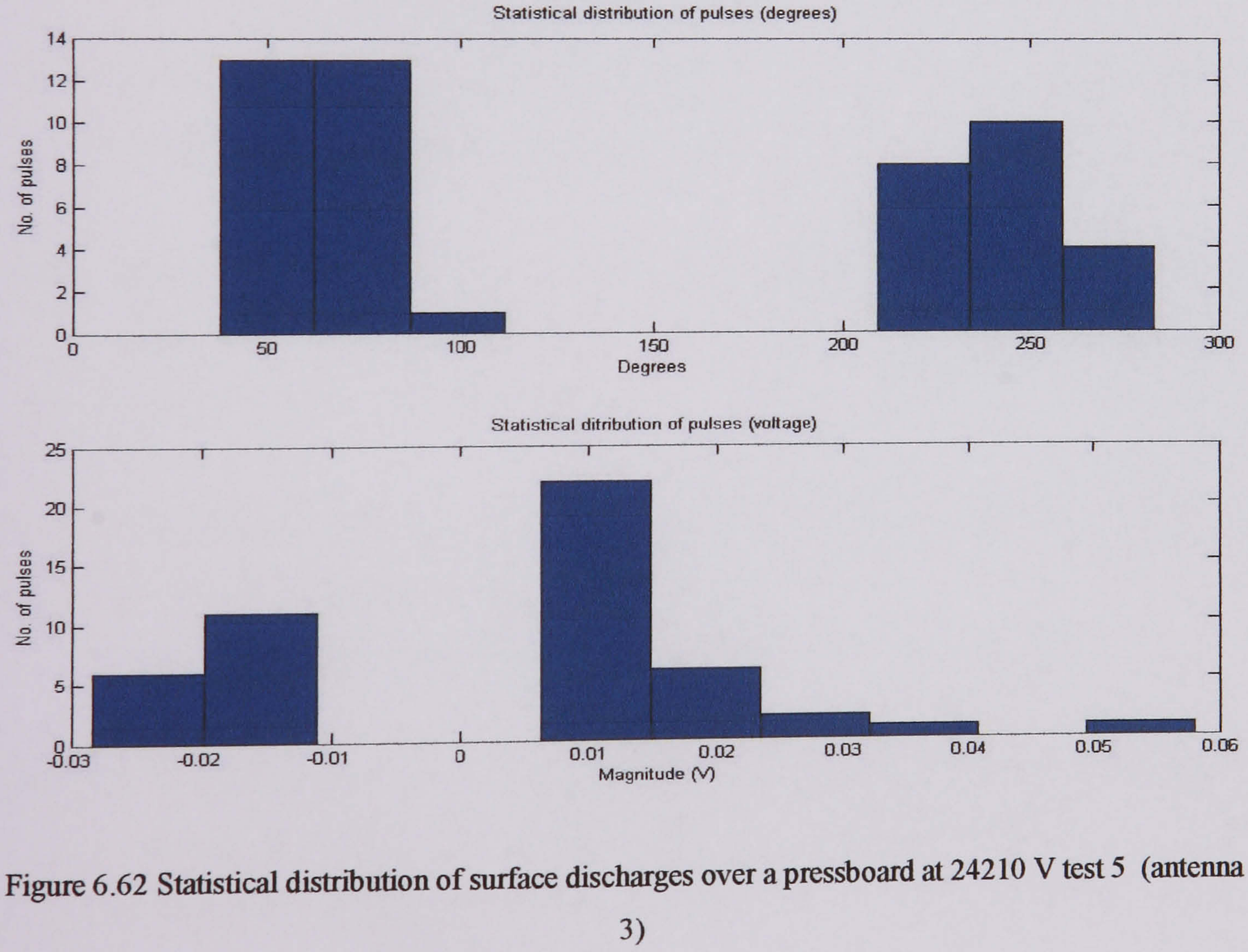

Figure 6.62 Statistical distribution of surface discharges over a pressboard at 24210 V test 5 (antenna 3)

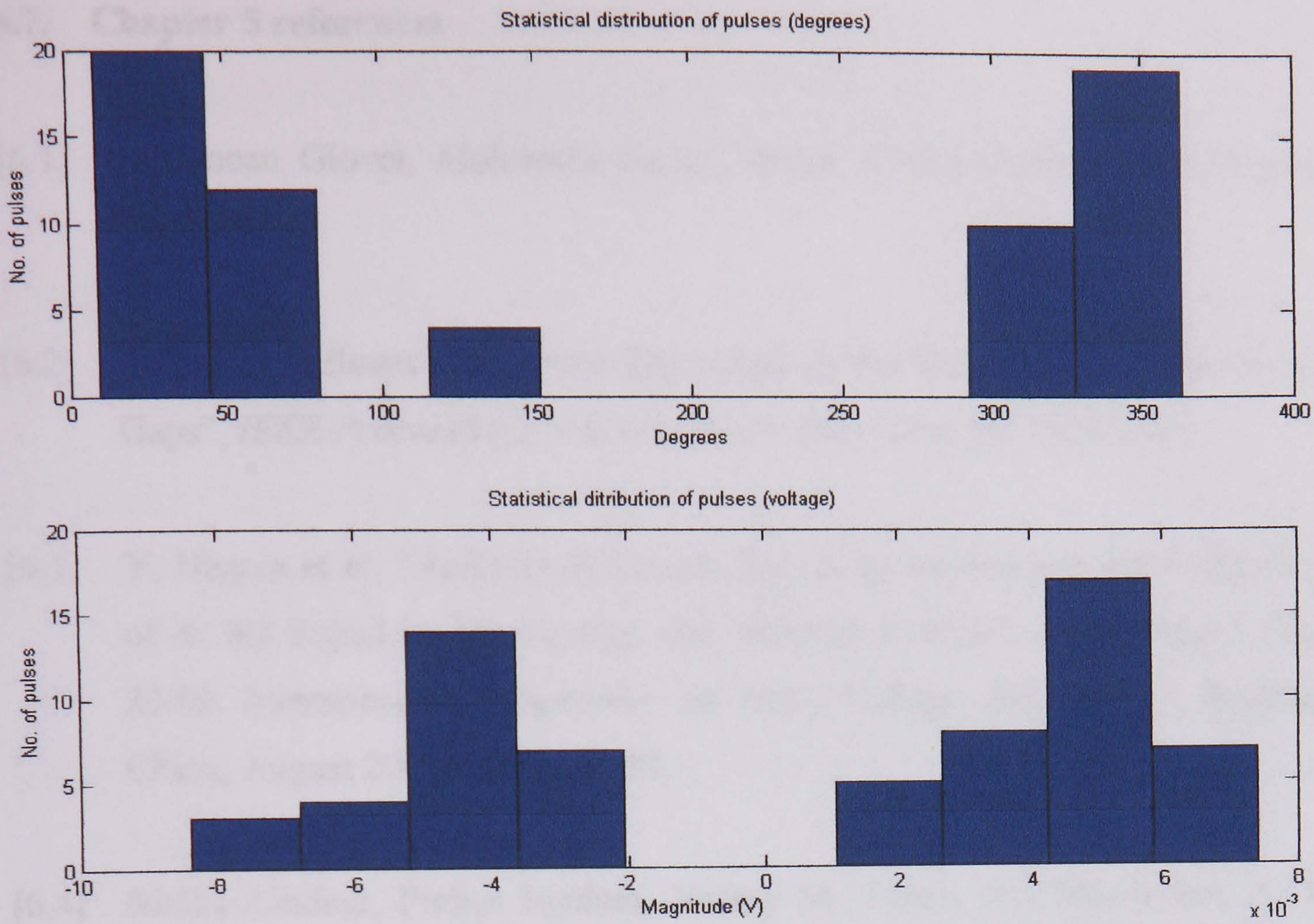

Figure 6.63 Statistical distribution of cavity discharges at 14230 V test 5 (antenna 3)

6.7. Chapter 5 references

[6.1] J. Duncan Glover, Mulukutla Sarma, *Power System Analysis and Design*, PWS, 1994.

[6.2] K. Feser, "Influence of Corona Discharges on the Breakdown Voltage of Air Gaps", *IEEE Proceedings*, Vol.118, No. 9, Sept 1971, pp: 1309-1313.

[6.3] Y. Negara et al, "Analysis of Corona Discharge Mechanism and Evaluation of its PD Signal in AC Air Gap with Metallic Particle", *Proceedings of the XIVth International Symposium on High Voltage Engineering*, Beijing, China, August 2005, session H-59.

[6.4] Malka Lindner, Pinhas Lindner, Jeremy M. Topaz, Avi Mendelson, A. J. Philips, "Daycor - A Dual Spectrum Camera for Daytime Corona Detection", *Daycor Systems*, http://www.daycor.com/camera-arc.html.

[6.5] Steven A. Boggs, "Partial Discharge: Overview and Signal Generation", *IEEE Electrical Insulation Magazine*, Vol.6, No.4 Jul./Aug., 1990, pp: 13-39.

[6.6] Steven A. Boggs, "Partial Discharge – Part VII: Practical Techniques for measuring PD in operating Equipment, *IEEE Electrical Insulation Magazine*, Vol.7, No.4 Jul/Aug, 1991, pp: 9-19.

[6.7] E. Lemke, P. Schmiegel, "Introduction to Fundamentals of PD Diagnostics", *Lemke Diagnostics*, website: http://www.hvtechnologies.com/images/publications/intro-us.pdf.

[6.8] R. S. Gorur and J. W. Chang, "Surface Hydrophobicity of Polymers Used For Outdoor Insulation", *IEEE Transactions on Power Delivery*, Vol.5, No.4 November, 1990, pp: 1923-1933.

[6.9] James P. Hall, "History and bibliography of polymeric insulators for outdoor applications", *IEEE Transactions on Power Delivery*, Vol.8, No.1 January, 1991, pp: 376-385.

[6.10] *IEC High Voltage Test Techniques*, International Electrotechnical Commission International, Standard, IEC 60-1, 1989.

[6.11] *IEEE Trial – Use Guide for the Detection of Acoustic Emissions from Partial Discharges in Oil – Immersed Power Transformers*, Transformer Committee of the IEEE Power Engineering Society,IEEE, 2000.

[6.12] N. H. Malik, A. A. Al-Arainy, M. I. Qureshi, *Electrical Insulation in Power Systems*, Marcel Dekker, 1998.

[6.13] Steven A. Boggs, "Partial Discharge – Part III: Cavity-Induce PD in Solid Dielectrics, *IEEE Electrical Insulation Magazine*, Vol.6, No.6 Nov./Dec., 1990, pp: 11-20.

[6.14] E.M. Bazelyan, Yu. P. Raizer, *Spark Discharge*, CRC Press LLC, 1998

[6.15] A. Krivda, Recognition of discharges: Discrimination and classification, Ph. D. dissertation, Delft University of Technology, The Netherlands 1995.

DISCRIMINATION OF THE GENERATED PARTIAL DISCHARGES

This chapter explains the need to implement a discrimination method for recognition of the generated partial discharges, the latter can be achieved through the introduction of statistical operators and discrimination techniques. These techniques will prove that radiated discharge signals preserves the basic characteristics of conducted discharge signals and leads to a suitable discrimination between the different samples used in this research.

7.1. The need of discrimination techniques.

Chapter 6 gave us an overview of the differences found between the different samples used in this research for conducted and radiated discharges; the analysis was basically made observing the different patterns of the discharges and its characteristics using the AC waveform (point on wave information) since the frequency content of the samples does not contain enough information to differentiate the discharges, however the simple observation of the pattern generated by the PD's is not enough to ensure a correct classification although different methods has been developed [7.1], its analysis becomes even more difficult when a three dimensional graph is generated, hence a suitable method in two dimensions to simplify analysis and detect subtle differences between samples becomes necessary. A reliable action is the analysis of quantifiable parameters obtained during the numerical processing of the acquired partial discharges, after the numerical

processing of those parameters, the application of statistical tools must follow, the result is known as statistical operators [7.2]. Statistical operators approach the numerous differences in magnitude, shape, angle and pulse distribution using point on wave information. This research uses typical statistical operators and introduces different ones; the next section is a description of the statistical operators used for discrimination of partial discharges.

7.2. Statistical operators.

Statistical operators are used mainly for the identification of phase-time resolved data patterns. They allow the recognition of different kinds of patterns that contain quantifiable information using several statistical methods to help discriminate the analyzed partial discharges. A brief description of the statistical operators used in this research will follow:

Skewness.- Skewness is a measure of the degree of asymmetry of the distribution with respect to a normal distribution [7.3,7.4], if the left tail is more pronounced than the right tail, the function is said to have a negative skewness, if the opposite happens is said to have positive skewness, if they are equal the function have cero skewness. Skewness is defined as:

$$S_k = \frac{\sum_{i=1}^{n}(x_i - \mu)^3 f(x_i)}{\sigma^3 \sum_{i=1}^{n} f(x_i)} \tag{7.1}$$

Were x_i is the recorded value, μ is the mean value and σ is the variance.

Kurtosis.- Kurtosis is an indication of the "peakedness" or sharpness of the distribution with respect to a normal distribution [7.3,7.5], high kurtosis means that most of the variance is due to infrequent extreme deviations (sharp distribution) and low kurtosis means small deviations (flat distribution). Kurtosis is defined as:

$$k_u = \frac{\sum_{i=1}^{n}(x_i - \mu)^4 f(x_i)}{\sigma^4 \sum_{i=1}^{n} f(x_i)} - 3 \qquad (7.2)$$

Were x_i is the recorded value, μ is the mean value and σ is the variance.

Cross correlation (cc) factor.- Cross correlation (sometimes called cross covariance) measure the similarity between two distributions of the positive and the negative half cycles of the AC signal taken as reference [7.6], a cc factor of 1 means 100 % shape symmetry, a cc factor of 0 means total asymmetry. The cross correlation factor is defined as:

$$cc = \frac{\sum_{i=1}^{n} x_i^+ x_i^- - \sum_{i=1}^{n} x_i^+ \sum_{i=1}^{n} x_i^- / n}{\sqrt{\left[\sum_{i=1}^{n}(x_i^+)^2 - (\sum_{i=1}^{n} x_i^+)^2 / n\right]\left[\sum_{i=1}^{n}(x_i^-)^2 - (\sum_{i=1}^{n} x_i^-)^2 / n\right]}} \qquad (7.3)$$

In the above equation x_i^+ is the average discharge magnitude in the i-th window of the positive half cycle and x_i^- the average discharge magnitude in the corresponding window in the negative half cycle; n is the number of phase windows per half cycle. Since pulse peaks can be positive or negative and can happen in both negative and positive half cycle of the AC waveform used as reference, skewness has to be computed separately.

Average distance between pulses.- The average distance between pulses indicates the occurrence of pulses within a positive or negative half cycle. It measures the average distance between the first pulse and the following one along the positive or negative half cycle of the analyzed samples in degrees, a distance of 0 means no pulse or a single pulse has occurred. The Average distance between pulses is defined as:

$$P_o = \frac{\sum_{i=1}^{n} P_i - P_{i+1}}{n-1} \tag{7.4}$$

Where P_i is the recorded pulse and n the number of recorded pulses.

Average pulse magnitude (D_{pn}) between positive and negative half cycles.- The average magnitude of pulses occurring in the positive and negative half cycles, is an indication of pulse magnitude in relationship with its position in the AC wave form. This is an important parameter for measure the severity of the discharge. This parameter is defined as:

$$D_{pn} = ABS(\sum \overline{M}_p - \sum \overline{M}_n) \tag{7.5}$$

Where $\overline{M}$ is the average magnitude of the positive half cycle pulses or the average magnitude of the negative half cycle pulses.

The above statistical operators were used for pattern recognition of the conducted and radiated partial discharges generated in this research.

7.3 Pattern recognition using statistical operators.

The graphical representation of the statistical operators, also known as the fingerprint of the discharge [7.7], is an important guidance in PD recognition since there are particular patterns for every kind of discharge. Once the statistical operators have been determined, the next step in the development of a method for PD recognition is the creation of a database that include as many patterns of different PD's as possible. In this research the initial database is formed mainly by the conducted partial discharges generated in the HV laboratory and they will serve as a reference when compare to the radiated ones. Appendix H shows the generated data base included the computed statistical operator from the radiated discharges.

7.3.1 Computing of statistical operators.

As it was described in section 4.3 the software used for the computation of point on wave information from the oscilloscope data file was made in MATLAB, the main characteristics are:

- Graphic user interface (GUI)
- Data acquisition
- Processing of point of wave information
- Detection of positive and negative peaks along the AC wave form used as reference
- Pulse counting
- PD average magnitude
- Average PD occurrence
- Computation of statistical operators
- Graphic output of computed parameters
- Data storage in excel datasheets
- Database storage of computed parameters

The figures 7.1-7.5 show the characteristics patterns of the acquired samples using the 50 Ω resistor, the patterns of the statistical operators for the used samples in antenna 1 and 3 are shown in appendix I. Note that the kurtosis and skewness operators were applied to the positive pulses, negative pulses, point-on-wave and magnitudes. In figures 7.1-7.5 these are shown as:

Kurtosisma(bkmap).- Kurtosis positive magnitude

Kurtosisdg(bkdgp).- Kurtosis positive point on wave

Skewnessma(bsmap).- Skewness positive magnitude

Skewnessdg(bsdgp).- Skewness positive point on wave

Kurtosisma(ckman).- Kurtosis negative magnitude

Kurtosisdg(ckdgn).- Kurtosis negative point on wave

Skewnessma(csman).- Skewness negative magnitude

Skewnessdg(csdgn).- Skewness negative point on wave

Avr distance pulses(distpn)/360.- Average distance between pulses occurring each half cycle.

Avr pos/neg relationship(diffpn).- Ratio between average pulses occurring each half clycle.

Correlation(ccr1).- Cross correlation factor

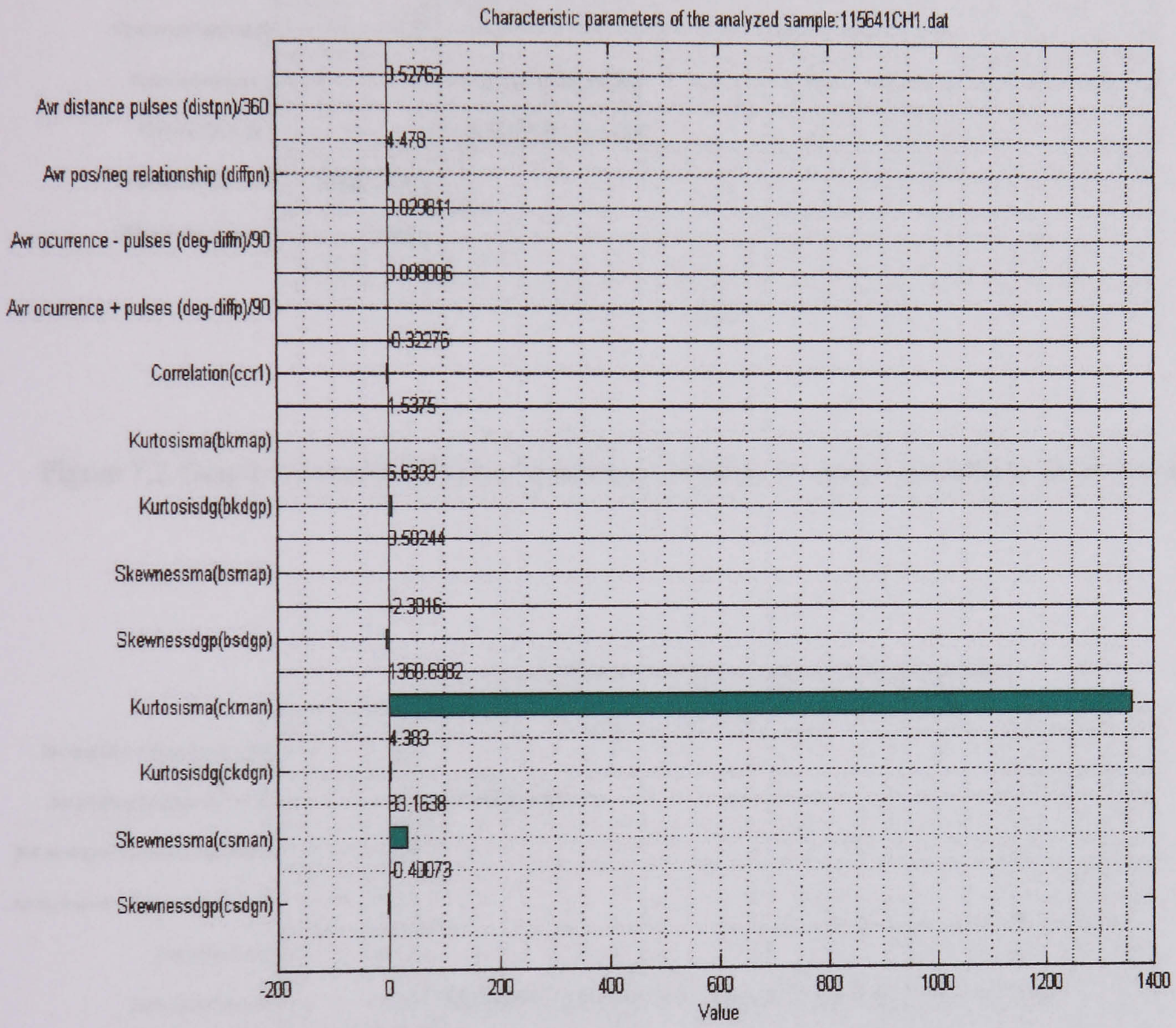

Figure 7.1 Graphical representation of statistical operators for corona discharge in the 50 Ω resistor

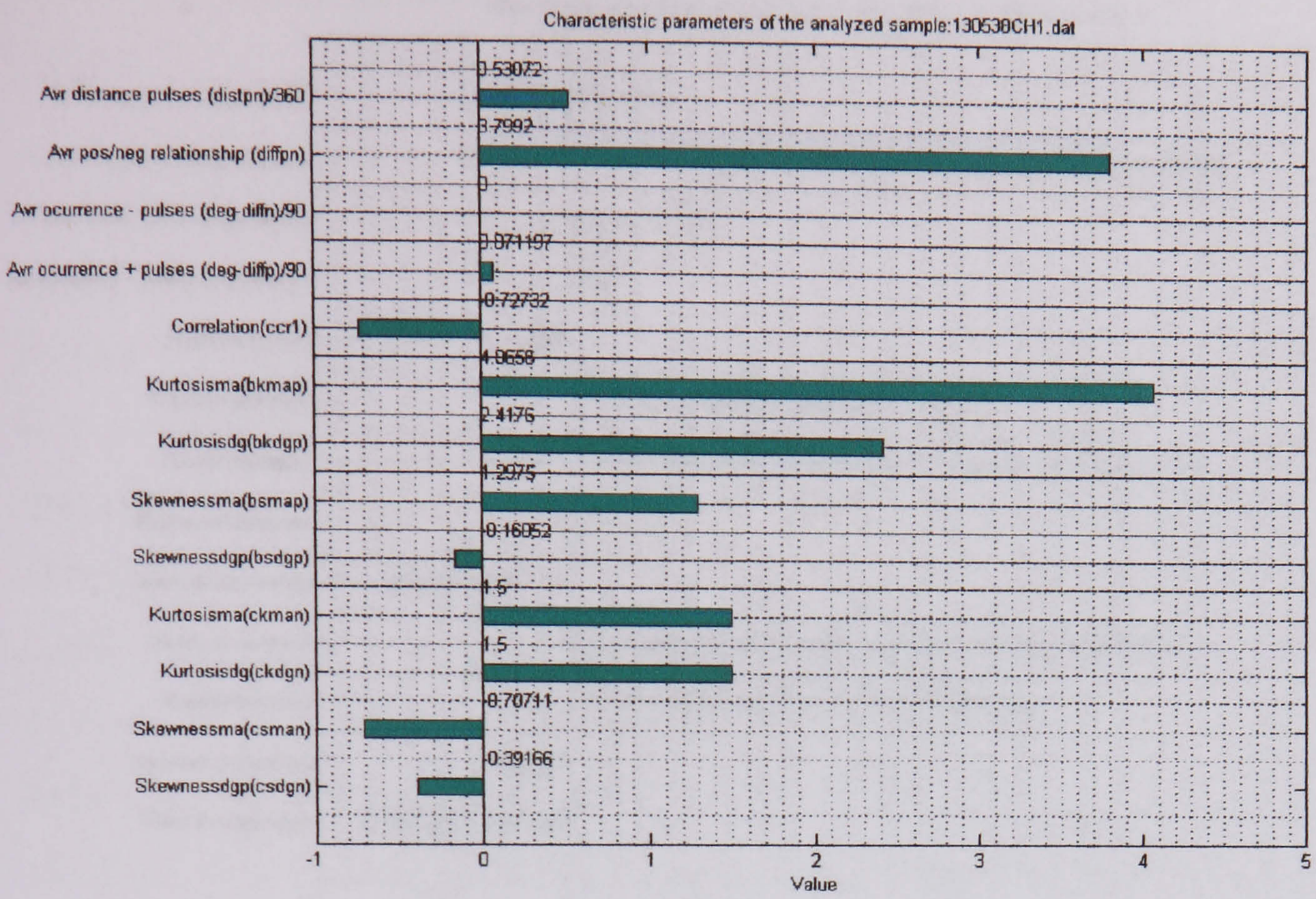

Figure 7.2 Graphical representation of statistical operators for a new insulator in the 50 Ω resistor

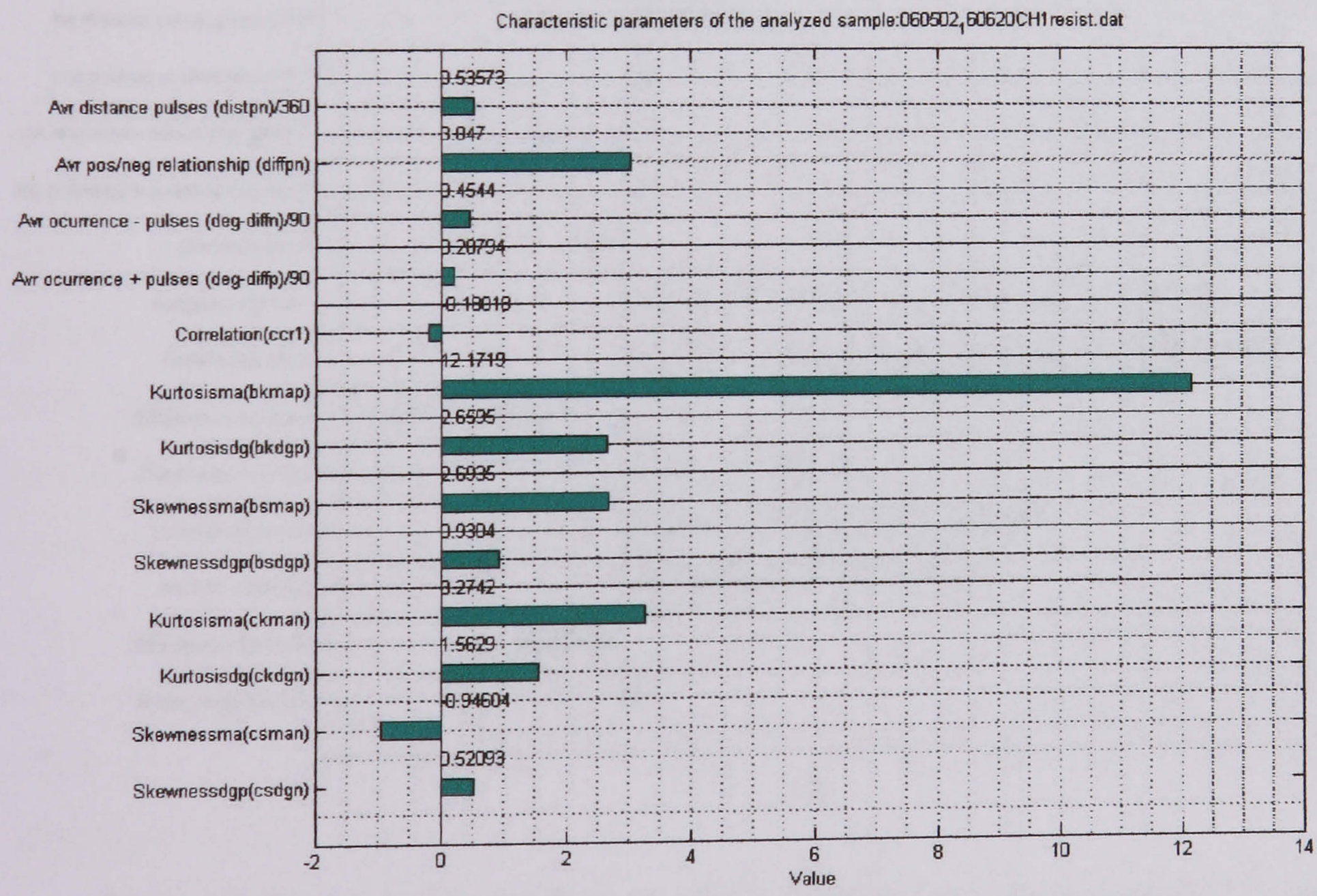

Figure 7.3 Graphical representation of statistical operators for an aged insulator in the 50 Ω resistor

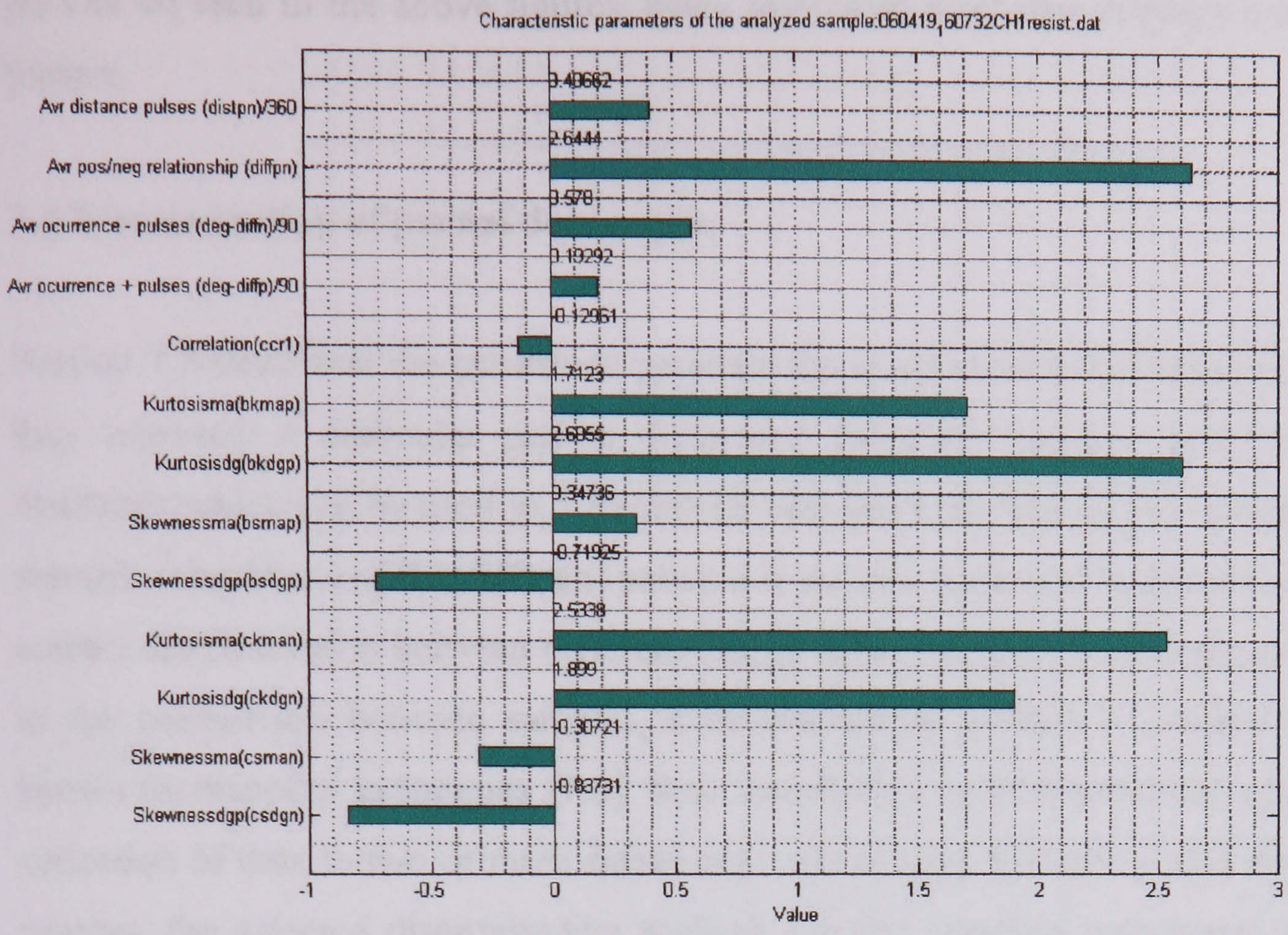

Figure 7.4 Graphical representation of statistical operators for a pressboard in the 50 Ω resistor

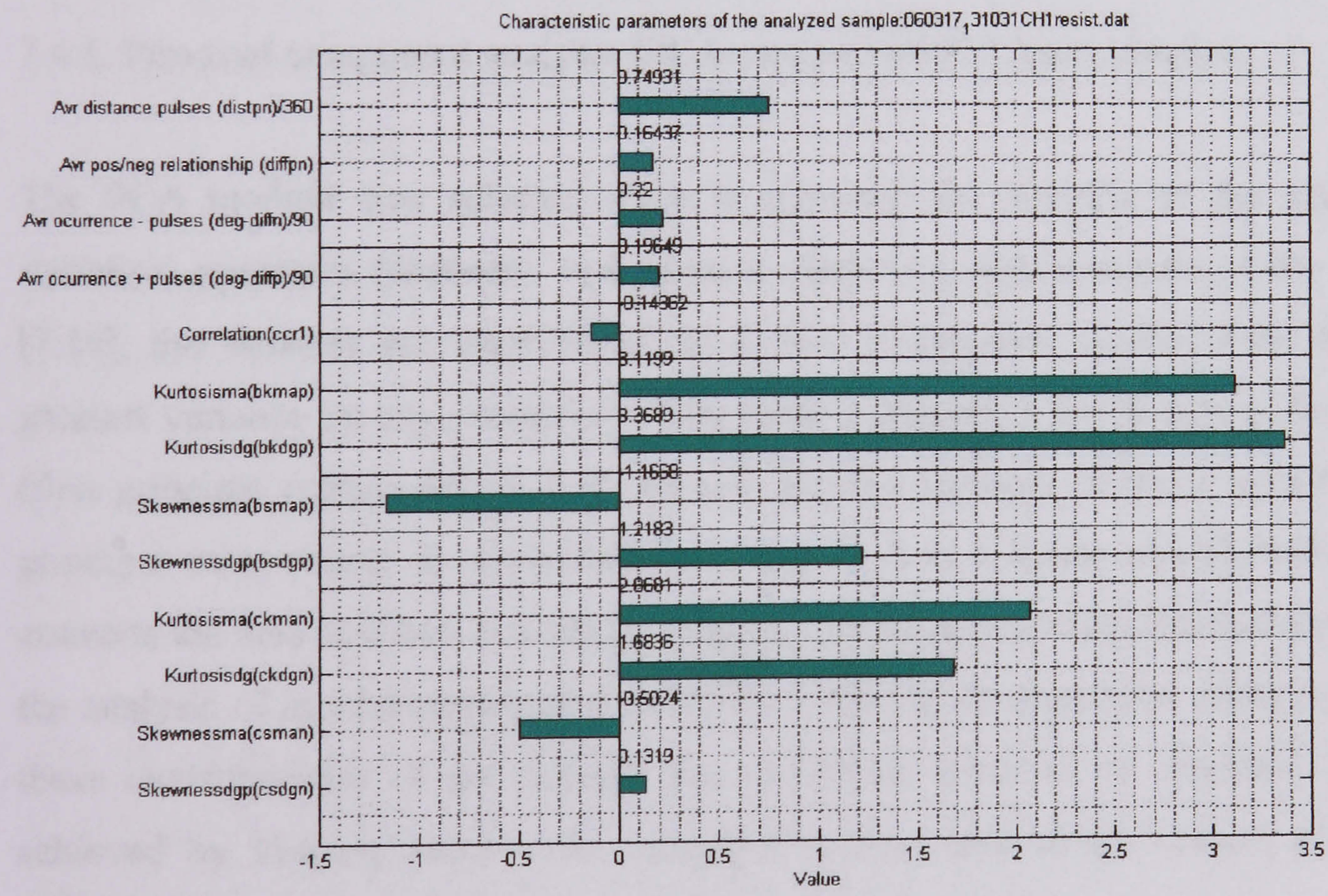

Figure 7.5 Graphical representation of statistical operators for a cavity in the 50 Ω resistor

As can be seen in the above figures, every generated discharge displays a different pattern.

7.4 Discrimination of partial discharges.

Section 7.3 described the process to generate the characteristic statistical operators, they represent a particular pattern distinctive for every radiated and conducted discharge which can be used to differentiate between each type of PD. However the manual comparison of the different patterns is tedious work and does not ensure the correct discrimination between different PD. In order to facilitate and give accuracy to the comparison between samples, a discrimination method is introduced, also known as mapping techniques [7.8], they transform a multidimensional space of a collection of data to two or three dimensions minimizing the loss of data during the process; the selected discrimination method was the principal component analysis (PCA) [7.9]. The following section will describe this method in detail.

7.4.1. Principal component analysis (PCA) method for PD discrimination.

The PCA method was selected since it approach the benefits of the generated statistical operators (datasets), and gives a clustering representation of the results [7.10], the datasets are transformed to a new coordinated system such that the greatest variance by any projection of the data is located in the X axis of the graph (first principal component) and the second greatest variance in the Y axis (second principal component). In statistical terms the PCA is a linear transformation that converts the data to a new coordinate system. The PCA is a technique that simplifies the analysis of multidimensional datasets by reducing its dimension while retaining those characteristics of the dataset that contribute most to its variance. This is achieved by keeping lower order principal components which contain the most important aspects of the data and ignoring higher order ones.

The first step in the application of the PCA algorithm using the covariance method [7.9,7.11] is to subtract the mean from each of the data dimensions m = 1…M, then each mean value can be described by a vector u of dimensions M x 1.

$$u[M] = \frac{1}{N}\sum_{n=1}^{N} X[m,n] \tag{6.5}$$

The covariance matrix can be used to calculate the spread of the data in the M dimensional space, its elements are $\sigma_x(i,k)$:

$$\sigma_x(i,k) = \frac{1}{m-1}\sum_{j=1}^{m}(x(i,j) - mean_x(i))(x(k,j) - mean_x(k))^t \tag{6.6}$$

For $i = 1,\ldots,N$ and $k = i,\ldots,N$

If the non-diagonal elements of the covariance matrix are larger compared to the diagonal elements (positive), a correlation between the responses of two features of the datasets is expected. On the other hand if the difference is near to zero then little correlation is expected.

The deviation from the mean can be calculated in terms of the correlation matrix R whose elements are related to the covariance matrix by:

$$R(i,j) = \sigma(i,j)/\sqrt{\sigma(i,i)\sigma(j,j)} \tag{6.7}$$

For $i = 1,\ldots..N$ and $k = i,\ldots..N$

The next step in the computation of the PCA is to find the eigenvectors and eigenvalues of the covariance matrix, the eigenvalues represent the relative variance of the data in the respective transformed coordinates, they are represented by:

$$\begin{bmatrix} \lambda_1 & 0 & 0 & . & . & 0 \\ 0 & \lambda_2 & 0 & . & . & 0 \\ 0 & 0 & \lambda_3 & . & . & 0 \\ . & . & . & . & . & . \\ 0 & 0 & 0 & . & . & \lambda_N \end{bmatrix} \tag{6.8}$$

Where the diagonal elements $(\lambda_1, \lambda_2, ..., \lambda_N)$ are the eigenvalues of the covariance matrix σ_x. The first value of the eigenvalues (λ_1) represents the maximum variance and the last values represent the minimum variance. The principal components are represented by the eigenvectors associated with these eigenvalues.

7.4.2. Application of the PCA method to the generated statistical operators data sets.

For the calculation of the principal component analysis method a separate MATLAB program was coded, it calls the data base of the reference discharges and the evaluated discharges, finally the results are displayed graphically. Figures 7.6, 7.7 and 7.8 shows the results of the PCA using the samples in the 50 Ω resistor, antenna 1 and antenna 3 respectively.

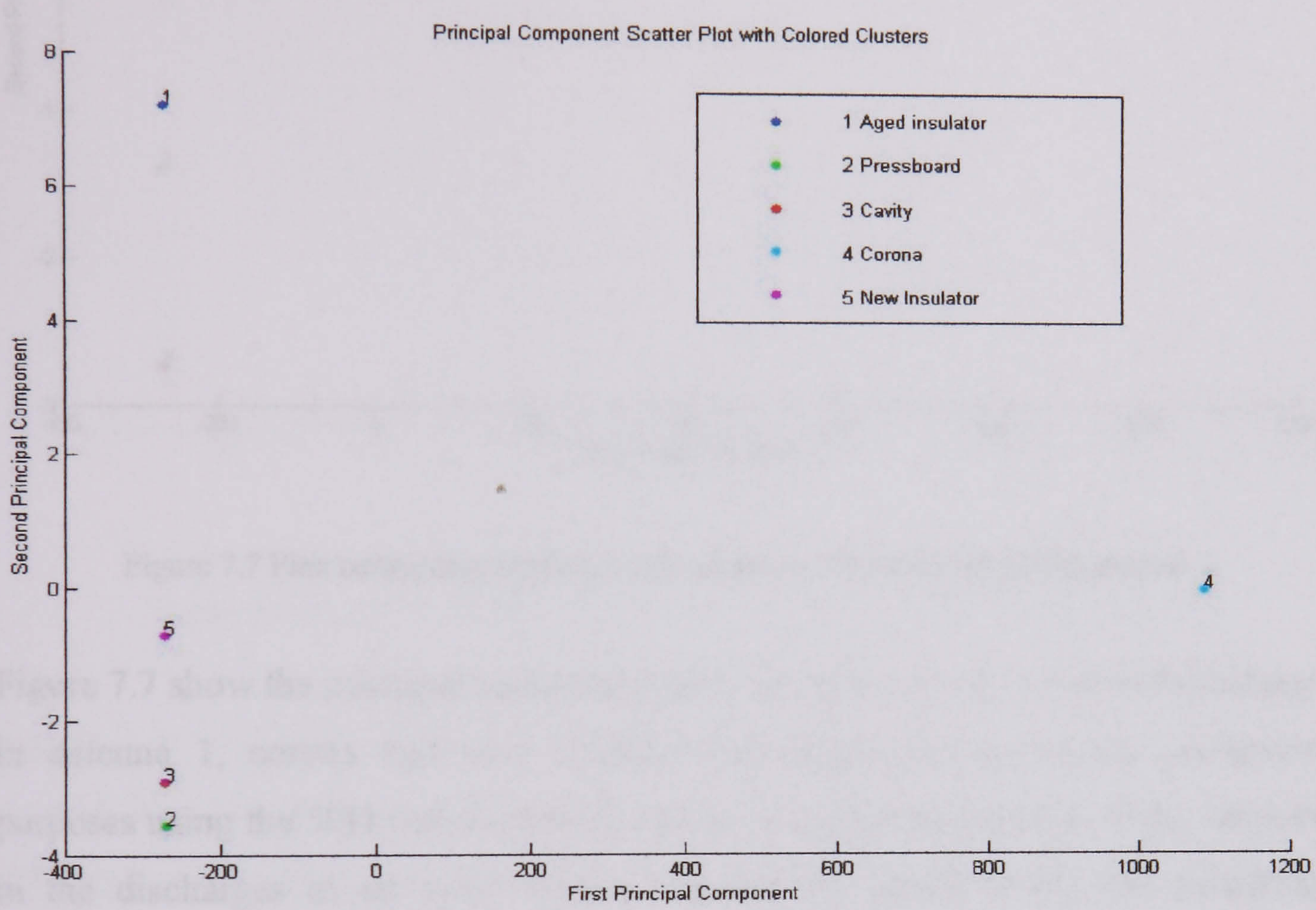

Figure 7.6 First component analysis of the acquired discharge data in the 50 Ω resistor

Figure 7.6 shows that the acquired samples in the 50 Ω resistor are clearly identified; corona discharges and surface discharges over an aged insulator are located far away from the rest of the samples, the variance of the new insulator discharges tend to be separated from the rest of the samples and cavity and pressboard discharges are clustered in the negative region of the graph and stay close.

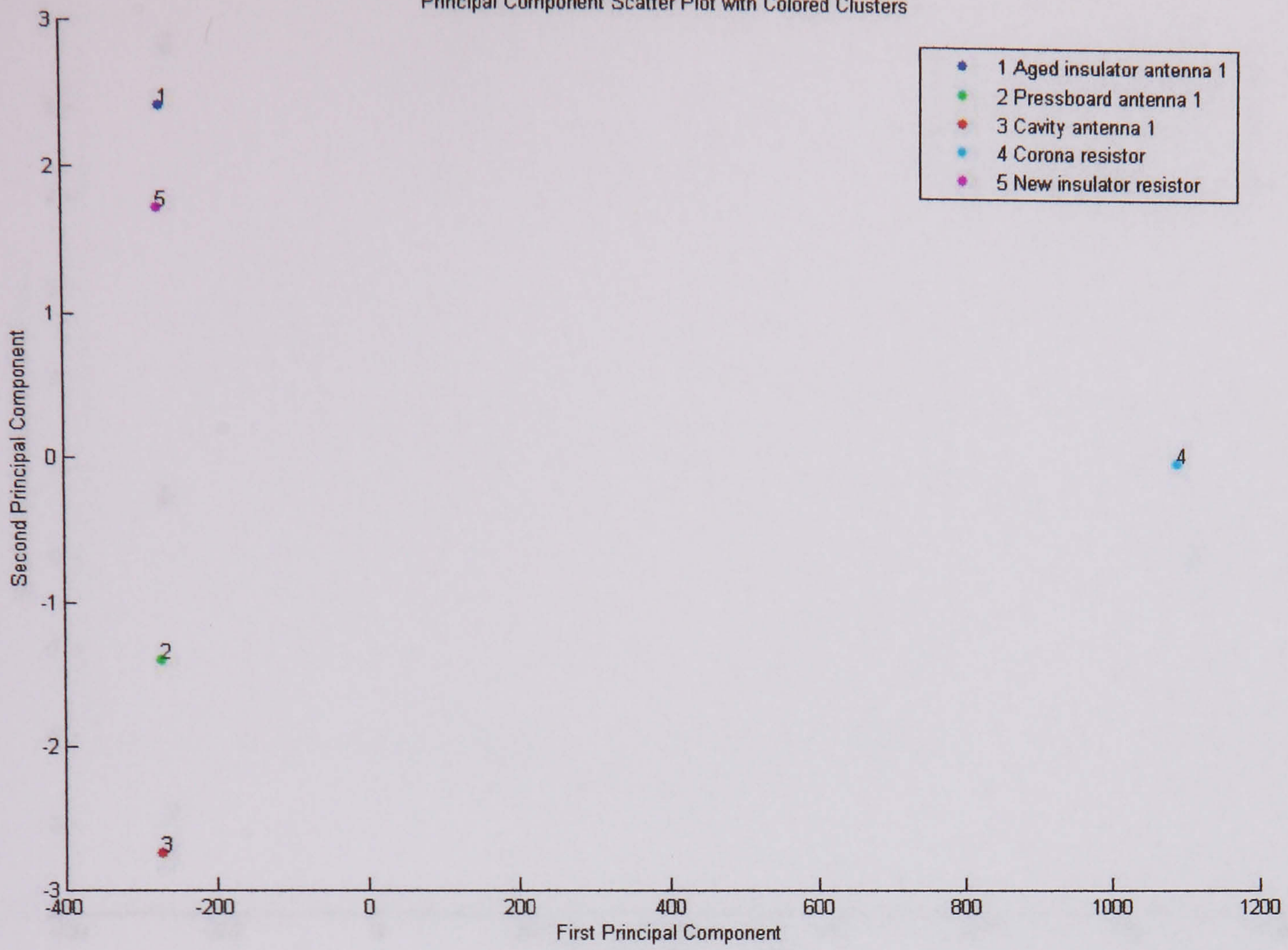

Figure 7.7 First component analysis of the acquired discharge data in the antenna 1

Figure 7.7 show the principal component analysis of the acquired radiated discharges in antenna 1, corona and new insulator discharges are shown for comparison purposes using the 50Ω resistor data. It can be seen that the position of the variances in the discharges in an aged insulator remain the same; cavity and pressboard discharges stay in the negative region of the variances but they switch position with respect to the conducted ones. The value of the variances has been reduced in the radiated discharges because of the smaller signal magnitude compared to the conducted discharges.

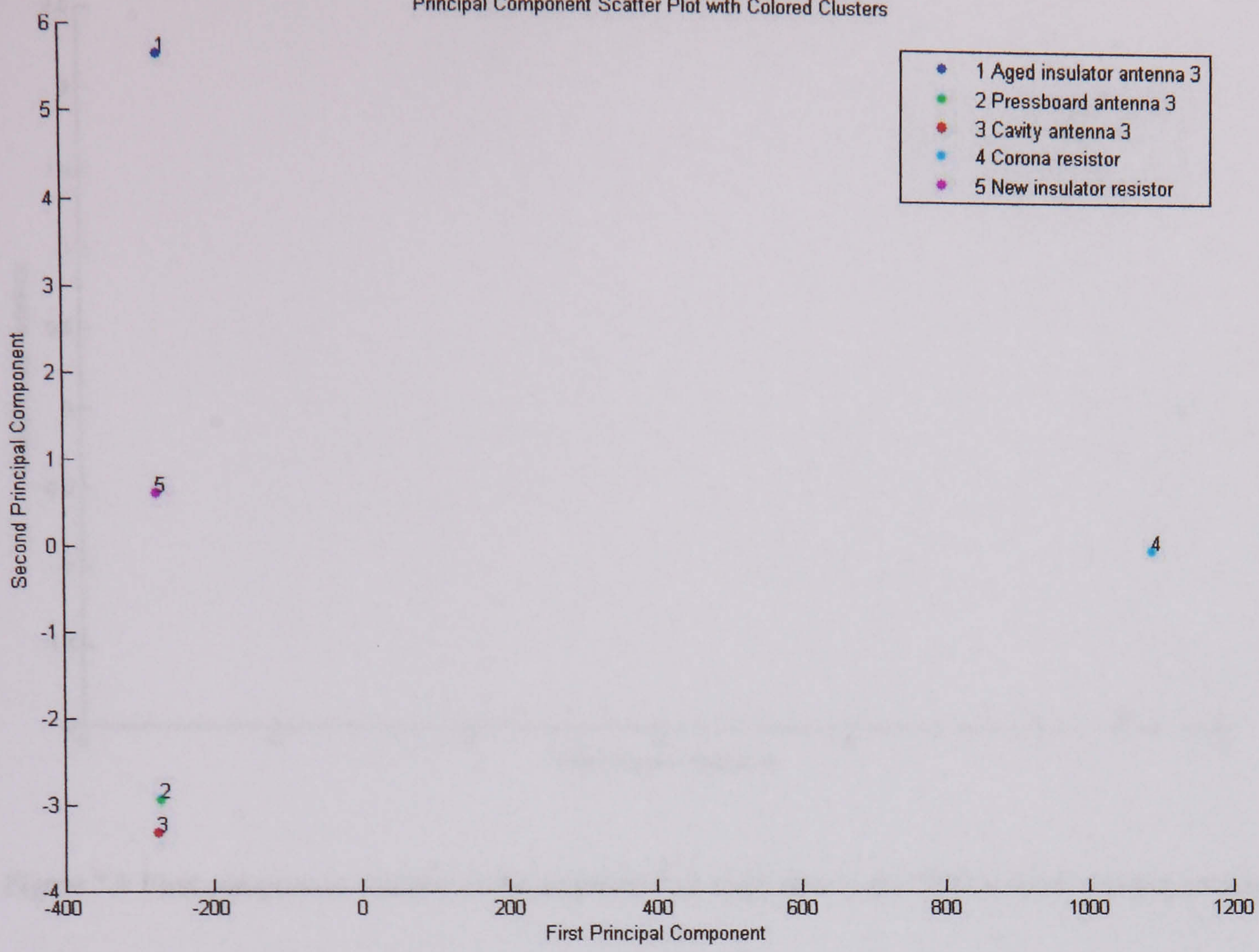

Figure 7.8 First component analysis of the acquired discharges in the antenna 3

Figure 7.8 show the PCA of the acquired discharges data from antenna 3. An appreciable reduction in magnitude of the variances occurs but the position of the discharges in the graph remain the same when compare with data from the antenna 1. Figures 7.9, 7.10 and 7.11 shows the results of the PCA using the samples in the 50 Ω resistor, antenna 1 and antenna 3 respectively without the effect of corona discharge.

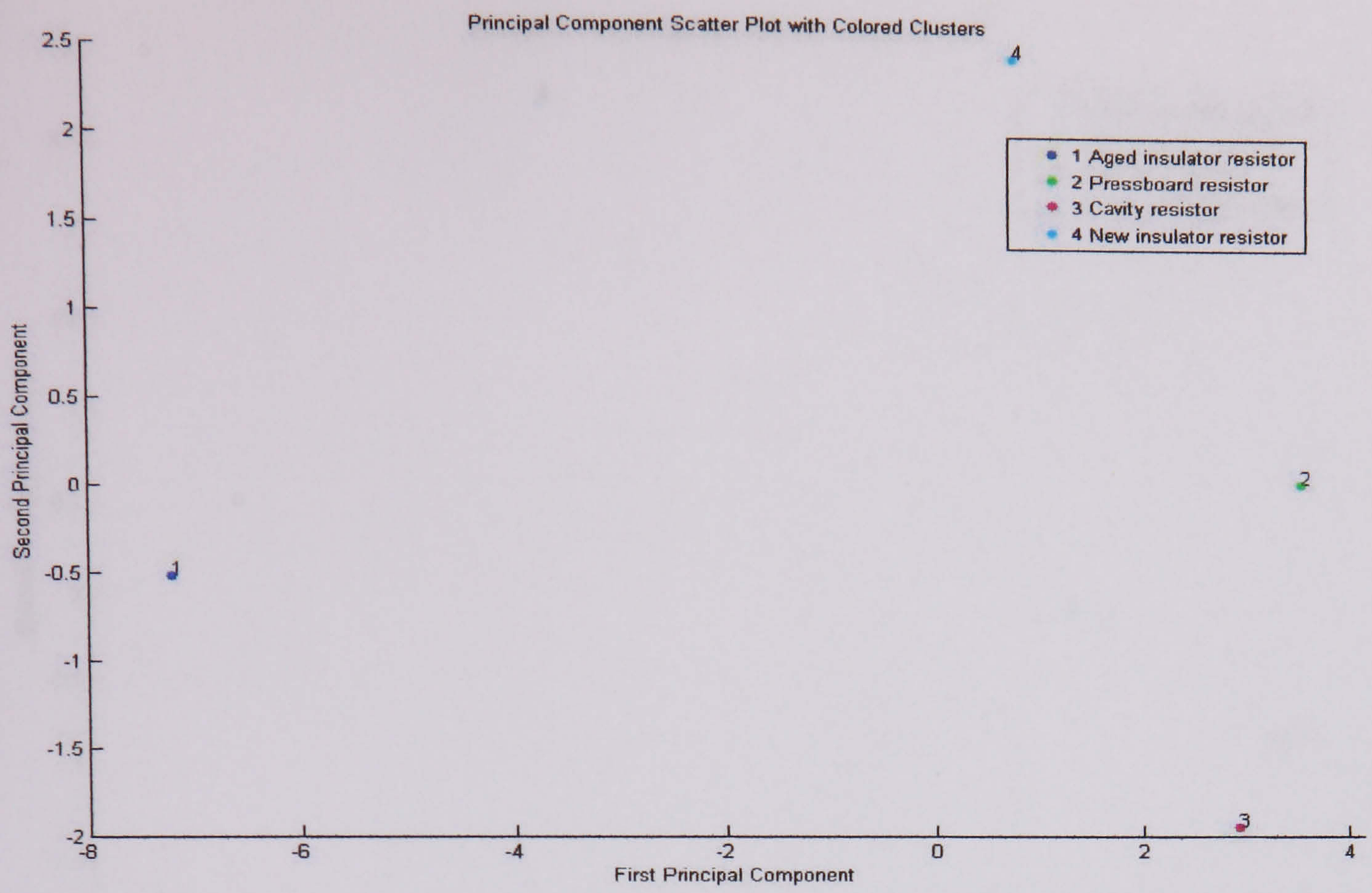

Figure 7.9 First component analysis of the acquired discharge data in the 50 Ω resistor without corona

Figure 7.9 shows that disregarding the effect of corona discharge, the positions of the different insulation defects change completely when compared with figure 7.6, however, cavity and pressboard PD's tend to cluster together and discharges in aged insulator is separated from new insulator discharges.

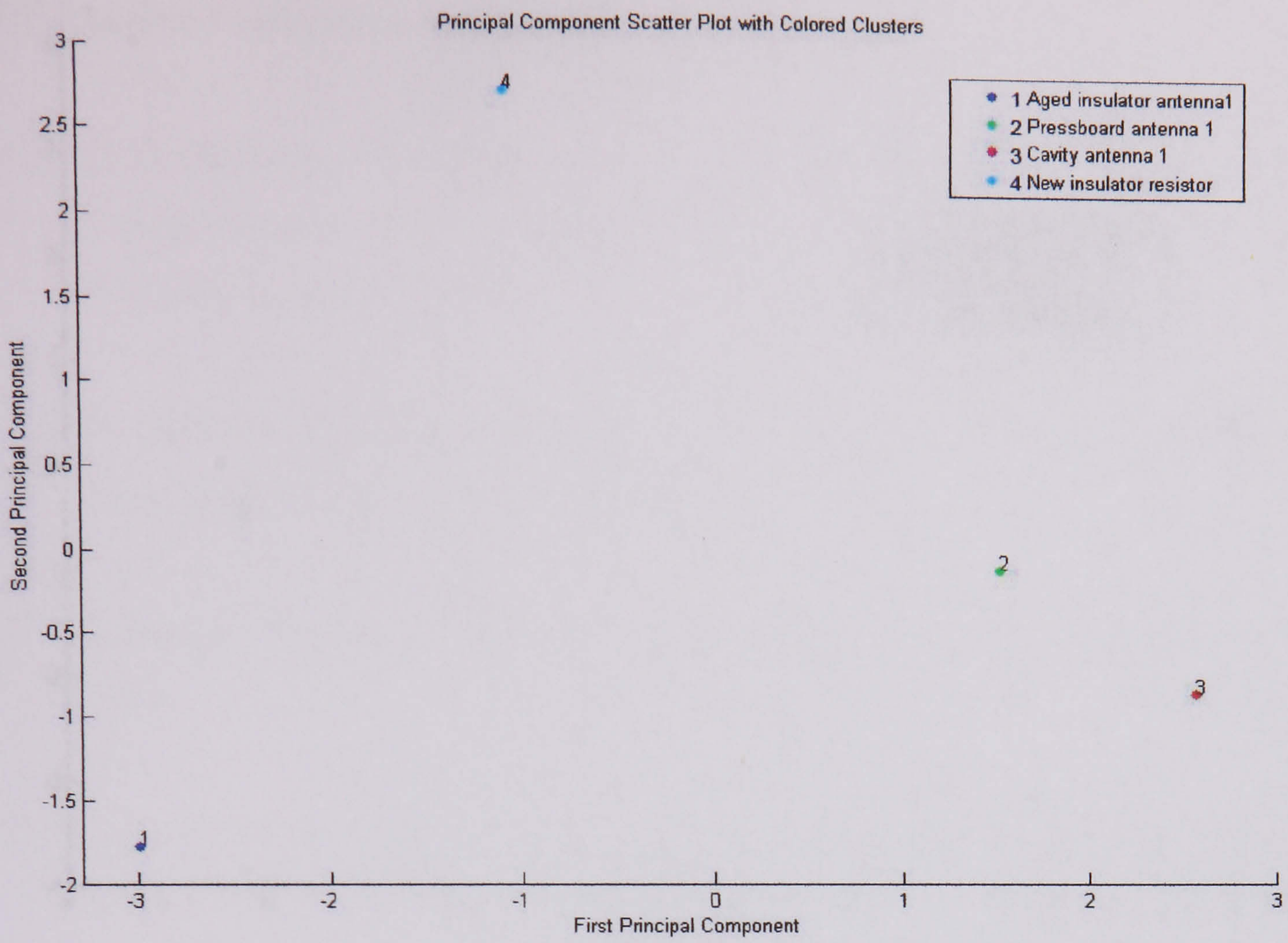

Figure 7.10 First component analysis of the acquired discharge data in the antenna 1 without corona

Figure 7.10 show the PCA of the acquired discharges in antenna 1 without the effect of corona, it can be observe that as in the case of the resistor the positions have changed completely when compare to figure 7.7, but cavity and pressboard PD's tend to cluster together and very well differentiated from PD's in aged insulator. When compared to figure 7.9, positions of insulation defects in figure 7.10 it is observe that PD's in pressboard and cavity have switched positions over the x axis but remain close.

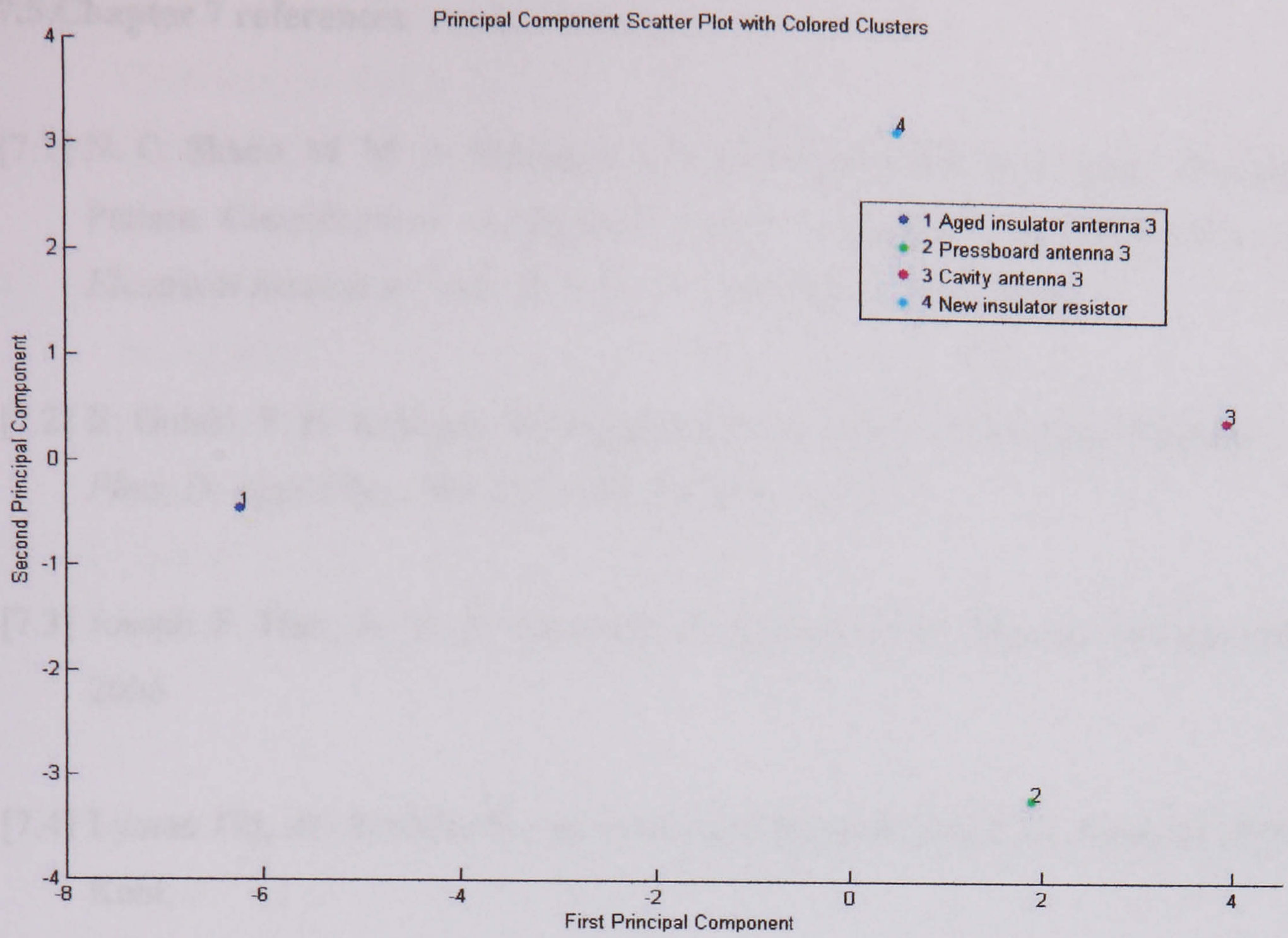

Figure 7.11 First component analysis of the acquired discharges in the antenna 3 without corona

Figure 7.11 shows the PCA of the acquired discharges in antenna 3 without the effect of corona, it can be observed that when compared to figure 7.8, positions of different insulation defects have change completely, however they remain very similar when compared to figure 7.10 (antenna 1) the main difference is in magnitude of the first and second components.

This demonstrate that changing the position of the antenna with respect to the discharge source, the position of the variances of the radiated discharges does not change, only the magnitude is affected. Disregarding the effect of corona discharge does not affect the distribution of the different insulation defects and they can be differentiated each other. Although this may appear to be a disadvantage, the use of a radiometric PD locating system [7. 12] allows an accurate assessment of the distance between the PD source and the antenna. From this distance the absolute, rather than relative PD signal magnitude may be calculated. By the use of a distance compensated PD signal magnitudes, the recognition of differing PD effects may be achieved at any arbitrary antenna position.

7.5 Chapter 7 references

[7.1] N. C. Shaoo, M. M. A. Salama and R. Bartnikas, "Trends in Partial Discharge Pattern Classification: A Survey", *IEEE Transactions on Dielectrics and Electrical Insulation*, Vol. 12, No. 2, April 2005, pp 248 – 264.

[7.2] E. Gulski, F. H. Kreuger, "Computer-aided Analysis of Discharge Patterns", *J. Phys, D: Appl Phys* , No. 23, 1990, pp 1569 – 1575.

[7.3] Joseph F. Hair, Jr. et al, *Multivariate Data Analysis,* Pearson Prentice Hall, 2006

[7.4] Lyman Olt, *An Introduction to Statistical Methods and Data Analysis,* PWS-Kent,
1998

[7.5] Richard J. Larson, Morris L. Marx, *An Introduction to Mathematical Statistics and Its Applications,* Prentice Hall, 1986

[7.6] Julius S. Bendat, Allan G. Piersol, *Engineering Applications of Correlation an Spectral Analysis,* John Wiley & Sons Inc., 1993

[7.7] A Krivda, E. Gulski, "Classification of Discharge Patterns During Ageing of Insulation", *IEEE 5th International Conference on Conduction and Breakdown in Solid Dielectrics,* 1995, pp 254 – 258.

[7.8] Anil K. Jain et al, "Statistical Pattern Recognition: A Review", *IEEE Transactions On Pattern Analysis and Machine Intelligence*, Vol. 22, No. 1, January 2000, pp 4 – 37.

[7.9] M. K. Abdul Rahman, R. Arora, S. C. Srivastava, "Partial Discharge Classification Using Principal Component Transformation", *IEE Proc-Sci. Meas Technol*, Vol. 147, No. 1, January 2000, pp 7-13.

[7.10] Yujing Zeng, Janusz Starzyk, "Statistical Approach to Clustering in Pattern Recognition", *Proceedings of the 33rd Southeastern Symposium on System Theory*, March 2001, pp 177-181.

[7.11] Lindsey Smith, "A tutorial on Principal Component Analysis", 2002, http://www.cs.otago.ac.nz/cosc453/student_tutorials/principal_components.pdf.

[7.12] Moore P J, Portugues I, Glover I A, "A Non-Intrusive Partial Discharge Measurement System Based on RF Technology", *Power Engineering Society Meeting*, June 2003, pp 627 – 633.

CONCLUSIONS

This thesis has investigated the intrinsic characteristics and the different factors that affect radiated PD. This has allowed the development of an identification and discrimination system for radiated partial discharges based on pattern classification this is the most significant finding of the thesis and is novel. The results obtained in this investigation are limited to laboratory environment however they constitute the basis for a reliable non-invasive diagnosis system. The investigation has included literature research, the design of a laboratory test set, experiments carried on using various samples, the analysis of the results using specialized software and its feasibility, and the development of a discrimination system based in point on wave information. The present chapter gives a summary of the conclusions of this research and the direct consequences of the results over the development of other research projects. The conclusions are presented as a compilation of results of the different investigations undertaken in this research.

8.1. Collation of evidence for identification of partial discharges.

Chapters 2 and 3 discussed the state of the art regarding partial discharges and its identification; following the literature review the next conclusions can be established:

- Conducted partial discharges use the structures of the primary equipment were they are originated to radiate into the atmospheric air, these radiated discharges have been described as PD sferics.

- Radiated discharges possess intrinsic characteristics such as frequency, duration, phase and magnitude.

- The intrinsic characteristics of radiated discharges can be modified by several factors such as objects placed in the vicinity, relative distance to the origin of the discharge, weather, etc.

- The detection of radiated partial discharges in substations and laboratory is limited to its early detection and location.

- No suitable pattern classification system for radiated partial discharges has been reported so far.

- To create a suitable classification of radiated discharges based on its intrinsic characteristics the development of a laboratory test set system to generate reliable radiated discharges is necessary.

8.2. Development of a test set system for generation of conducted and radiated partial discharges

Chapter 3 showed a general review of the methods for partial discharge generation and detection; those methods are used when a fundamental analysis of partial discharges become necessary, most of the methods used in laboratory use partial discharge detectors that evaluate the apparent charge of the conducted discharge. The use of partial discharge of this kind implies the measurement of the apparent charge of the conducted discharges; however the parameters used to measure the energy of radiated discharges are volts and dB's, having this in mind it was decided the use of a reliable test set that will allow the study of radiated partial discharges and compare the latter with conducted discharges using the same measured parameters, the latter requirements can be achieved with the use of a 50 Ω resistor placed in the grounded connection of the test sample as it measures directly the current of the discharge, the main characteristics of the developed tests set can be summarized as follow:

- Generation of AC High Voltage up to 45 kV
- Test set PD and corona free
- Flexibility for the use of different samples for PD generation
- Accurate control of the generated voltage (step up and step down voltage)
- Reliable acquisition of conducted and radiated discharges

The developed test set was installed in the High Voltage Laboratory of the University accordingly to the required safety regulations.

8.3. Analysis of the laboratory results

- *Frequency response tests.*- Frequency response tests show that by using the compensation method applied to radiated discharges, the frequency spectra can be filtered and the real frequency response unwrapped, this is particularly useful when different antennas in different position and different acquisitions are analyzed, as the method make uniform the peak value of the frequency spectra, also it can differentiate between oil and air emissions as the latter show higher frequencies, however this method is only applicable in laboratory tests and the antenna must be place as close as possible to the PD source otherwise a false frequency peak can be obtained since the received signal is too small.

- *Corona discharges.*- The point on wave information and the pattern of corona discharges show that the most significant characteristic is the distribution of negative and positive discharges when the voltage of the source is raised gradually, the first pulses to appear are negative and their value remains relative constant until the breakdown of the gap, a *region of transition* with

positive and negative discharges is observed, as the voltage is increased the magnitude and recurrence of positive pulses increase until the complete breakdown of the gap, its pattern is very distinctive as the majority of positive and negative pulses stay grouped around the maximum of the half positive and negative half cycles of the AC reference. Conducted discharges can be observed all the time however, it is not possible to observe radiated corona discharges until just before the complete breakdown of the air gap.

- *Surface discharges over new and aged insulators.*- There is a remarkable difference between new and aged insulators in terms of generated surface discharges and its characteristics in frequency and time. Aged insulator causes strong surface activity that can be received in the 50 Ω resistor and the antennas. The analysis of the generated pattern using point on wave information showed that negative and positive pulses are observed and they group in the first half of the positive and negative half cycles of the AC waveform. The pattern of conducted and radiated discharges is very similar, differing only in magnitude as the radiated discharges tend to be attenuated by the surrounding media. The new insulator produced only small magnitude discharges that could not be received with the antennas. This difference in behavior between the new and the aged insulator can be attributable to the loss of hydrophobicity of the aged insulator, which allows surface discharges to incept easily and spread along the surface of the insulator.

- *Surface discharges over a pressboard submerged in oil.*- Conducted and radiated surface discharges over a pressboard were observed. The detected pulses show both positive and a negative and tend to group in the first half of the positive and negative half cycle of the AC reference. The pattern of the conducted and radiated discharge is similar differing only in magnitude - radiated discharges are smaller.

- *Cavity discharges.*- Cavity discharges are received in the antennas and the 50 Ω resistor. Conducted and radiated cavity discharges of positive and negative

polarity are received, they tend to group around the cero crossing of the descending slope of the AC reference, i.e. every 360 degrees, and have a relatively constant spacing. The magnitude of the conducted pulses as expected is higher than the radiated pulses. The pattern of the conducted and radiated discharges is similar differing only in recurrence and magnitude.

- *Influence of the antenna position over the radiated discharges.*- The different tests in radiated samples show that the magnitude of the received discharge is a function of the relative distance between the antenna and the discharge source, hence the position of the antenna influence the magnitude of the radiated discharges, the magnitude and components of the frequency spectra of the radiated discharges also is affected by the position of the antenna, they always show a higher frequency than the conducted ones, this effect is caused by the reflections of the radiated discharges over the surrounding objects.

- *Polarity of the radiated discharges.*- In all the tests the radiated discharge shift its polarity when received by the antenna, to positive if the discharge is negative or negative if it is positive. This is attributed mainly to the antenna design and does not affect the pattern distribution of the discharges.

- *Pattern classification of radiated discharges.*- A pattern classification of radiated partial discharges is possible as the intrinsic characteristics of the conducted and radiated discharges are similar. However the sole observation of these patterns is insufficient for a reliable identification, and the use of a discrimination method become necessary.

- *Recognition of radiated discharges.*- The use of discrimination methods using statistical operators and cluster classification (PCA) for PD recognition proved to be reliable for conducted and radiated discharges, since the relative position of the antenna with respect to the discharge source does not affect the final result.

FUTURE WORK

Possible future work that undergraduate and postgraduate projects can feasibly carry on has been identified as a result of the findings in this research; this chapter presents a summary of possible future work.

9.1. Development of a reliable method to compensate the effect of the surrounding objects over the radiated discharges.

It was demonstrated that the equipment and structures nearby to the origin of the radiated discharge affects its frequency spectra, angle and phase. In the laboratory this effect was compensated by applying the compensation method described in section 5.3. This allowed an identification of radiated discharges, using its frequency spectra. However in substation the application of the method in its present state is unreliable since the identification of the frequency spectra of the surrounding objects requires the precise location of the partial discharges, and the application of a sweep signal from this location to generate the frequency spectra of the area, and then the application of the compensation method, hence a system for the identification of partial discharges through the analysis of its frequency spectra that include the latter characteristics is suggested. As an example, the required sweep signal to generate the frequency spectra can be injected with PLC equipment using a voltage transformer with capacitive coupling and placing the antennas nearby the equipment under test.

9.2. Increase of the existed data base with more tests in laboratory and substations.

The samples used in this research for the generation of corona and partial discharges represent some of the basic kinds of partial discharges, hence the use of other samples is recommended.

The generation of more conducted and radiated discharges such as internal PD's in power transformers, CT's, circuit breakers etc. can be used to increase the created data base. The follow arrangements are suggested:

Corona discharges:

- Gap configuration plane-plane
- Gap configuration plane-tip rod

Surface discharges:

- Surface discharges over aged silicon rubber insulators
- Surface discharges over polluted glass and ceramic insulators
- Surface discharges over a bounded polymeric sample
- Surface discharges over a pressboard submerged in used oil (plane to pressboard configuration)
- Surface discharges over a pressboard in SF_6 (plane to pressboard and tip rod to pressboard configuration)

Treeing discharges

- Inside a polymeric sample (EPDM)

- Inside a polymeric sample (Silicon Rubber)

Cavity discharges

- Single cavity sample (different sizes)

- Multi-cavity sample (different sizes)

Floating particle in air, SF_6 and oil

- Floating particle in a tip-plane configuration

- Floating particle in a plane to plane configuration

- Floating particle in a tip rod to tip rod configuration

Conducting particle in air, SF_6 and oil

- Conducting particle in a tip-plane configuration

- Conducting particle in a plane to plane configuration

- Conducting particle in a tip rod to tip rod configuration

Additional to the above test, an evaluation of surface and cavity discharges inside an experimental transformer and power cables is suggested.

9.3 Further evaluation of partial discharges using different discrimination methods

In order to increase the reliability in diagnosing radiated partial discharges, the use of additional discrimination methods is suggested, the possible discrimination methods to be considered are:

- Cluster classification of partial discharges
- Fractal features for discrimination
- Neuronal networks for discrimination
- Recognition rate
- Centour score

9.4 Development of automated diagnostic software for partial discharges

Based on the software for discrimination of PD's developed in this investigation, specialized software for the diagnostic and evaluation of radiated discharges is recommended. The suggested software may include:

- Full Graphic Interface (GUI) for data loading and analysis
- Integrated data base with the propose PD defects
- Graphic analysis of partial discharge pattern using point on wave information
- Graphic analysis of partial discharge discrimination using different methods
- Automated diagnose of partial discharges

The proposed software must be integrated to the acquisition system and must be tested using field tests in a mobile vehicle for a full non-invasive diagnosis of partial discharges or it can be integrated to a fixed diagnostic system.

Appendix A: Interpolation method used in MATLAB.

1-D data interpolation (table lookup)

Syntax

```
yi = interp1(x,Y,xi)
yi = interp1(Y,xi)
yi = interp1(x,Y,xi,method)
yi = interp1(x,Y,xi,method,'extrap')
yi = interp1(x,Y,xi,method,extrapval)
pp = interp1(x,Y,method,'pp')
```

Description

yi = interp1(x,Y,xi) interpolates to find yi, the values of the underlying function Y at the points in the vector or array xi. x must be a vector. Y can be a scalar, a vector, or an array of any dimension, subject to the following conditions:

- If Y is a scalar or vector, it must have the same length as x. A scalar value for Y is expanded to have the same length as x. xi can be a scalar, a vector, or a multidimensional array, and yi has the same size as xi.
- If Y is an array that is not a vector, the size of Y must have the form [n,d1,d2,...,dk], where n is the length of x. The interpolation is performed for each d1-by-d2-by-...-dk value in Y. The sizes of xi and yi are related as follows:
    - If xi is a scalar or vector, size(yi) equals [length(xi), d1, d2, ..., dk].
    - If xi is an array of size [m1,m2,...,mj], yi has size [m1,m2,...,mj,d1,d2,...,dk].

yi = interp1(Y,xi) assumes that x = 1:N, where N is the length of Y for vector Y, or size(Y,1) for matrix Y.

yi = interp1(x,Y,xi,method) interpolates using alternative methods:

'nearest'	Nearest neighbor interpolation
'linear'	Linear interpolation (default)
'spline'	Cubic spline interpolation
'pchip'	Piecewise cubic Hermite interpolation
'cubic'	(Same as 'pchip')
'v5cubic'	Cubic interpolation used in MATLAB 5. This method does not extrapolate. Also, if x is not equally spaced, 'spline' is used/

For the 'nearest', 'linear', and 'v5cubic' methods, interp1(x,Y,xi,method) returns NaN for any element of xi that is outside the interval spanned by x. For all other methods, interp1 performs extrapolation for out of range values.

yi = interp1(x,Y,xi,method,'extrap') uses the specified method to perform extrapolation for out of range values.

yi = interp1(x,Y,xi,method,extrapval) returns the scalar extrapval for out of range values. NaN and 0 are often used for extrapval.

pp = interp1(x,Y,method,'pp') uses the specified method to generate the piecewise polynomial form (ppform) of Y. You can use any of the methods in the preceding table, except for 'v5cubic'. pp can then be evaluated via ppval. ppval(pp,xi) is the same as interp1(x,Y,xi,method,'extrap').

The interp1 command interpolates between data points. It finds values at intermediate points, of a one-dimensional function $f(x)$ that underlies the data. This function is shown below, along with the relationship between vectors x, Y, xi, and yi.

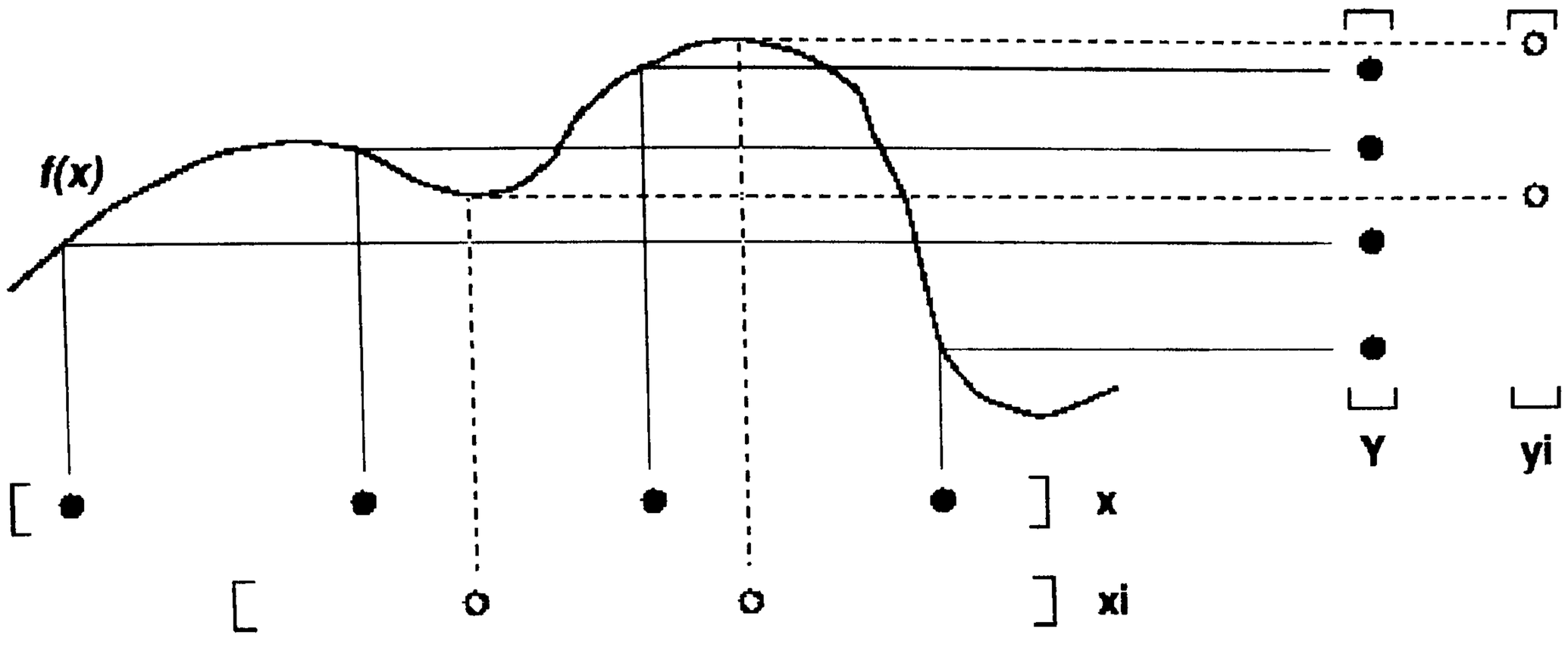

Interpolation is the same operation as *table lookup*. Described in table lookup terms, the *table* is [x,Y] and interp1 *looks up* the elements of xi in x, and, based upon their locations, returns values yi interpolated within the elements of Y.

Appendix B: Oscilloscope settings for acquired epochs for the analyzed samples

Frequency response test for all samples						
Device	**Channel**	**Time**	**Sampling**	**Length**	**Freq. Count**	**Coupling**
Antenna 1	**1**	**200 ns**	**2.5 Gs/s**	**5000**	**5**	**50 Ω**
Antenna 2	**2**	**200 ns**	**2.5 Gs/s**	**5000**	**5**	**50 Ω**
50 Ω Resistor	**3**	**200 ns**	**2.5 Gs/s**	**5000**	**5**	**1M**
Antenna 3	**4**	**200 ns**	**2.5 Gs/s**	**5000**	**5**	**50 Ω**
Time domain test for all samples						
50 Ω Resistor	**1**	**10 ms**	**10 Ms/s**	**$1x10^6$**	**2**	**50 Ω**
Antenna 1	**2**	**10 ms**	**10 Ms/s**	**$1x10^6$**	**2**	**50 Ω**
AC reference	**3**	**10 ms**	**10 Ms/s**	**$1x10^6$**	**2**	**1M**
Antenna 3	**4**	**10 ms**	**10 Ms/s**	**$1x10^6$**	**2**	**50 Ω**

Appendix C: Patterns for corona in air gap and their statistical distributions

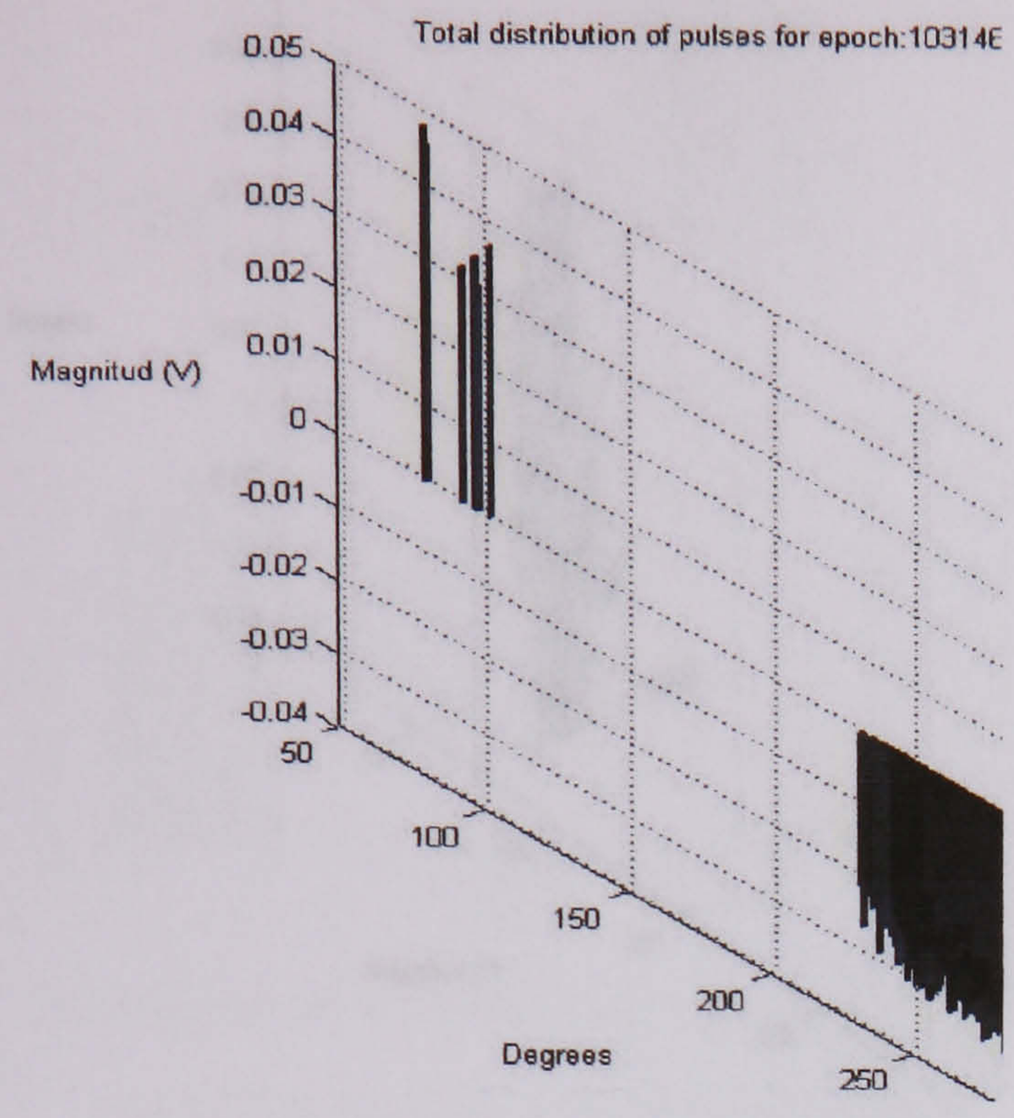

Distribution of corona pulses at 2860 V with a 10mm air gap

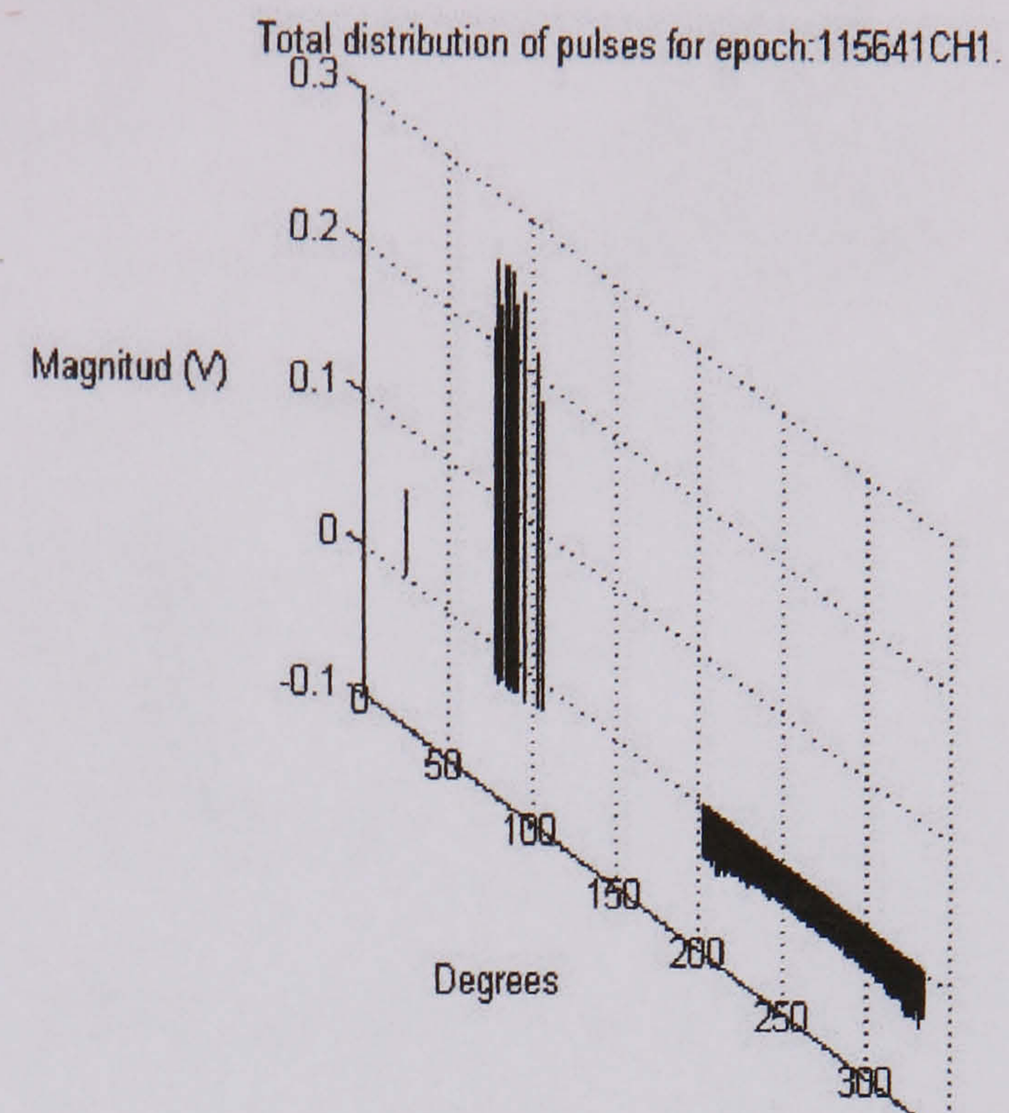

Distribution of corona pulses at 6540 V with a 10mm air gap

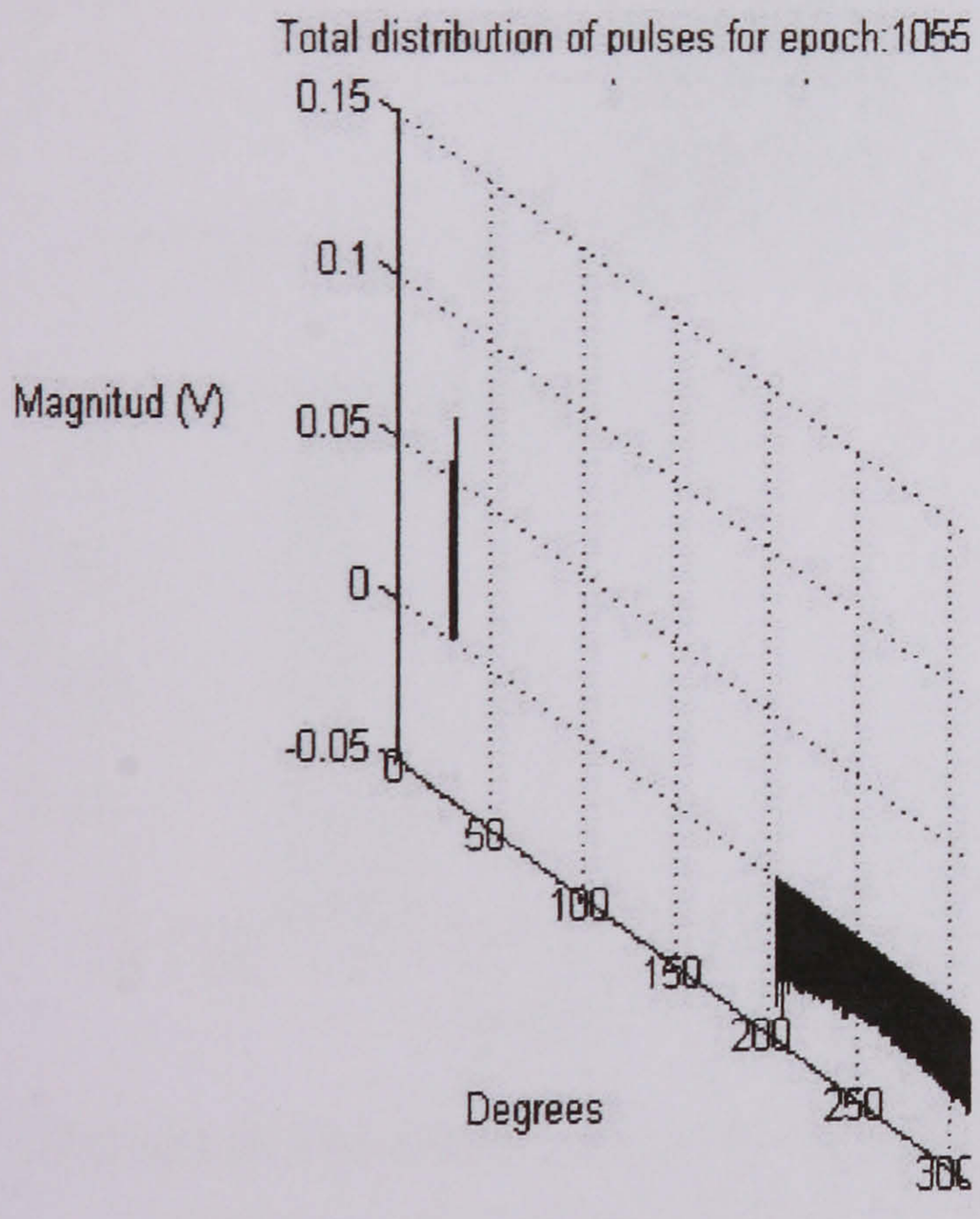

Distribution of corona pulses at 5740 V with a 10mm air gap

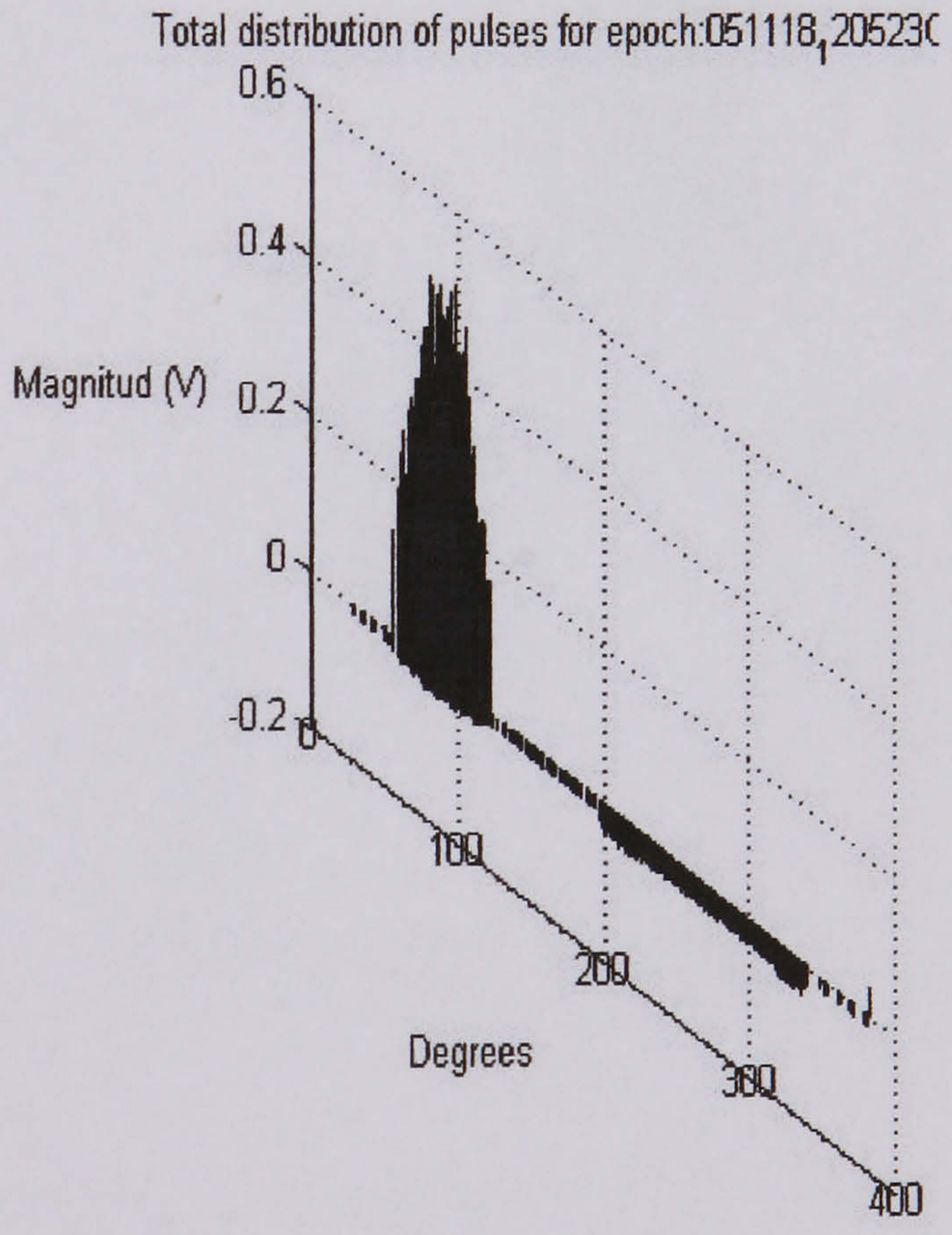

Distribution of corona pulses at 7370 V with a 10mm air gap

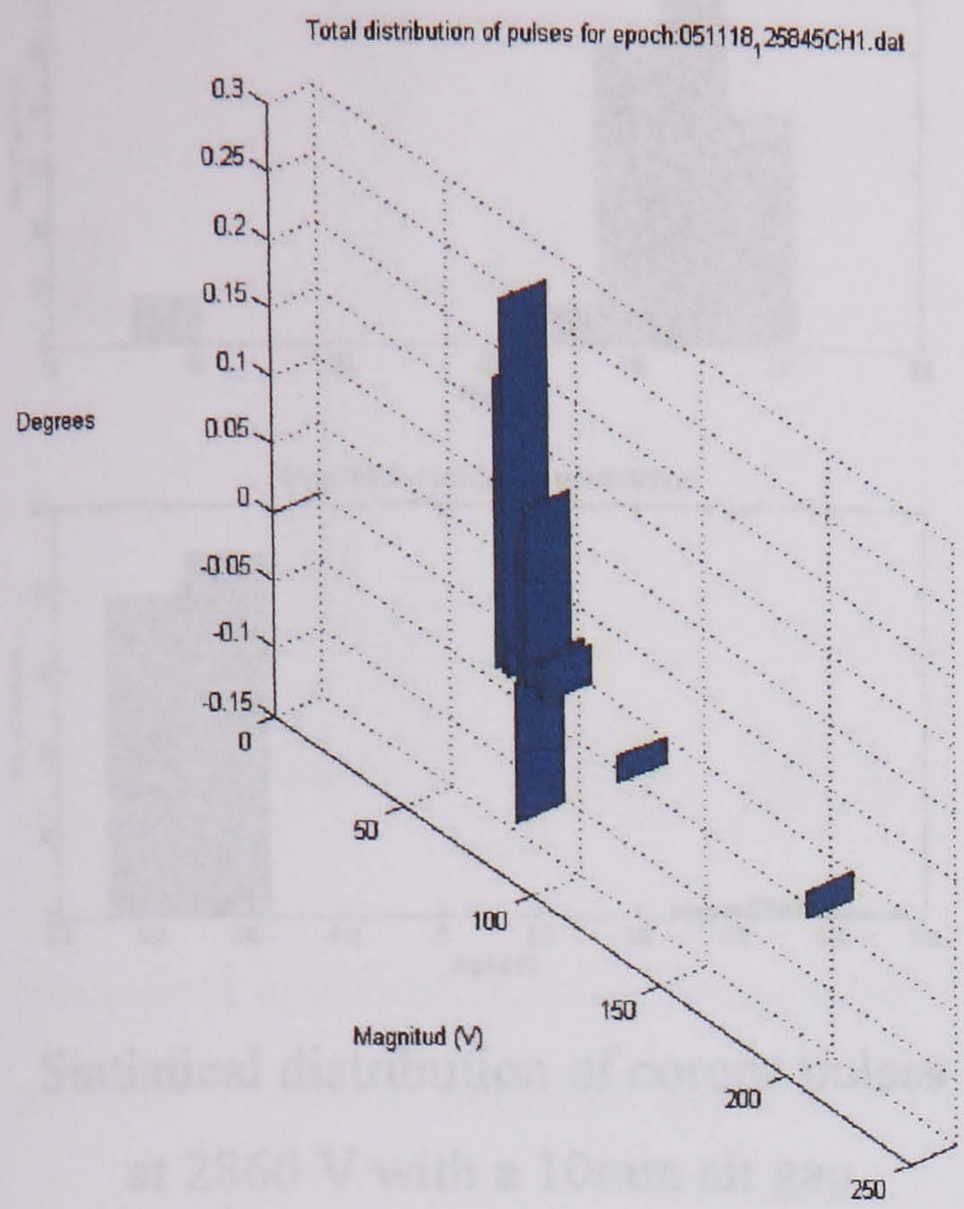

Distribution of corona pulses at 8610 V (discharge) with a 10mm air gap

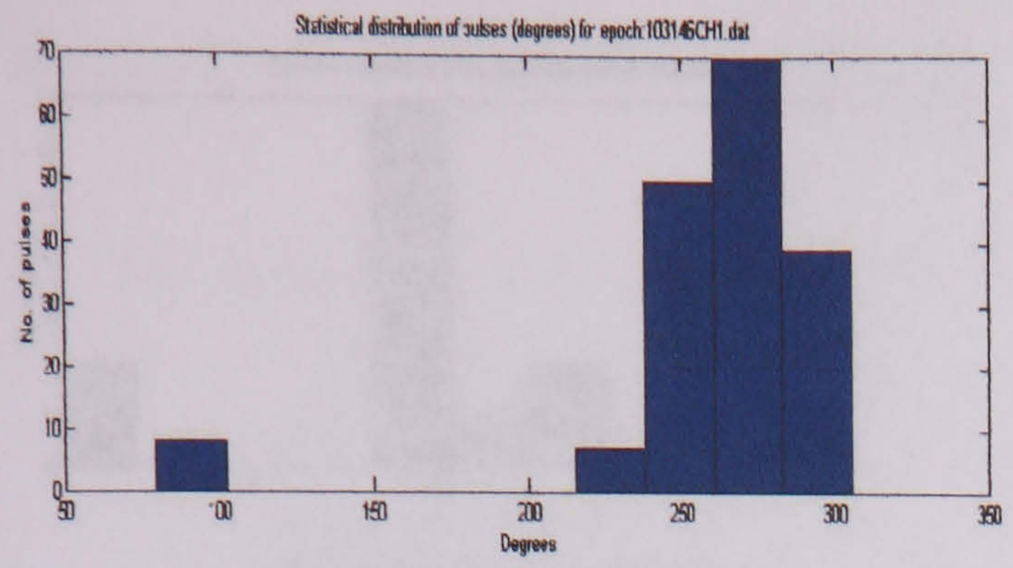

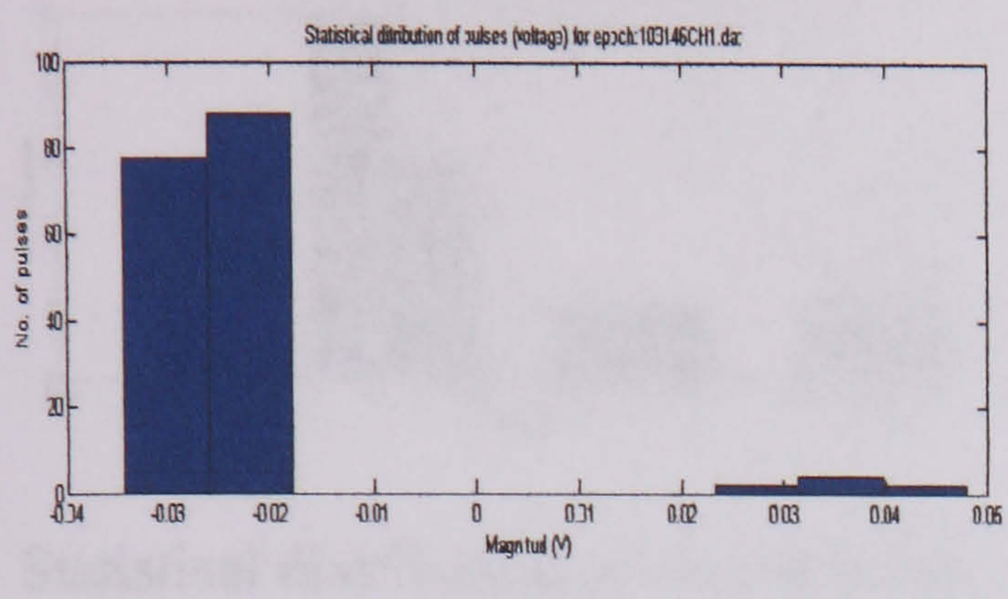

Statistical distribution of corona pulses at 2860 V with a 10mm air gap

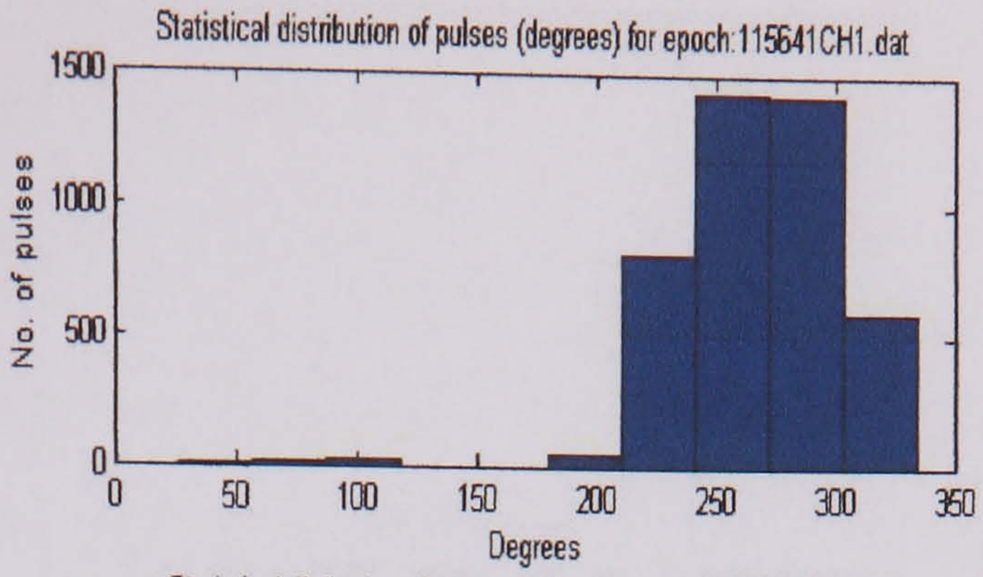

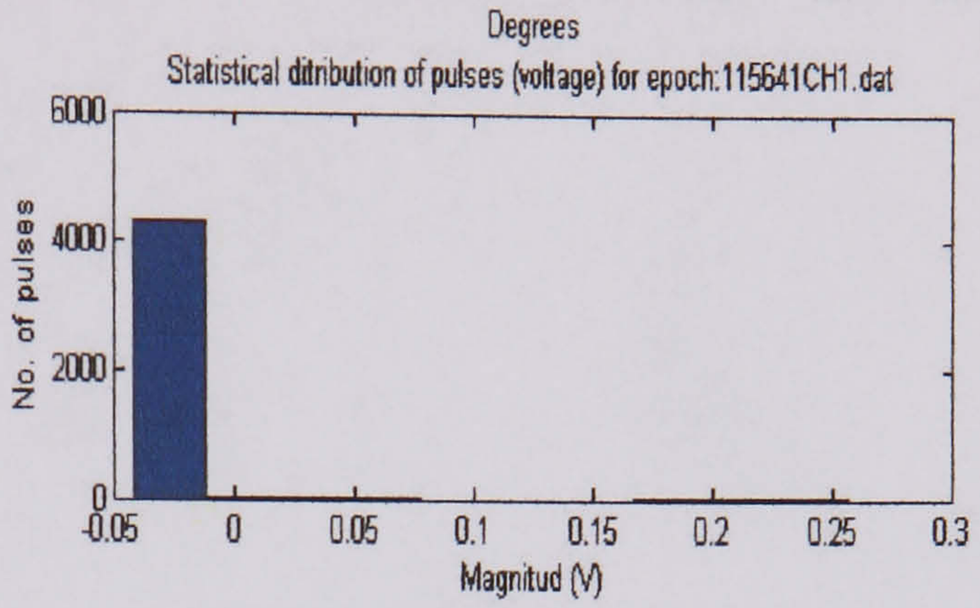

Statistical distribution of corona pulses at 6540 V with a 10mm air gap

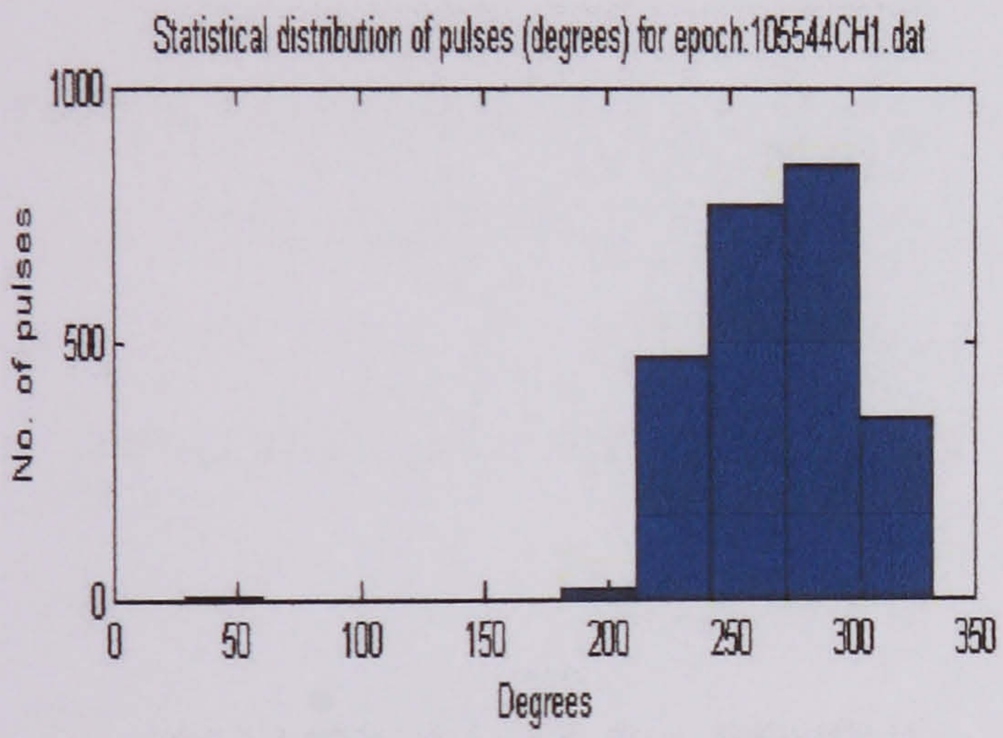

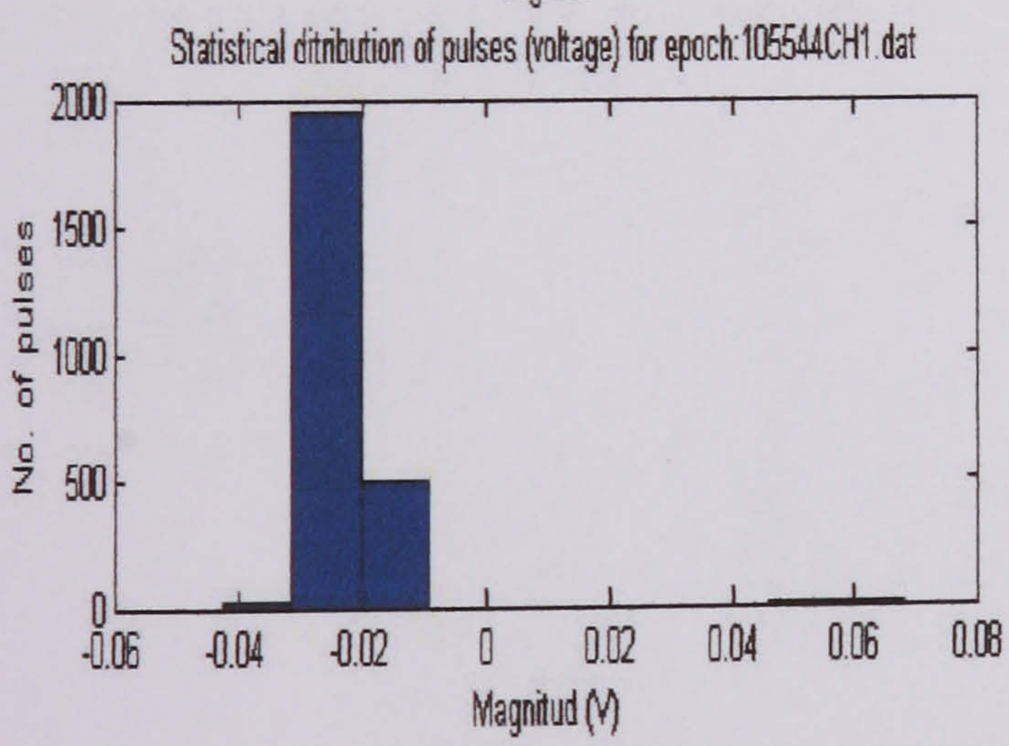

Statistical distribution of corona pulses at 5740 V with a 10mm air gap

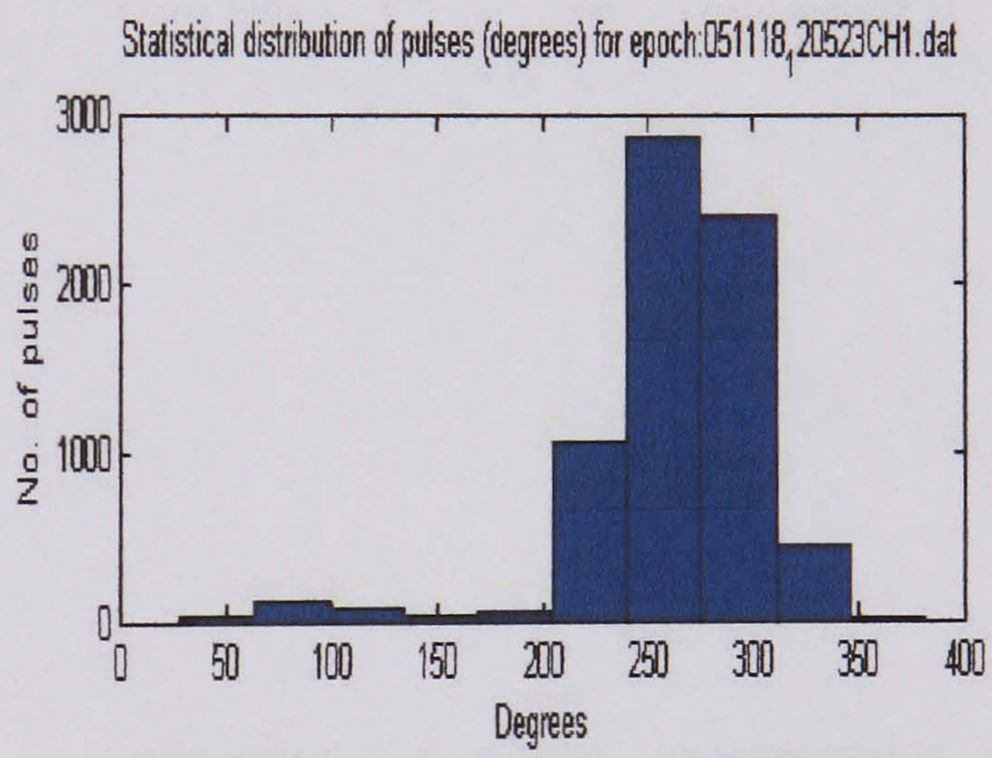

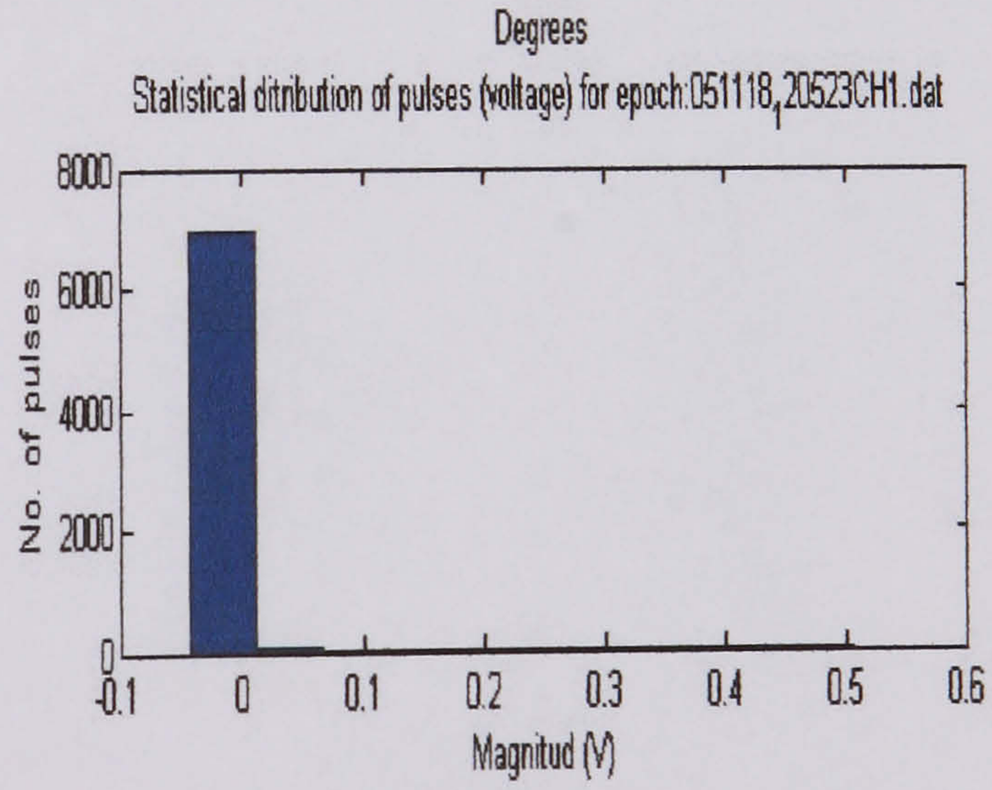

Statistical distribution of corona pulses at 7370 V with a 10mm air gap

Statistical distribution of corona pulses

at 7370 V with a 10mm air gap

Appendix D: Patterns for new insulator and their statistical distribution

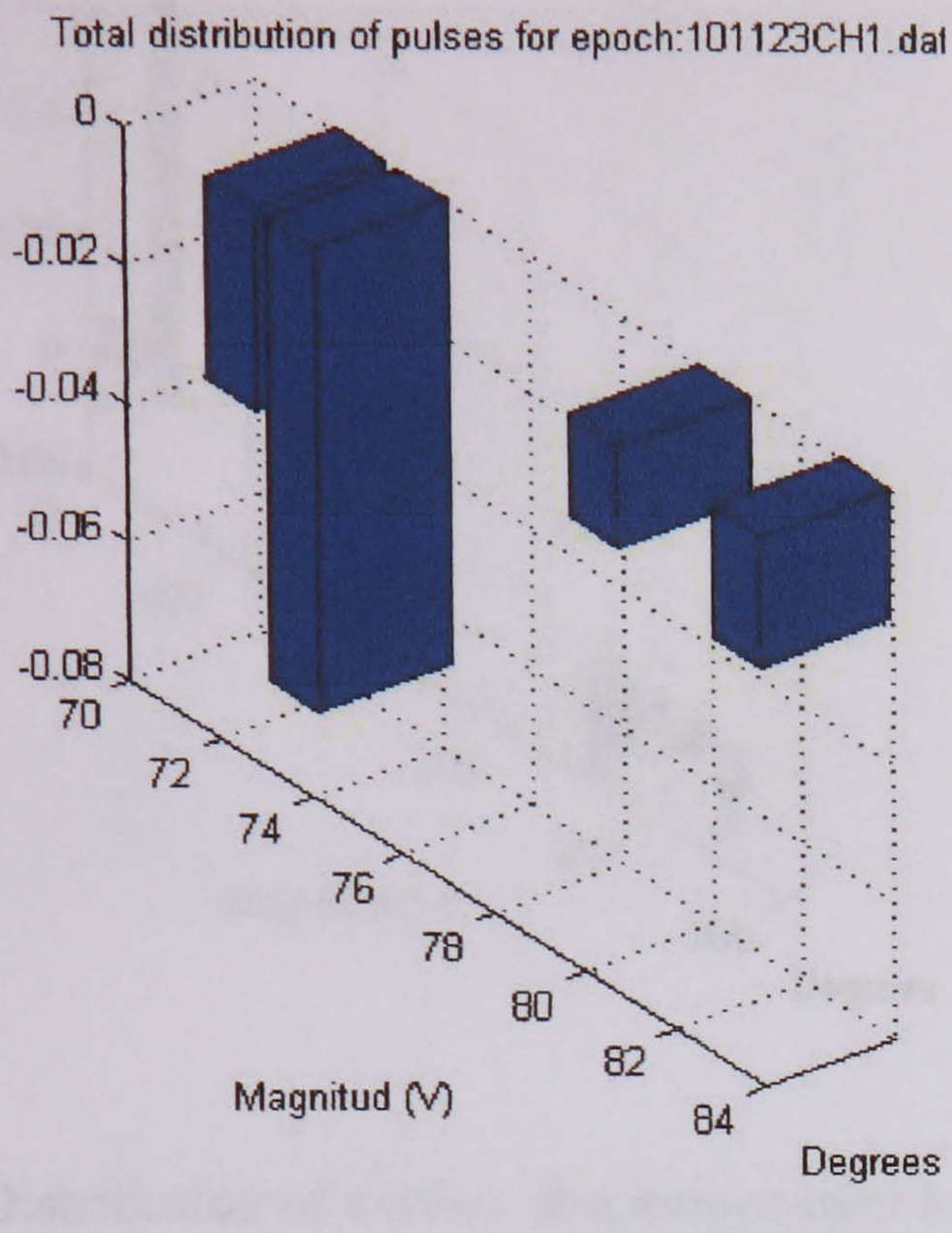

Distribution of surface discharges over a new insulator at 28700 V

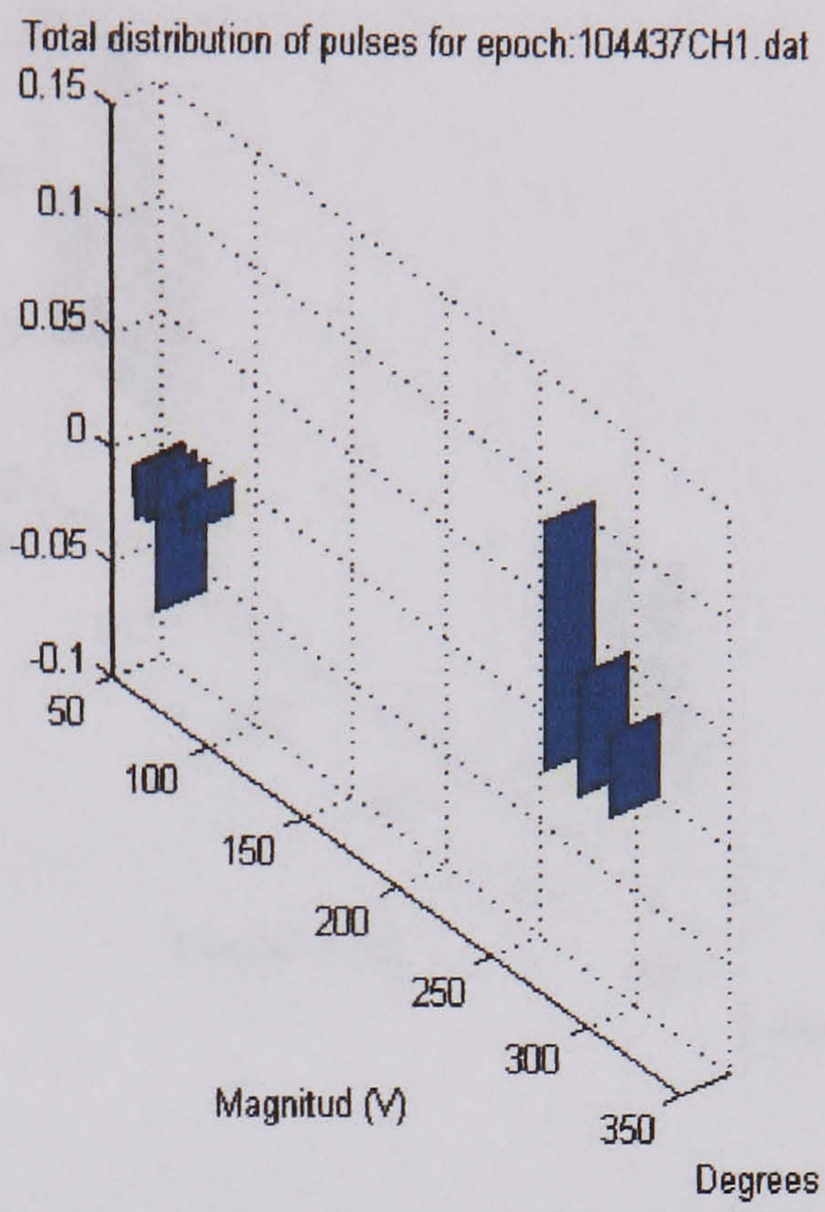

Distribution of surface discharges over a new insulator at 34830 V

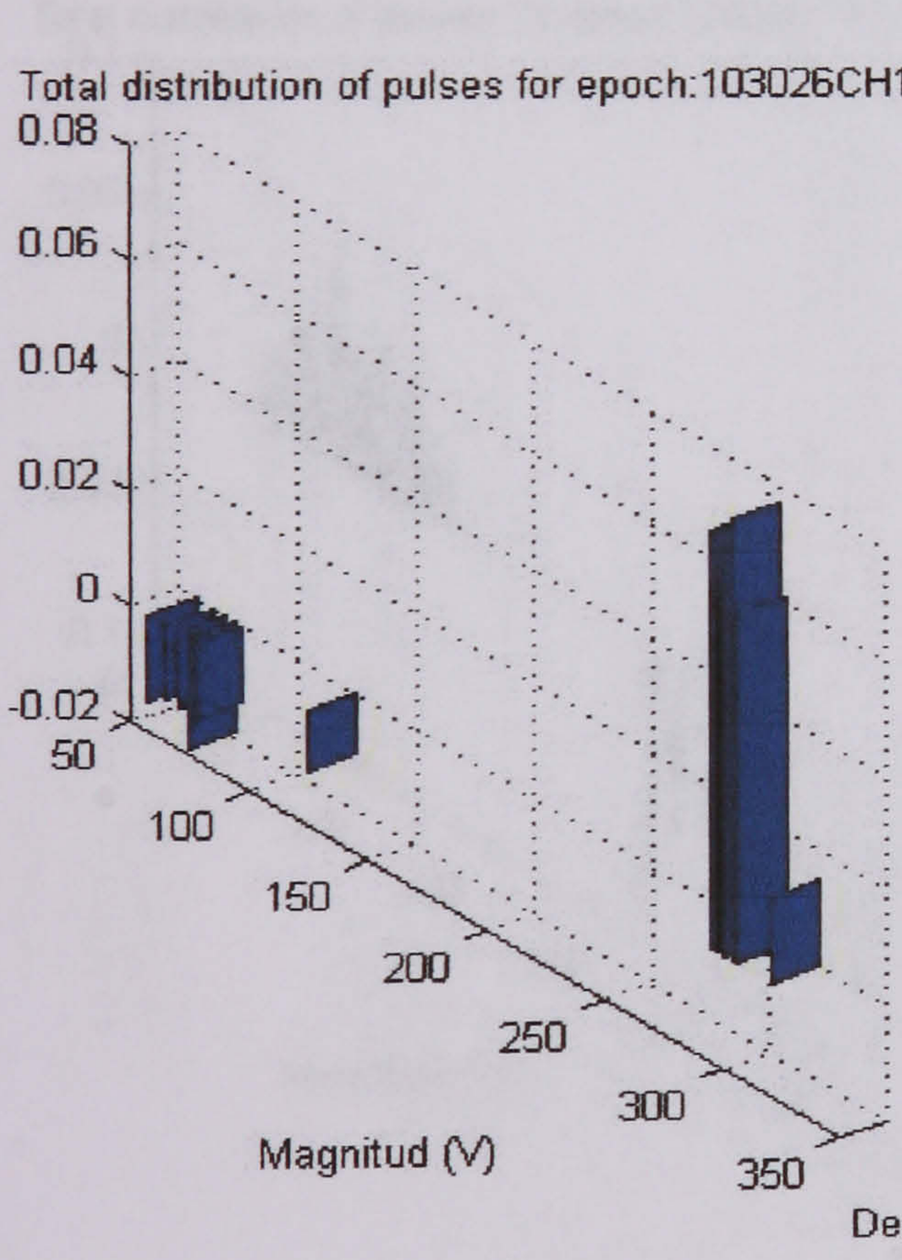

Distribution of surface discharges over a new insulator at 32810 V

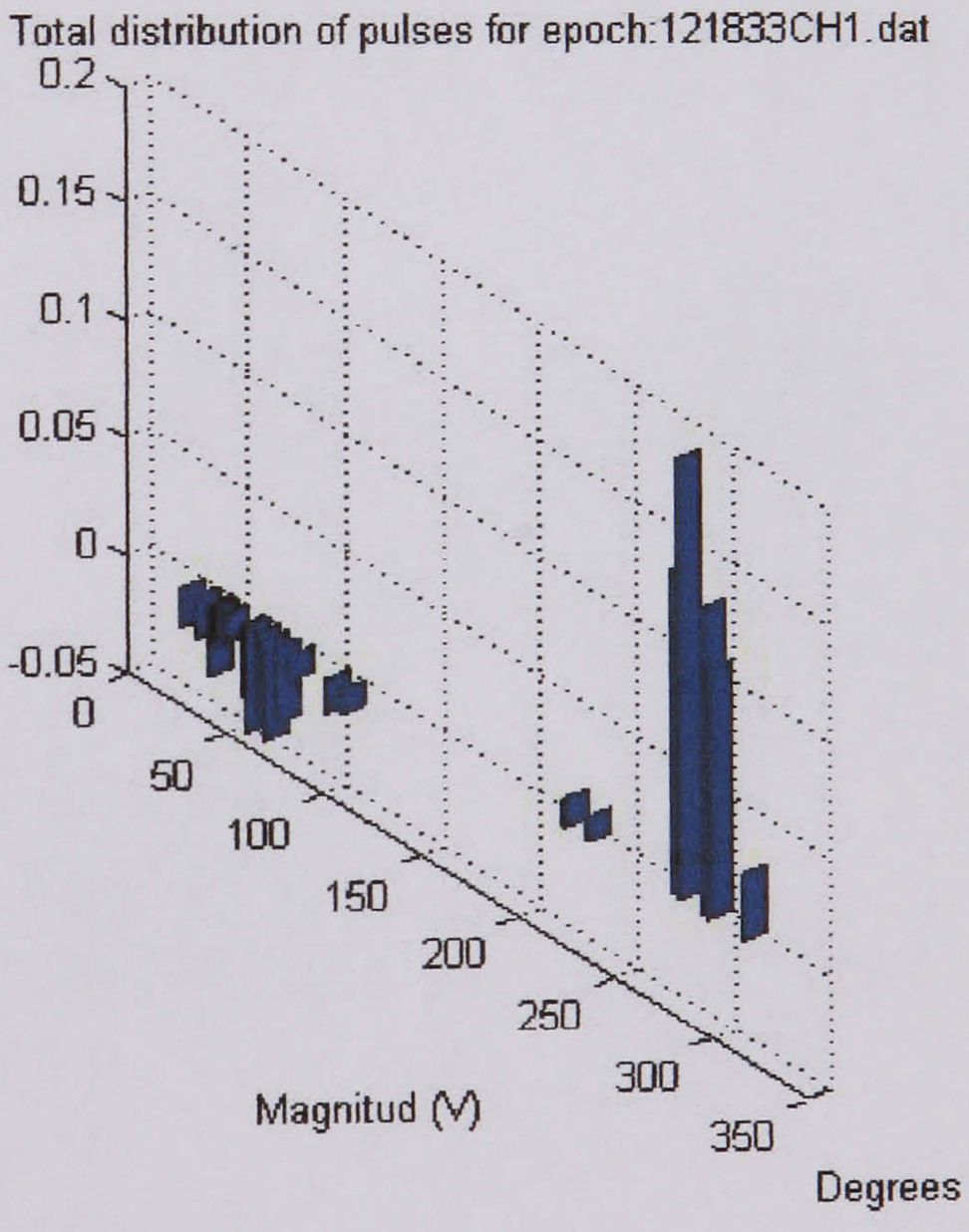

Distribution of surface discharges over a new insulator at 36900 V

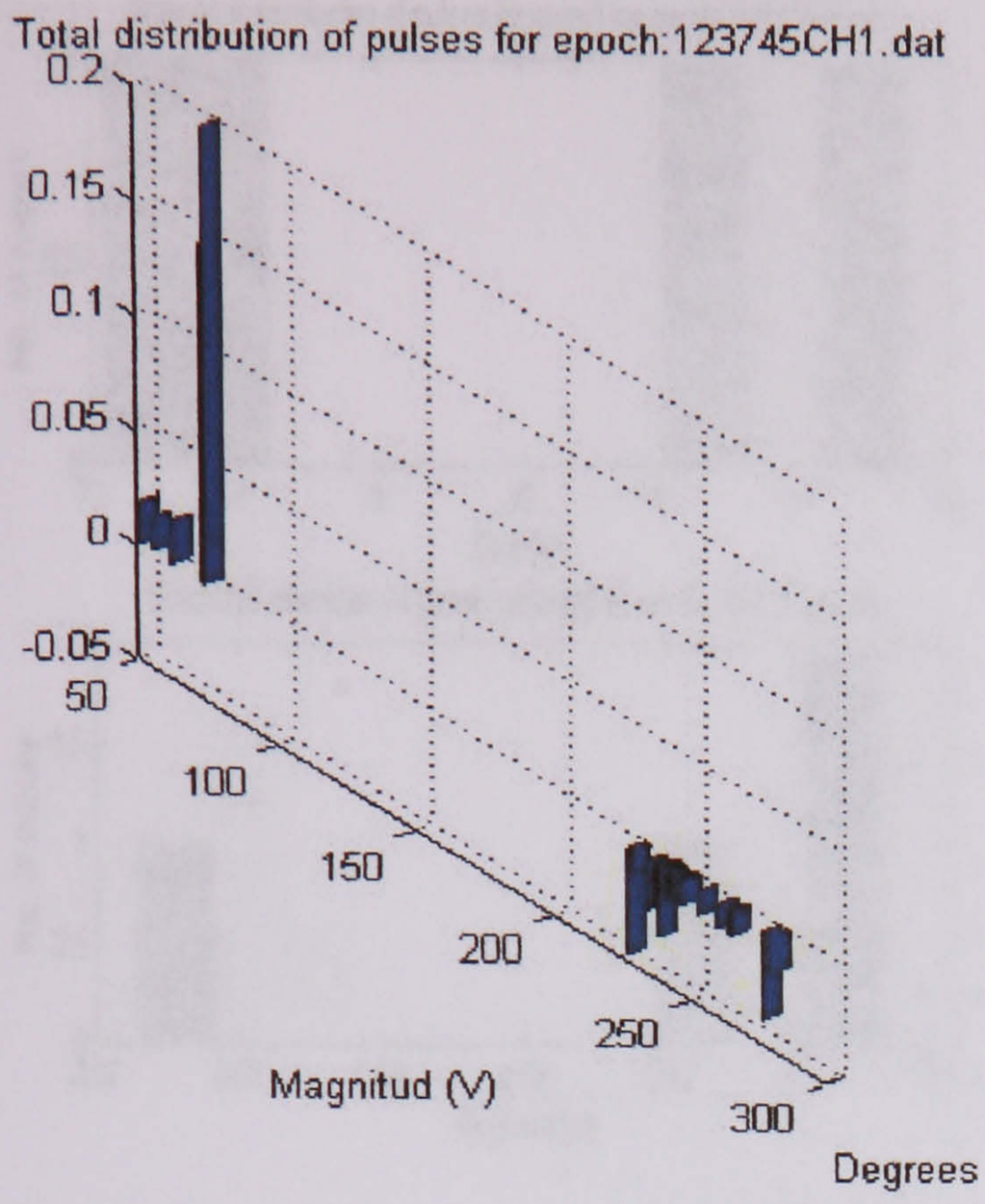

Distribution of surface discharges over a new insulator at 38800 V

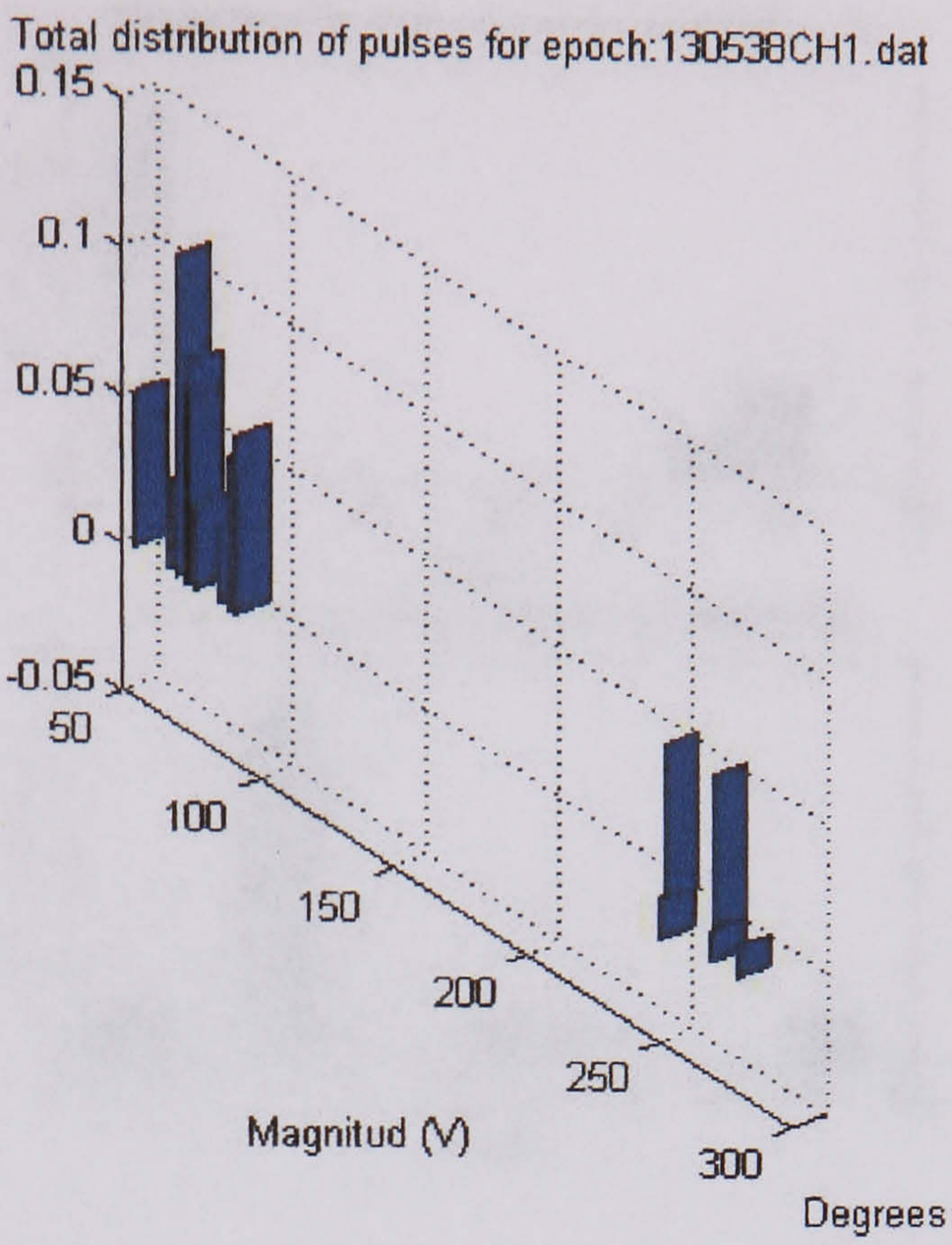

Distribution of surface discharges over a new insulator at 42500 V

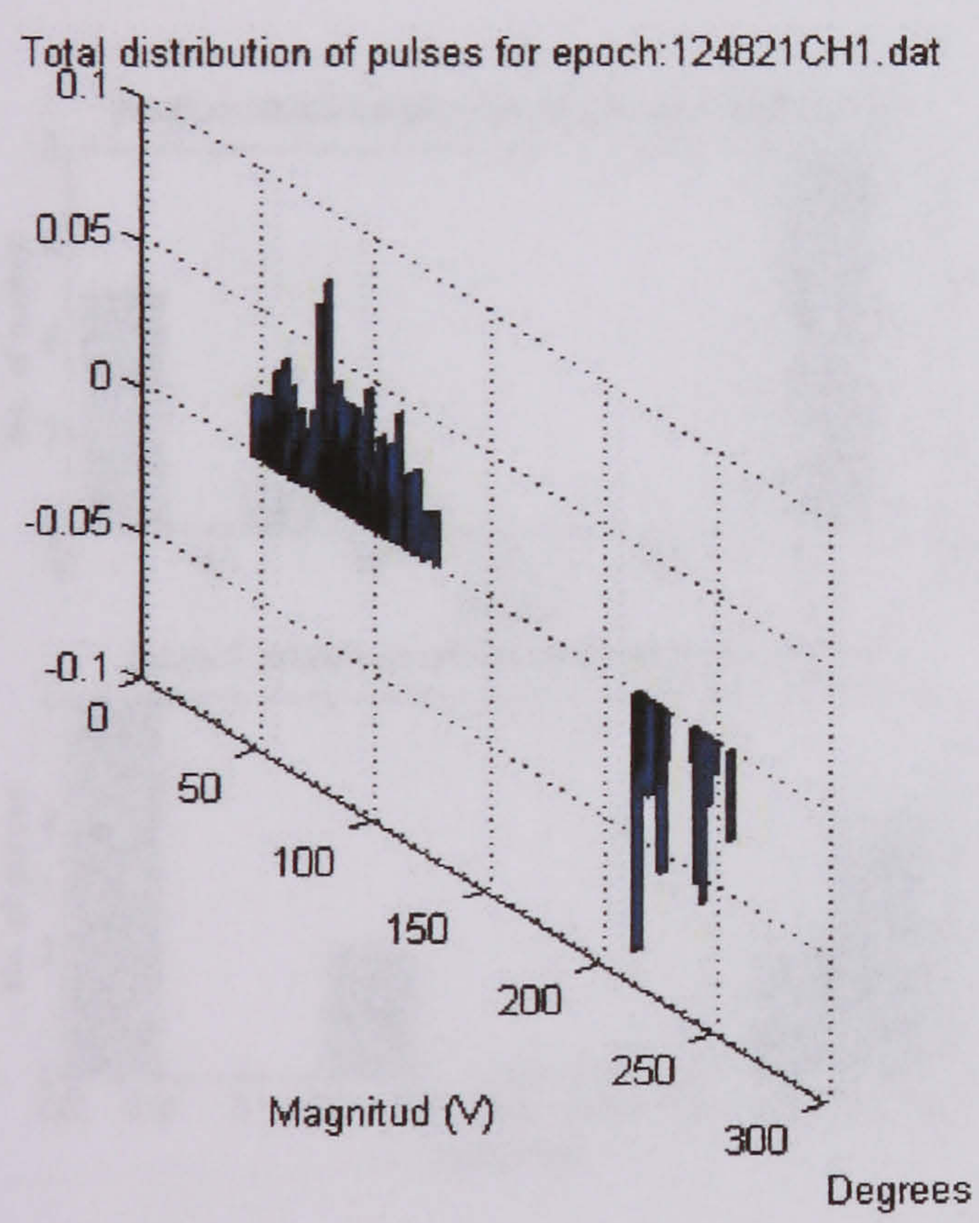

Distribution of surface discharges over a new insulator at 40800 V

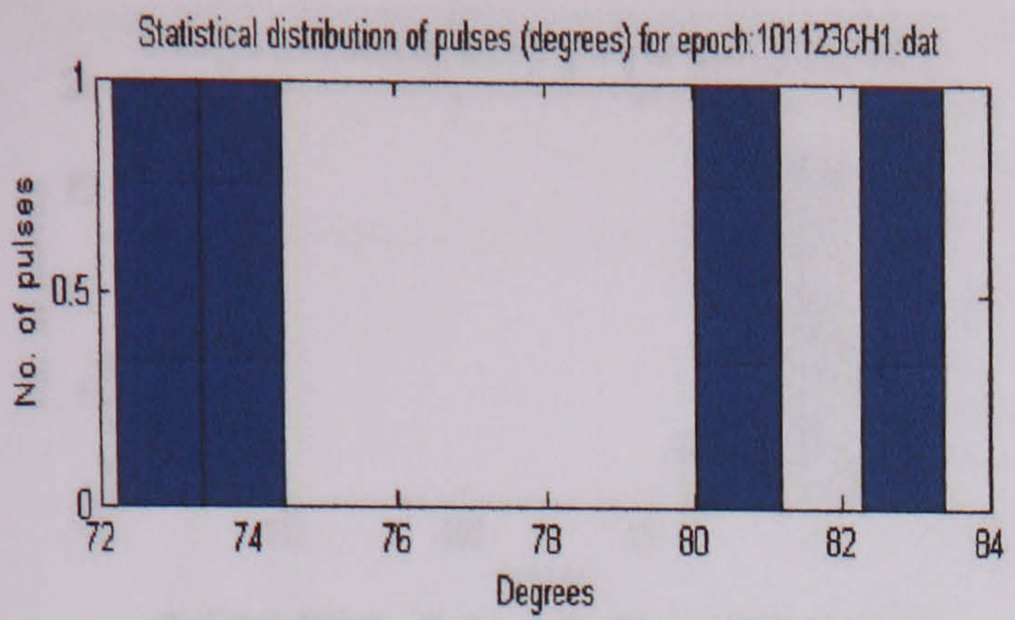

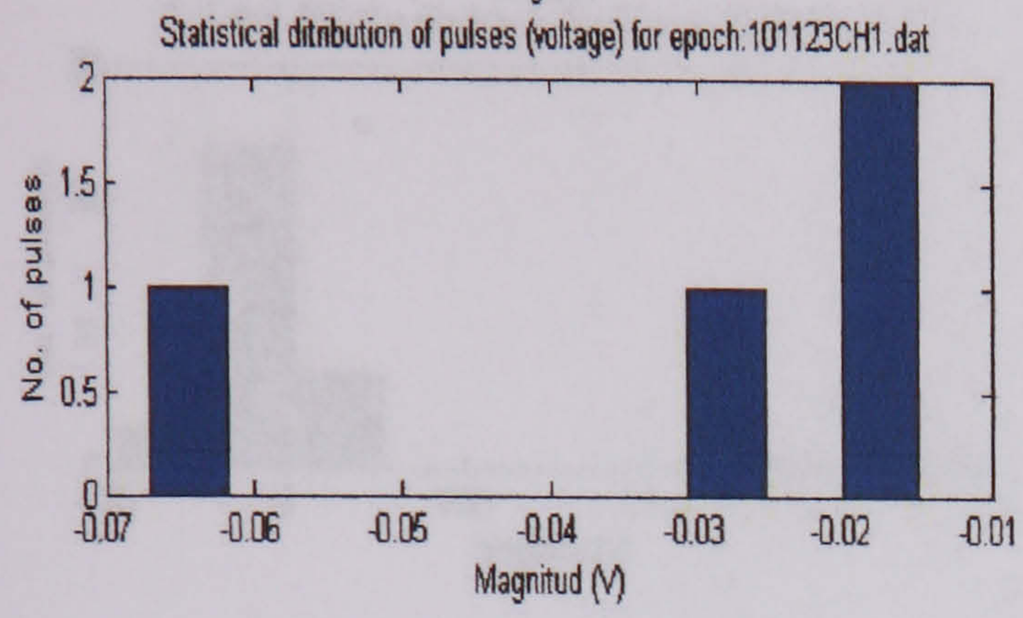

Statistical distribution of surface discharges over a new insulator at 28700 V

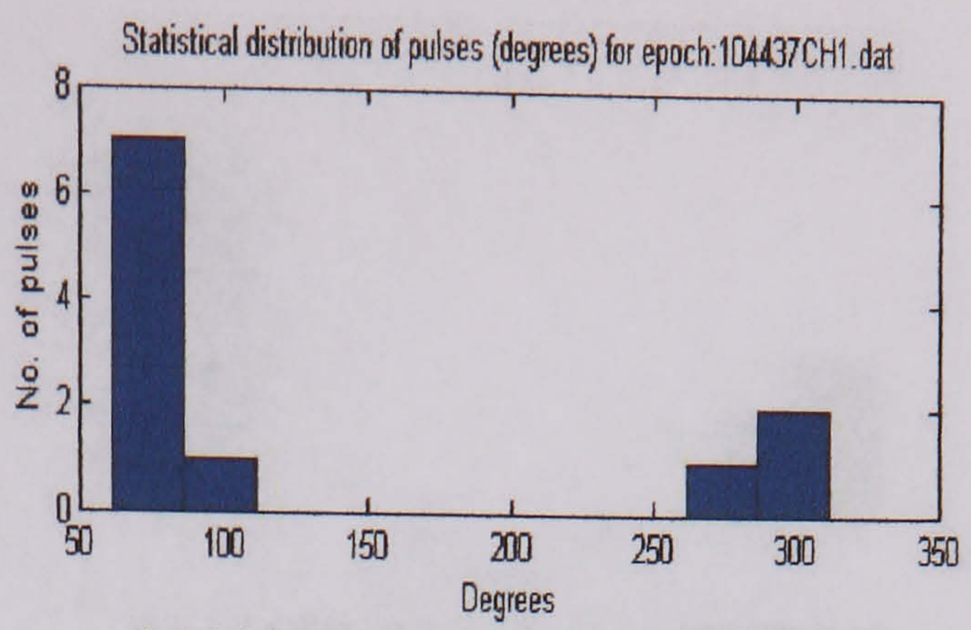

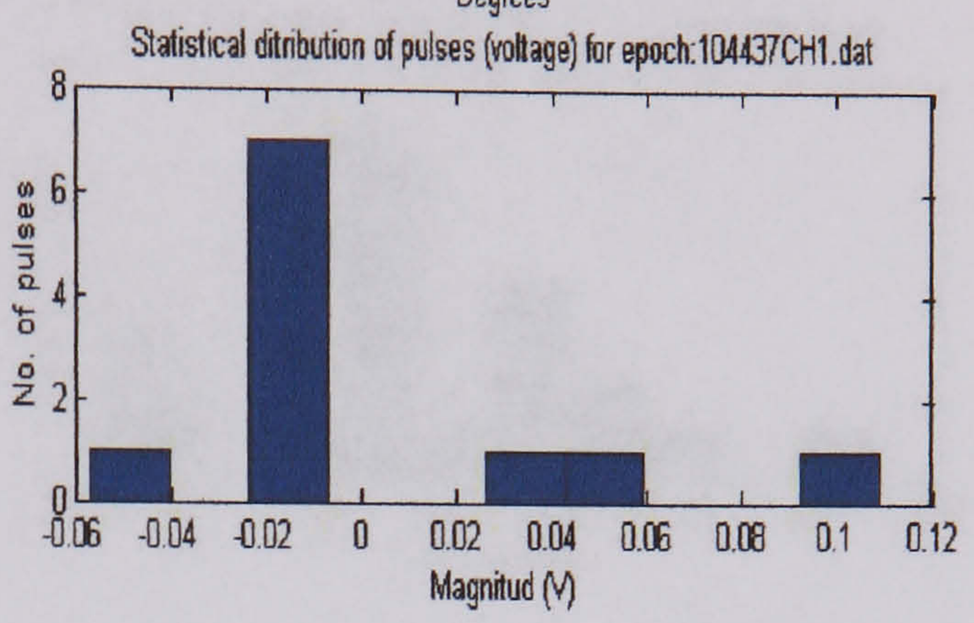

Statistical distribution of surface discharges over a new insulator at 34830 V

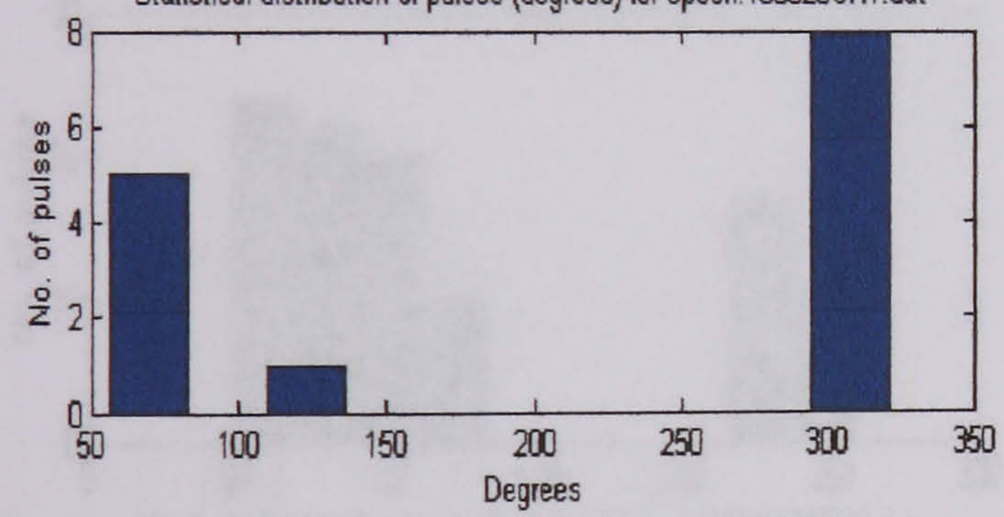

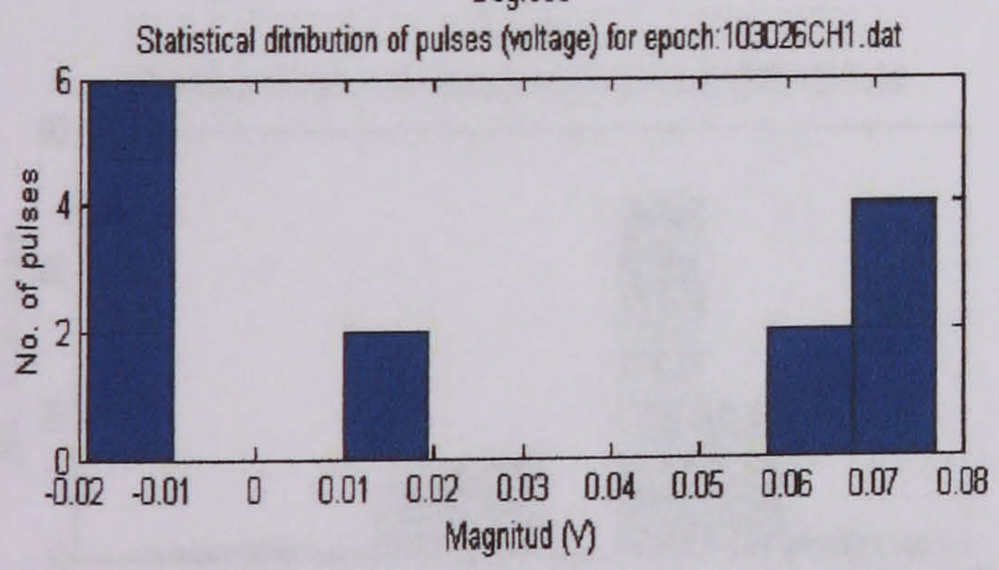

Statistical distribution of surface discharges over a new insulator at 32810 V

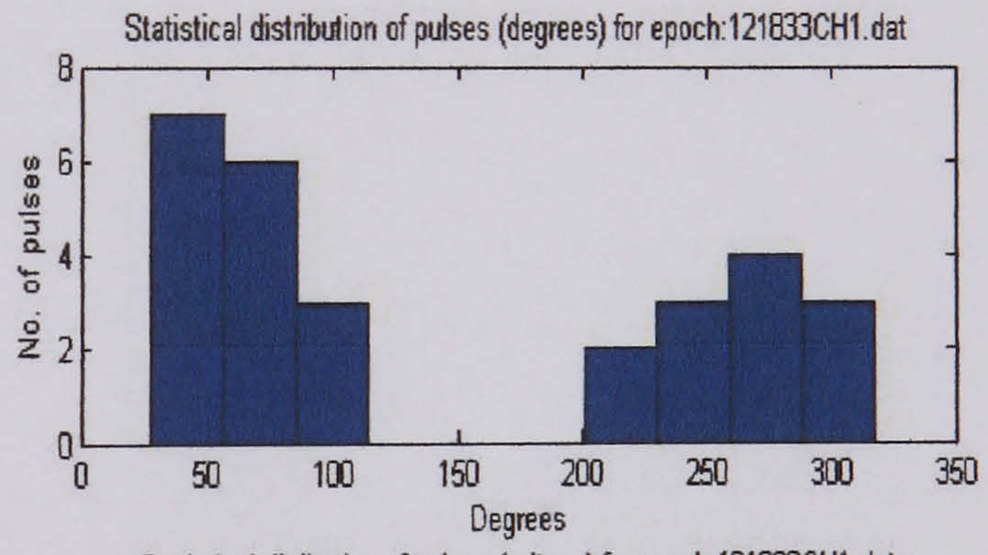

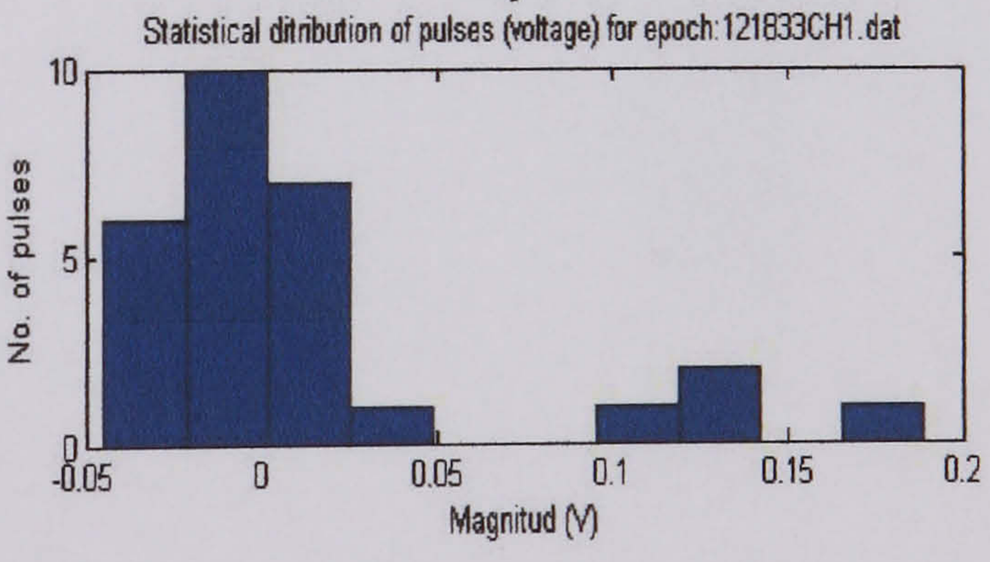

Statistical distribution of surface discharges over a new insulator at 36900 V

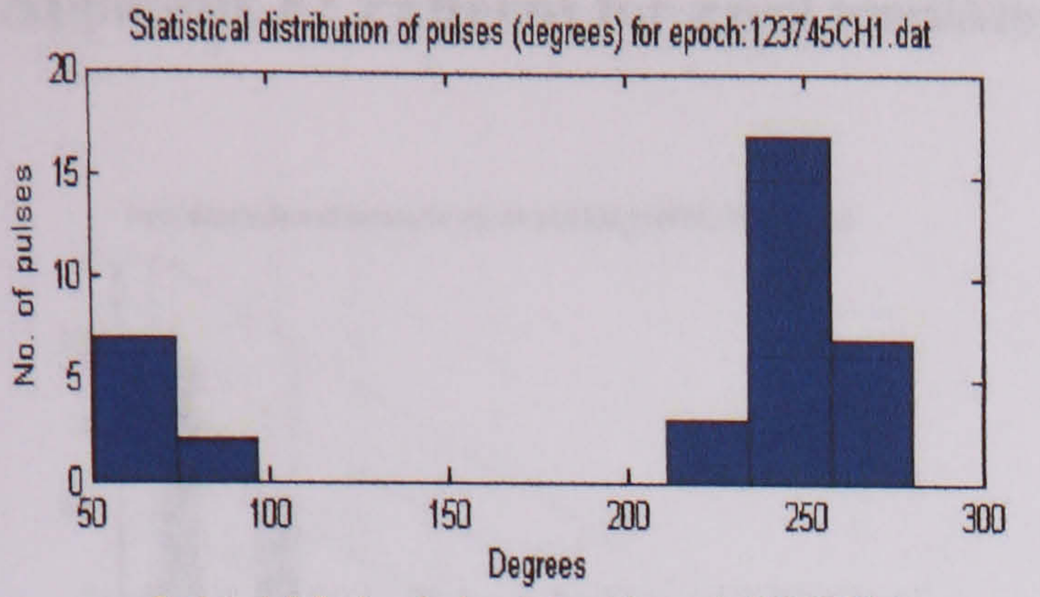

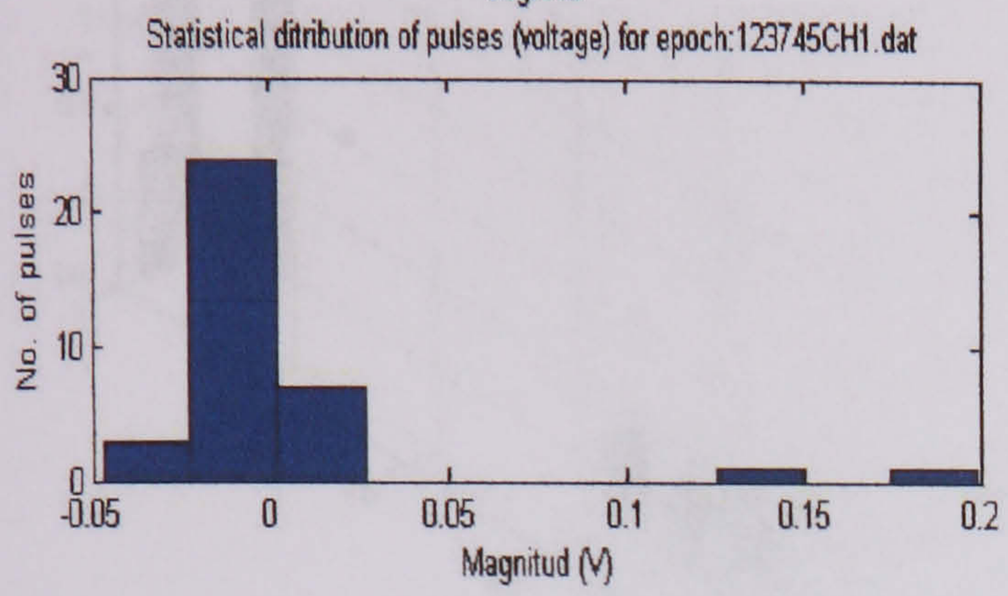

Statistical distribution of surface discharges over a new insulator at 38800 V

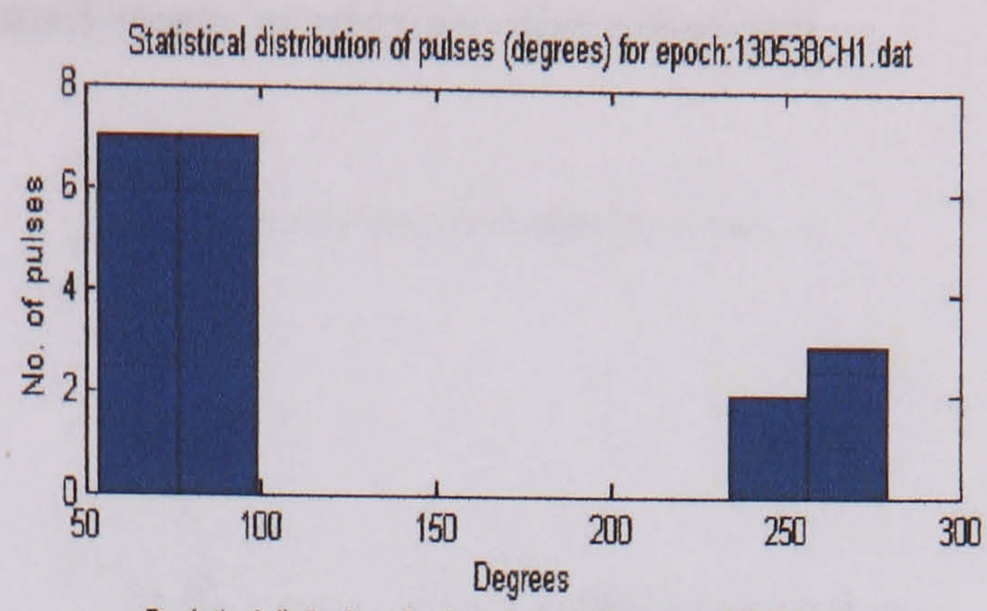

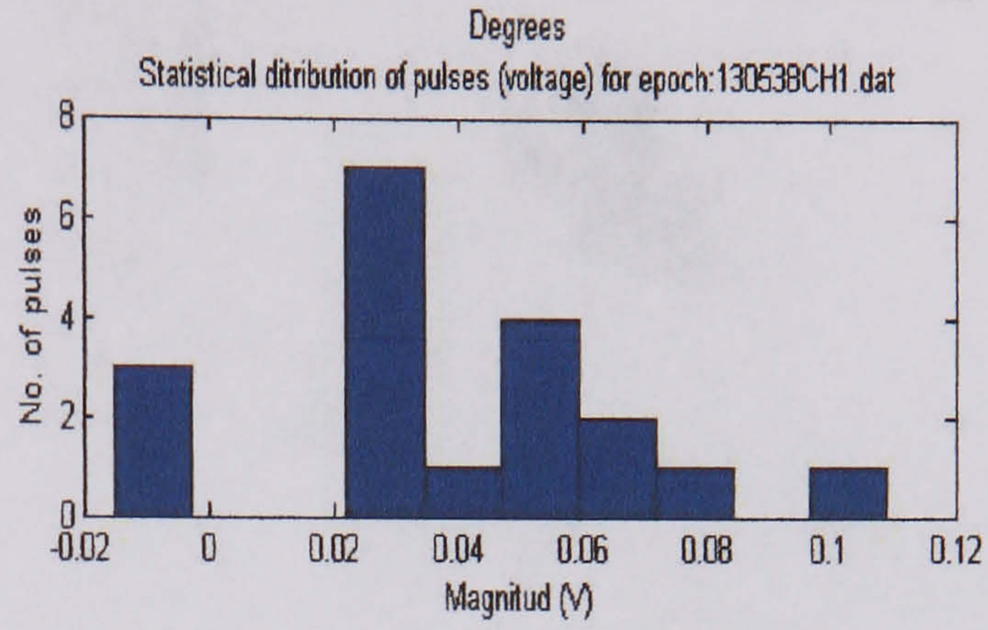

Statistical distribution of surface discharges over a new insulator at 42500 V

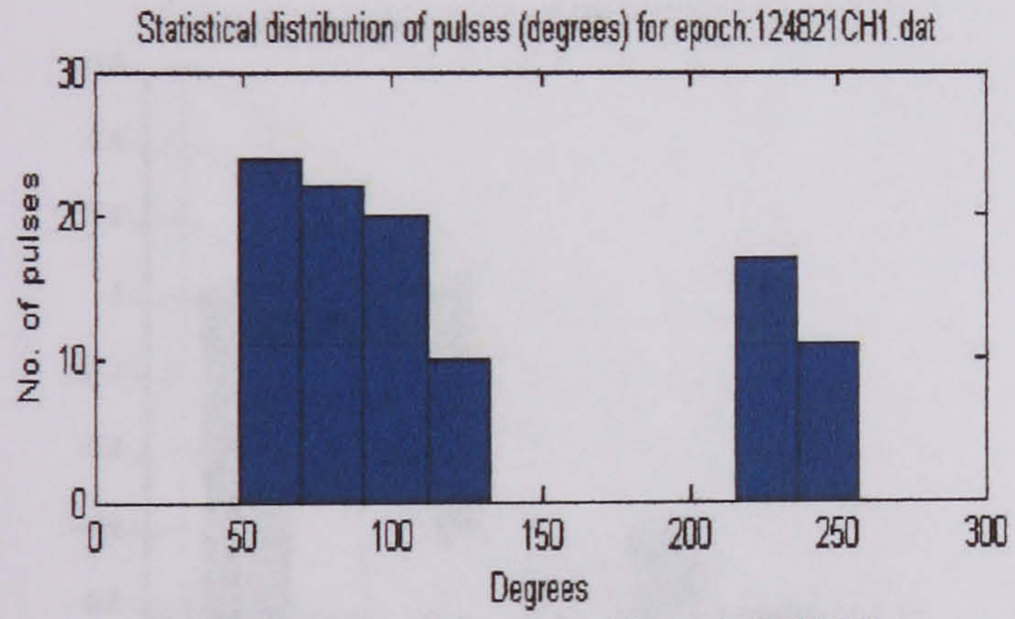

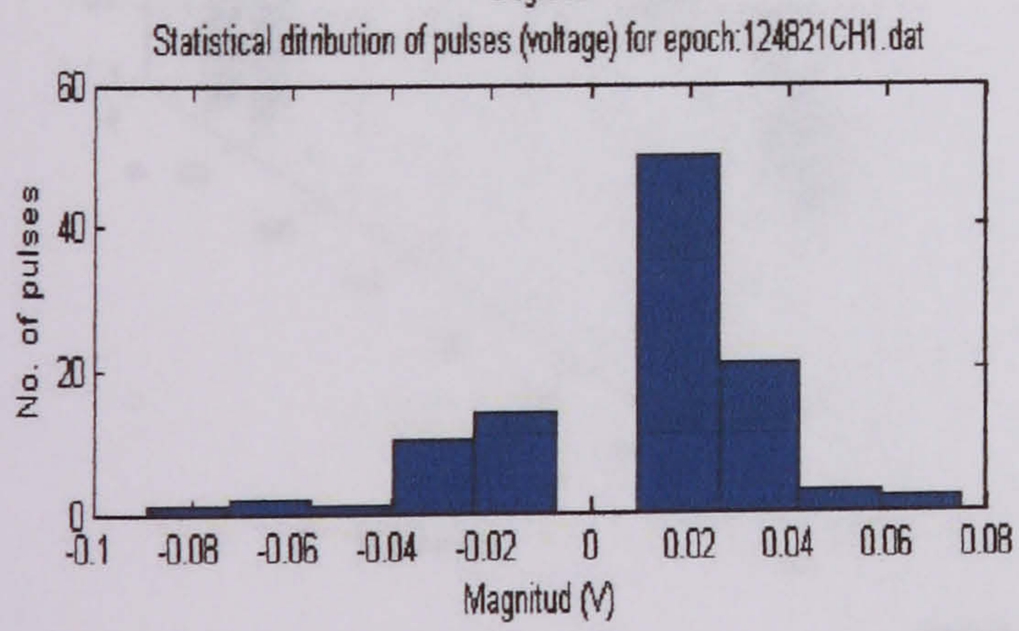

Statistical distribution of surface discharges over a new insulator at 40800 V

Appendix E: Patterns for aged insulator and their statistical distribution

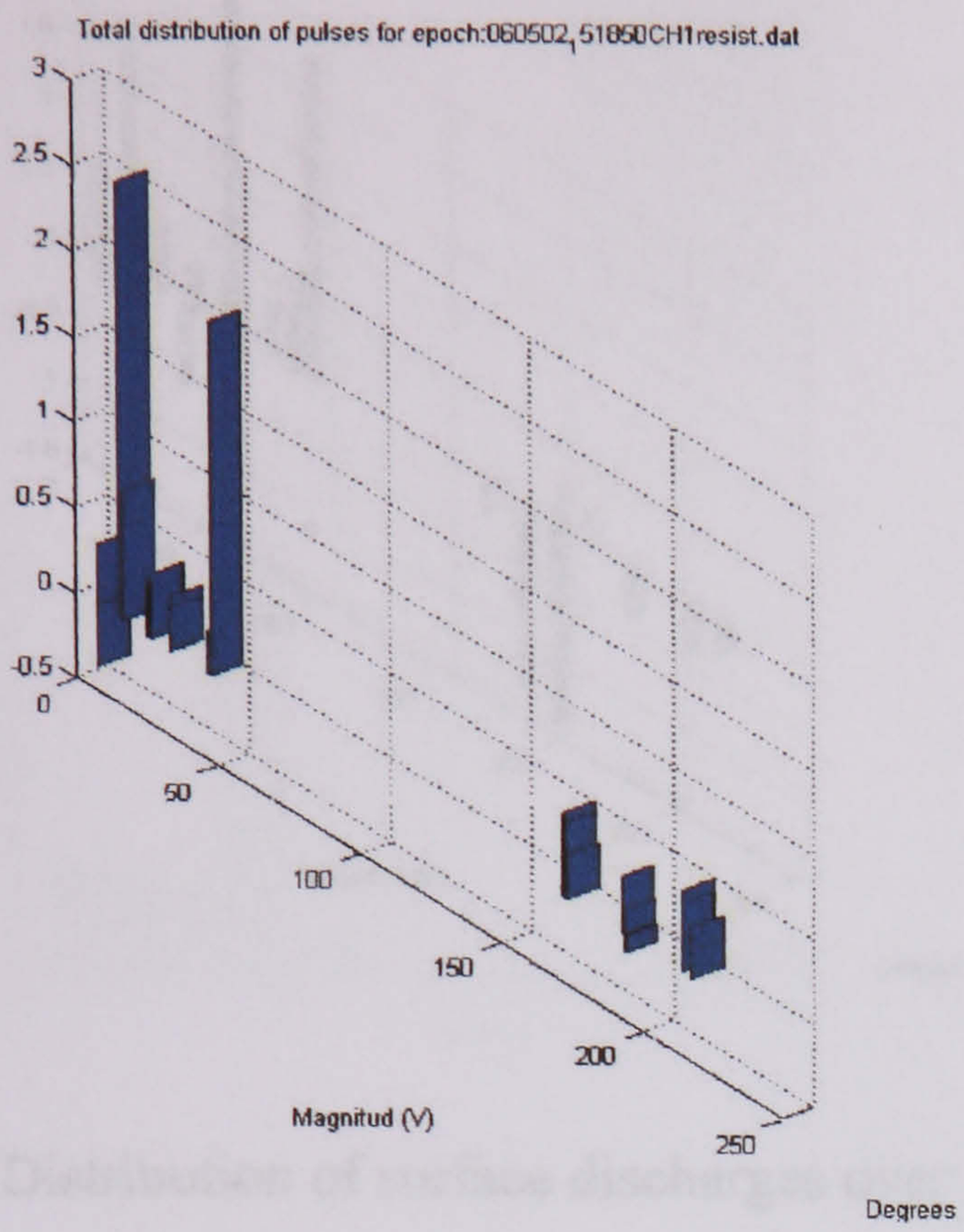

Distribution of surface discharges over an aged insulator at 30760 V (resistor)

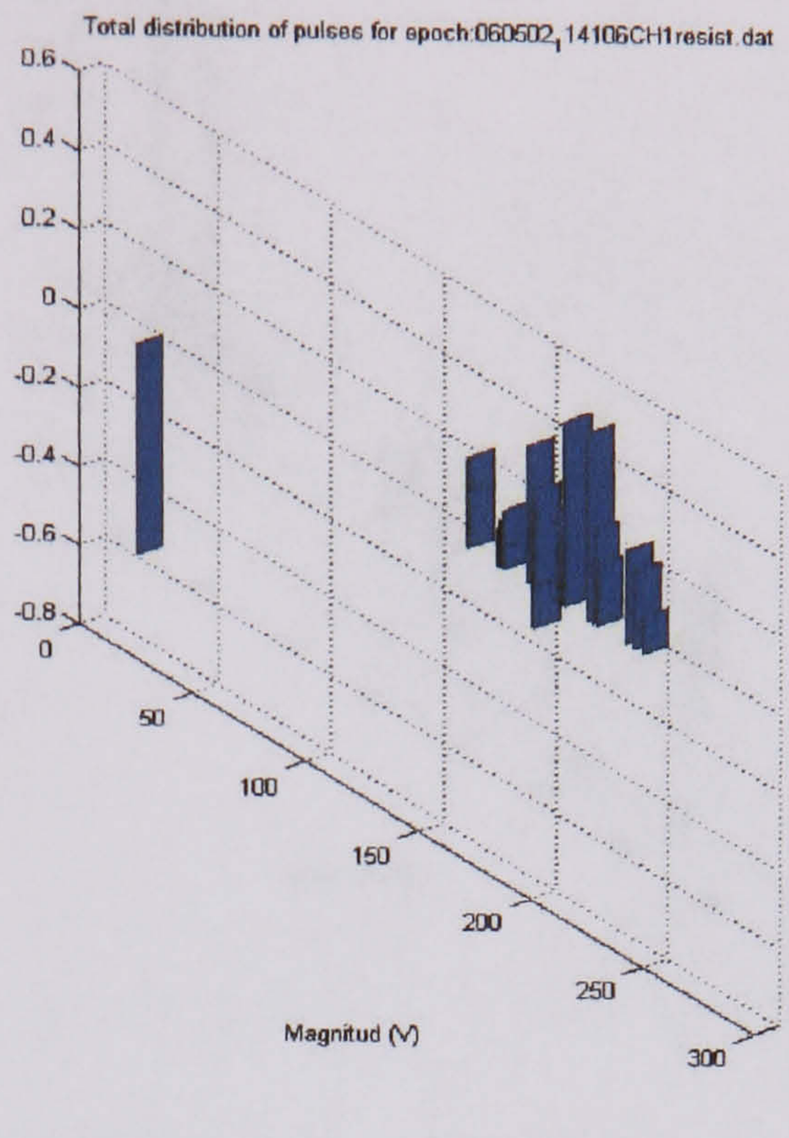

Distribution of surface discharges over an aged insulator at 34830 V (resistor)

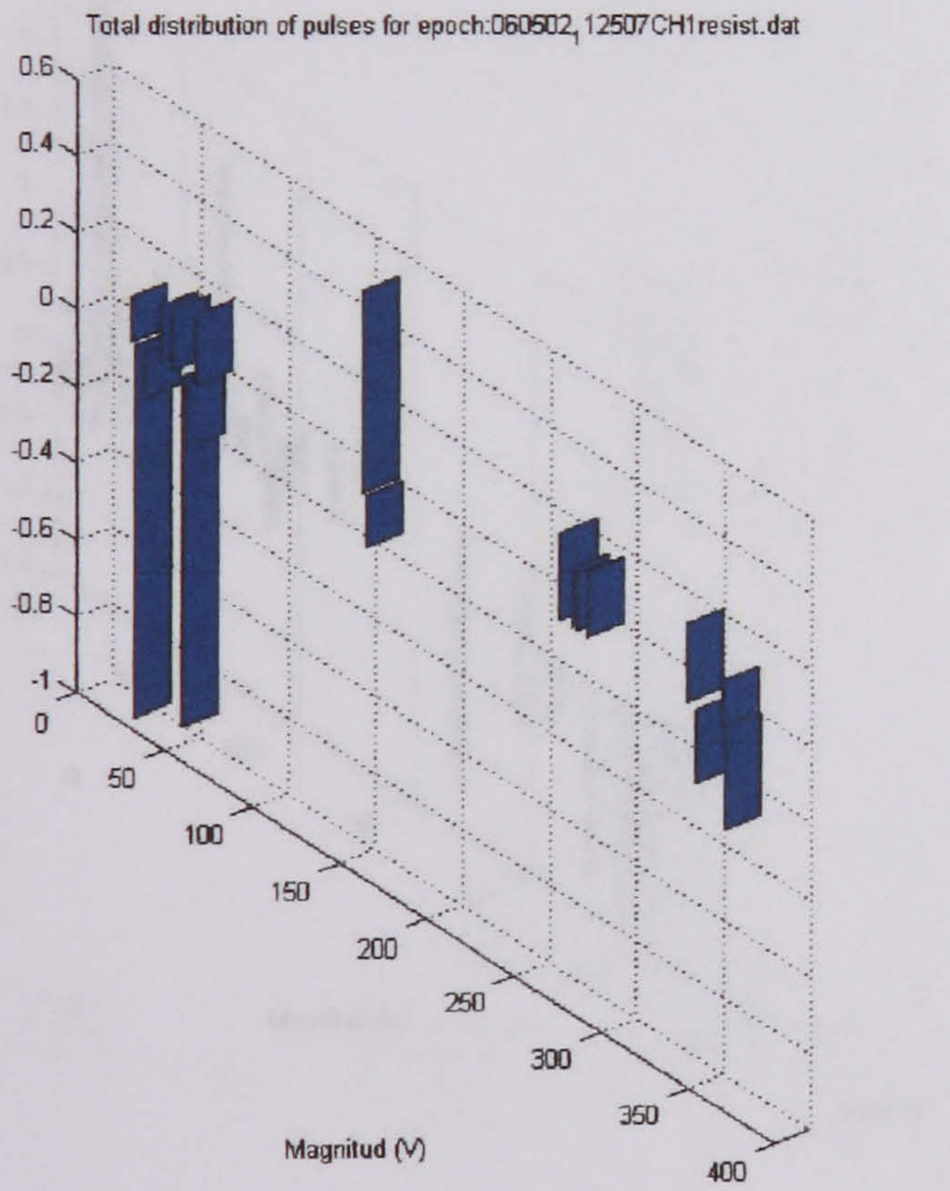

Distribution of surface discharges over an aged insulator at 32810 V (resistor)

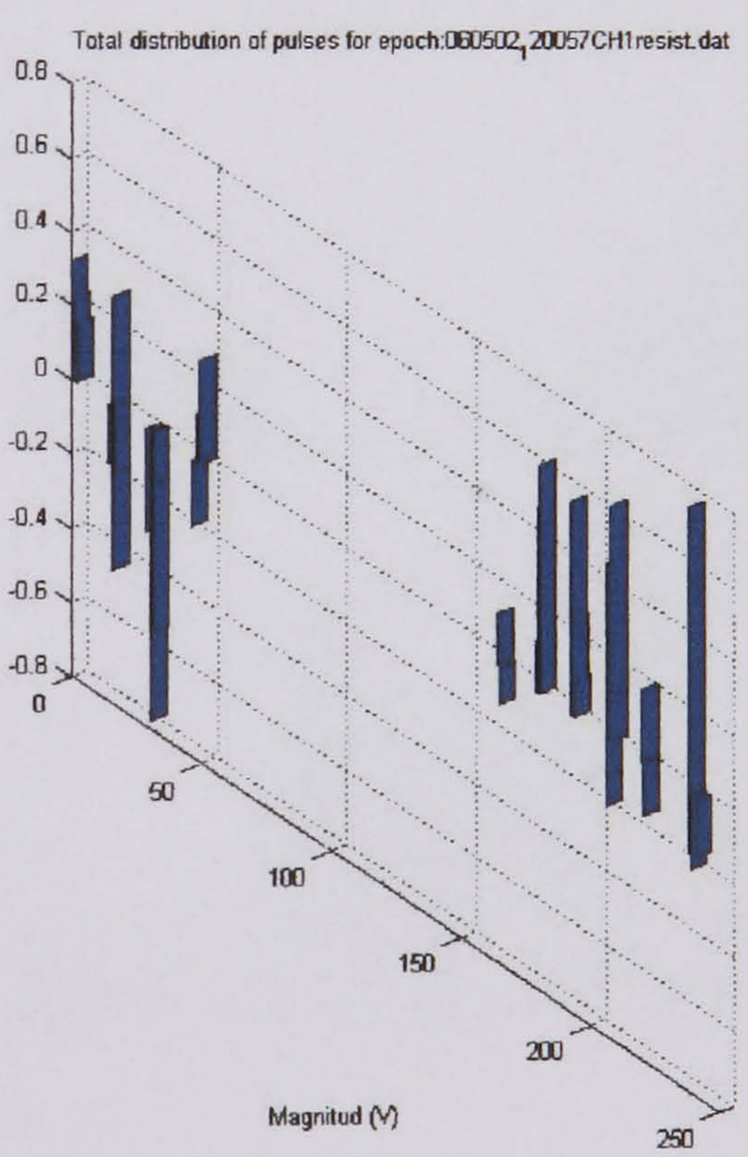

Distribution of surface discharges over an aged insulator at 36900 V (resistor)

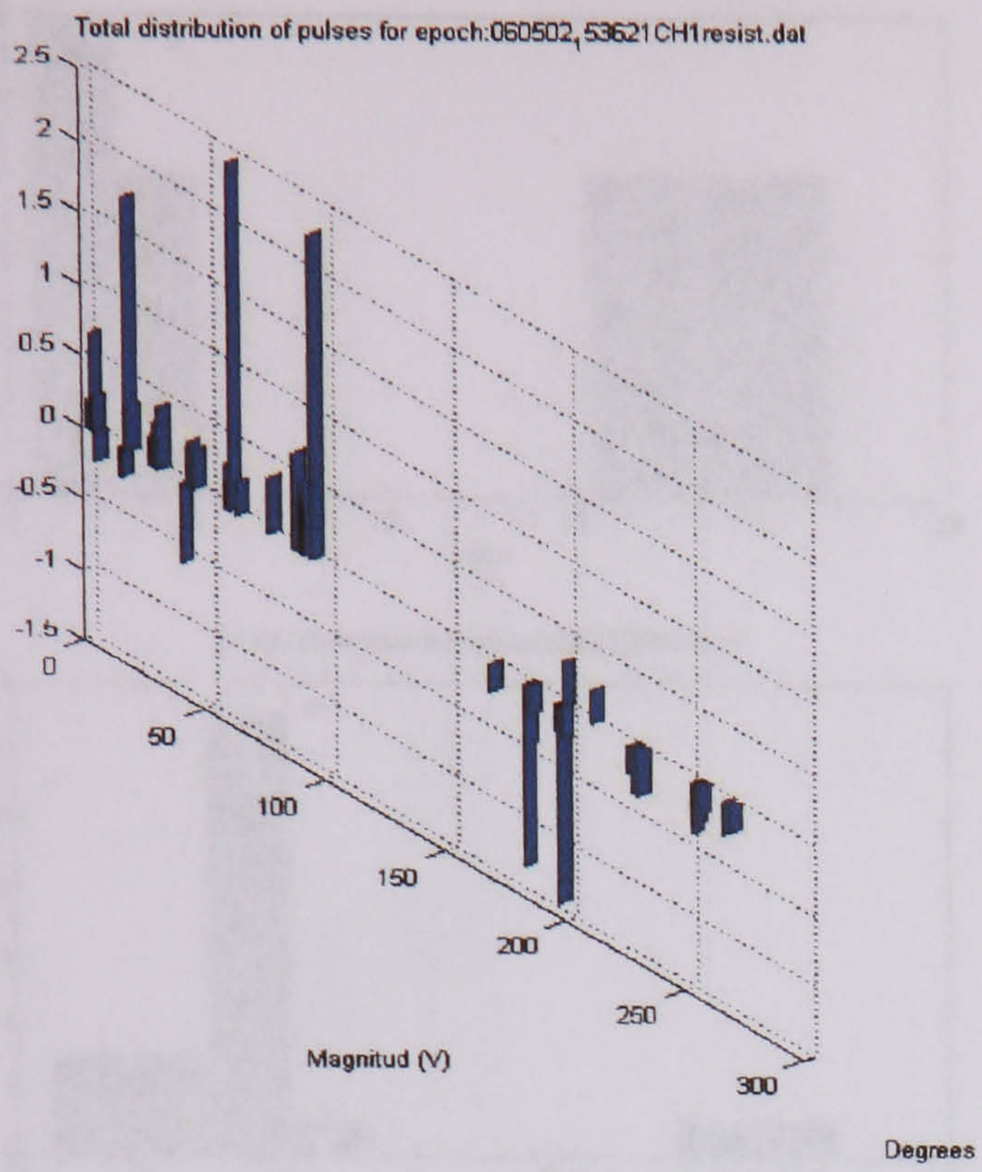

Distribution of surface discharges over an aged insulator at 38800 V (resistor)

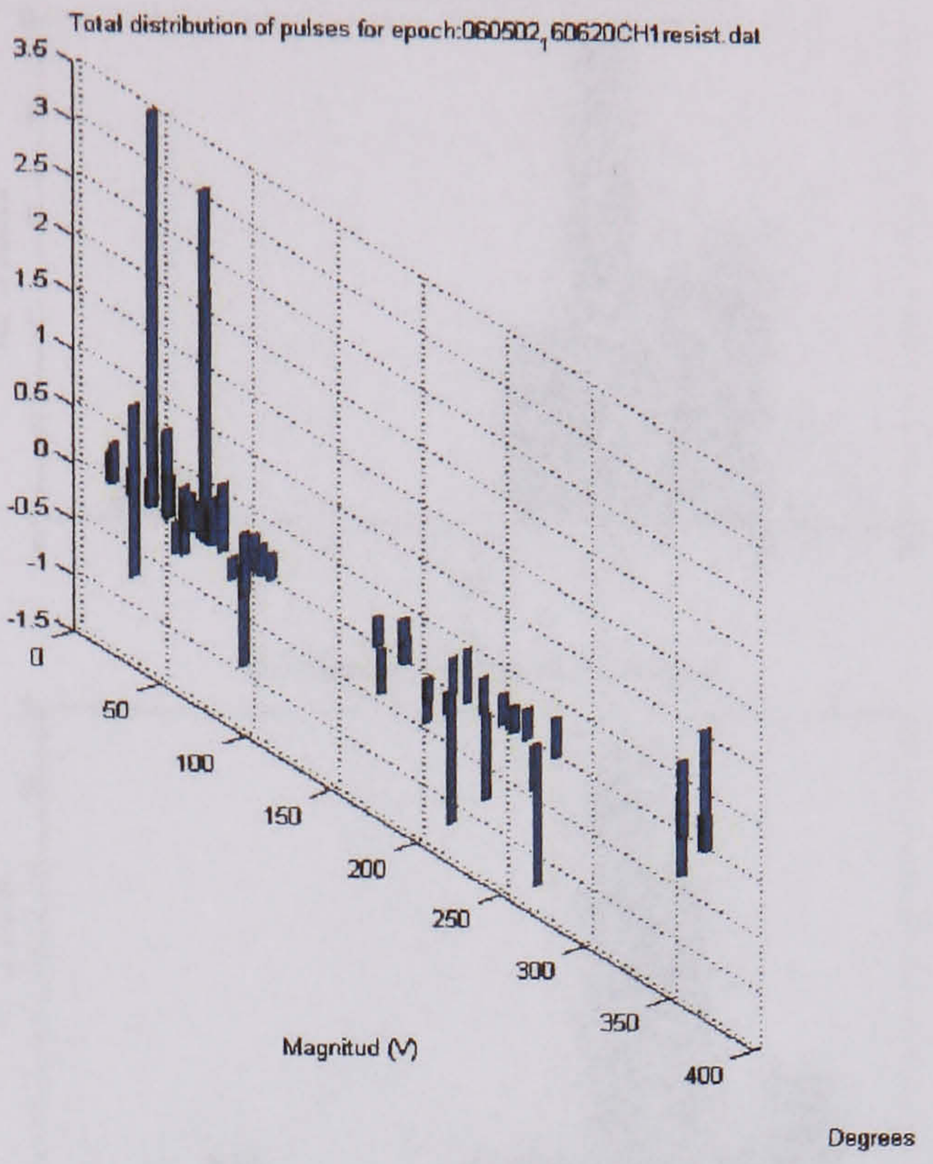

Distribution of surface discharges over an aged insulator at 42500 V (resistor)

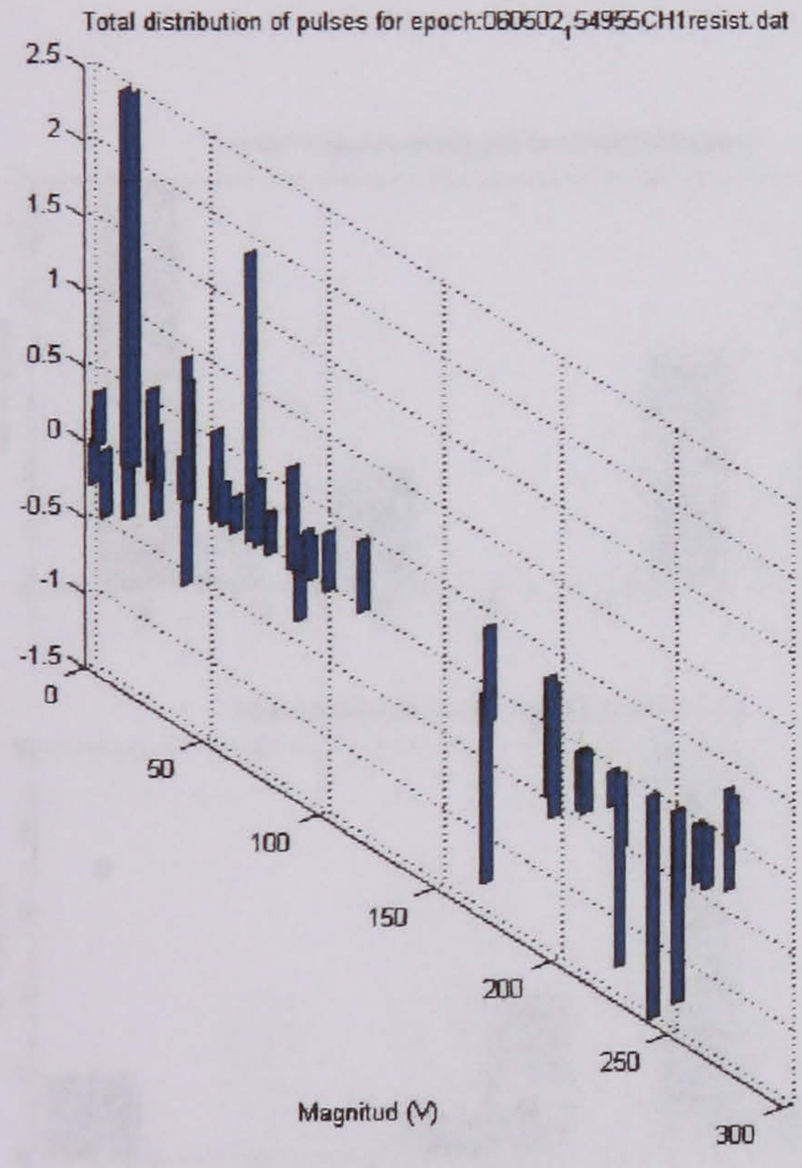

Distribution of surface discharges over an aged insulator at 40800 V (resistor)

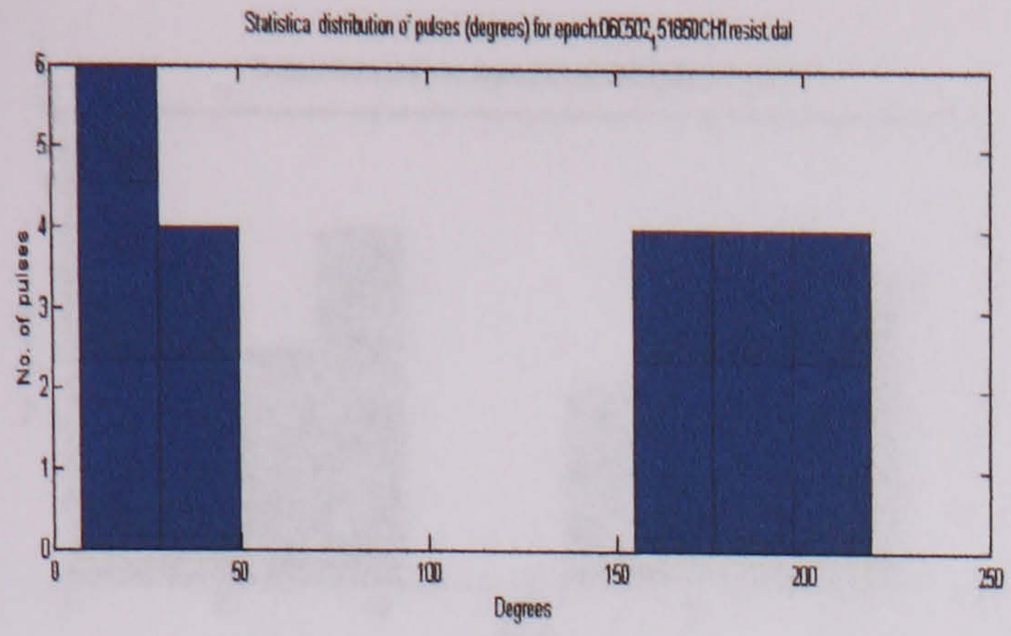

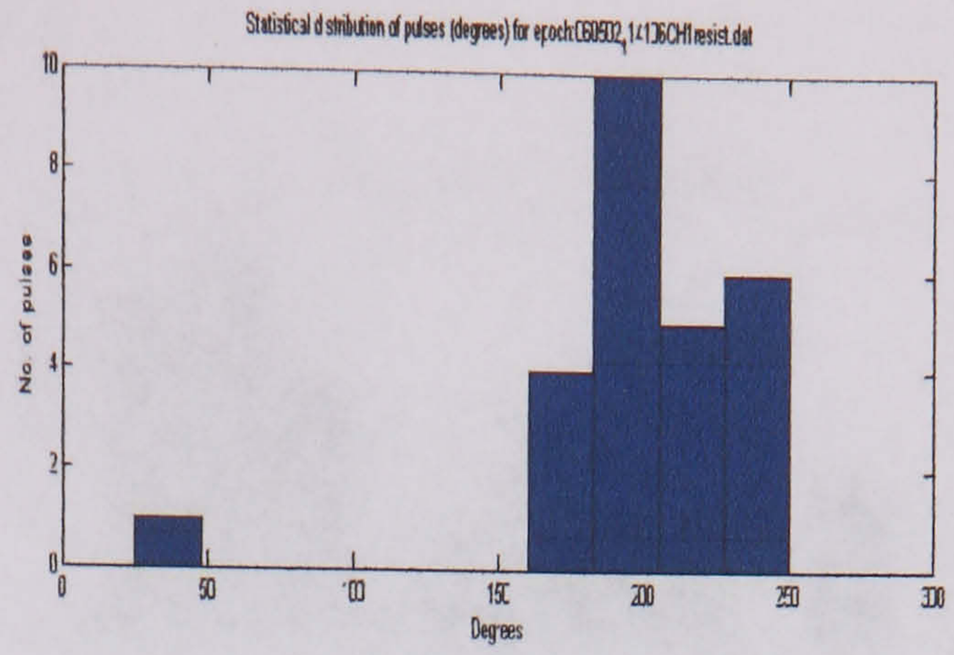

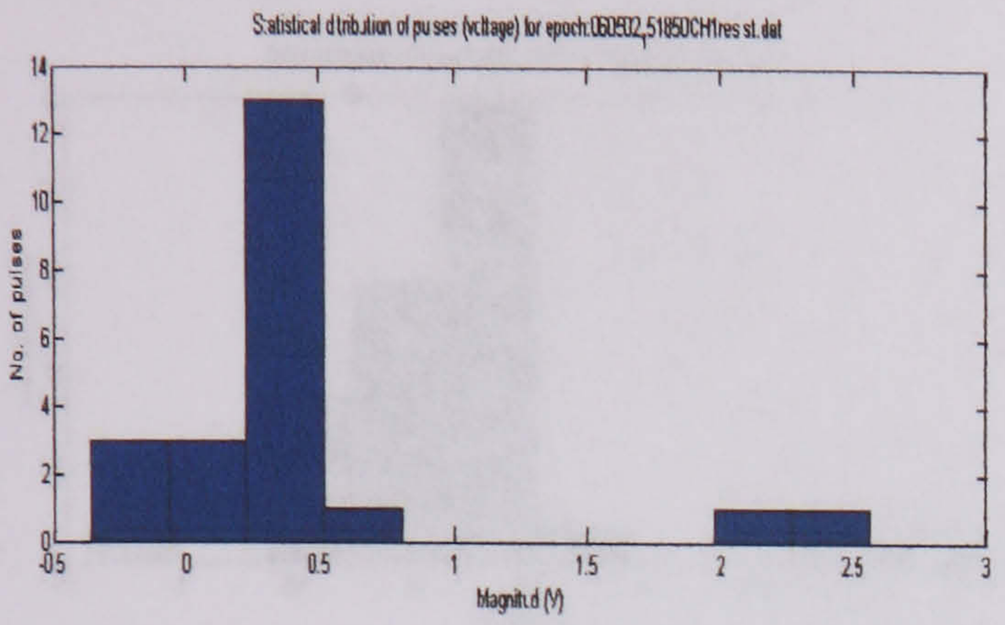

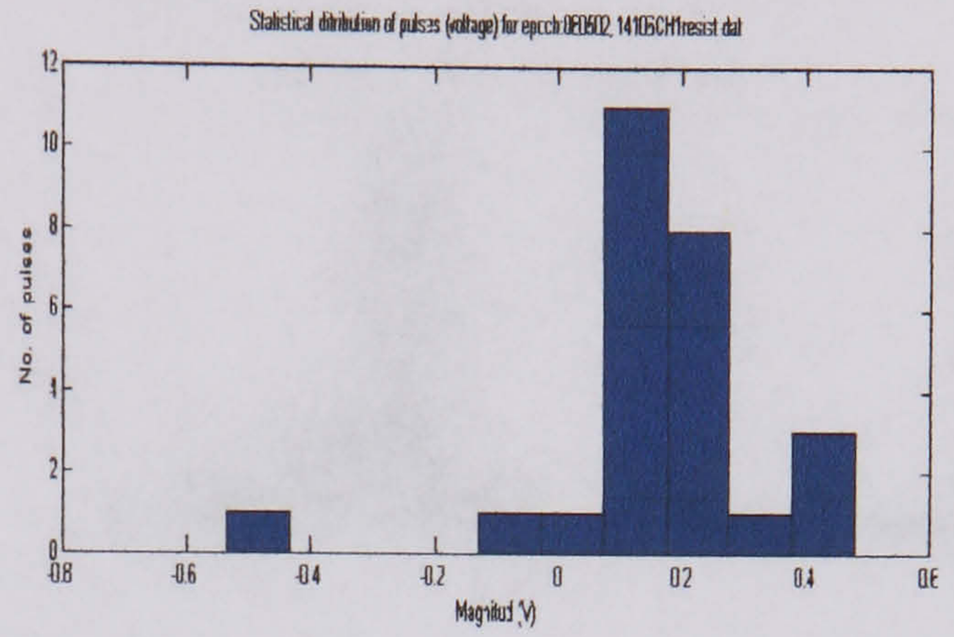

Distribution of surface discharges over an aged insulator at 30760 V (resistor)

Statistical distribution of surface discharges over an aged insulator at 34830 V (resistor)

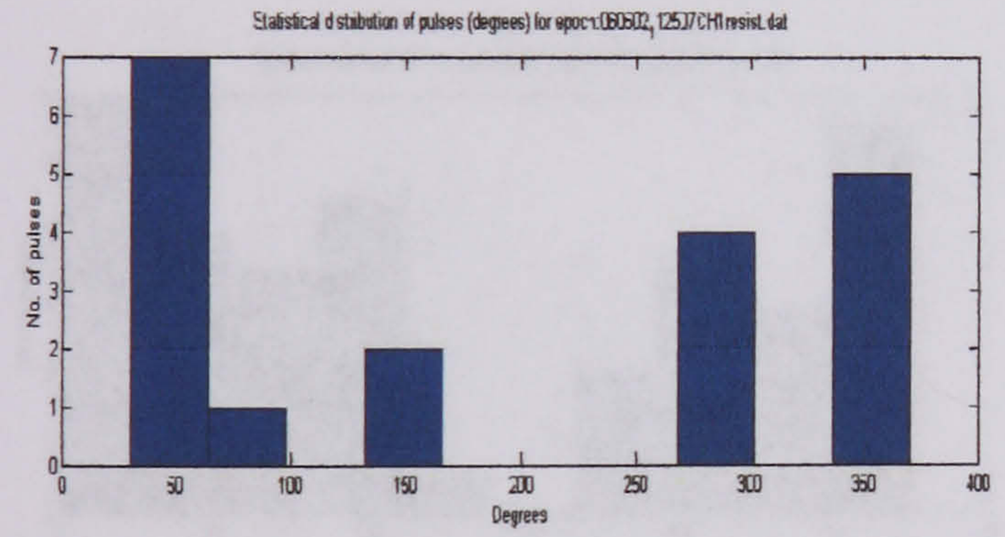

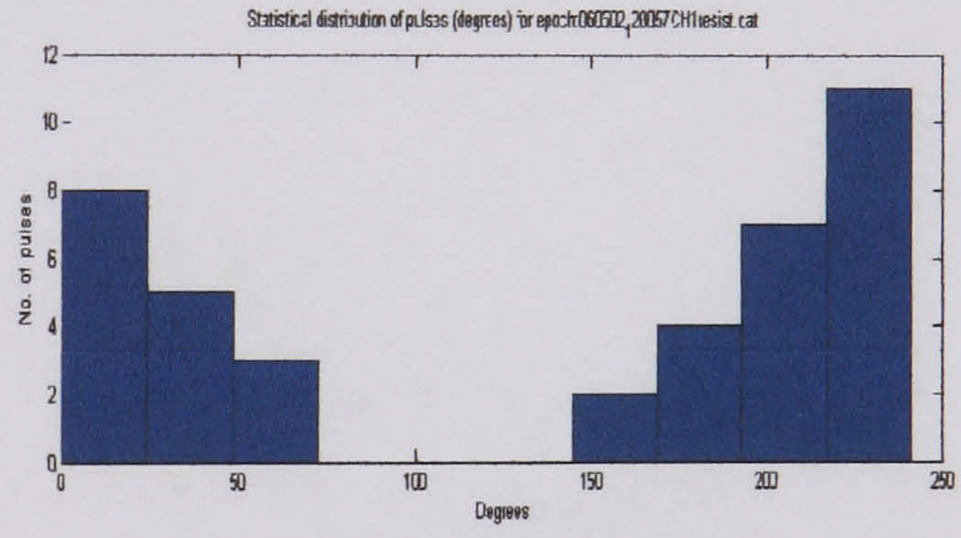

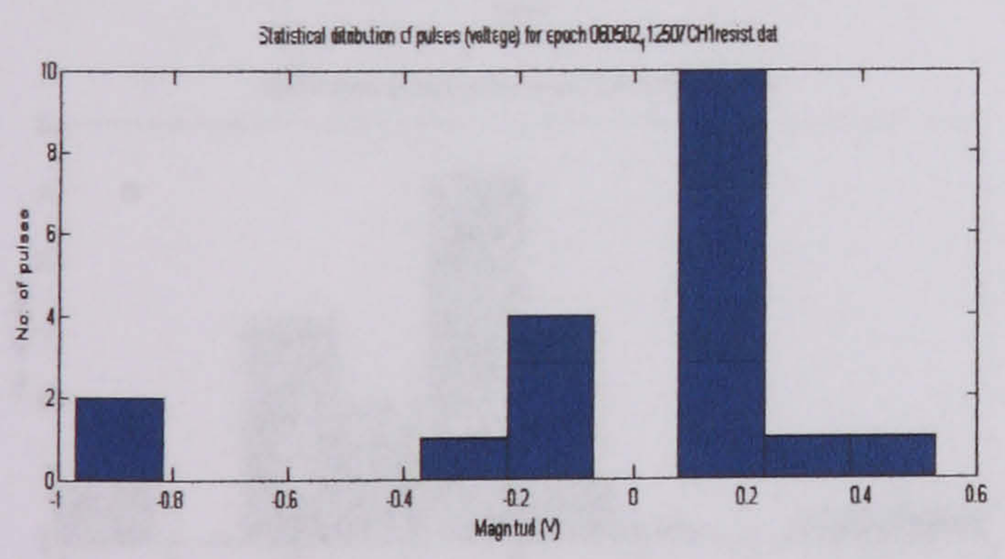

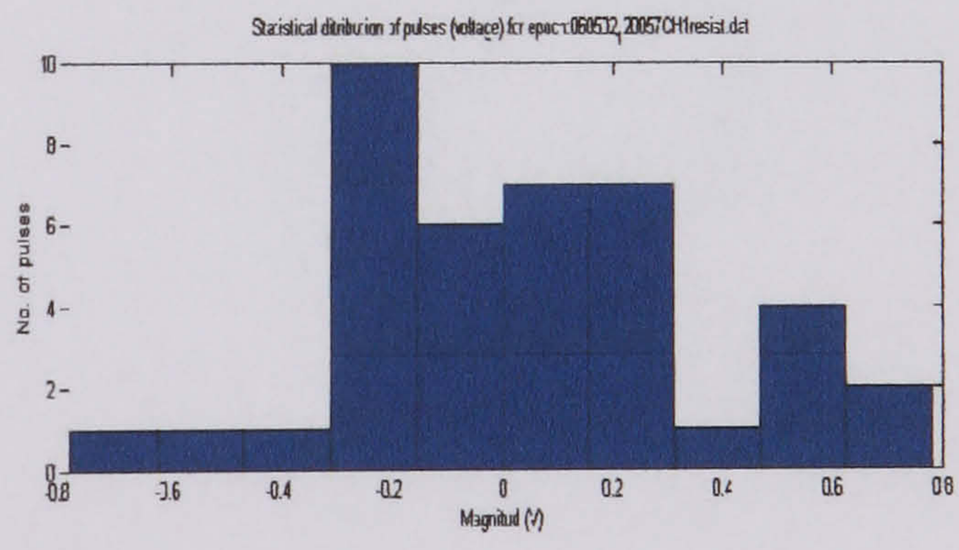

Statistical distribution of surface discharges over an aged insulator at 32810 V (resistor)

Statistical distribution of surface discharges over an aged insulator at 36900 V (resistor)

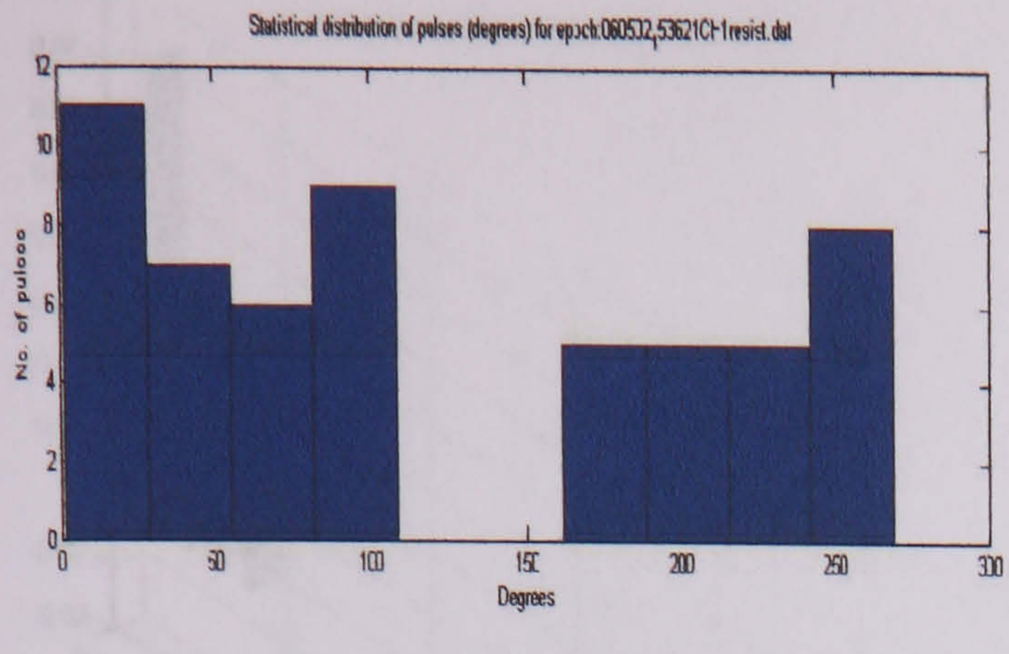

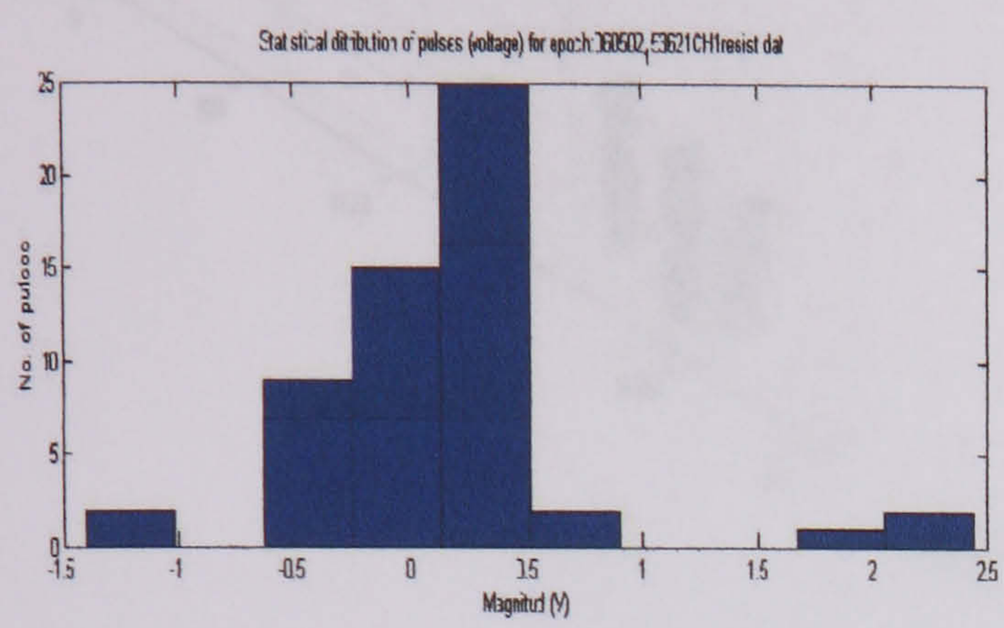

Statistical distribution of surface discharges over an aged insulator at 38800 V (resistor)

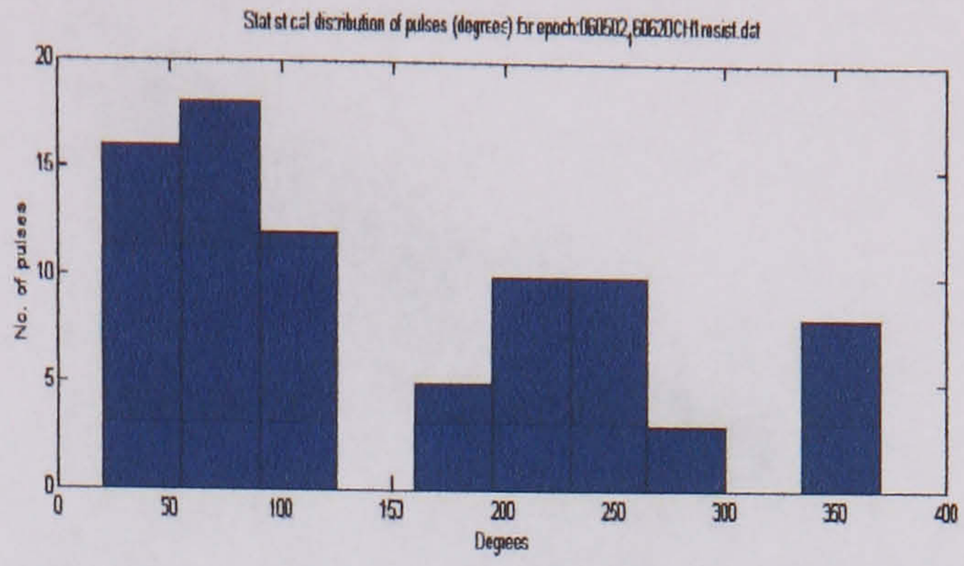

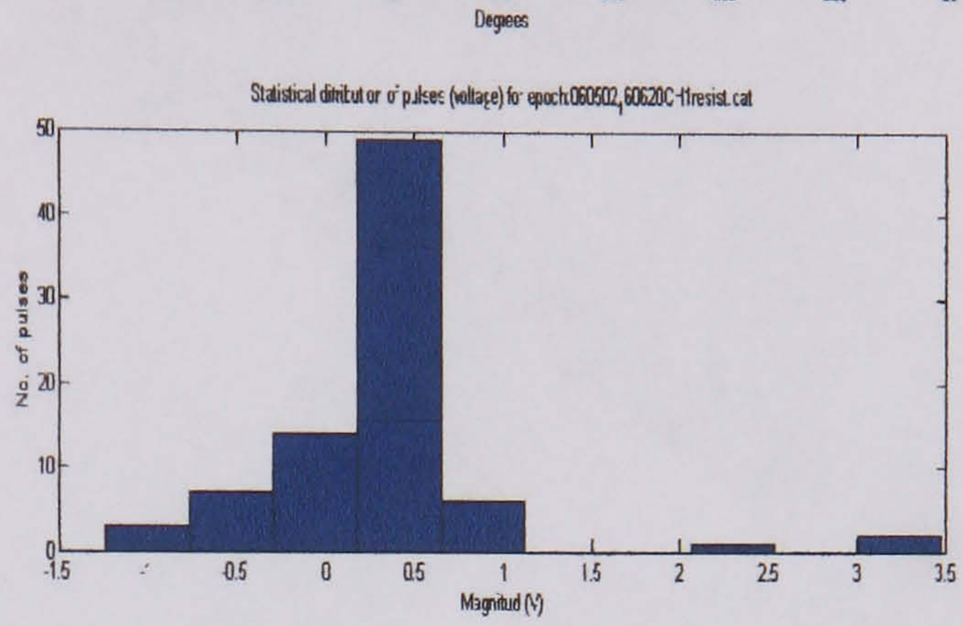

Statistical distribution of surface discharges over an aged insulator at 42500 V (resistor)

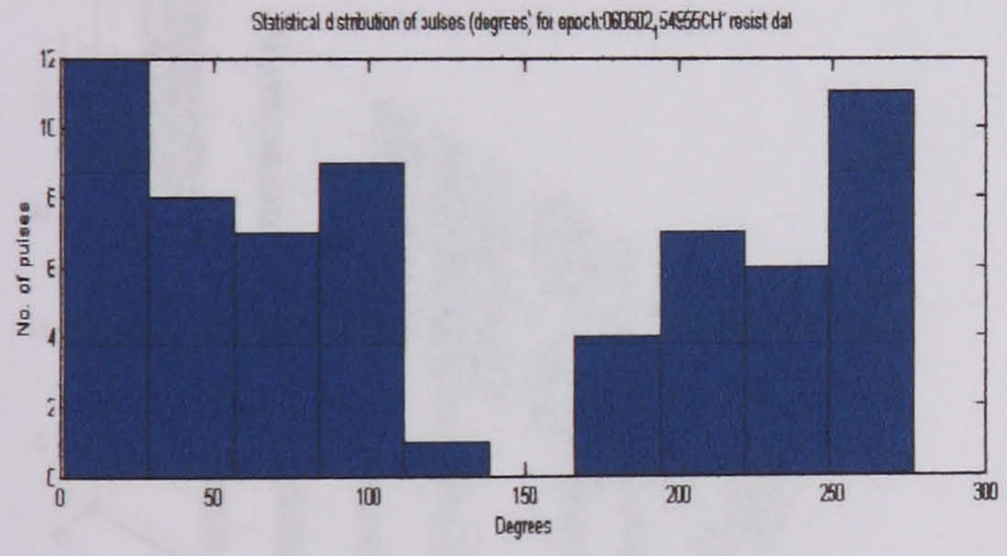

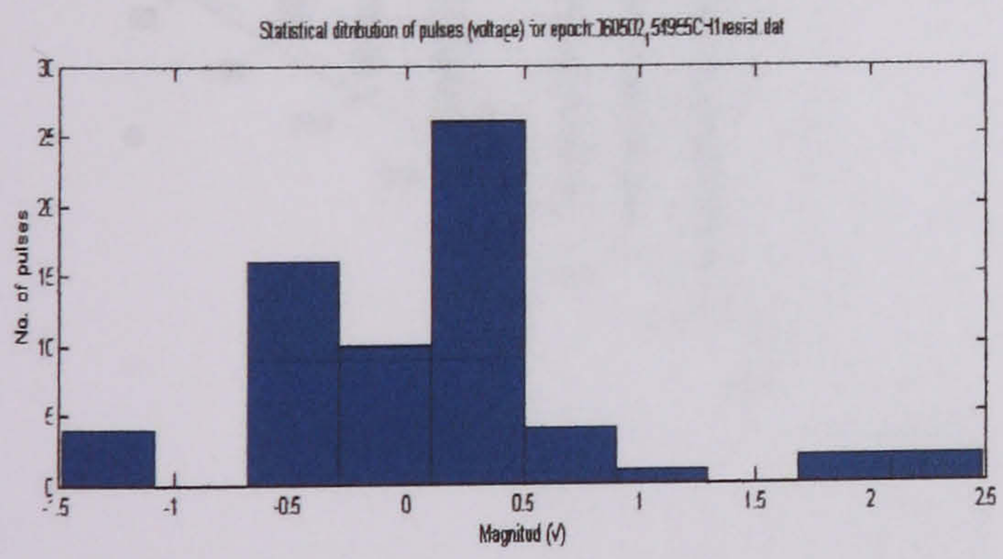

Statistical distribution of surface discharges over an aged insulator at 40800 V (resistor)

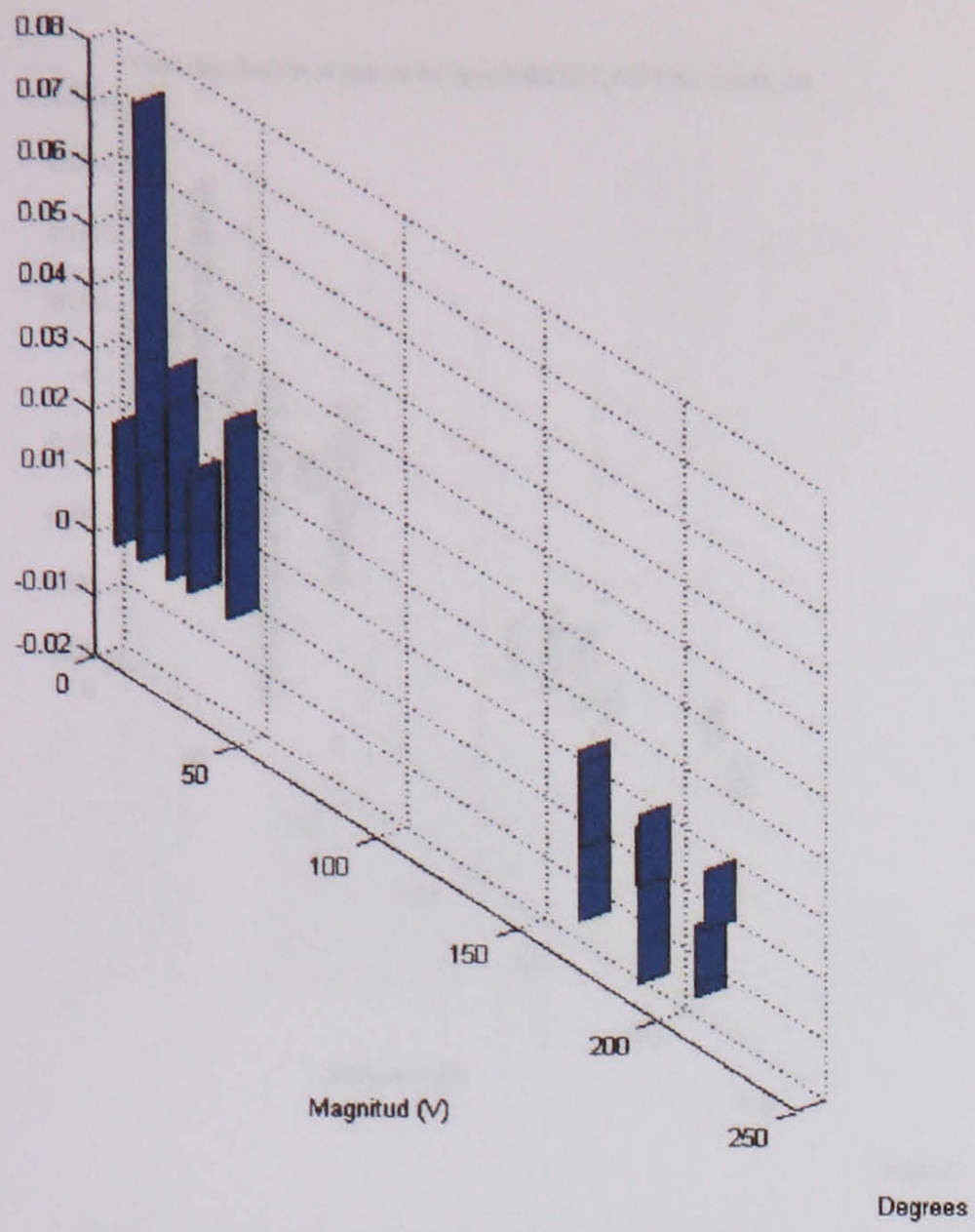

Distribution of surface discharges over an aged insulator at 30760 V (antenna 1)

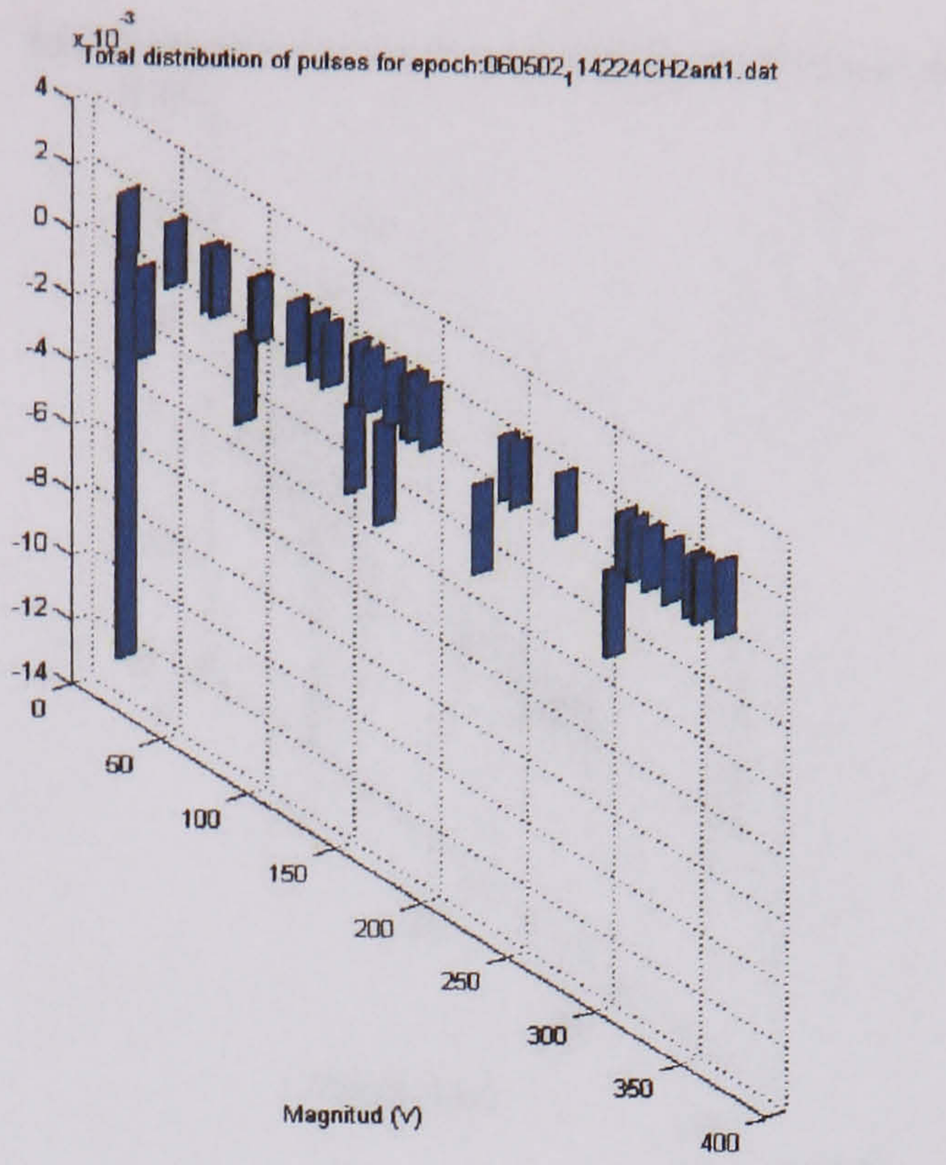

Distribution of surface discharges over an aged insulator at 34830 V (antenna 1)

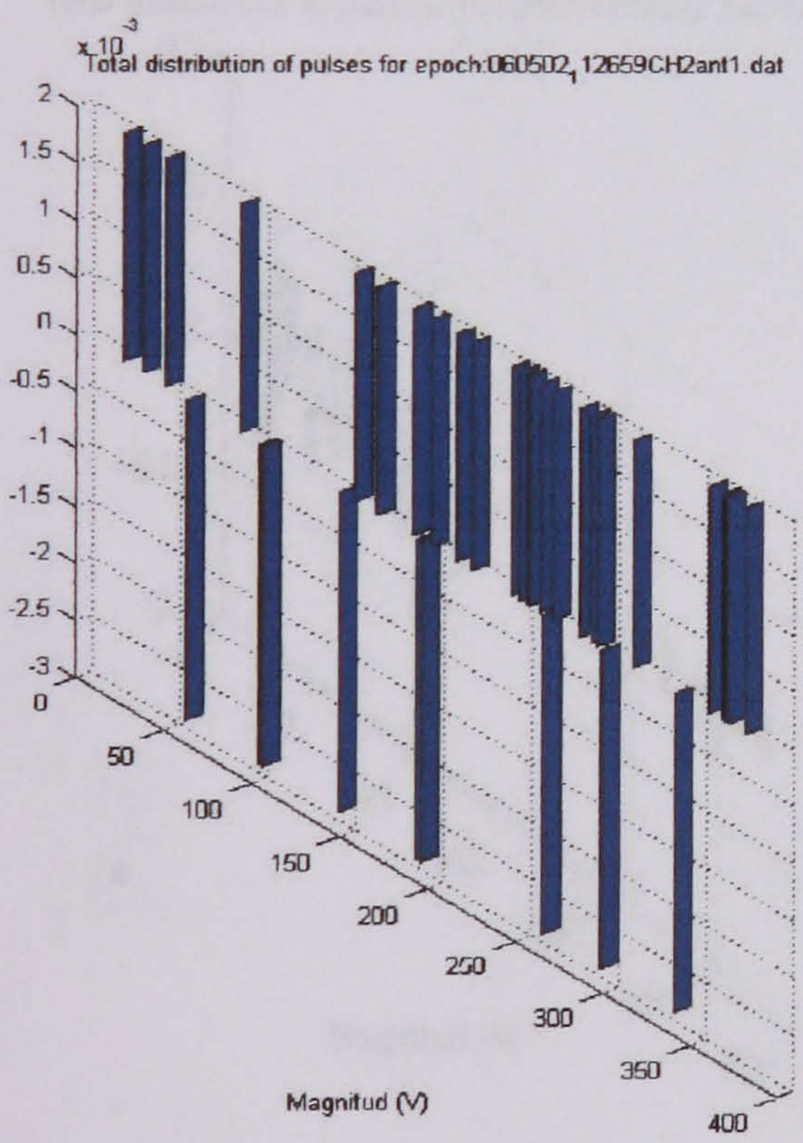

Distribution of surface discharges over an aged insulator at 32810 V (antenna 1)

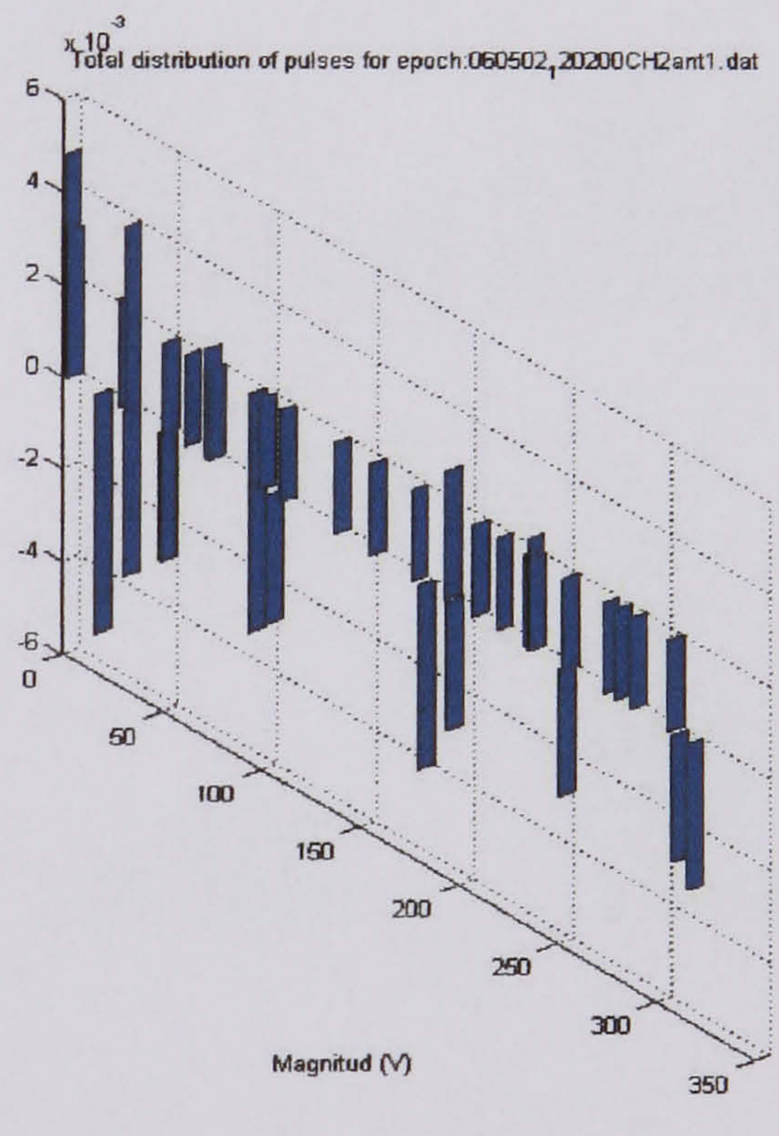

Distribution of surface discharges over an aged insulator at 36900 V (antenna 1)

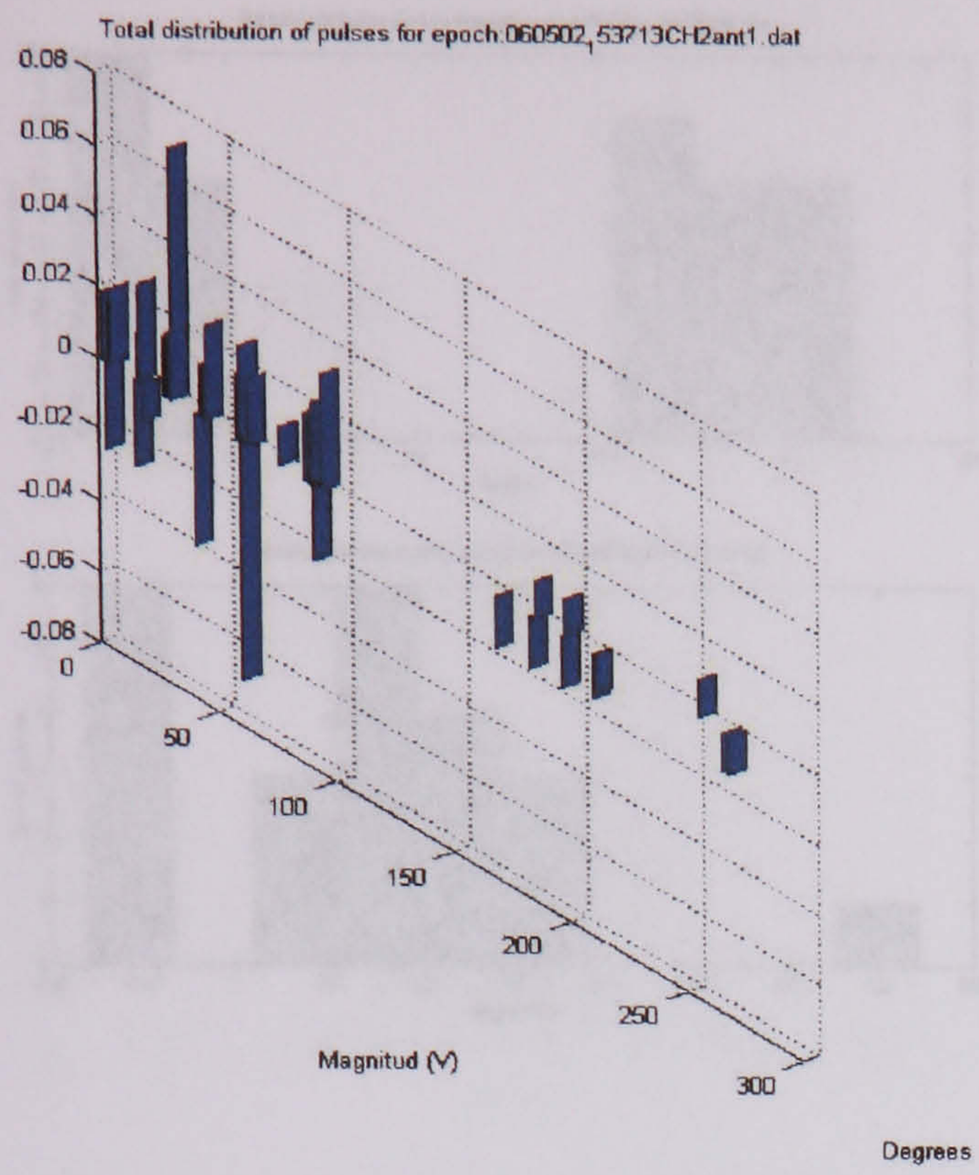

Distribution of surface discharges over an aged insulator at 38800 V (antenna 1)

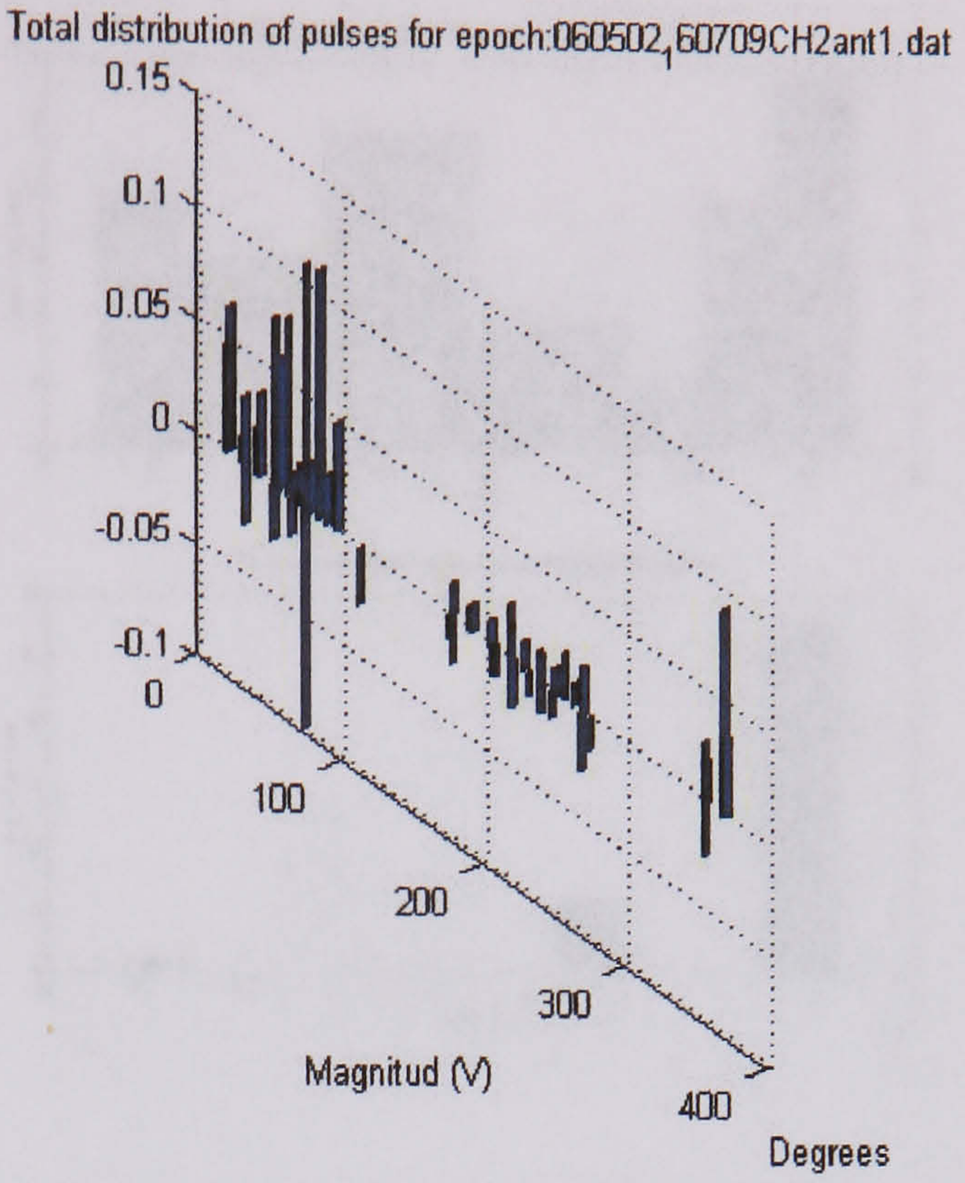

Distribution of surface discharges over an aged insulator at 42500 (antenna 1)

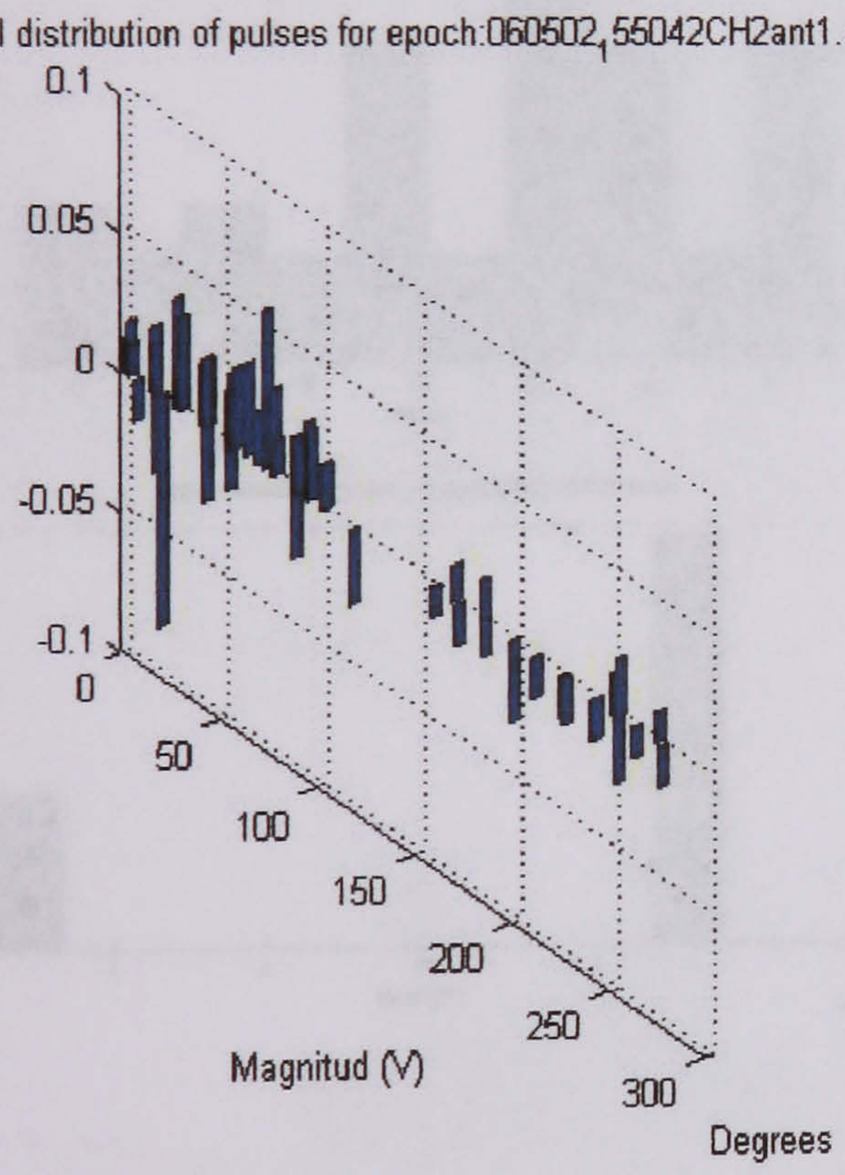

Distribution of surface discharges over an aged insulator at 40800 (antenna 1)

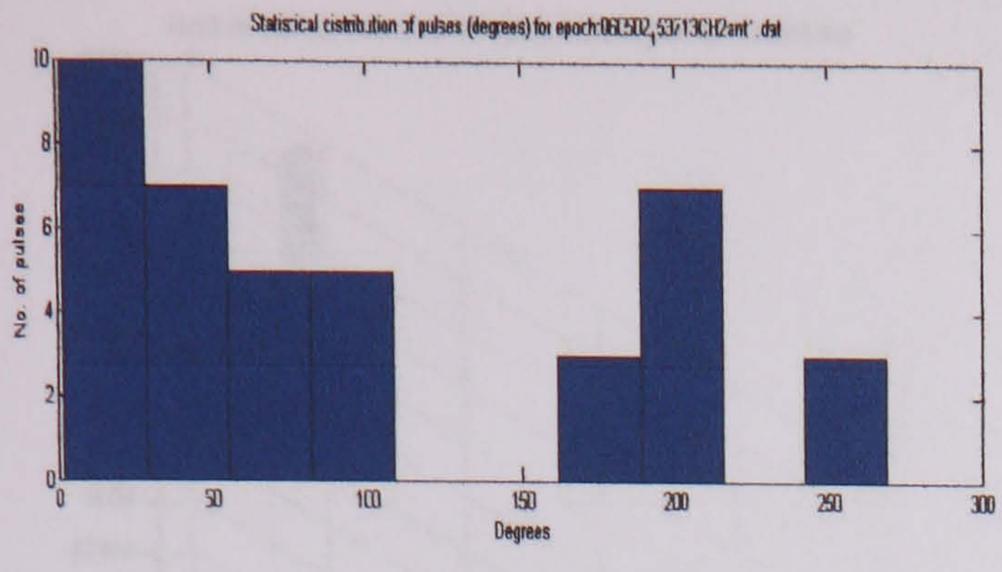

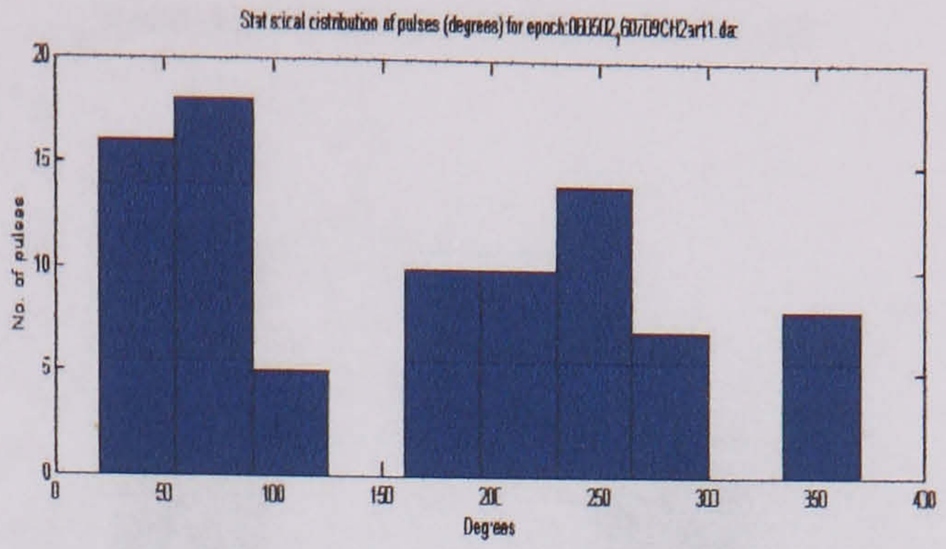

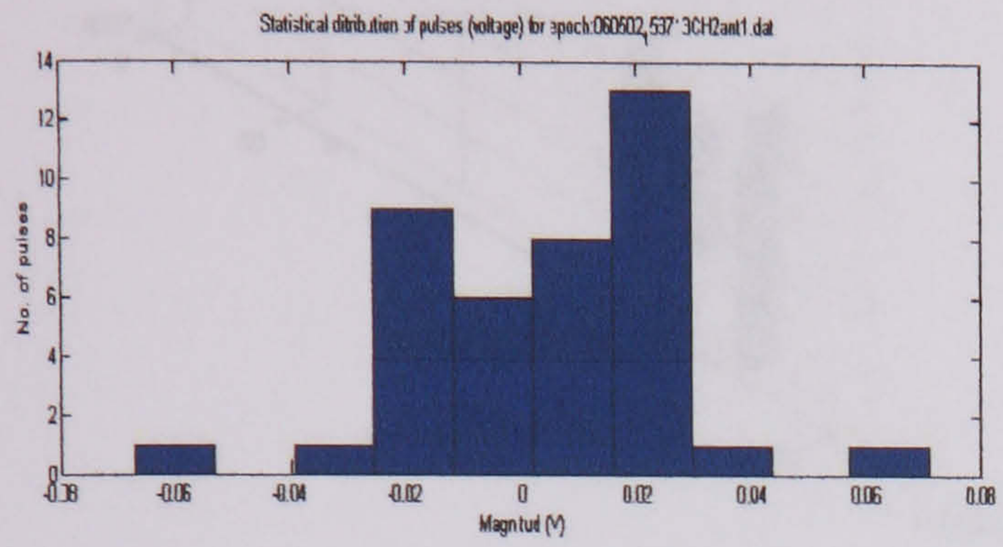

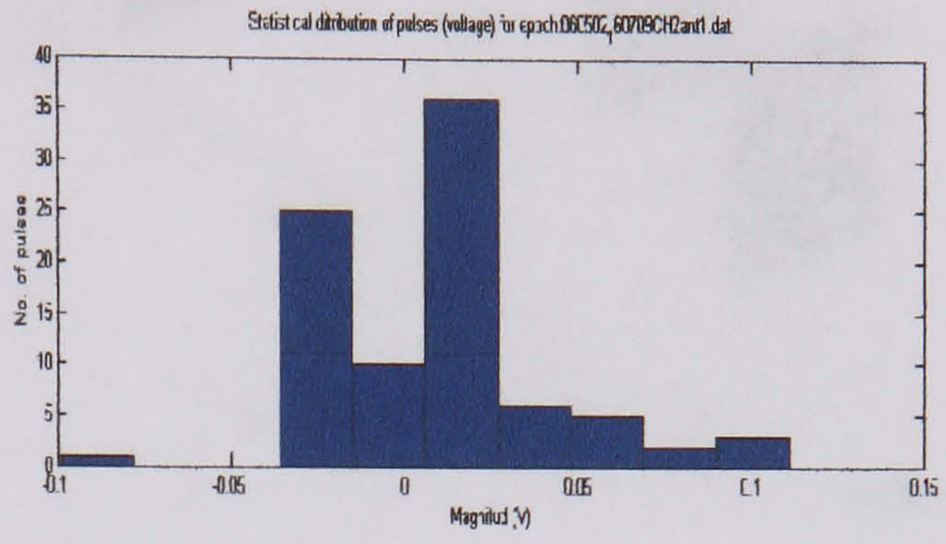

Distribution of surface discharges over an aged insulator at 38800 V (antenna 1)

Distribution of surface discharges over an aged insulator at 42500 V (antenna 1)

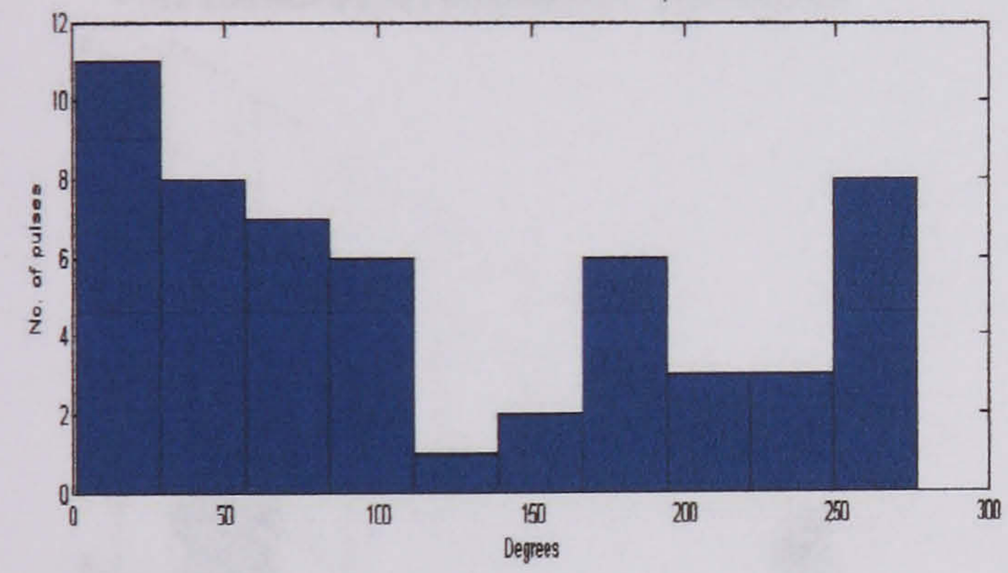

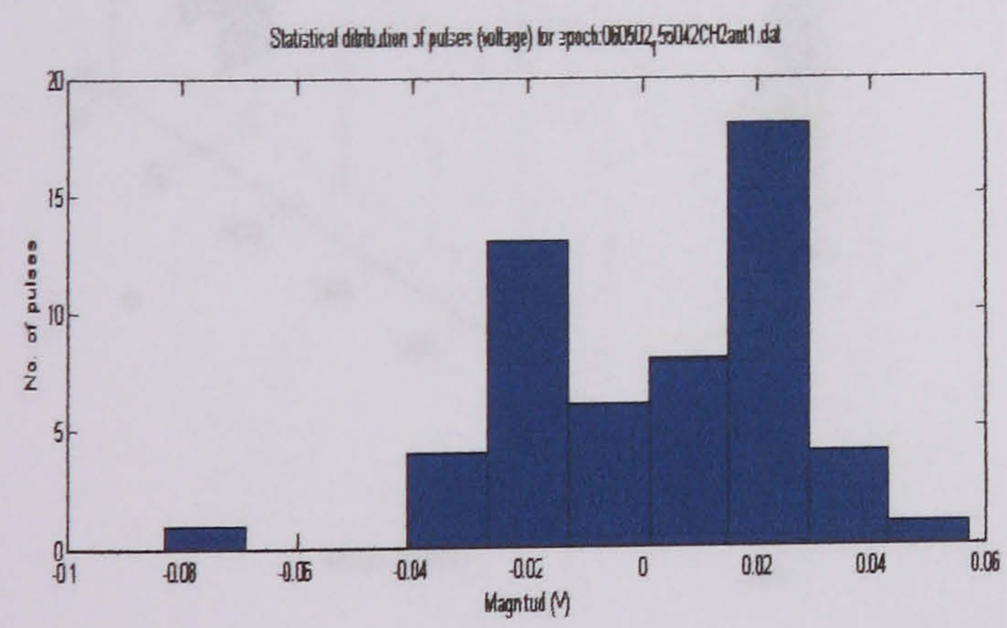

Distribution of surface discharges over an aged insulator at 40800 V (antenna 1)

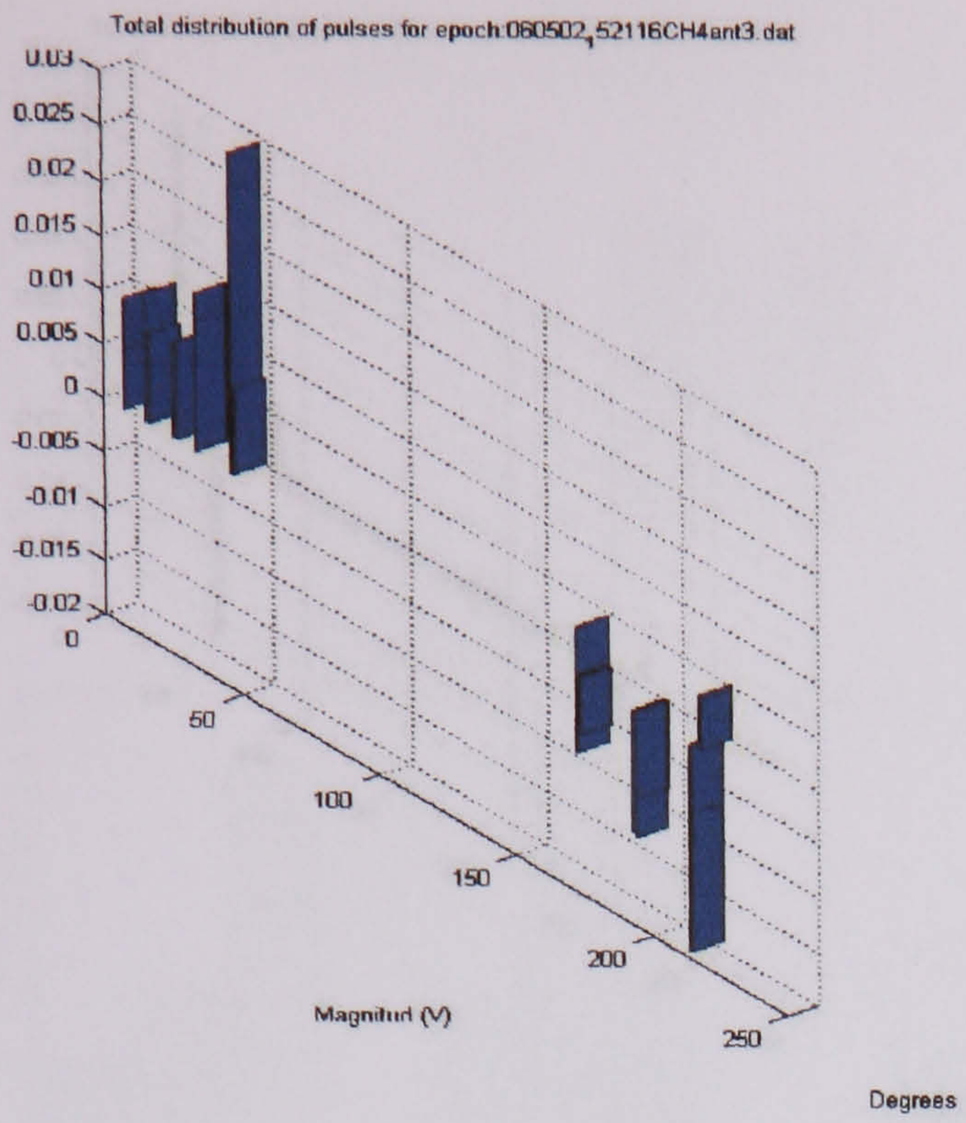

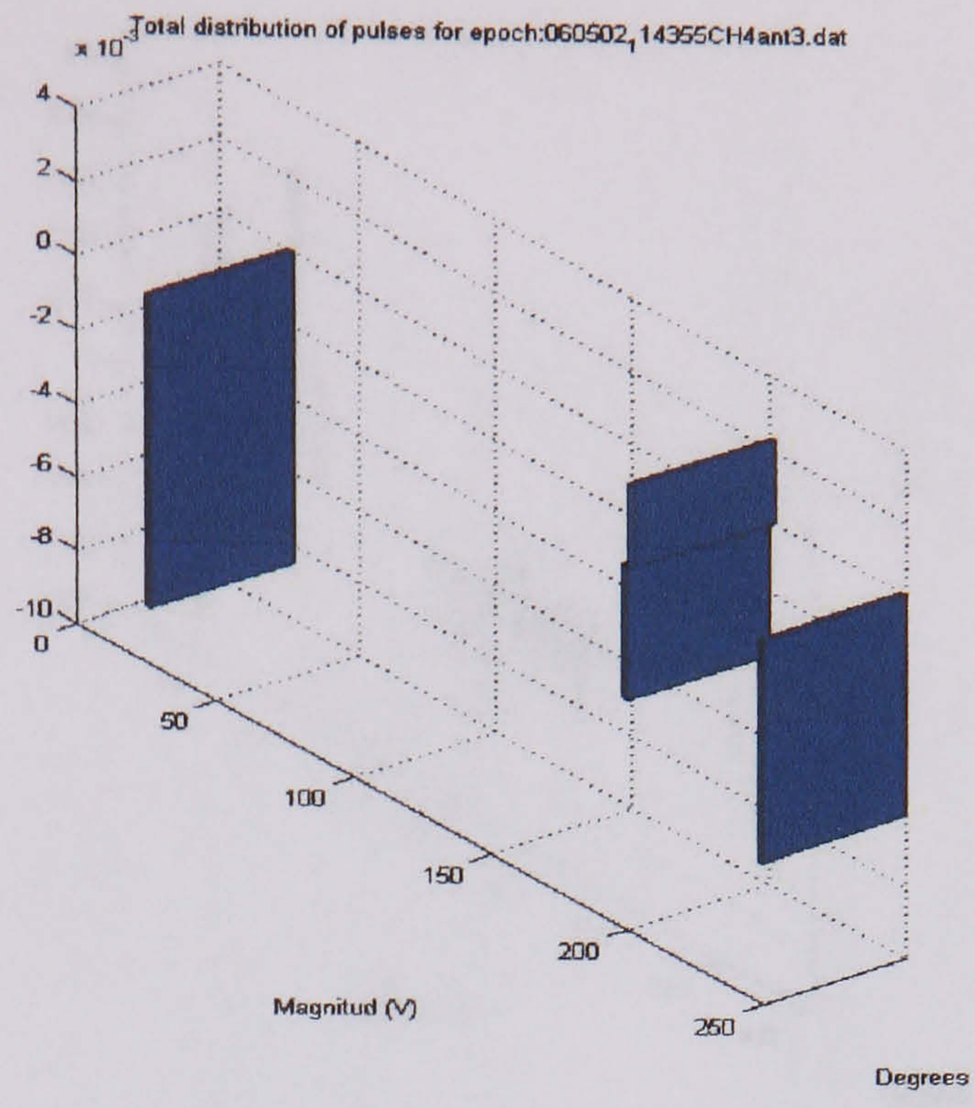

Distribution of surface discharges over an aged insulator at 30760 V (antenna3)

Distribution of surface discharges over an aged insulator at 34830 V (antenna3)

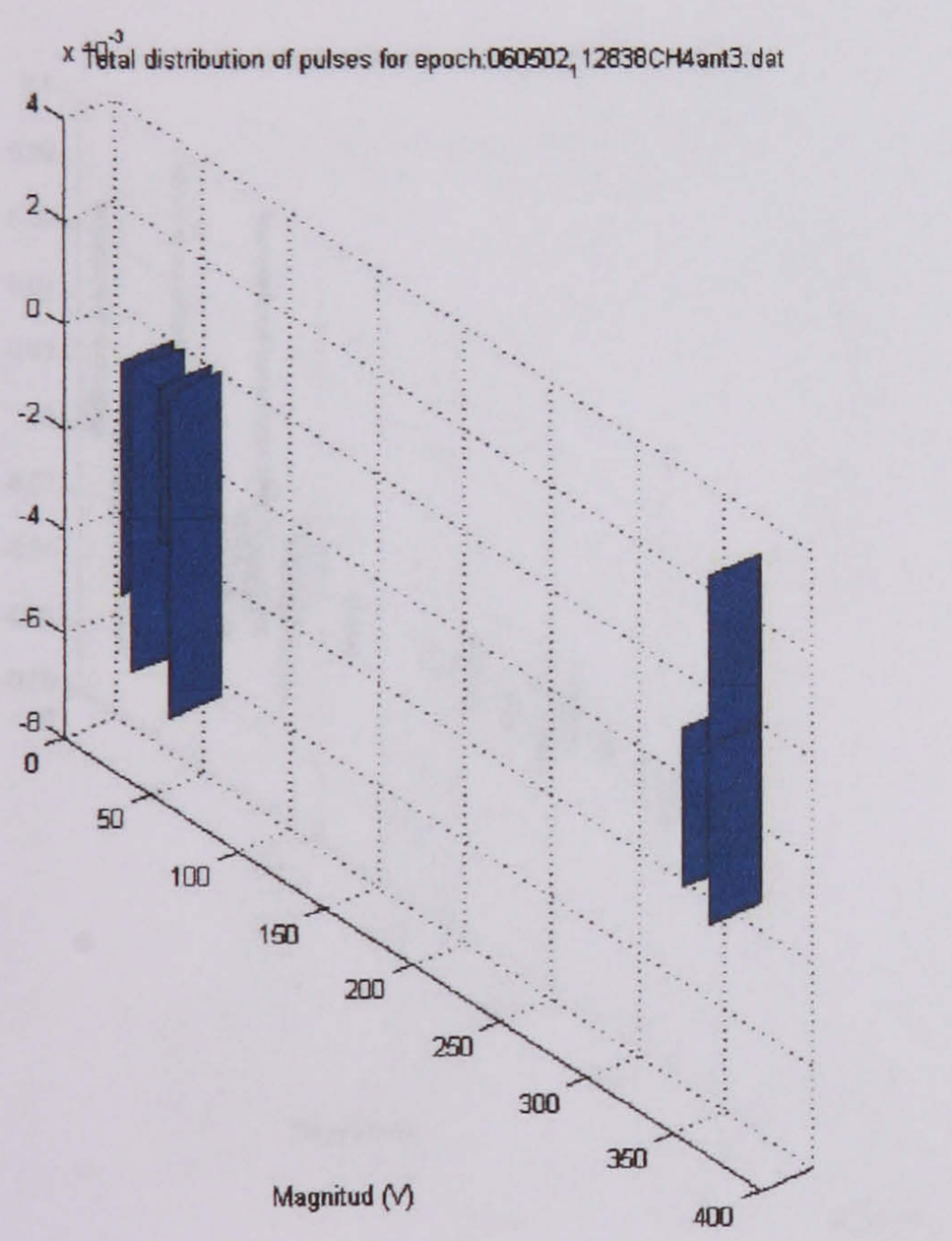

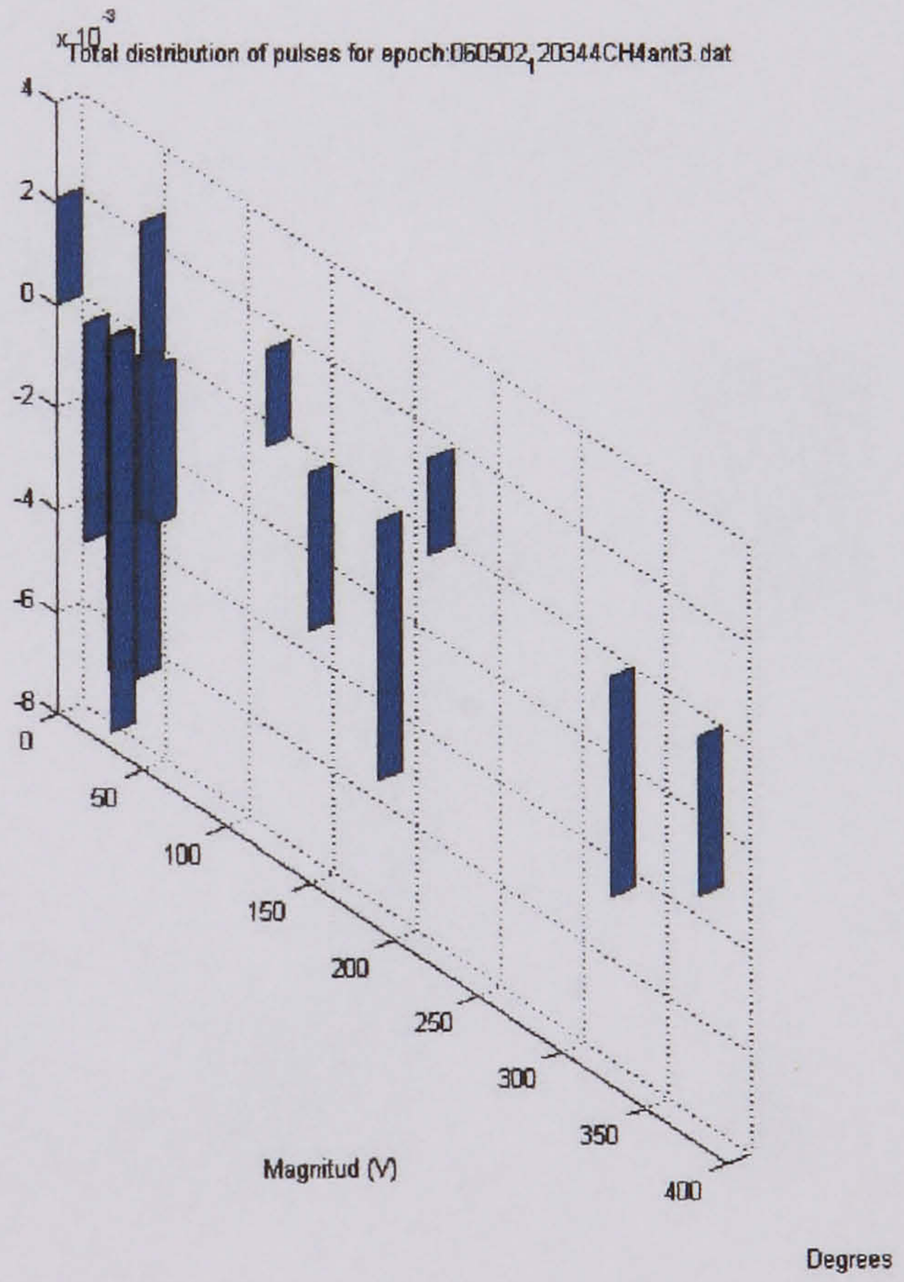

Distribution of surface discharges over an aged insulator at 32810 V (antenna3)

Distribution of surface discharges over an aged insulator at 36900 V (antenna3)

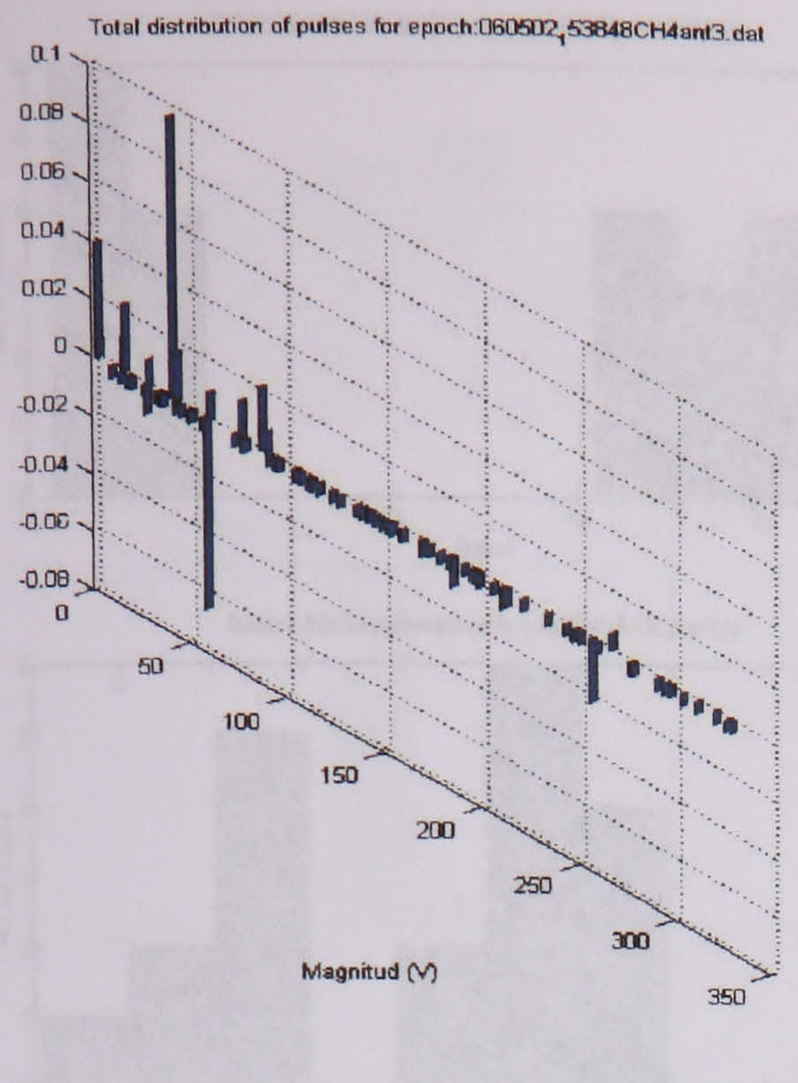

Distribution of surface discharges over an aged insulator at 38800 V (antenna3)

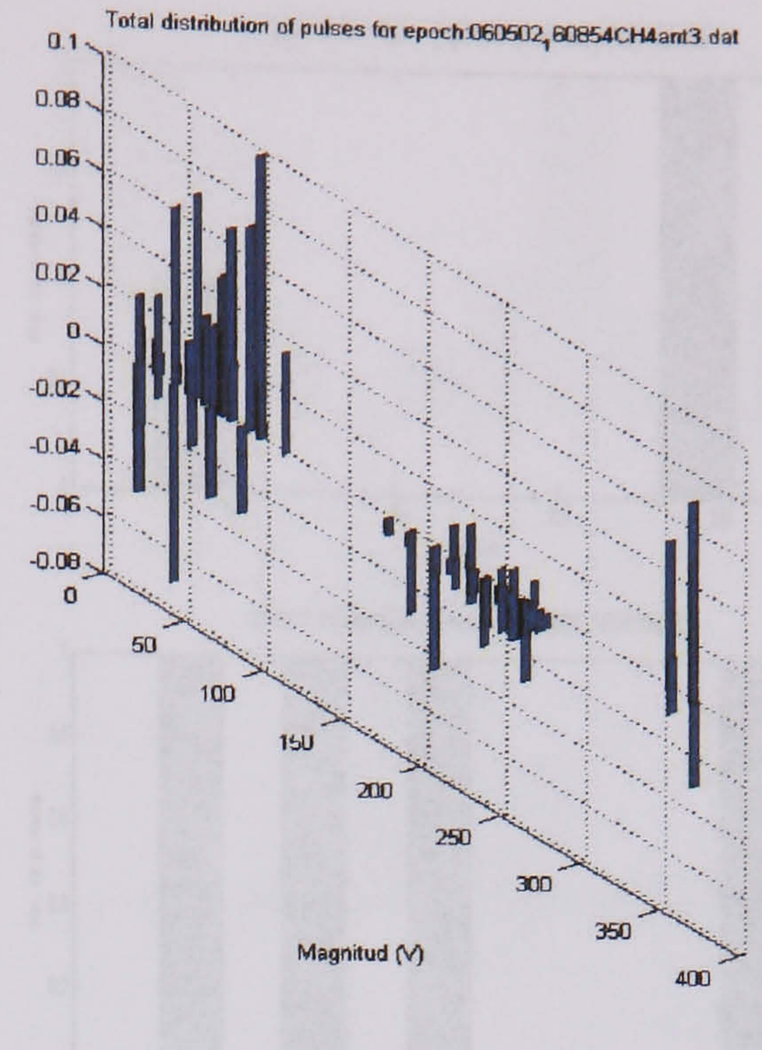

Distribution of surface discharges over an aged insulator at 42500 V (antenna3)

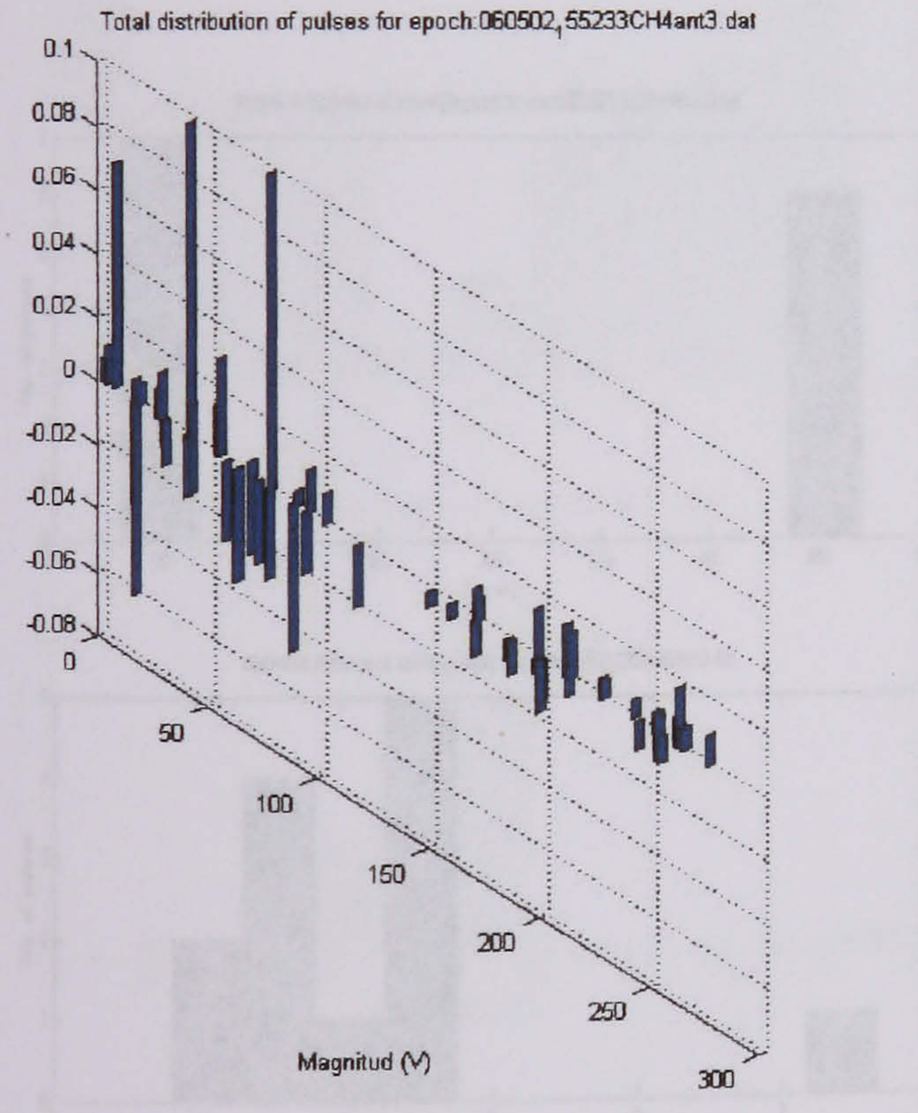

Distribution of surface discharges over an aged insulator at 40800 V (antenna3)

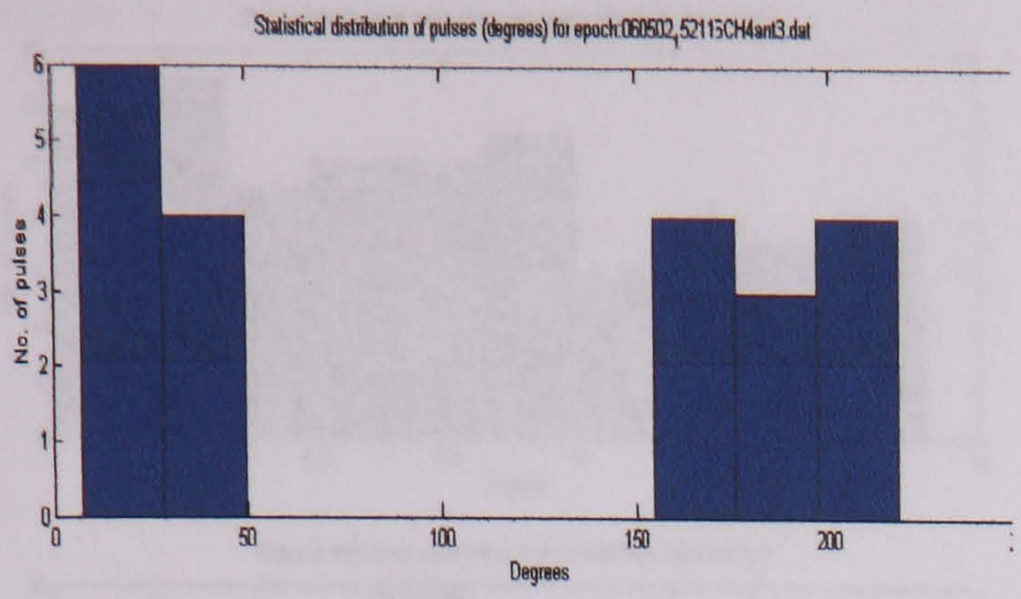

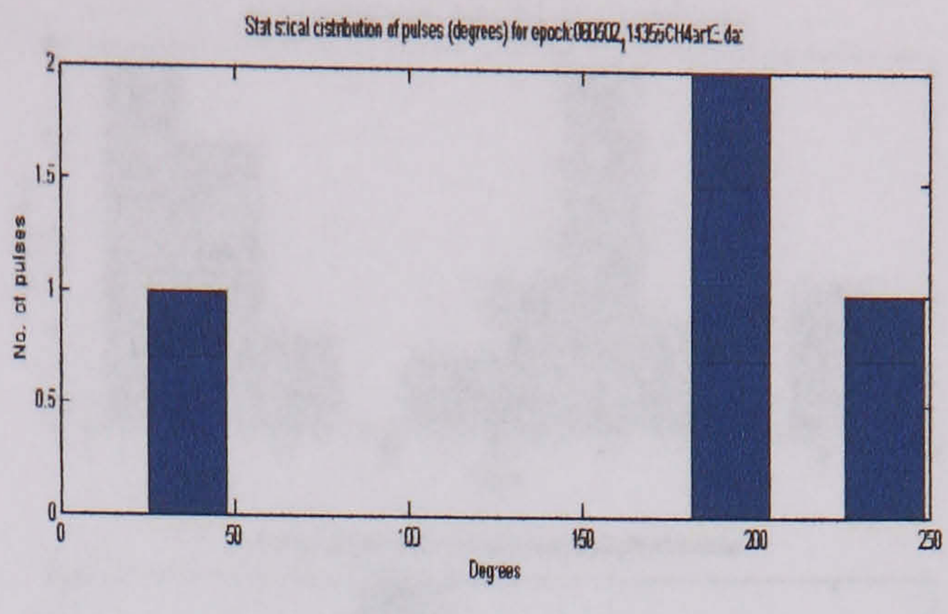

Distribution of surface discharges over an aged insulator at 30760 V (antenna3)

Distribution of surface discharges over an aged insulator at 34830 V (antenna3)

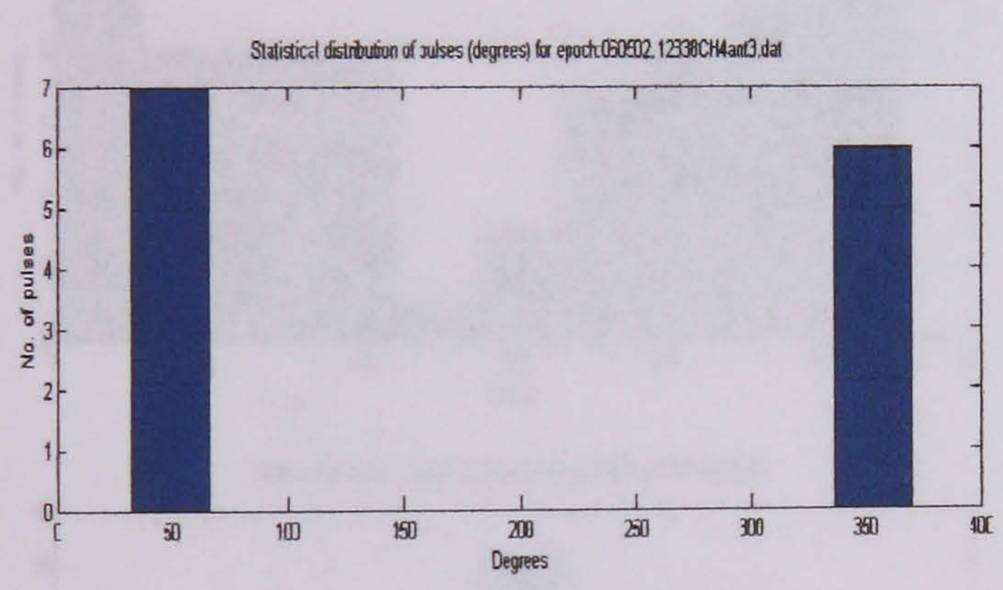

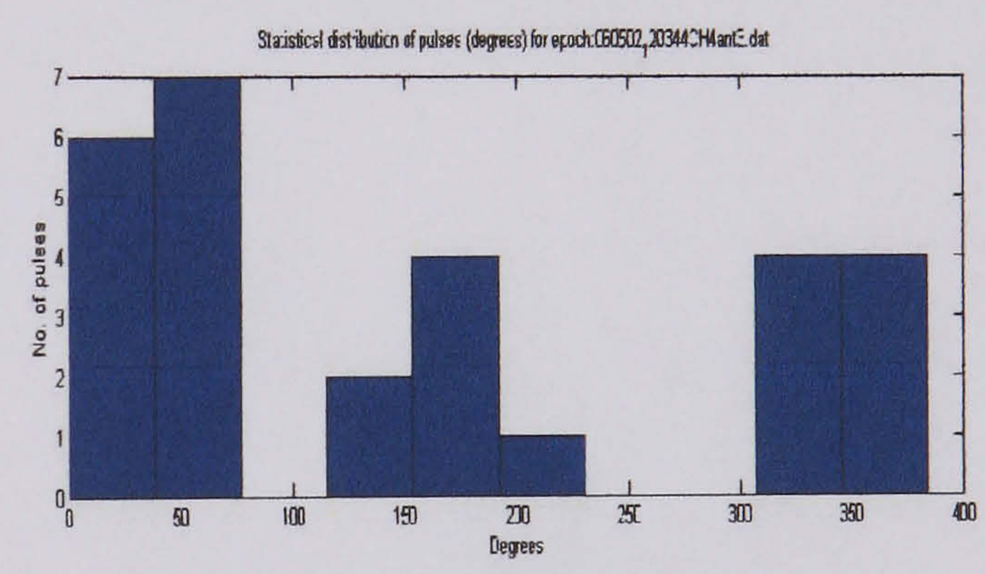

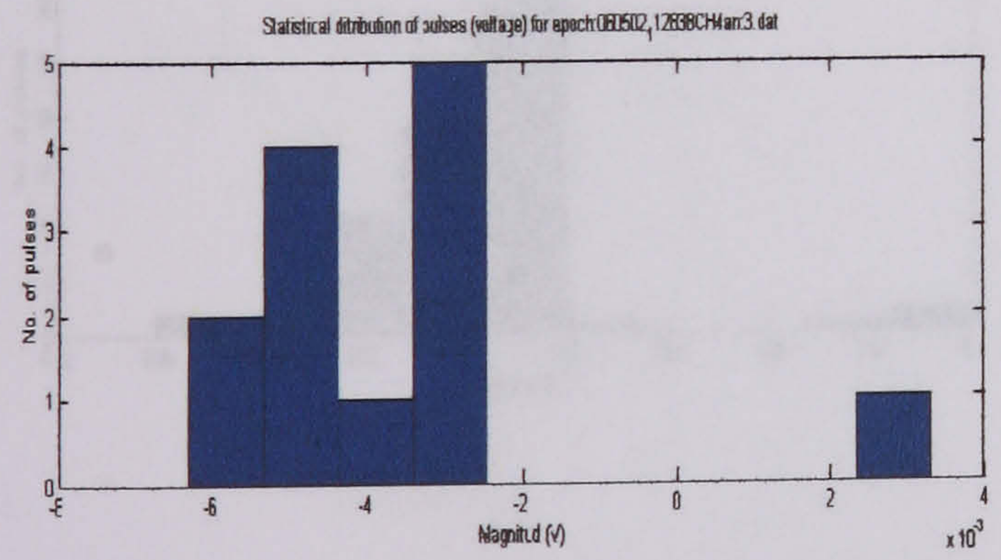

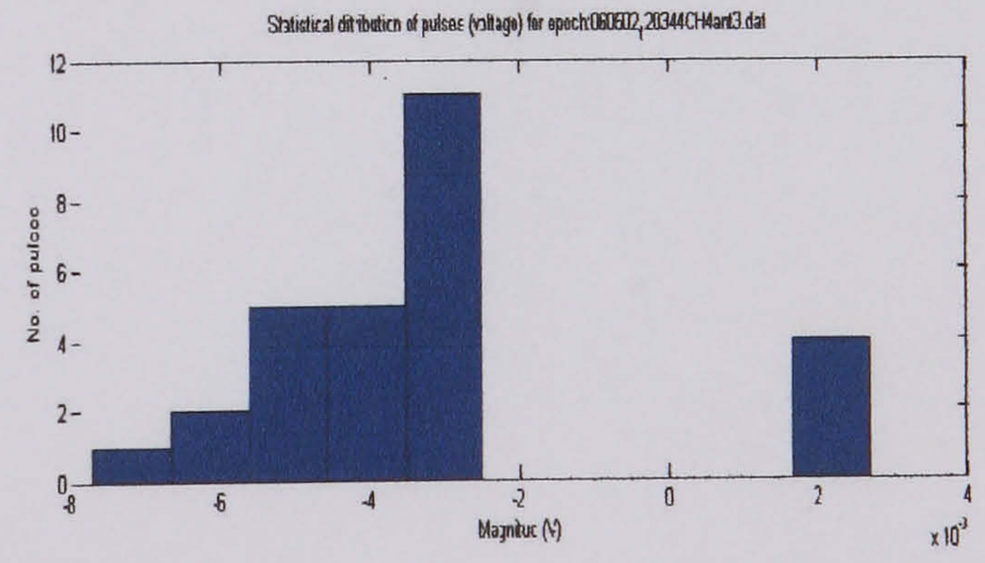

Distribution of surface discharges over an aged insulator at 32810 V (antenna3)

Distribution of surface discharges over an aged insulator at 36900 V (antenna3)

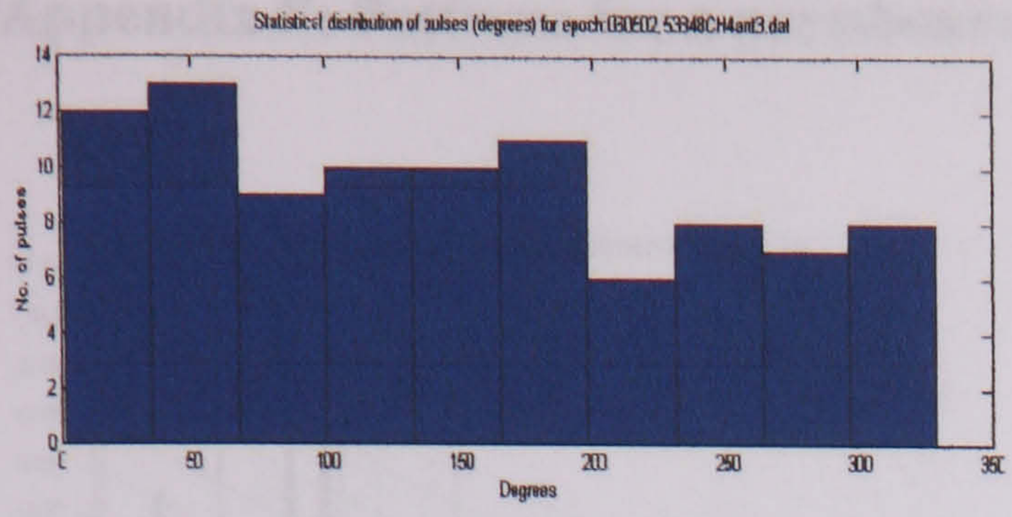

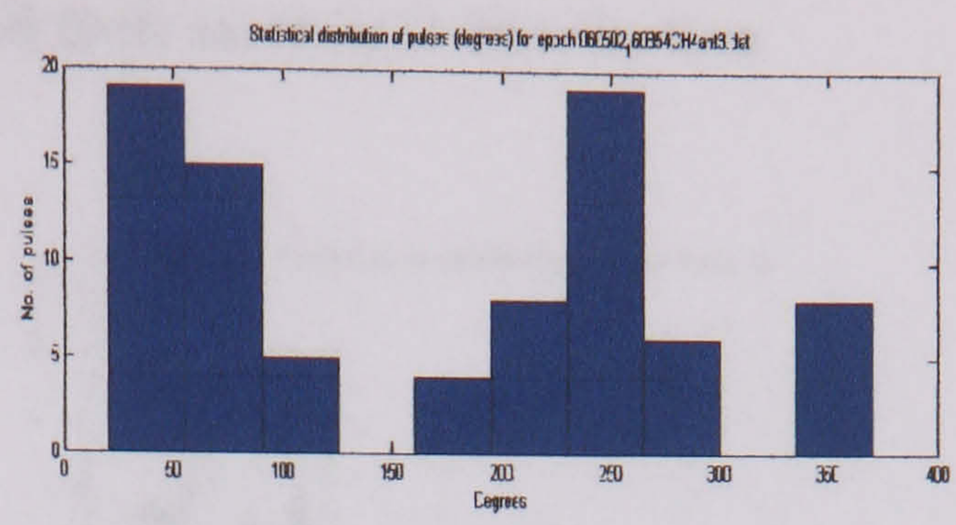

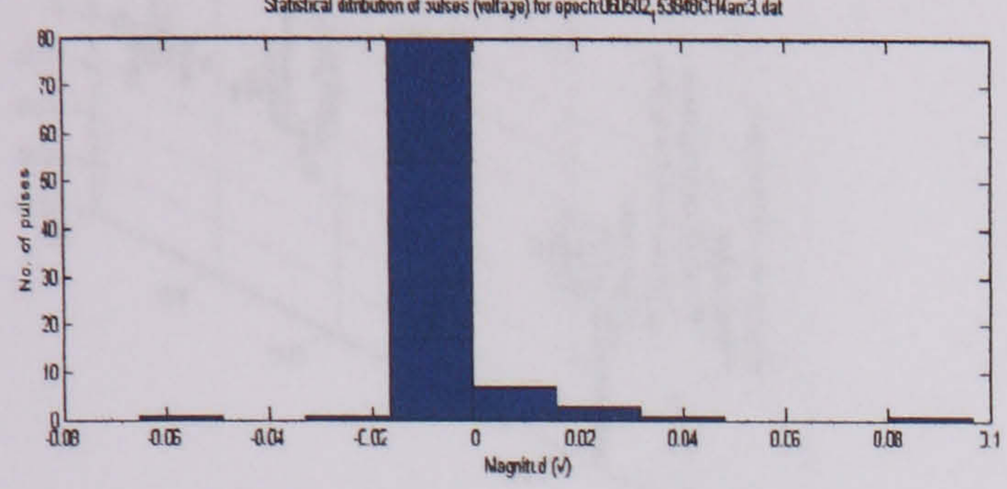

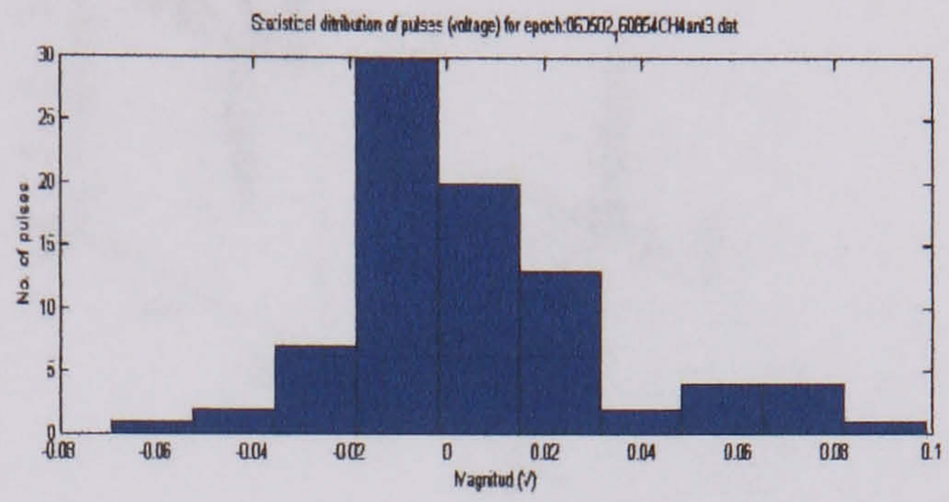

Distribution of surface discharges over an aged insulator at 38800 V (antenna3)

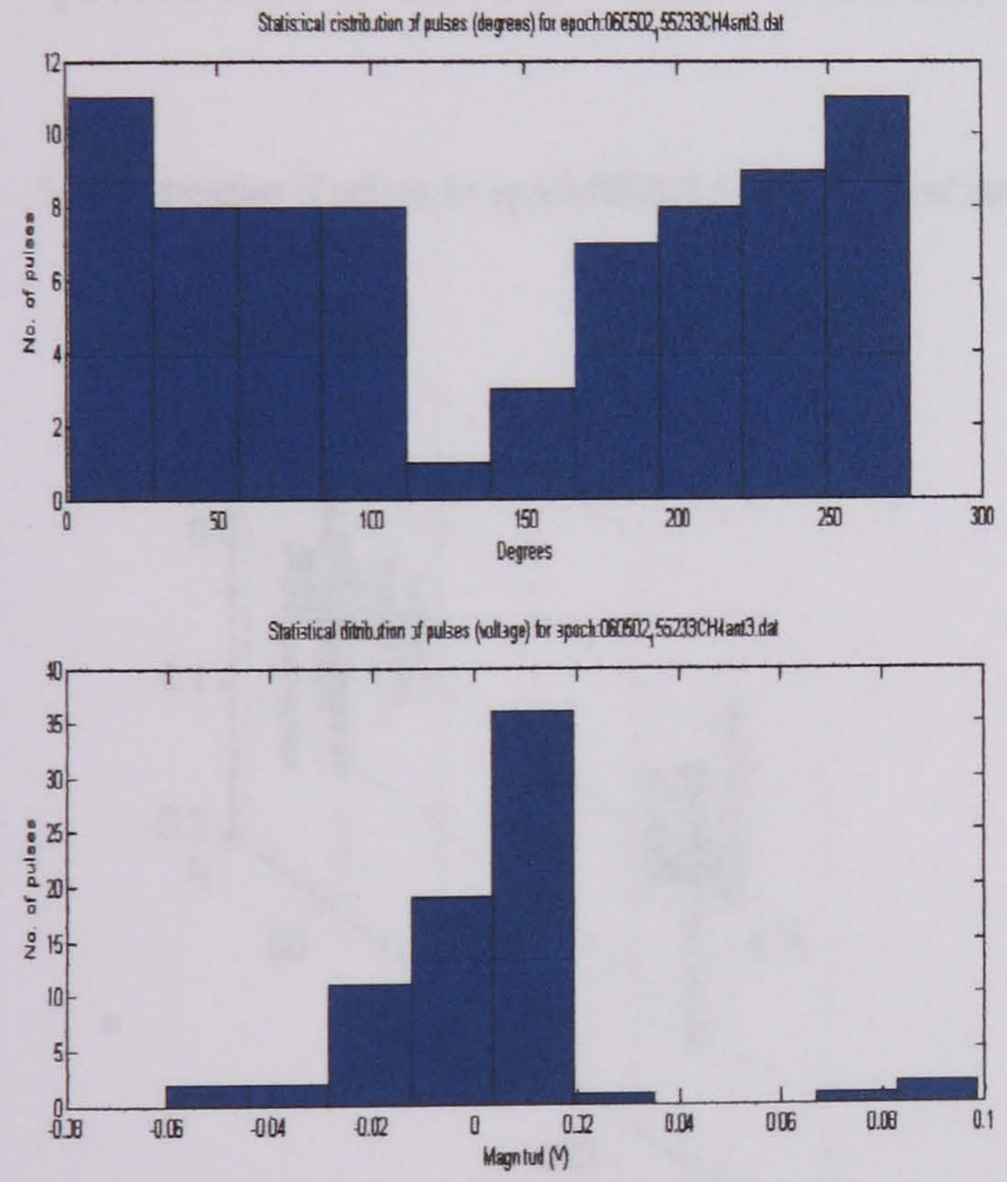

Distribution of surface discharges over an aged insulator at 42500 V (antenna3)

Distribution of surface discharges over an aged insulator at 40800 V (antenna3)

Appendix F: Patterns for a pressboard and their statistical distribution

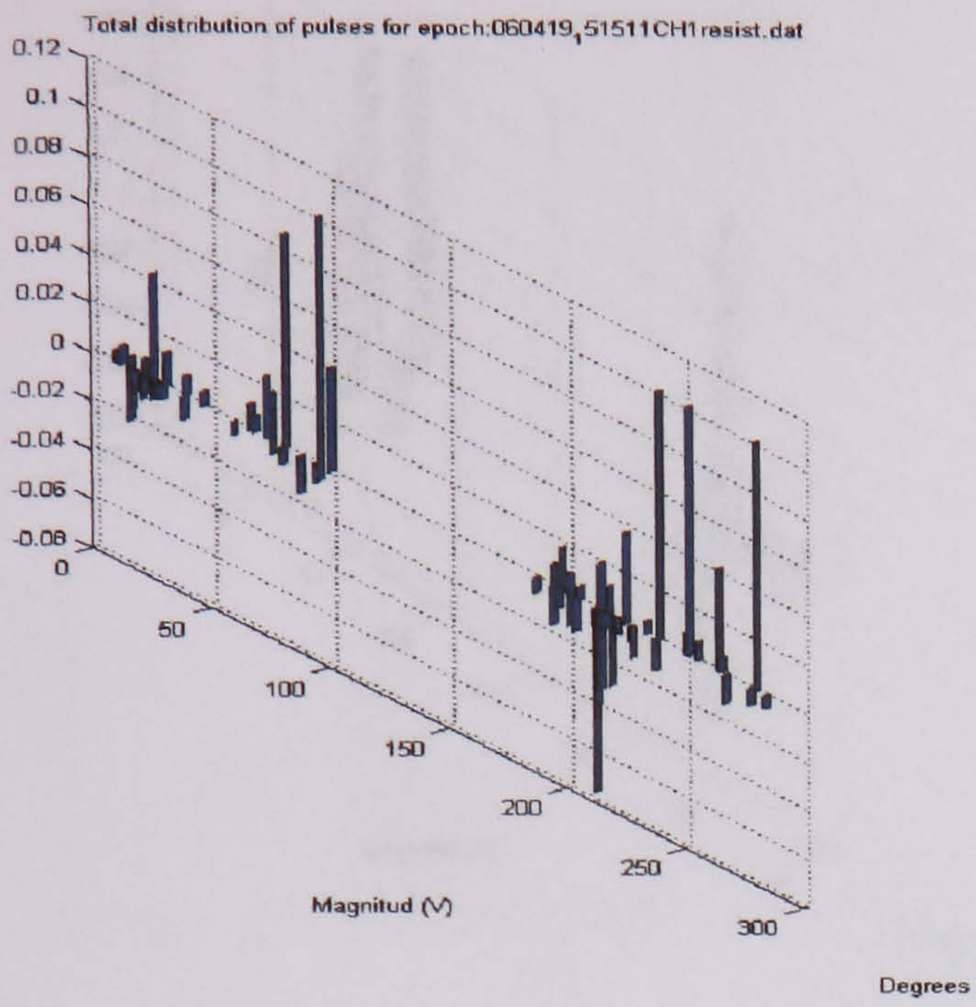

Distribution of surface discharges over a pressboard at 24210 V test 1 (resistor)

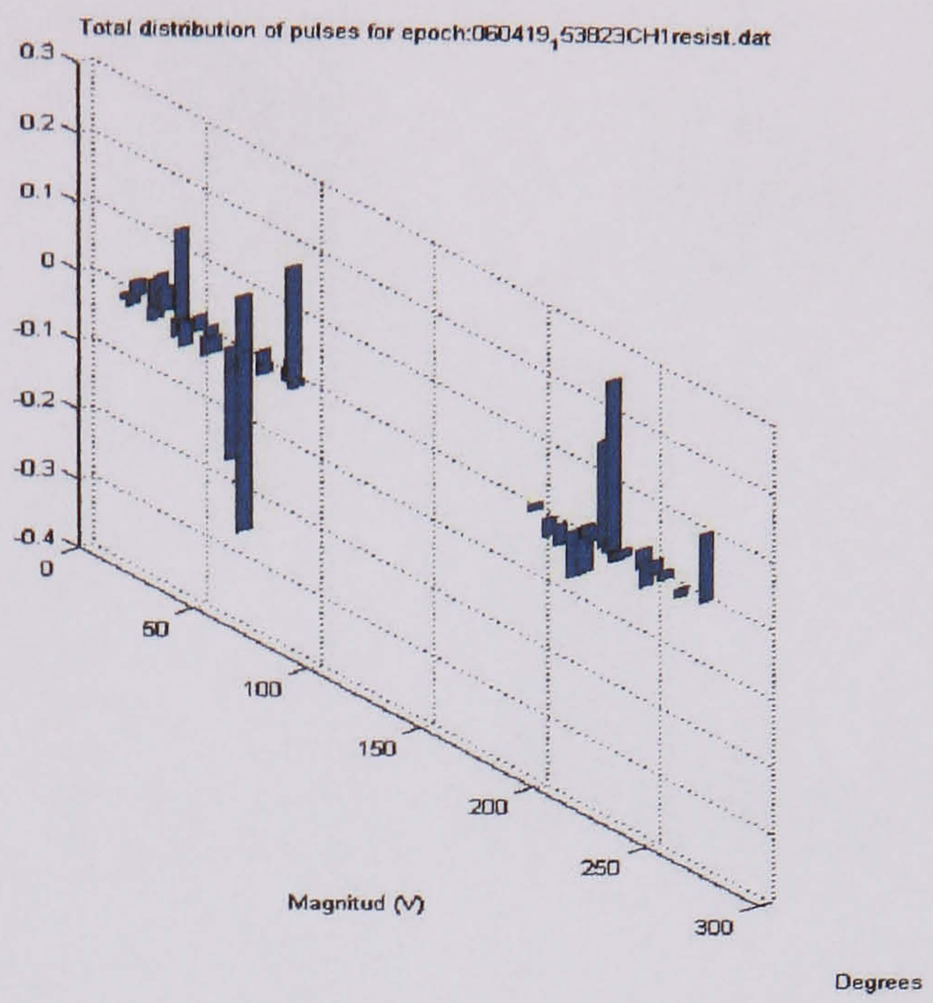

Distribution of surface discharges over a pressboard at 24210 V test 3 (resistor)

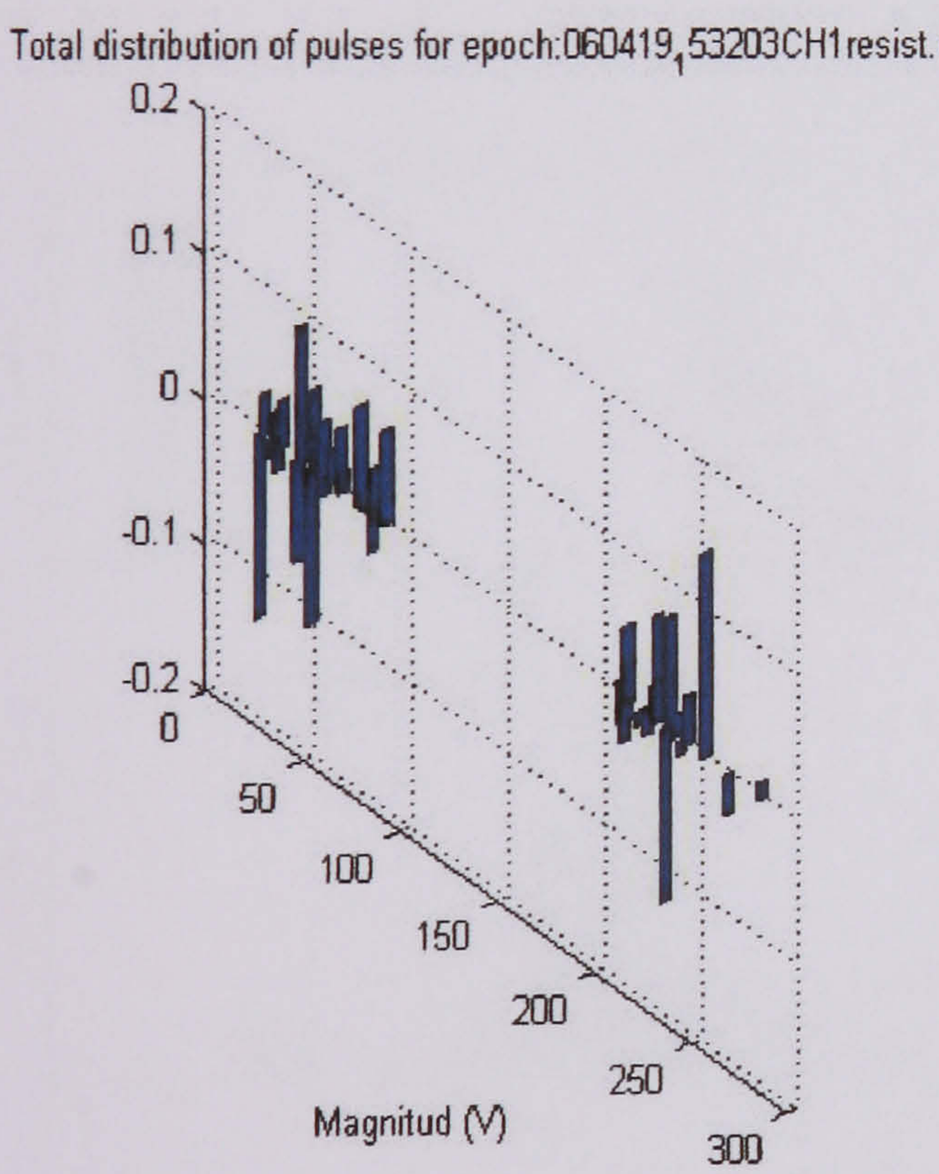

Distribution of surface discharges over a pressboard at 24210 V test 2 (resistor)

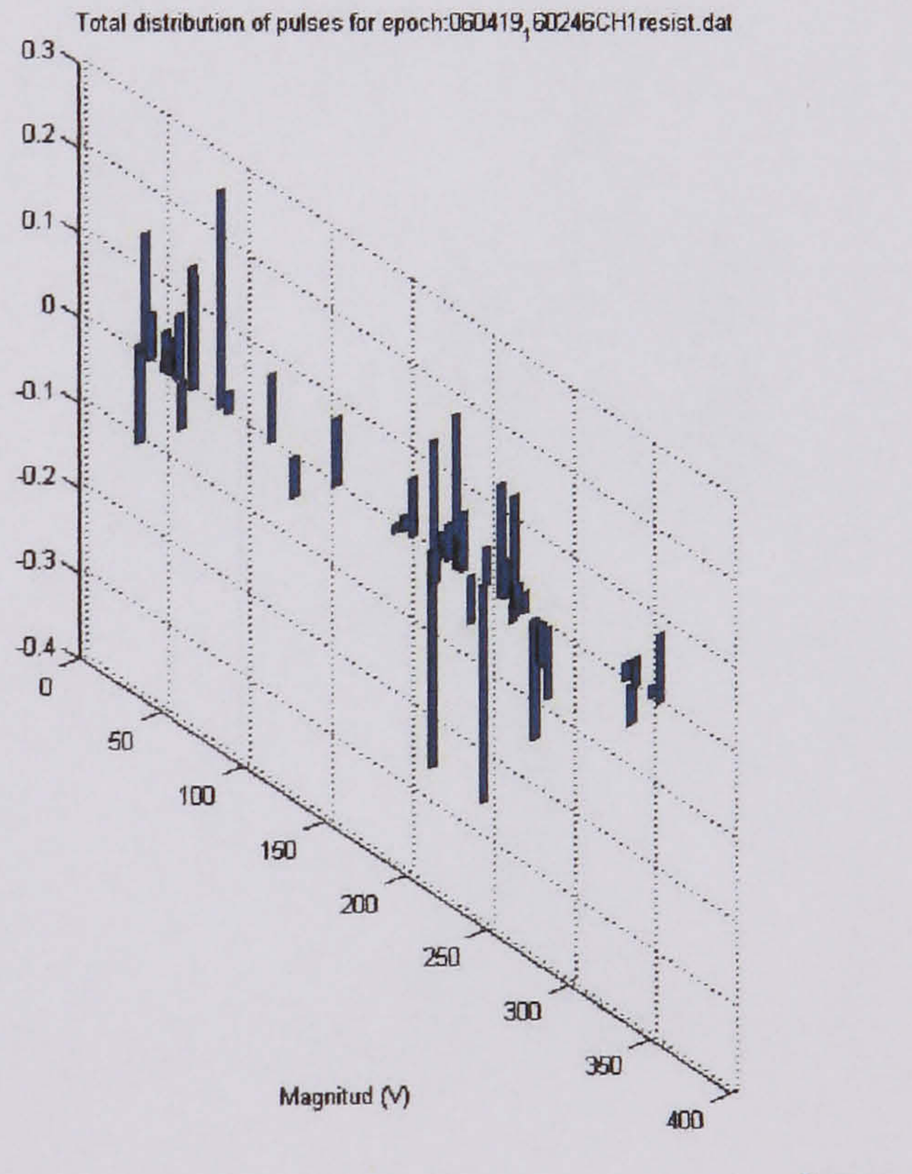

Distribution of surface discharges over a pressboard at 24210 V test 4 (resistor)

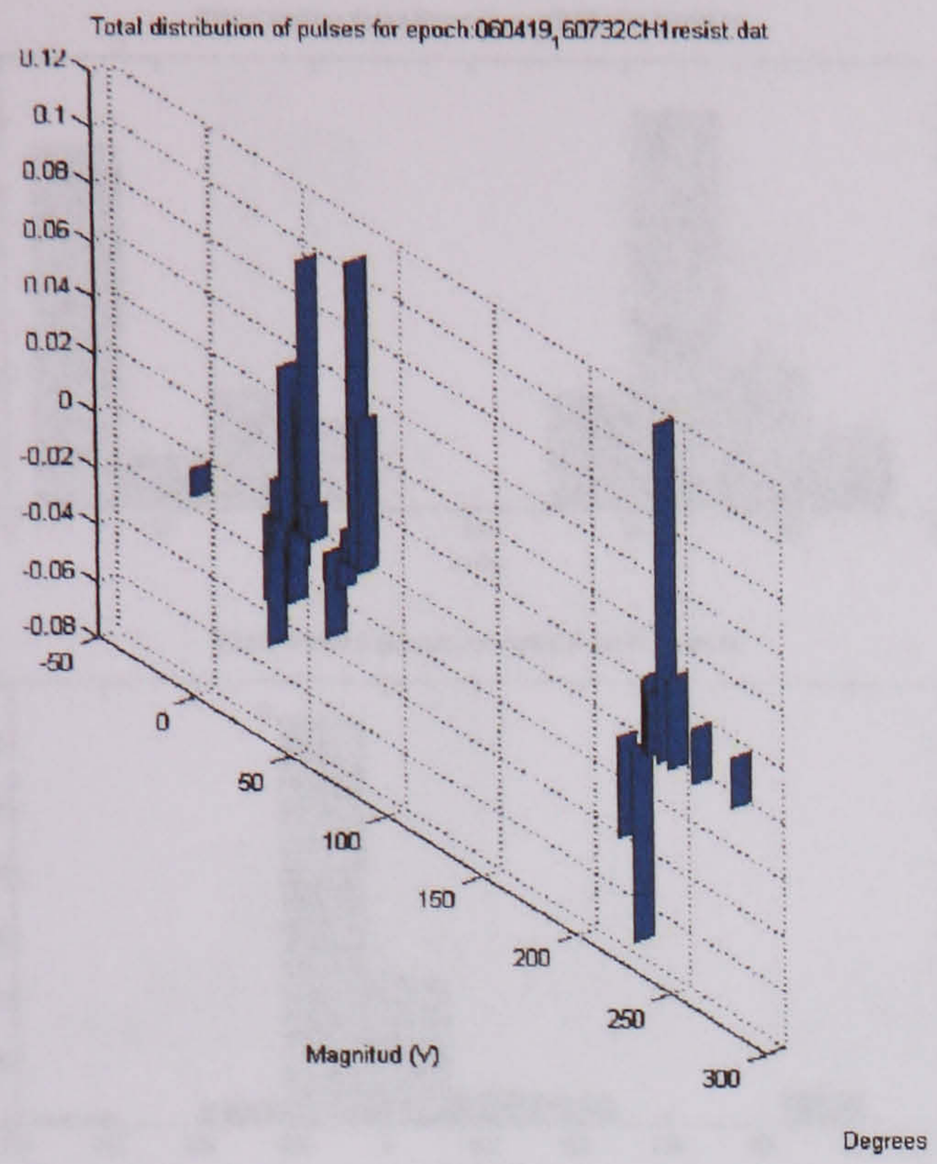

Distribution of surface discharges over a pressboard at 24210 V test 5 (resistor)

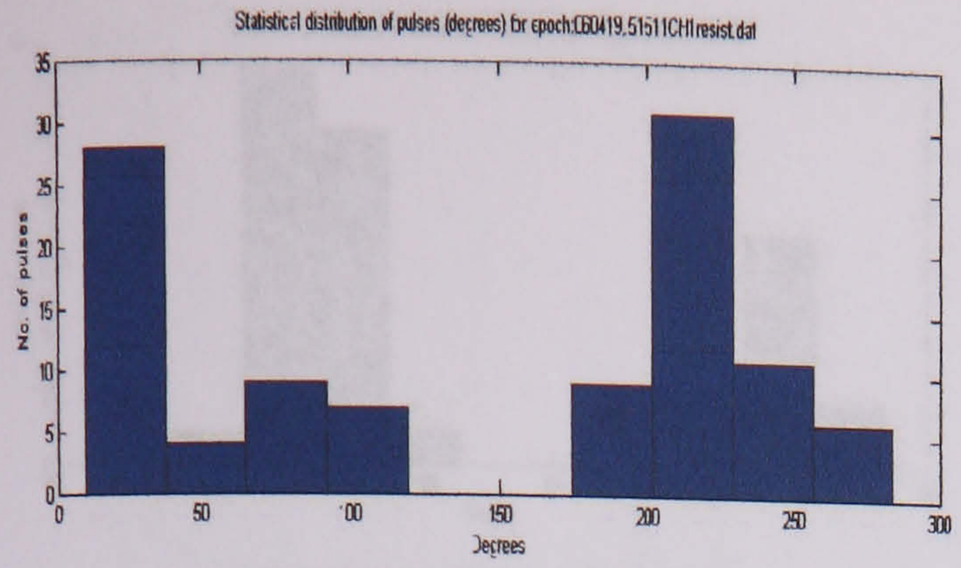

Statistical distribution of surface discharges over a pressboard at 24210 V test 1 (resistor)

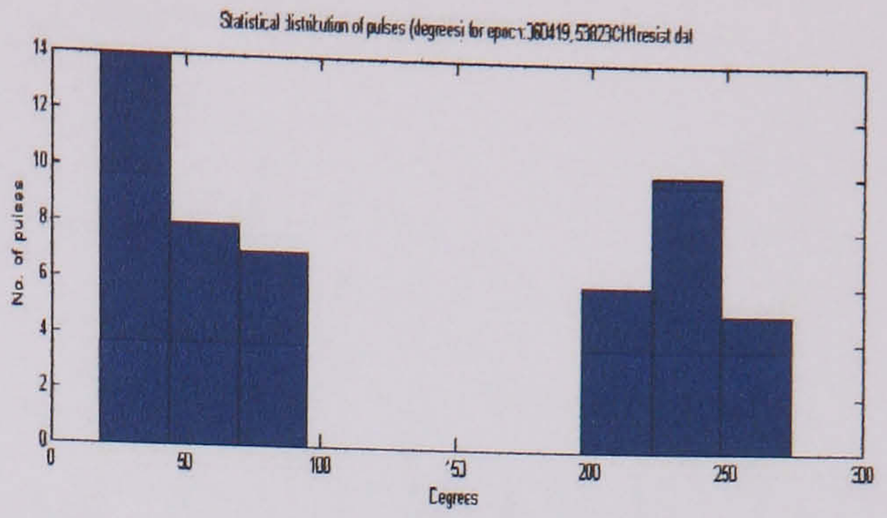

Statistical distribution of surface discharges over a pressboard at 24210 V test 3 (resistor)

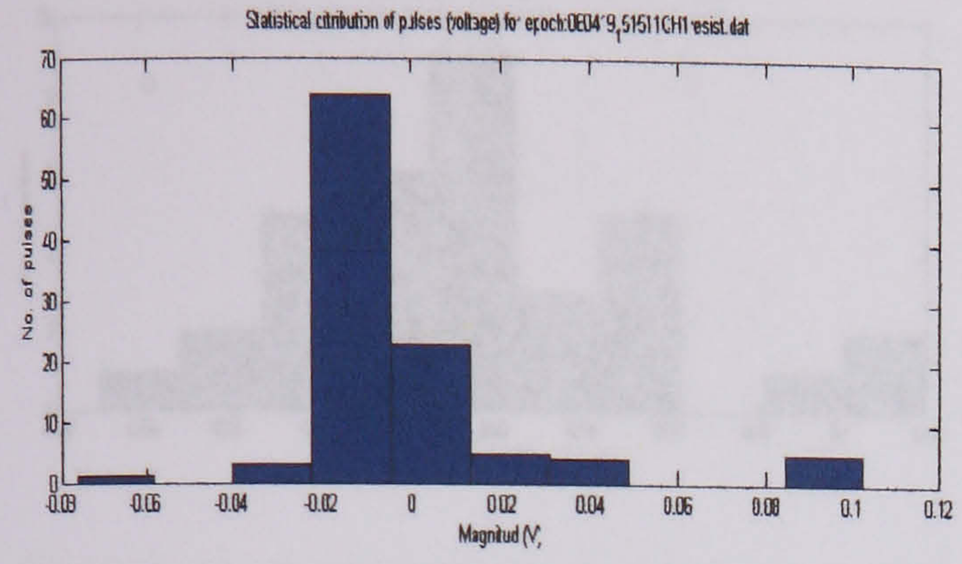

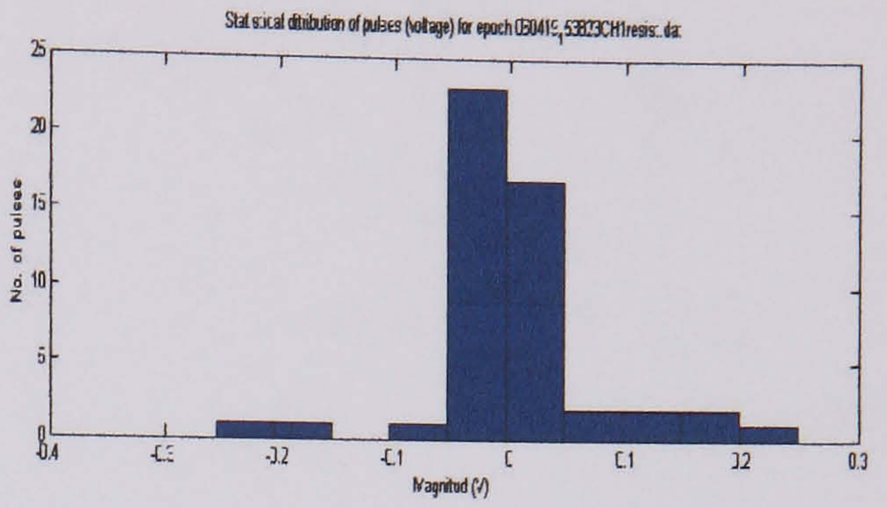

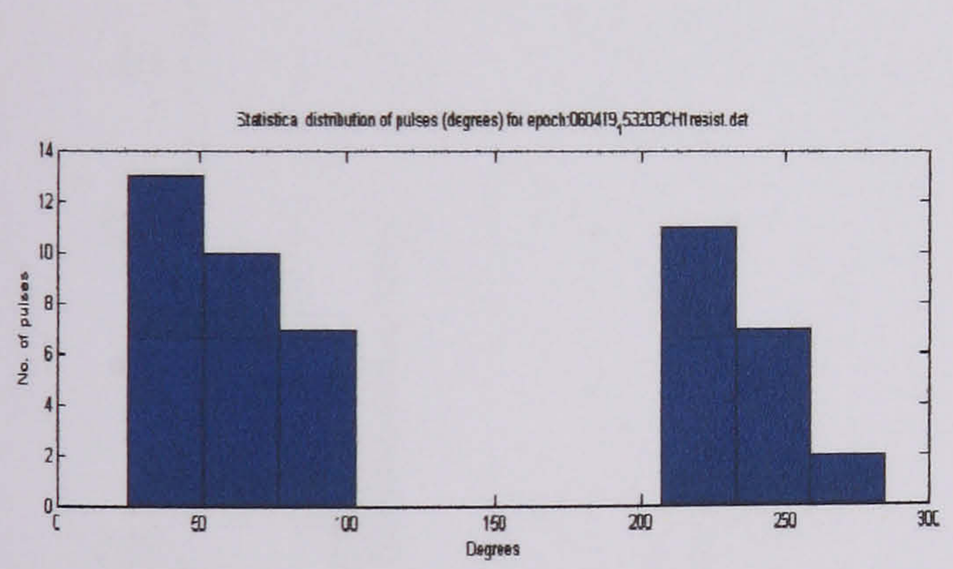

Statistical distribution of surface discharges over a pressboard at 24210 V test 2 (resistor)

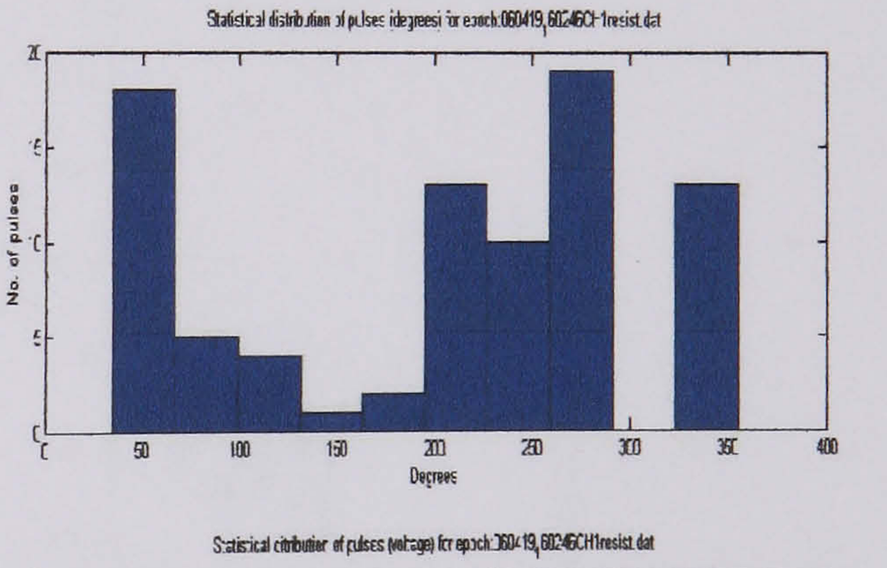

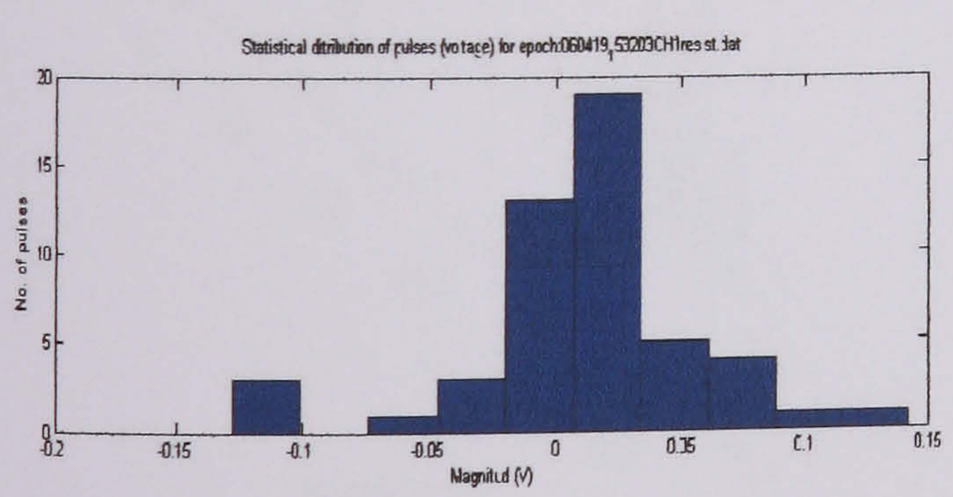

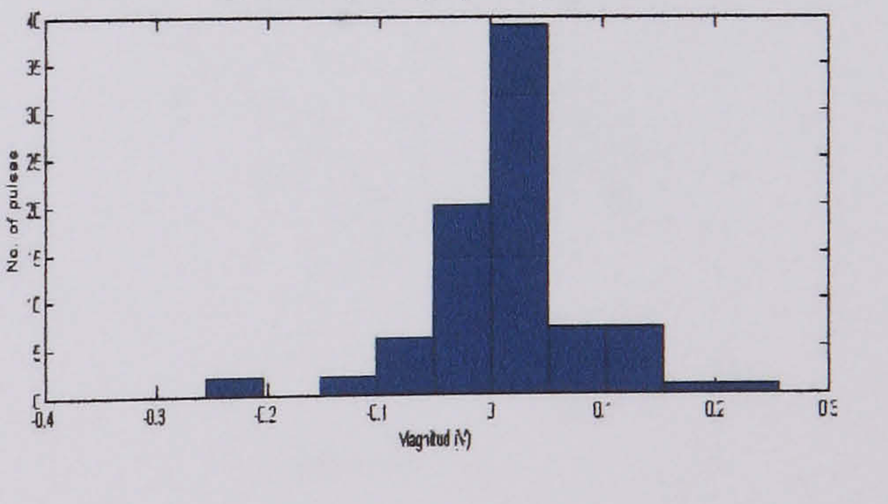

Statistical distribution of surface discharges over a pressboard at 24210 V test 4 (resistor)

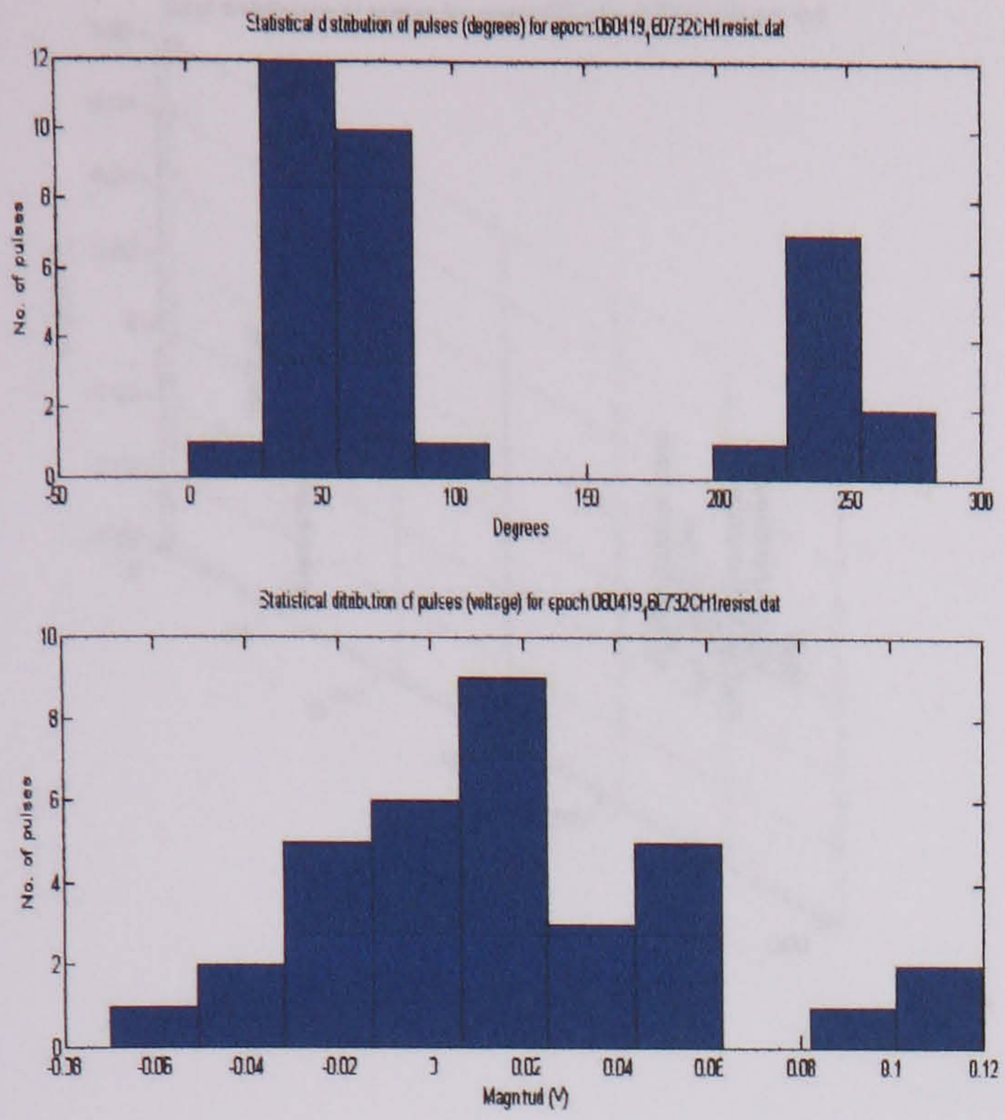

Statistical distribution of surface discharges over a pressboard at 24210 V test 5 (resistor)

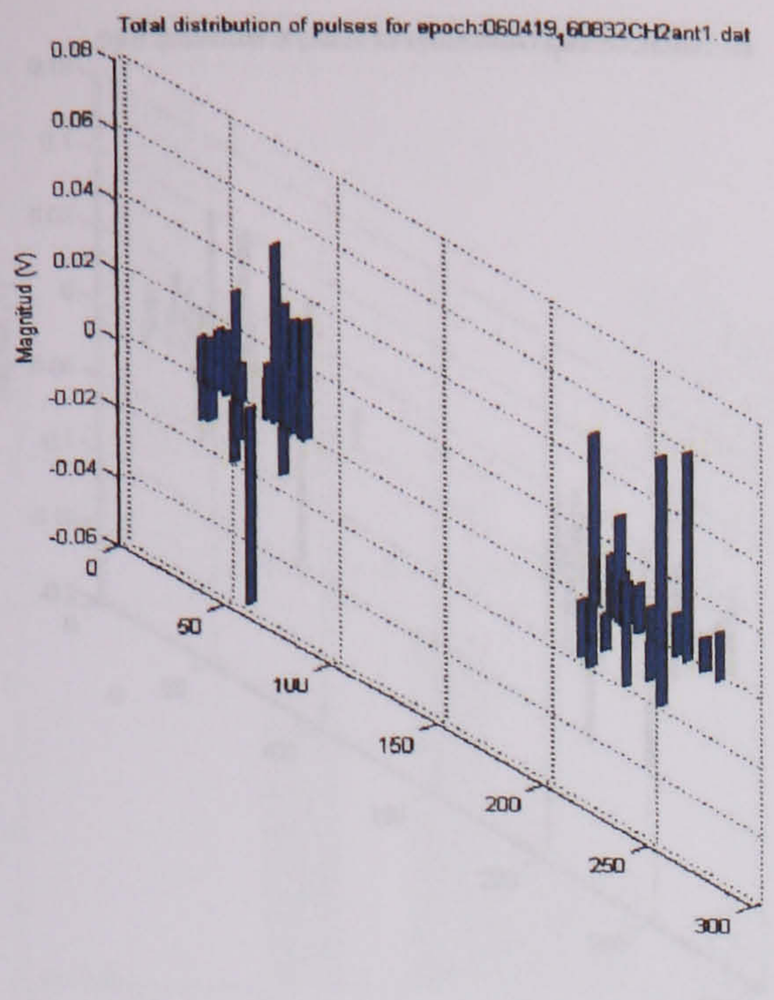

Distribution of surface discharges over a pressboard at 24210 V test 1 (antenna 1)

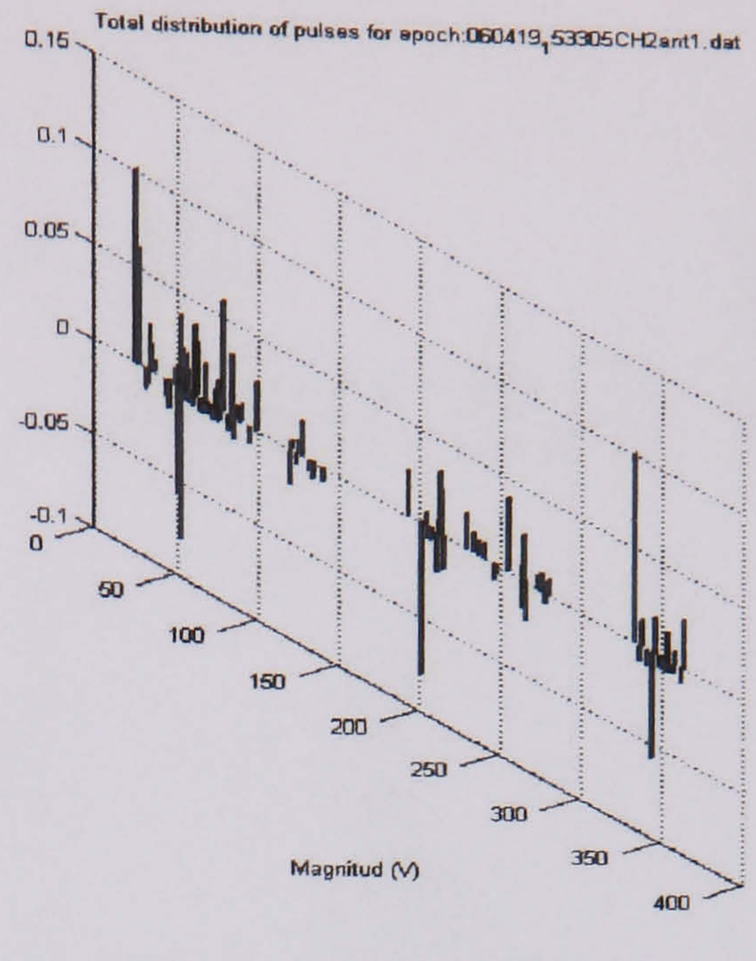

Distribution of surface discharges over a pressboard at 24210 V test 3 (antenna 1)

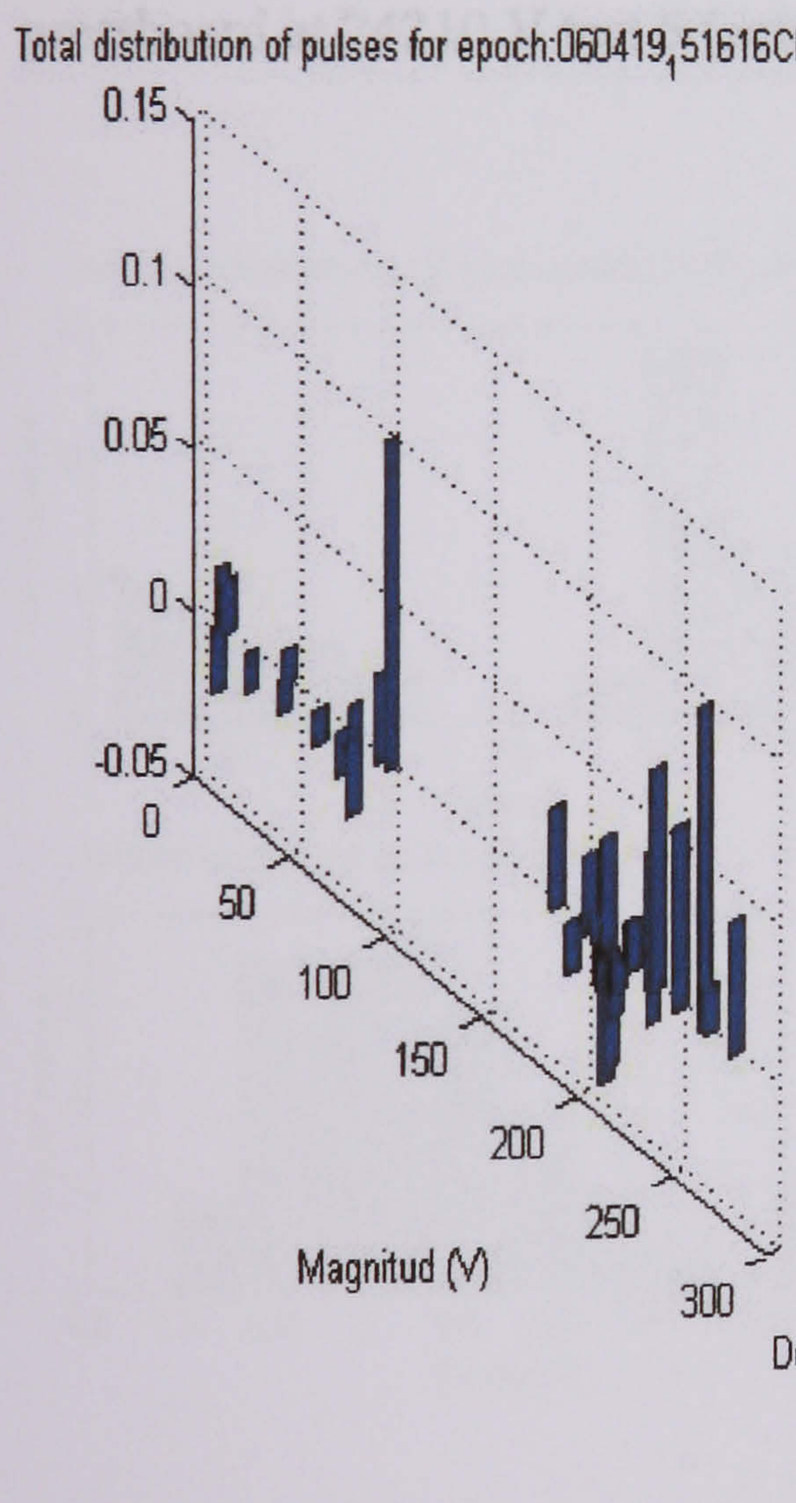

Distribution of surface discharges over a pressboard at 24210 V test 2 (antenna 1)

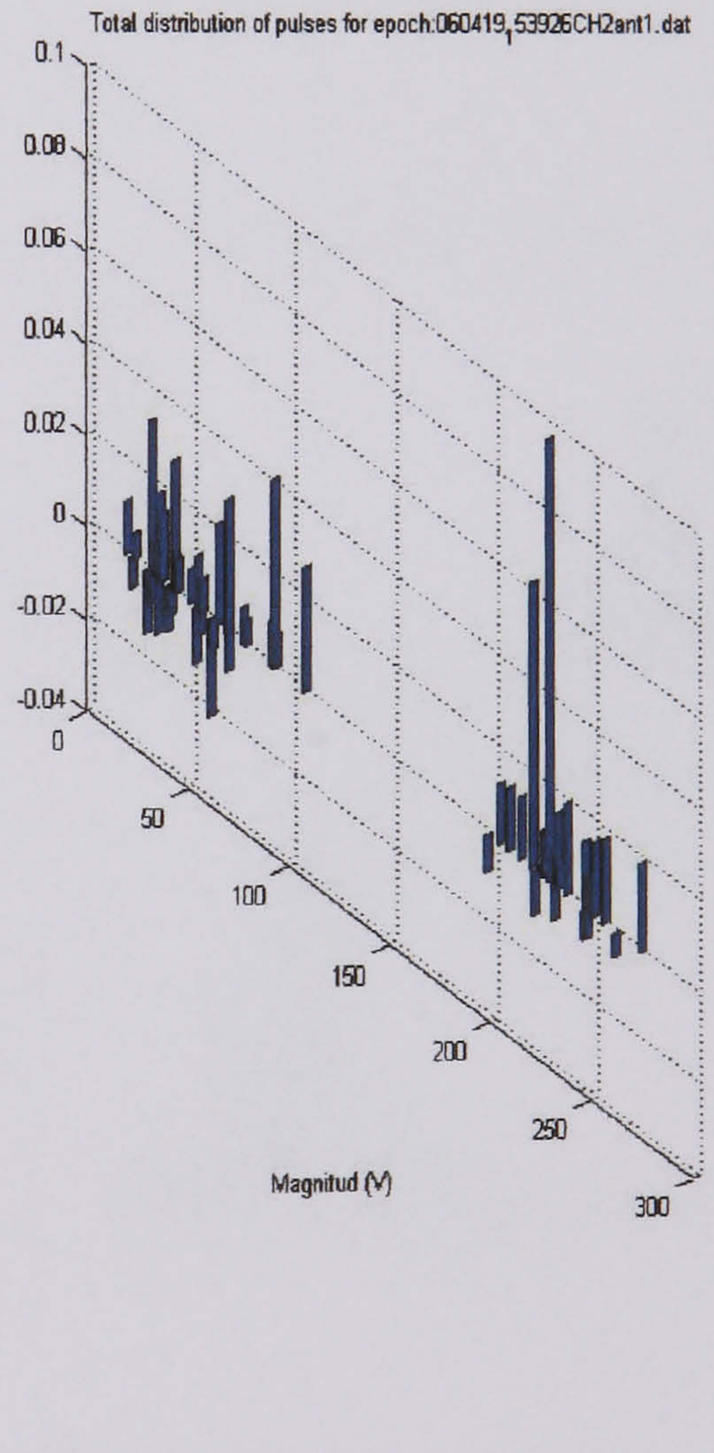

Distribution of surface discharges over a pressboard at 24210 V test 4 (antenna 1)

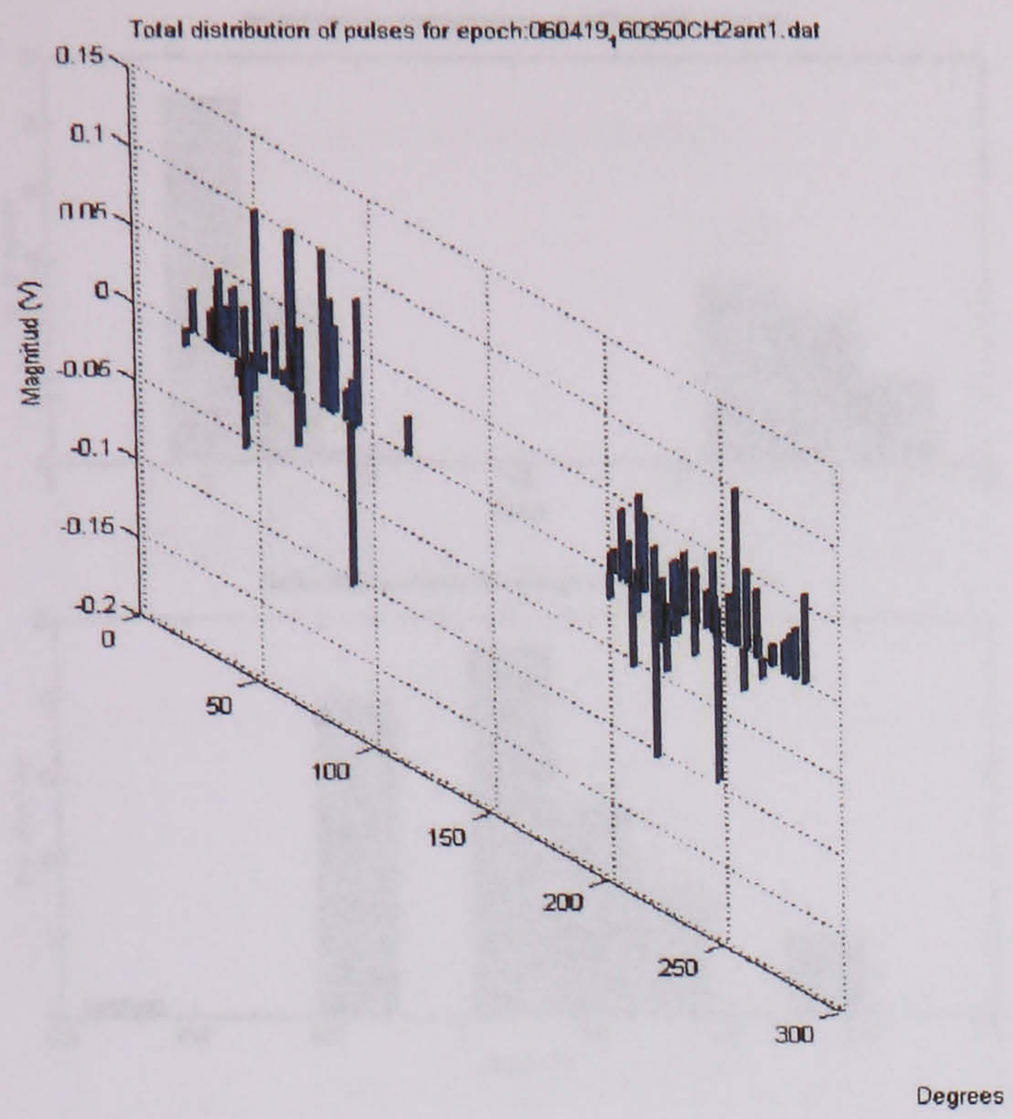

Distribution of surface discharges over a pressboard at 24210 V test 5 (antenna 1)

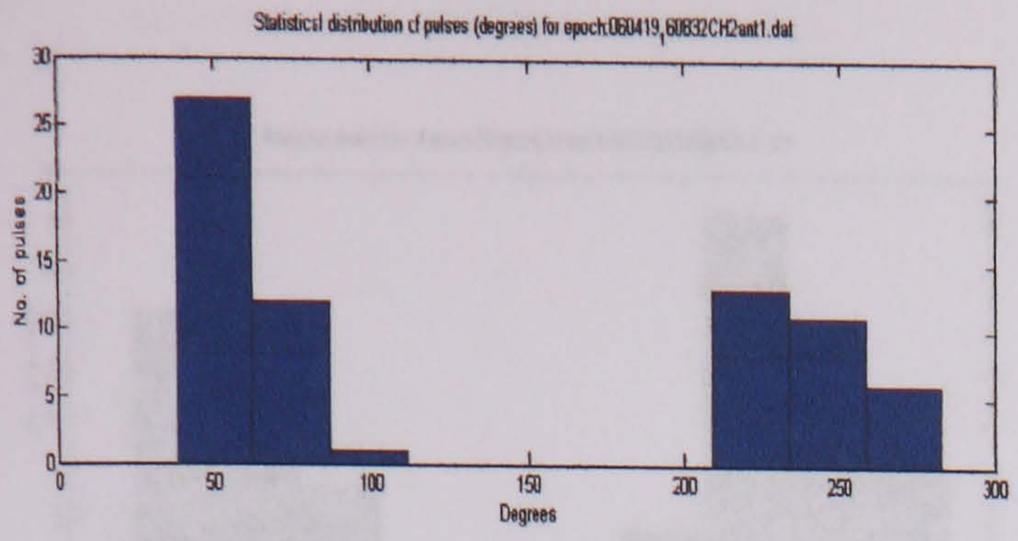

Statistical distribution of surface discharges over a pressboard at 24210 V test 1 (antenna 1)

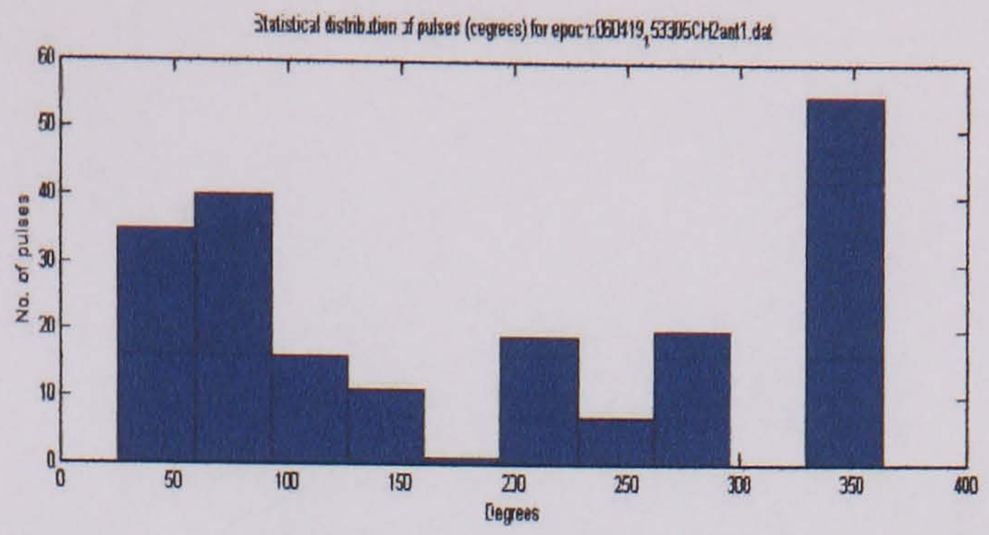

Statistical distribution of surface discharges over a pressboard at 24210 V test 3 (antenna 1)

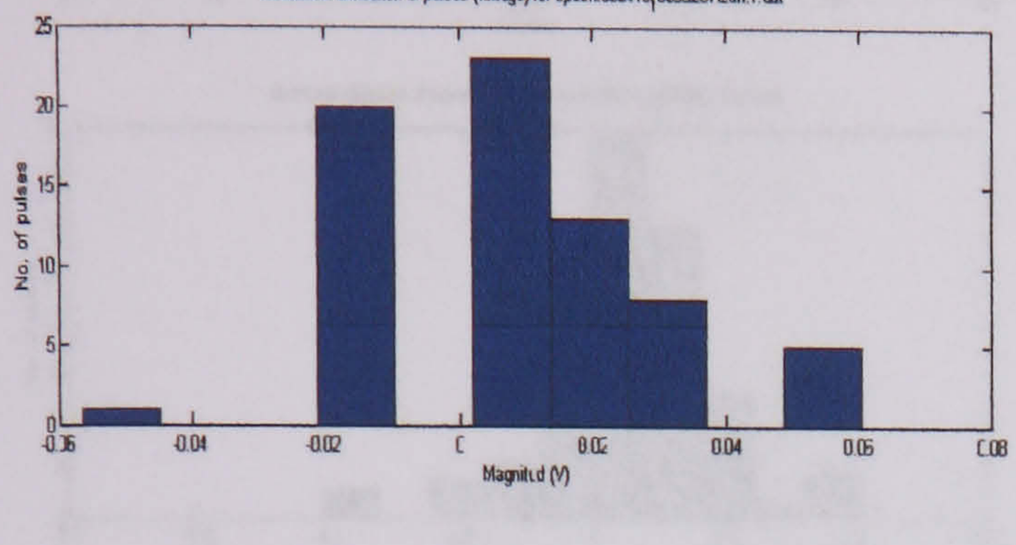

Statistical distribution of surface discharges over a pressboard at 24210 V test 2 (antenna 1)

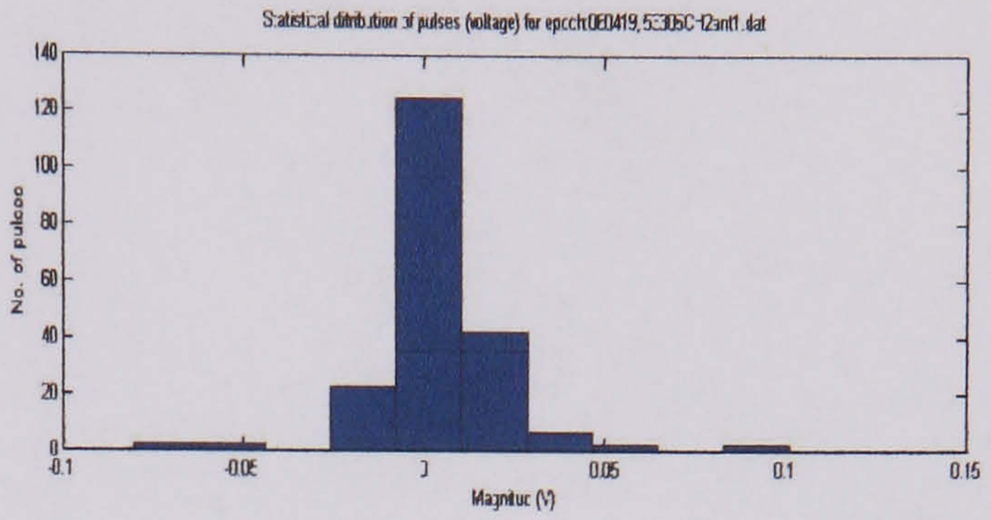

Statistical distribution of surface discharges over a pressboard at 24210 V test 4 (antenna 1)

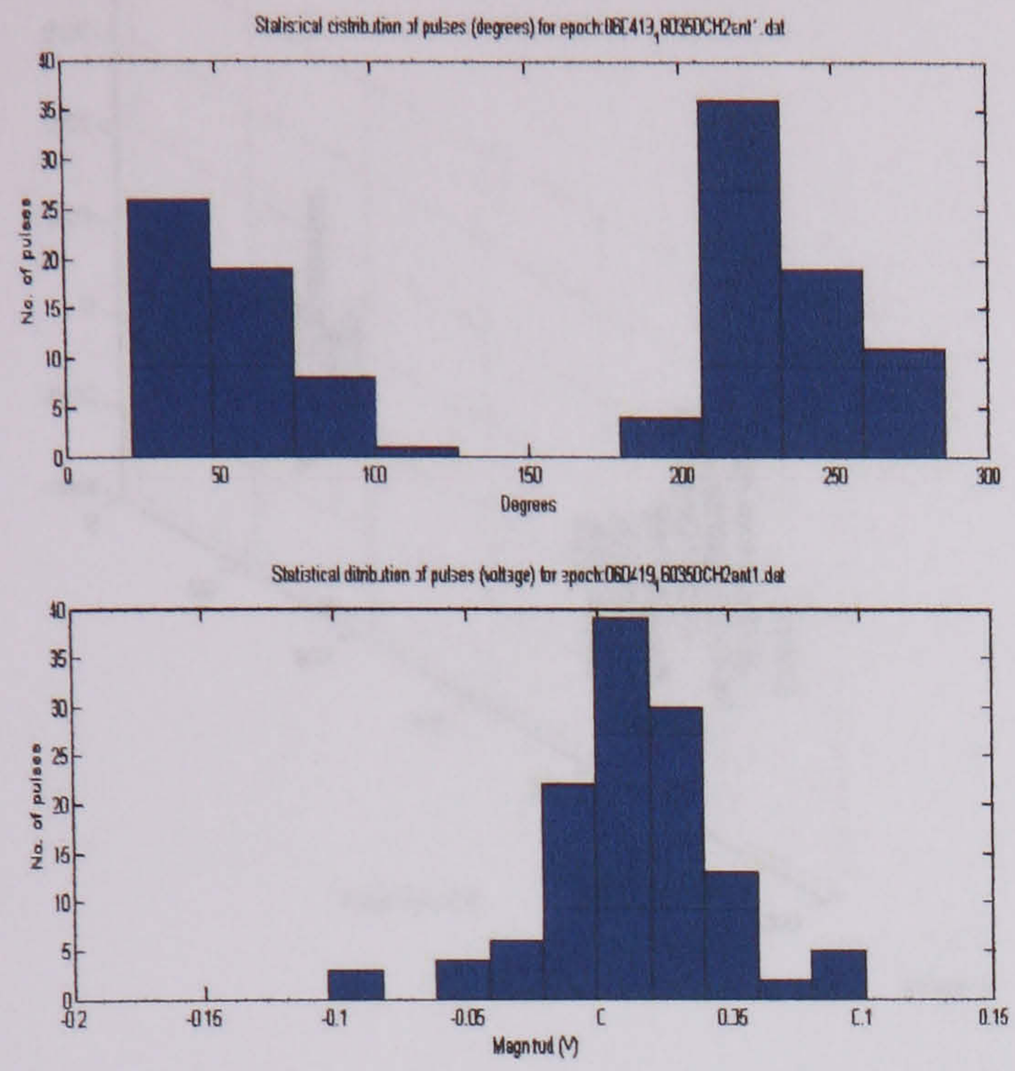

Statistical distribution of surface discharges over a pressboard at 24210 V test 5 (antenna 1)

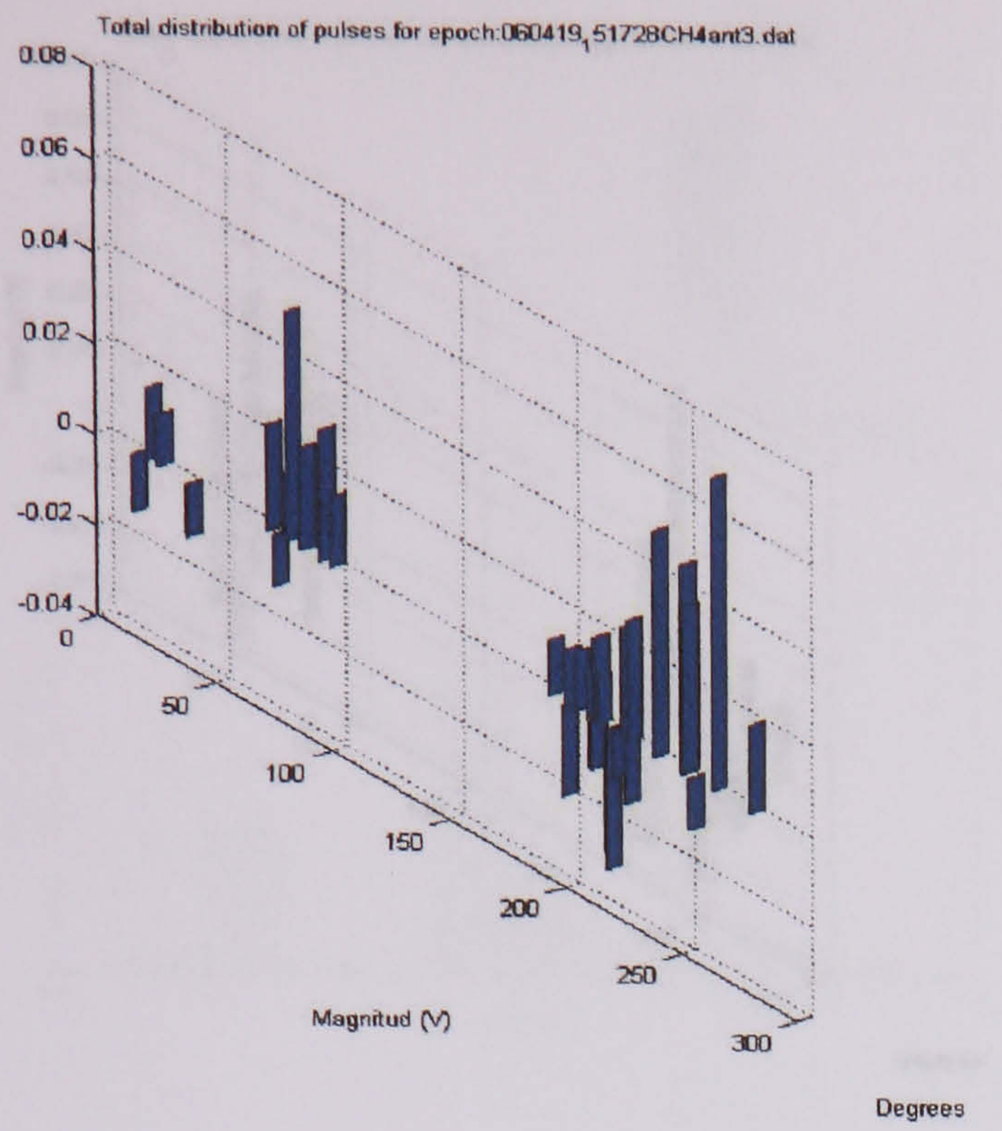

Distribution of surface discharges over a pressboard at 24210 V test 1 (antenna 3)

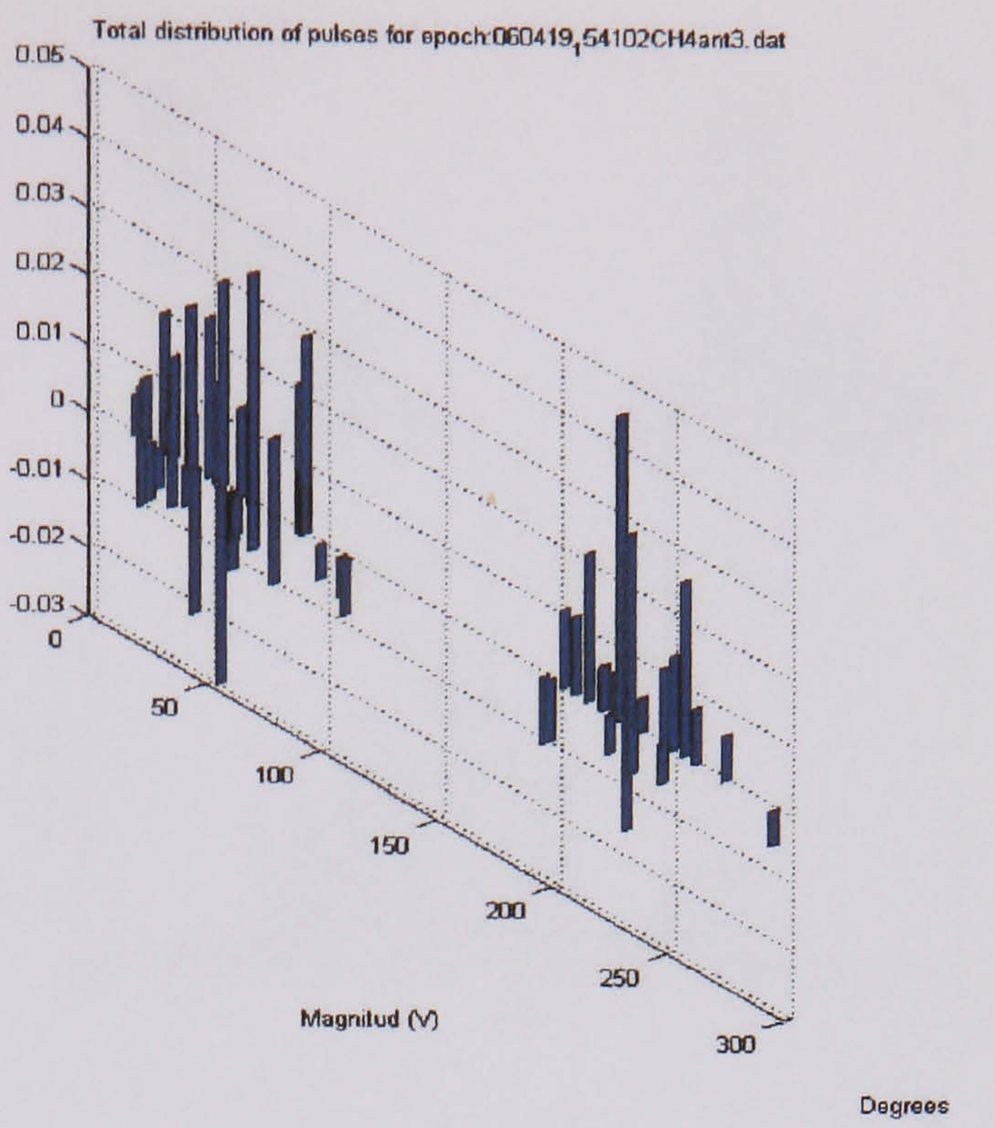

Distribution of surface discharges over a pressboard at 24210 V test 3 (antenna 3)

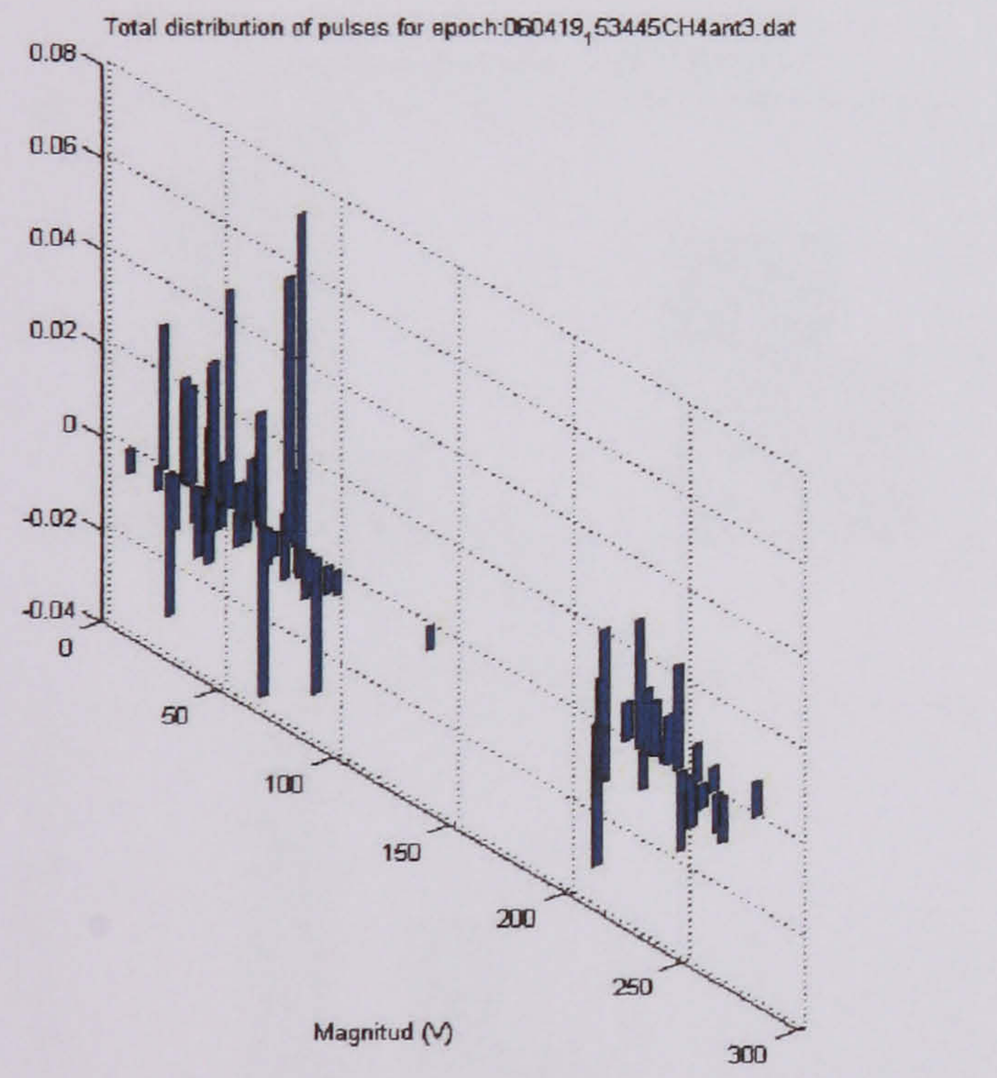

Distribution of surface discharges over a pressboard at 24210 V test 2 (antenna 3)

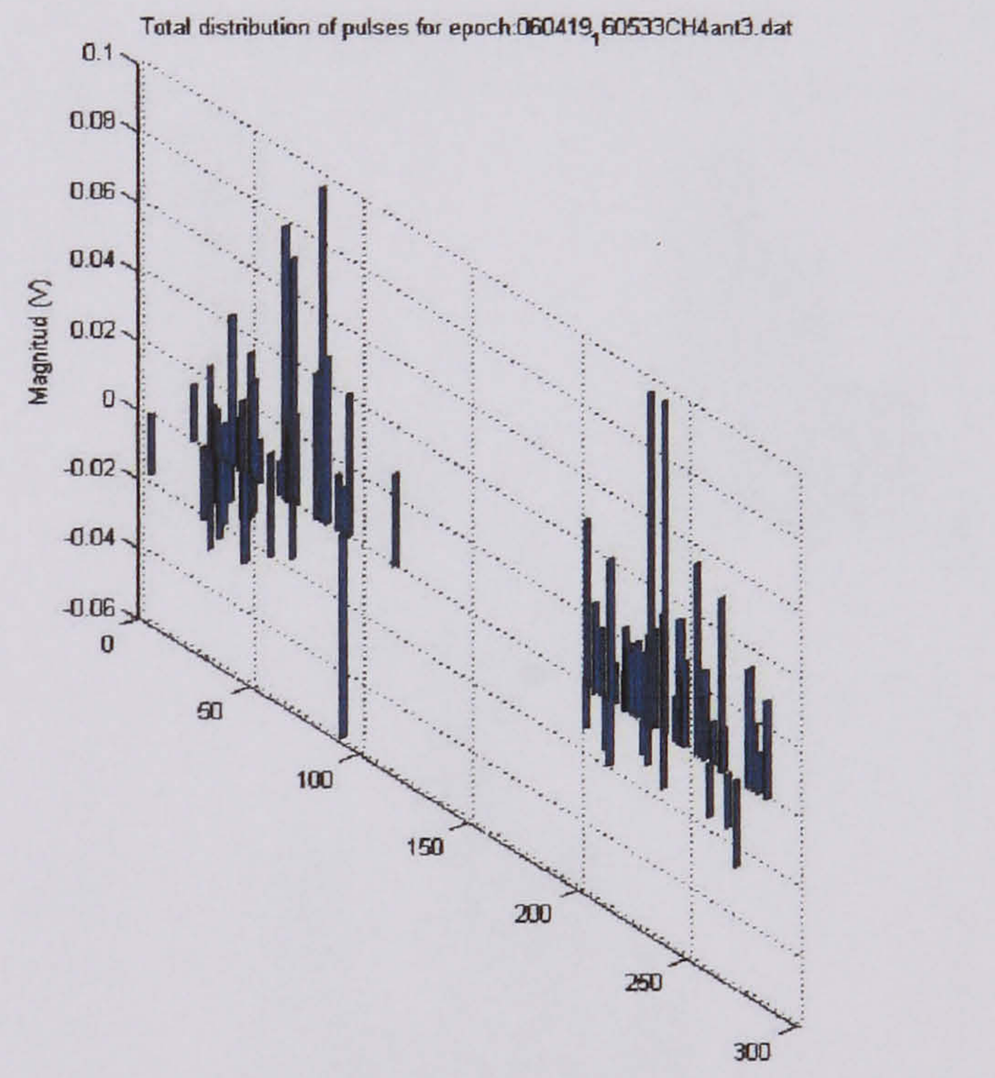

Distribution of surface discharges over a pressboard at 24210 V test 4 (antenna 3)

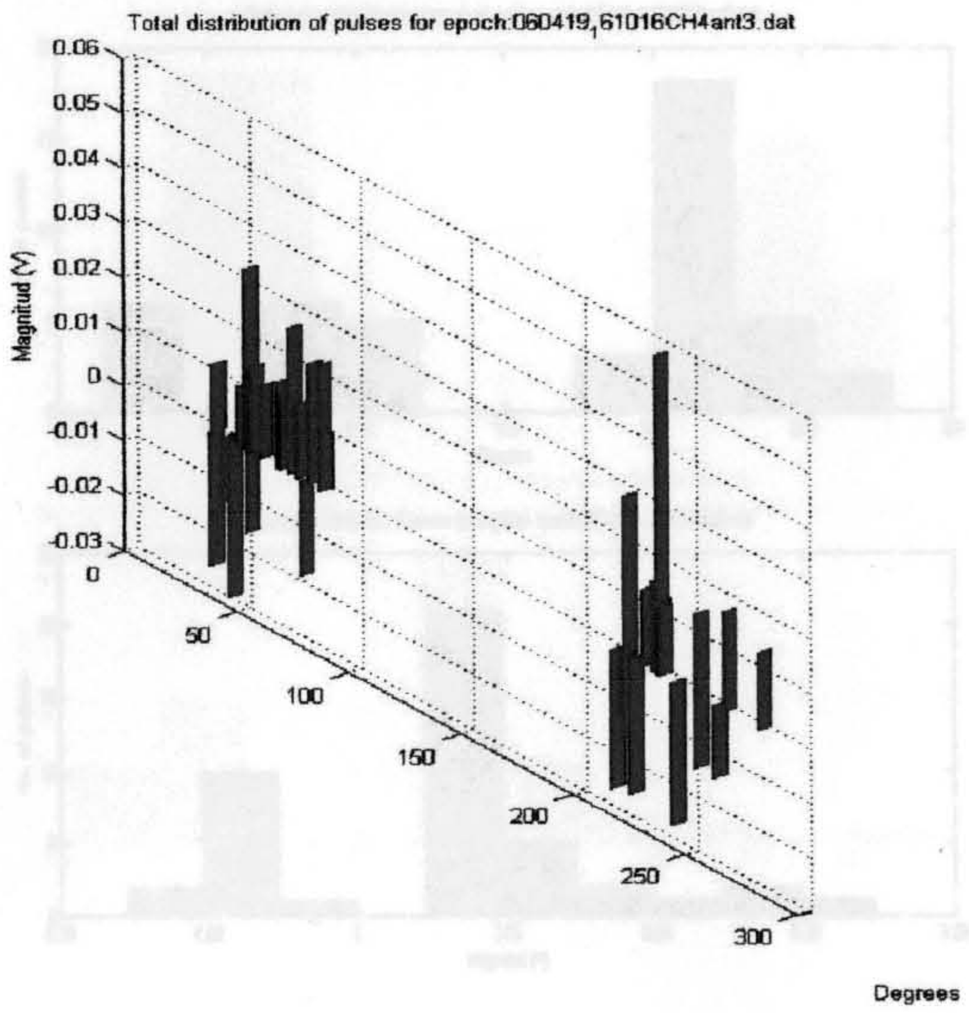

Distribution of surface discharges over a pressboard at 24210 V test 5 (antenna 3)

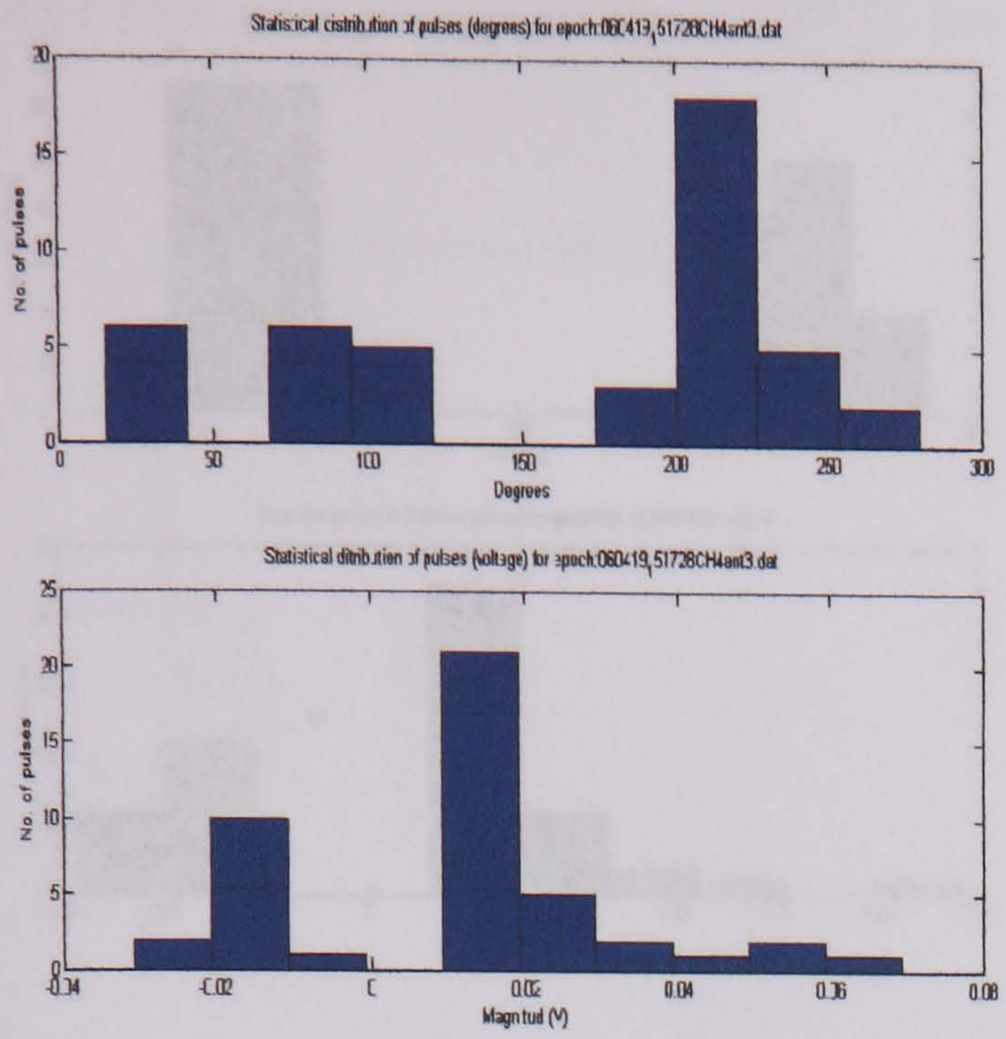

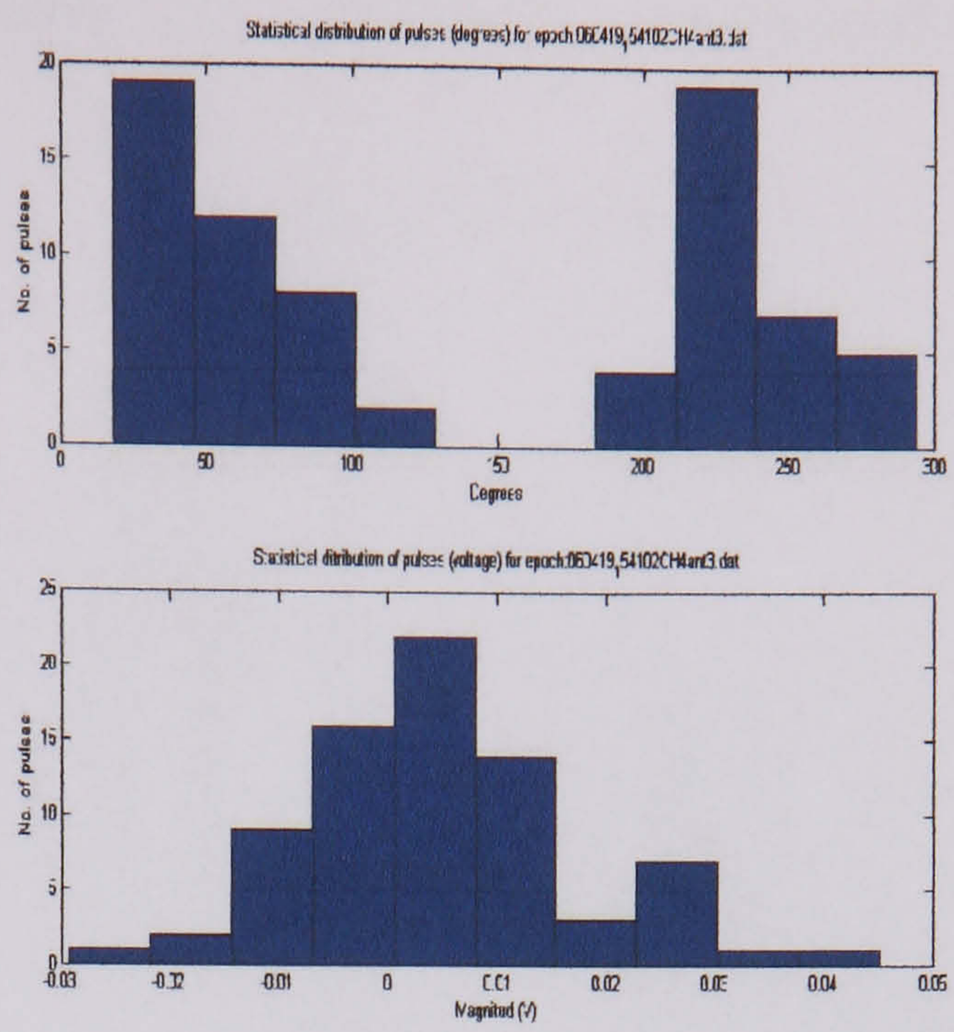

Statistical distribution of surface discharges over a pressboard at 24210 V test 1 (antenna 3)

Statistical distribution of surface discharges over a pressboard at 24210 V test 3 (antenna 3)

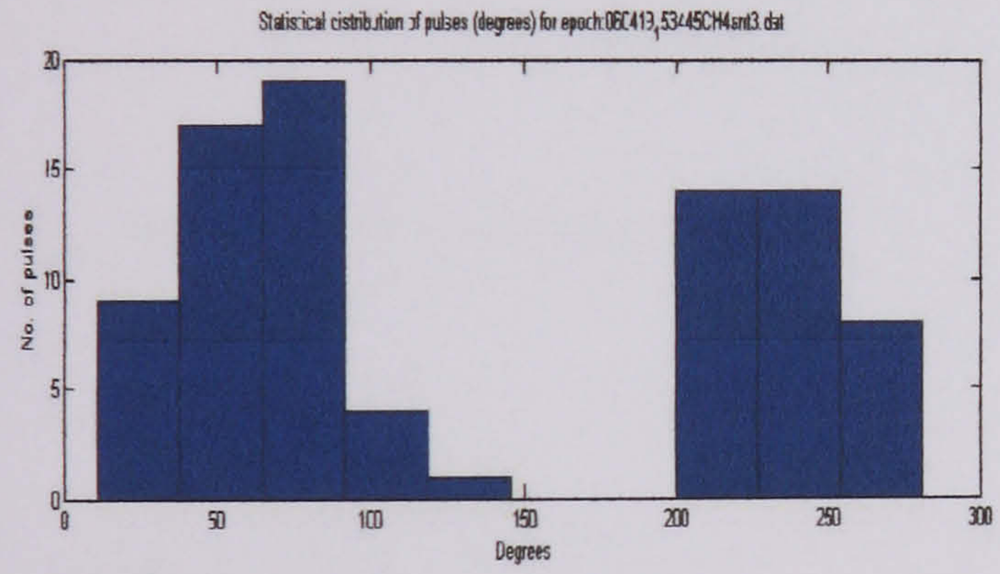

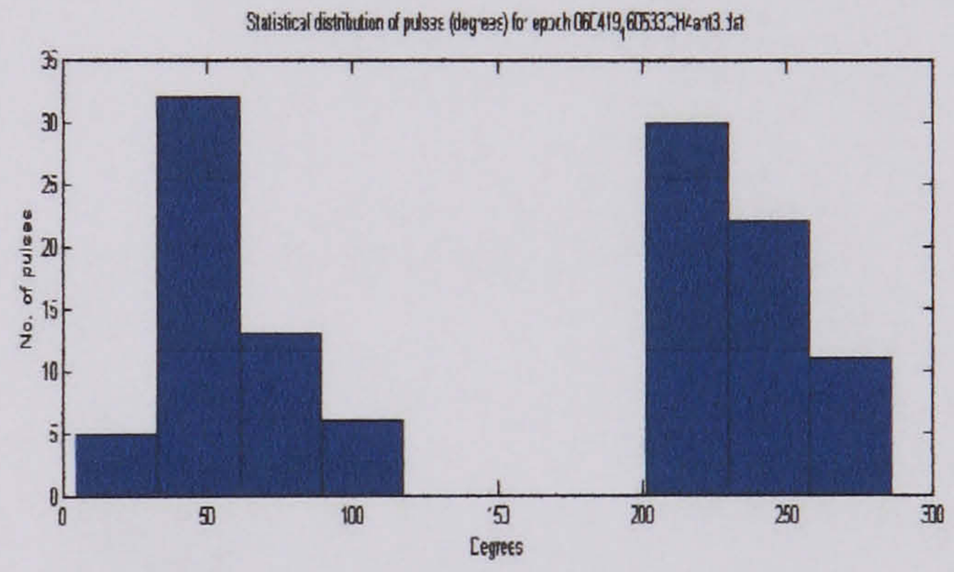

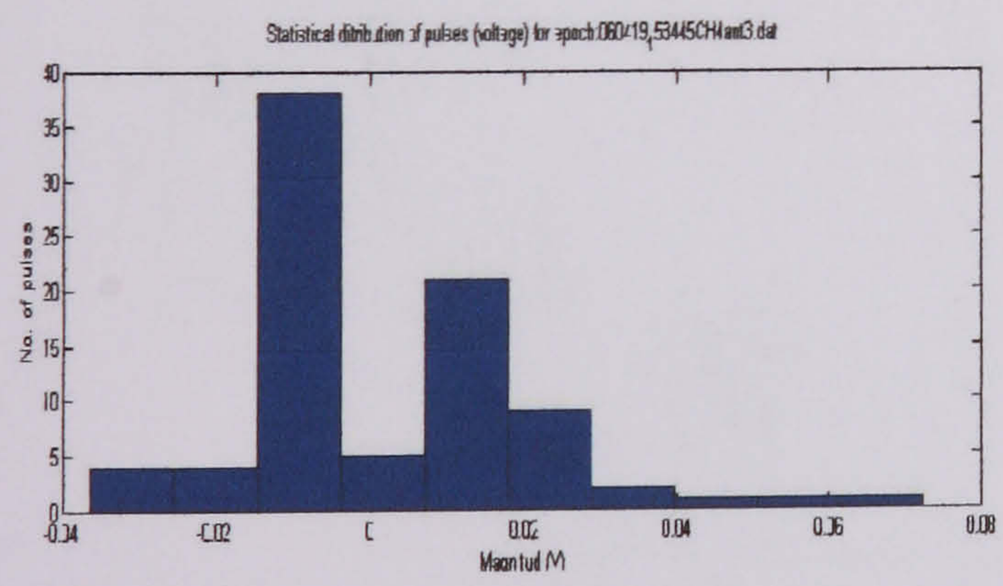

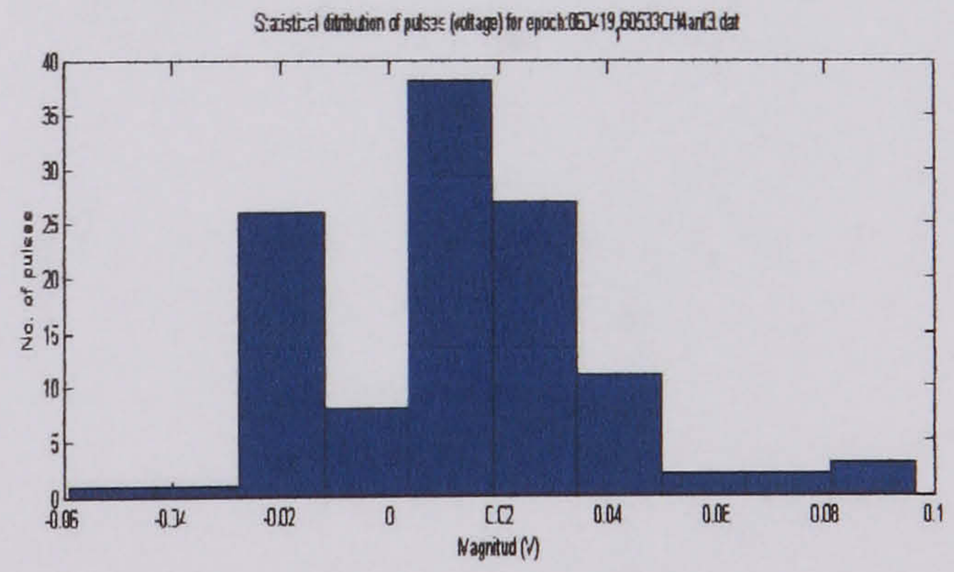

Statistical distribution of surface discharges over a pressboard at 24210 V test 2 (antenna 3)

Statistical distribution of surface discharges over a pressboard at 24210 V test 4 (antenna 3)

Statistical distribution of surface discharges over a pressboard at 24210 V test 5 (antenna 3)

Appendix G: Patterns for a cavity and their statistical distribution

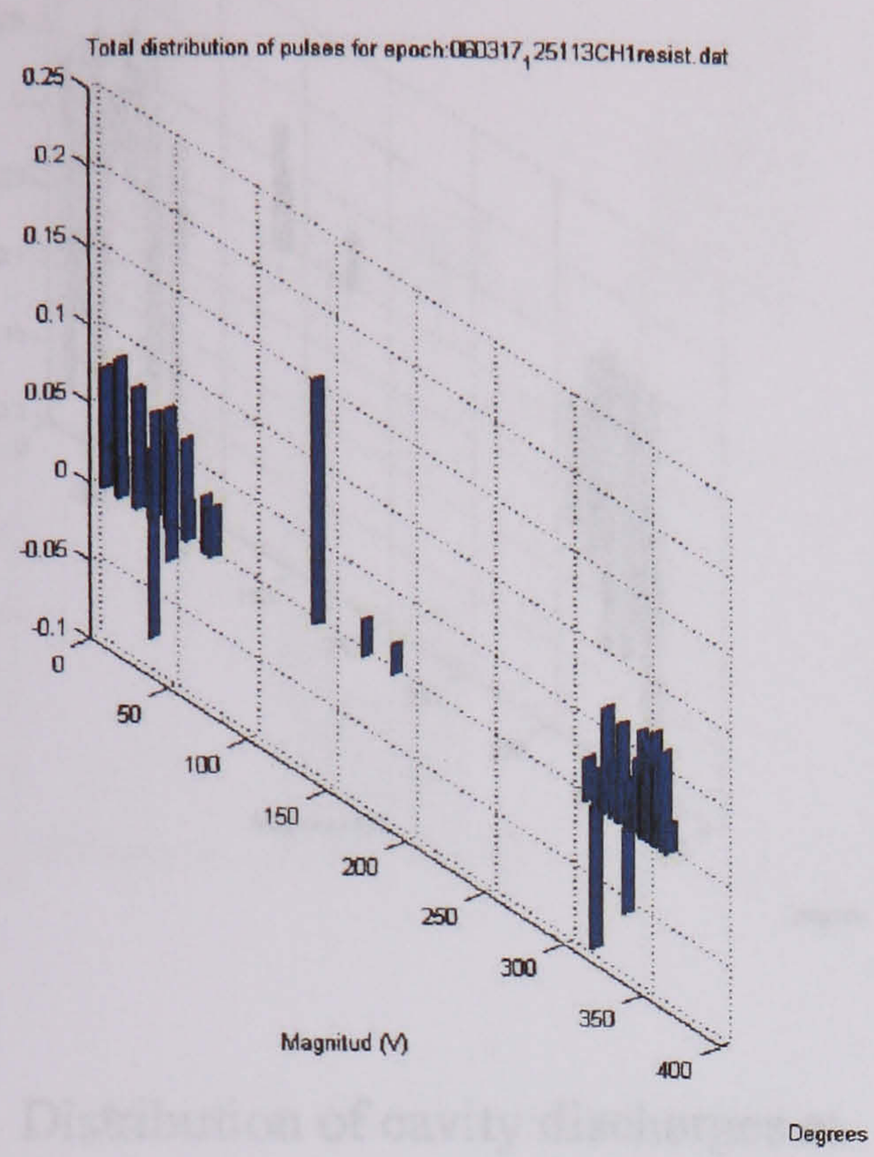

Distribution of cavity discharges at 14320 V test 1 (resistor)

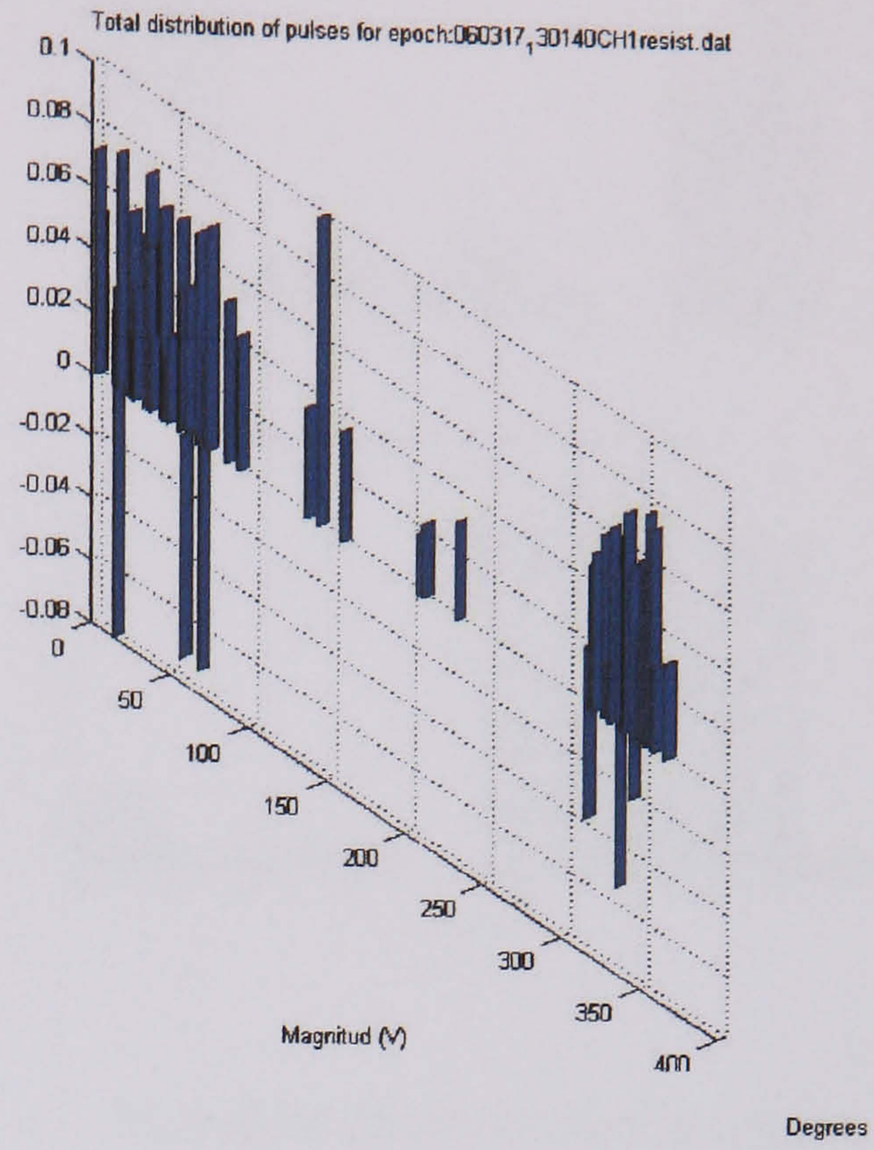

Distribution of cavity discharges at 14320 V test 3 (resistor)

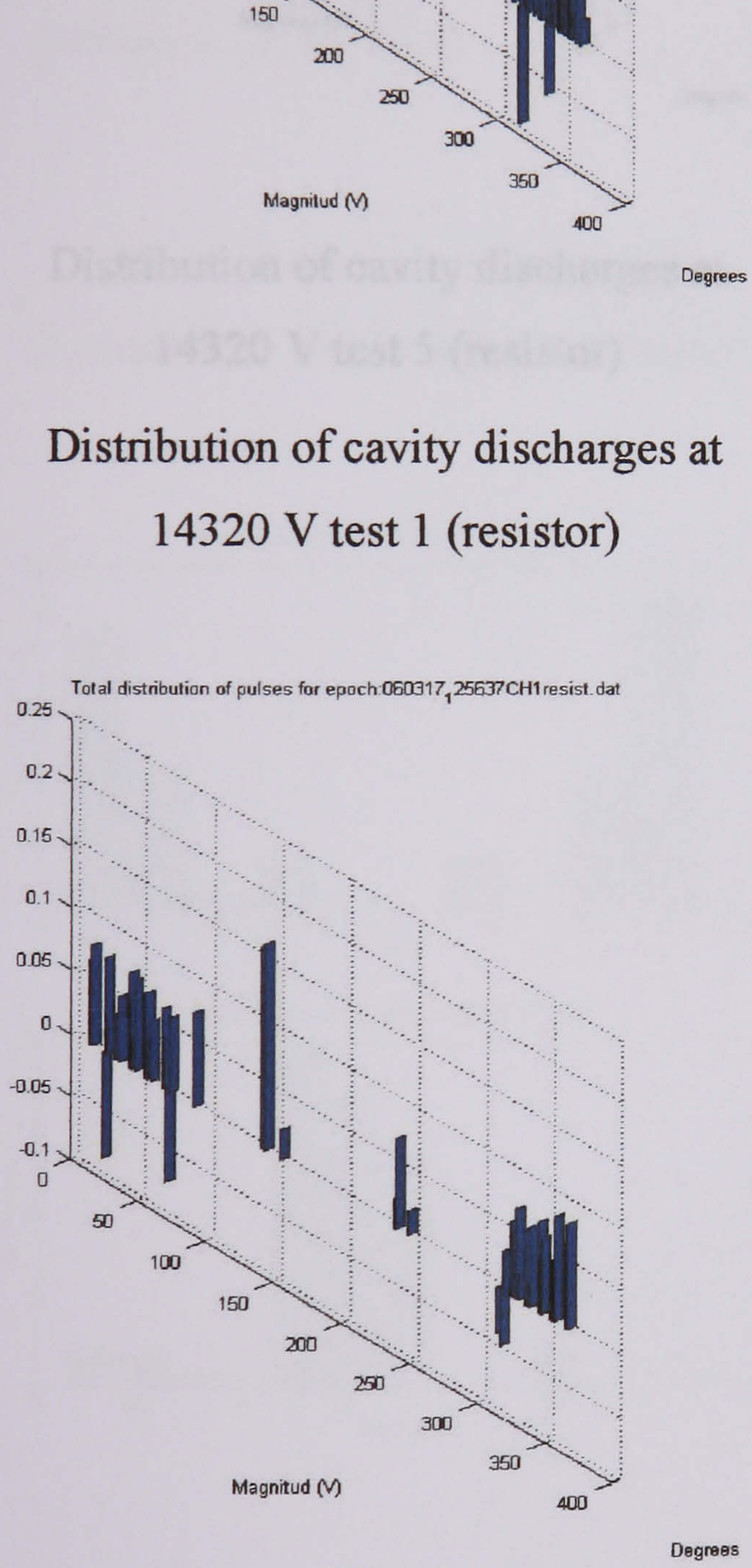

Distribution of cavity discharges at 14320 V test 2 (resistor)

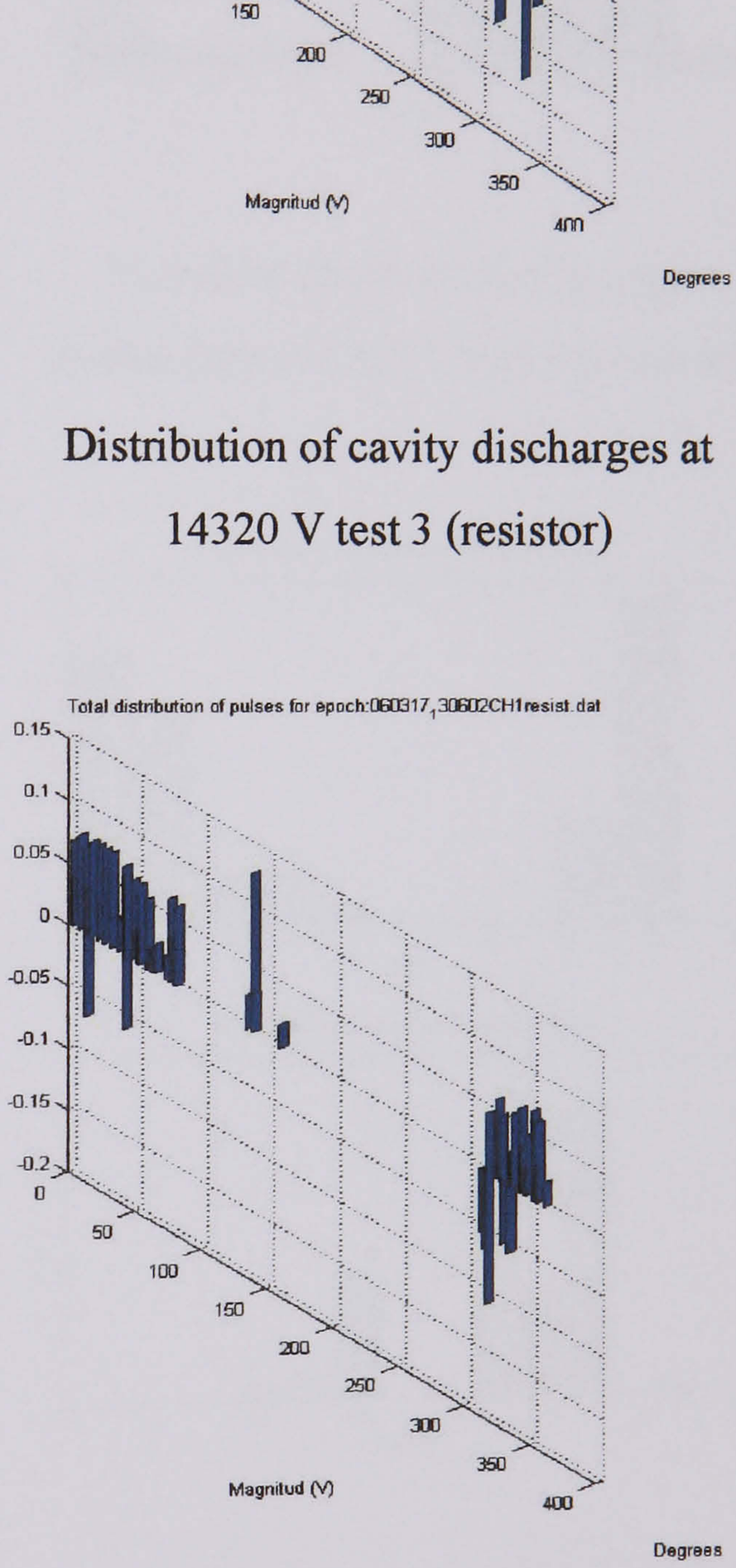

Distribution of cavity discharges at 14320 V test 4 (resistor)

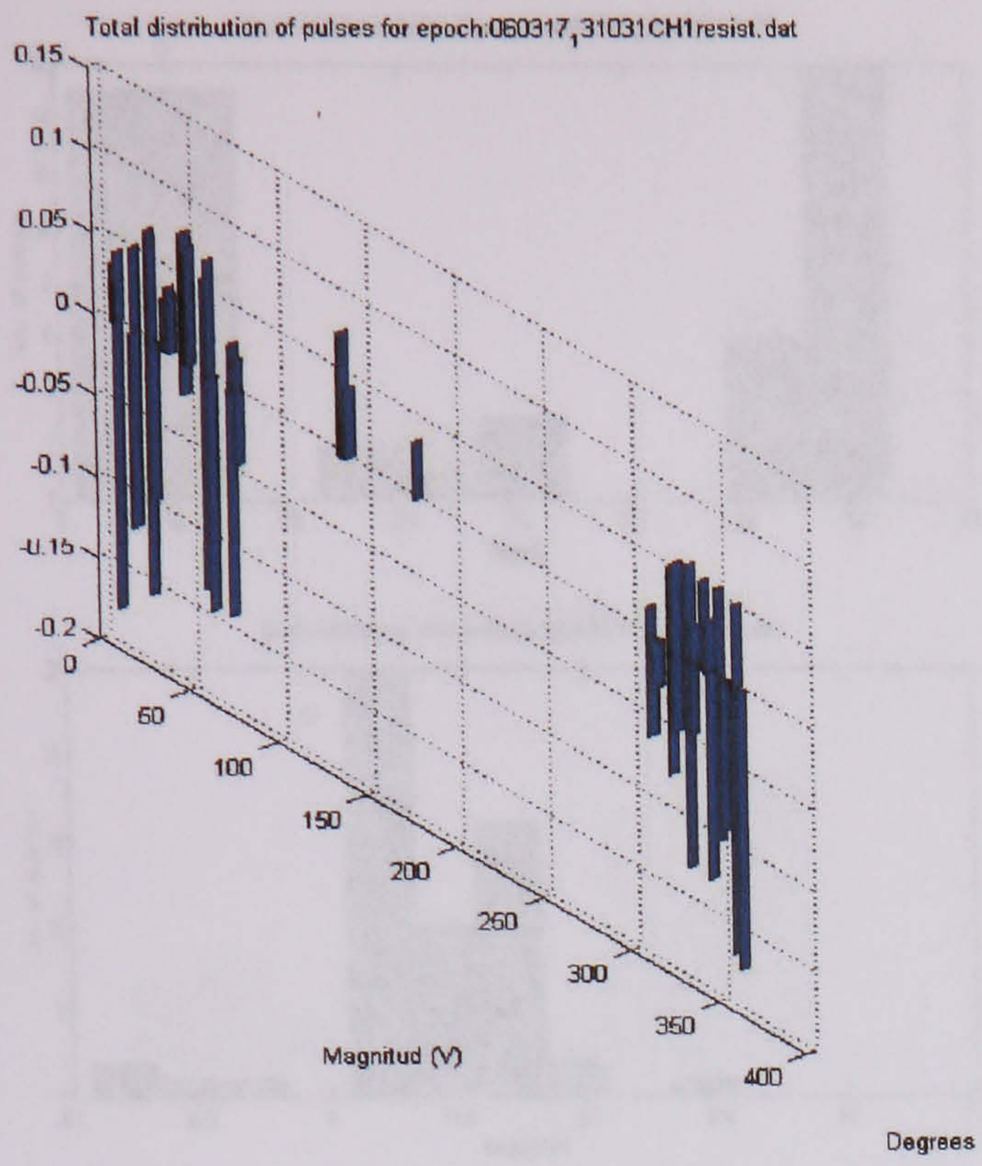

Distribution of cavity discharges at

14320 V test 5 (resistor)

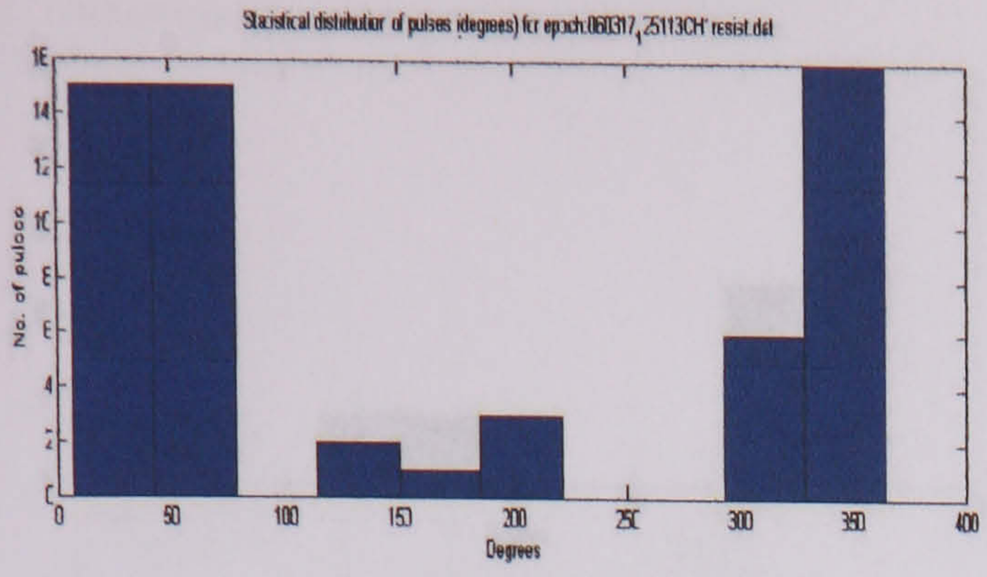

Statistical distribution of cavity discharges at 14320 V test 1 (resistor)

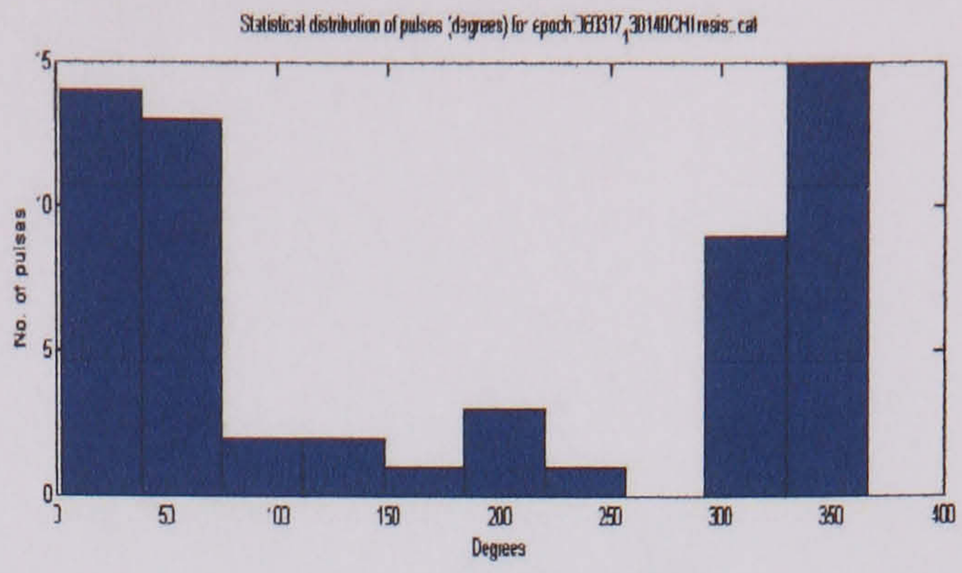

Statistical distribution of cavity discharges at 14320 V test 3 (resistor)

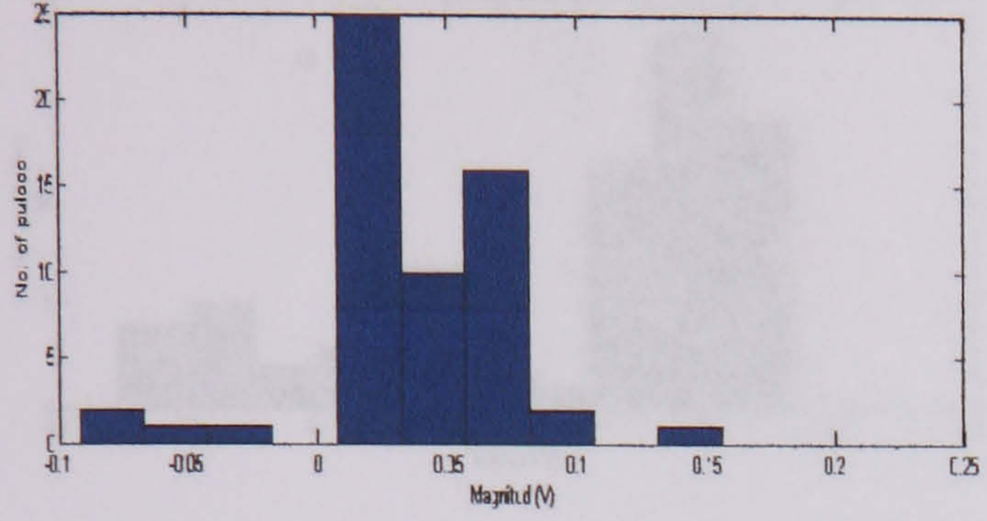

Statistical distribution of cavity discharges at 14320 V test 2 (resistor)

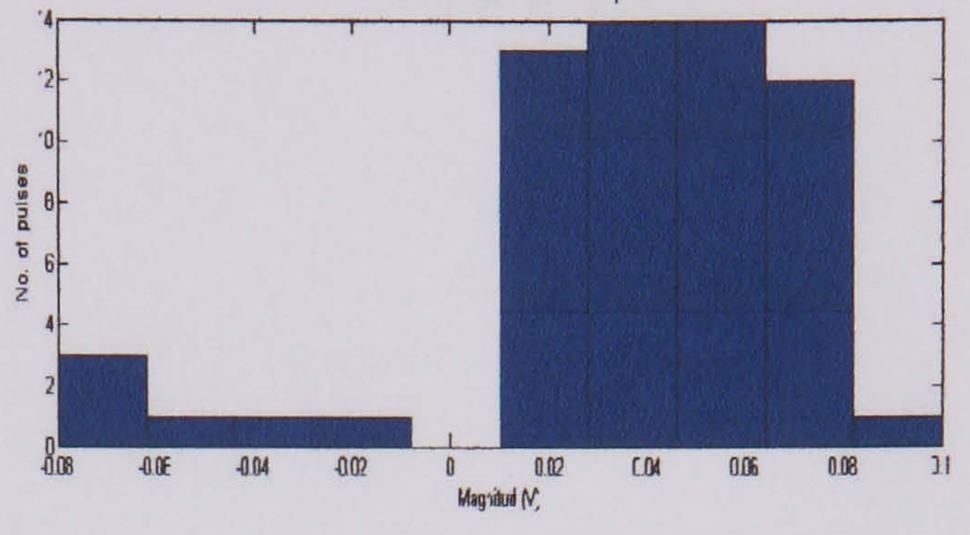

Statistical distribution of cavity discharges at 14320 V test 4 (resistor)

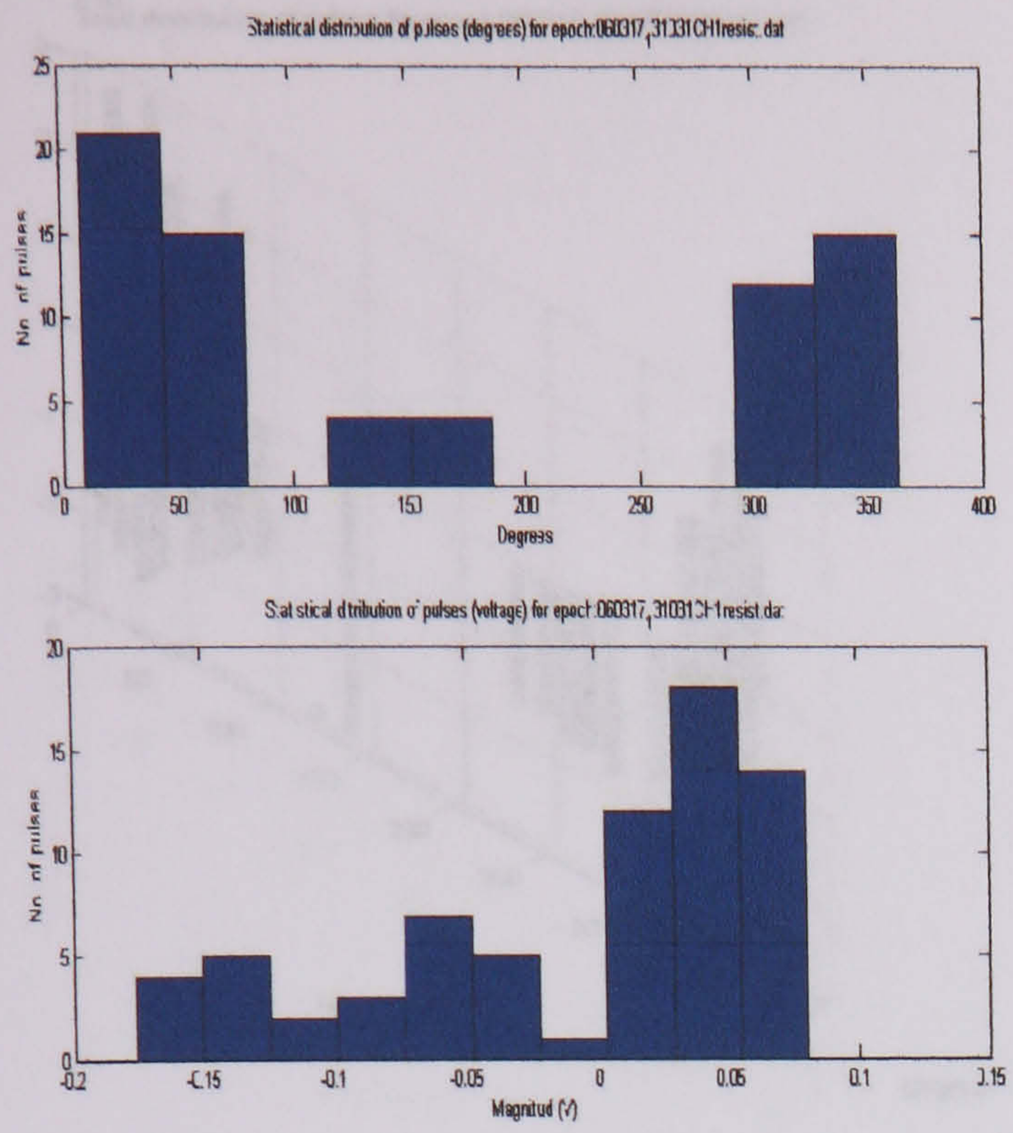

Statistical distribution of cavity discharges at 14320 V test 5 (resistor)

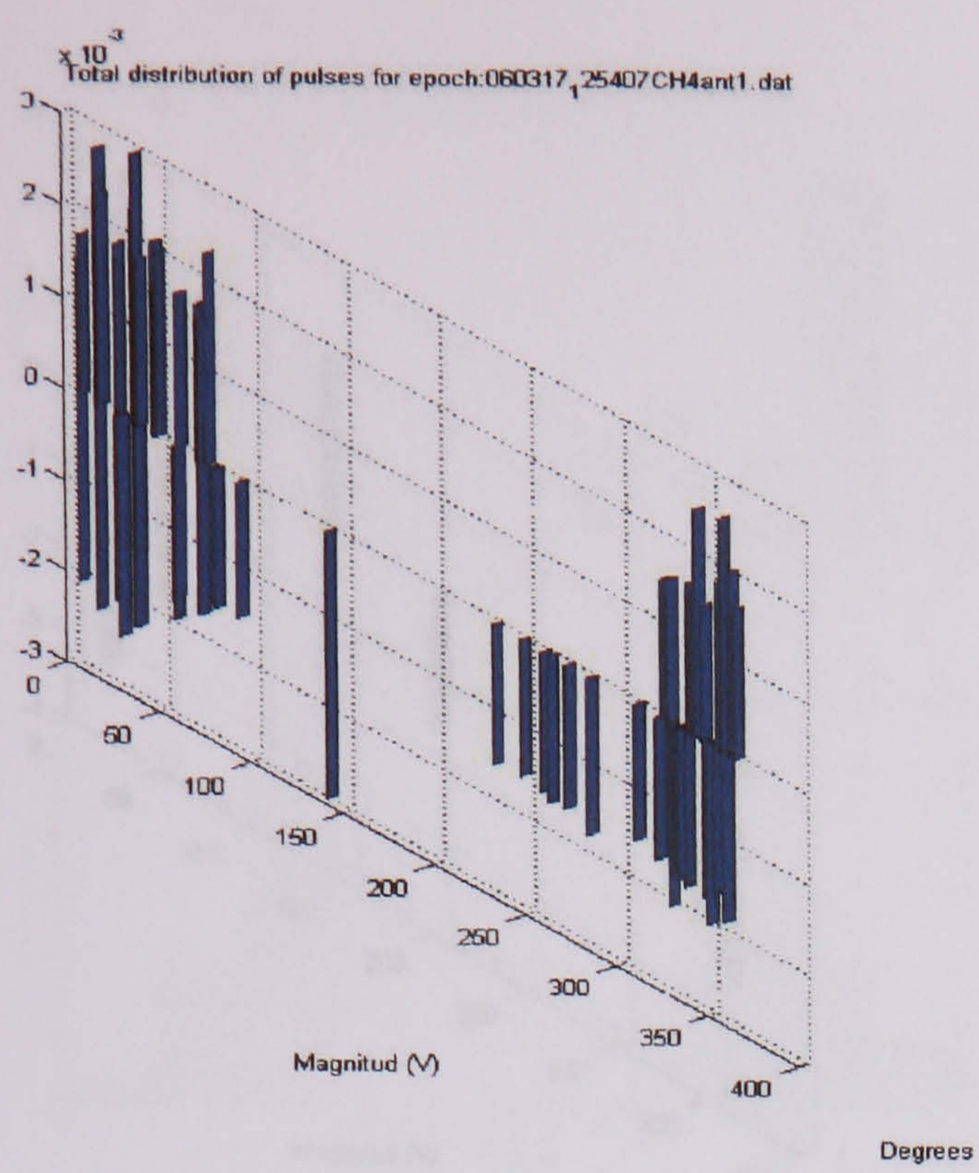

Statistical distribution of cavity discharges at 14320 V test 1 (antenna 1)

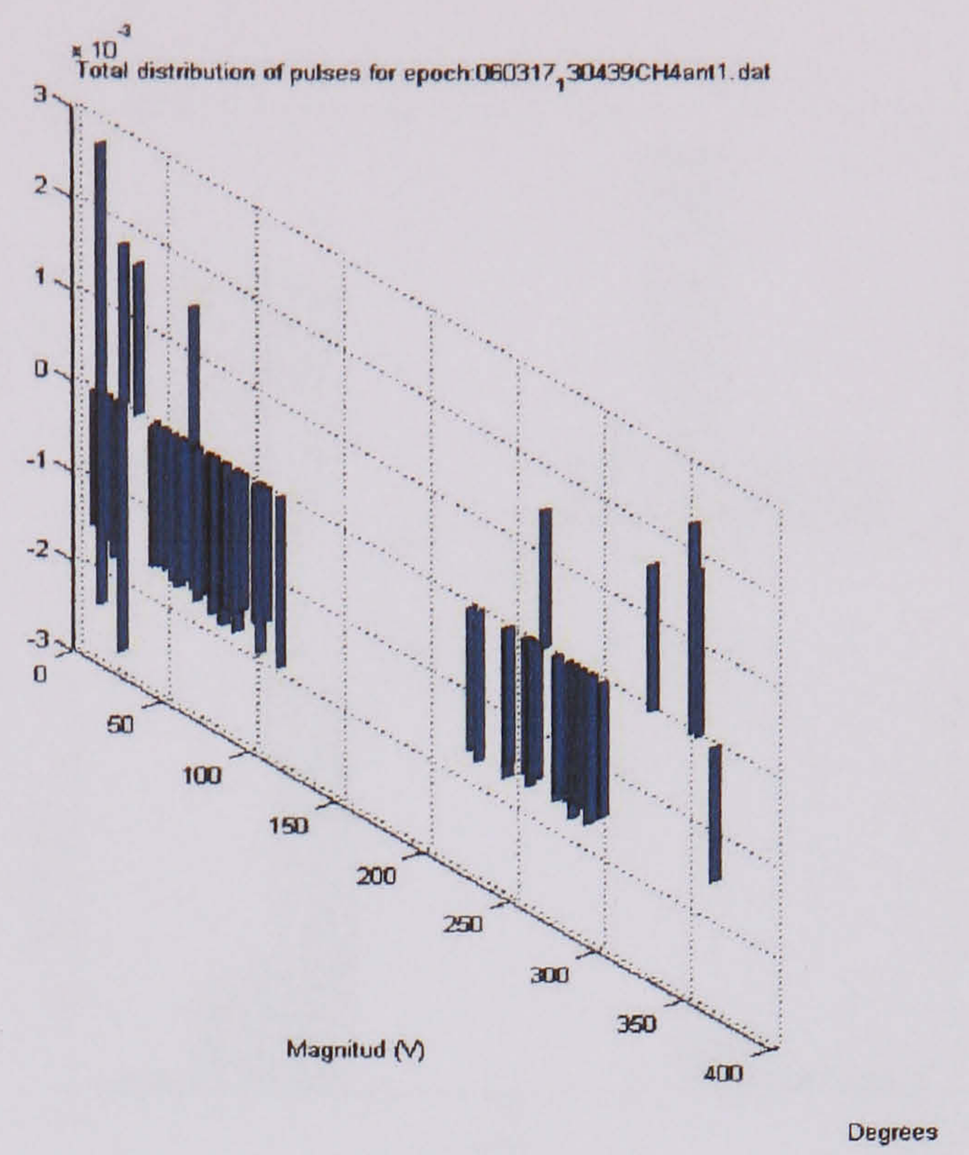

Statistical distribution of cavity discharges at 14320 V test 3 (antenna 1)

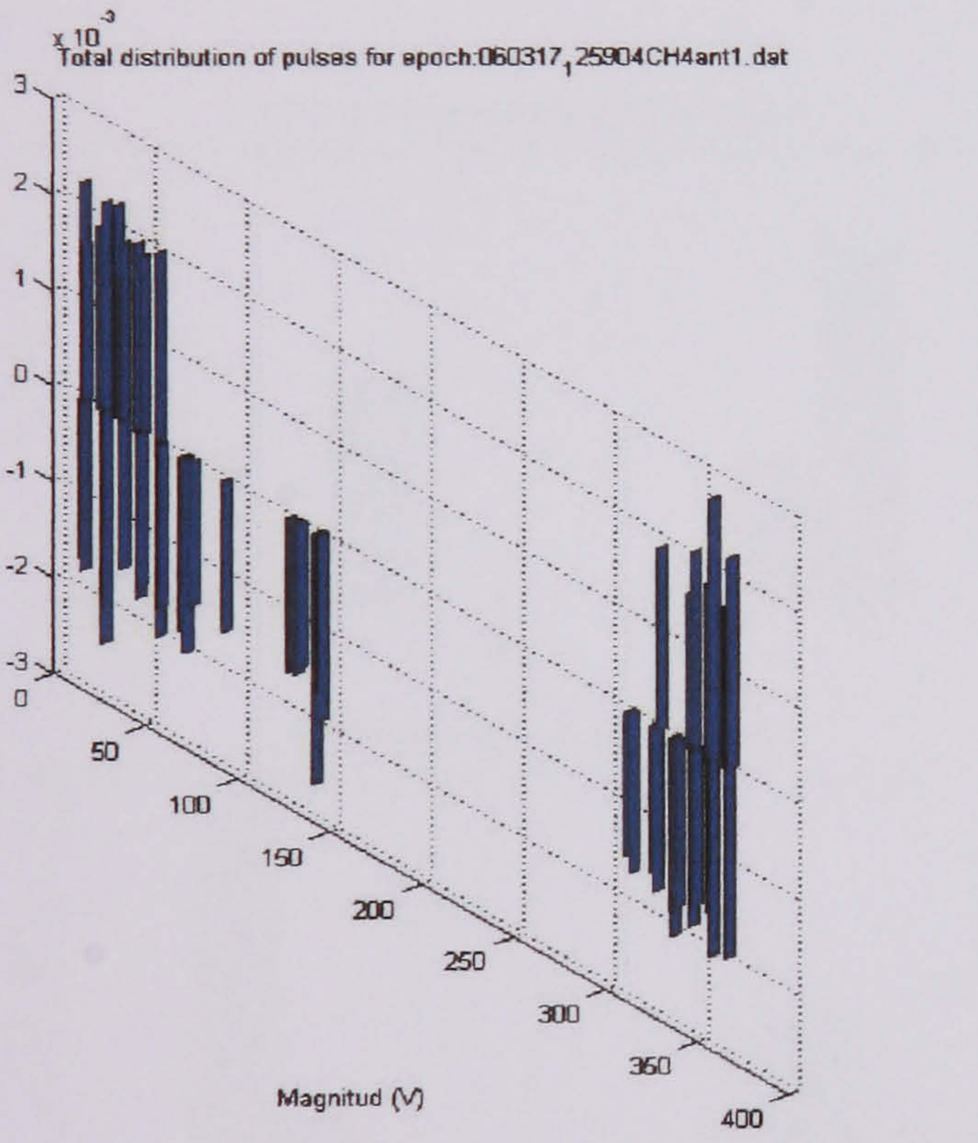

Statistical distribution of cavity discharges at 14320 V test 2 (antenna 1)

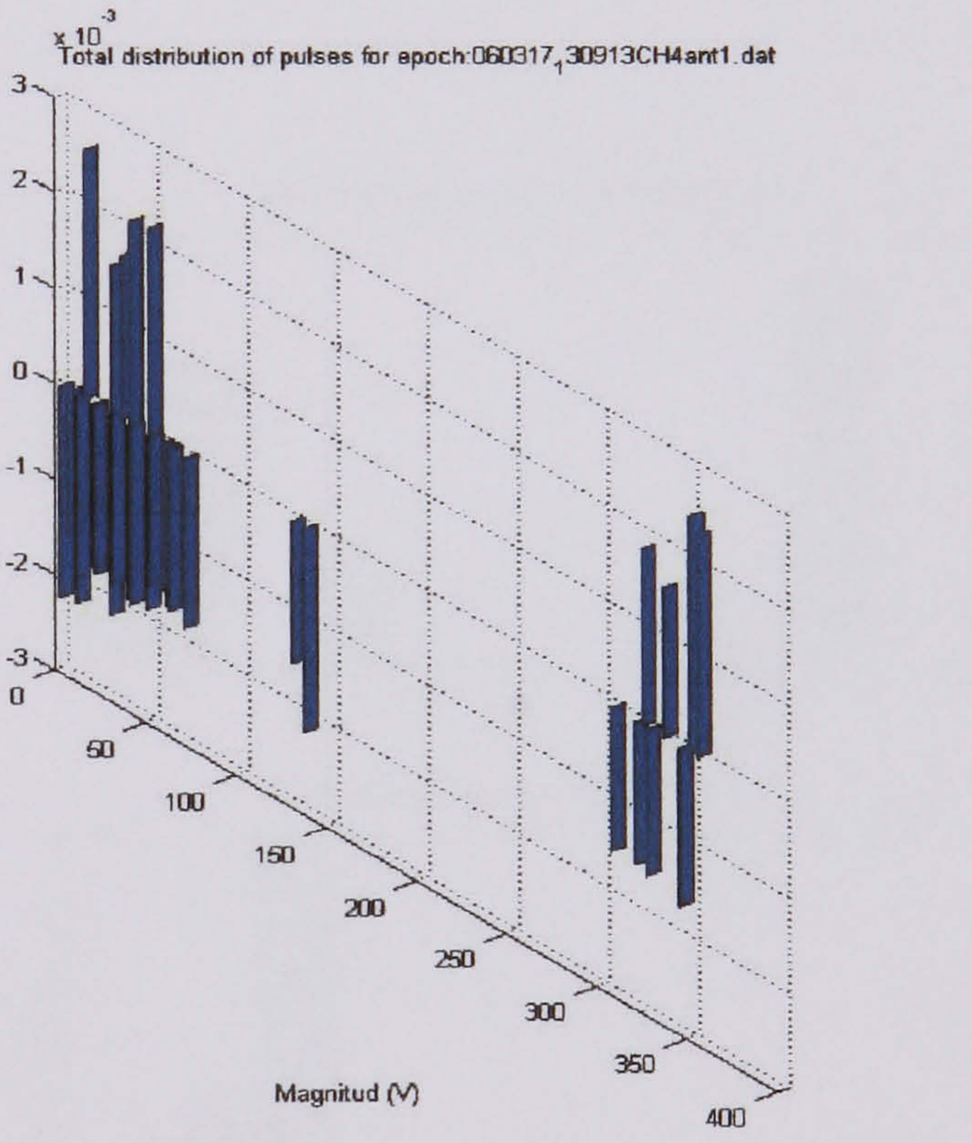

Statistical distribution of cavity discharges at 14320 V test 4 (antenna 1)

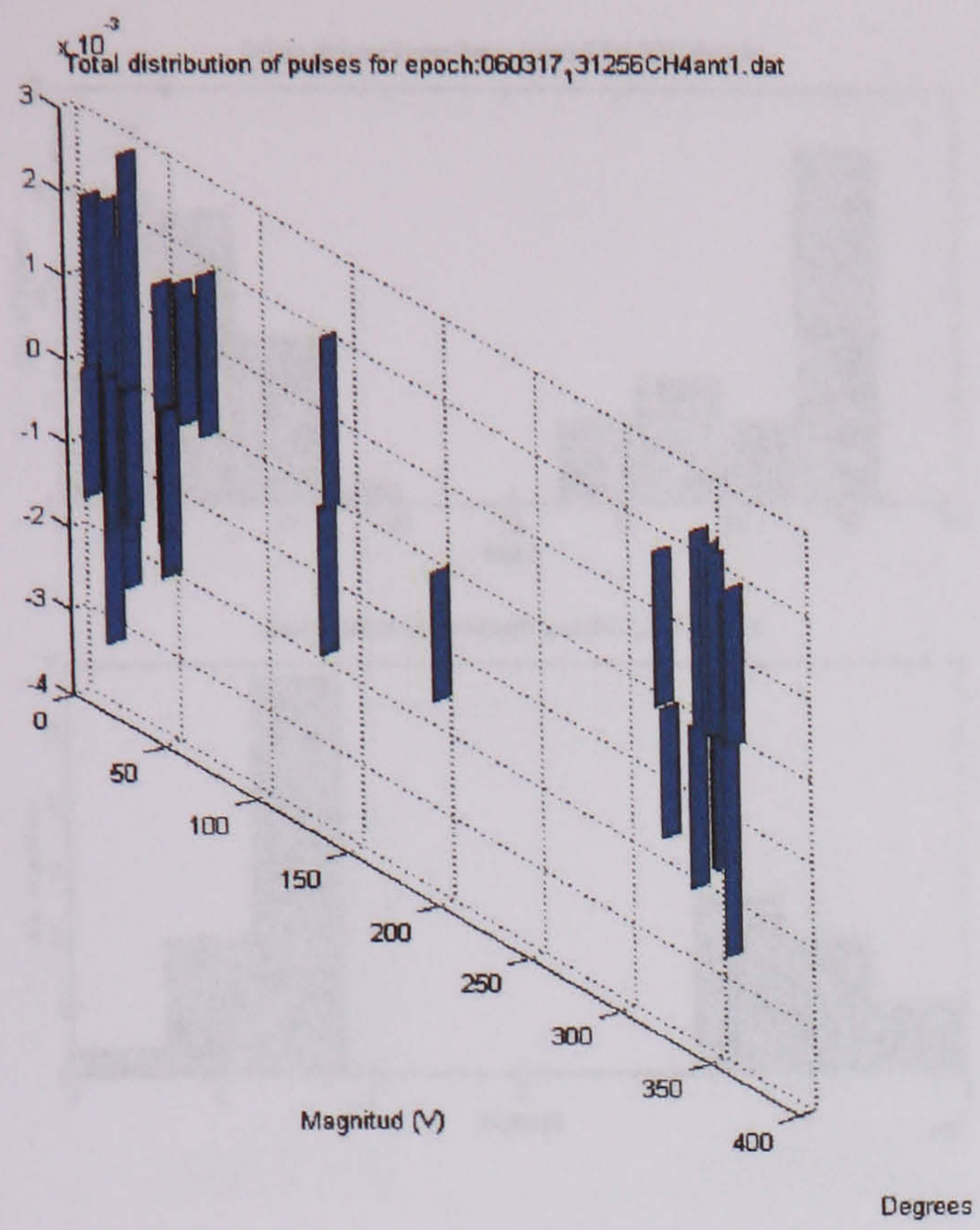

Statistical distribution of cavity discharges at 14320 V test 5 (antenna 1)

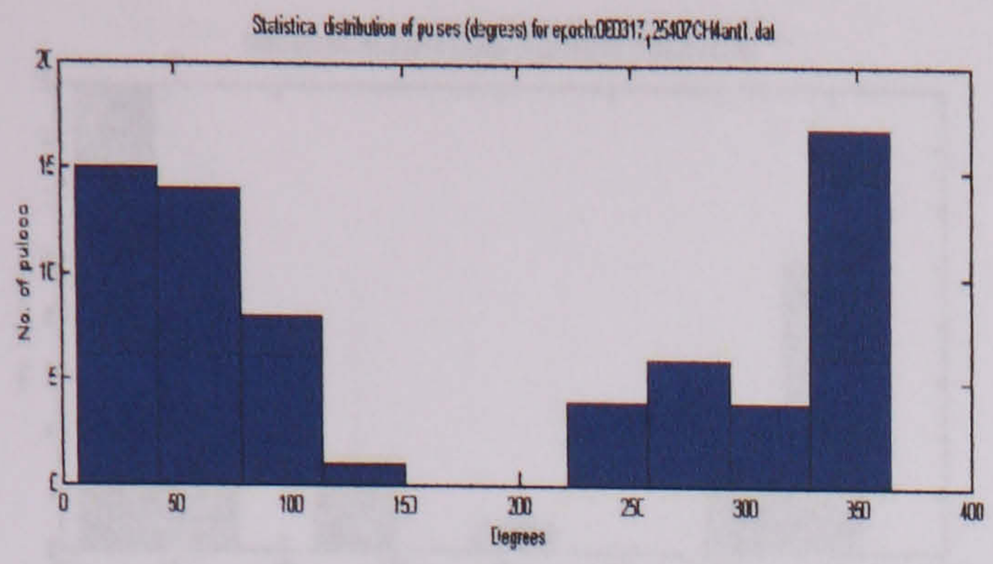

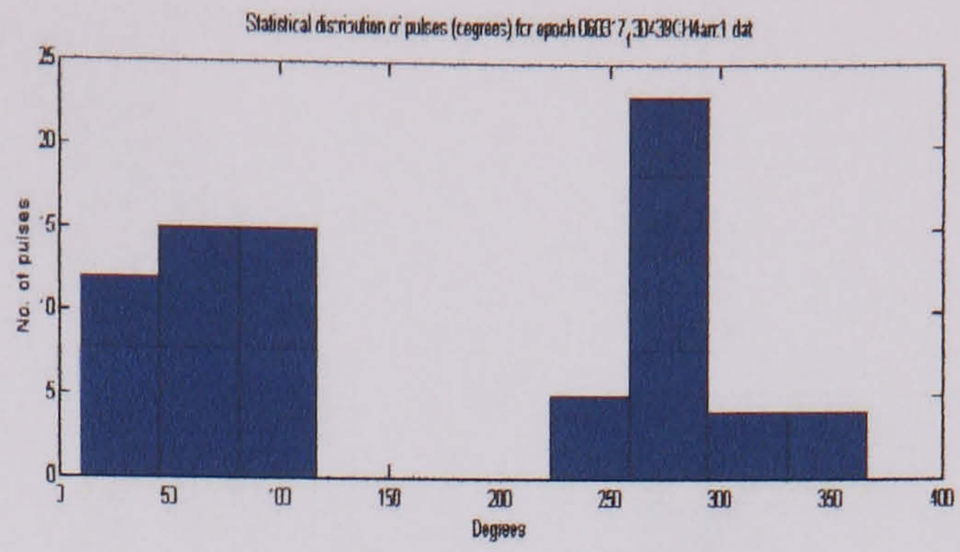

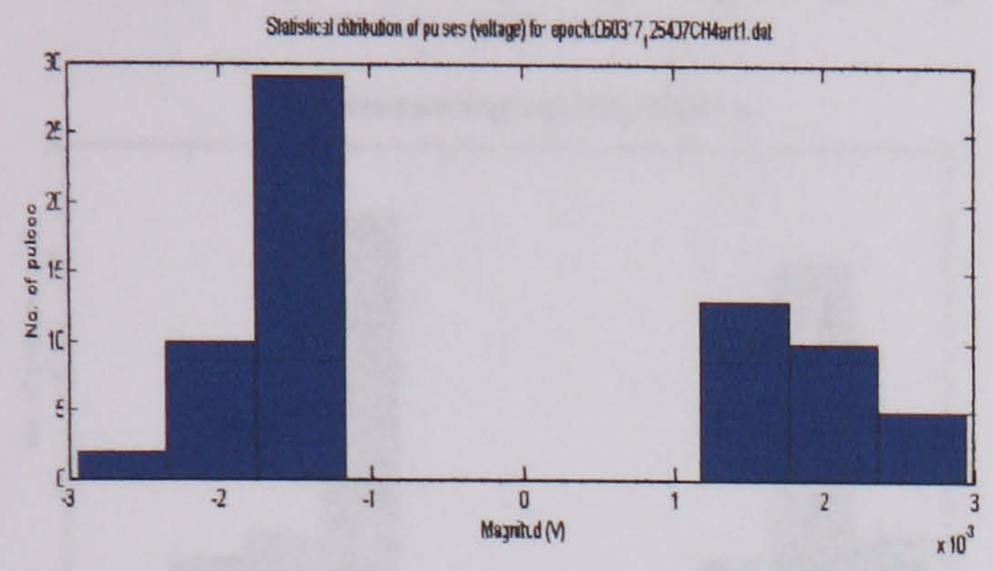

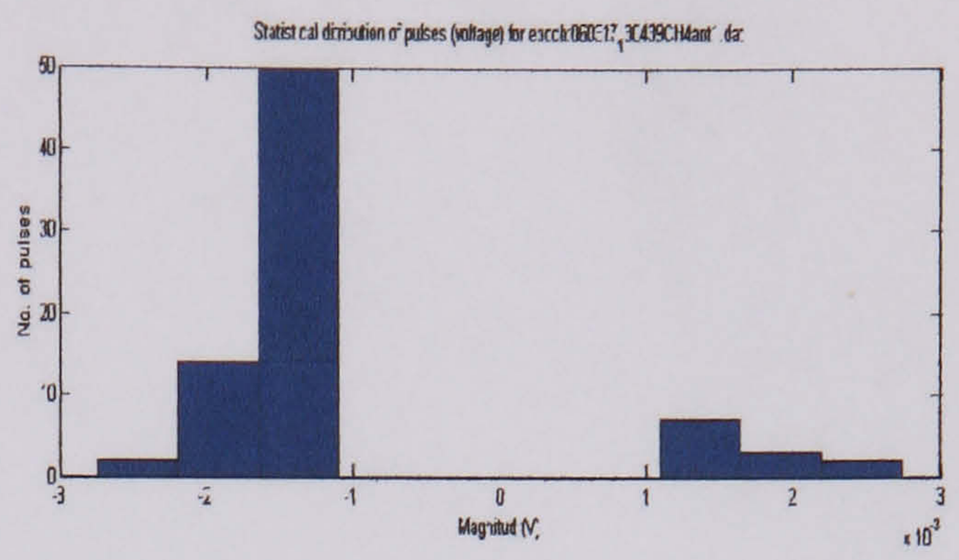

Statistical distribution of cavity discharges at 14320 V test 1 (antenna 1)

Statistical distribution of cavity discharges at 14320 V test 3 (antenna 1)

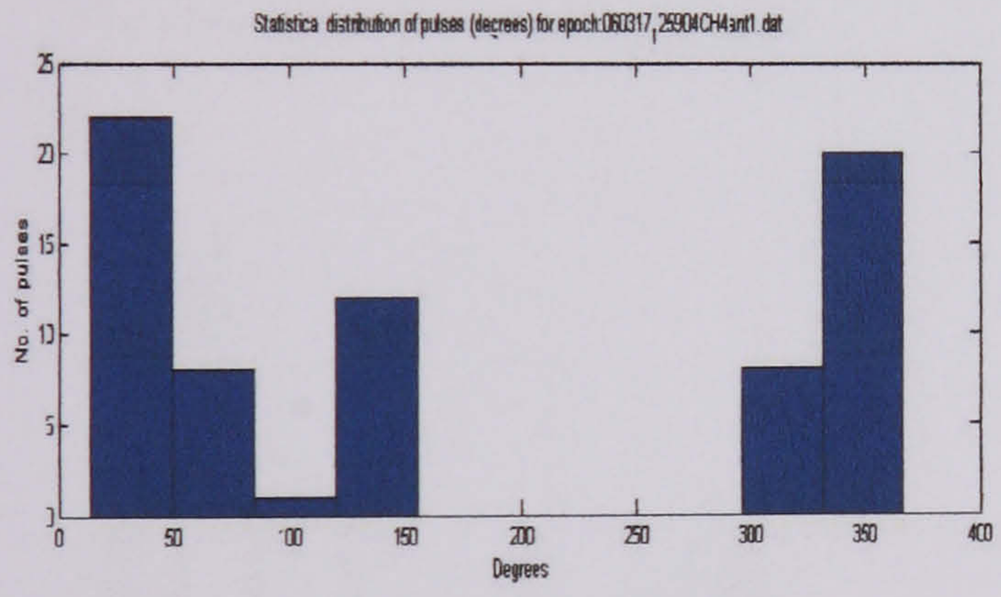

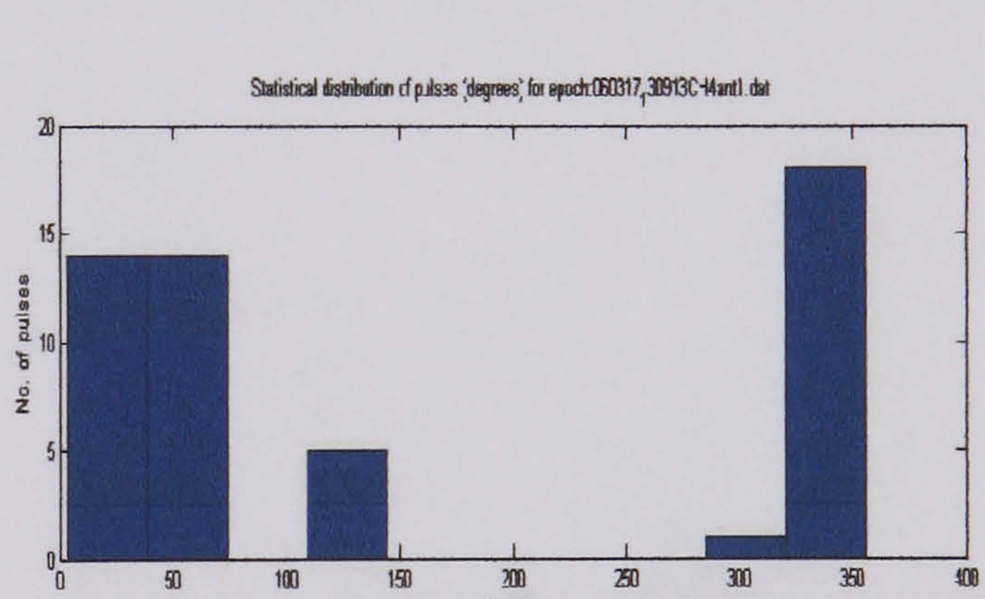

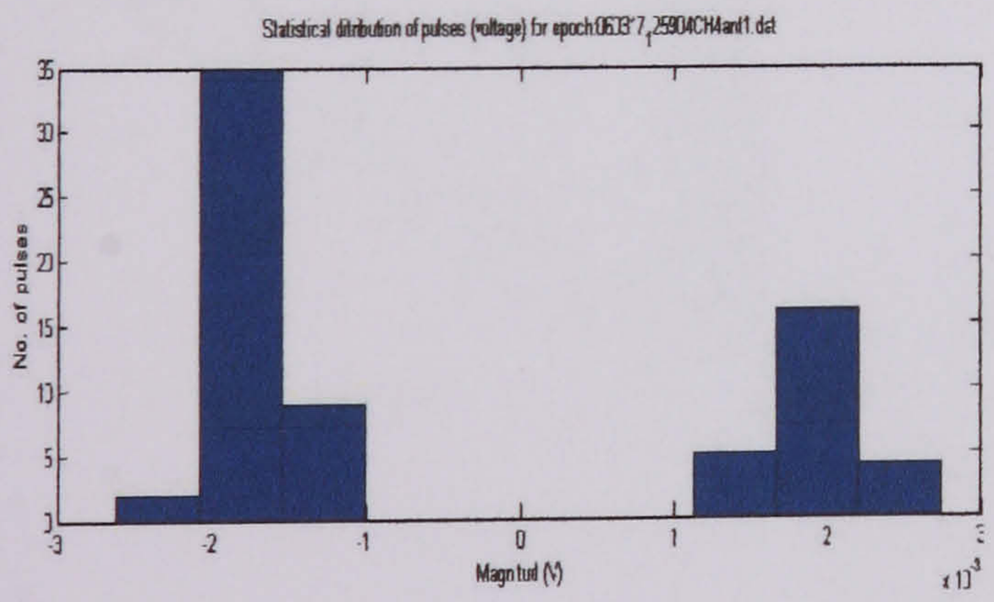

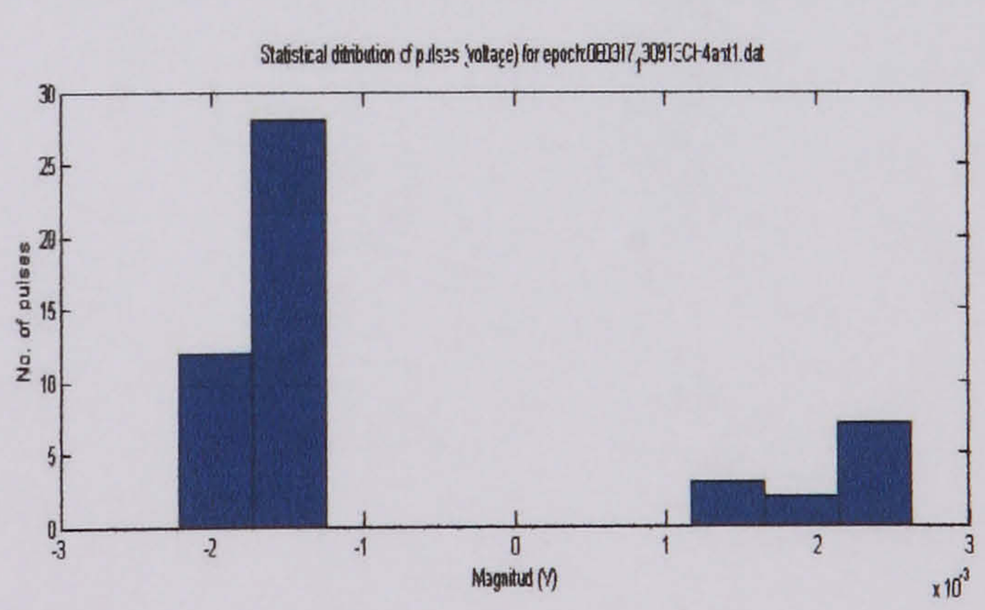

Statistical distribution of cavity discharges at 14320 V test 2 (antenna 1)

Statistical distribution of cavity discharges at 14320 V test 4 (antenna 1)

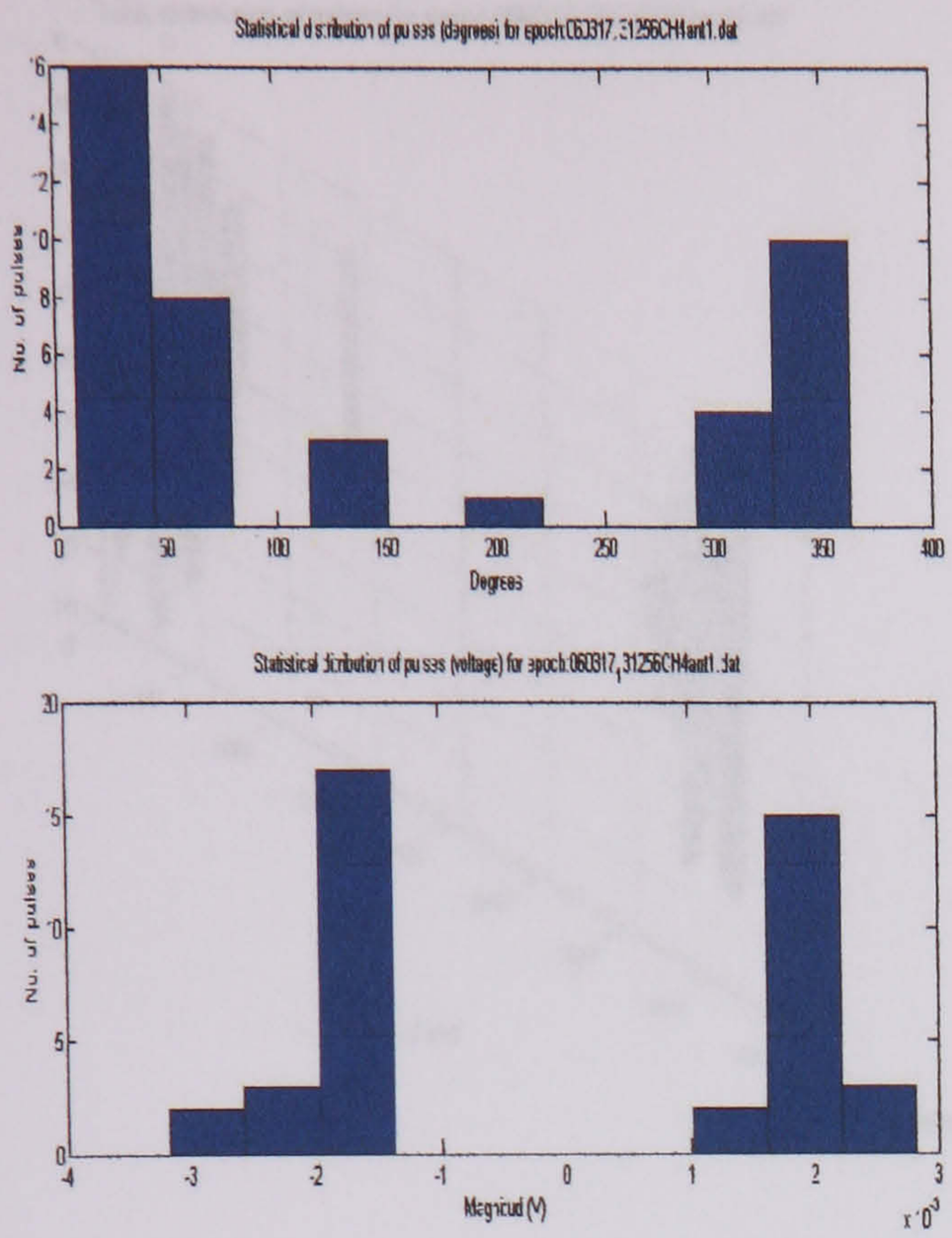

Statistical distribution of cavity discharges at 14320 V test 5 (antenna 1)

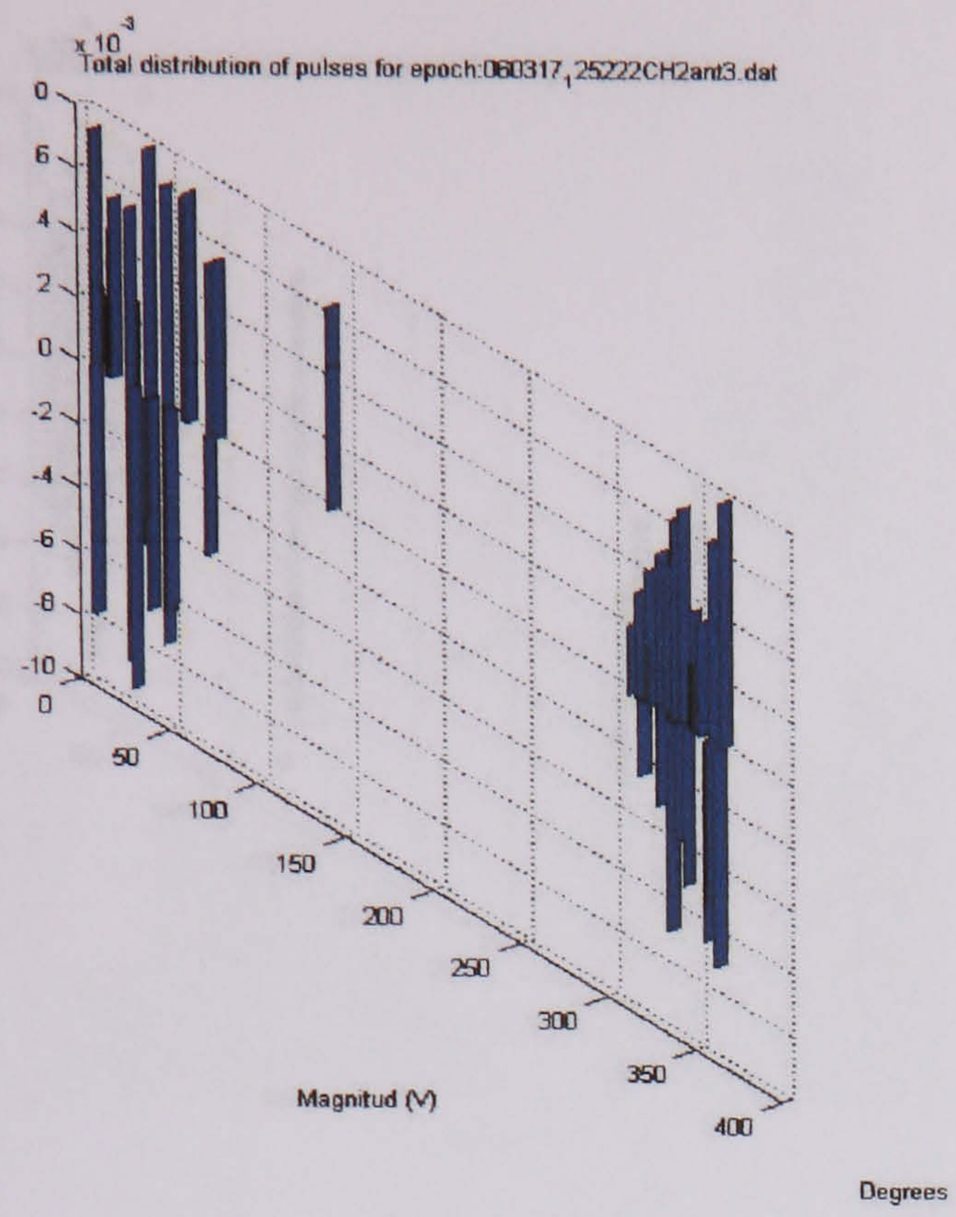

Statistical distribution of cavity discharges at 14320 V test 1 (antenna 3)

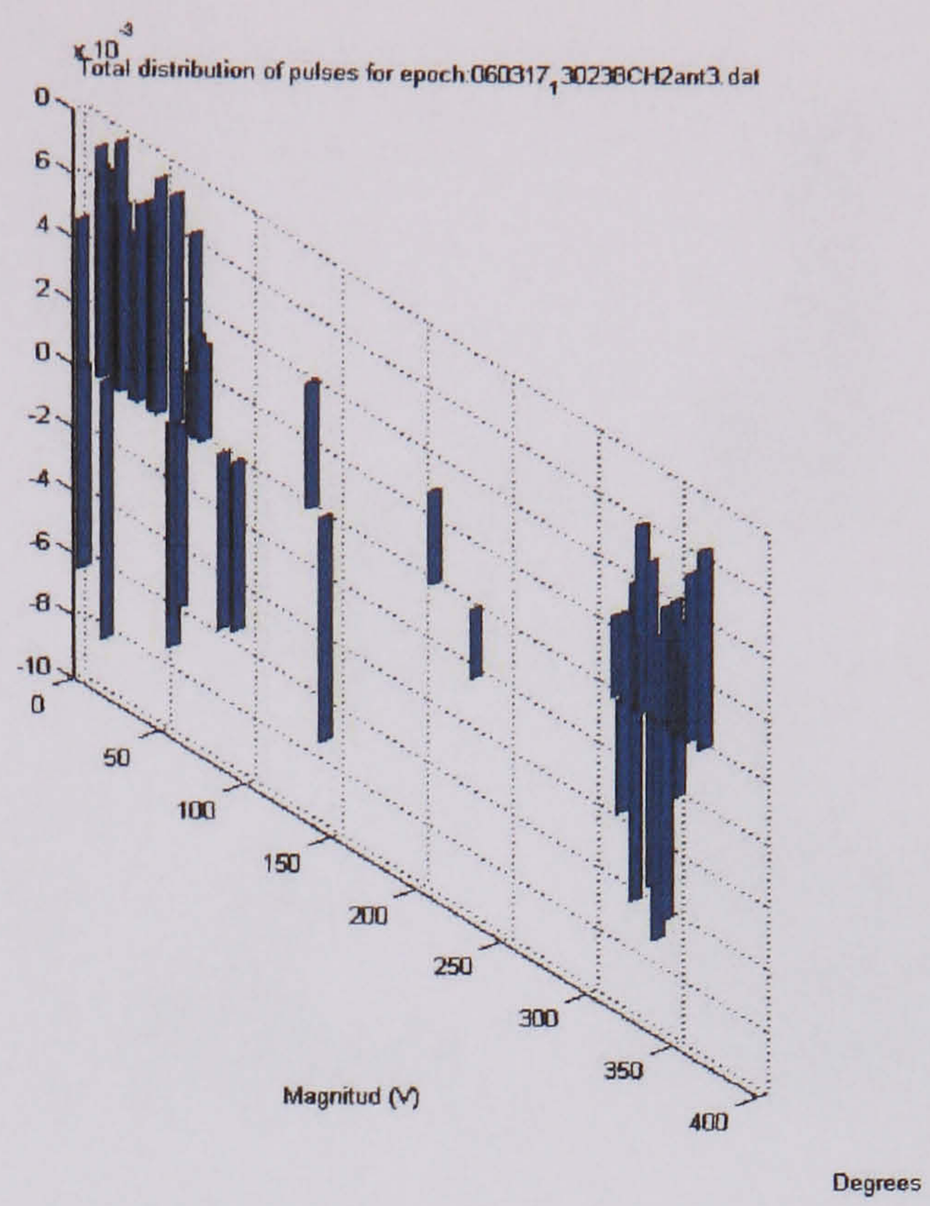

Statistical distribution of cavity discharges at 14320 V test 3 (antenna 3)

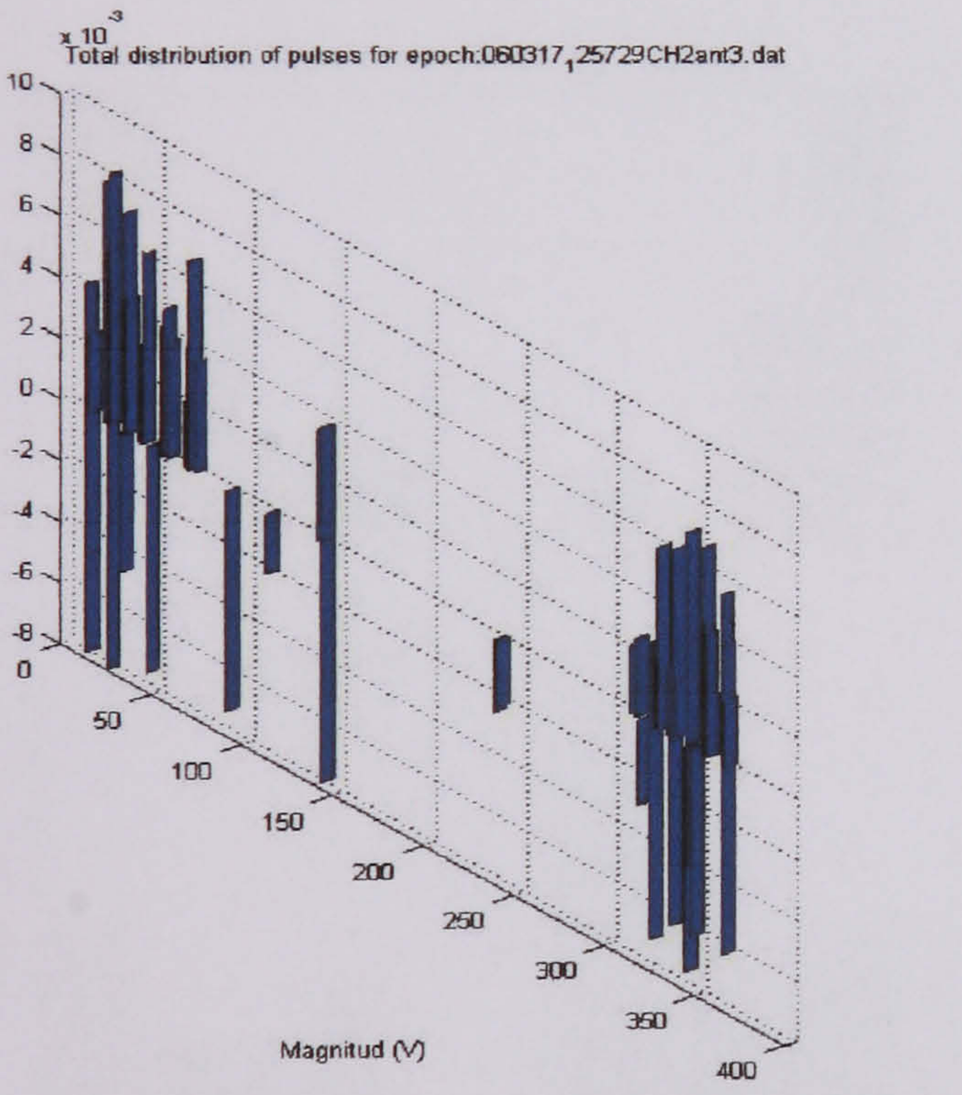

Statistical distribution of cavity discharges at 14320 V test 2 (antenna 3)

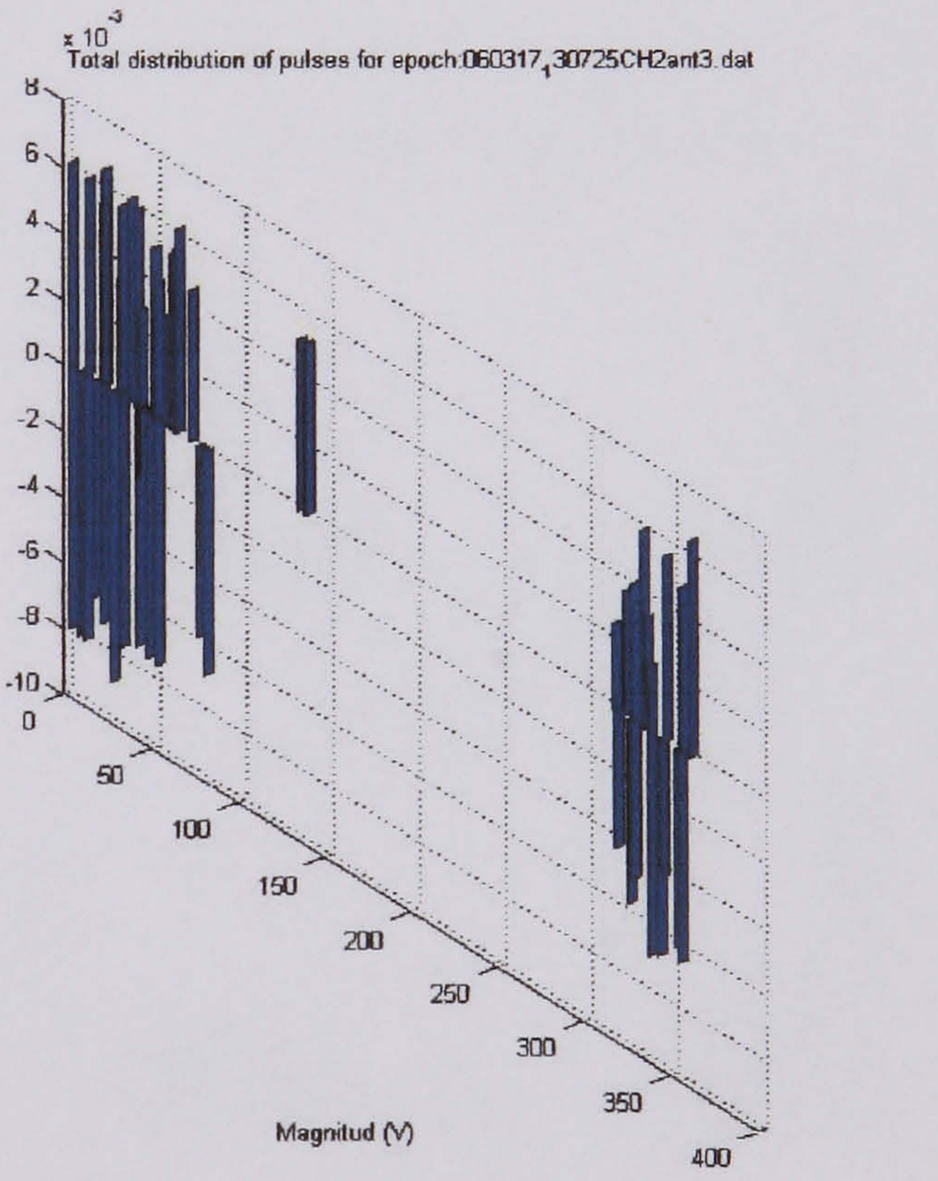

Statistical distribution of cavity discharges at 14320 V test 4 (antenna 3)

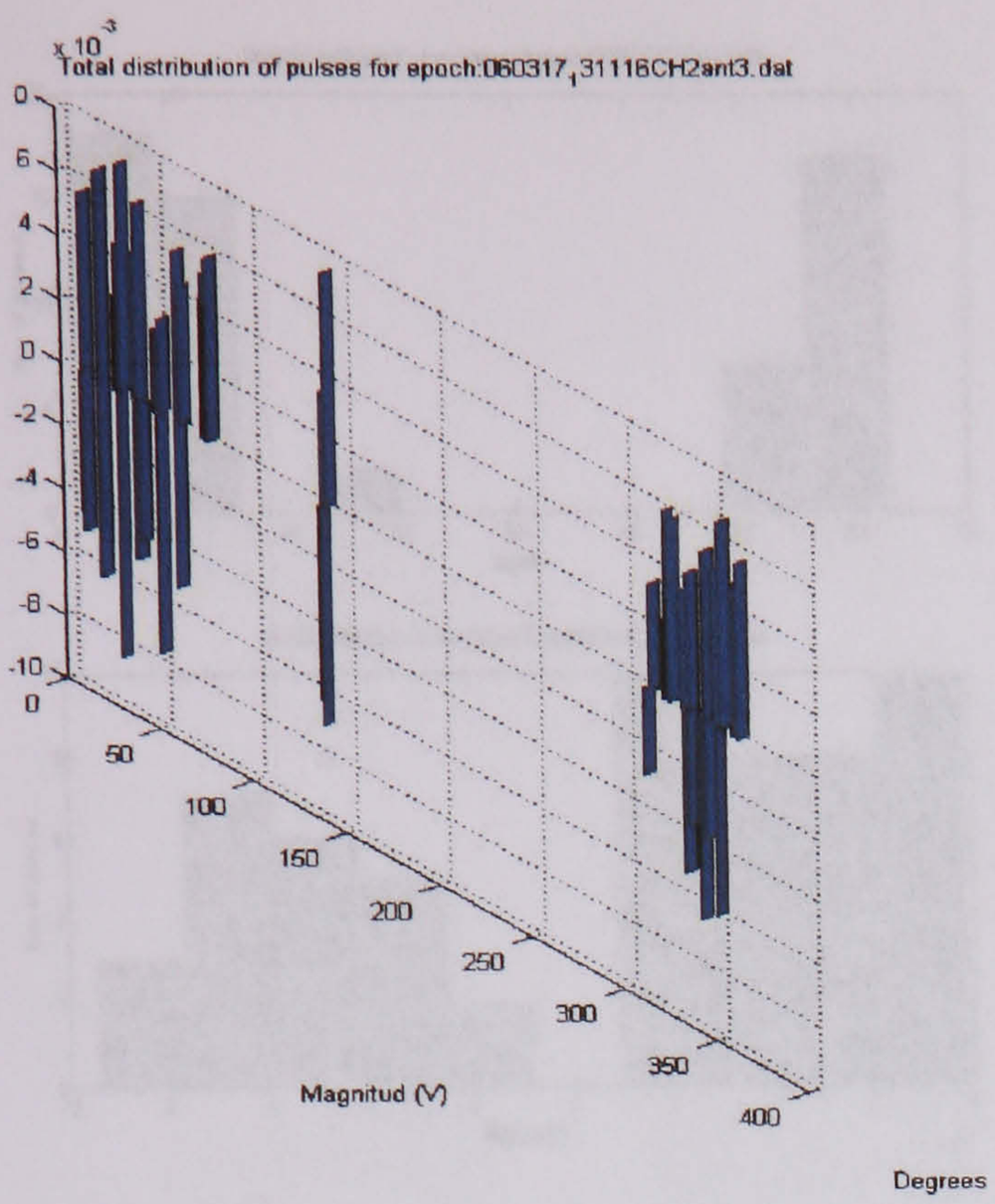

Statistical distribution of cavity discharges at 14320 V test 5 (antenna 3)

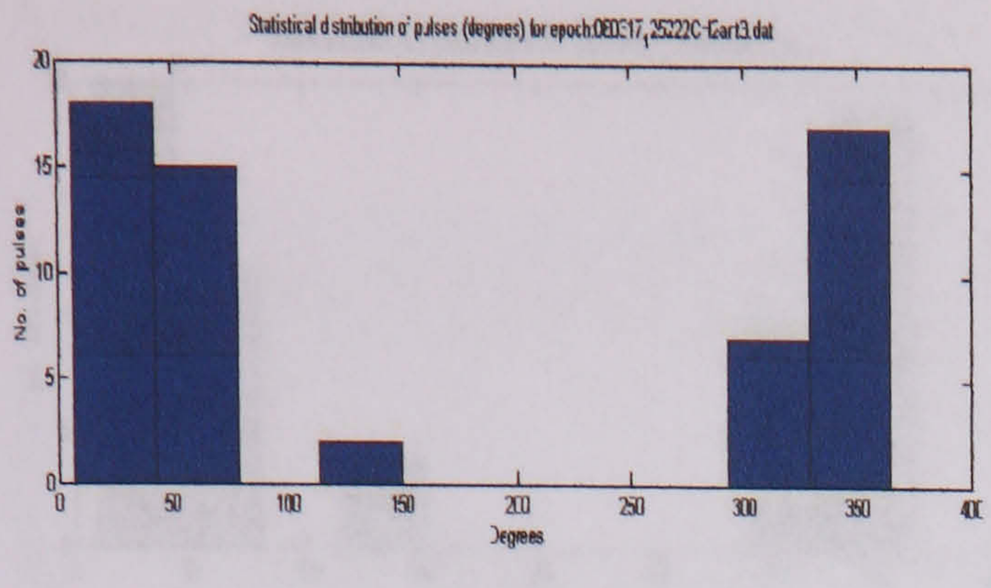

Statistical distribution of cavity discharges at 14320 V test 1 (antenna 3)

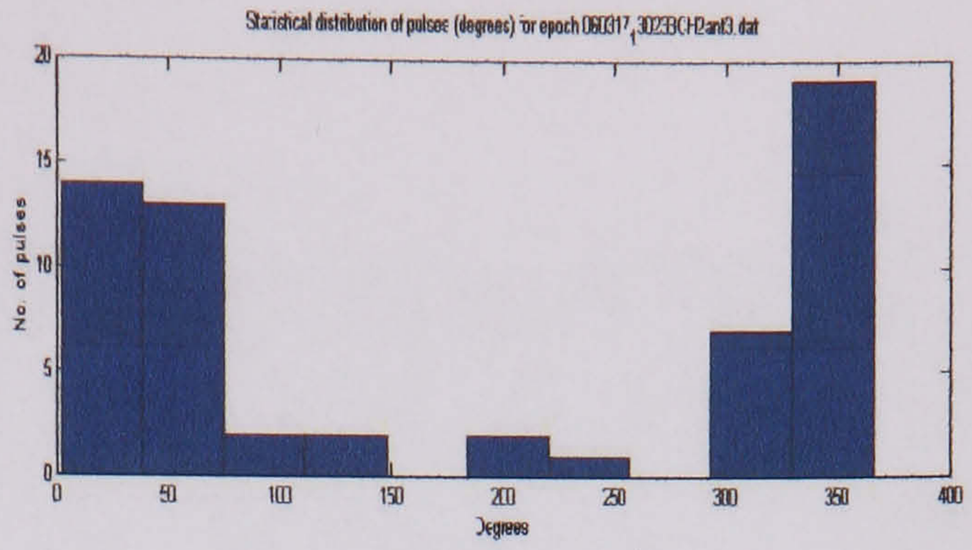

Statistical distribution of cavity discharges at 14320 V test 3 (antenna 3)

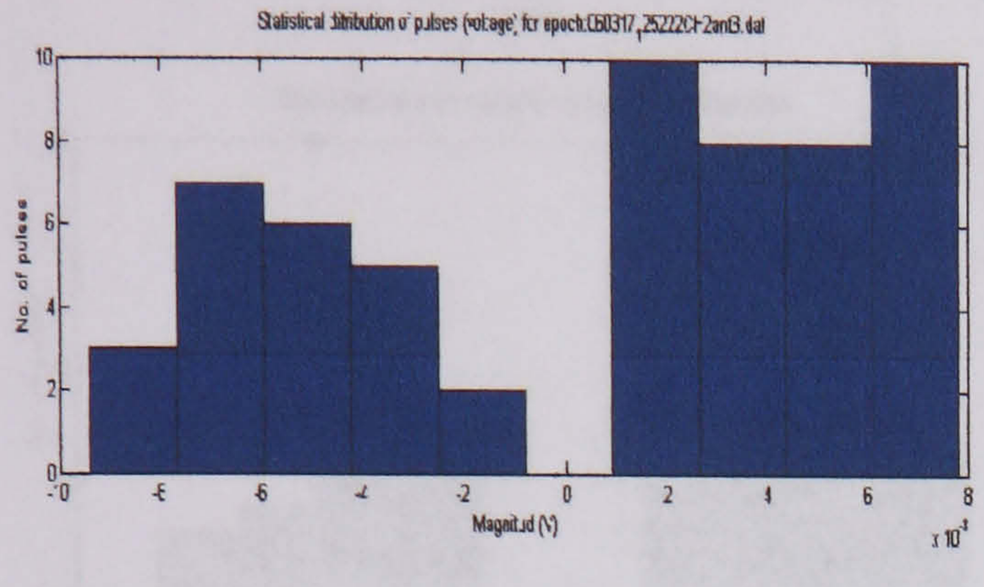

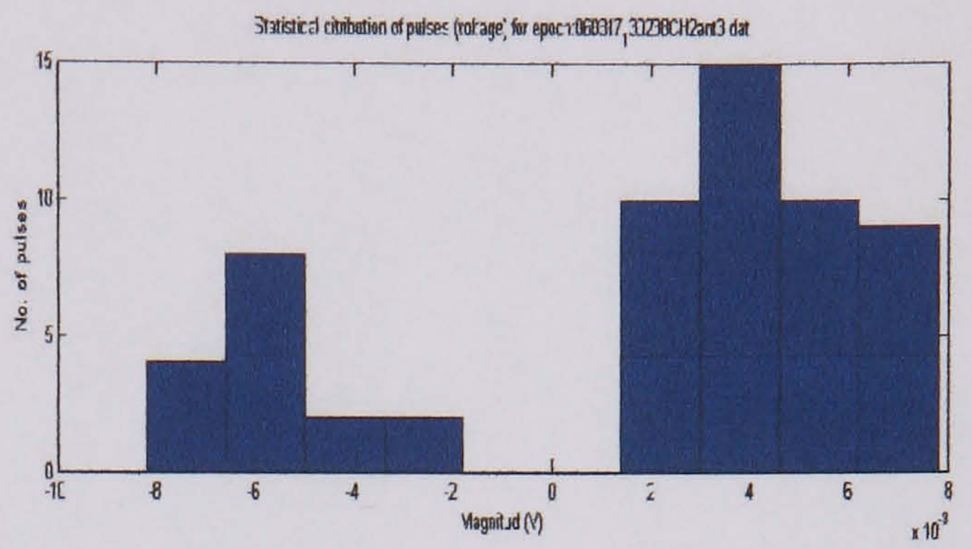

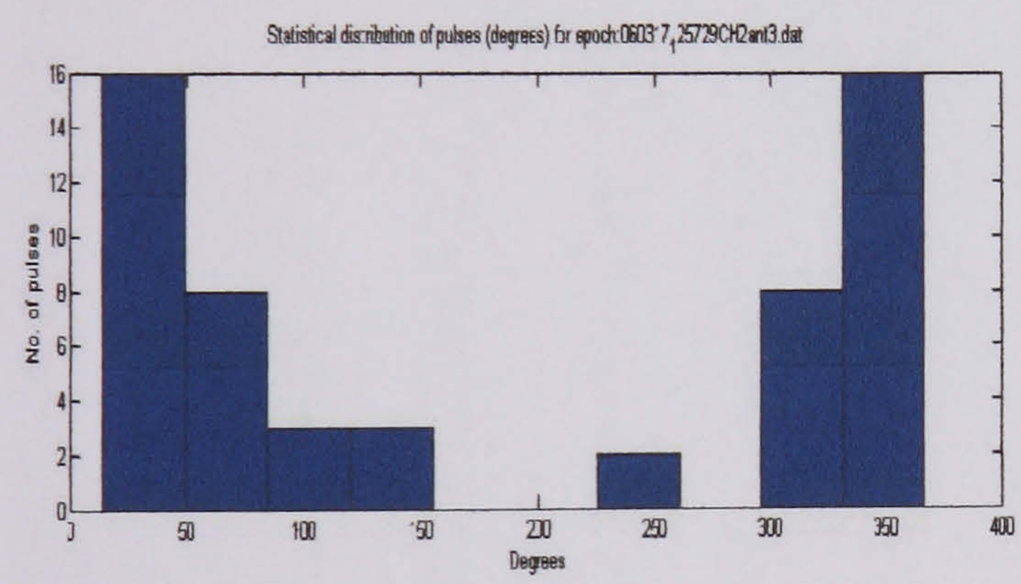

Statistical distribution of cavity discharges at 14320 V test 2 (antenna 3)

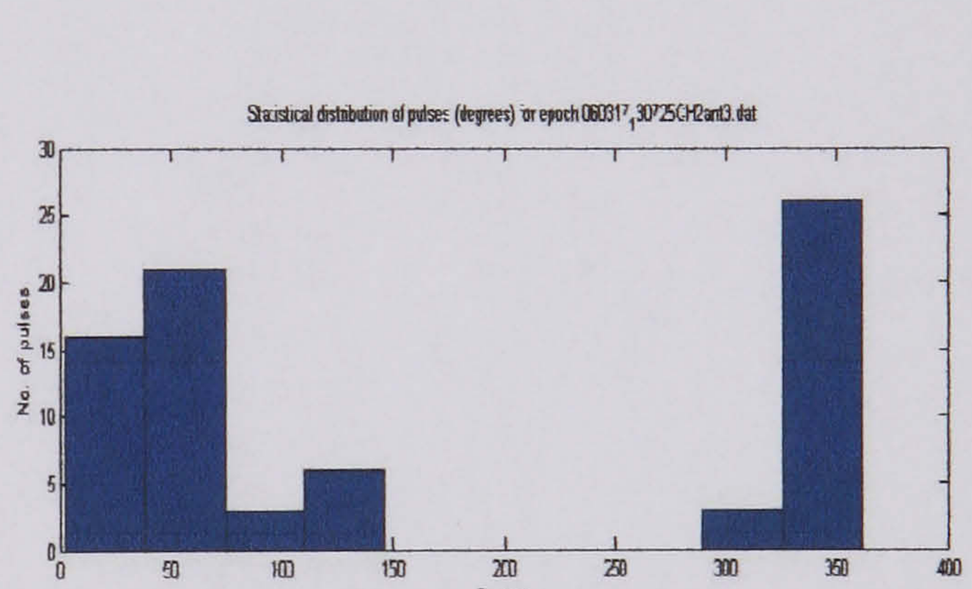

Statistical distribution of cavity discharges at 14320 V test 4 (antenna 3)

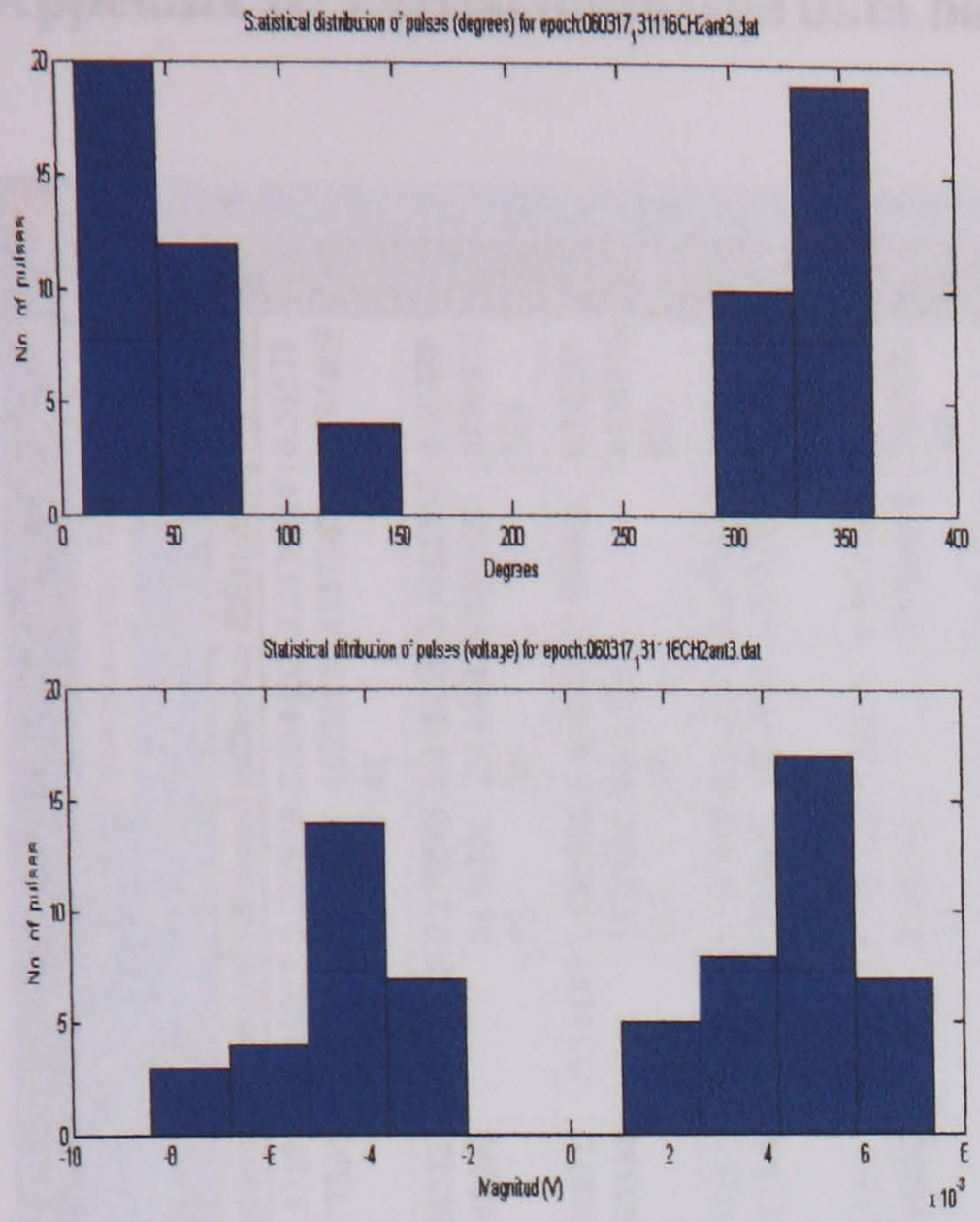

Statistical distribution of cavity discharges at 14320 V test 5 (antenna 3)

Microsoft Access - [pds : Table]

File Edit View Insert Format Records Tools Window Help Adobe PDF

Type a question for help

No	PD_Type	Epoch_no	skewness	skewness	kurtossis	kurtossis	skewness	skewness	kurtossis	kurtossi	correlatio	differenc	differenc	difference	distance
1	Agedins	060502_160620CH1resist.dat	0.520929	-0.94604	1.562937	3.274222	0.930395988106447	2.69348748878294	2.65946974847576	12.171903773314	-0.18018	0.2079395	0.4544028623188 41	3.04702194357367	0.535731184403 34
2	Agedins	060502_160709CH2ant1.dat	0.900499	1.299674	2.418885	5.270313	0.783072446720849	0.27452265783842 6	2.18495611267255	4.6818214886904 41	-0.1506	0.2705030170301 95	0.4784292014468 56	3.33825079030559	0.494896890972 123
3	Agedins	060502_160854CH4ant3.dat	0.882507	1.408442	2.912361	6.114039	1.271675836707 67	0.09648587909695 36	6.00850567819347	3.5987112953362 4	-0.15137	0.0904665125652 255	0.6316428571428 57	7.539961	0.562314426133 833
4	pressboard	060419_160732CH1resist.dat	0.044194	0.738712	1.105647	4.014121	-0.469961391629209	0.33692178495735 8	1.73661173275649	2.0716700825416 6	0.080033	0.1914566666666 67	0.2141431034025 58	1.01187403200826	0.305796063726 666
5	pressboard	060419_160832CH2ant1.dat	-0.04935	-0.07764	1.146811	2.335676	0.813363965796815	-0.67039502938157	2.54382205460698	2.4180141883912	-0.2281	0.1563233333333 33	0.35319	0.939130434782609	0.321077012104 307
6	pressboard	060419_161016CH4ant3.dat	-1.56409	1.280643	4.128375	5.467513	0.259119335050632	-0.38368075031288	1.74592848170169	3.2260157095970 2	0.143752	0.24012	0.32332	0.588619855495137	0.452829529425 028
7	Cavity	060317_131031CH1resist.dat	0.131895	-0.50240	1.683564	2.068132	1.21829815236855	-1.16684827782058	3.36893101428958	3.1199325455151 9	-0.14362	0.1964889556851 32	0.2200006492506 16	0.164366883116883	0.749309845040 817
8	Cavity	060317_131256CH4ant1.dat	-0.13964	-1.36419	1.536041	3.606024 92961294	-0.238781629927998	0.13217923795019 8	1.89641383343454	1.4904349811902 2	0.151592	0.2952613333333 33	0.4059709070174 43	0.274661508704062	0.522914174711 882
9	Cavity	060317_131116CH2ant3.dat	-1.38803	-0.25982	3.169703	1.402542	-0.018672368713564	-0.22599575819170	2.00057989003797	1.3529741477312 1	-0.01294	0.1248652	0.3090596141510 54	0.357367475292004	0.696459434432 939
10	Corona	115641CH1.dat	-0.40073	33.16377	4.383006	1360.698	-2.30160391891168	0.50243596663767 3	6.63929564753643	1.5375195986990 6	-0.32276	0.0980055	0.0298109527131 783	4.47795505038103	0.527620834003 609
11	Newins	130538CH1.dat	-0.39166	-0.70711	1.5	1.5	-0.160515974822418	1.2974719890667	2.41764041543551	4.0656252190011	-0.72732	0.0711973348169 23	0	3.7992277992278	0.530724110223 638
*															

Record: 8 of 11

Datasheet View

Appendix I: Graphical representation of statistical operators

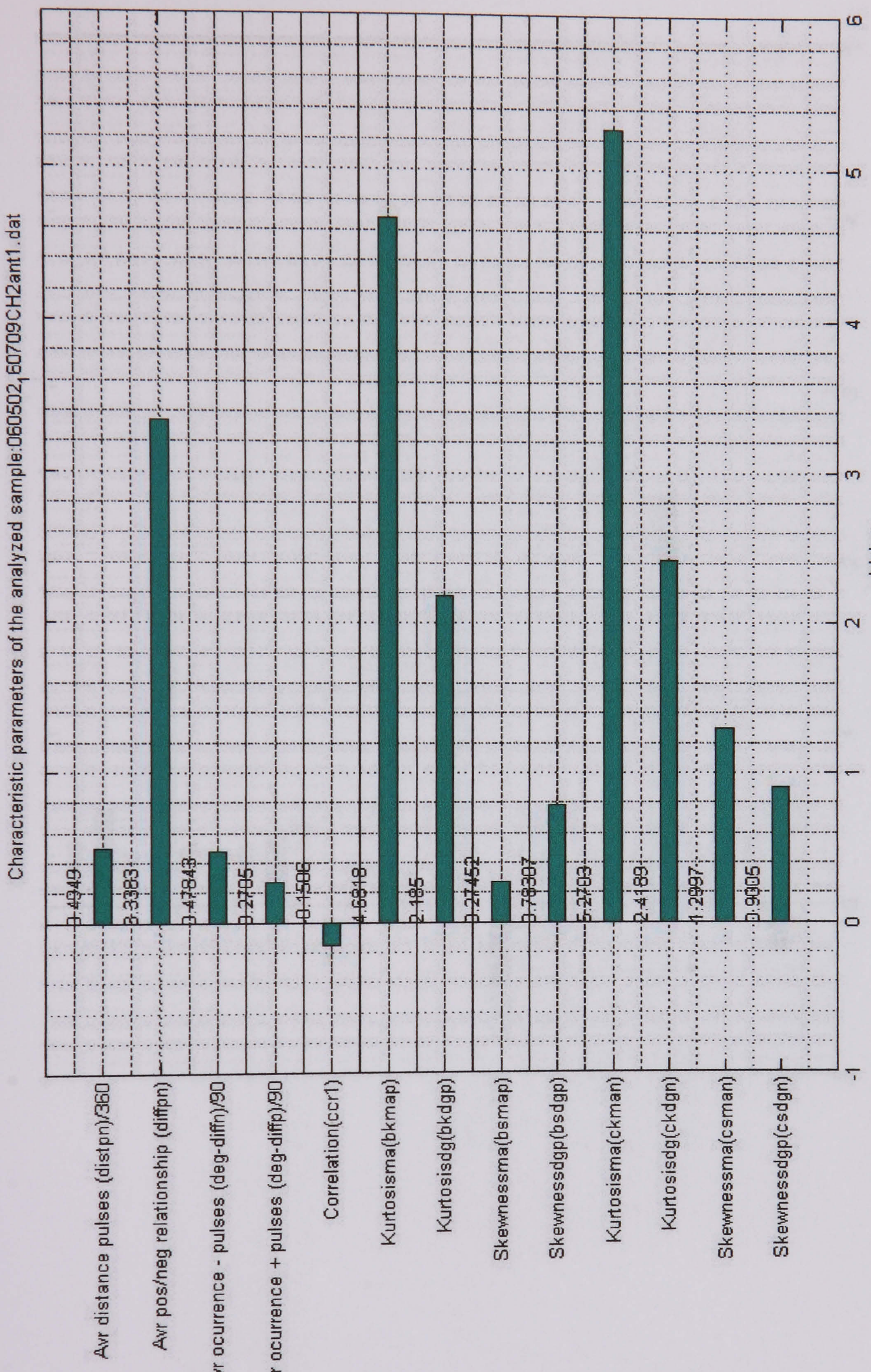

Graphical representation of statistical operators for an aged insulator in antenna 1

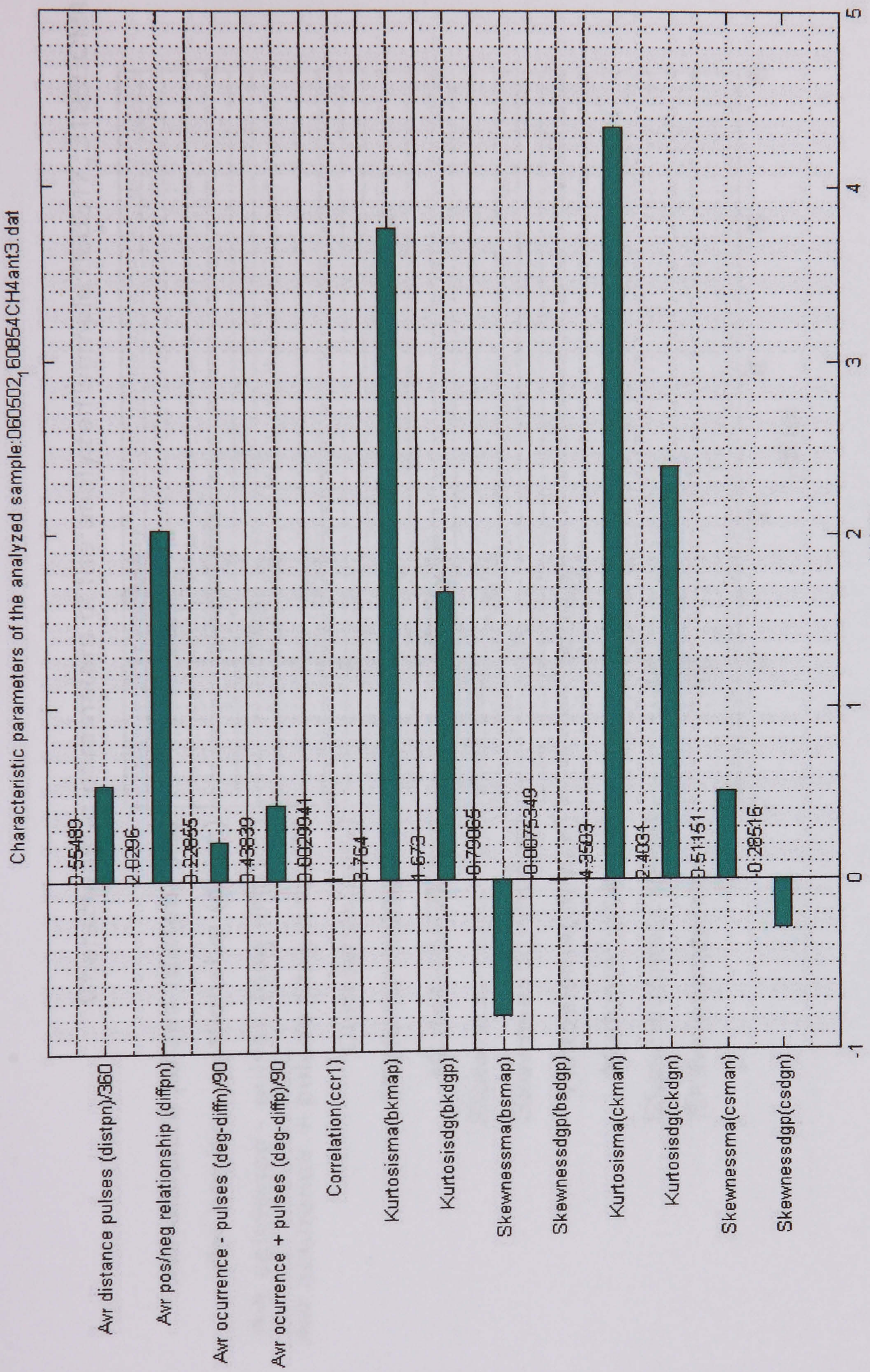

Graphical representation of statistical operators for an aged insulator in antenna 3

Graphical representation of statistical operators for cavity discharges in antenna 1

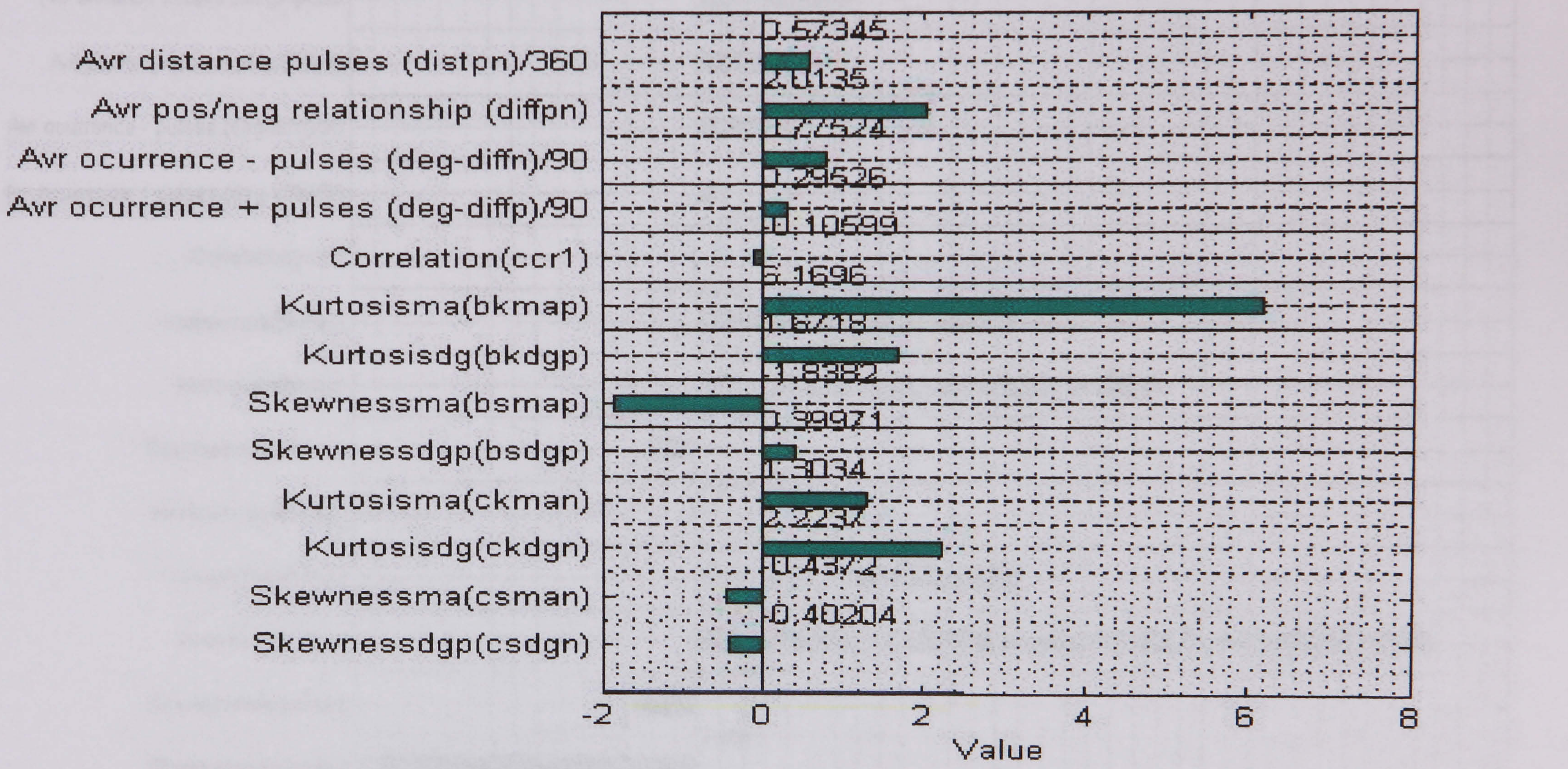

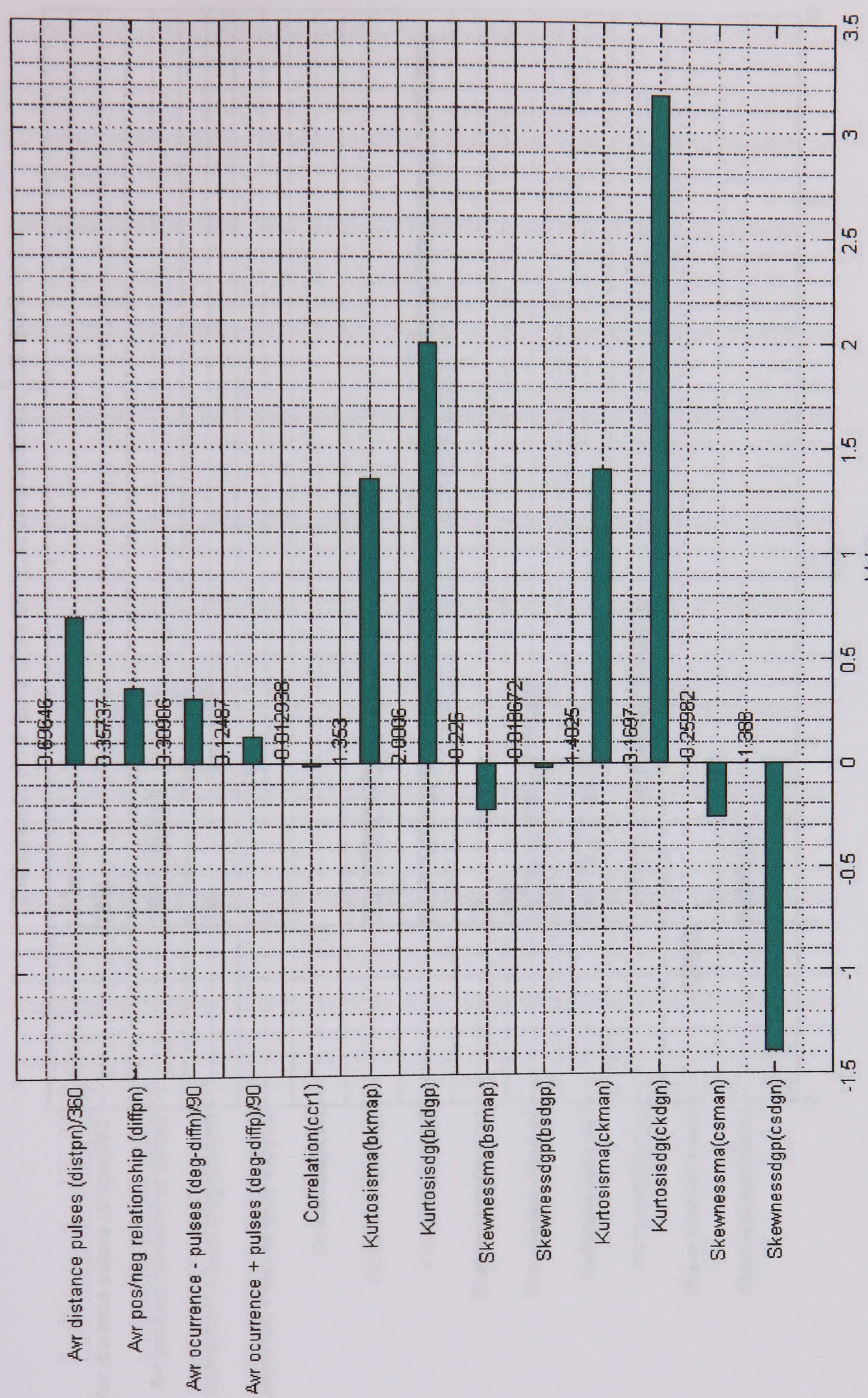

Graphical representation of statistical operators for cavity discharges in antenna 3

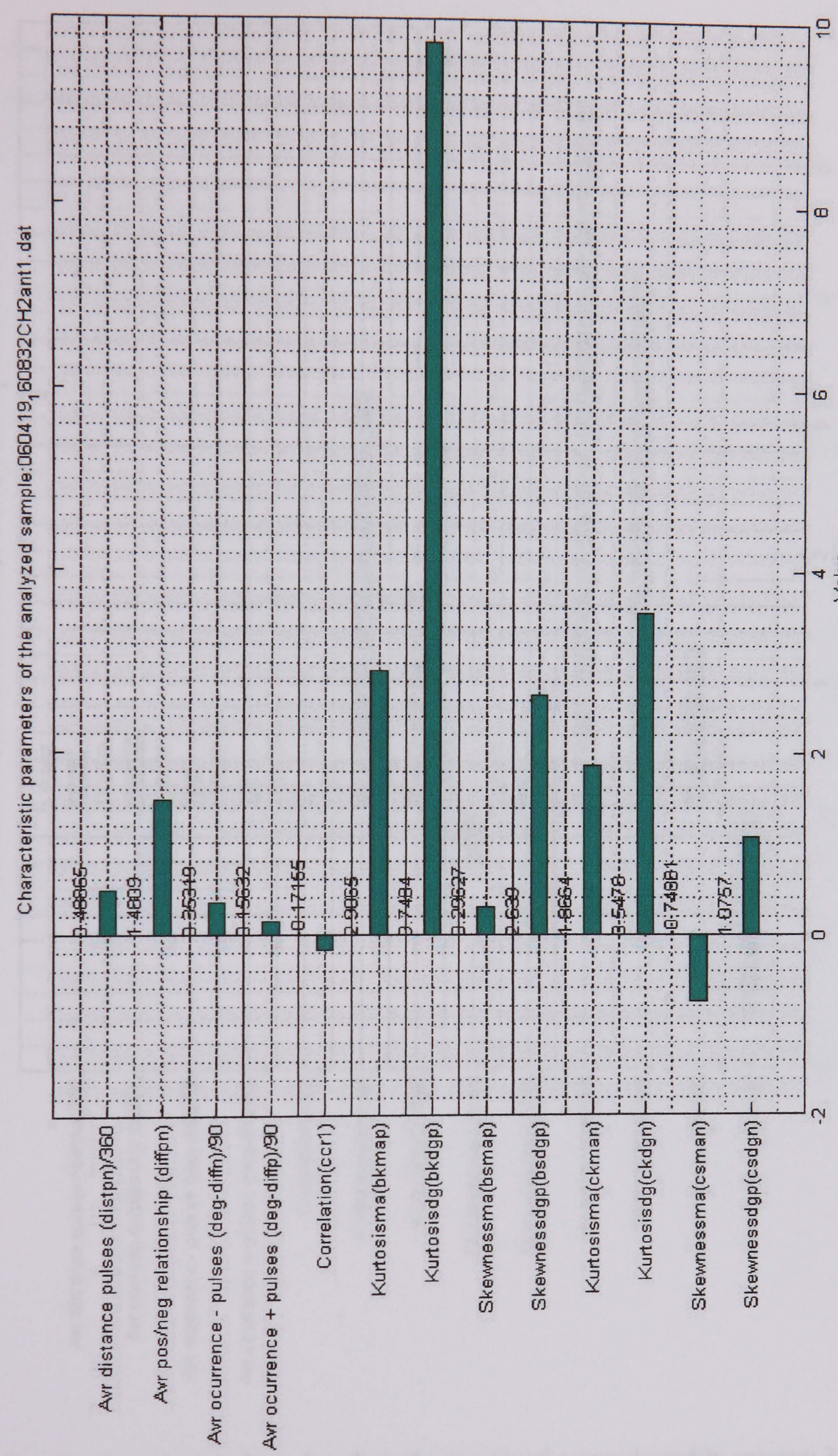

Graphical representation of statistical operators for pressboard in antenna 1

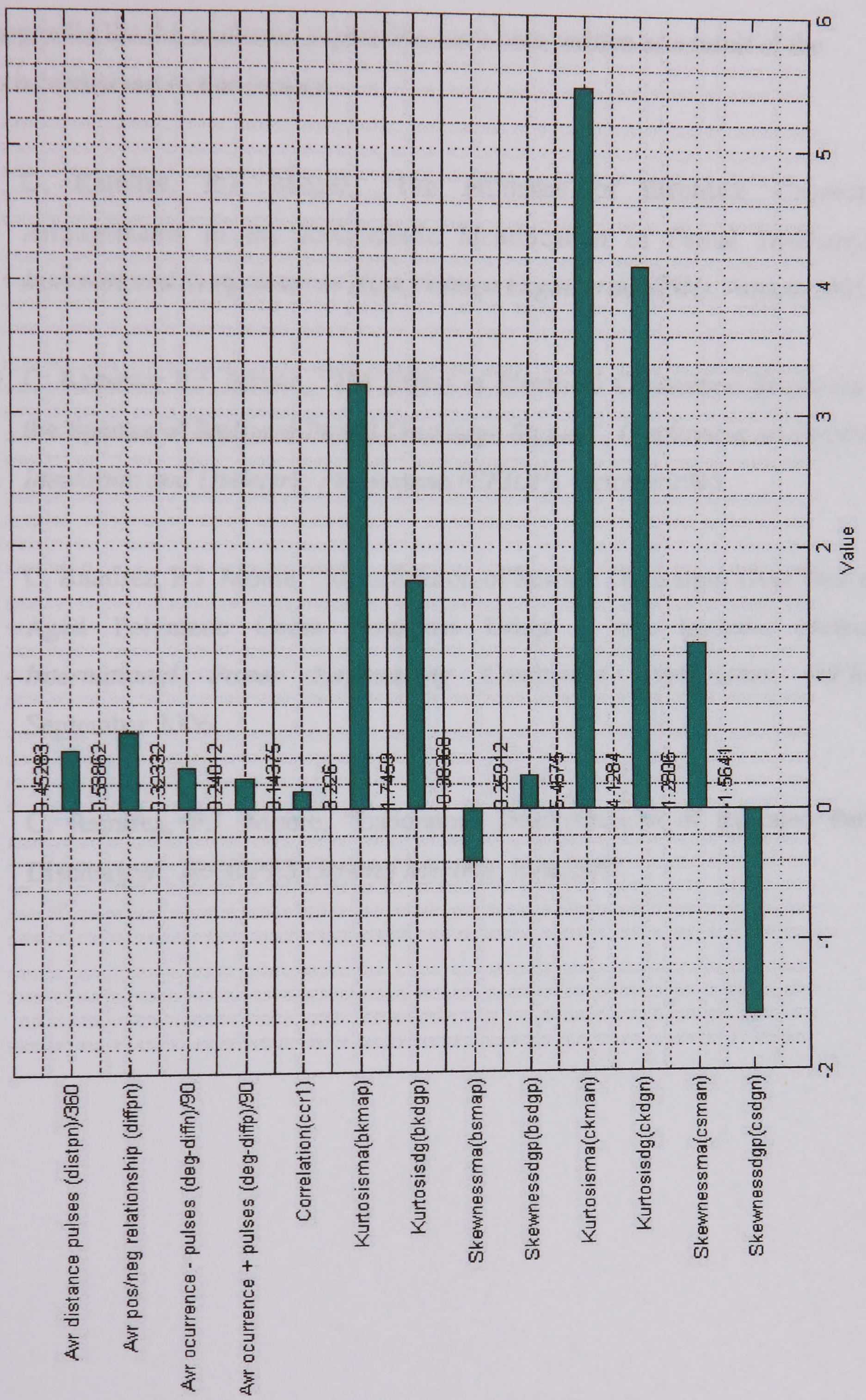

Graphical representation of statistical operators for pressboard in antenna 3

Appendix J: Academic papers

This appendix list the academic papers that have been written as a result of the research carried out in this project.

[1] C. Ramirez, P.J. Moore, "The Influence of Electrical Connection Arrangements in the Radiometric Identification of Partial Discharges", *International Symposium in High Voltage Engineering (ISH)*, August 2005.

[2] C. Ramirez, P.J. Moore, "The Effect of Electrical Connection Structures on the Spectra of Radiated Partial Discharge Signals", *Conference on Electrical Insulation and Dielectric Phenomena (CEIDP)*, October 2005.

[3] C. Ramirez, P.J. Moore, "Identification of Surface Discharges Over New and Aged Polymeric Chain Insulators Using a non Invasive Method", *International Power Engineering Conference Universities (UPEC)*, September 2006.

[4] C. Ramirez, P.J. Moore, "Laboratory Discrimination of Radiated Partial Discharges", *IEEE PES General Meeting*, June 2007.